[03]

Eur. J. Inorg. Chem. 2012, 337–584

D 3715

EurJIC

European Journal of Inorganic Chemistry

3/2012

3rd January Issue

Cluster Issue: Cooperative & Redox Non-Innocent Ligands in Directing Organometallic Reactivity

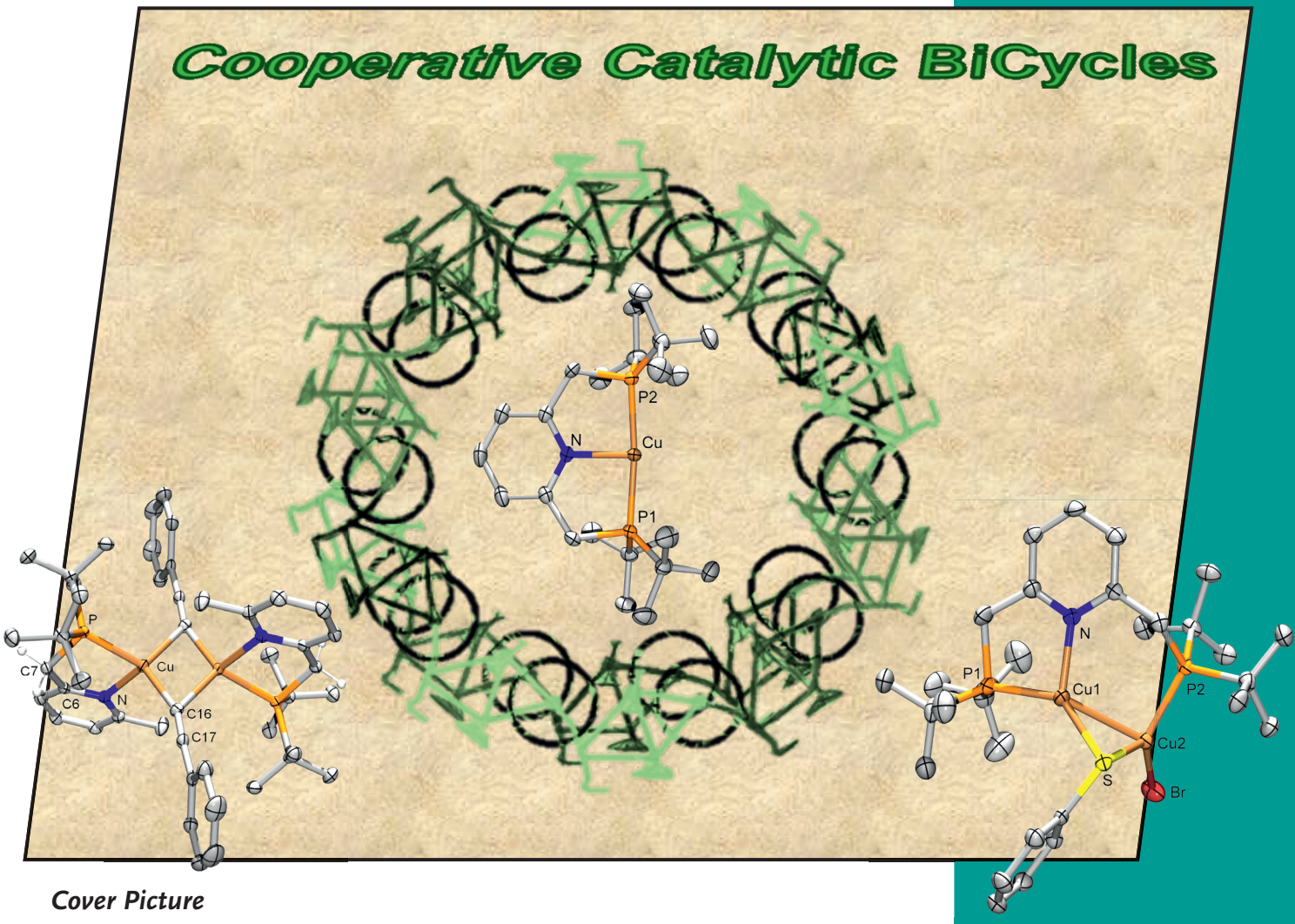

Cover Picture

Jarl Ivar van der Vlugt

Cooperative Catalysis with First-Row Late Transition Metals

Microreviews by

Jarl Ivar van der Vlugt; Marine Desage-El Murr, Louis Fensterbank, Max Malacria et al.; Paul J. Low et al.; Sven Schneider et al.; X. Peter Zhang et al.; Kenneth G. Caulton; Peter Burger et al.

A Journal of ChemPubSoc Europe

WILEY-VCH

www.eurjic.org

EJICFK (03) 337–584 (2012) · ISSN 1434-1948 · No. 03/2012

EurJIC
European Journal of Inorganic Chemistry

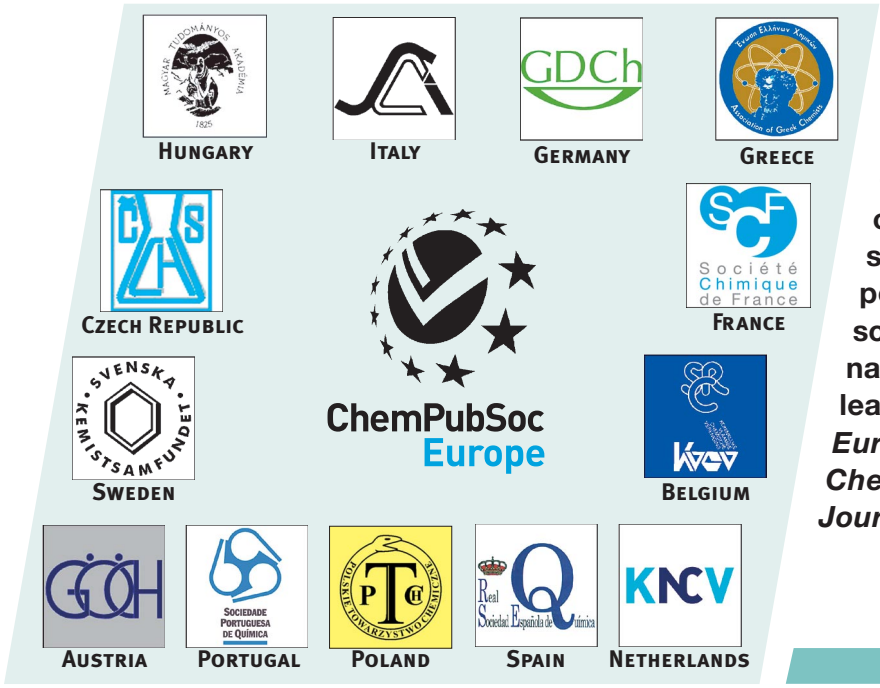

EurJIC is a journal of ChemPubSoc Europe, a union of 16 European chemical societies formed for the purpose of publishing high-quality science. All owners merged their national journals to form two leading chemistry journals, the *European Journal of Inorganic Chemistry* and the *European Journal of Organic Chemistry*.

Other ChemPubSoc Europe journals are *Chemistry – A European Journal*, *ChemBioChem*, *ChemPhysChem*, *ChemMedChem*, *ChemSusChem* and *ChemCatChem*.

FRONT COVER PICTURE

The front cover picture shows selected examples of solid-state structures, combining a cheap metal (here copper) with smart ligands (here lutidinyl-based PN and PNP systems), amenable to bifunctional bond activation of (small molecule) substrates and cooperative catalysis. Financial support for this work from the Netherlands' Research Council (NWO) is gratefully acknowledged. These structures are accompanied by perpetual 'tandem-bicycles'. Miss Christine Czauderna is thanked for the inspirational design. Progress and potential for the emerging field of cooperative catalysis with first-row transition metals is outlined in the Microreview by J. I. van der Vlugt on p. 363ff.

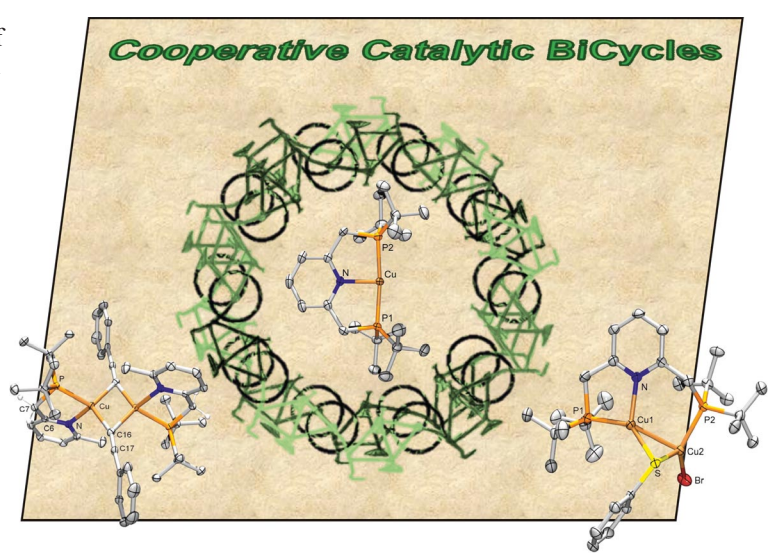

 © 2012 Wiley-VCH Verlag GmbH & Co. KGaA, Weinheim

Cooperative & Redox Non-Innocent Ligands in Directing Organometallic Reactivity

Karen Hindson
Editor, EurJIC

This Cluster Issue covers a buzz topic in the reactivity of complexes, a core theme for *EurJIC*. It is thus an ideal subject for a cluster issue and I'd like to thank *EurJIC*'s Editorial Board member, Bas de Bruin, for taking on the job of Guest Editor and doing it with such enthusiasm. The issue provides something for a broad range of chemists, not only those already active in the field, as the comprehensive Editorial by the Guest Editor and the Essay by one of the leaders in the field, Wolfgang Kaim, shows: for those who stumble over the term "non-innocence" as it personifies the metal and the ligand, you will discover that in this chemistry there is indeed something like a dialogue between metal and ligand; confused about the difference between cooperative and non-innocent ligands? – Bas puts it in a nutshell; if you simply want to know what all the fuss is about, the Essay will draw together the threads, from small molecule radicals through molecular conductors to high-temperature superconducting cuprates. These two introductory articles cover the ground comprehensively. I am sure that after reading them, you will be eager for more. I'll not keep you any longer from the pleasure.

Guest Editorial

Bas de Bruin
***EurJIC* Editorial Board Member**
University of Amsterdam
The Netherlands

This special issue focuses on the properties and application of two special ligand-types: 'cooperative' and 'redox non-innocent' ligands. These ligands have attracted much attention in coordination chemistry, and more recently also in the field of catalysis.

The properties of a metal complex as a whole are the result of the interaction of the metal centre with its surrounding ligands. Ligands strongly influence the reactivity and selectivity of metal complexes, but in most cases they play spectator roles, maintaining their original structure, while the reactivity takes place at the metal centre. In catalysis, for example, the traditional approach is to change the steric and electronic properties of the ligands in order to influence the performance of the catalyst. Although a sub-classification of ligands, including hemilabile, hybrid or supramolecular systems, may be useful to emphasize certain ligand properties, the basic idea of 'catalysis controlled by ligand design' is always the same: modification of the steric and electronic properties *of the metal centre*, thus effecting chemo- and enantioselectivity by enhancing the rate of a desired pathway over non-desired ones. Recently, new approaches have emerged that deviate from this traditional concept, by allowing *reactive* ligands to play a much more prominent role in elementary bond-making and bond-breaking steps at a rather distant position from the metal. The central idea of these new approaches is that the metal and the ligand can cooperate in a synergistic manner and that their interplay facilitates the chemical process. In this light, complexes based on so-called 'cooperative' and 'redox non-innocent' ligands have shown remarkable catalytic activities, and they hold the promise to uncover many exciting new (catalytic) reactions.

New approaches that challenge traditional concepts

 © 2012 Wiley-VCH Verlag GmbH & Co. KGaA, Weinheim

Cooperative ligands may be defined as those that participate directly in a bond-activation reaction and undergo reversible chemical transformations.[1] Besides the reactive ligand, the metal also bears its intrinsic reactivity, or, at the least, functions as a binding site to bring substrates together. Thus, the metal and the ligand cooperate in a synergistic manner and their interplay facilitates a chemical process.

Cooperation exploits synergism

Redox non-innocent ligands are redox-active ligands, which can be easily oxidized or reduced by one or more electrons, and can serve as electron reservoirs. Often these ligands transform into ligand radicals upon binding to transition metals. This can lead to confusion about the electronic structure of the complex. For example, seemingly closed-shell, diamagnetic $Fe^{II}(L^0)$ species may in reality be open-shell diamagnetic ligand radical complexes $Fe^{\cdot III}(L^{-1\cdot})$ with antiferromagnetically coupled metal and ligand electrons. These are distinct 'redox isomers' (not just resonance structures) with very different properties and reactivities. Therefore, a detailed understanding of these electronic structures is of utmost importance. Hence, for complexes with 'redox non-innocent' ligands the actual d-electron configuration of the metal (which defines the 'real' or 'spectroscopic' metal oxidation state) may differ from the formal oxidation state. However, this is not always the case, as it depends on the total oxidation level of the complex and the type of other ligands that are present. This ambiguity in 'real' oxidation state assignments of the metal and the redox-active ligands is the origin of the name of these ligands: 'redox non-innocent'.[2] Redox non-innocent ligands can, among others, initiate and control radical-type transformations or serve as electron reservoirs to allow multi-electron transformations for metals that are reluctant to undergo such transformations otherwise. Some redox non-innocent ligands can also be classified as 'cooperative' ligands. Since part of the bond-activation processes and/or redox processes can take place at the *ligand*, these reactive or 'actor' ligands can be used to replace expensive 2nd or 3rd row transition metals by much cheaper and less toxic 1st row transition metals in catalysis. Furthermore, cooperative effects make it possible to enhance activities and increase selectivities in catalytic reactions.

Redox isomers can play a role

Activation by cheaper metals in catalysis

This special issue focuses on such new applications (catalysis) and novel developments (and model studies) of 'cooperative and redox non-innocent' ligands in inorganic chemistry and catalysis. The issue contains a nice blend of viewpoints, descriptions and original new work in the form of short reviews, short communications and full papers.

The issue starts with an excellent Essay by Wolfgang Kaim, one of the pioneers in the field, in which he gives his view on the concept of redox non-innocent ligands, including current developments. A set of seven reviews complement this essay, and all together they provide a nice overview over the field of 'cooperative and redox non-innocent ligands'.

Overview of the field

The review of Jarl Ivar van der Vlugt gives a general overview of current metal–ligand cooperative reactivity in catalytic reactions employing first-row transition metals and of future opportunities to complement or replace noble-metal systems. The review of Ken Caulton provides a tutorial overview of the systematics, warnings and future projections concerning the use of redox non-innocent amide/imine ligands in transition-metal coordination chemistry, and discusses the factors which favour oxidized versus reduced ligand forms. The review of Phil Schauer and Paul Low summarizes the chemical behaviour of redox non-innocent σ-alkynyl ligands that easily form ligand radical species, which are crucial to understand the reactivity of these interesting open-shell organometallic complexes. Marine Desage-El Murr, Louis Fensterbank, Max Malacria and co-workers review the chemistry and synthetic (catalytic) applications of low-valent iron complexes bearing redox non-innocent ligands. For some of the compounds discussed, the authors have reinvestigated the DFT electronic structure themselves, and they provide additional information based on a comparative analysis of the available spectroscopic data. The microreview of Peter Zhang and co-workers summarizes his work on enantioselective cyclopropanation reactions with metallo-radical cobalt–porphyrin complexes, in which the redox non-innocence of carbene ligands plays an important role. The microreview is complemented with original new data that focus on ligand effects on the (enantio)selectivity of the reactions. The review of Sven Schneider gives a nice overview of the coordination chemistry of electron-rich metal complexes containing the aliphatic, anionic diphosphanylamido ligand $\{N(CH_2CH_2PR_2)_2\}$ in comparison with related anionic PEP (E = C, N) pincer ligands. The use of these ligands in cooperative bifunctional stoichiometric bond-activation reactions and catalysis is discussed for several examples. Peter Burger reviews his recent work on Rh and Ir complexes with redox non-innocent pyridine-2,6-diimine (PDI) ligands.

Beside the above reviews, the issue contains a wide variety of original new work from prominent researchers in the field. The importance of metal–ligand cooperativity in catalysis is illustrated by contributions from the following pioneers: Thomas Rauchfuss shows that ligand protonation is an effective method to increase the Lewis acidity of iridium(III) complexes. Joost Reek, Albrecht Berkessel and co-workers describe the use of P-stereogenic sulfonamide-phosphinamides as new acid/base type cooperative ligand building-blocks used in Rh-based enantioselective hydrogenation reactions, and Takao Ikariya, Shigeki Kuwata and co-workers describe the metal–ligand cooperativity effects in transfer hydrogenation of ketones with alcohols, employing organometallic oxime complexes as novel bifunctional catalysts.

Scope of the contributions

 © 2012 Wiley-VCH Verlag GmbH & Co. KGaA, Weinheim

Several authors, among them many well-known experts in the field, have contributed to this special *EurJIC* issue with excellent, original research papers about the (catalytic) application of redox-active ligands. This clearly illustrates the importance of redox non-innocent ligands and shows a strong motivation to further develop this research area. Paul Chirik, Karl Wieghardt and co-workers report interesting new data on the redox non-innocence of the pyridine-2,6-diimine ligand (PDI) and describe the properties of a variety of isolated manganese carbonyl complexes containing 1e- and 2e-reduced forms of the PDI ligand. Peter Budzelaar reports a DFT study on the reactions of imine/pyridine ligands with main-group metal alkyl compounds, in which the redox non-innocence of the ligand plays an important role, thus explaining the experimentally observed radical-type reactions. Frank Neese and Patrick Holland discuss the redox non-innocence of end-on and side-on coordinated nitrile ligands in low-valent Fe complexes and show how one-electron transfer to ligands and two-electron backbonding to ligands may be distinguished. A somewhat related study by Cristina Tejel and co-workers shows that π-coordinated imine ligands are redox non-innocent. These imines are involved in a highly unusual redox equilibrium involving several associated modes of isomerism. Klaus Theopold discusses the redox non-innocence of diimine ligands in chromium chemistry and shows that imine insertion into chromium-alkyl bonds easily takes place in the case of the neutral, oxidized form of the ligand, but is prevented after electron transfer to the redox non-innocent diimine ligand. Craig Grapperhaus makes efficient use of the redox non-innocence of thiolato ligands to capture alkynes, which have the tendency to bind selectively/preferentially to the sulfur-radical ligands of oxidized ruthenium-thiyl complexes. Claudio Verani, Richard Lord and co-workers report an unexpected aerobic cyclization reaction of the *N*,*N*′-bis(3,5-di-*tert*-butyl-2-hydroxyphenyl)-1,2-phenylenediamine ligand in the coordination sphere of cobalt(II) to form a new mixed phenolate/phenoxazinylate radical species. They further discuss the properties of the thus formed new redox-active ligands as electron reservoirs. Very unusual electrochemical behaviour of [Re(bipy)(imidazole)] complexes is reported by František Hartl, Antonín Vlček Jr. and co-workers. Electrochemical reduction of the bipy ligand leads to unexpected "deprotonation" of the rhenium-coordinated imidazole ligand. Pierre Braunstein, Biprajit Sarkar and co-workers report new Ru complexes with redox non-innocent catechol/quinone-type ligands in different oxidation states of the ligand and apply these complexes in transfer hydrogenation reactions. Jake Soper discusses the use of oxorhenium(V) complexes with redox non-innocent catechol/quinone-type ligands for the aerobic oxidation of alcohols, and Alan Heyduk reports the use of a redox non-innocent ONO pincer-type ligand that functions as an electron- and proton reservoir in the unusual activation of dioxygen at a d^0 Zr^{IV} site. John Berry reports catalytic amination reactions of benzylic C−H bonds mediated by dinuclear Rh complexes bearing redox-active ligands. Related catalytic amination reactions of allylic C−H bonds mediated by ruthenium-porphyrin complexes are reported by Emma Gallo and co-workers, while Kin Shing Chan reports catalytic benzene functionalization reactions mediated by metalloradical cobalt-porphyrin complexes.

It is clear that the research field of cooperative and redox non-innocent ligands has developed enormously from a limited focus-area for a selected group of spectroscopists to an energetic 'bioinspired' research area covering diverse topics ranging from catalysis, materials for energy storage/conversion, electrosynthesis, gas purification, biomimetic transformations and sustainable synthesis. A bright future is ahead of us, and I expect much from forthcoming reactivity studies based on cooperative 'actor' ligands. It has given me joy to collect these contributions; I hope it gives you at least equal joy to read and discover the content of this special issue.

Bright future ahead

[1] H. Grützmacher, *Angew. Chem. Int. Ed.* **2008**, *47*, 1814; J. I. van der Vlugt, J. N. H. Reek, *Angew. Chem. Int. Ed.* **2009**, *48*, 8832.
[2] C. K. Jørgensen, *Coord. Chem. Rev.* **1966**, *1*, 164.

 © 2012 Wiley-VCH Verlag GmbH & Co. KGaA, Weinheim

DOI: 10.1002/ejic.201101359

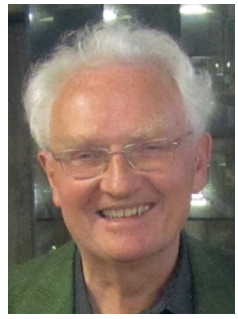

The Shrinking World of Innocent Ligands: Conventional and Non-Conventional Redox-Active Ligands

Wolfgang Kaim*

Keywords: Cyanides / Non-innocent ligands / Organometallic chemistry / Oxido ligands

This essay for EurJIC's cluster issue on cooperative and redox non-innocent ligands introduces the reader to redox-active ligands, which range from the small archetypical $NO^{+/\bullet/-}$ and $O_2^{0/\bullet-/2-}$systems via the classical 1,4-dihetero-1,3-diene chelates (e.g. α-diimine, dithiolene, or *o*-quinone redox series) to π-conjugated macrocycles. The increased attention paid recently to the redox activity of ligands in coordination chemistry has now prompted wider successful searches, resulting in the establishing of less-conventional examples such as cyanide, carbon monoxide, thioethers, or acetylacetonate derivatives as non-innocently behaving ligands. By considering situations with significantly covalent metal–ligand bonding, the cases of metal–oxo, metal–hydrido, and organometallic compounds will also be addressed, with a perspective on how pervasive non-innocent ligand behavior is. The materials and reactivity potential of redox-active ligands will be pointed out.

Although viewed by some as just a convenient fiction,[1] the oxidation states[2] continue to serve their double role in inorganic chemistry, both as a means of electron bookkeeping as well as an indicator of the electron configuration and thus of expected physical properties and corresponding chemical or biochemical functionality.[3]

Relating to redox-active ("non-innocent"[2]) and thus, literally, ambi-valent ligands (either in electronic hybrid or valence-tautomeric complexes), a significant section of *applied* non-innocent ligand science thus concerns their function in materials with sought-after physical properties. Prime examples include:
(1) molecular conductors and switches such as Cu^{n+}-$TCNQ^{n-}$[4] or high-temperature superconductors such as $YBa_2Cu_3O_{7-x}$ with partially oxidized "oxide" bridges,[5]
(2) molecular magnets with redox-active ligands such as monoatomic $O^{2-/\bullet-}$, diatomic cyanide, or polyatomic $TCNQ^{n-}$ as spin carriers or superexchange mediators,[6] and
(3) photoactive components such as sensitizers or emitters with metal-to-ligand, ligand-to-metal, or ligand-to-ligand charge-transfer excited states, which involve readily oxidized or reduced ligands.[7]

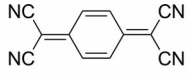

7,7,8,8-tetracyano-p-quinodimethane (TCNQ)

[a] Institut für Anorganische Chemie, Universität Stuttgart, Pfaffenwaldring 55, 70550 Stuttgart, Germany
E-mail: kaim@iac.uni-stuttgart.de

Even closer to the center of chemistry, the recognition of non-innocent ligand behavior[8] has opened new pathways for synthetic conversions, for instance, by permitting the use of inert[9] or otherwise unsuitable metal sites in molecules for transformations that were previously limited, e.g. to precious metal complexes.[10] In contrast to innocent "spectator" or "reporter" ligands, the so-called "cooperative ligands"[11] (possibly but not necessarily redox-active) are distinguished by synergistic metal–ligand interactions leading to transformation of a substrate.

There are many different manifestations of non-innocent ligand behavior that have been reviewed.[12] From a functional viewpoint, redox-active ligands can serve as:
(1) substrates of reactions (such as O_2 or quinones/catechols in oxygenations),
(2) reactive intermediates (such as H-abstracting oxyl or oxidizing phenoxyl radicals), or
(3) controlling electron reservoirs (such as dithiolene or porphyrin π systems).

Among the typical redox non-innocent ligands are several biologically relevant examples.[13] These include small molecular species $NO^{+/\bullet/-}$ and $O_2^{0/\bullet-/2-}$, medium-size 4-center chelate redox systems (Scheme 1) with *o*-quinone/*o*-semiquinone/catecholate,[14] α-iminocarbonyl[15] or α-dithiolene/ene-1,2-dithiolate functions[16] of corresponding cofactors,[13] and larger heterocyclic π systems such as the tetrapyrrole ligands (porphyrins, corroles). Non-biorelevant examples are the α-dicarbonyl, α-diimine,[17,18] and α-azo-functional[19] 4-center systems as well as the N=N containing tetrazine ligands,[20] or acceptor-substituted olefins such as TCNE and TCNQ.[21] The latter has been shown to act

 © 2012 Wiley-VCH Verlag GmbH & Co. KGaA, Weinheim

either completely innocently as a tetradentate tetranitrile bridge to four carbonyl-metal entities or as redox-active, considerably reduced ligand towards oxidizable complex fragments, which produce mixed-valent metal situations.[22] Thus, innocence or non-innocence is not the permanent attribute of a ligand, but molecules can *behave*[8] as innocent or non-innocent ligands towards redox-active metals under specific circumstances, in a certain situation.

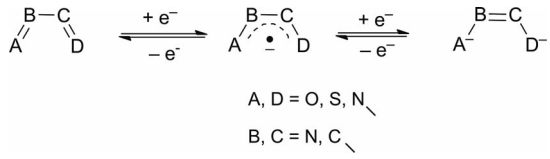

Scheme 1. The chelating 1,4-dihetero-1,3-diene redox system.

While the potential for non-innocent ligand behavior is obvious for the very easily reducible and correspondingly employed TCNQ acceptor,[21] or for nitrosoarenes,[23] there are ligands with less eye-catching non-innocence. For instance, the substitutional modification[24] of the "NacNac" ligand[24] in $[MeNC(Me)C(H)C(Me)NMe]^-$ has made it potentially redox-active, i.e. susceptible to one-electron oxidation in a nickel complex, as indirectly deduced from physical properties such as magnetism. Such an assignment, referred to as "hidden non-innocence",[24a] raises the questions what other, perhaps even more commonly and widely used, ligands can be tweaked to exhibit non-innocent behavior and what consequences this might have for electronic structure, physical properties, and reactivity.

As another example, sulfur-based non-innocent ligands can involve sulfenyl ("thiyl") radicals, $RS^\bullet$ (one-electron oxidized thiolates),[25] or radical cations $[RSR]^{\bullet+}$ from thioethers. In the form of 1,4,7-triheterononacycle ligands, the latter are predominantly involved in spin accommodation for complexes that have, sometimes, been advertised as compounds with unusual metal oxidation states such as Pt^{III} or Au^{II}:[26] $[M^{n+1}(RSR)] \leftrightarrow [M^n(RSR^{\bullet+})]$, e.g. M = Pt and $n = 2$, or M = Au and $n = 1$. Depending on the chemist's perspective, one may find an even greater satisfaction in proving the stabilization of organosulfur radical cations by transition metals in their *normal* oxidation states.

Three of the most common but outwardly very different kinds of ligands will be referred to here with respect to their little-discussed potential for non-innocence, viz.:
(1) cyanide as the oldest synthetic ligand and one of the purportedly best-understood ligands in coordination chemistry,[27]
(2) the oxo ligand[28] with its ubiquity in geochemistry and materials science, and
(3) the hydride and alkyl ligands and other organic molecules from organometallic chemistry.[29–31]

All these ligands are biorelevant, and their "hidden" non-innocence may be essential for their biochemical functioning.[32] While cyanide has been established, less than two decades ago, as a ligand for iron in hydrogenases,[33] the role of the oxo ligand beyond a mere inert oxide function has been recognized, especially for P450-dependent enzymes[34] and copper-containing monooxygenases.[35] Metal alkyl functions were established for cobalamines (B_{12} coenzymes)[36] and for methane-producing nickel-dependent enzymes.[32,37]

Non-Innocent Diatomics

The classical non-innocent ligand[2] is NO with its distinctly different, well-established charge states NO^+, $NO^\bullet$, and NO^-,[38] which play a major role in the biological function of "NO" as frequently iron-coordinated species for the synthesis, release, transfer, and selective uptake of nitric oxide.[39] However, even in this well-researched field, there may be surprises: On the basis of the recognition of a three-electron-reduced dinitrogen species, $N_2^{\bullet 3-}$, in an electronically and sterically confined situation,[40] the isoelectronic radical dianion $NO^{\bullet 2-}$, the fourth member in the NO^k series, was envisaged,[41] prepared, and characterized recently.[42] The ions $N_2^{\bullet 3-}$ and $NO^{\bullet 2-}$ are isoelectronic with the superoxide radical, $O_2^{\bullet -}$, the intermediate of a redox series $O_2^{0/\bullet -/2-}$ with a long non-innocent ligand history[43] and with enormous biological relevance.[44]

Very recently,[26,45] a completely documented case of reduced cyanide, viz., three $CN^{1.67-}$ ions stabilized by cobalt(–I) in $M_3[Co(CN)_3]$, M = Sr, Ba, was reported. The material was obtained by a high-temperature (1200 K) "solid-state" route and not by a conventional coordination chemistry procedure. The diamagnetic compounds contain $[Co(CN)_3]^{6-}$ with trigonal-planar tricyanocobaltate and significantly lengthened C–N bonds of about 1.24 Å relative to the typical[27] 1.15 Å for coordinated CN^-.

The results for $[Co^{-I}\{CN^{(5/3)-}\}_3]^{6-}$ demonstrate that the cyanide ligand, while always acknowledged as a π acceptor,[27] can exhibit a hitherto undocumented non-innocent behavior,[26,45] supported by the 18 valence electron configuration for $[Co(CN)_3]^{6-}$, by the d^{10} closed-shell stabilization for Co^{-I}, and by charge compensation through the metal dications. Other super-reduced diatomics like paramagnetic $N_2^{\bullet 3-}$[40,41] or $NO^{\bullet 2-}$[41,42] are also stabilized by higher-valent metal species, as is the carbon monoxide radical anion,[46] which can dimerize to form a strong covalent bond in bridging $(\mu\text{-}\eta^1{:}\eta^1\text{-}C_2O_2)^{2-}$.[46a,46b,46e]

Non-Innocent Oxide

The non-innocent ligand potential of the oxide dianion, O^{2-}, implies that it can be oxidized to the reactive oxyl radical anion, $O^{\bullet -}$ (Scheme 2).

The oxyl radical anion has been invoked as a conceivable ligand for oxidized heme- or nonheme-iron intermediates and for the O_2-producing step of photosystem II.[34] Even if metal-stabilized, the monoatomic oxyl radical would be expected to exhibit typical spin-localized radical reactivity such as H abstraction from C–H bonds. Such an abstraction is commonly believed to be the first step of the "rebound" mechanism of monooxygenation.[32,34a] While most

 © 2012 Wiley-VCH Verlag GmbH & Co. KGaA, Weinheim

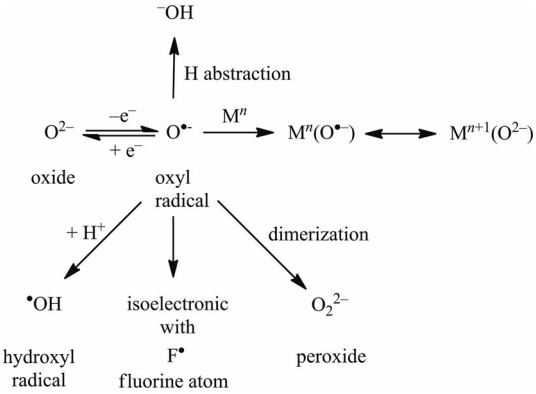

Scheme 2. Elementary oxyl radical reactivity.

polyatomic radical anion ligands[47] with some persistence are spin and charge delocalized π systems that prefer electron-transfer reactivity to free radical-type hydrogen abstraction, the concentration of spin at one atom favors the latter in the case of oxyliron intermediates.

Oxyl was also postulated as a ligand of ruthenium in a semiquinone complex,[48] which was later associated with water oxidation catalysis.[49,50] Extensive calculations have led to a reassignment,[49] taking into account the presence of a similarly non-innocent catecholate/quinone ligand. The mechanism of water oxidation has been formulated as involving the catechol/quinone and H_2O/O_2 redox systems as non-innocent ligands at a largely redox-invariant but not inactive ruthenium center.[49]

Given the affinity of copper to radical ligands,[51] the role of copper(II) oxyl in copper-dependent monooxygenation catalysis was debated,[35] but there is no firm experimental evidence yet. For instance, a $[Cu(L)(O)]^+$ species as conceivable for monooxygenation can be described with a copper(III)/oxo or copper(II)/oxyl oxidation state combination. The latter offers a further alternative between singlet or triplet ground state.[52]

To add a further metal for complication, in the recent discussion on the mechanism of action of copper-dependent particulate methane monooxygenase, which converts one of the strong C–H bonds of CH_4 to form methanol (CH_3OH), there has been evidence for a dinuclear Cu–O–Cu active site[53] with either a Cu^{II}–(μ-O^{2-})–Cu^{III} (mixed-valent) or Cu^{II}–($O^{\bullet-}$)–Cu^{II} radical-bridge formulation.[54] Such mixed-valency vs. radical bridge alternatives have been known for some time in coordination chemistry, e.g. as Ru^{II}(μ-BL^{2-})–Ru^{III} vs. the Ru^{II}–(μ-$BL^{\bullet-}$)–Ru^{II} alternative.[12]

In connection with the Cu^nO^m oxidation state ambiguity, the high-temperature superconducting cuprates cannot be overlooked. Applying conventional oxidation state assignments to the prototypical $Y^{III}(Ba^{II})_2Cu_3O_{7-x}$, the $\{Cu_3O_{7-x}\}^{7-}$ entity has to involve $Cu^{III}Cu^{II}$ mixed valency and/or partial oxidation of the oxide ions. In fact, attempts to understand the conduction properties from a chemical viewpoint have suggested that the nonmetallic O^{n-} constituents of the cuprates are hole centers that carry significant spin, ferromagnetically coupled to Cu^{II}.[5]

Non-Innocent Organic Ligands and Hydride

The potential of organometallic ligands for non-innocent behavior may be introduced by remembering the principal bonding patterns:

(1) π bonding, organic ligands include potentially non-innocent[55] alkenes such as electron-accepting tetracyanoethene, $(NC)_2C{=}C(CN)_2$ = TCNE, which can act as η^2-$TCNE^{2-}$ towards platinum metals,[55] or cyclopentadienides $C_5R_5^-$ (with oxidized $C_5R_5^\bullet$ acting as true cyclopentadien*yl* radicals),[56]

(2) σ- and π bonding, ligands include reducible CO (→ oligomerization[46]), non-innocent carbenes,[57] or metal-capped C_n chains,[58] and

(3) σ bonding dominates the interaction of metals with hydride, alkyl, and aryl groups.

By invoking at least partial covalency, the concept of oxidation states has found less popularity in organometallic chemistry. Apparently, relevant terms such as "carbanion" or "carbocation" have largely been used to describe reactivity, i.e. kinetic aspects. However, the importance of this research area and its attraction for scientists from different disciplines create the need and opportunity to apply several complementary concepts in the analysis of reactivity and properties. When discussing such concepts, the pioneering work by Kochi, Fukuzumi, and Astruc have to be cited, summarized in excellent volumes.[29,30] This groundwork and the more recent approaches by de Bruin and Budzelaar[57,59d] on M–C bond uses relying on electron transfer allow me to add just a few thoughts.

By considering alkyl (simplest version: methyl) as a *bona fide* ligand in coordination chemistry, Scheme 3 indicates the limiting formulations of carbanion and free radical ligands, and, for the latter, its propensity for H abstraction and dimerization. Dimerization of radical intermediates of non-innocently behaving ligands was also noted for the carbon monoxide radical anion,[46b] and even the dimerized thiyl radical anion $2\ S^{\bullet-} \rightarrow S_2^{2-}$ in pyrite, FeS_2, can be included in this category (note that $S^{\bullet-}$ is the heavier homologue of oxyl, $O^{\bullet-}$).

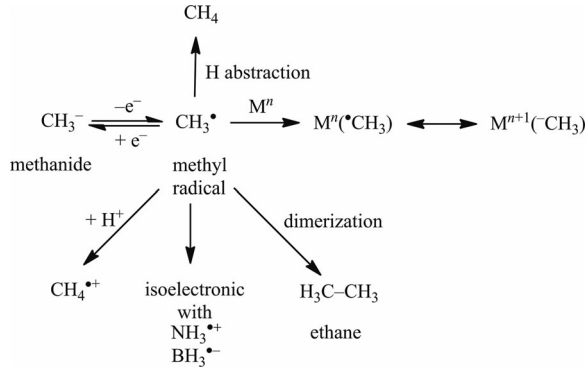

Scheme 3. Elementary methyl radical reactivity.

 © 2012 Wiley-VCH Verlag GmbH & Co. KGaA, Weinheim

When bonded to electropositive metals, "alkyl" ligands are more fittingly described as alkanido ligands, R^-, strong σ donors. This and the coordinative saturation distinguish R^- from the oxide/oxyl ligands, which can thus act as bridges or directly attack substrates. The donor effect of R^- supports high metal oxidation states, and the characteristic ambivalence for a situation with non-innocent ligand behavior in a coordination compound involves ambiguities such as M^n–(R^-) ↔ M^{n-1}–($R^\bullet$). The radical ligand formulation has been discussed in connection with general electron-transfer reactivity of organometallics.[29,30,59] Obtained by photoexcitation or thermally, the two-spin system as obtained from a spin-paired precursor can react by an internal rearrangement ("cage") process or dissociate into separate "escape" compounds, leading to characteristic products in each case.[59] In fact, the instability of many transition-metal alkyls may be connected to the internal electron transfer, producing both reactive ligand radicals and possibly reactive metal oxidation states.

The prime example for this kind of organometallic reactivity is the cobalamin ("B_{12}") coenzyme, which contains a corrin-chelated [Co^{III}](CH_2R') entity.[36] Ionic alkylation of substrates or homolytic radical generation for H abstraction from rearranging substrates in mutase enzymes are the two kinds of biochemical functions associated with cobalamins (Scheme 4).

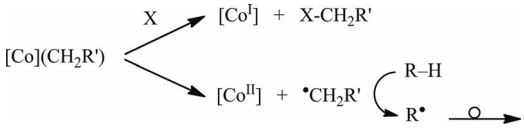

Scheme 4. B_{12} reactivity pathways.

While the conventional formulation involves trivalent cobalt (low spin d^6) and a carbanionic axial ligand, the reactivity options (Scheme 4) betray the non-innocent potential of the alkyl ligand.

The requirement for the otherwise uncommon biometal cobalt comes from the necessity to perform the classical d^6/d^8 oxidative-addition/reductive-elimination sequence under physiological conditions and with bioavailable ligands, i.e. involving the physiologically accessible oxidation states (+I)–(+III). Neither iron with oxidation states (0)–(+II) nor nickel with (+II)–(+IV) would be suitable, while the heavier homologues of cobalt are not bioavailable.

In connection with the coordination chemistry of cobalt,[60] the simplest ligand of all, H, is also notoriously redox ambivalent – the "hydride" = H^- designation is a frequent source for misunderstanding when discussing hydridocobalt species between L_nCo^{III}–(H^-) and $(OC)_4Co^{-I}$–(H^+) formulations.

Ubiquity of Non-Innocence?

From the above, it may appear that only a few classes of ligands are completely free of "guilt" in the sense that they will *never* become redox active in the coordinated form under ordinary laboratory conditions. Under the right circumstances, non-innocent ligand behavior is thus more universal than previously thought. While the earlier disregard of radical ligands, variously described in the past as oddities, laboratory curiosities, or exotic intermediates, may have been caused by the chemists' strong intuitive bias for electron-paired situations, the recognition of hidden or conspicuous open-shell configurations may now foster a better understanding of new kinds of reactivity in attractive areas such as H_2 conversion.[61] Although this may not herald the "end of all innocence", the now recognized role of redox-active ligands in the biochemical context, in electronically functional materials for energy and information transfer, and in the development of synthetic strategies ("radical ligands confer nobility on base-metal catalysts",[10] "cheap metals for noble tasks") illustrates that the scientists' imagination must not be restricted by too limited views of the ligands' capability.

[1] a) R. Resta, *Nature* **2008**, *453*, 735; b) M. Jansen, U. Wedig, *Angew. Chem.* **2008**, *120*, 10176; *Angew. Chem. Int. Ed.* **2008**, *47*, 10026.
[2] a) C. K. Jørgensen, *Coord. Chem. Rev.* **1966**, *1*, 164; b) C. K. Jørgensen, *Oxidation Numbers and Oxidation States*, Springer, Berlin, **1969**; c) P. J. Chirik, *Inorg. Chem.* **2011**, *50*, 9737.
[3] P. Chaudhuri, C. N. Verdani, E. Bill, E. Bothe, T. Weyhermüller, K. Wieghardt, *J. Am. Chem. Soc.* **2001**, *123*, 2213.
[4] R. S. Potember, T. O. Poehler, D. O. Cowan, *Appl. Phys. Lett.* **1979**, *34*, 405.
[5] Y. Guo, J.-M. Langlois, W. A. Goddard, *Science* **1988**, *239*, 896.
[6] a) H. Zhao, M. J. Bazile Jr., J. R. Galán-Mascarós, K. R. Dunbar, *Angew. Chem.* **2003**, *115*, 1045; *Angew. Chem. Int. Ed.* **2003**, *42*, 1015; b) T. D. Harris, C. Coulon, R. Clérac, J. R. Long, *J. Am. Chem. Soc.* **2011**, *133*, 123.
[7] G. L. Geoffroy, M. S. Wrighton, *Organometallic Photochemistry*, Academic Press, New York, **1979**.
[8] M. D. Ward, J. A. McCleverty, *J. Chem. Soc., Dalton Trans.* **2002**, 275.
[9] a) K. J. Blackmore, J. W. Ziller, A. F. Heyduk, *Inorg. Chem.* **2005**, *44*, 5559; b) M. R. Haneline, A. F. Heyduk, *J. Am. Chem. Soc.* **2006**, *128*, 8410; c) N. A. Ketterer, H. Fan, K. J. Blackmore, X. Yang, J. W. Ziller, M.-H. Baik, A. F. Heyduk, *J. Am. Chem. Soc.* **2008**, *130*, 4364; d) R. A. Zarkesh, J. W. Ziller, A. F. Heyduk, *Angew. Chem.* **2008**, *120*, 4793; *Angew. Chem. Int. Ed.* **2008**, *47*, 4715; e) A. L. Smith, K. I. Hardcastle, J. D. Soper, *J. Am. Chem. Soc.* **2010**, *132*, 14358; f) F. Lu, R. A. Zarkesh, A. F. Heyduk, *Eur. J. Inorg. Chem.*, **2012**, 467–470; g) C. A. Lippert, K. Riener, J. D. Soper, *Eur. J. Inorg. Chem.*, **2012**, 554–561; h) W. I. Dzik, J. I. van der Vlugt, J. N. H. Reek, B. de Bruin, *Angew. Chem.* **2011**, *123*, 3416; *Angew. Chem. Int. Ed.* **2011**, *50*, 3356.
[10] P. J. Chirik, K. Wieghardt, *Science* **2010**, *327*, 794.
[11] a) H. Grützmacher, *Angew. Chem.* **2008**, *120*, 1838; *Angew. Chem. Int. Ed.* **2008**, *47*, 1814; b) J. I. van der Vlugt, *Eur. J. Inorg. Chem.*, **2012**, 363–375; c) S. Schneider, J. Meiners, B. Askevold, *Eur. J. Inorg. Chem.*, **2012**, 412–429.
[12] W. Kaim, *Inorg. Chem.* **2011**, *50*, 9752.
[13] a) W. Kaim, B. Schwederski, *Coord. Chem. Rev.* **2010**, *254*, 1580; b) W. Kaim, B. Schwederski, *Bioinorganic Chemistry*, Wiley, Chichester, **1994**.
[14] a) C. G. Pierpont, C. W. Lange, *Prog. Inorg. Chem.* **1994**, *41*, 331; b) A. L. Balch, *J. Am. Chem. Soc.* **1973**, *95*, 2723.

 © 2012 Wiley-VCH Verlag GmbH & Co. KGaA, Weinheim

[15] a) C. Bessenbacher, W. Kaim, *Z. Anorg. Allg. Chem.* **1989**, *577*, 39; b) C. C. Lu, E. Bill, T. Weyhermüller, E. Bothe, K. Wieghardt, *Inorg. Chem.* **2007**, *46*, 7880; c) H. P. Nayek, N. Arleth, I. Trapp, M. Löble, P. Oña-Burgos, M. Kuzdrowska, Y. Lan, A. K. Powell, F. Breher, P. W. Roesky, *Chem. Eur. J.* **2011**, *17*, 10814.

[16] a) A. Vlcek, *Coord. Chem. Rev.* **2010**, *254*, 1357, and following articles in that issue; b) R. Eisenberg, H. B. Gray, *Inorg. Chem.* **2011**, *50*, 9741; c) R. P. Mtei, E. Perera, B. Mogesa, B. Stein, P. Basu, M. L. Kirk, *Eur. J. Inorg. Chem.*, **2012**, *1*, 5467–5470.

[17] a) E. Uhlig, *Pure Appl. Chem.* **1988**, *60*, 1235; b) C. C. Scarborough, K. Wieghardt, *Inorg. Chem.* **2011**, *50*, 9773.

[18] a) K. G. Caulton, *Eur. J. Inorg. Chem.*, **2012**, 435–443; b) K. A. Kreisel, G. P. A. Yap, K. H. Theopold, *Eur. J. Inorg. Chem.*, **2012**, 520–529; c) W. Kaim, M. Sieger, S. Greulich, B. Sarkar, J. Fiedler, S. Záliš, *J. Organomet. Chem.* **2010**, *695*, 1052.

[19] W. Kaim, *Coord. Chem. Rev.* **2001**, *219–221*, 463.

[20] W. Kaim, *Coord. Chem. Rev.* **2002**, *230*, 127.

[21] W. Kaim, M. Moscherosch, *Coord. Chem. Rev.* **1994**, *129*, 157.

[22] a) H. Hartmann, W. Kaim, I. Hartenbach, Th. Schleid, M. Wanner, J. Fiedler, *Angew. Chem.* **2001**, *113*, 2927; *Angew. Chem. Int. Ed.* **2001**, *40*, 2842; b) A. N. Maity, B. Schwederski, B. Sarkar, S. Záliš, J. Fiedler, S. Kar, G. K. Lahiri, C. Duboc, M. Grunert, P. Gütlich, W. Kaim, *Inorg. Chem.* **2007**, *46*, 7312; c) S. Záliš, B. Sarkar, C. Duboc, W. Kaim, *Chem. Monthly* **2009**, *140*, 765.

[23] N. C. Tomson, L. A. Labios, T. Weyhermüller, J. S. Figueroa, K. Wieghardt, *Inorg. Chem.* **2011**, *50*, 5763.

[24] a) M. M. Khusniyarov, E. Bill, T. Weyhermüller, E. Bothe, K. Wieghardt, *Angew. Chem.* **2011**, *123*, 1690; *Angew. Chem. Int. Ed.* **2011**, *50*, 1652; b) R. E. Cowley, G. J. Christian, W. W. Brennessel, F. Neese, P. L. Holland, *Eur. J. Inorg. Chem.*, **2012**, 479–483.

[25] K. Ouch, M. S. Mashuta, C. A. Grapperhaus, *Eur. J. Inorg. Chem.*, **2012**, 475–478.

[26] a) E. Stephen, A. J. Blake, E. S. Davies, J. McMaster, M. Schröder, *Chem. Commun.* **2008**, 5707; b) E. Stephen, D. Huang, J. L. Shaw, A. J. Blake, D. Collison, E. S. Davies, R. Edge, J. A. K. Howard, E. J. L. McInnes, C. Wilson, J. Wolowska, J. McMaster, M. Schröder, *Chem. Eur. J.* **2011**, *17*, 10246.

[27] a) H. B. Gray, N. A. Beach, *J. Am. Chem. Soc.* **1963**, *85*, 2922; b) K. R. Dunbar, R. A. Heintz, *Prog. Inorg. Chem.* **1997**, *45*, 283; c) G. M. Chiarella, D. Y. Melgarejo, S. A. Koch, *J. Am. Chem. Soc.* **2006**, *128*, 1416; d) W. Kaim, *Angew. Chem.* **2011**, *123*, 10682; *Angew. Chem. Int. Ed.* **2011**, *50*, 10498.

[28] C. J. Ballhausen, H. B. Gray, *Inorg. Chem.* **1962**, *1*, 111.

[29] D. Astruc, *Organometallic Chemistry and Catalysis*, Springer, Berlin, **2007**.

[30] a) J. K. Kochi, *Organometallic Mechanisms and Catalysis*, Academic Press, New York, **1978**; b) S. Fukuzumi in *Electron Transfer in Chemistry*, Vol. 4 (Ed.: V. Balzani), Wiley-VCH, Weinheim, **2001**, p. 3.

[31] R. H. Crabtree, *The Organometallic Chemistry of the Transition Metals*, 5th ed., Wiley, Hoboken, **2009**.

[32] W. Kaim, B. Schwederski, *Bioinorganic Chemistry*, Wiley, Chichester, **1994**.

[33] S. Reissmann, E. Hochleitner, H. Wang, A. Paschos, F. Lottspeich, R. S. Glass, A. Böck, *Science* **2003**, *299*, 1067.

[34] a) B. Meunier, J. Bernadou, *Top. Catal.* **2002**, *21*, 47; b) S. Shaik, H. Hirao, D. Kumar, *Acc. Chem. Res.* **2007**, *40*, 532; c) S. Ye, F. Neese, *Proc. Natl. Acad. Sci. USA* **2011**, *108*, 1228; d) W. Ames, D. A. Pantazis, V. Krewald, N. Cox, J. Messinger, W. Lubitz, F. Neese, *J. Am. Chem. Soc.* **2011**, *133*, 19743.

[35] a) E. I. Solomon, P. Chen, M. Metz, S.-K. Lee, A. E. Palmer, *Angew. Chem.* **2001**, *113*, 4702; *Angew. Chem. Int. Ed.* **2001**, *40*, 4570; b) L. Que Jr., W. B. Tolman, *Nature* **2008**, *455*, 333; c) S. Hong, PhD Thesis, University of Minnesota, 2010; http://purl.umn.edu/94402.

[36] B. Kräutler in *Metal-Carbon Bonds in Enzymes and Cofactors*, Vol. 6 (Eds.: A. Sigel, H. Sigel, R. K. O. Sigel), The Royal Society of Chemistry, Cambridge, **2009**, p. 1.

[37] S. W. Ragsdale, *J. Inorg. Biochem.* **2007**, *101*, 1657.

[38] J. A. McCleverty, *Chem. Rev.* **2004**, *104*, 403.

[39] P. G. Wang, T. B. Cai, N. Taniguchi (Eds.), *Nitric Oxide Donors*, Wiley-VCH, Weinheim, **2005**.

[40] W. J. Evans, M. Fang, G. Zucchi, F. Furche, J. W. Ziller, R. M. Hoekstra, J. I. Zink, *J. Am. Chem. Soc.* **2009**, *131*, 11195.

[41] W. Kaim, B. Sarkar, *Angew. Chem.* **2009**, *121*, 9573; *Angew. Chem. Int. Ed.* **2009**, *48*, 9409.

[42] W. J. Evans, M. Fang, J. E. Bates, F. Furche, J. W. Ziller, M. D. Kiesz, J. I. Zink, *Nature Chem.* **2010**, *2*, 644.

[43] a) S. Schmidt, F. W. Heinemann, A. Grohmann, *Eur. J. Inorg. Chem.* **2000**, 1657; b) C. Würtele, E. Gaoutchenova, K. Harms, M. C. Holthausen, J. Sundermeyer, S. Schindler, *Angew. Chem.* **2006**, *118*, 3951; *Angew. Chem. Int. Ed.* **2006**, *45*, 3867.

[44] A. F. Miller, *Curr. Opin. Chem. Biol.* **2004**, *8*, 162.

[45] P. Höhn, F. Jach, B. Karabiyik, S. Agrestini, Y. Prots, F. R. Wagner, M. Ruck, L. H. Tjeng, R. Kniep, *Angew. Chem.* **2011**, *123*, 9533; *Angew. Chem. Int. Ed.* **2011**, *50*, 9361.

[46] a) E. Weiss, W. Büchner, *Chem. Ber.* **1965**, *98*, 126; b) A. S. Frey, F. G. N. Cloke, P. B. Hitchcock, I. J. Day, J. C. Green, G. Aitken, *J. Am. Chem. Soc.* **2008**, *130*, 13816; c) J. E. Ellis, P. T. Barger, M. L. Winzenburg, G. F. Warnock, *J. Organomet. Chem.* **1990**, *383*, 521; d) Z. Chen, Y. Deng, J. Bian, L. Li, G. Xu, *THEOCHEM* **1998**, *434*, 155; e) G. Aitken, N. Hazari, A. S. P. Frey, F. G. N. Cloke, O. Summerscales, J. C. Green, *Dalton Trans.* **2011**, *40*, 11080; f) B. B. Wayland, A. E. Sherry, G. Pozmik, A. G. Bunn, *J. Am. Chem. Soc.* **1992**, *114*, 1673.

[47] W. Kaim, *Coord. Chem. Rev.* **1987**, *76*, 187.

[48] K. Kobayashi, H. Ohtsu, T. Wada, T. Kato, K. Tanaka, *J. Am. Chem. Soc.* **2003**, *125*, 6729.

[49] a) J. T. Muckerman, D. E. Polyansky, T. Wada, K. Tanaka, E. Fujita, *Inorg. Chem.* **2008**, *47*, 1787; b) J. L. Boyer, J. Rochford, M.-K. Tsai, J. T. Muckerman, E. Fujita, *Coord. Chem. Rev.* **2010**, *254*, 309.

[50] S. Ghosh, M.-H. Baik, *Inorg. Chem.* **2011**, *50*, 5946.

[51] a) W. Kaim, J. Rall, *Angew. Chem.* **1996**, *108*, 47; *Angew. Chem. Int. Ed. Engl.* **1996**, *35*, 43; b) W. Kaim, *Dalton Trans.* **2003**, 761.

[52] A. Vega, J. Manzur, M. Sieger, J. Schnödt, J. Fiedler, W. Kaim, unpublished results.

[53] R. Balasubramanian, S. M. Smith, S. Rawat, L. A. Yatsunyk, T. L. Stemmler, A. C. Rosenzweig, *Nature* **2010**, *465*, 115.

[54] R. A. Himes, K. Barnese, K. D. Karlin, *Angew. Chem.* **2010**, *122*, 6864; *Angew. Chem. Int. Ed.* **2010**, *49*, 6714.

[55] a) B. de Bruin, D. G. H. Hetterscheid, *Eur. J. Inorg. Chem.* **2007**, *2*, 211; b) D. G. H. Hetterscheid, H. Grützmacher, A. J. J. Koekoek, B. de Bruin, *Prog. Inorg. Chem.* **2007**, *55*, 247; c) W. H. Baddley, *Inorg. Chim. Acta Rev.* **1968**, *2*, 7; d) S. Záliš, L. Steudle, W. Kaim, unpublished results.

[56] a) H. Sitzmann, H. Bock, R. Boese, T. Dezember, Z. Havlas, W. Kaim, M. Moscherosch, L. Zanathy, *J. Am. Chem. Soc.* **1993**, *115*, 12003; b) H. Sitzmann, T. Dezember, W. Kaim, F. Baumann, D. Stalke, J. Kärcher, E. Dormann, H. Winter, C. Wachter, M. Kelemen, *Angew. Chem.* **1996**, *108*, 3013; *Angew. Chem. Int. Ed. Engl.* **1996**, *35*, 2872.

[57] W. I. Dzik, X. P. Zhang, B. de Bruin, *Inorg. Chem.* **2011**, *50*, 9896.

[58] a) S. N. Semenov, O. Blacque, T. Fox, K. Venkatesan, H. Berke, *J. Am. Chem. Soc.* **2010**, *132*, 3115; b) P. Low, *Eur. J. Inorg. Chem.*, **2012**, 390–411.

[59] a) W. Kaim, *Acc. Chem. Res.* **1985**, *18*, 160; b) W. Kaim, *Top. Curr. Chem.* **1994**, *169*, 231; c) S. Hasenzahl, W. Kaim, T. Stahl, *Inorg. Chim. Acta* **1994**, *225*, 23; d) D. Zhu, I. Thapa, I. Korobkov, S. Gambarotta, P. H. M. Budzelaar, *Inorg. Chem.* **2011**, *50*, 9879; e) P. H. M. Budzelaar, *Eur. J. Inorg. Chem.*, **2012**, 530–534.

 © 2012 Wiley-VCH Verlag GmbH & Co. KGaA, Weinheim

[60] a) V. Artero, M. Chavarot-Kerlidou, M. Fontecave, *Angew. Chem.* **2011**, *123*, 7376; *Angew. Chem. Int. Ed.* **2011**, *50*, 7238; b) R. M. Bullock, *Catalysis without Precious Metals*, Wiley-VCH, Weinheim, **2010**.

[61] a) M. R. Ringenberg, M. J. Nilges, T. B. Rauchfuss, S. R. Wilson, *Organometallics* **2010**, *29*, 1956; b) M. R. Ringenberg, T. B. Rauchfuss, *Eur. J. Inorg. Chem.*, **2012**, 490–495.

Received: December 5, 2011
Published Online: January 5, 2012

 © 2012 Wiley-VCH Verlag GmbH & Co. KGaA, Weinheim

EurJIC
European Journal of Inorganic Chemistry

BACK COVER PICTURE

The back cover picture shows the structure of a dinuclear organometallic oxime complex, which exhibits metal−ligand bifunctional reactivity upon dissociation to the mononuclear hydrido−oxime complex and coordinatively unsaturated oximato complex. These mononuclear species are easily converted to each other through proton-coupled hydride transfer with alcohols and ketones. Owing to metal−ligand cooperation, the dinuclear complex efficiently catalyzes the transfer hydrogenation of ketones with 2-propanol. Details are discussed in the article by S. Kuwata, T. Ikariya et al. on p. 504ff.

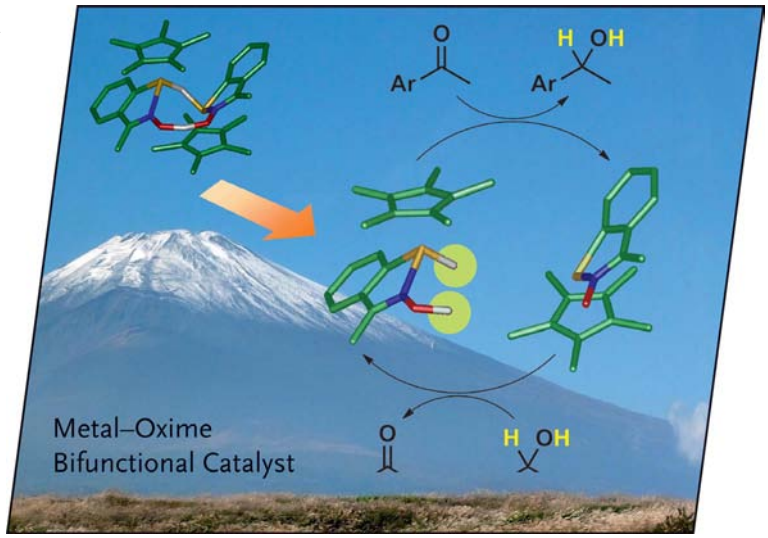

 © 2012 Wiley-VCH Verlag GmbH & Co. KGaA, Weinheim

EurJIC
European Journal of Inorganic Chemistry

3/2012
3rd January Issue

Cluster Issue:
Cooperative & Redox Non-Innocent Ligands in Directing Organometallic Reactivity

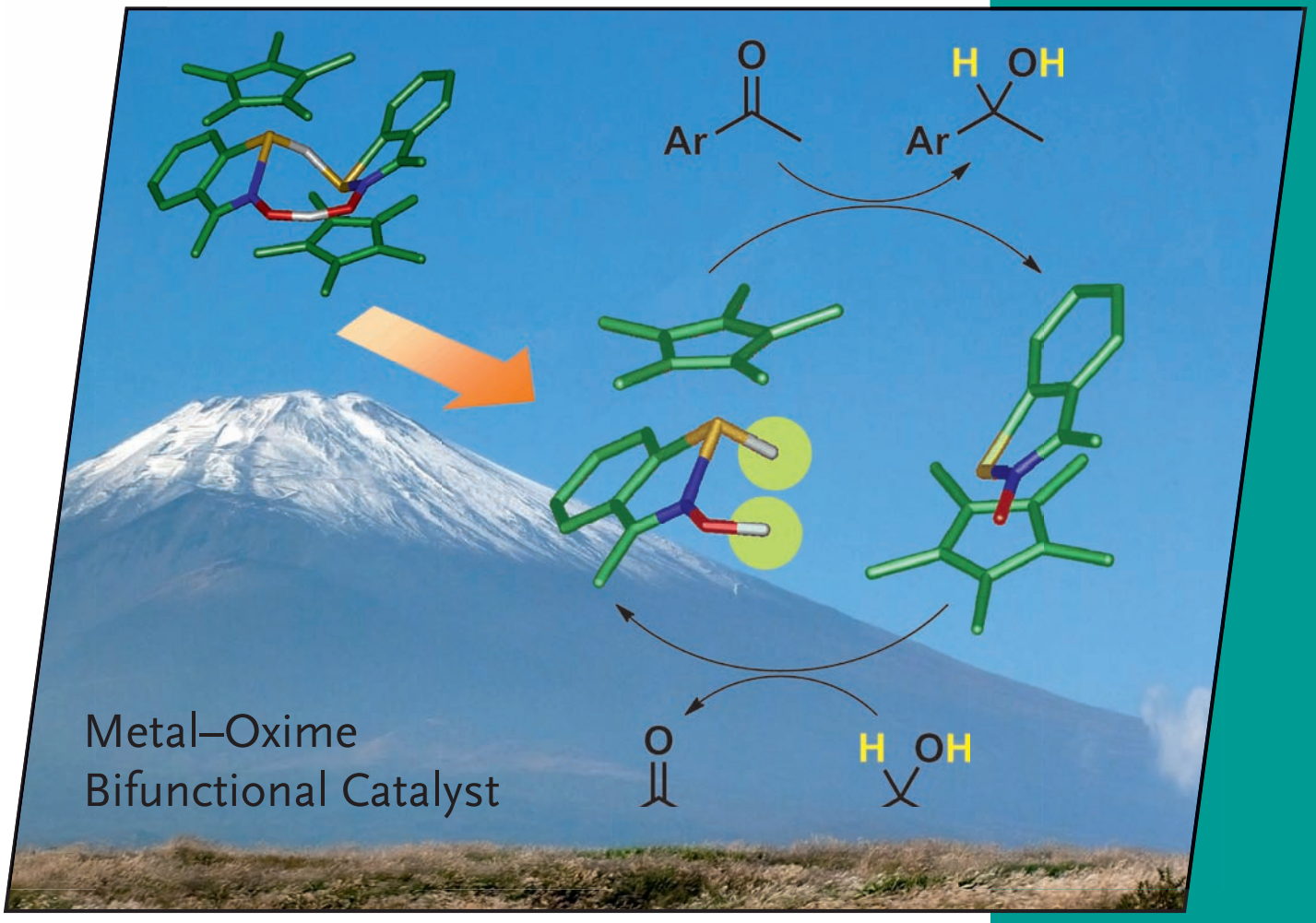

Back Cover Picture
Shigeki Kuwata, Takao Ikariya et al.
Iridium Complexes Bearing a C–N Chelate Oxime Ligand

A Journal of
ChemPubSoc Europe

WILEY-VCH
www.eurjic.org

CONTENTS

ESSAY

Scope of Non-Innocent Ligands

W. Kaim* **343–348**

The Shrinking World of Innocent Ligands: Conventional and Non-Conventional Redox-Active Ligands

Keywords: Cyanides / Non-innocent ligands / Organometallic chemistry / Oxido ligands

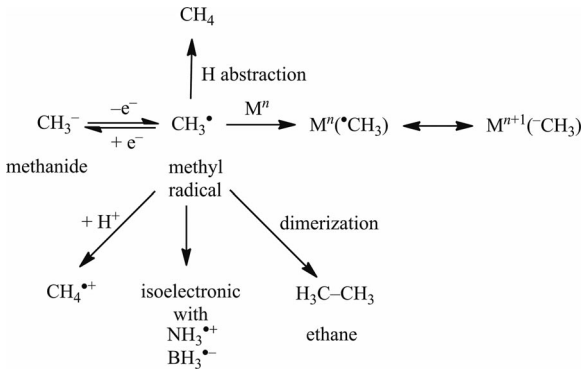

Evidence for non-innocent ligand behavior is being found for an increasing number of coordination compounds, including those with seemingly unassuming ligands. The recognition of such situations can be exploited for supporting attractive material properties and for understanding and developing chemical reactivity.

MICROREVIEWS

Cooperative Catalysis

J. I. van der Vlugt* **363–375**

Cooperative Catalysis with First-Row Late Transition Metals

Keywords: Homogeneous catalysis / Cooperative catalysis / First-row metals / Ligand–metal cooperativity / Dinuclear complexes / Noninnocent ligands / Hemilabile ligands

A helping hand. This microreview describes recent developments and opportunities in the rapidly expanding field of bioinspired first-row late transition metal catalysis with cooperative ligand systems. Particular emphasis is placed on hemilabile, redox-noninnocent and adaptive ligand scaffolds and on particular bimetallic strategies.

Iron Catalysis

S. Blanchard, E. Derat, M. Desage-El Murr,* L. Fensterbank,* M. Malacria,* V. Mouriès-Mansuy **376–389**

Non-Innocent Ligands: New Opportunities in Iron Catalysis

Keywords: Non-innocent ligands (NILs) / Redox chemistry / Iron / Density functional calculations / Low-valent iron complexes

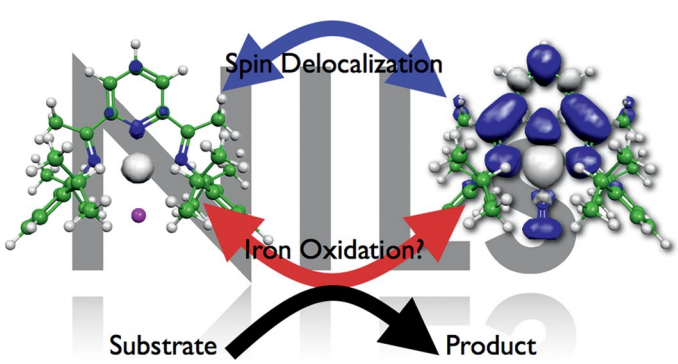

The ability of non-innocent ligands (NILs) to act as a storage/supply unit of electrons promotes one- or two-electron transfers, allowing iron catalysts to perform reactions that were previously restricted to catalysts based on noble metals. Progress in this promising area of research is reviewed with special emphasis on DFT calculations and analysis of spectroscopic data.

 © 2012 Wiley-VCH Verlag GmbH & Co. KGaA, Weinheim

Transition-Metal Alkynyl Complexes

P. A. Schauer, P. J. Low* 390–411

Ligand Redox Non-Innocence in Transition-Metal σ-Alkynyl and Related Complexes

Keywords: Redox chemistry / Radical reactions / Ligand effects / Alkyne ligands / Rutheniu

Many transition-metal σ-alkynyl complexes are redox-active, undergoing facile oxidation (reduction) at moderate potentials to generate radical cations (anions). This review summarises the diverse chemical behaviour of metal-supported σ-alkynyl radicals, which can often be rationalised in terms of the distribution of electron-spin density over the metal alkynyl scaffold.

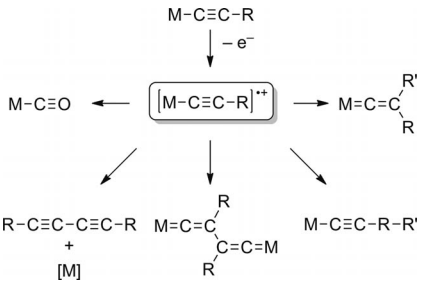

Cooperative Pincer Ligands

S. Schneider,* J. Meiners, B. Askevold 412–429

Cooperative Aliphatic PNP Amido Pincer Ligands – Versatile Building Blocks for Coordination Chemistry and Catalysis

Keywords: Cooperative catalysis / Pincer complexes / N ligands / Homogeneous catalysis / C–H activation

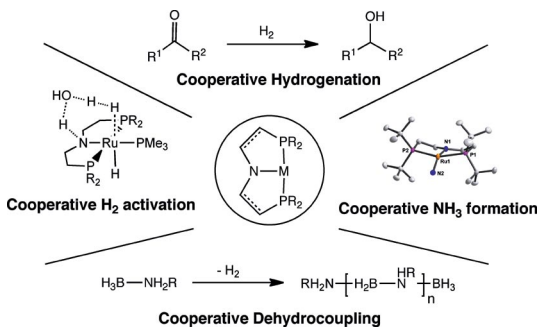

Aliphatic PNP pincer ligands, $HN(CH_2CH_2PR_2)_2$, and ligands derived from them by backbone functionalization, are versatile chelating ligands for metal–ligand cooperative small molecule activation and catalysis. This microreview covers the recent work with these ligands and provides a comprehensive comparison with related pincer systems.

Asymmetric Cyclopropanation

S. Zhu, X. Cui, X. P. Zhang* 430–434

Ligand Effect on Cobalt(II)-Catalyzed Asymmetric Cyclopropanation with Diazosulfones – Approaching High Stereoselectivity through Modular Design of D_2-Symmetric Chiral Porphyrins

Keywords: Cyclopropanation / Chiral porphyrins / Cobalt / Ligand effects / Asymmetric catalysis

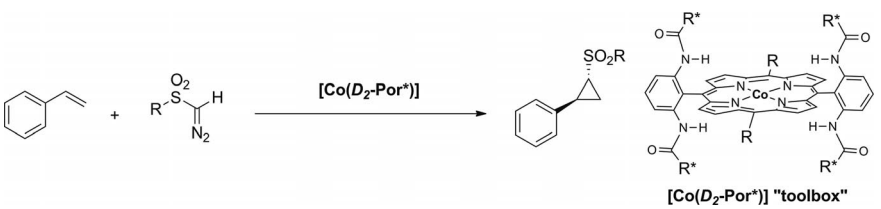

Systematic studies of the ligand effect of Co^{II} complexes of D_2-symmetric chiral porphyrins on catalytic asymmetric cyclopropanation with diazosulfones are reviewed. Ligand structures have significant influence on both the reactivity and enantioselectivity of the reaction. Catalysts with rigidity have been shown to have high asymmetric induction.

Redox-Active Ligands

K. G. Caulton* 435–443

Systematics and Future Projections Concerning Redox-Noninnocent Amide/Imine Ligands

Keywords: Redox-noninnocent ligands / N ligands / Conjugation / Pincer ligands

Core features of redox-active ligands are analysed and generalized.

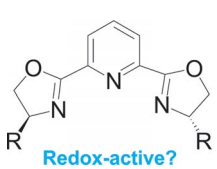

 © 2012 Wiley-VCH Verlag GmbH & Co. KGaA, Weinheim

CONTENTS

Metal−Ligand Electron Transfer

D. Sieh, M. Schlimm, L. Andernach, F. Angersbach, S. Nückel, J. Schöffel, N. Šušnjar, P. Burger* ..... 444−462

Metal−Ligand Electron Transfer in 4d and 5d Group 9 Transition Metal Complexes with Pyridine, Diimine Ligands

Keywords: Charge transfer / NMR spectroscopy / Density functional calculations / Rhodium / Iridium

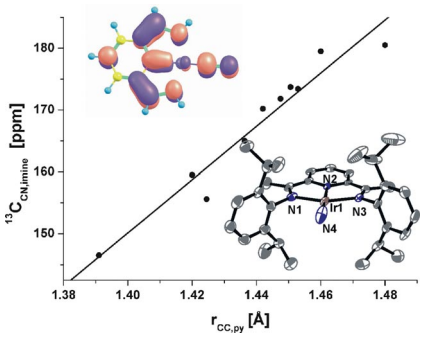

The syntheses, X-ray crystal structures, and spectroscopic data for rhodium and iridium pyridine, diimine (PDI) complexes (PDI)Rh,Ir−$L_n^{0,1+}$ (n = 1−3) are reported for a large variety of ligands L and different coordination numbers (CN = 4−6). The extent of metal−ligand electron transfer in these diamagnetic complexes was evaluated by experimental and theoretical methods.

SHORT COMMUNICATIONS

Metal-radical Chemistry

F. D. Lesh, R. L. Lord,* M. J. Heeg, H. B. Schlegel, C. N. Verani* .... 463−466

Unexpected Formation of a Cobalt(III) Phenoxazinylate Electron Reservoir

Keywords: Coordination chemistry / Redox-active ligands / Cobalt / Electrochemistry / Density functional calculations

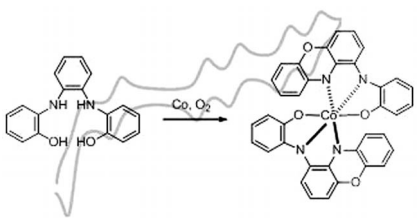

An unexpected aerobic cyclization of the popular redox active *N*,*N*′-bis(3,5-di-*tert*-butyl-2-hydroxyphenyl)-1,2-phenylenediamine ligand occurs in the presence of a cobalt(II) salt to form a new mixed phenolate/phenoxazinylate radical species. Experimental and computational studies elucidate the properties of the resultant bisligated cobalt(III) complex that traverses redox levels from 2+ to 3−.

Electron and Proton Reservoirs

F. Lu, R. A. Zarkesh, A. F. Heyduk* ..... 467−470

A Redox-Active Ligand as a Reservoir for Protons and Electrons: O_2 Reduction at Zirconium(IV)

Keywords: Redox-active ligands / Zirconium / Oxygen reduction / Redox chemistry / Structure elucidation

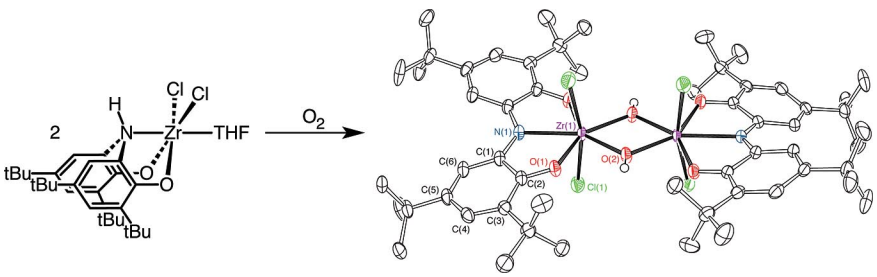

The redox-active [ONO] ligand platform coordinates zirconium(IV) to form (ONO^{cat})$ZrCl(THF)_2$ (**1**) and (ONHO)-$ZrCl_2$(THF) (**2**). In **2**, the ligand retains one proton in addition to its redox-active pair of electrons. Exposure of **2** to O_2 results in a four-electron, two-proton reaction to form [(ONO^{q})$ZrCl_2$(μ-OH)]$_2$ (**3**). This reaction occurs because the ligand platform serves as a reservoir for both electrons and protons in small-molecule activation reactions.

Spectroelectrochemistry

Q. Zeng, M. Messaoudani, A. Vlček Jr.,* F. Hartl* ..... 471−474

Electrochemical Reductive Deprotonation of an Imidazole Ligand in a Bipyridine Tricarbonyl Rhenium(I) Complex

Keywords: Rhenium / Imidazole / N ligands / Heterocycles / Electrochemistry

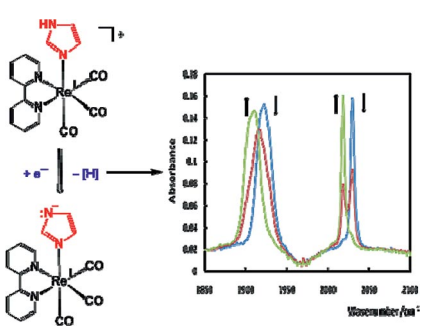

The first example of electrochemical reductive conversion of coordinated imidazole (imH) to the terminal 3-imidazolato (3-im⁻) ligand is reported for *fac*-[Re^{I}-(imH)$(CO)_3$(bpy)]$^+$ (bpy = 2,2′-bipyridine). Its cathodic conversion to *fac*-[Re^{I}-(3-im⁻)$(CO)_3$(bpy)] was studied by variable-temperature UV/Vis/NIR−IR spectroelectrochemistry in an OTTLE cell.

 © 2012 Wiley-VCH Verlag GmbH & Co. KGaA, Weinheim

Oxidation of Thiyl Radicals

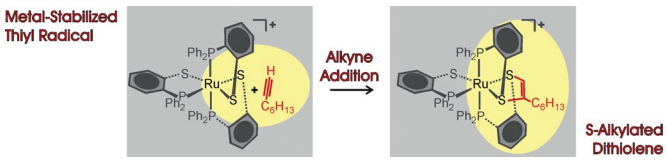

The addition of 1-octyne to an electrophilic metal-stabilized thiyl radical complex has been induced through chemical and electrochemical oxidation. The alkyne adds irreversibly across the *cis*-sulfur sites of the metal-thiolate precursor to yield an *S*-alkylated dithiolene product complex.

K. Ouch, M. S. Mashuta, C. A. Grapperhaus* 475–478

Alkyne Addition to a Metal-Stabilized Thiyl Radical: Carbon–Sulfur Bond Formation between 1-Octyne and $[Ru(SP)_3]^+$

Keywords: Alkynes / C–S bond formation / Oxidation / Sulfur / Electrochemistry

Electronic Structure

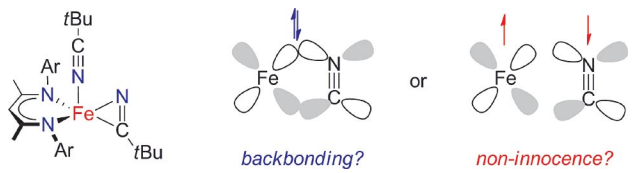

In the $S = 3/2$ molecule $L^{Me}Fe(NCtBu)_2$, the side-on nitrile ligand has N–C–C bending and N–C weakening that suggests partial reduction of the nitrile group. Even though the molecule has three unpaired spins, the interaction between the iron atom and the nitrile ligand is two-electron backbonding rather than redox non-innocence.

R. E. Cowley, G. J. Christian, W. W. Brennessel, F. Neese,* P. L. Holland* 479–483

A Reduced (β-Diketiminato)iron Complex with End-On and Side-On Nitriles: Strong Backbonding or Ligand Non-Innocence?

Keywords: Nitriles / Iron / Density functional calculations / Pi interactions

FULL PAPERS

Cobalt(II)–Porphyrin Catalysis

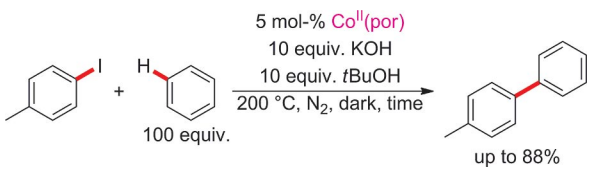

The electronic effects of porphyrin ligands on the cobalt(II)–porphyrin-catalyzed direct C–H arylation were studied. The reaction rates were found to be dependent on the electronic richness of the porphyrin ligands. Additional axial ligands did not aid the rate-determining abstraction of the iodine atom.

T. L. Chan, C. T. To, B.-S. Liao, S.-T. Liu,* K. S. Chan* 485–489

Electronic Effects of Ligands on the Cobalt(II)–Porphyrin-Catalyzed Direct C–H Arylation of Benzene

Keywords: Electronic effects / Cobalt / C–H arylation / Rate-determining step / Ligand effects / Steric hindrance

Protons and Noninnocence

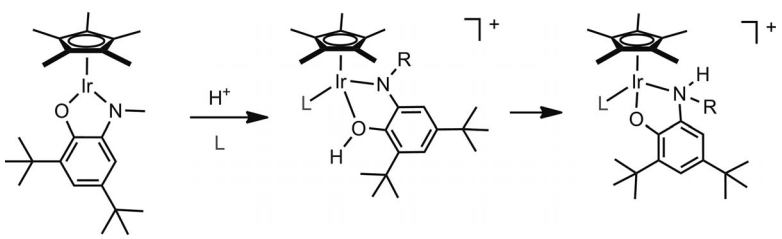

Not just redox: Noninnocent ligands exhibit rich acid–base behavior. Protonation of noninnocent anilidophenolates induces the binding of Lewis bases (CO, PR_3, MeCN). Bulky Lewis bases stabilize *O*-protonation, whereas smaller bases give *N*-protonated products.

M. R. Ringenberg, T. B. Rauchfuss* 490–495

Protonation-Enhanced Lewis Acidity of Iridium Complexes Containing Noninnocent Amidophenolates

Keywords: Protonation / Noninnocent ligand / Carbonylation / Amides / Phenoxide

 © 2012 Wiley-VCH Verlag GmbH & Co. KGaA, Weinheim

CONTENTS

P-Chirogenic Tautomers

F. W. Patureau, M. A. Siegler, A. L. Spek, A. J. Sandee, S. Jugé, S. Aziz, A. Berkessel, J. N. H. Reek* 496–503

Supramolecular Hydrogen-Bonding Tautomeric Sulfonamido–Phosphinamides: A Perfect P-Chirogenic Memory

Keywords: Tautomerism / Rhodium / Hydrogenation / Phosphorus / Chirality

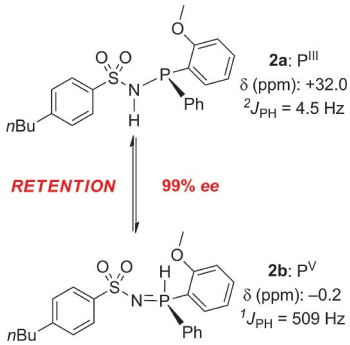

Supramolecular hydrogen-bonding sulfonamido–phosphinamides exist as a mixture of tautomers (P^{III}/P^{V}) in slow equilibrium on the NMR spectroscopic timescale (METAMORPhos). The tautomeric process retains the configuration at the P centre, even in protic solvents. Their resolution allowed up to 99% *ee*.

Bifunctional Catalysts

M. Watanabe, Y. Kashiwame, S. Kuwata,* T. Ikariya* 504–511

Synthesis, Structures, and Transfer Hydrogenation Catalysis of Bifunctional Iridium Complexes Bearing a C–N Chelate Oxime Ligand

Keywords: Homogeneous catalysis / Iridium / Hydrogen bonds / Hydride ligands / Cooperative effects

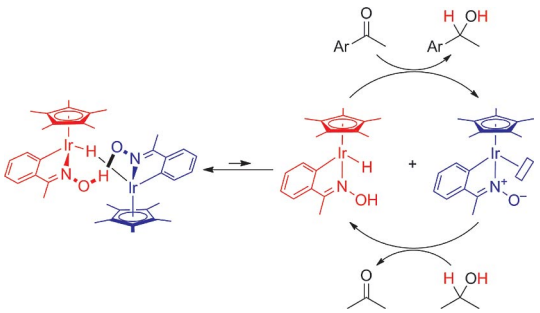

A series of organometallic oxime complexes featuring a β-protic OH group have been synthesized. The hydrido-bridged oxime–oximato complex (pictured) dissociates into two mononuclear species, which are interconvertible through reactions with hydrogen donors and acceptors. Owing to the metal–ligand cooperation, catalytic transfer hydrogenation of ketones with 2-propanol has been achieved.

Multifaceted Reversible Isomerism

C. Tejel,* L. Asensio, M. Pilar del Río, B. de Bruin, J. A. López, M. A. Ciriano 512–519

Snapshots of a Reversible Metal–Ligand Two-Electron Transfer Step Involving Compounds Related by Multiple Types of Isomerism

Keywords: Rhodium / Iridium / Mixed-valent compounds / Imines / Electron transfer / Redox noninnocent ligands

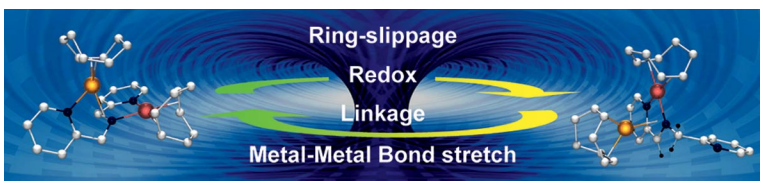

Four different types of isomerism are involved in the reversible conversion of two isolated isomeric species of the heterodinuclear complex [(cod)Rh(bpa − 2H)Ir(cod)], which contains a redox noninnocent 2-iminopyridine-type ligand. Enthalpy stabilizes the $Rh^{-I}\{(bpa - 2H)^{0}\}$ isomer (left), whereas entropy is the driving force to generate the $Rh^{I}\{(bpa - 2H)^{2-}\}$ isomer (right).

Organochromium Complexes

K. A. Kreisel, G. P. A. Yap, K. H. Theopold* 520–529

Organochromium Complexes Bearing Noninnocent Diimine Ligands

Keywords: Chromium complexes / Diimine ligands / N ligands / Alkylation / Insertion

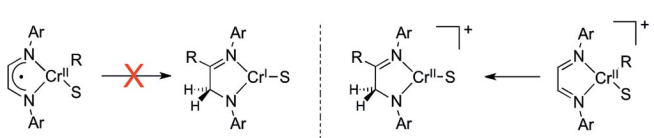

A series of organochromium complexes bearing α-diimine ligands has been prepared. The compounds contain diimine ligands in the neutral, singly, and doubly reduced states. All the complexes resist alkyl migration to the diimine backbone, except for a cationic alkyl-Cr^{II} species that features a neutral diimine ligand. A C=N insertion mechanism followed by a hydride shift is proposed.

 © 2012 Wiley-VCH Verlag GmbH & Co. KGaA, Weinheim

Metal–Alkyl Homolysis

Ligands containing at least two imine or pyridine ligands in conjugation reduce the energy required for metal–alkyl homolysis dramatically; ligand alkylation reactions are best explained via free alkyl radicals.

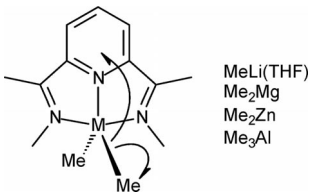

P. H. M. Budzelaar* 530–534

Radical Chemistry of Iminepyridine Ligands

Keywords: N ligands / Imines / Radicals / Electron transfer / Density functional calculations

Manganese Compounds

The chemistry of reduced aryl-substituted bis(imino)pyridine manganese complexes has been explored with the goal of elucidating the role of the redox-active chelate. The bis(THF) derivative [(^{iPr}PDI)Mn(THF)$_2$] is a high-spin Mn^{II} complex antiferromagnetically coupled to a bis(imino)pyridine diradical, while the related dicarbonyl complex is a low-spin Mn^{I}, d^6 derivative with a ligand-based SOMO.

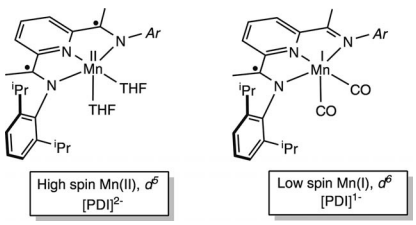

S. K. Russell, A. C. Bowman, E. Lobkovsky, K. Wieghardt, P. J. Chirik* 535–545

Synthesis and Electronic Structure of Reduced Bis(imino)pyridine Manganese Compounds

Keywords: Manganese / Catalysts / Chelates / Redox chemistry / Non-innocent ligands

Ruthenium Hydride Complexes

Ruthenium hydride complexes derived from zwitterionic quinonoid ligands have been synthesized, and their isomers have been separated and structurally characterized. Cyclic voltammetry of the complexes showed the redox noninnocent nature of the quinonoid ligands. One of the complexes showed good activity as a catalyst for the transfer hydrogenation of acetophenone.

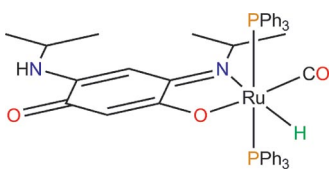

S. Hohloch, P. Braunstein,* B. Sarkar* 546–553

Ruthenium Hydride Complexes with Zwitterionic Quinonoid Ligands – Isomer Separation, Structural Properties, Electrochemistry, and Catalysis

Keywords: Quinones / Ruthenium / Hydrides / Noninnocent ligands / Redox chemistry / Transfer hydrogenation catalysis

Redox-Active Ligand Catalysis

The capacity of oxorhenium(V) anions with redox-active catecholate ligands to homolyze O_2 and generate dioxorhenium(VII) products is utilized for oxidase-type alcohol oxidations. Formation of the active oxidant requires both the dioxo and monooxo species. The scope and limitations of this redox-active ligand-mediated catalysis are discussed.

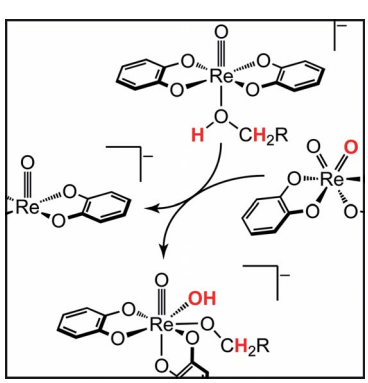

C. A. Lippert, K. Riener, J. D. Soper* 554–561

Aerobic Alcohol Oxidations Catalyzed by Oxorhenium Complexes Containing Redox-Active Ligands

Keywords: Redox-active ligands / Homogeneous catalysis / Oxidation / Rhenium / Proton-coupled electron transfer

 © 2012 Wiley-VCH Verlag GmbH & Co. KGaA, Weinheim

CONTENTS

C−H Amination

K. P. Kornecki, J. F. Berry* ..... 562−568

Dirhodium Catalysts That Bear Redox Noninnocent Chelating Dicarboxylate Ligands and Their Performance in Intra- and Intermolecular C−H Amination

Keywords: Rhodium / Homogeneous catalysis / Amination / Redox chemistry / Chelates

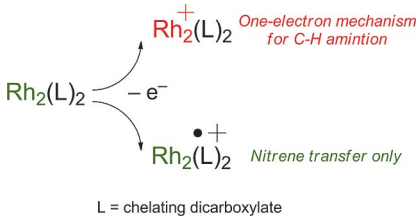

Two new analogues of the well-known C−H amination catalyst [Rh_2(esp)$_2$] (esp = α,α,α′,α′-tetramethyl-1,3-benzenedipropanoate) are reported that bear redox-active supporting ligands that are structurally similar to esp. The dissimilar electrochemistry of the three catalysts and their different performance in intra-/intermolecular reactions support two mechanisms for the C−H amination reaction.

C−H Bond Amination

D. Intrieri, A. Caselli, F. Ragaini, P. Macchi, N. Casati, E. Gallo* ..... 569−580

Insights into the Mechanism of the Ruthenium−Porphyrin-Catalysed Allylic Amination of Olefins by Aryl Azides

Keywords: Amination / C−H activation / Azides / Metalloporphyrins / Porphyrinoids / Homogeneous catalysis

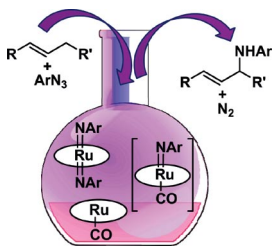

The [Ru(TPP)CO]-catalysed synthesis of allylic amines was performed by employing aryl azides (ArN_3) as nitrogen sources. A mechanistic hypothesis for the nitrene transfer reaction to cyclohexene was proposed on the basis of synthetic, spectroscopic and kinetic studies.

* Author to whom correspondence should be addressed.

Supporting information on the WWW (see article for access details).

This article is available online free of charge (Open Access).

If not otherwise indicated in the article, papers in issue 2 were published online on December 30, 2011

 © 2012 Wiley-VCH Verlag GmbH & Co. KGaA, Weinheim

On these pages, we feature a selection of the excellent work that has recently been published in our sister journals. If you are reading these pages on a computer, click on any of the items to read the full article. Otherwise please see the DOIs for easy online access through Wiley Online Library.

Gas-Phase Chemistry

R. Kretschmer, M. Schlangen, H. Schwarz*

Mechanistic Aspects and Elementary Steps of N–H Bond Activation of Ammonia and C–N Coupling Induced by Gas-Phase Ions: A Combined Experimental/Computational Exercise

Step by step: Due to its extraordinary potential, N–H bond activation and C–N coupling processes have formed the focus of broad research activities. This Minireview will describe examples of these processes mediated by gaseous "bare" or ligated ions and provide detailed insights into the underlying mechanisms and elementary steps.

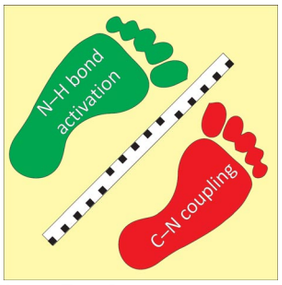

Chem. Eur. J.
DOI: **10.1002/chem.201102494**

Organometallic Complexes

B. T. Loughrey,* B. V. Cunning, P. C. Healy, C. L. Brown, P. G. Parsons, M. L. Williams

Selective, Cytotoxic Organoruthenium(II) Full-Sandwich Complexes: A Structural, Computational and In Vitro Biological Study

Ru positive? A diverse range of lipophilic, cationic full-sandwich complexes of ruthenium(II) have been prepared and structurally characterized. Computational experiments predict each molecule to possess a delocalized δ+ electrostatic potential, and in vitro cytotoxicity studies demonstrate these lipophilic cations to be potent and selective growth inhibitors of tumorigenic cells lines.

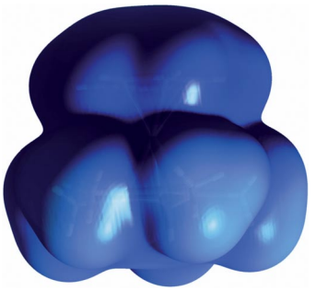

Chem. Asian J.
DOI: **10.1002/asia.201100637**

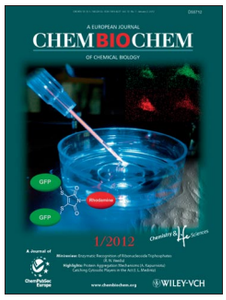

Protein Prenylation

Y.-W. Wu,* R. S. Goody, K. Alexandrov*

Intein-Mediated Construction of a Library of Fluorescent Rab GTPase Probes

Taking the Rab: Expressed protein ligation allows site-specific incorporation of unnatural functionalities, such as fluorophores, into proteins. This requires synthesis of peptides with such functionalities and their subsequent ligation onto proteins. To construct a library of fluorescent RabGTPase sensors we developed an alternative approach in which proteins are labeled on a free cysteine and then ligated to an unlabeled peptide.

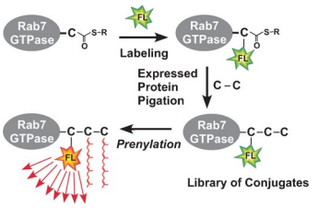

ChemBioChem
DOI: **10.1002/cbic.201100377**

 © 2012 Wiley-VCH Verlag GmbH & Co. KGaA, Weinheim

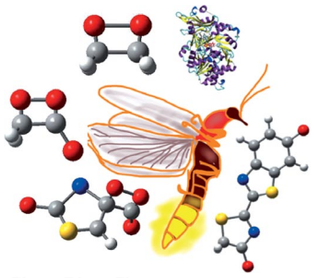

ChemPhysChem
DOI: **10.1002/cphc.201100504**

Bioluminescence

I. Navizet,* Y.-J. Liu, N. Ferré, D. Roca-Sanjuán, R. Lindh

The Chemistry of Bioluminescence: An Analysis of Chemical Functionalities

Evolution of oxyluciferin: Starting from simple models expanding to more complex ones (see picture) this review shows how theoretical calculations give insights for the color modulation of firefly luciferin.

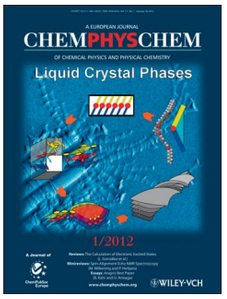

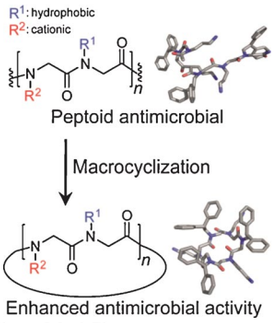

ChemMedChem
DOI: **10.1002/cmdc.201100358**

Peptidomimetics

M. L. Huang, S. B. Y. Shin, M. A. Benson, V. J. Torres, K. Kirshenbaum*

A Comparison of Linear and Cyclic Peptoid Oligomers as Potent Antimicrobial Agents

Cycling builds endurance! A family of linear N-substituted glycine "peptoid" oligomers bearing cationic and hydrophobic side chains were subjected to macrocyclization, thereby enhancing antimicrobial potency. These compounds are active against Gram-negative and Gram-positive bacteria and are non-hemolytic toward human erythrocytes.

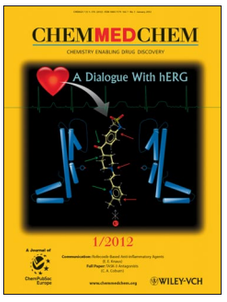

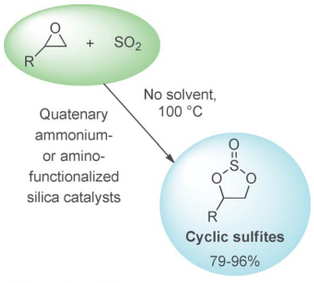

ChemSusChem
DOI: **10.1002/cssc.201100492**

Sustainable Chemistry

Y. Takenaka,* T. Kiyosu, G. Mori, J.-C. Choi, N. Fukaya, T. Sakakura, H. Yasuda*

Synthesis of Cyclic Sulfites from Epoxides and Sulfur Dioxide with Silica-Immobilized Homogeneous Catalysts

Immobilized for crimes of pyrolysis: Quaternary ammonium- and amino-functionalized silica catalysts promote the cycloaddition of sulfur dioxide to epoxides to produce cyclic sulfites in high yields (79–96 %) that are comparable to those with the homogeneous catalysts. Separation of the functionalized silica catalyst from the product solution by filtration avoids pyrolysis of the cyclic sulfites during purification by distillation.

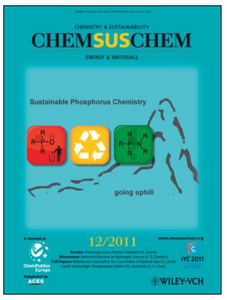

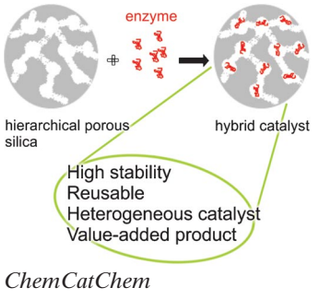

ChemCatChem
DOI: **10.1002/cctc.201100174**

Enzyme Immobilization

C. Bernal, L. Sierra, M. Mesa*

Application of Hierarchical Porous Silica with a Stable Large Porosity for β-Galactosidase Immobilization

Pin that enzyme down: Hierarchical porous silica, synthesized by using sodium silicate, is used as support for immobilization of β-galactosidase by the adsorption pathway. Their loading capacity and enzyme retention are explained in terms of their large mesopores and macropores and the surface silanol groups. Under extreme conditions, the hybrid biocatalyst is more stable than the soluble β-galactosidase.

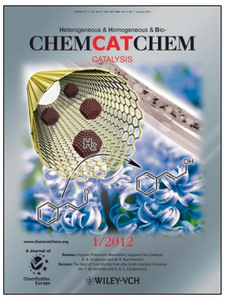

 © 2012 Wiley-VCH Verlag GmbH & Co. KGaA, Weinheim

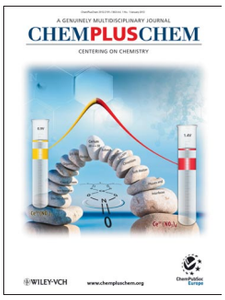

Polymers

B. Zhang, G. Liu, Y. Chen,* C. Wang, K.-G. Neoh, T. Bai, E.-T. Kang*

Electrical Bistability and WORM Memory Effects in Donor–Acceptor Polymers Based on Poly(*N*-vinylcarbazole)

Make the switch: Poly(*N*-vinylcarbazole) derivatives with pendant donor–trap–acceptor structures exhibit electrical effects. The origin of the electrical bistability, which arises from the intramolecular charge transfer, trapping, and conformational relaxation of the electrostatic energy of the Al/polymer/indium tin oxide sandwich structure (see figure), was established by spectroscopic, microscopic, and molecular computational techniques.

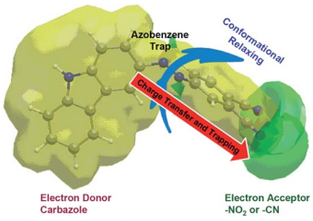

ChemPlusChem
DOI: **10.1002/cplu.201100007**

History of Science

F. Stern*

Fritz Haber: Flawed Greatness of Person and Country

Onkel Fritz: In his lecture at the Centennial Celebration of The Fritz Haber Institute, Fritz Stern reflects on the strengths and flaws of the Institute's founder. Can we judge a person without considering the historical and cultural context? In a sense, Haber's life encompassing triumph and tragedy is a reflection of his country at that time.

Angew. Chem. Int. Ed.
DOI: **10.1002/anie.201107900**

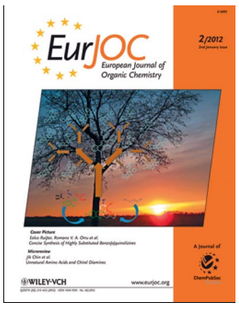

Helical Peptides

F. Formaggio,* M. Crisma, C. Peggion, A. Moretto, M. Venanzi, C. Toniolo*

Looking for a Robust, Synthetic, Fully-Extended (2.0_5-Helical) Peptide Structure – Effect of Terminal Groups

The fully-extended structure, albeit appealing for its potential applications, is the least investigated among polypeptide conformations. Here, we show that this 3D structure is stabilized by a C-terminal ester moiety. However, C-termination with a –CONHR (R = H, alkyl) group will convert it into the much more contracted 3_{10} helix.

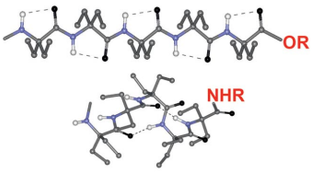

Eur. J. Org. Chem.
DOI: **10.1002/ejoc.201101273**

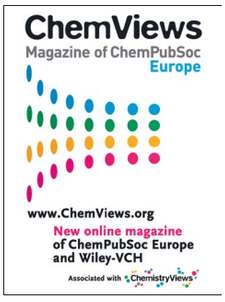

Design by Evolution

Vera Köster

Design by Evolution

Caltech Professor Frances H. Arnold sees laboratory evolution designing biology as solution to human problems. In her interview she also talks about creating proteins that expand the alphabet beyond the 20 natural amino acids and the few prosthetic groups that biology uses. If you use chemical knowledge, say from organocatalysis or inorganic chemistry, you can expand the chemical palette that's accessible to biology. There is a lot of room for creativity and imagination in these ideas that we are going to see developed in the near future.

ChemViews magazine
DOI: **10.1002/chemv.201000143**

 © 2012 Wiley-VCH Verlag GmbH & Co. KGaA, Weinheim

DOI: 10.1002/ejic.201100752

Cooperative Catalysis with First-Row Late Transition Metals

Jarl Ivar van der Vlugt*[a]

Keywords: Homogeneous catalysis / Cooperative catalysis / First-row metals / Ligand–metal cooperativity / Dinuclear complexes / Noninnocent ligands / Hemilabile ligands

Cooperative catalysis with first-row transition metals holds much promise for future developments regarding sustainable, selective transformations, including e.g. alkenes, dienes and a variety of small molecules such as CO_2, N_2 and water. This non-exhaustive analysis of the current state-of-the-art aims to give a comprehensive overview of the various design strategies and applications of first-row transition metal cooperative reactivity and to provide leads for new research initiatives in order to expand this emerging field. The main aspects covered involve bimetallic cooperativity, redox-noninnocent ligands in combination with first-row transition metal complexes, otherwise reactive or noninnocent scaffolds that can induce metal-ligand bifunctional substrate activation and the design of adaptive ligands and complexes thereof, wherein hemilability is a key factor for selective reactivity. The metals under review are primarily the late transition metals Fe, Co, Ni and Cu.

1. Introduction

Many elements from the Periodic Table are available in very limited supply, whilst resources are increasingly depleted as a result of the ever-growing global population, the rising average level of welfare and related demands for energy and chemical products. Catalysis is *the* key technology for the efficient conversion of raw materials into valuable products, but many catalysts themselves are based on scarce, expensive and noble materials such as second- and third-row transition metals. This is not sustainable for the future application of catalysts and new approaches and concepts need to be developed.

Nature has perfected the application of cheap, earth-abundant first-row transition metals for the execution of noble tasks such as small molecule activation or the functionalization and selective conversion of challenging substrates.[1] However, the (metallo)enzyme active sites employed very often rely on the reactivity of neighbouring ligand scaffolds and second coordination sphere interactions, i.e. Nature makes use of *cooperative catalysis* and "bifunctional activation" is an ubiquitous concept in the chemistry of biological systems.[2] This principle covers many seemingly unrelated types of functionalities wherein the protein scaffold or co-factors around the active site actively facilitate substrate turnover in a way that would not be possible or not as efficiently achieved without the element of cooperativity.

The mode of action of e.g. the enzymes galactose oxidase[3] and the hydrogenases[4] are based (in part) on cooperative effects induced by the ligand sphere around the metal active site. Similar arguments can be used to qualify the bi- or oligonuclear nature of many active sites to steer and control substrate activation and functionalization processes, often also involving multi-electron redox events as well as proton-coupled electron-transfer phenomena. Many metalloenzymes utilize such multimetallic cooperative systems for selective transformations, including copper-based oxidases and oxygenases,[5] non-heme iron-based active sites,[6,7] dinuclear nickel-containing systems[8] as well as many mixed-metal biocatalysts.[9] The use of "flexidentate" or hemilabile ligation[10] can also be included as a commonly observed strategy to regulate accessibility to the active site and thereby control reactivity.

[a] Supramolecular & Homogeneous Catalysis, van't Hoff Institute for Molecular Sciences, University of Amsterdam,
Science Park 904, 1098 XH Amsterdam, The Netherlands
Fax: +31-20-5255604
E-mail: j.i.vandervlugt@uva.nl

Jarl Ivar van der Vlugt (1975) earned his PhD with Prof. Vogt at the Eindhoven University of Technology (TUle) in 2003, working on ligand design and homogeneous catalysis, for which he received the 2004 KNCV Catalysis prize. After postdoctoral research with prof. Rauchfuss (UIUC) and with Prof. Meyer (Göttingen), as an Alexander-von-Humboldt Fellow, he obtained an NWO-CW VENI Grant to start his independent career at the TUle in 2007. Late 2008 he became assistant professor at the van't Hoff Institute for Molecular Sciences at the University of Amsterdam (UvA). His scientific interests are in small molecule activation, hydroamination, CO_2 functionalization, catalysis for green energy applications, (bimetallic) cooperative catalysis and ligand design. He was recently awarded an ERC Starting Grant to expand his research in the area of cooperative first-row transition metal catalysis.

 © 2012 Wiley-VCH Verlag GmbH & Co. KGaA, Weinheim

In contrast to the many very successful examples of cooperative catalysis based on abundant metals for selective transformations in biological systems,[13] the design and utilization of synthetic cooperative systems is still in its infancy, especially with respect to applications in catalysis. Only relatively recently has the targeted design of adaptive, cooperative ligand frameworks been recognized as a promising way to approach synthetic problems related to the selective conversion of substrates and the uncovering of new reactivity and previously unknown transformations.

This microreview is intended to survey four bioinspired strategies (Scheme 1) to induce and utilize cooperative reactivity in the context of (small molecule) substrate activation and homogeneous catalysis. Attention will be given to the use of redox-noninnocent ligands, to ligand–metal bifunctional substrate activation, to favorable interactions in bimetallic complexes and to adaptive, hemilabile coordination strategies. Particular emphasis on recent and ongoing efforts to combine these design concepts with earth-abundant late transition metals (Fe, Co, Ni and Cu). The nascent research field of supramolecular cooperative catalysis is introduced separately at the end of this non-exhaustive but rather illustrative overview of this emerging research field.

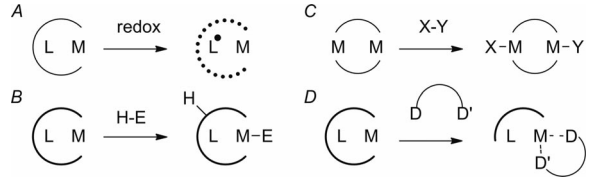

Scheme 1. Overview of cooperative reactivity strategies: *A* redox-noninnocent ligand scaffolds; *B* bifunctional substrate activation; *C* bimetallic substrate activation; *D* adaptive, hemilabile ligand coordination.

2. Cooperative Homogeneous Catalysis

One of the big focus points in present-day catalysis is the search for catalysts based on earth-abundant metals for green energy production and applications.[11] As such, the production of dihydrogen from a renewable resource like water and at low overpotentials, utilizing solar energy, is at the forefront of these developments. These attempts are driven by the desire to decipher ways to obviate the need for scarce, expensive Pt (electro)catalysts and to replace them with base-metal systems. Initial progress was made on the use of diiron systems as electrocatalysts for the reduction of protons to dihydrogen.[4] Even more timely and with pronounced usefulness for catalytic applications are ligand-metal assemblies that operate via an intramolecular acid/base functionality located in the ligand framework, akin to the hydrogenase active site.[12] The introduction of a biorelevant azadithiolate co-factor allowed the investigation of cooperative proton reduction events, involving intramolecular proton-hydride coupling processes to generate H_2 via a bifunctional pathway.

Ligand-assisted reactivity has so far proven particularly attractive for hydrogenation-related catalysis, involving heterolytic H_2 activation as a key step in the overall processes. Most of these cooperative catalytic systems incorporate alcohol–ketone[14] or amine–amide functionalities.[15] Impressive catalytic activities and mechanistic insights have been obtained for a number of these bioinspired molecular systems and for various types of substrates.

These developments in turn allow for a wider range of activity than traditionally provided for by metal-based catalysis alone. However, the vast majority of catalytic systems developed and applied to date are based on expensive, noble metals. However, it is essential and thus believed to be only a matter of time before combinations of earth-abundant first-row transition metals and cooperative ligand scaffolds will show to be equally powerful as or even to surpass current noble metal based methodologies and will enable also completely new reactivity to be utilized in catalytic transformations.

2.1 Redox Noninnocent Systems

First-row transition metals often display one-electron reactivity rather than the more common two-electron pathways typically observed with second- and third-row analogues. However, the use of these earth-abundant metals in combination with ligand-based redox-activity is still underdeveloped in catalysis, as the main focus in the past decade has been on detailed understanding of electronic structures of both metal and ligand fragments in stoichiometric reactivity studies.[16,17,18] It is foreseen that these powerful combinations of both metal and ligand redox-noninnocent systems will lead to new catalytic reactions and improvements in existing processes.

Many different types of ligand scaffolds[19] have proven to engage in ligand-based redox-processes when coordinated to (late) transition metals, which often strongly complicates formal oxidation state assignments as well as the overall electronic structure determination of the resulting species. Well-known and thoroughly investigated examples of these so-called redox-noninnocent ligand systems include *inter alia* quinones, dithiolenes or α-dimines.[20] More recently, ligands such as bis(imino)pyridines, diphenylamine-based systems and even Fischer carbenes have been shown to be susceptible to redox-chemistry in the coordination sphere of a transition metal.

Bis(imino)pyridines have been shown to undergo ligand-based redox-events, which do not affect the formal oxidation state of the coordinated metal.[21] This makes scenarios possible wherein the electron storage capacity of ligands supplies the redox-equivalents necessary to drive reactions such as selective C–C bond formation in the hydrovinylation of alkenes and the cyclization of diynes with iron (Scheme 2).[22,23] As such, it is a very powerful type of catalytic approach, that may be expandable to other metals as well, such as cobalt.[24] Both the "oxidative addition" and "reductive elimination" processes associated with the two C–C bond forming processes lead to oxidation and reduction of the ligand rather than the metal (which stays in

 © 2012 Wiley-VCH Verlag GmbH & Co. KGaA, Weinheim

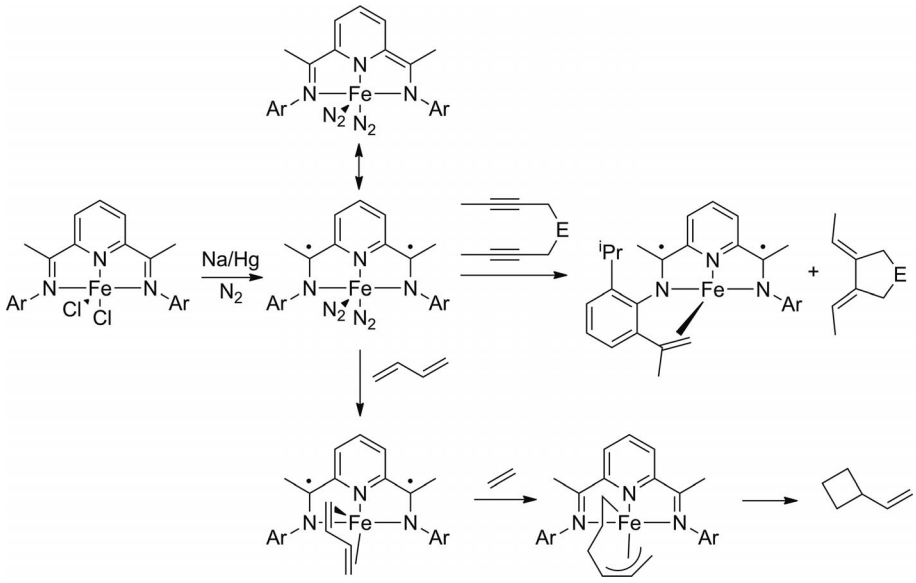

Scheme 2. Formation of a Fe complex based on bis(imino)pyridine and its reactivity in the cyclization and hydrovinylation of unsaturated hydrocarbons.

the Fe^{II} spectroscopic oxidation state throughout the entire catalytic cycle), and thereby the redox-active bis(imino)-pyridine ligand imposes some noble character to iron. This concept is highly compelling and suggests that it could well be possible to replace noble metals currently used in several types of organometallic catalytic reactions by cheaper and more abundant first-row TM's (perhaps even main-group metals). The Chirik group has expanded the chemistry of Fe-based bis(imino)pyridine complexes also to hydrogenations, polymerizations and stoichiometric bond-activation reactions.[25]

Soper and co-workers recently showed that metal-carbon bond formation can occur via metal-centered oxidative addition steps but *without* changing the d-electron configuration of the metal.[26] This was made possible by using redox active ligands that offer selective and fast electron transfer to the metal. The particular Co^{III} complex, which is a *square-planar* Co^{III} species (Scheme 3), featured two robust, redox noninnocent amidophenolate ligands. These ligands are easily, yet reversibly oxidized by one electron, thereby forming stable imino-semiquinone radical ligands. The (stoichiometric) cross-coupling of alkylzinc reagents with alkylhalides was demonstrated to be facilitated by this innovative "electron-borrowing" methodology. Eventually this could lead to cross-coupling transformations with earth-abundant metals instead of the expensive noble transition metals utilized extensively at the present time.

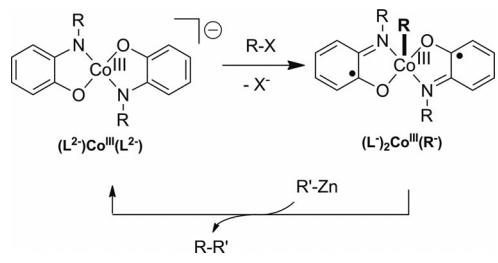

Scheme 3. Schematic representation of the "electron borrowing" methodology of redox-active amidophenolate ligands coordinated to a Co^{III} metal center.

Mindiola has described the redox-activity of specific monoanionic PNP-pincer scaffolds.[27] Starting from neutral square-planar NiCl(PNP^{iPr}), this species reacts with FcOTf (Fc = ferrocenium) to induce oxidation of the ligand backbone rather than the metal center (also certain Ag-salts are amenable to afford this redox-reaction), generating a ligand-centered radical anion coordinated to the unaltered square-planar Ni^{II} center (Scheme 4). The electronic structure of this unusual complex was investigated via a combined X-ray crystallographic, spectroscopic (UV, EPR, multi-edge XAS) and computational DFT study, indicating that the radical character is most pronounced at the nitrogen atom, with further contributions from the two phenyl rings. Although the authors speculate on the usefulness of this ligand based redox-switching event for catalysis, no further investigations on this matter have been reported to date. It is likely that this type of ligand cooperativity may find applications in certain types of bond activation processes, potentially even with further functionalization.

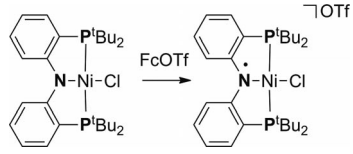

Scheme 4. Redox noninnocent behaviour of diphenylamide derived PNP ligand when coordinated to Ni^{II}.

It may be speculated that the all-nitrogen donor NNN analogues[28] also facilitate such ligand-centered redox-behaviour during e.g. Ni-catalyzed Kumada coupling of alkyl

 © 2012 Wiley-VCH Verlag GmbH & Co. KGaA, Weinheim

Grignards and alkyl halides rather than going proceeding through the intermediacy of a formal Ni^{IV} species.[29] It was recently established that the same nickel catalyzed cross-coupling reactions using related bidentate NN analogues followed a radical mechanism.[30]

The group of Zhang recently introduced Co^{II}(por*) complexes, wherein por* represents C_2-symmetric porphyrins functionalized with chiral auxiliaries that are also able to interact with suitable substrates via H-bonding.[31] This has resulted in unprecedented high enantioselectivity for the Co^{II}-catalyzed cyclopropanation of electron-poor alkenes with diazoesters.[32] It was subsequently established, through combined spectroscopic and theoretical studies using ethyl diazoacetate as model substrate, that the relevant cobalt(carbene) intermediate displays radical character at the carbene carbon atom rather than the d^7 cobalt center, making it a one-electron reduced Fischer carbene (Scheme 5). This effectively implied that metal-carbenes can display redox-noninnocent behaviour.[33] Subsequent computational investigations have identified ligand-based radical reactivity in the strongly related aziridination of electron-poor alkenes with azides {as well as PhI = NTs – [*N*-(*p*-tolylsulfonyl)imino]phenyl-iodinane} as nitrene source.[34] Follow-up reactivity studies will establish if this observed noninnocence in these neutral ligand fragments, previously thought to be mere innocent substrates or spectator ligands at best, will reach beyond these C–H and C=C bond activation reactions. It can be envisioned that one-electron reduced Fisher or one-electron oxidized Schrock carbenes could lead to alternative reaction pathways for various reactions, also toward C–heteroatom bond formation processes. For the moment, the limited accessibility of suitable precursors for these carbenes (diazo compounds) and nitrenes (PhINTs or azides) might hamper progress, unless ways are found to convert alkyl or amine fragments into the corresponding six-valence electron species. These elegant systems could be regarded as examples of supramolecular cooperative catalysis, given the strong influence of the H-bonding motif between the ligand periphery and the substrate, both with respect to enantiodiscrimination and stabilization of the radical nature of the carbene fragment.

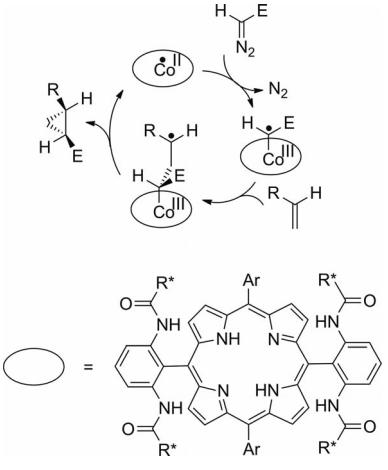

Scheme 5. Co-catalyzed asymmetric cyclopropanation of electron-poor alkenes occurs via carbene radical anion species, with aided stability provided by a functionalized chiral porphyrin.

2.2 Bifunctional Substrate Activation

Pincer ligands have been studied intensively ever since their inception in the 1970's by Shaw.[35] Many variations of these rigid, meridional tridentate ligand scaffolds have been developed, including many that do not exhibit rigid pincer-like binding characteristics but induce a more flexible coordination sphere around the metal center of choice.[36] The original design featured a central (pivotal) deprotonated sp^2 carbon flanked by two heteroatom donor groups, but over the years various other classes have emerged, the latest being EBE with a deprotonated boryl group.[37] Formally neutral tridentate pincer ligand systems have become very popular in the last decade(s), such as those based on 2,6-diaminopyridine[38] or 2,6-dihydroxypyridine.[39] They offer complementary chemistry to their monoanionic derivatives, e.g. when focusing on low-valent metal centers (e.g. Rh^I, Ir^I) or if coordinatively unsaturated dicationic complexes (such as Pt^{II}) are targeted.

Recently, a specific class of aromatic, neutral tridentate ligands based on lutidine, and close analogues thereof, has received much attention. One special feature of these 2,6-lutidine-derived systems is their ease of deprotonation of the methylene spacer group, effectively making this a "non-innocent" class of ligands.[40] The mode of action and type of reactions accessible with this kind of ligand-metal cooperative reactivity differs significantly from that observed in previously studied acid/base switching systems. Other types of deprotonatable ligand structures have appeared in the literature in recent years, but again research initially focussed mainly on proven second- and third-row group 8–10 transition metals, which will not be further discussed here.[41]

Given the cooperative nature of the lutidine-derived **PNP^R** class of ligands and their close PNN analogues, which was elegantly utilized for stoichiometric reactivity and catalytic transformations using second- and third-row transition metals,[40] it is somewhat remarkable to notice that only very recently the first reports of first-row transition metal based chemistry with this reactive type of scaffold was reported. Mononuclear Fe^{II} and Fe^0 complexes were investigated by Milstein,[42] Goldman[43] and Chirik.[44] Interestingly, subtle but significant differences were noted in the actual geometry around the Fe-center, depending on the substitution on the phosphane side-groups (Scheme 6). With the sterically less encumbered ligand PNP^{iPr}, the Fe center shows a trigonal bipyramidal structure, while for the bulkier analogue PNP^{tBu} a square-pyramidal geometry is obtained, both for the Fe^{II} as well as the formal Fe^0 state.

To date, only one example of cooperative catalysis with Fe has been detailed using this type of ligand framework (Scheme 7).[45] The hydrogenation of ketones was reported

 © 2012 Wiley-VCH Verlag GmbH & Co. KGaA, Weinheim

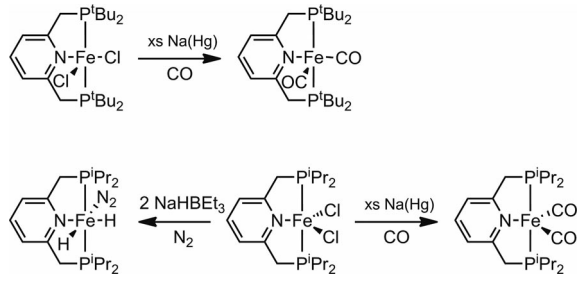

Scheme 6. Subtle influence of the R group in **PNP^{R}** on the geometry of the Fe complex.

to be quite efficient with [FeBr(H)(CO)(**PNP^{tBu}**)] as precursor and speculated to behave in a cooperative manner, reminiscent to the classic Noyori-type mechanism. As iron-catalyzed hydrogenations are gaining in importance, due to the obvious advantages gained over other more established metals,[46] it is expected that various types of ligand scaffolds will be successfully probed to display reactivity toward susceptible C=C and C=X groups (X = O, N).

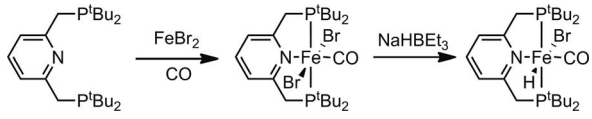

Scheme 7. Preparation of Fe(Br)(H)(CO)(**PNP^{tBu}**), which is a catalyst for the cooperative hydrogenation of ketones.

Chemistry and catalytic reactivity of nickel with cooperative ligand-scaffolds is still far from developed. Initial results using the same **PNP^{tBu}** framework as for Fe (vide supra) have been obtained starting from dicationic Ni^{II} precursors via a sequential dearomatization-reprotonation protocol to generate terminal thiolate complexes as well as nickel-alkyl species (Scheme 8).[47] Nickel alkyl complexes are inferred as catalytic intermediates for a range of organic transformations, such as hydrovinylation, Heck and Kumada coupling and polymerization reactions. Their targeted synthesis, via sequential ligand-based activation and metal-based substitution reactions, in combination with dual-mode reactivity options at both ligand and metal *and* the potential to switch the catalyst on or off during catalysis might aid the development of more active or selective systems.

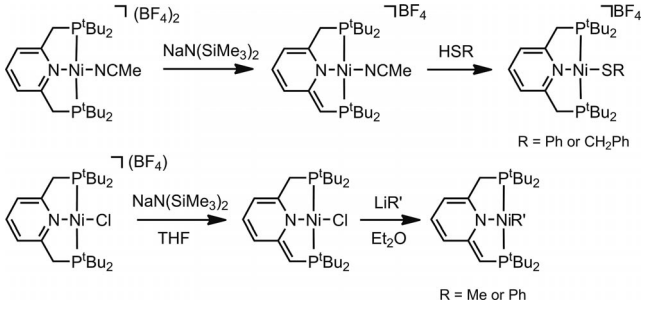

Scheme 8. Synthesis of the Ni-alkyl complexes featuring a deprotonated version of ligand **PNP^{tBu}**.

The first example of hemilability of the central N-atom of the cooperative, neutral pincer ligand **PNP^{tBu}** was recently discussed; pyridyl nitrogen coordination could be monitored using IR spectroscopy and was shown to be dependent on charge as well as steric arguments (Scheme 9).[48] Only in case of a cationic species was N-coordination observed. Furthermore, selective alkylation of the dearomatized ligand backbone {obtained after treatment of the complex [CuBr(**PNP^{tBu}**)] with base} was described, highlighting the reactive nature of these charge-switching scaffolds.[49] This might lead to new opportunities for the synthesis and exploration of modified, perhaps even chiral analogues of this cooperative ligand scaffold.

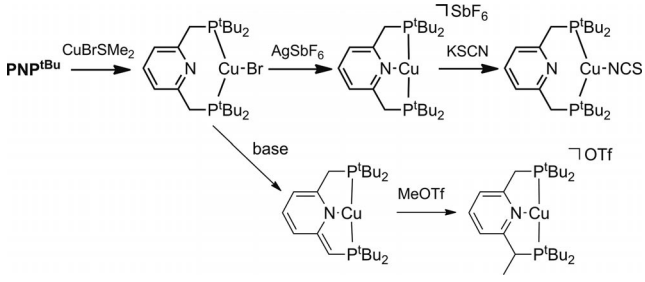

Scheme 9. Hemilabile coordination and reactivity of the dearomatized T-shaped complex Cu(**PN^{-}P^{tBu}**) with electrophiles.

Apart from the preferred coordination as a typical meridional, tridentate "pincer" ligand, recent evidence from X-ray crystallography proved that this framework can also act as a dinucleating scaffold, bridging two Cu^{I} centers in an unprecedented κ^2–*P*,*N*-κ^1–*P* mode (Scheme 10).[50] We recently demonstrated the use of these Cu complexes with cooperative PNP-ligands to be active in the [2+3] dipolar addition reaction between azides and alkynes. The intermediacy of complex **2** was strongly suggested by stoichiometric reactivity studies. Initial formation of a phenyl acetylide derivative after reaction of complex **2** with HCCPh (the acetylenic proton is acidic enough to reprotonate the dearomatized ligand) and subsequent addition of benzyl azide led to generation of the triazole product through intramolecular ligand-to-triazole proton transfer.[51]

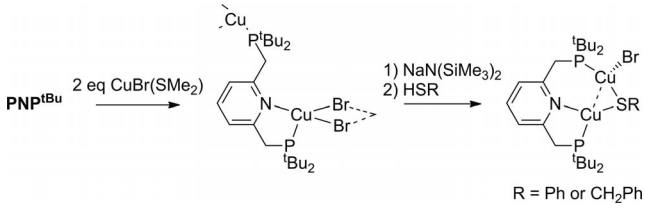

Scheme 10. Generation of unusual dinuclear Cu^{I} complexes with a bridging **PNP^{tBu}** ligand via sequential dearomatization-reprotonation.

Besides reversible deprotonation or dearomatization in order to induce cooperative reactivity, some systems can act as intramolecular base in tandem with first-row transition metals, much like the classic Noyori Ru-catalysts.[13,52] This concept is e.g. explored in the context of hydrogenase modeling. DuBois and co-workers have employed bioinspired

 © 2012 Wiley-VCH Verlag GmbH & Co. KGaA, Weinheim

bis(phosphanylmethyl)amines to play a crucial cooperative role during the generation of dihydrogen at mononuclear Co^{II} and Ni^{II} centers (Scheme 11).[53] Square-planar starting compounds carrying either one or two PNP ligands have been prepared, whereby the cooperating ligand furnishes a proton-accepting pocket in close proximity to an axial coordination site at the metal center, that may bind a hydride. Two sequential proton-coupled electron transfer steps furnish the hydride-ammonium species that can lead to the formation of H_2.

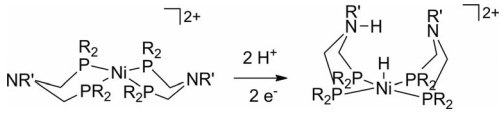

Scheme 11. Cooperative production of dihydrogen through bifunctional proton activation.

The same catalyst system has subsequently been covalently anchored and immobilized on electron-conducting carbon nanotubes by the group of Palacin, Fontecave and Artero, who demonstrated the highly efficient use of these devices in the reversible oxidation of H_2, with turnovers of up to 100,000 at very low overpotentials.[54] In subsequent work the non-covalent adsorption onto carbon nanotubes using pyrene-functionalized PNP scaffolds was shown.[55]

Recently, the groups of Holland and Eisenberg demonstrated the photocatalytic production of dihydrogen from water using this type of Ni complexes featuring cooperative ligands.[56] It is clear that the combination of an intramolecular proton-docking site close to an hydridophilic metal site creates a powerful cooperative combination for this deceptively simple but complex reaction, as it reduces the required overpotential needed to drive this reaction. It is paramount for the development of catalysts and devices for solar fuel production to utilize and incorporate the same principles.

The group of Talarmin, Schollhammer and Gloaguen has reported on a diphosphanyl-amine ligand resembling the naturally occurring azadithiolate co-factor with regards to its potential for proton-binding whilst being in close proximity to a metal-hydride site.[57] This PNP-system can act as a bridging or a chelating ligand (depending on reaction conditions) to a diiron system reminiscent of the $[Fe_2]$-H_2-ase active site (Scheme 12). Addition of acids to this biomimetic model system led to initial protonation at the intramolecular basic nitrogen, with subsequent proton-transfer to the diiron core.

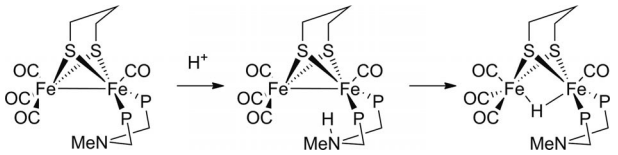

Scheme 12. Cooperative proton-transfer within a bioinspired diiron model system relevant for H2ase activity.

Recently, a new twist to this strategy was presented by the group of Ott.[58] Using a particular *mononuclear* Fe^{II} system featuring a chelating dithiolate ligand (Scheme 13), which in itself is already noteworthy, they observed that one of the thiolate-sulfur atoms could be reversibly protonated. This example of ligand reactivity was then used to facilitate cooperative dihydrogen production. Electrocatalytic proton reduction was shown to be very efficient at relatively low overpotentials.

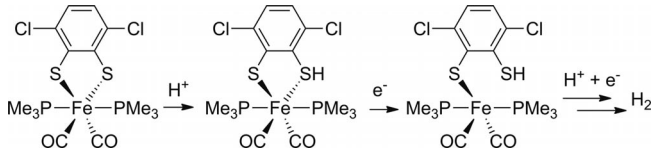

Scheme 13. Cooperative (noninnocent) reactivity of a dithiolate ligand on a mononuclear Fe^{II} species, relevant for bioinspired dihydrogen production.

2.3 Bimetallic Catalysis

Cooperativity in a di- or polynuclear metal system is mainly useful and productive if the activity exhibited by the multimetallic core either surpasses results obtained for the mononuclear analogue or if the cluster induces a reactivity that is not possible otherwise.[59] For some time now, bimetallic cooperative catalysis has been established in the field of polymer catalysis, with landmark contributions by the group of Coates on CO_2-propylene oxide copolymerization systems that outperform their mononuclear analogues.[60] Jacobsen pioneered the use of dicobalt species for the ring opening of epoxides.[61] Recently, some adaptations of this proven concept have been elaborated on, using supramolecular bowl-shaped structures.[62] The area of "click chemistry", originally defined by Sharpless[63] to include 100% atom-efficient, thermodynamically favored and very selective coupling reactions between two reactive coupling partners, is dominated by the copper-catalyzed azide–alkyne coupling to generate bioorthogonal triazole fragments. The group of Marks has made elegant contributions using well-designed dinickel complexes based on dinucleating phenoxyiminato ligands, which were shown to induce cooperative catalysis in both the homopolymerization of ethylene *and* the copolymerization of ethylene with polar comonomers (norbornadiene and acrylates).[64] This has led to high levels of comonomer incorporation, significantly higher branch-content in PE and hence in different polymer microstructures. Meyer has developed innovative dinucleating ligands based on functionalized pyrazolate scaffolds and the corresponding Ni, Cu and Zn bimetallic complexes thereof, which are active models for urease (Ni),[65] phosphatase (Zn)[66] and e.g. polyphenolether synthesis (Cu).[67,68]

Ozerov has described the formation of specific Pd^{I}(PNP) dimers – PNP = bis[2-(diisopropyl- phosphanyl)-4-methylphenyl]amido – via photolytic activation of the corresponding mononuclear Pd(PNP)(alkyl) species and utilized these systems (Scheme 14), which feature an unsupported

 © 2012 Wiley-VCH Verlag GmbH & Co. KGaA, Weinheim

Pd–Pd single bond and can thus be viewed as two-electron reductants, for the bimetallic, homolytic activation of particular H–E bonds, most notably H_2O and NH_3.[69] It remains to be seen if similar strategies may be fruitful with first-row analogues, especially in combination with redox-active ligands (vide infra).

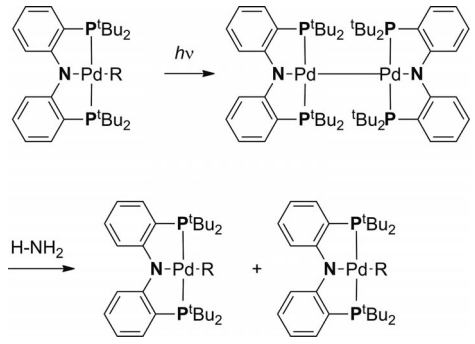

Scheme 14. Dinuclear activation of ammonia at a Pd^I–Pd^I dimer.

Peters has developed dinuclear copper species based on the same PNP ligand scaffold as well as its close structural PPP derivative [PPP = bis(2-diisopropylphosphanyl)phenylphosphane],[80] which showed very interesting electronic behaviour, allowing the isolation of mixed-valent states as well as spectacular, long-lived luminescence.[71,72] Using the same PNP framework (Scheme 15), Mindiola disclosed the synthesis and follow-up reduction of the mononuclear CoCl(PNP) complex, which revealed some interesting chemistry, most notably the fact that the one-electron reduced Co^I species Co(PNP) rapidly dimerized, with the PNP ligand acting as a bridging dinucleating scaffold in the resulting diamanoid structure.[73] Under an atmosphere of CO, the related mononuclear species was again obtained. When the reduction was performed under an N_2 atmosphere, the end-on coordinated dinuclear dinitrogen complex could be isolated. To date, no further reactivity with any these species has been reported; it can be expected that ultimately these types of species may be utilized for dinitrogen functionalization.

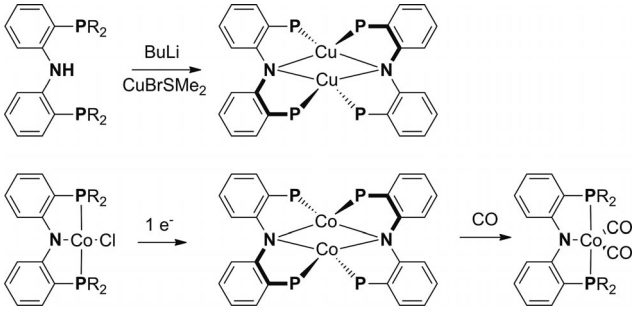

Scheme 15. Formation of dinuclear Cu^I and Co^I species with a bridging PNP ligand.

The group of Agapie recently adapted the ligand backbone design, originally described by Vilar[74] to prepare mono- and dinuclear Pd^I complexes, based on terphenylphosphanes in order to arrive at dinuclear Ni^I-dimeric systems facilitate stoichiometric C–C bond formation reactions between bis(orthometallated) biphenyls and CO (Scheme 16).[75] The two Ni-centers actively cooperate during the essential steps of this transformation, and one potential mechanism includes formal two-electron reduction of the Ni^I-dimer core after initial association and insertion of CO in a Ni–C bond. Indeed, dinuclear Ni^0 species have been observed in the reaction mixture. Strikingly, the same dinickel biphenyldiyl complex was also reactive toward geminal dichloroalkanes, leading to the formation of substituted fluorenes. This suggests an oxidative mechanism for the dinickel core, with oxidative C–Cl addition over the metal-metal bond as one option (radical mechanisms to form mixed-valent Ni^I–Ni^{II} species are another viable possibility). Therefore, there seems to be much versatility in the type of bimetallic scaffolds and the electronic state of the metal–metal bond to induce selective bond forming reactions. Key aspect for further development is the transformation from stoichiometric to catalytic turnover, with regeneration of the active dinickel species. Furthermore, it is potentially also possible that such dimers actually break up into reactive mononuclear entities. Similar dinuclear nickel species and their reactivity were reported by the groups of Hillhouse and Johnson very recently.[76]

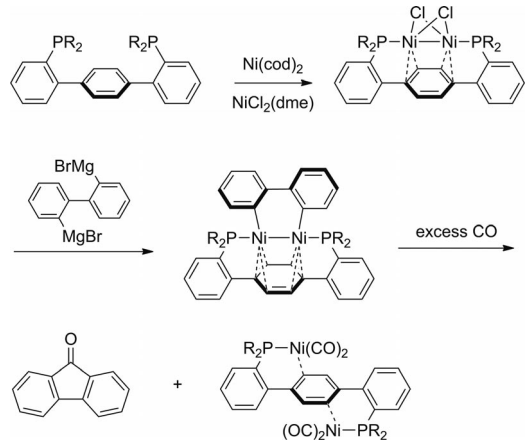

Scheme 16. Formation and C–C bond forming reactivity of a dinuclear Ni^I–Ni^I complex with a *trans*-spanning terphenyldiphosphane ligand (xs = excess).

Betley has reported elegant polydentate, C_3-symmetric[77] hexaamine ligand design strategies to prepare tri- and hexanuclear iron clusters.[78] The former was shown to be a suitable platform for the generation of nucleophilic μ^3-nitrido species that smoothly reacted with MeI to generate the corresponding methylimide. The iron centers in the hexanuclear clusters showed a high level of electronic cooperativity, which translated into a highly delocalized electronic structure of the Fe ions. The stoichiometric reduction of NO_2 was described, which indicates that reactivity is possible with these clusters, concomitant with noticeable structural changes to the hexanuclear geometry.[78d] These bioinspired clusters may prove useful for small molecule activation, in the spirit of e.g. nitrogenase or as homogeneous models for heterogeneous catalysis such as the Haber-Bosch process.[79] The group of Agapie has reported on similar polynuclear

 © 2012 Wiley-VCH Verlag GmbH & Co. KGaA, Weinheim

clusters accommodated by polydentate ligand scaffolds and the resulting electronic communication between the metal centers.[80]

Bouwman et al. recently showed that CO_2 can be reductively coupled to form oxalate using a dinuclear Cu^I species, wherein each copper center has an N_3S coordination sphere, with the two metal centers bridged merely by a disulfide linkage (Scheme 17).[81] This system showed remarkable selectivity for CO_2 over O_2 and regeneration of the active precursor was feasible through electrocatalytic reduction. The proposed mechanism involves initial reduction of CO_2 in the coordination sphere of Cu^I to the $CO_2^{\bullet-}$ radical ion, which occurs at a significantly lower potential than for the non-metal mediated process, concomitant formation of Cu^{II}. Dimerization (with generation of a tetranuclear copper-species) results in oxalate formation, which could be liberated from the Cu_4 core by addition of Li salt.

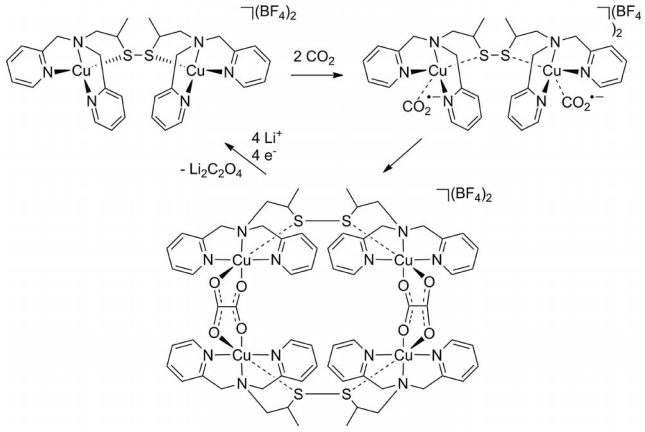

Scheme 17. Reductive coupling of CO_2 to oxalate by a dinuclear Cu^I complex.

2.4 Hemilabile Ligands for Cooperative Catalysis

Biology often employs donor groups and ligating fragments that show variable coordination to the metal center. This adaptive coordination behaviour (termed hemilability or flexidenticity)[82] allows the regulation of vacant sites and the selective conversion of reactive substrates. Adaptive ligand systems that can accommodate different stages for a catalytically active complex during turnover, e.g. creating and masking vacant sites depending on external stimuli (reagents, substrates) are very promising to induce selective cooperative catalysis, provided the characteristics of the hemilabile group can be properly tuned. The group of Braunstein has developed many bi- and tridentate scaffolds that feature weakly coordinating donor groups, which easily dissociate from the metal center in the presence of exogenous ligand or substrate.[83]

Allosteric catalysis on the basis of hemilabile coordination of a hybrid ligand to a secondary metal site, whereafter a nearby primary catalytic site is transformed from a dormant to an active catalyst state, has been demonstrated by Mirkin and co-workers in a number of systems.[84] They developed cleft-like dinuclear systems that operate via a "weak-link" concept based on P,S-ligation to a transition metal (typically Rh), that is connected to a first-row metal based (Mn, Zn) catalyst site (Scheme 18). One of their elegant designs features two Mn-salen units sandwiched between these P,S-ligated Rh hinges. Introduction of an exogenous substrate resulting in opening of the cleft, which led to higher accessibility of the bis-Mn-salen core and subsequently to catalytic activity in the acyl transfer reaction involving acetic anhydride and pyridyl carbinol as the substrates, generating acetate as product. Furthermore, a system was devised where this product was the exogenous trigger to induce catalyst activity (autocatalysis). More recently, triple-decker catalytic systems have been developed, wherein two side-arm functionalities act as "hinges" to selectively mask the catalytically active metal site, which was an Al-salen unit capable of catalyzing the ring-opening of ε-caprolactone.[85]

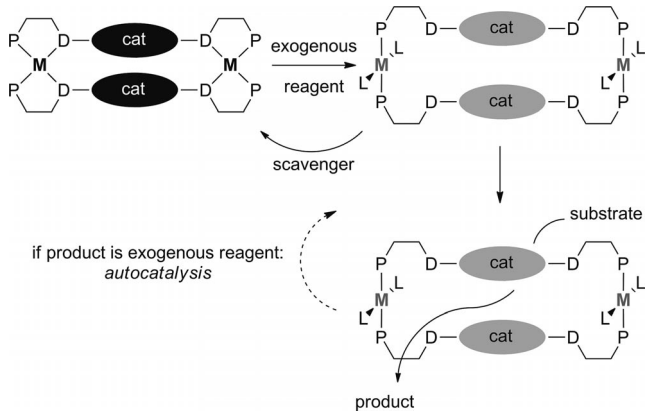

Scheme 18. Mechanism of autocatalysis at a primary catalytic site made possible by selective hemilabile coordination at a secondary metal site.

Recently, new hybrid meridional tridentate ligands have been introduced, that feature two distinctly different side-arm donor groups. The use of such hemilabile *pincer* ligands was pioneered by Milstein, who developed neutral hybrid PNN systems that were amenable to induce unprecedented dehydrogenative coupling reactions involving alcohols.[86] Also hybrid, asymmetrically substituted monoanionic ligands have been developed that display selective dissociation of one of the side-arms, thereby vacating a coordination site at the metal center (Scheme 19).[87] To

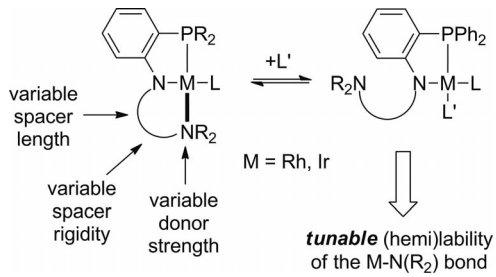

Scheme 19. Concept of tunable hemilability to induce cooperative reactivity.

 © 2012 Wiley-VCH Verlag GmbH & Co. KGaA, Weinheim

date, this ligand design has not been combined with first-row transition metals but has only been tested with Rh, Ir and Ru.

3. Supramolecular Cooperative Catalysis

Supramolecular catalysis is a rapidly expanding field within homogeneous catalysis, wherein self-assembly via non-covalent interactions (i.e. H-bonding, metal templation, anion templation or other types of weak interactions) is employed to construct the desired ligand scaffold and/or to generate the supramolecular catalyst species. This also includes examples dealing with self-complementary monophosphorus ligands.[88] To date, this concept has been mainly explored with second- and third-row metals, although first-row metals such as Zn or Cu are frequently employed as metal template.[89] However, merging this strategy with ligand based noninnocence has been ill-explored to date.

Apart from the system of Zhang (vide supra), only a few ligand scaffolds combine non-covalent ligand-substrate interactions with first-row transition metal complexes. Borovik and co-workers developed tripodal ligand scaffolds adorned with H-bonding patterns along the periphery.[90] These ligands have allowed the selective construction of e.g. Fe-oxo and Co-hydroxo species, wherein the oxygen-containing fragment is stabilized by H-bonding to the amide units in the ligand side-arms. This may ultimately be a useful strategy for selective catalytic oxygenation or oxidation reactions.

Breit and co-workers reported on the Ni-catalyzed hydrocyanation of styrenes using self-assembled bidentate phosphane ligands.[91] Although this provides a very elegant way to prepare new ligand systems, with the advantage of creating larger libraries due to the higher availability of building blocks, the self-assembly does not extend to the level of cooperative catalysis, as the ligands do not actively participate during substrate conversion but are merely configured using non-covalent H-bonding interactions. In general, despite the "synzymatic" nature of some of these supramolecular catalysts, there is no true cooperative aspect as yet incorporated in most of these concepts, nor are first-row transition metals exploited in this way. However, it is envisioned that such favorable design features may well come into existence in the near future, as more control over the preparation and behaviour of these supramolecular systems is gained.[92]

Crabtree and Brudvig developed a Mn-based oxidation catalyst for C–H oxygenation reactions, wherein substrate recognition and preorganization induced by multiple hydrogen bonding were essential to achieve the observed high chemoselectivity.[93] The bimetallic catalyst featured a bioinspired Mn_2 reactive center with bridging oxo-ligands and a functionalized terpyridyl ligand adorned with a carboxylic acid moiety capable of interacting with the carboxylic acid group of the substrate ibuprofen, thereby positioning the desired C–H bond directly above the active Mn_2 center. Control experiments supported the role of hydrogen bonding in orienting the substrate to achieve high selectivity.

The use of other types of cooperative ligand structures so far has been limited to noble metal chemistry. For instance, the elegant systems employed by the group of Jun[94] and Breit et al.,[95] wherein the ligand interacts strongly with the substrate of choice – be it an aldehyde to infer selective hydroacylation, through the formation of a reversible imine bond, or the hydroformylation of α,β-unsaturated carboxylic acids, making use of directing H-bonding – have been tested mainly with Rh and Ru. Related approaches using bifunctional substrate activation have been developed by Reek et al., wherein hydrogen bonding interactions[96] between the ligands and the substrates were shown to enhance the asymmetric hydrogenation of functionalized substrates. The use of an anion-binding pocket as the backbone of a diphosphorus ligand was able to regulate the regioselectivity during the rhodium-catalyzed hydroformylation of unsaturated carboxylate substrates.[97]

In general, despite the obvious advances developed and the complementary or beneficial aspects of various complex or supramolecular (cooperative) systems recently reports, e.g. in terms of reactivity, tunability and selectivity, to date no attention is given at all to applying these concepts with first-row metals and there is a whole field waiting to be explored.

4. Conclusions

The field of transition metal cooperative catalysis has seen much fascinating progress in the last decade, but the first-row transition metals are still far from well-developed in this respect. It is believed that combining cooperative ligands, either featuring redox-activity, proton-transfer abilities or coordinative adaptivity with earth-abundant metals such as Fe, Co, Ni or Cu, either as mononuclear or bimetallic species, will prove to be very efficient for both new reactivity as well as the use of cheap metals for noble tasks. This will include processes to facilitate the cooperative, catalytic activation and functionalization of small molecules for which currently no methodologies are available or that can only be mediated by expensive metals.[98,99,100]

Acknowledgments

The author's research in the area of cooperative chemistry and first-row transition metal catalysis has been made possible by the Netherlands' Research Council - Chemical Sciences (NWO CW VENI Innovative Research, grant number 700.56.403) and the University of Amsterdam. Additional financial support from NWO-CW, NWO-ACTS, NRSC-C, the SmartMix program CATCHBIO and the BioSolarCells consortium is also acknowledged. Ongoing research in this area will be funded by the European Research Council (ERC Starting Grant, agreement 279097). The author thanks the collaborative EU COST network PhoSciNet (CM802) for additional resources and his colleagues Prof. Dr. Joost Reek and Dr. Bas de Bruin at UvA for scientific discussions.

 © 2012 Wiley-VCH Verlag GmbH & Co. KGaA, Weinheim

[1] a) I. Bertini, H. B. Gray, S. J. Lippard, J. S. Valentine, *Bioinorganic Chemistry*, University Science Books, Mill Valley, CA, **1994**.

[2] a) J. Stubbe, W. A. van der Donk, *Chem. Rev.* **1998**, *98*, 705–762; b) G. Parkin, *Chem. Rev.* **2004**, *104*, 699–768; c) J. Weston, *Chem. Rev.* **2005**, *105*, 2151–2174; d) D. Voet, J. G. Voet, *Biochemistry*, Wiley, New York, **2008**.

[3] a) N. Ito, S. E. V. Phillips, C. Stevens, Z. B. Ogel, M. J. McPherson, J. N. Keen, K. D. S. Yadav, P. F. Knowles, *Nature* **1991**, *350*, 87–90; b) N. Ito, S. E. V. Phillips, K. D. S. Yadav, P. F. Knowles, *J. Mol. Biol.* **1994**, *238*, 794–814; c) Y. Wang, J. L. DuBois, B. Hedman, K. O. Hodgson, T. D. P. Stack, *Science* **1998**, *279*, 537–540; d) J. Müller, T. Weyhermüller, E. Bill, P. Hildebrandt, L. Ould-Moussa, T. Glaser, K. Wieghardt, *Angew. Chem.* **1998**, *110*, 637; *Angew. Chem. Int. Ed.* **1998**, *37*, 616–619; e) J. W. Whittaker, *Chem. Rev.* **2003**, *103*, 2347–2363.

[4] For natural systems, see: a) P. M. Vignais, B. Billoud, *Chem. Rev.* **2007**, *107*, 4206–4272; b) J. C. Fontecilla-Camps, A. Volbeda, C. Cavazza, Y. Nicolet, *Chem. Rev.* **2007**, *107*, 4273–4303. For model systems, see: c) C. Mealli, T. B. Rauchfuss, *Angew. Chem.* **2007**, *119*, 9100; *Angew. Chem. Int. Ed.* **2007**, *46*, 8942–8944; d) F. Gloaguen, T. B. Rauchfuss, *Chem. Soc. Rev.* **2009**, *38*, 100–108; e) C. Tard, C. J. Pickett, *Chem. Rev.* **2009**, *109*, 2245–2274.

[5] For recent reviews, see: a) I. A. Koval, P. Gamez, C. Belle, K. Selmeczi, J. Reedijk, *Chem. Soc. Rev.* **2006**, *35*, 814–840; b) J. I. van der Vlugt, F. Meyer, *Top. Organomet. Chem.* **2007**, *22*, 191–240; for a recent model system, see: c) M. Rolff, J. N. Hamann, F. Tuczek, *Angew. Chem. Int. Ed.* **2011**, *50*, 6924–6927.

[6] Such as sMMO, see: a) A. C. Rosenzweig, C. A. Frederick, S. J. Lippard, P. Nordlund, *Nature* **1993**, *366*, 537–543; b) B. J. Wallar, J. D. Lipscomb, *Chem. Rev.* **1996**, *96*, 2625–2657; c) S. Friedle, E. Reisner, S. J. Lippard, *Chem. Soc. Rev.* **2010**, *39*, 2768–2779; d) C. E. Tinberg, S. J. Lippard, *Acc. Chem. Res.* **2011**, *44*, 280–288. For a bioinspired NiFe system, see: S. Yao, C. Herwig, Y. Xiong, A. Company, E. Bill, C. Limberg, M. Driess, *Angew. Chem. Int. Ed.* **2010**, *49*, 7054–7058.

[7] a) J. S. Rieske, D. H. MacLennan, R. Coleman, *Biochem. Biophys. Res. Commun.* **1964**, *15*, 338–344; b) J. S. Rieske, *J. Biol. Chem.* **1968**, *239*, 3017–3022; c) T. A. Link, O. M. Hatzfeld, M. Saynovits, in *Bioinorganic Chemistry* (Ed.: A. X. Trautwien), Wiley-VCH, Weinheim, Germany, **1997**, p. 312–325. For a synthetic structural model, see: J. C. Ballmann, A. Albers, S. Demeshko, S. Dechert, E. Bill, E. Bothe, U. Ryde, F. Meyer, *Angew. Chem.* **2008**, *120*, 9680; *Angew. Chem. Int. Ed.* **2008**, *47*, 9537–9541. For a functional model, see: K. Chen, L. Que Jr., *Angew. Chem.* **1999**, *111*, 2365; *Angew. Chem. Int. Ed.* **1999**, *38*, 2227–2229.

[8] J. I. van der Vlugt, F. Meyer, *Met. Ions Life Sci.* **2007**, *2*, 181–240.

[9] a) I. Bertini, A. Sigel, H. Sigel, *Handbook on Metalloproteins*, Marcel Dekker, New York, **2001**; b) R. C. Linck, T. B. Rauchfuss, in: *Bioorganometallics* (Ed.: G. Jaouen), Wiley-VCH, Weinheim, Germany, **2005**.

[10] a) T. G. Traylor, C. K. Chang, J. Geibel, A. Berzinis, T. Mincey, J. Cannon, *J. Am. Chem. Soc.* **1979**, *101*, 6716–6731; b) E. B. Springman, E. L. Angleton, H. Birkedal-Hansen, H. E. van Wart, *Proc. Natl. Acad. Sci. USA* **1990**, *87*, 364–368; c) H. E. van Wart, H. Birkedal-Hansen, *Proc. Natl. Acad. Sci. USA* **1990**, *87*, 5578–5582; d) J. Wuerges, J.-W. Lee, Y.-I. Yim, H.-S. Yim, S.-O. Kang, K. Djinovic Carugo, *Proc. Natl. Acad. Sci. USA* **2004**, *101*, 8569–8574; e) D. P. Barondeau, C. J. Kassmann, C. K. Bruns, J. A. Tainer, E. D. Getzoff, *Biochemistry* **2004**, *43*, 8038–8047.

[11] N. S. Lewis, D. G. Nocera, *Proc. Natl. Acad. Sci. USA* **2006**, *103*, 15729–15735.

[12] a) A. Silakov, B. Wenk, E. J. Reijerse, W. Lubitz, *Phys. Chem. Chem. Phys.* **2009**, *11*, 6592–6599; b) O. F. Erdem, L. Schwartz, M. Stein, A. Silakov, S. Kaur-Ghumaan, P. Huang, S. Ott, E. J. Reijerse, W. Lubitz, *Angew. Chem. Int. Ed.* **2011**, *50*, 1439–1443. For some relevant structural and functional models of the Fe_2H_2ase, see: c) C. A. Boyke, J. I. van der Vlugt, T. B. Rauchfuss, S. R. Wilson, G. Zampella, L. De Gioia, *J. Am. Chem. Soc.* **2005**, *127*, 11010–11018; d) J. I. van der Vlugt, T. B. Rauchfuss, C. M. Whaley, S. R. Wilson, *J. Am. Chem. Soc.* **2005**, *127*, 16012–16013; e) J. I. van der Vlugt, T. B. Rauchfuss, S. R. Wilson, *Chem. Eur. J.* **2006**, *12*, 90–98; f) A. K. Justice, G. Zampella, L. De Gioia, T. B. Rauchfuss, J. I. van der Vlugt, S. R. Wilson, *Inorg. Chem.* **2007**, *46*, 1655–1664; g) F. Wang, M. Wang, X. Liu, K. Jin, W. Dong, G. Li, B. Åkermark, L. Sun, *Chem. Commun.* **2005**, 3221–3223; for a recent dicobalt-catalyst, see: N. K. Szymczak, L. A. Berben, J. C. Peters, *Chem. Commun.* **2009**, 6729–6731.

[13] Breakthrough examples and reviews: a) R. Noyori, T. Ohkuma, *Angew. Chem.* **2001**, *113*, 40; *Angew. Chem. Int. Ed.* **2001**, *40*, 40–73; b) D. B. Grotjahn, *Chem. Eur. J.* **2005**, *11*, 7146–7153; c) M. R. Ringenberg, S. L. Kokatam, Z. M. Heiden, T. B. Rauchfuss, *J. Am. Chem. Soc.* **2008**, *130*, 788–789; d) F. W. Patureau, M. Kuil, A. J. Sandee, J. N. H. Reek, *Angew. Chem.* **2008**, *120*, 3224; *Angew. Chem. Int. Ed.* **2008**, *47*, 3180–3183; e) T. Zweifel, J.-V. Naubron, J. Grützmacher, *Angew. Chem.* **2009**, *121*, 567; *Angew. Chem. Int. Ed.* **2009**, *48*, 559–563; f) S. W. Kohl, L. Weiner, L. Schwartsburd, L. Konstantinovski, L. J. W. Shimon, Y. Ben-David, M. A. Iron, D. Milstein, *Science* **2009**, *324*, 74–77; g) Y. Kashiwame, S. Kuwata, T. Ikariya, *Chem. Eur. J.* **2010**, *16*, 766–770.

[14] a) Y. Blum, D. Czarkie, Y. Rahamim, Y. Shvo, *Organometallics* **1985**, *4*, 1459–1461; b) A. L. E. Larsson, B. A. Persson, J.-E. Bäckvall, *Angew. Chem.* **1997**, *109*, 1256; *Angew. Chem. Int. Ed. Engl.* **1997**, *36*, 1211–1212; c) J. S. M. Samec, A. H. Éll, J. B. Åberg, T. Privalov, L. Eriksson, J.-E. Bäckvall, *J. Am. Chem. Soc.* **2006**, *128*, 14293–14305; d) C. P. Casey, H. Guan, *J. Am. Chem. Soc.* **2007**, *129*, 5816–5817; e) C. P. Casey, T. B. Clark, I. A. Guzei, *J. Am. Chem. Soc.* **2007**, *129*, 11821–11827; f) C. P. Casey, H. Guan, *J. Am. Chem. Soc.* **2009**, *131*, 2499–2507.

[15] a) R. C. Linck, R. J. Pafford, T. B. Rauchfuss, *J. Am. Chem. Soc.* **2001**, *123*, 8856–8857; b) J. S. M. Samec, J. E. Bäckvall, P.-G. Andersson, P. Brandt, *Chem. Soc. Rev.* **2006**, *35*, 237–248; c) M. Ito, T. Ikariya, *Chem. Commun.* **2007**, 5134–5142; d) Z. M. Heiden, T. B. Rauchfuss, *J. Am. Chem. Soc.* **2007**, *129*, 14303–14310; e) M. Ito, A. Sakaguchi, C. Kobayashi, T. Ikariya, *J. Am. Chem. Soc.* **2007**, *129*, 290–291; f) M. R. Ringenberg, S. L. Kokatam, Z. M. Heiden, T. B. Rauchfuss, *J. Am. Chem. Soc.* **2008**, *130*, 788–789; g) Z. M. Heiden, T. B. Rauchfuss, *J. Am. Chem. Soc.* **2009**, *131*, 3593–3600.

[16] W. Kaim, *Inorg. Chem.* **2011**, *50*, DOI: 10.1021/ic2003832.

[17] W. I. Dzik, X. P. Zhang, B. de Bruin, *Inorg. Chem.* **2011**, *50*, DOI: 10.1021/ic200043a.

[18] a) C. S. Scarborough, K. Wieghardt, *Inorg. Chem.* **2011**, *50*, DOI: 10.1021/ic2005419; b) S. Sproules, K. Wieghardt, *Coord. Chem. Rev.* **2010**, *254*, 1358–1382; c) C. C. Lu, T. Weyhermüller, E. Bill, K. Wieghardt, *Inorg. Chem.* **2009**, *48*, 6055–6064; d) S. Sproules, K. Wieghardt, *Dalton Trans.* **2007**, 1552–1566.

[19] A. M. Allgeier, C. A. Mirkin, *Angew. Chem.* **1998**, *110*, 936; *Angew. Chem. Int. Ed.* **1998**, *37*, 894–908.

[20] K. Caulton, *Eur. J. Inorg. Chem.* **2012**, DOI: 10.1002/ejic.201100623.

[21] B. de Bruin, E. Bill, E. Bothe, T. Weyhermüller, K. Wieghardt, *Inorg. Chem.* **2000**, *39*, 2936–2947. See also: a) V. C. Gibson, C. Redshaw, G. A. Solan, *Chem. Rev.* **2007**, *107*, 1745–1776; b) G. J. P. Britovsek, S. A. Cohen, V. C. Gibson, P. J. Maddox, M. van Meurs, *Angew. Chem.* **2002**, *114*, 507; *Angew. Chem. Int. Ed.* **2002**, *41*, 489–491; c) T. M. Kooistra, Q. Knijnenburg, J. M. M. Smits, A. D. Horton, P. H. M. Budzelaar, A. W. Gal, *Angew. Chem.* **2001**, *113*, 4855; *Angew. Chem. Int. Ed.* **2001**, *40*, 4719–4722; d) G. J. P. Britovsek, V. C. Gibson, B. S. Kimberley, P. J. Maddox, S. J. McTavish, G. A. Solan, A. J. P.

 © 2012 Wiley-VCH Verlag GmbH & Co. KGaA, Weinheim

White, D. J. Williams, *Chem. Commun.* **1998**, 849–850; e) B. L. Small, M. Brookhart, A. M. A. Bennett, *J. Am. Chem. Soc.* **1998**, *120*, 4049–4050.

[22] a) W. I. Dzik, J. I. van der Vlugt, J. N. H. Reek, B. de Bruin, *Angew. Chem. Int. Ed.* **2011**, *50*, 3356–3358; b) P. J. Chirik, K. Wieghardt, *Science* **2010**, *327*, 794–795.

[23] a) S. K. Russell, E. Lobkovsky, P. J. Chirik, *J. Am. Chem. Soc.* **2011**, *133*, 8858–8861; b) S. K. Russell, C. Milsmann, E. Lobkovsky, T. Weyhermüller, P. J. Chirik, *Inorg. Chem.* **2011**, *50*, 3159–3169; c) A. M. Tondreau, C. Milsmann, E. Lobkovsky, P. J. Chirik, *Inorg. Chem.* **2011**, *50*, doi: 10.1021/ic200730k; d) S. K. Russell, J. M. Darmon, E. Lobkovsky, P. J. Chirik, *Inorg. Chem.* **2010**, *49*, 2782–2792; e) K. T. Sylvester, P. J. Chirik, *J. Am. Chem. Soc.* **2009**, *131*, 8777–8779.

[24] M. M. P. Grutters, J. I. van der Vlugt, Y. Pei, A. M. Mills, M. Lutz, A. L. Spek, C. Müller, C. Moberg, D. Vogt, *Adv. Synth. Catal.* **2009**, *351*, 2199–2208. See also: M. M. P. Grutters, C. Müller, D. Vogt, *J. Am. Chem. Soc.* **2006**, *128*, 7414–7415.

[25] a) A. M. Tondreau, C. Milsmann, A. D. Patrick, H. M. Hoyt, E. Lobkovsky, J. Wieghardt, P. J. Chirik, *J. Am. Chem. Soc.* **2010**, *132*, 15046–15059; b) B. M. Wile, R. J. Trovitch, S. C. Bart, A. M. Tondreau, E. Lobkovsky, C. Milsmann, E. Bill, K. Wieghardt, P. J. Chirik, *Inorg. Chem.* **2009**, *48*, 4190–4200; c) A. C. Bowman, S. C. Bart, F. W. Heinemann, K. Meyer, P. J. Chirik, *Inorg. Chem.* **2009**, *48*, 5587; d) S. K. Russell, E. Lobkovsky, P. J. Chirik, *J. Am. Chem. Soc.* **2009**, *131*, 36; e) R. J. Trovitch, E. Lobkovsky, M. W. Bouwkamp, P. J. Chirik, *Organometallics* **2008**, *27*, 6264–6278; f) R. J. Trovitch, E. Lobkovsky, P. J. Chirik, *J. Am. Chem. Soc.* **2008**, *130*, 11631–11640; g) M. W. Bouwkamp, A. C. Bowman, E. Lobkovsky, P. J. Chirik, *J. Am. Chem. Soc.* **2006**, *128*, 13340–13341; h) M. W. Bouwkamp, E. Lobkovsky, P. J. Chirik, *Inorg. Chem.* **2006**, *45*, 2–4.

[26] A. L. Smith, K. I. Hardcastle, J. D. Soper, *J. Am. Chem. Soc.* **2010**, *132*, 14358. See also: A. L. Smith, L. A. Clapp, K. I. Hardcastle, J. D. Soper, *Polyhedron* **2010**, *29*, 164–169.

[27] D. Adhikari, S. Mossin, F. Basuli, J. C. Huffman, R. K. Szilagyi, K. Meyer, D. J. Mindiola, *J. Am. Chem. Soc.* **2008**, *130*, 3676–3682.

[28] a) J. C. Peters, S. B. Harkins, S. D. Brown, M. W. Day, *Inorg. Chem.* **2001**, *40*, 5083–5091; b) S. B. Harkins, J. C. Peters, *Organometallics* **2002**, *21*, 1753–1755; c) S. B. Harkins, J. C. Peters, *Inorg. Chem.* **2006**, *45*, 4316–4318; d) T. A. Betley, B. A. Qian, J. C. Peters, *Inorg. Chem.* **2008**, *47*, 11570–11582; e) D. L. M. Suess, J. C. Peters, *Chem. Commun.* **2010**, *46*, 6554–6556.

[29] a) O. Vechorkin, V. Proust, X. Hu, *J. Am. Chem. Soc.* **2009**, *131*, 9756–9766; b) O. Vechorkin, Z. Csok, R. Scopelliti, X. Hu, *Chem. Eur. J.* **2009**, *15*, 3889–3999.

[30] P. Ren, O. Vechorkin, K. von Allmen, R. Scopelliti, X. Hu, *J. Am. Chem. Soc.* **2011**, *133*, 7084–7095.

[31] For a recent review on catalytic C–H activation using metalloporphyrins, see: H. Lu, X. P. Zhang, *Chem. Soc. Rev.* **2011**, *40*, 1899–1909. For other reviews on metal-carbenoid based C–H functionalization, see: a) H. M. L. Davies, R. E. J. Beckwith, *Chem. Rev.* **2003**, *103*, 2861; b) C. J. Moody, *Angew. Chem. Int. Ed.* **2007**, *46*,9148–9150; c) M. P. Doyle, *Angew. Chem.* **2009**, *121*, 864; *Angew. Chem. Int. Ed.* **2009**, *48*, 850–852; d) M. P. Doyle, R. Duffy, M. Ratnikov, L. Zhou, *Chem. Rev.* **2010**, *110*, 704–724; e) H. M. L. Davies, D. Morton, *Chem. Soc. Rev.* **2011**, *40*, 1857–1869.

[32] a) Y. Chen, K. B. Fields, X. P. Zhang, *J. Am. Chem. Soc.* **2004**, *126*, 14718–14719; b) Y. Chen, J. V. Ruppel, X. P. Zhang, *J. Am. Chem. Soc.* **2007**, *129*, 12074–12075; c) S. Zhu, J. V. Ruppel, H. Lu, L. Wojtas, X. P. Zhang, *J. Am. Chem. Soc.* **2008**, *130*, 5042–5043.

[33] a) W. I. Dzik, X. Xu, X. P. Zhang, J. N. H. Reek, B. de Bruin, *J. Am. Chem. Soc.* **2010**, *132*, 10891–10902; b) H. J. Lu, W. I. Dzik, X. Xu, L. Wojtas, B. de Bruin, X. P. Zhang, *J. Am. Chem. Soc.* **2011**, *133*, 8518–8521.

[34] a) A. I. Olivos-Suarez, H. Jiang, X. P. Zhang, B. de Bruin, *Dalton Trans.* **2011**, *40*, 5697–5705; b) V. Lyaskovskyy, A. I. Olivos-Suarez, H. Lu, H. Jiang, X. P. Zhang, B. de Bruin, *J. Am. Chem. Soc.* **2011**, *133*, 12264–12273.

[35] A. D. Pryde, B. L. Shaw, B. Weeks, *J. Chem. Soc., Dalton Trans.* **1976**, 322–327.

[36] For general reviews, see: a) M. T. Whited, R. H. Grubbs, *Acc. Chem. Res.* **2009**, *42*, 1607–1616; b) D. Morales-Morales, C. M. Jensen, in *the Chemistry of Pincer Compounds*, Elsevier, Amsterdam, **2007**; c) L.-C. Liang, *Coord. Chem. Rev.* **2006**, *250*, 1152–1177; d) M. van der Boom, D. Milstein, *Chem. Rev.* **2003**, *103*, 1759–1792.

[37] a) J. I. van der Vlugt, *Angew. Chem. Int. Ed.* **2010**, *49*, 252–255; b) Y. Segawa, M. Yamashita, K. Nozaki, *J. Am. Chem. Soc.* **2009**, *131*, 9201–9203; c) A. M. Spokoyny, M. G. Reuter, C. L. Stern, M. A. Ratner, T. Seideman, C. A. Mirkin, *J. Am. Chem. Soc.* **2009**, *131*, 9482–9483.

[38] a) D. Benito-Garagorri, E. Becker, J. Wiedermann, W. Lackner, M. Pollak, K. Mereiter, J. Kisala, K. Kirchner, *Organometallics* **2006**, *25*, 1900–1913; b) D. Benito-Garagorri, K. Kirchner, *Acc. Chem. Res.* **2008**, *41*, 201–213; c) W. Schirmer, U. Flörke, H.-J. Haupt, *Z. Anorg. Allg. Chem.* **1987**, *545*, 83–97.

[39] a) W. H. Bernskoetter, S. Kloek Hanson, S. K. Buzak, Z. Davis, P. S. White, R. Swartz, K. I. Goldberg, M. Brookhart, *J. Am. Chem. Soc.* **2009**, *131*, 8603–8613; b) H. Salem, L. J. W. Shimon, Y. Diskin-Posner, G. Leitus, Y. Ben-David, D. Milstein, *Organometallics* **2009**, *28*, 4791–4806.

[40] J. I. van der Vlugt, J. N. H. Reek, *Angew. Chem.* **2009**, *121*, 8990; *Angew. Chem. Int. Ed.* **2009**, *48*, 8832–8846.

[41] a) B. Askervold, J. Torres Nieto, S. Tussupbayev, M. Diefenbach, E. Herdtweck, M. C. Holthausen, S. Schneider, *Nature Chem.* **2011**, *3*, 532–537; b) S. Musa, I. Shaposhnikov, S. Cohen, D. Gelman, *Angew. Chem. Int. Ed.* **2011**, *50*, 3533–3537; c) K. Muñiz, A. Lishchynskyi, J. Streuff, M. Nieger, E. C. Escudero-Adán, M. Martínez Belmonte, *Chem. Commun.* **2011**, *47*, 4911–4913; d) N. Nebra, N. Saffon, L. Maron, B. Martin-Vaca, D. Bourissou, *Inorg. Chem.* **2011**, *50*, 6378–6383; e) N. Nebra, J. Lisena, N. Saffon, L. Maron, B. Martin-Vaca, D. Bourissou, *Dalton Trans.* **2011**, *40*, 8912–8921; f) N. Tsoureas, Y.-Y. Kuo, M. F. Haddow, G. R. Owen, *Chem. Commun.* **2011**, *46*, 484–486; g) P. Oulie, N. Nebra, N. Saffon, L. Maron, B. Martin-Vaca, D. Bourissou, *J. Am. Chem. Soc.* **2009**, *131*, 3493–3498.

[42] J. Zhang, M. Gandelman, D. Herrman, G. Leitus, L. J. W. Shimon, Y. Ben-David, D. Milstein, *Inorg. Chim. Acta* **2006**, *359*, 1955–1960.

[43] E. M. Pelczar, T. J. Emge, K. Krogh-Jespersen, A. S. Goldman, *Organometallics* **2008**, *27*, 5759–5767.

[44] R. J. Trovitch, E. Lobkovsky, P. J. Chirik, *Inorg. Chem.* **2006**, *45*, 7252–7260.

[45] a) R. Langer, G. Leitkus, Y. Ben-David, D. Milstein, *Angew. Chem. Int. Ed.* **2011**, *50*, 2120–2124; comprehensive highlight: b) G. Bauer, K. A. Kirchner, *Angew. Chem. Int. Ed.* **2011**, *50*, 5798–5800.

[46] R. M. Bullock, *Catalysis without Precious Metals*, Wiley-VCH, Weinheim, Germany, **2010**. See also: a) B. D. Sherry, A. Fürstner, *Acc. Chem. Res.* **2008**, *41*, 1500–1511; b) B. Plietker, *Iron Catalysis in Organic Synthesis; Reactions and Applications*, **2008**, Wiley-VCH; c) A. A. O. Sarhan, C. Bolm, *Chem. Soc. Rev.* **2009**, *38*, 2730–2744.

[47] a) J. I. van der Vlugt, M. Lutz, E. A. Pidko, D. Vogt, A. L. Spek, *Dalton Trans.* **2009**, 1016–1023; b) M. Lutz, J. I. van der Vlugt, D. Vogt, A. L. Spek, *Polyhedron* **2009**, *28*, 2341–2346.

[48] J. I. van der Vlugt, E. A. Pidko, D. Vogt, M. Lutz, A. L. Spek, A. Meetsma, *Inorg. Chem.* **2008**, *47*, 4442–4444.

[49] J. I. van der Vlugt, E. A. Pidko, D. Vogt, M. Lutz, A. L. Spek, *Inorg. Chem.* **2009**, *48*, 7513–7515.

[50] J. I. van der Vlugt, E. A. Pidko, R. C. Bauer, Y. Gloaguen, M. K. Rong, M. Lutz, *Chem. Eur. J.* **2011**, *17*, 3850–3854.

[51] S. Y. de Boer, Y. Gloaguen, M. Lutz, J. I. van der Vlugt, *Inorg. Chim. Acta* **2011**; DOI: 10.1016/j.ica.2011.10.037.

 © 2012 Wiley-VCH Verlag GmbH & Co. KGaA, Weinheim

[52] The classic Shvo-catalyst is another landmark example of cooperative catalysis with Ru, see ref. [14] and: a) Y. Shvo, D. Czarkie, Y. Rahamim, D. F. Chodosh, *J. Am. Chem. Soc.* **1986**, *108*, 7400–7402; b) B. L. Conley, M. K. Pennington-Boggio, E. Boz, T. J. Williams, *Chem. Rev.* **2010**, *110*, 2294–2312; c) T. C. Johnson, G. H. Clarkson, M. Wills, *Organometallics* **2011**, *30*, 1859–1868; d) H. Zhang, D. Chen, Y. Zhang, G. Zhang, J. Liu, *Dalton Trans.* **2010**, *39*, 1972–1978.

[53] a) U. J. Kilgore, J. A. S. Roberts, D. H. Pool, A. M. Appel, M. P. Stewart, M. Rakowski DuBois, W. G. Dougherty, W. S. Kassel, R. M. Bullock, D. L. DuBois, *J. Am. Chem. Soc.* **2011**, *133*, 5861–5872; b) D. L. DuBois, R. M. Bullock, *Eur. J. Inorg. Chem.* **2011**, 1017–1027; c) M. Rakowski DuBois, D. L. DuBois, in: *Catalysis without Precious Metals* (Ed.: R. M. Bullock), Wiley-VCH, Weinheim, Germany, **2010**, p. 165–180; d) E. S. Wiedner, J. Y. Yang, W. G. Dougherty, W. S. Kassel, R. M. Bullock, M. Rakowski DuBois, D. L. DuBois, *Organometallics* **2010**, *29*, 5390–5401; e) M. Rakowski DuBois, D. L. DuBois, *Acc. Chem. Res.* **2009**, *42*, 1974–1982; f) M. Rakowski DuBois, D. L. DuBois, *Chem. Soc. Rev.* **2009**, *38*, 62–72; g) G. M. Jacobsen, J. Y. Yang, B. Twamley, A. D. Wilson, R. M. Bullock, M. Rakowski DuBois, D. L. DuBois, *Energy Environ. Sci.* **2008**, *1*, 167–174; h) M. Rakowski DuBois, D. L. DuBois, *C. R. Chim.* **2008**, *11*, 805–817.

[54] A. Le Goff, V. Artero, B. Jousselme, P. D. Tran, N. Guillet, R. Métayé, A. Fihri, S. Palacin, M. Fontecave, *Science* **2009**, *326*, 1384–1387.

[55] P. D. Tran, A. Le Goff, J. Heidkamp, B. Jousselme, N. Guillet, S. Palacin, H. Dau, M. Fontecave, V. Artero, *Angew. Chem. Int. Ed.* **2011**, *50*, 1371–1374.

[56] M. P. McLaughlin, T. M. McCormick, R. Eisenberg, P. L. Holland, *Chem. Commun.* **2011**, *47*, 7989–7991.

[57] a) S. Ezzaher, J.-F. Capon, F. Gloaguen, F. Pétillon, P. Schollhammer, J. Talarmin, N. Kervarec, *Inorg. Chem.* **2009**, *48*, 2–4; see also: b) N. Wang, M. Wang, T. Zhang, P. Li, J. Liua, L. Sun, *Chem. Commun.* **2008**, 5800–5802; c) N. Wang, M. Wang, T. Zhang, P. Li, J. Liua, L. Sun, *Inorg. Chem.* **2009**, *48*, 11551–11558.

[58] S. Kaur-Ghumaan, L. Schwartz, R. Lomoth, M. Stein, S. Ott, *Angew. Chem. Int. Ed.* **2010**, *49*, 8033–8036.

[59] R. D. Adams, F. A. Cotton, *Catalysis by Di- and Polynuclear Metal Cluster Complexes*, Wiley-VCH, New York, **1998**.

[60] For a recent review, see: M. R. Kember, A. Buchard, C. K. Williams, *Chem. Commun.* **2011**, *47*, 141–163. See also: M. Cheng, E. B. Lobkovsky, G. W. Coates, *J. Am. Chem. Soc.* **1998**, *120*, 11018–11019.

[61] a) R. G. Konsler, J. Karl, E. N. Jacobsen, *J. Am. Chem. Soc.* **1998**, *120*, 10780–10781; b) R. Breinbauer, E. N. Jacobsen, *Angew. Chem. Int. Ed.* **2000**, *39*, 3640–3607.

[62] a) R. M. Haak, S. J. Wezenberg, A. W. Kleij, *Chem. Commun.* **2010**, *46*, 2713–2723; b) R. M. Haak, M. Martínez Belmonte, E. C. Escudero-Adán, J. Benet-Buchholz, A. W. Kleij, *Dalton Trans.* **2010**, *39*, 593–602.

[63] a) H. C. Kolb, M. G. Finn, K. B. Sharpless, *Angew. Chem.* **2001**, *113*, 2056; *Angew. Chem. Int. Ed.* **2001**, *40*, 2004–2021; b) M. Meldal, C. W. Tornøe, *Chem. Rev.* **2008**, *108*, 2952–3015; c) J. E. Hein, V. V. Fokin, *Chem. Soc. Rev.* **2010**, *39*, 1302–1315; d) L. Liang, D. Astruc, *Coord. Chem. Rev.* **2011**, DOI:10.1016/j.ccr.2011.06.028.

[64] B. A. Rodriguez, M. Delferro, T. J. Marks, *J. Am. Chem. Soc.* **2009**, *131*, 5902–5919.

[65] For a general review, see: J. Klingele, S. Dechert, F. Meyer, *Coord. Chem. Rev.* **2009**, *253*, 2698–2741. For specific examples for Ni, see: a) T. Graef, J. Galezowska, S. Dechert, F. Meyer, *Eur. J. Inorg. Chem.* **2011**, 4161–4167; b) A. Sachse, S. Demeshko, S. Dechert, V. Daebel, A. Lange, F. Meyer, *Dalton Trans.* **2010**, *39*, 3903–3914; c) S. V. Kryatov, E. V. Rybak-Akimova, F. Meyer, H. Pritzkow, *Eur. J. Inorg. Chem.* **2003**, 1581–1590.

[66] a) M. Jarenmark, E. Csapó, J. Singh, S. Wöckel, E. Farkas, F. Meyer, M. Haukka, E. Nordlander, *Dalton Trans.* **2010**, *39*, 8183–8194; b) M. Jarenmark, M. Haukka, S. Demeshko, F. Tuczek, L. Zuppiroli, F. Meyer, E. Nordlander, *Inorg. Chem.* **2011**, *50*, 3866–3887; c) L. V. Penkova, A. Maciag, E. V. Rybak-Akimova, M. Haukka, V. A. Pavlenko, T. S. Iskenderov, H. Kozlowski, F. Meyer, I. O. Fritzky, *Inorg. Chem.* **2009**, *48*, 6960–6971; d) B. Bauer-Siebenlist, S. Dechert, F. Meyer, *Chem. Eur. J.* **2005**, *11*, 5343–5352; e) B. Bauer-Siebenlist, F. Meyer, E. Farkas, D. Vidovic, S. Dechert, F. Meyer, *Chem. Eur. J.* **2005**, *11*, 4349–4360; f) B. Bauer-Siebenlist, F. Meyer, E. Farkas, D. Vidovic, J. A. C. Seijo, R. Herbst-Irmer, H. Pritzkow, *Inorg. Chem.* **2004**, *43*, 4189–4202.

[67] a) A. Prokofieva, S. Dechert, C. Grosse, G. M. Sheldrick, F. Meyer, *Chem. Eur. J.* **2009**, *15*, 4994–4997; b) A. Prokofieva, A. I. Prikhod'ko, S. Dechert, F. Meyer, *Chem. Commun.* **2008**, 1005–1007; c) J. Ackermann, S. Buchler, F. Meyer, *C. R. Chim.* **2007**, *10*, 421–432; d) J. Ackermann, F. Meyer, E. Kaifer, H. Pritzkow, *Chem. Eur. J.* **2002**, *8*, 247–258.

[68] For other Cu-systems with dinucleating pyrazolate ligands, see: a) M. Stollenz, H. Gehring, V. Konstanzer, S. Fischer, S. Dechert, C. Grosse, F. Meyer, *Organometallics* **2011**, *31*, 3708–3725; b) A. K. Singh, J. I. van der Vlugt, S. Demeshko, S. Dechert, F. Meyer, *Eur. J. Inorg. Chem.* **2009**, 3431–3439; c) J. I. van der Vlugt, S. Demeshko, S. Dechert, F. Meyer, *Inorg. Chem.* **2008**, *47*, 1576–1585; d) M. Stollenz, C. Grosse, F. Meyer, *Chem. Commun.* **2008**, 1744–1746.

[69] C. M. Fafard, D. Adhikari, B. M. Foxman, D. J. Mindiola, O. V. Ozerov, *J. Am. Chem. Soc.* **2007**, *129*, 10318–10319.

[70] a) S. B. Harkins, J. C. Peters, *J. Am. Chem. Soc.* **2004**, *126*, 2885–2893; b) S. B. Harkins, J. C. Peters, *J. Am. Chem. Soc.* **2005**, *127*, 2030–2031; c) N. P. Mankad, E. Rivard, S. B. Harkins, J. C. Peters, *J. Am. Chem. Soc.* **2005**, *127*, 16032–16033; d) S. B. Harkins, N. P. Mankad, A. J. M. Miller, R. K. Szilagyi, J. C. Peters, *J. Am. Chem. Soc.* **2008**, *130*, 3478–3485; e) J. C. Deaton, S. C. Switalski, D. Y. Kondakov, R. H. Young, T. D. Pawlik, D. J. Giesen, S. B. Harkins, A. J. M. Miller, S. F. Mickenberg, J. C. Peters, *J. Am. Chem. Soc.* **2010**, *132*, 9499–9508.

[71] For other applications of this PPP-scaffold with second- and third-row metals, see: a) M. Mazzeo, M. Lamberti, A. Massa, A. Scettri, C. Pellecchia, J. C. Peters, *Organometallics* **2008**, *27*, 5741; b) M. Mazzeo, M. Lamberti, I. d'Auria, S. Milione, J. C. Peters, C. Pellecchia, *J. Polym. Sci. Polym. Chem. Ed.* **2010**, *48*, 1374; c) M. Mazzeo, M. Strianese, O. Kühl, J. C. Peters, *Dalton Trans.* **2011**, *40*, 9026–9033.

[72] R. C. Bauer, Y. Gloaguen, M. Lutz, J. N. H. Reek, B. de Bruin, J. I. van der Vlugt, *Dalton Trans.* **2011**, *40*, 8822–8829.

[73] A. R. Fout, F. Bauli, H. Fan, J. Tomaszewski, J. C. Huffman, M.-H. Baik, D. J. Mindiola, *Angew. Chem.* **2006**, *118*, 3369; *Angew. Chem. Int. Ed.* **2006**, *45*, 3291–3295.

[74] a) U. Christmann, R. Vilar, A. J. P. White, D. J. Williams, *Chem. Commun.* **2004**, 1294–1295; b) U. Christmann, D. A. Pantazis, J. Benet-Buchholz, J. E. McGrady, F. Maseras, R. Vilar, *J. Am. Chem. Soc.* **2006**, *128*, 6376–390.

[75] a) A. Velian, S. Lin, A. J. M. Miller, M. W. Day, T. Agapie, *J. Am. Chem. Soc.* **2010**, *132*, 6296–6297; b) S. Lin, M. W. Day, T. Agapie, *J. Am. Chem. Soc.* **2011**, *133*, 3828–3831; c) S. T. Chao, N. C. Lara, S. Lin, M. W. Day, T. Agapie, *Angew. Chem. Int. Ed.* **2011**, *50*, 7529–7532. For related terphenyl-based diphosphanes, see: J. I. van der Vlugt, R. van Duren, G. D. Batema, R. den Heeten, A. Meetsma, J. Fraanje, K. Goubitz, P. C. J. Kamer, P. W. N. M. van Leeuwen, D. Vogt, *Organometallics* **2005**, *24*, 5377–5382.

[76] a) C. A. Laskowski, G. L. Hillhouse, *Chem. Sci.* **2011**, *2*, 321–325; b) R. Beck, S. A. Johnson, *Chem. Commun.* **2011**, *47*, 9233–9235.

[77] For reviews on the use of C_3-symmetric systems in catalysis, see: a) C. Moberg, *Angew. Chem.* **1998**, *110*, 260; *Angew. Chem. Int. Ed.* **1998**, *37*, 248–268; b) S. E. Gibson, M. P. Castaldi, *Chem. Commun.* **2006**, 3045–3062; see also: c) J. Wassenaar, M. A. Siegler, A. L. Spek, B. de Bruin, J. N. H. Reek, J. I. van der Vlugt, *Inorg. Chem.* **2010**, *49*, 6495–6508; d) M. M. P.

 © 2012 Wiley-VCH Verlag GmbH & Co. KGaA, Weinheim

Grutters, J. I. van der Vlugt, Y. Pei, A. M. Mills, M. Lutz, A. L. Spek, C. Müller, C. Moberg, D. Vogt, *Adv. Synth. Catal.* **2009**, *351*, 2199–2208; e) M. Ciclosi, J. Lloret, F. Estevan, P. Lauerta, M. Sanaú, J. Pérez-Prieto, *Angew. Chem.* **2006**, *118*, 6893; *Angew. Chem. Int. Ed.* **2006**, *45*, 6741–6744; f) G. Ionescu, J. I. van der Vlugt, H. C. L. Abbenhuis, D. Vogt, *Tetrahedron: Asymmetry* **2005**, *16*, 3970–3975; g) J. I. van der Vlugt, M. M. P. Grutters, J. Ackerstaff, R. W. J. M. Hanssen, H. C. L. Abbenhuis, D. Vogt, *Tetrahedron Lett.* **2003**, *44*, 8301–8305.

[78] a) Q. Zhao, T. A. Betley, *Angew. Chem. Int. Ed.* **2011**, *50*, 709–712; b) T. M. Powers, A. R. Fout, S.-L. Zheng, T. A. Betley, *J. Am. Chem. Soc.* **2011**, *133*, 3336–3338; c) Q. Zhao, T. D. Harris, T. A. Betley, *J. Am. Chem. Soc.* **2011**, *133*, 8293–8306; d) T. D. Harris, T. A. Betley, *J. Am. Chem. Soc.* **2011**, *133*, doi: 10.1021/ja2052655.

[79] This approach of mimicking heterogeneous catalysts using homogeneous model systems is reminiscent of the modeling of silica surfaces using silsesquioxane frameworks, see: a) R. Duchateau, *Chem. Rev.* **2002**, *102*, 3525–3542; b) J. R. Severn, J. C. Chadwick, R. Duchateau, N. Friederichs, *Chem. Rev.* **2005**, *105*, 4073–4147; see also: c) J. I. van der Vlugt, J. Ackerstaff, T. W. Dijkstra, A. M. Mills, H. Kooijman, A. L. Spek, A. Meetsma, H. C. L. Abbenhuis, D. Vogt, *Adv. Synth. Catal.* **2004**, *346*, 399–412; d) J. I. van der Vlugt, M. Fioroni, J. Ackerstaff, R. W. J. M. Hanssen, A. M. Mills, A. L. Spek, A. Meetsma, H. C. L. Abbenhuis, D. Vogt, *Organometallics* **2003**, *22*, 5297–5306; e) H. C. L. Abbenhuis, *Chem. Eur. J.* **2000**, *6*, 25–32.

[80] a) E. Y. Tsui, M. W. Day, T. Agapie, *Angew. Chem. Int. Ed.* **2011**, *50*, 1668–1672; b) E. Y. Tsui, J. S. Kanady, M. W. Day, T. Agapie, *Chem. Commun.* **2011**, *47*, 4189–4191. See also: J. S. Kanady, E. Y. Tsui, M. W. Day, T. Agapie, *Science* **2011**, *333*, 733–736.

[81] R. Angamuthu, P. Byers, M. Lutz, A. L. Spek, E. Bouwman, *Science* **2010**, *327*, 313–315.

[82] J. C. Jeffrey, T. B. Rauchfuss, *Inorg. Chem.* **1979**, *18*, 2658. This paper described the first hemilabile coordination of (*o*-diphenylphosphanyl)anisole. For related bisphosphanes with this motif, see: a) J. I. van der Vlugt, J. M. Bonet, A. M. Mills, A. L. Spek, D. Vogt, *Tetrahedron Lett.* **2003**, *44*, 4389–4392; b) J. I. van der Vlugt, M. M. P. Grutters, A. M. Mills, H. Kooijman, A. L. Spek, D. Vogt, *Eur. J. Inorg. Chem.* **2003**, 4361–4369.

[83] a) P. Braunstein, F. Naud, *Angew. Chem.* **2001**, *113*, 702; *Angew. Chem. Int. Ed.* **2001**, *40*, 680–699; b) P. Braunstein, *J. Organomet. Chem.* **2004**, *689*, 3953–3967; c) C. S. Slone, D. A. Weinberger, C. A. Mirkin, *Prog. Inorg. Chem.* **1999**, *48*, 233; d) G. W. Parshall, S. D. Ittel, in: *Homogeneous Catalysis: The Applications and Chemistry of Catalysis by Soluble Transition Metal Complexes*, 2nd ed., Wiley-Interscience, New York, **1992**, pp. 70; e) W. Keim, *Angew. Chem.* **1990**, *102*, 251; *Angew. Chem. Int. Ed. Engl.* **1990**, *29*, 235–244.

[84] a) M. J. Wiester, P. A. Ulmann, C. A. Mirkin, *Angew. Chem. Int. Ed.* **2011**, *50*, 114–137; b) H. Jae Yoon, C. A. Mirkin, *J. Am. Chem. Soc.* **2008**, *130*, 11590–11591; c) C. G. Oliveri, P. I. A. Ulmann, M. J. Wiester, C. A. Mirkin, *Acc. Chem. Res.* **2008**, *41*, 1618–1629; d) H. J. Yoon, J. Heo, C. A. Mirkin, *J. Am. Chem. Soc.* **2007**, *129*, 14182–14183; e) M. S. Masar III, N. C. Gianneschi, C. G. Oliveri, C. L. Stern, S. T. Nguyen, C. A. Mirkin, *J. Am. Chem. Soc.* **2007**, *129*, 10149–10158.

[85] H. J. Yoon, J. Kuwabara, J.-H. Kim, C. A. Mirkin, *Science* **2010**, *330*, 66–69.

[86] C. Gunanathan, D. Milstein, *Acc. Chem. Res.* **2011**, *44*, 588–602.

[87] R. Lindner, B. van den Bosch, M. Lutz, J. N. H. Reek, J. I. van der Vlugt, *Organometallics* **2011**, *30*, 499–510. For related examples of such hybrid PNN-ligands (but without studies on their hemilabile character), see: a) N. G. Leonard, P. G. Williard, W. H. Bernskoetter, *Dalton Trans.* **2011**, *40*, 4300–4306; b) A. Choualeb, A. J. Lough, D. G. Gusev, *Organometallics* **2007**, *26*, 5224–5229; c) W.-Y. Lee, L.-C. Liang, *Dalton Trans.* **2005**, 1952–1956.

[88] a) J. I. van der Vlugt, J. N. H. Reek, in: *Phosphorus Ligands: Design and Synthesis* (Eds.: P. C. J. Kamer, P. W. N. M. van Leeuwen), Wiley-VCH, Weinheim, Germany, **2011**, in press; b) F. W. Patureau, S. de Boer, P.-A. R. Breuil, J. Meeuwissen, M. A. Siegler, A. L. Spek, A. J. Sandee, B. de Bruin, J. N. H. Reek, *J. Am. Chem. Soc.* **2009**, *131*, 6683–6685.

[89] General reviews introducing the area: a) W. Seiche, B. Breit, in: *Phosphorus Ligands in Asymmetric Catalysis* (Ed.: A. Börner), Wiley-VCH, Weinheim, Germany, **2008**, p. 1379–1404; b) B. Breit, in: *Supramolecular Catalysis* (Ed.: P. W. N. M. van Leeuwen), Wiley-VCH, Weinheim, Germany, **2008**, p. 29–56; c) J. N. H. Reek, in: *Supramolecular Catalysis* (Ed.: P. W. N. M. van Leeuwen), Wiley-VCH, Weinheim, Germany, **2008**, p. 199–234.

[90] a) A. S. Borovik, *Chem. Soc. Rev.* **2011**, *40*, 1870–1874; b) R. L. Shook, A. S. Borovik, *Chem. Commun.* **2008**, 6095–6107; c) R. L. Shook, S. M. Peterson, J. Greaves, C. Moore, A. L. Rheingold, A. S. Borovik, *J. Am. Chem. Soc.* **2011**, *133*, 5810–5817.

[91] M. de Greef, B. Breit, *Angew. Chem.* **2009**, *121*, 559; *Angew. Chem. Int. Ed.* **2009**, *48*, 551–554.

[92] J. Meeuwissen, J. N. H. Reek, *Nature Chem.* **2010**, *2*, 615–621.

[93] S. Das, C. D. Incarvito, R. H. Crabtree, G. W. Brudvig, *Science* **2006**, *312*, 1941–1943.

[94] a) J.-W. Park, J.-H. Park, C.-H. Jun, *J. Org. Chem.* **2008**, *73*, 5598–5601; b) J.-H. Park, J.-W. Park, C.-H. Jun, *Acc. Chem. Res.* **2008**, *41*, 222–234.

[95] a) N. R. Vautravers, D. D. Regent, B. Breit, *Chem. Commun.* **2011**, *47*, 6635–6637; b) T. Šmejkal, D. Gribkov, J. Geier, M. Keller, B. Breit, *Chem. Eur. J.* **2010**, *16*, 2470–2478; c) L. Diab, T. Šmejkal, J. Geier, B. Breit, *Angew. Chem.* **2009**, *121*, 8166; *Angew. Chem. Int. Ed.* **2009**, *48*, 8022–8026.

[96] P.-A. R. Breuil, F. W. Patureau, J. N. H. Reek, *Angew. Chem.* **2009**, *121*, 2196; *Angew. Chem. Int. Ed.* **2009**, *48*, 2162–2165.

[97] P. Dydio, W. I. Dzik, M. Lutz, B. de Bruin, J. N. H. Reek, *Angew. Chem. Int. Ed.* **2011**, *50*, 396–400.

[98] NH_3: a) J. I. van der Vlugt, *Chem. Soc. Rev.* **2010**, *39*, 2302–2322; b) J. L. Klinkenberg, J. F. Hartwig, *Angew. Chem. Int. Ed.* **2011**, *50*, 86–95; c) E. Khaskin, M. A. Iron, L. J. W. Shimon, J. Zhang, D. Milstein, *J. Am. Chem. Soc.* **2010**, *132*, 8542–8543.

[99] H_2: a) M. R. Ringenberg, S. Latha Kokatam, Z. M. Heiden, T. B. Rauchfuss, *J. Am. Chem. Soc.* **2008**, *130*, 788–789; b) W. Cui, B. B. Wayland, *J. Am. Chem. Soc.* **2004**, *126*, 8266–8274; c) J. Wassenaar, B. de Bruin, M. A. Siegler, A. L. Spek, J. N. H. Reek, J. I. van der Vlugt, *Chem. Commun.* **2010**, *46*, 1232–1234.

[100] D. G. H. Hetterscheid, J. I. van der Vlugt, B. de Bruin, J. N. H. Reek, *Angew. Chem.* **2009**, *121*, 8324; *Angew. Chem. Int. Ed.* **2009**, *48*, 8178–818.

Received: July 19, 2011
Published Online: September 29, 2011

 © 2012 Wiley-VCH Verlag GmbH & Co. KGaA, Weinheim

DOI: 10.1002/ejic.201100985

Non-Innocent Ligands: New Opportunities in Iron Catalysis

Sébastien Blanchard,[a] Etienne Derat,[a] Marine Desage-El Murr,*[a] Louis Fensterbank,*[a] Max Malacria,*[a] and Virginie Mouriès-Mansuy[a]

Keywords: Non-innocent ligands (NILs) / Redox chemistry / Iron / Density functional calculations / Low-valent iron complexes

Introduced in the late sixties, non-innocent (or redox) ligands have been extensively studied for their unusual and intriguing chemical behavior. Their ability to delocalize and/or provide electrons to the metal center of organometallic complexes confers them undisputable chemical interest and has proved valuable in the development of novel synthetic methodologies. This review will focus on the chemistry and applications of low-valent iron complexes bearing potentially non-innocent ligands. Because of the elusive nature of these ligands, and whenever possible, theoretical calculations and analysis of spectroscopic data will be presented in an effort to provide insights into the catalytic activity of the complexes.

1. Introduction

From an organic chemist's perspective, a ligand is the cornerstone of a catalytic system and allows for fine-tuning of reactivity and selectivity through steric and/or electronic interactions during the catalytic cycle. However, and although optimization of a catalytic system often requires in-depth and extensive structural modifications, a ligand has so far been a well-characterized closed-shell molecule that performs well-defined tasks, and in this prospect, the less-defined and intriguing electronic structure of non-innocent ligands (NILs) holds promises as to their use in innovative organometallic catalysis.[1]

The "non-innocent" terminology was introduced in 1966 in a seminal work by Jørgensen[2] stating that "ligands are innocent when they allow oxidation states of the central atom to be defined".

Although more a definition of what a NIL is not, this assertion clearly shows that NILs are molecular scaffolds that are able to delocalize part of the electronic density of the complexes to which they belong, becoming – in addition to the metal center – a place where redox processes can also take place. The reasons for this are the higher energy HOMO (or alternatively a low-lying LUMO) levels of these ligands as compared to those of typical ligands, and NILs will therefore participate in electronic transfer through an inverted bonding process.[3] This specificity can broaden the scope of redox events that a metal can perform by overcoming the limitations imparted by its original electronic structure. Since their introduction in the field of inorganic chemistry, redox ligands (or NILs) and complexes thereof have attracted much attention, mainly devoted to the identification, extensive studies, and rationalization of their unusual electronic properties.[4] However, NILs are now emerging as synthetically useful and attractive scaffolds with broad and exciting perspectives as their use could open up the field of reactivity of easily accessible base metals. This microreview will focus on the recent developments of iron complexes bearing such ligands and their application in synthetic methodologies.

[a] Institut Parisien de Chimie Moléculaire (IPCM, UMR CNRS 7201), Université Pierre & Marie Curie (UPMC),
cc 229, 4, place Jussieu, 75252 Paris Cedex 05, France
Fax: +33-1-44277360
E-mail: marine.desage-el_murr@upmc.fr
louis.fensterbank@upmc.fr
max.malacria@upmc.fr

Supporting information for this article is available on the WWW under http://dx.doi.org/10.1002/ejic.201100985.

2. Context and Limitations

Noble metals such as palladium, rhodium, and platinum – to name but a few – occupy a prominent position in numerous synthetic methodologies and industrial processes.[5] Their landmark is to engage in well-defined two-electron redox reactions, while typical base metals (Fe, Cu) will favor one-electron redox changes that might result in uncontrolled reactivities and less stable catalytic intermediates. However, noble metals are mostly not abundant on the earth, neither are they cheap, and they can generate toxic waste, even though in moderate amounts. They also tend to become scarcer and sometimes are the hostages of problematic geopolitical contexts. Recently, the search for more cost-effective alternatives and increasingly compelling environmental issues have triggered a trend to reinvestigate the use of both cheaper and more environmentally benign metals, among which iron is one of the most popular.

While iron is one of the very metals that operate in Nature's catalysts (metalloenzymes), iron catalysis is still in its early days relative to its well-established noble metal cousins. The classical chemistry of iron has long been associated

© 2012 Wiley-VCH Verlag GmbH & Co. KGaA, Weinheim

with the belief that this metal was not as versatile and unable to perform as well as noble metals in terms of catalytic applications, and its applications were mainly confined to its use as a Lewis acid or stoichiometric reagent. Fortunately, the last two decades have proved this assumption wrong, as the field of iron catalysis has witnessed exciting developments.[6] The well-documented reactivity of iron and complexes thereof is nevertheless inherently limited in terms of catalytic processes, because of the electronic structure of iron, which favors one-electron redox changes over two-electron redox processes. The latter must be favored over the former if chemists are to develop the use of iron com-

Sébastien Blanchard received his Ph.D. in Inorganic Chemistry in 2002 from the Université Paris XI in Orsay, working on Artificial Photosynthesis with Prof. J.-J. Girerd and Dr. G. Blondin. He then spent almost two years in Prof. K. Wieghardt's group at the MPI fuer Bioanorganische Chemie in Muelheim an der Ruhr. After a brief stint in the Life Science department of the CEA in Saclay, he became as an Assistant Professor in 2005 at the Université Pierre & Marie Curie in the polyoxometalate team of IPCM.

Etienne Derat studied chemistry in Reims (Champagne-Ardennes), followed by a Ph.D. at the same university under the direction of Prof. Stéphane Humbel, working on theoretical organometallic chemistry. In 2004, he started postdoctoral research with Prof. Sason Shaik in Jerusalem on QM/MM and metalloenzymes. In 2006, he became Assistant Professor in the group of Prof. Max Malacria (IPCM-UPMC). In February 2011, he was invited professor at the University of Tokyo.

Marine Desage-El Murr was born in Paris and grew up in Nantes. In 2000, she graduated from the Ecole Supérieure de Chimie Physique et Electronique de Lyon (CPE Lyon), while spending her third year at the Ecole Nationale Supérieure de Chimie de Paris (ENSCP). She went on to work under the supervision of Dr. Charles Mioskowski at the Commissariat à l'Energie Atomique (CEA Saclay) and obtained her Ph.D. in 2003. Then, she joined the group of Profs. R. J. Griffin and B. T. Golding at the University of Newcastle-upon-Tyne (UK), as a post-doctoral research associate. Since 2007, she is Assistant Professor in Prof. Max Malacria's team at the Institut Parisien de Chimie Moléculaire (IPCM) of the Université Pierre & Marie Curie (UPMC). Her research interests encompass new synthetic methodologies, natural products, and organometallic catalysis.

Louis Fensterbank was born in Poitiers in 1967 and was raised in Tours. After graduating from the Ecole Supérieure de Chimie Industrielle de Lyon (ESCIL) in 1990, he joined the team of Scott Sieburth at SUNY Stony Brook, worked on silicon-tethered reactions, and obtained his Ph.D. in 1993. After a temporary lecturer position at the Université Pierre & Marie Curie (UPMC) in 1994, he was appointed by the CNRS in 1995 as a Chargé de Recherche in Max Malacria's team. In 2004, he obtained a professorship at UPMC, and in 2008 he was nominated junior member at the Institut Universitaire de France. In 2009, he was a visiting scientist at the Australian National University (Canberra, Australia). His research interests concern the discovery of new molecular transformations relying on radical or organometallic processes and their applications to the synthesis of substrates with relevant properties (natural products, probes, ligands, and so on).

Max Malacria was born in 1949 in Marseille, France. He obtained his Ph.D. from the University of Aix-Marseille III with Prof. Marcel Bertrand in 1974. He was appointed Assistant in 1974 at the University of Lyon I with Prof. J. Goré. After almost two years as a postdoctoral fellow with Prof. K. P. C. Vollhardt at Berkeley, he went back to the University of Lyon as Assistant Professor in 1983. In 1988, he was appointed Full Professor at the UPMC. In 1991, he was elected junior member of the Institut Universitaire de France and promoted to senior member in 2001. His research interests include the development of new domino processes in both organometallic and radical chemistry and applications in synthesis, asymmetric synthesis, new stereoselective reactions involving heteroelements, and developing physical chemistry interfaces. His work was rewarded with the prize of the Organic Chemistry Division of the French Chemical Society (1997), the Grammaticakis-Neuman prize from the French Academy of Sciences (2000), médaille d'argent du CNRS (2001), and recently, the Franco-Spanish Catalan-Sabatier prize from the Real Sociedad Española de Química (2009).

Virginie Mouriès-Mansuy was born in Toulon (France) in 1970. She graduated from the Université Pierre & Marie Curie (UPMC) and obtained her Ph.D. at the Ecole Polytechnique in 1998 under the supervision of Prof. F. Mathey. Her Ph.D. focused on the synthesis of chiral diphosphanes and their application in asymmetric catalysis. After a postdoctoral position at the Université René Descartes and a temporary lecturer position at the UPMC, she obtained an Assistant Professor position in 2002 in Prof. Lhommet's team (IPCM-UPMC), working on the total synthesis of alkaloids. In 2010, she joined Prof. Louis Fensterbank's group (IPCM-UPMC), where she works in the field of organometallic catalysis and on the design of new ligands for asymmetric synthesis.

 © 2012 Wiley-VCH Verlag GmbH & Co. KGaA, Weinheim

plexes as mimics of noble metals and provide new synthetic methods by expanding their chemistry. As a matter of fact, recent developments regarding low-valent iron complexes have drawn attention from the community of synthetic chemists,[7] and specifically the synthetic applications of low-valent iron complexes bearing non-innocent ligands appear promising.[1]

The challenge facing this development is double, as both iron complexes and redox ligands are usually associated with mechanisms that are unclear at best and unknown mostly. While tuning the electronic structure of metal complexes by playing with ligand properties is a classical tool to adjust reactivity, the unusual electronic effects exerted by the redox ligands on the metal center make a full understanding of the catalytic cycle difficult and require thorough and detailed spectroscopic studies coupled with DFT calculations.

Classically, slight electronic or steric modifications on the ligands are expected to alter the electronic properties of the metal center where the catalysis happens. However, in the context of this review, a far more fundamental question arises: where do the electrons reside? This is a critical issue, as the global electronic structure of the entire organometallic complex including the ligands can actually participate by receiving and/or supplying electrons at various stages of the catalytic cycle, as clearly evidenced in the case of bis(imino)pyridine–iron complexes (see the following sections).[8] It is thus of paramount interest to be able to unravel the actual site of reduction (or oxidation, accordingly) in the catalytic species. In order to do so, several groups[9] showed that a careful combination of spectroscopic, electrochemical, and when available, X-ray diffraction studies, in conjunction with theoretical calculations, allows for the determination of the actual (or spectroscopic as sometimes coined) oxidation state of both the metal center and the ligands.

This microreview aims at presenting the recent developments and applications of catalytic systems containing NILs in the field of iron catalysis and is divided into two sections. Formation of carbon–carbon bonds will first be presented, followed by creation of carbon–heteroatom bonds.

3. C–C Bond Formation

3.1. Polymerization

Inspired by previous Pd^{II} and Ni^{II} α-diimine polymerization catalysts, Brookhart[10] and Gibson[11] introduced in 1998 the 2,6-bis(imino)pyridyl ligands (or PDI: Pyridine Di-Imine), in which the imine moieties are bulky *ortho*-substituted aryl imines.[12] These ligands are easily obtained from the Schiff base condensation of two equivalents of the desired aniline with 2,6-diacetylpyridine (Scheme 1).

A variety of coordination complexes with various transition metals have been prepared.[13,14] They rapidly elicited great excitement about their structure and electronic properties.[15] Some of them proved to be very robust and active

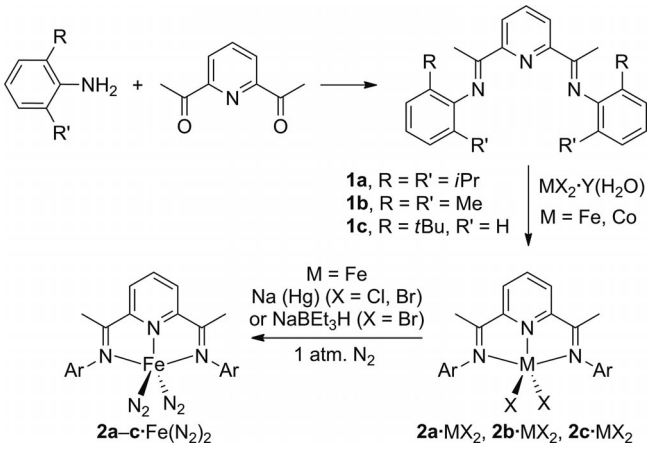

Scheme 1. Synthetic preparation of the bis(imino)pyridine iron complexes. **1a** = *i*PrPDI.

catalysts – especially the iron complexes – for the polymerization of ethylene to linear, high-density polyethylene, and they could improve the performances obtained from the metallocene-based catalysts.[16,17,18] The parameter crucial to the production of high-molecular-weight polymers is the presence of highly bulky aryl substituents (Ar = 2,6-$C_6H_3Me_2$, or 2,6-$C_6H_3iPr_2$), which presumably retards the rate of chain transfer. Iron complexes with bis(imino)pyridine ligands bearing only one *ortho* substituent on the aryl ring in the presence of MMAO (a modified methylaluminoxane activator) proved to be excellent catalysts of oligomerization of ethylene into linear α-olefins.[19] Significant advances on related systems affording various applications then followed, and they have been reviewed.[13,14]

Following these seminal works, Chirik developed a new family of complexes (Scheme 2) based on the alkylation of **2a**·$FeCl_2$ with 2 equiv. of $LiCH_2SiMe_3$ to give complex **3**.[20] The latter was then treated with $[PhMe_2NH][BPh_4]$ to produce new complexes **4a** or **4b** – depending on the solvent – and with $B(C_6F_5)_3$ to give complex **5**. Among these three complexes, **5** proved to be more active and produced olefin end groups containing polymers with higher molecular weight (MW) and narrower polydispersity than with MAO-activated catalysts, which is consistent with chain termination by β-H elimination. Interestingly, Gambarotta and Budzelaar reexamined the alkylation of **2a**·$FeCl_2$ with $LiCH_2SiMe_3$, provided evidence for the formation of side products **6**–**9**,[21,22] and rationalized their formation. Thus, **6** and **7** presumably originate from a homolytic addition of the R moiety. It was also observed that **6** could transform into **3** in ether at room temperature. They showed that all the resulting species **3** and **6**–**9** exhibited high catalytic activity for olefin polymerization with MAO activation, the nature of the formed polymer depending on the oxidation state of the metal center.

In 2010, Chirik[8b] enlarged the family of bis(imino)-pyridine iron alkyl complexes that can behave as single-component ethylene polymerization catalysts.

It is generally admitted that the "Brookhart" catalyst involved in polymerization is an iron(II) ion complexed by a

 © 2012 Wiley-VCH Verlag GmbH & Co. KGaA, Weinheim

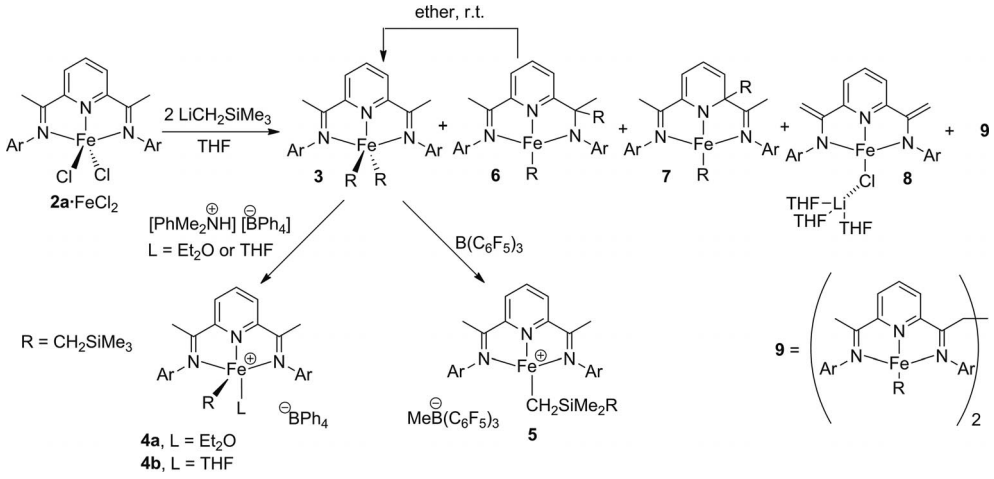

Scheme 2. Bis(imino)pyridine complexes for olefin polymerization.

bis(imino)pyridine ligand bearing an alkyl chain (at least a methyl group). It has been suggested in some reports[23] that an iron(III) ion can also be an effective catalyst. But even if an iron(III) catalyst seems to be more effective during the propagation steps according to DFT-calculated barriers [10.8 kcal/mol for iron(III) vs. 14.2 kcal/mol for iron(II)],[23a] the termination/propagation ratio and experimental polymer MW favor an iron(II) catalyst.

Our own DFT calculations[24] show that the fundamental spin state for the iron alkyl monocation is indeed a quintet corresponding to a high-spin iron(II) coordinated by an innocent ligand.[8b] However, we have calculated a low-lying triplet excited state 4.27 kcal/mol above the quintet ground state (see Supporting Information for details on DFT methodology used). These results differ from previously reported ones[25] but are in agreement with the most recent and elaborate calculations.[23a,26] These discrepancies arise from the diversity of theoretical treatments for iron catalysts, where multiple spin states are involved. In this triplet state, it appears very clearly (Scheme 3) that an unpaired electron is delocalized on the bis(imino)pyridine ligand, and one can find three unpaired electrons with α spin localized in d orbitals on iron, according to Mulliken analysis. Since the molecular spin state is a triplet, one unpaired electron with β spin must be present, and is indeed, but localized on the ligand. Participation of this low-lying spin state with a non-innocent character in the catalysis cannot be excluded.

As stated in Scheme 3, the polymerization mechanism proceeds through ethylene binding on iron, followed by insertion of the ethylene fragment into the Fe–C bond. The DFT barriers found for this step in different studies[25] are rather small and between 7 and 14 kcal/mol. For the termination process, two mechanisms can be found in the literature, one involving a β-hydrogen elimination and another involving a hydrogen atom transfer between the alkyl chain and ethylene. The β-hydrogen elimination process is

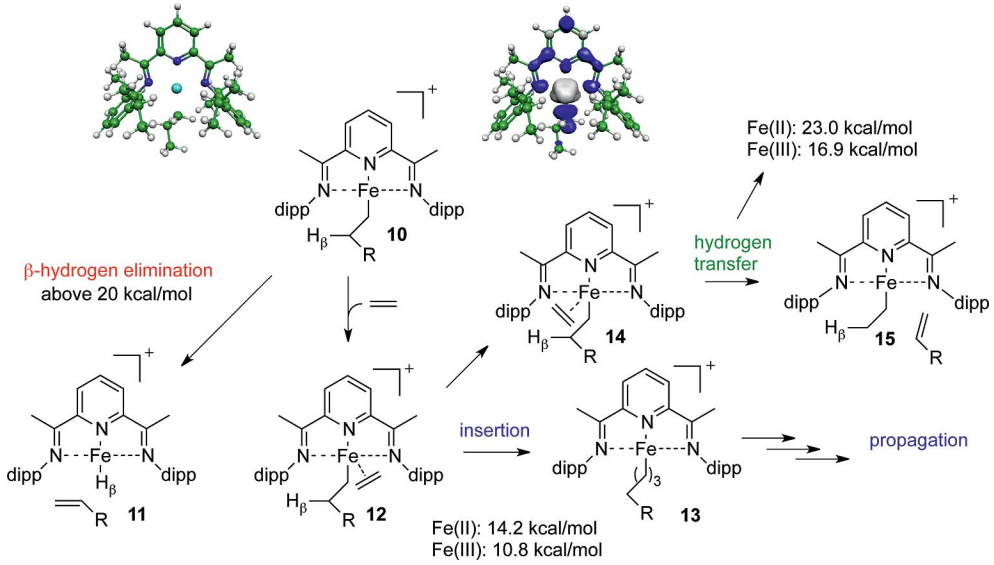

Scheme 3. Proposed mechanisms for polymerization with a bis(imino)pyridine catalyst. The DFT [UB3LYP/SV(P), triplet state] structure and corresponding spin density are given for the starting point with R = Me. (dipp = 2,6-diisopropylphenyl).

 © 2012 Wiley-VCH Verlag GmbH & Co. KGaA, Weinheim

clearly disfavored, as the formation of a hydrido–iron complex is not thermodynamically favored. For the mechanism of hydrogen transfer, the barriers found[26] are usually 4–5 kcal/mol higher in energy than those for the corresponding insertion, thus explaining correctly the experimental MW distribution. Recently, it has been shown that experimental product distribution can be rationalized by theoretical methods, by using a Fe^{III} model with a quartet spin configuration.[27] In that contribution, by computing the gap between the activation energies of insertion and hydrogen transfer, a linear relationship with the logarithm of a coefficient (named Schulz–Flory) describing the experimental ratio of polymerization was found. It should be noted that this research area is still very active, because it represents a challenge for computational chemistry: large systems, steric effects,[28] open-shell wavefunctions, and the influence of counterions like MAO.[8b]

As mentioned earlier, establishing the real electronic structure necessitates a combination of spectroscopic and theoretical methods, in conjunction with high-quality X-ray structure determinations. The case of bis(imino)pyridine complexes has been studied in depth experimentally. Intrigued by the unusual reactivity of the reduced forms of cobalt, iron, or ruthenium complexes of these ligands described by the groups of Brookhart and Vrieze,[29] Wieghardt et al. studied in 2000 a series of $[M\{bis(imino)pyridine\}]^{2+}$ complexes (M = Co, Mn, Ni, Cu, Fe) and their mono- or direduced forms.[30] In the dicationic iron complex, X-ray diffraction studies clearly showed that the ligands were in a neutral form and therefore the cation truly Fe^{II}. Cyclic voltammetry of this complex displays two one-electron reversible waves in reduction. Thus, spectroscopic characterizations of the electrogenerated mono- and direduced species have been performed, which clearly indicated ligand-centered first and second reduction. Among the different hints that point toward this direction, one can highlight the following: the iron complex reduction wave potentials are the same as those of the Zn analogue, where the reduction can only be ligand-centered; the electrochemically reduced $[Fe\{bis(imino)pyridine\}]^{+}$ displays an EPR spectrum with g close to the free-electron value of 2 and low anisotropy (g_x = 1.996, g_y = 1.975, g_z = 1.961), characteristic of an organic-centered radical with low delocalization of the spin density on the d orbitals of the low-spin iron(II) metal center.[31]

For this particular system, the non-innocence of the bis(imino)pyridine ligand was further highlighted upon isolation by Gambarotta et al. of the triply reduced form of the ligand, stabilized with Li^{+} complexation.[32] Finally, collaborative work between Chirik's and Wieghardt's groups on the elucidation of the structure of the neutral bis(imino)pyridine–dinitrogen–iron complex relied notably on magnetic measurement and Mössbauer spectroscopy coupled to high-level DFT calculations on a parent neutral bis(imino)pyridinedimethylaminopyridine–iron complex. This rigorous work, in line with former studies in this field by Wieghardt's group,[8b,9b,33] led to a description of the complex as an intermediate-spin Fe^{II} coordinated by a diradical dianionic form of the bis(imino)pyridine ligand.

The structures of iron complexes synthesized by Chirik et al.[43] were investigated by DFT (B3LYP) calculations (Figure 1). The starting point is $FeCl_2$ complexed by a bis(imino)pyridine ligand (**2a**·$FeCl_2$). This structure is a classical square planar pyramid as shown in column B (Figure 1).

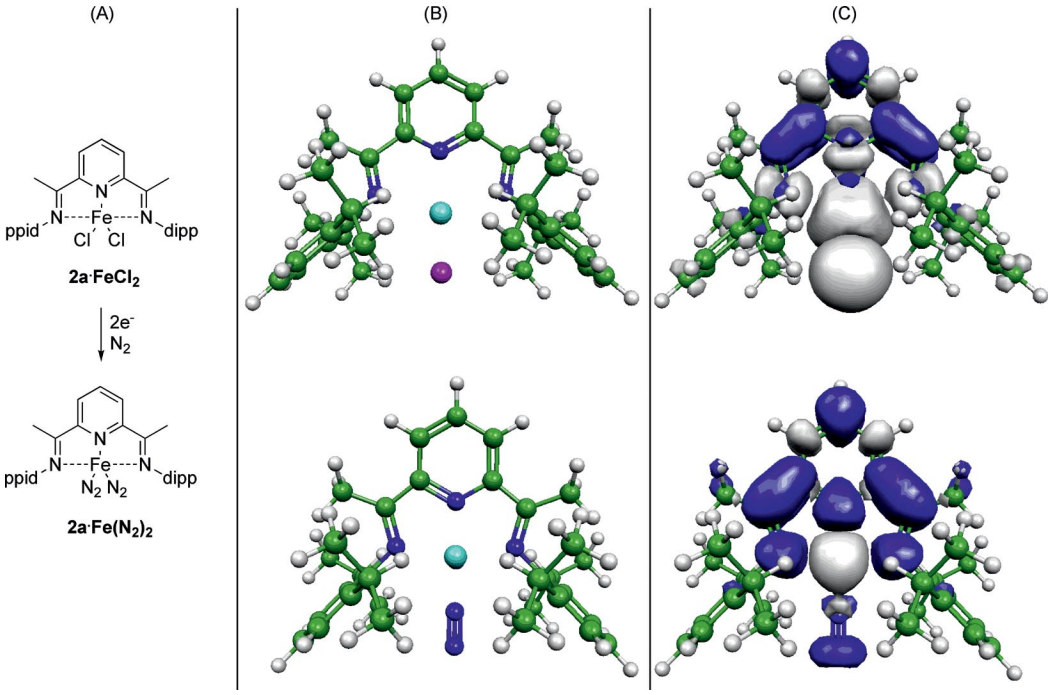

Figure 1. (A) Formation of the formal iron(0) structure as proposed by Chirik et al.[42] (B) DFT [UB3LYP/SV(P)] optimized structures, open-shell quintet (Cl_2 complex)/singlet [$(N_2)_2$ complex] ground state. (C) Spin density for the ground state for each complex.

 © 2012 Wiley-VCH Verlag GmbH & Co. KGaA, Weinheim

The ground state was found to be a quintet, as observed experimentally.[10,11] According to our DFT calculations, this d^6 complex has four unpaired electrons localized on iron [high-spin iron(II)], with small spin polarization on the bis(imino)pyridine (–0.1 e^- according to Mulliken analysis and natural orbitals analysis, see Figure 2). After reduction in the presence of dinitrogen, a formal iron(0) [**2a**·Fe$(N_2)_2$, Figure 1] was obtained. The complex geometry is quite similar to that of the dichlorido one. The electronic ground state is not a quintet anymore but rather an open-shell singlet, and although the spin densities for the two complexes look very similar, the spin distribution is totally different. There is only one unpaired electron localized on iron (0.73 e^- precisely according to Mulliken spin density analysis). Obviously, since the complex is a singlet, the same exact β spin distribution can be found on the ligand. The three nitrogen atoms share the majority of this β electron, the remaining part being distributed between the conjugated carbon atoms of the bis(imino)pyridine. This would be in agreement with an electronic configuration closer to an iron(I) coordinated to a radical anion ligand. However, even if this is formally an iron(0) complex, the calculated Mulliken charge on iron (+0.43 e^-) is close to the charge calculated in the case of Ritter's complex (see section 4.3.) and in agreement with an iron(II) electronic configuration. In this case, it appears difficult to assign a definite oxidation number to the iron and thus to the ligand. This can indicate a rather high covalent character of the metal–ligand bond. We therefore propose to represent the system through a classical mesomeric equilibrium (Scheme 4). Moreover, in view of other theoretical studies on iron reactivities,[34] this complex can be described in the framework of multi-state reactivities (MSR),[35] where the intrinsic reactivity of an iron complex emerges from different spin configurations. Depending on the chemistry performed, the bis(imino)pyridine ligand is thus able to act either as a classical innocent ligand (Brookhart's olefin polymerization catalyst) or as a non-innocent ligand with the same metal. This finding is in agreement with the variety of reactions observed by Gambarotta and Budzelaar (Scheme 2) and a good example of the adaptation of the iron spin state to its environment and its related reactivity.[36]

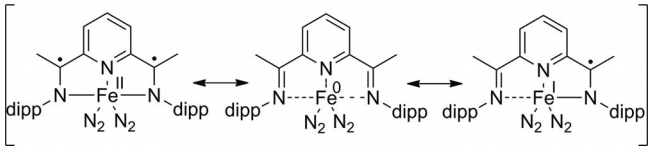

Scheme 4. Mesomeric electronic configurations of structure **2a**·Fe$(N_2)_2$.

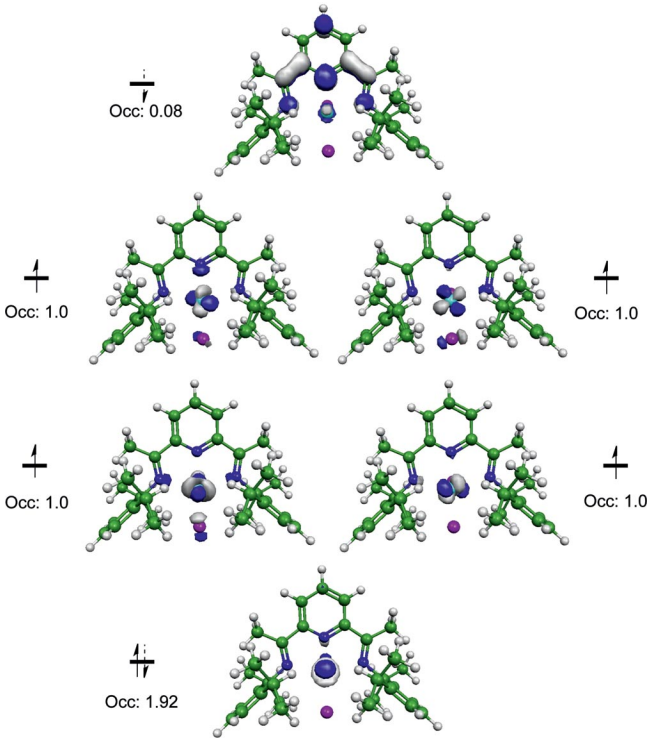

Figure 2. Frontier natural orbitals and their respective occupation numbers for complex **2a**·$FeCl_2$ in the open-shell quintet ground state.

3.2. Cycloadditions and Cycloisomerizations

Cycloaddition and cycloisomerization reactions share two specificities: allowing for rapid and efficient access to high molecular diversity as well as relying mostly on the use of noble metal complexes as catalysts in order to do so. However, in 2008 Fürstner's group reported efficient [4+2], [5+2], and [2+2+2] cycloaddition and cycloisomerization reactions of polyunsaturated substrates catalyzed by low-valent iron complexes.[37] Among numerous examples, the well-defined organometallic complexes {[CpFe$(C_2H_4)_2$][Li(tmeda)]} (**16**) and {[CpFe(COD)][Li(DME)]} (COD = cyclooctadiene) (**17**) efficiently promote Alder-ene reactions (Scheme 5).

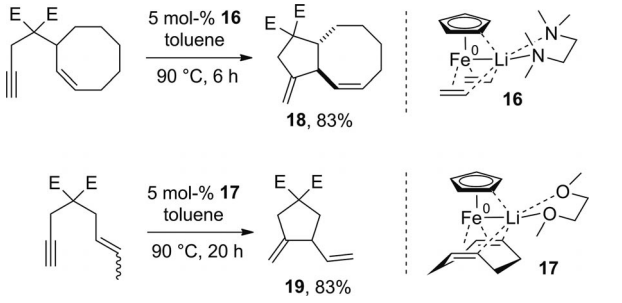

Scheme 5. Examples of Alder-ene reactions.

In this paper, Fürstner raises the question of the true electronic nature of this system, since, as the authors state, it was shown to exhibit "the capacity of the metal center to share electron density with the ligand environment" and we propose here to push further this analysis. The available characterizations are low-temperature ^{13}C NMR spectroscopic and X-ray diffraction studies. In the latter, a noticeable fact is the elongation of the olefin double bonds in both ethylene {[CpFe$(C_2H_4)_2$][Li(tmeda)]} (**16**) and COD

 © 2012 Wiley-VCH Verlag GmbH & Co. KGaA, Weinheim

{[CpFe(COD)] [Li(DME)]} (**17**). Indeed, in both complexes the C–C bond length lies between 1.421 and 1.449 Å, intermediate between a double bond, at about 1.337(6) Å, and a single bond at 1.541(3) Å.[38] This has been associated by Fürstner et al. with classical π-back-donation from the Fe^0 into the π* orbitals, but it could alternatively suggest a partial reduction of the olefins to a radical anion state, which then coordinates to a Fe central cation. Indeed, our open-shell calculations on this system lead to a singlet ground state. The system can also be described as a low-spin iron(II) formally coordinated with two ethenyl anions. This can be analyzed as a result of a three-orbital interaction involving the two π* orbitals of the ethylene ligands and one of the "d" orbital, leading to a doubly occupied HOMO-1 mainly centered on the ligands. In this process, a high-lying "d" orbital would allow to bypass the Woodward–Hoffmann [2π+2π] forbidden interaction.

However, further characterizations including Mössbauer measurements of these complexes would be needed in order to reinforce this hypothesis. Indeed, the calculated Mössbauer isomer shift at about 0.5 mm s^{-1} is typical for Fe^{II} cyclopentadienyl-enen/enyl complexes,[39] whereas the more reduced Fe^{I} Cp-polyene complexes display isomer shifts around 0.8 mm s^{-1}.[40] Besides Mössbauer studies, one could expect a quite intense ligand-to-ligand charge-transfer band in UV/Vis spectroscopy, as observed in various iron–diradical complexes.[33,41] Although these topics would need to be experimentally confirmed, it seems relevant to include this efficient catalytic system in this review.

[2+2] cycloaddition is one of the main strategies for the synthesis of cyclobutane derivatives. Chirik and colleagues reported the intramolecular [2+2] cyclization of α,ω-dienes promoted by iron complex **2a**·$Fe(N_2)_2$ (Scheme 6).[42] This group has described previously efficient hydrogenation of olefins, alkynes, and aryl azides with these iron systems.[43,44] In a first experiment, 1,5-hexadiene was submitted to 10 mol-% of **2a**·$Fe(N_2)_2$ under 0.5 atm of H_2. No [2+2] product was obtained, but a mixture of methylenecyclopentane, methylcyclopentane, and *n*-hexane. When **2a**·$Fe(H_2)_2$ was used as the catalyst, the reaction was more selective, and only methylenecyclopentane was obtained. A variety of α,ω-dienes **20** were then subjected to the same catalytic conditions [10 mol-% of **2a**·$Fe(N_2)_2$ under 0.5 atm of H_2], and the expected bicyclo[3.2.0] ring systems **21** were obtained in good yields. The reaction also tolerated a broad range of functionalities. The mechanism proposed by the authors is outlined in Scheme 6.

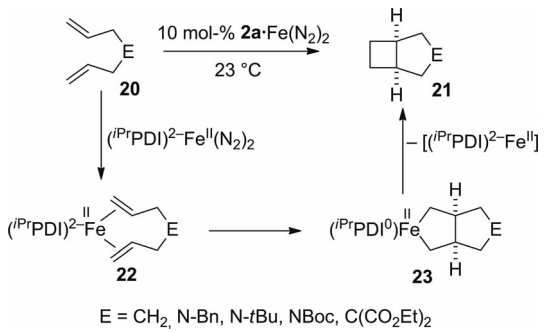

Scheme 6. Proposed mechanism for the [2+2] cycloaddition of α,ω-dienes. (^{iPr}PDI)$Fe(N_2)_2$ {^{iPr}PDI = 2,6-(2,6-$^{iPr2}C_6H_3NCMe)_2$-C_5H_3N}.

After substitution of the N_2 ligands by the diene, the resulting intermediate **22** undergoes oxidative cyclization to form metallacycle **23** by formal [2+2] cycloaddition, the needed electron being provided by the ligand. Subsequent formal reductive elimination yields the expected bicycle **21** and regenerates the iron complex.

In order to generalize the formation of the cyclobutane derivative by iron-catalyzed [2+2] cycloaddition, Chirik et al. reported preliminary results of intermolecular reactions between ethylene and various 1,3-butadienes (Scheme 7).[45] An equimolar mixture of ethylene and butadiene in the presence of 5 mol-% iron catalyst at 23 °C afforded the expected vinylcyclobutane in good yield. When a methyl group was introduced into the diene, a 1,4-addition of ethylene to the 1,3-diene occurred, as described previously by Ritter et al.[47] (see section 3.3.). In this study, the authors demonstrate that steric hindrance on the diene blocks the reaction (Scheme 7).

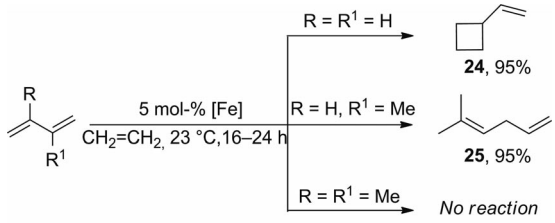

Scheme 7. Intermolecular [2+2] cycloaddition.

Based on deuterium-labeling experiments, the authors proposed the following mechanism (Scheme 8): coordination of butadiene occurs upon displacement of dinitrogen ligands from the initial **2b**·$Fe(N_2)_2$ iron complex, leading to η^4-butadiene complex **26**. Insertion of ethylene induced the formation of iron metallacycle **27**, which was well-charac-

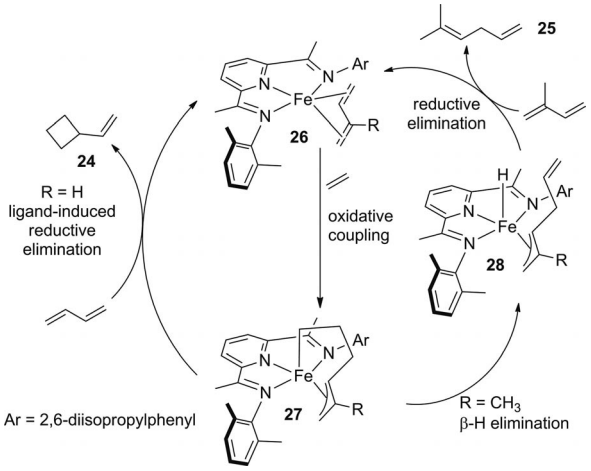

Scheme 8. Mechanistic proposal for the intermolecular [2+2] cycloaddition.

 © 2012 Wiley-VCH Verlag GmbH & Co. KGaA, Weinheim

terized, especially by single-crystal X-ray diffraction. In the presence of butadiene, the latter promoted C–C reductive elimination to furnish the corresponding vinylcyclobutane **24** and regenerate the propagating iron butadiene complex **26**.

The sterically more hindered isoprene is a weaker ligand, disfavoring ligand-induced reductive elimination and making the β-H elimination leading to intermediate **28** a competitive alternative pathway. This observation corroborates the results obtained by the Ritter group on the 1,4-addition of α-olefins to 1,3-dienes (see section 3.3.).

Aiming to extend the application of their iron-based catalytic systems, the Chirik group has explored the cycloisomerization of 1,6-enynes and diynes.[46] Indeed, organometallic cyclization of polyunsaturated substrates is a powerful method for the construction of a myriad of cyclic compounds. Enyne cyclization was first conducted with 5 mol-% of **2a**·$Fe(N_2)_2$ at 23 °C under 4 atm. dihydrogen (Scheme 9), which was necessary to promote the catalytic cycle and allow the final reductive elimination step. When enynes bearing terminal alkyne groups were used, the expected Alder-ene product **29** was formed, but the latter underwent further hydrogenation, leading to the reduced product **30**. However, when substrates bearing internal alkyne groups were involved in the cyclization, the Alder-ene product was isolated without further reduction, as the **2a**·$Fe(N_2)_2$ complex was unable to hydrogenate the unreactive trisubstituted alkene products. This iron-catalyzed system could be extended to diyne–amine derivatives, and the expected (*Z*,*Z*)-disubstituted pyrrolidine products were isolated in good yield.

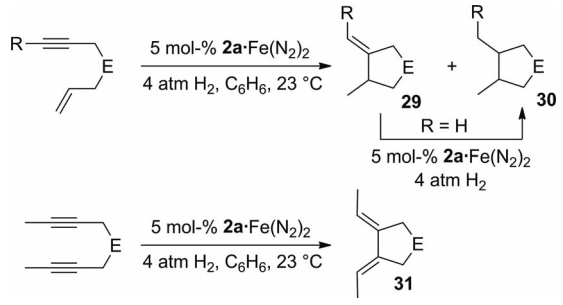

Scheme 9. Catalytic enyne and diyne cyclizations with **2a**·$Fe(N_2)_2$.

The mechanism proposed by the authors is depicted in Scheme 10. From previous studies on [2+2] cycloaddition, it can be concluded that metallacycle **32** is formed first, followed by a hydrogenation addition step. Deuterium-labeling studies established that both intermediates **33** and **34** are formed. Finally, reductive elimination of a carbon–hydrogen bond from these intermediates forms the observed product **29**.

On the basis of previous observations in [2+2] cycloadditions, the authors postulate that reductive cyclization to form the carbon–carbon bond involves electron transfer from the bis(imino)pyridine chelate and therefore results in formal oxidation of the ligand rather than the iron center. The formal oxidation state of the iron center is thus preserved throughout the catalytic cycle.

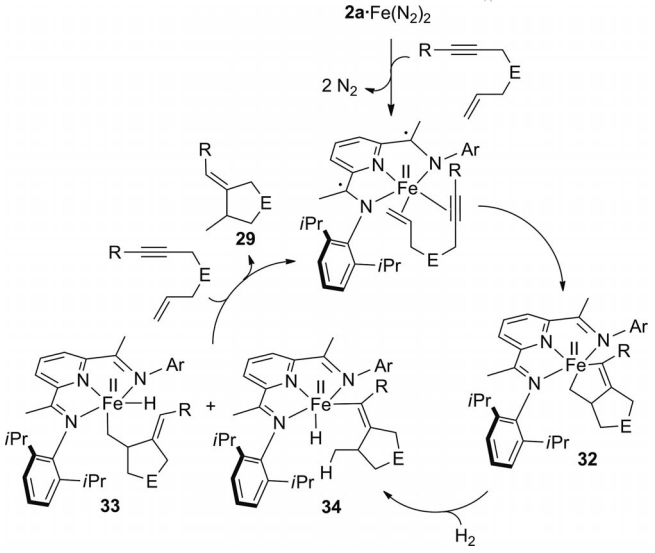

Scheme 10. Mechanistic proposal for the iron-catalyzed, hydrogen-mediated enyne cyclization.

3.3. Addition of Olefins to Dienes

In 2009, Ritter et al. introduced an efficient iron-catalyzed 1,4-addition of α-olefins to 1,3-dienes.[47] The method is highly stereo- and regioselective, and the coupling products are obtained in good yields (up to 94%). The α-olefins are mainly styrene derivatives and a wide range of electron-withdrawing and -donating groups at the *para* position are well tolerated. Both symmetrical and unsymmetrical dienes were investigated, among which were 2,3-dimethyl-1,3-butadiene, isoprene, and the more complex myrcene. The catalytic system relies on a low-valent 1:1 iminopyridine/Fe complex (either isolated, as proved by crystal structure, or generated in situ from $FeCl_2$), the iminopyridine ligand (**35** or **36**, Scheme 11), and a reducing agent (activated magnesium). The catalytic loading is low, as only 2 mol-% of precatalyst is sufficient for the reaction to proceed smoothly. The presence of all components (iron, reducing agent, and ligand) is mandatory, and removal of any of them fails to deliver a working catalytic cycle.

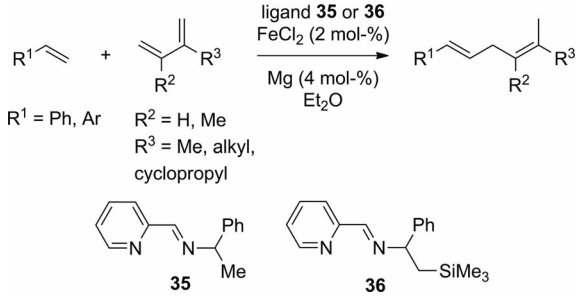

Scheme 11. Iron-catalyzed 1,4-addition of α-olefins to 1,3-dienes.

The authors provide a putative catalytic cycle for this transformation (Scheme 12), where the initial activation step is the in situ reduction of the $FeCl_2$ complex by magnesium, followed by coordination of the diene, thereby generating a catalytically competent low-valent iron species **37**.

 © 2012 Wiley-VCH Verlag GmbH & Co. KGaA, Weinheim

Subsequent coordination of the olefin to the iron center followed by oxidative coupling would afford an iron(II)–alkyl–allyl complex **39** that could undergo a π–σ rearrangement to form a seven-membered η^1-allyl ferracycle **40**. In the last two steps, *syn*-β-hydride elimination and subsequent reductive elimination would regenerate the active catalytic species **37** while releasing the expected coupling adduct. The iminopyridine ligand stays on the metal throughout the whole cycle, and, even though no rationalization has yet been provided, it was observed that slight modifications of the ligand structure can have a dramatic impact on both yield and regioselectivity of the reaction. The proposed catalytic cycle complies with deuterium-labeling experiments carried out by the authors.

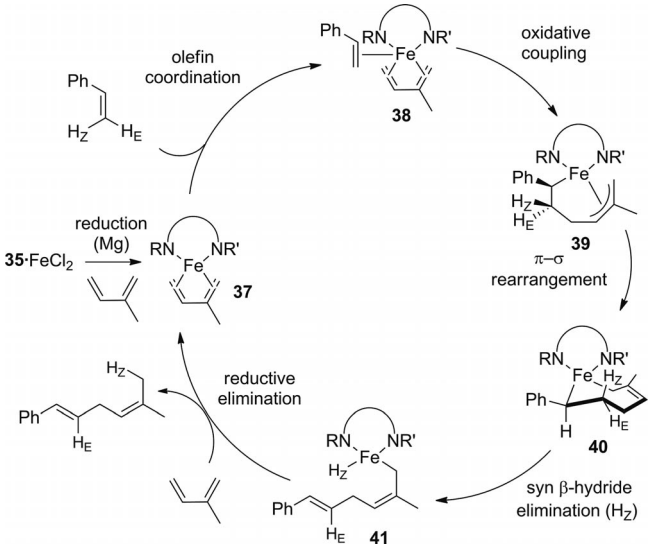

Scheme 12. Proposed catalytic cycle for the 1,4-addition of α-olefins to 1,3-dienes.

In order to probe the proposed catalytic cycle, we performed DFT calculations by using the X-ray crystallographic structure obtained by the authors for complex **42**, bearing an *ortho*-methylated analogue of ligand **35**. Iron(II) structure **42**, taken as a starting point for calculations, is in a quintet state without any unpaired electrons delocalized on the ligand. If formally two electrons are added to the complex, while maintaining the other structural parameters, one can see in Figure 3 (**43**, right-hand side) that unpaired

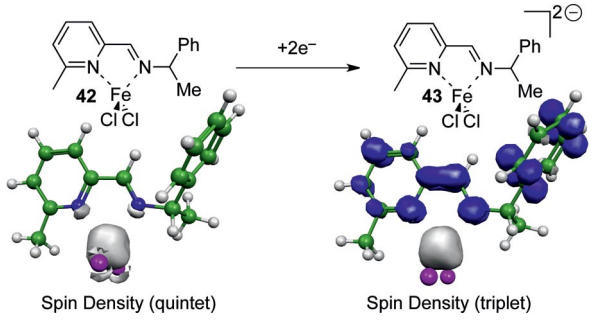

Figure 3. Calculated spin densities of $FeCl_2$·iminopyridine complexes before and after $2e^-$ reduction.

electrons can be found on the iminopyridine ligand. Thus, in situ reduction of the catalyst by magnesium confers non-innocence to the catalytic system based on iron iminopyridine.

3.4. Tandem C–H Activation and C–C Coupling

C–H activation is a much sought-after synthetic transformation that has been actively developed in the last decade, mostly with noble metals such as palladium, rhodium, and ruthenium. However, iron-catalyzed alternatives are emerging,[48] and Nakamura has been developing a system that enables activation of aromatic C–H bonds in diverse settings, followed by C–C coupling.[49] This systems builds on previous reports by this group on low-valent iron catalysis including early works on carbometalation and cross-coupling of alkyl halides with Grignard reagents and/or zinc reagents.[50] The reaction conditions involve $Fe(acac)_3$ as the metal source in 10 mol-% loading, along with dtbpy (4,4′-di-*tert*-butyl-2,2′-bipyridyl) in 10 to 15 mol-% loading (Scheme 13). Excess of the Grignard partner (two equivalents at least) is required, as when only one equivalent is used, the reaction conversion stops at 47%, suggesting that one equivalent of the Grignard reagent is used for the C–C bond formation step and the second could be of use as a hydrogen acceptor in the C–H activation step.[51] Also, two equivalents of 1,2-dichloro-2-methylpropane as external oxidant are necessary to sustain the catalytic system, as previously shown through optimization studies. Mechanistic considerations seem to suggest the formation of a ferracycle intermediate resulting from the initial C–H activation step. However, to the best of our knowledge, no clear intermediate or precatalyst has been identified. Technically, the catalytic system is quite complex, and although the bipyridinyl nature of dtbpy might raise the question of the valency of the iron center in the course of the reaction and point to a possible non-innocent mode of action, no supporting evidence for such behavior has yet been disclosed.

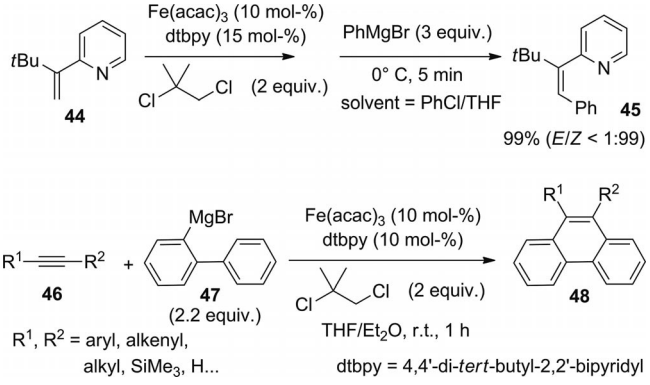

Scheme 13. Application of tandem C–H activation and C–C coupling.

4. C–Y Bond Formation

4.1. Hydrogenation

The previously described bis(imino)pyridine iron complex system used in polymerization and cycloisomerization

 © 2012 Wiley-VCH Verlag GmbH & Co. KGaA, Weinheim

(see sections 3.1. and 3.2., respectively) was also successfully applied to the hydrogenation of alkenes.[43] The catalyst loading was as low as 0.3 mol-%, and various substrates were tested (Scheme 14). A variety of olefins could be efficiently hydrogenated, and terminal alkenes such as 1-hexene and styrene were the most reactive substrates. Although slightly longer reaction times were necessary, hydrogenation of internal and *gem*-disubstituted olefins was also possible.

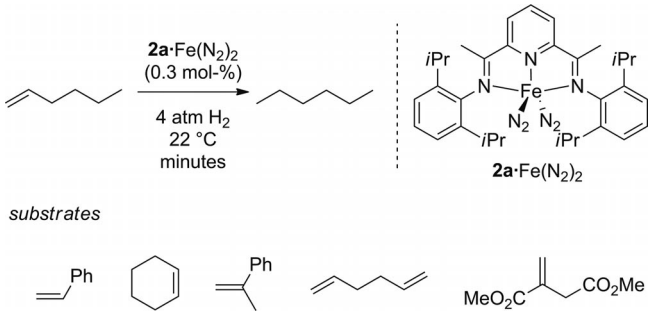

Scheme 14. Hydrogenation of alkenes with bis(imino)pyridine iron complexes.

Experimental findings provide evidence for a stereoselective *syn*-addition. On the basis of experimental data including isotopic labeling studies, the authors propose a mechanism involving a first olefin coordination step followed by oxidative addition of dihydrogen to generate an 18-electron olefin dihydride intermediate **50** (Scheme 15). Presumably, direct olefin coordination is preferred over oxidative addition of dihydrogen as the first step, because of the sensitivity of species **2a**·FeH_2 to nitrogen, coupled with the fact that an intermediate resulting from the direct olefin coordination of an alkyne was previously identified and isolated.

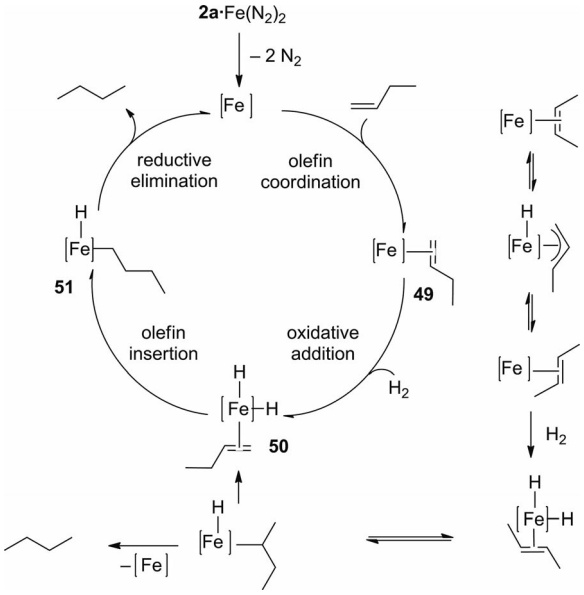

Scheme 15. Proposed catalytic cycle for the hydrogenation of alkenes.

4.2. Hydroboration

Carbon–boron bond formation has been investigated by the Ritter group. The catalytic system is similar[52] to the one they had previously reported for the C–C bond forming 1,4-addition of α-olefins to 1,3-dienes, except for a slight modification of the iminopyridine ligand for which fine-tuning of the substitution by a bis(aromatic) or a bulky dipp ligand (ligands **54** and **55**, respectively) gave optimal results (Scheme 16). The boron source is H–BPinacol and selectivity of linear product **52** over branched product **53** was achieved together with (*E*) stereoselectivity.

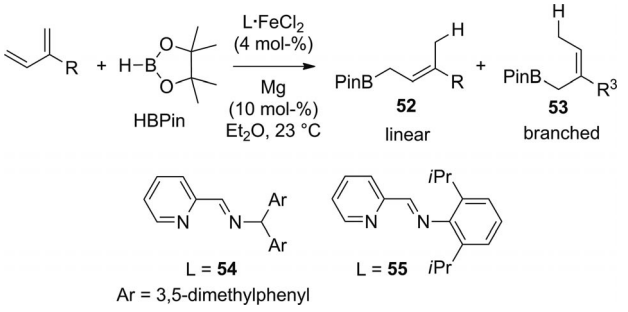

Scheme 16. Hydroboration of alkenes with iminopyridine ligands.

Referring to previous work[53] by Wieghardt on bis(iminopyridine) metal complexes, the authors hint at the probability of a non-innocent behavior of the ligands, stating that "the redox activity of iminopyridine ligands may play a role in effecting efficient catalysis", which is also in agreement with our results on this family of complexes (see sections 3.3. and 4.3.). The putative catalytic cycle (Scheme 17) mirrors the one previously proposed for the 1,4-addition of olefins in which pinacol borane undergoes oxidative addition to the iron center. Again, deuterium-labeling experiments with deuteriated pinacol borane strongly support the proposed mechanism (Scheme 17).

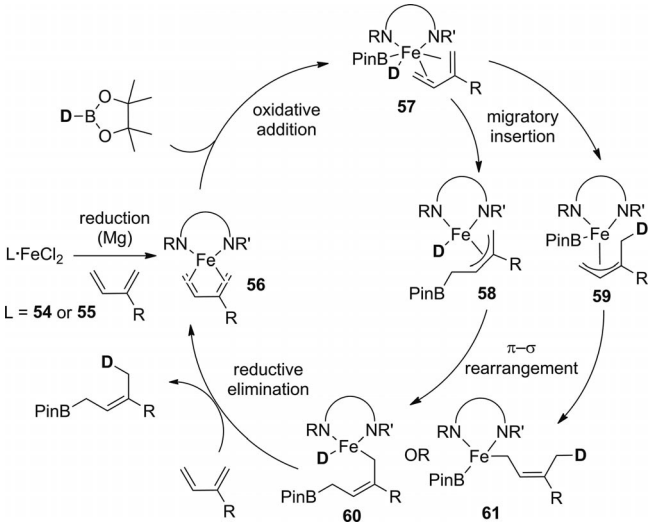

Scheme 17. Deuterium-labeling experiments supporting the proposed mechanism for the hydroboration of alkenes.

 © 2012 Wiley-VCH Verlag GmbH & Co. KGaA, Weinheim

4.3. Hydrosilylation

Hydrosilylation is a useful transformation, which has also been targeted by redox ligand systems. In this context, both iminopyridine and bis(imino)pyridine ligands have been successful. Along with their studies on the hydrogenation of alkenes (see section 4.1.), the Chirik group reported a hydrosilylation catalyzed by complex **2a**·$Fe(N_2)_2$ (Scheme 18).

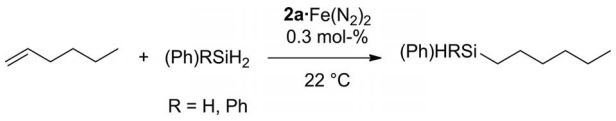

Scheme 18. Hydrosilylation of alkenes with bis(imino)pyridine iron complexes.

Both $PhSiH_3$ and Ph_2SiH_2 were found to be efficient silylation reagents, delivering the anti-Markovnikov addition products in minutes, and reactions with $PhSiH_3$ were even faster. The relative rates of hydrosilylation are close to those observed for the hydrogenation reaction, terminal alkenes reacting more rapidly than *gem*-disubstituted and internal olefins. Reactivity of alkynes was also investigated and these were found to undergo monosilylation to yield the corresponding silylated olefins. Reaction of **2a**·$Fe(N_2)_2$ with excess $PhSiH_3$ provided an iron(0)–bis(silane) complex **2a**·Fe(η^2-$SiH_3Ph)_2$ {denoted **2a**·$Fe(Si)_2$}, which was isolated and recrystallized at –35 °C. This complex was also an effective precatalyst for the hydrosilylation reaction. Based upon these findings, the mechanism is postulated to proceed through the same pathway as previously proposed for the hydrogenation reaction (see Scheme 15, section 4.1.), an intermediate iron olefin complex undergoing oxidative addition of silane, thus generating an iron(II) olefin silyl hydride complex. The isolation of the iron(0)–bis(silane) complex would be in disfavor of a direct oxidative addition to the L·Fe^0 fragment. Worthy of note is the related hydrosilylation of ketones with iron complexes of bis(imino)pyridine and bis(oxazoline)pyridine ("Pybox") ligands, reported later by the authors.[54] The "Pybox" ligands were found to perform well, but measurement of the first reduction potential of their iron complexes demonstrated that they are more electron-donating that their bis(imino)-pyridine counterparts and thus less prone to engage in electron transfer with the iron center.

The carbon–silicon bond formation reaction was also studied by the Ritter group by using an improved methodology[55] (see sections 3.3. and 4.2.) relying on a better defined low-valent iron complex **62**. This catalyst is efficiently accessed through reductive elimination of two *N*,*N*-dimethylbenzylamine ligands from precatalyst **63** (Scheme 19). This strategy circumvents the use of an in situ reducing agent such as activated magnesium, which often requires optimization of the reaction conditions and sometimes results in ill-defined reactive species.

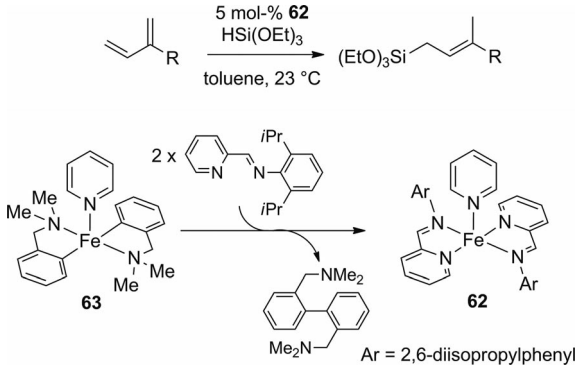

Scheme 19. Regioselective diene hydrosilylation (top) and preparation of catalyst (bottom).

Also, the use of precatalyst **63** allows to easily test a wide set of ligands with varied steric or electronic features. As in the previous studies reported by the authors,[47,52] modification of the ligands was found to have a dramatic influence on the regioselectivity of the reaction, allowing the selectivity to be switched from a 1:2 mixture (linear vs. branched), when using ligand **55**, to a 94:6 or higher ratio in favor of the linear product with ligands **35** and **36** (Figure 4).

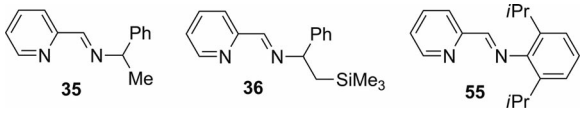

Figure 4. Iminopyridine ligands for regioselective hydrosilylation of alkenes.

In the case of bis(imino)pyridine–iron catalyst **62** used by Ritter for hydrosilylation,[55] the authors clearly opted for a potentially non-innocent ligand to tune the electronic properties of the catalyst (Scheme 20). According to Mössbauer measurements in correlation with previous work

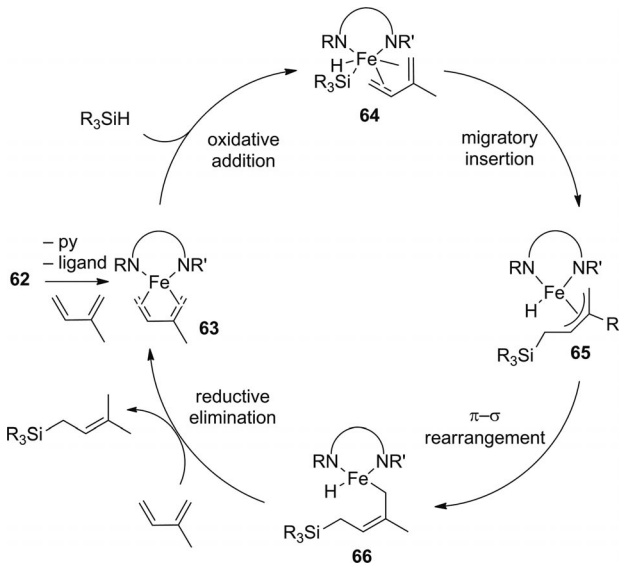

Scheme 20. Proposed catalytic cycle for the hydrosilylation of alkenes.

 © 2012 Wiley-VCH Verlag GmbH & Co. KGaA, Weinheim

on other bis(imino)pyridine complexes in Wieghardt's group,[53] Ritter et al. suggest an iron(II) coordinated to two iminopyridyl radical anions. Indeed, this proposal is reinforced by the careful analysis of the bond lengths within the ligands in the crystal structure (Figure 5): the C–N bond lengths at 1.343 ±0.015 Å in the imino functions are clearly intermediate between a C–N double bond (ca. 1.28 Å) and single bond (ca. 1.46 Å).[53] Similarly, the length of the C–C bond linking the pyridine group to the imino function is 1.382 ±0.015 Å, which is intermediate between the expected values for a single bond (1.47 Å) and a double bond (1.35 Å) in such systems. These parameters are clearly in favor of a radical anion state of the ligands.

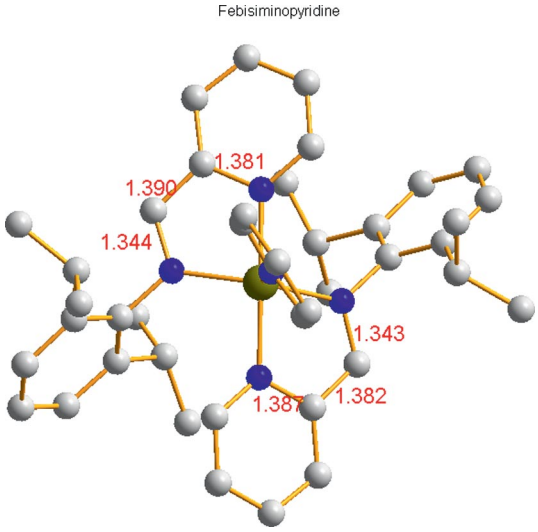

Figure 5. Relevant bond lengths in the [Fe(iminopyridine)$_2$(pyridine)]complex.

On the basis of X-ray crystallographic characterization of the pre-catalyst by Ritter's group, calculations of its electronic structure were conducted with standard DFT [namely UB3LYP and a double-ζ basis set SV(P)]. The total spin density surface (with a cut-off of 0.005 electron) can be seen in Figure 6. The total charge of complex **62** is zero, implying a formal iron(0) and three ligands are arranged around iron: two iminopyridines and one pyridine, in what can be seen as a square-planar pyramid. Our calculations support a non-innocent scenario. The pyridine has no single electrons and behaves as a classical apical ligand, like histidine in peroxidase.[56] On the other hand, the two iminopyridines have a totally distinct electronic behavior. One of the iminopyridine has one unpaired electron of α spin and the other one has one unpaired electron of β spin. The ground state is thus an open-shell singlet, the triplet configuration being 8.8 kcal/mol and the quintet 9.6 kcal/mol above the ground state. According to DFT calculations, there is nearly no spin density on iron (0.0008 e$^-$), and a Mulliken positive charge of 0.4490 e$^-$. Thus, the global structure could be described as that shown in Scheme 21.

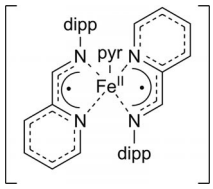

Scheme 21. Electronic structure for iminopyridine complex **62** (dipp = 2,6-diisopropylphenyl).

5. Conclusion

The recent contributions reported in this review clearly establish non-innocent ligands and iron catalysis as a good match for innovative organometallic chemistry. Although challenges – among which better understanding of the mechanistic rationale of the catalytic systems – remain to be addressed, overcoming these limitations will without doubt lead to the development of new catalysts and provide the synthetic community with powerful and improved alternatives to the hegemony of noble metal catalysis.

Supporting Information (see footnote on the first page of this article): Computational details.

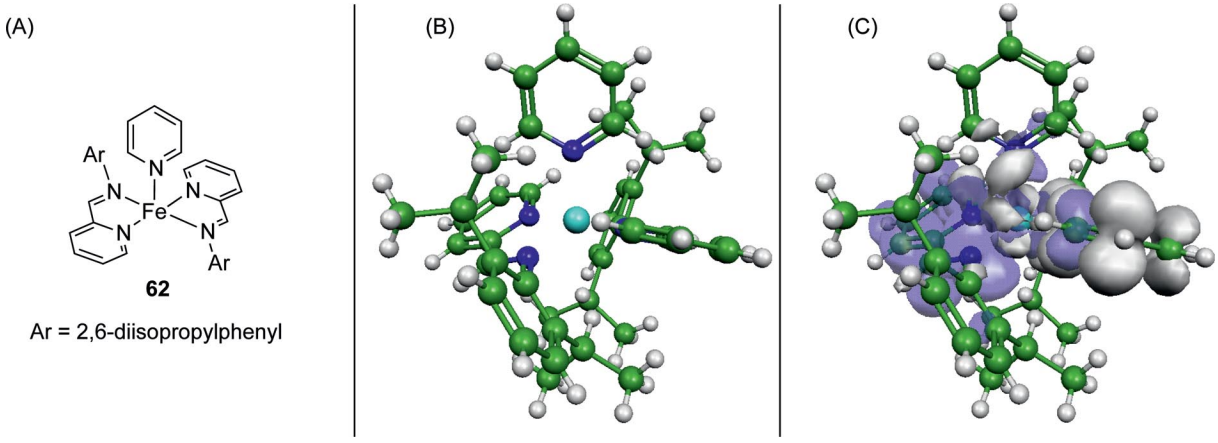

Figure 6. (A) X-ray structure of the catalyst prepared by Ritter et al. Worthy of note is the fact that the two iminopyridines are not coplanar. (B) Calculated spin density [UB3LYP/SV(P), open-shell singlet] for the same catalyst. The white lobes correspond to α spin density while the blue ones correspond to β spin density.

 © 2012 Wiley-VCH Verlag GmbH & Co. KGaA, Weinheim

Acknowledgments

Louis Fensterbank and Max Malacria thank the Institut Universitaire de France (IUF). The Agence Nationale pour la Recherche (ANR) is acknowledged for funding ("Unilversal" project, ANR JCJC 2011). The authors wish to thank the Université Pierre & Marie Curie (UPMC) and the Centre National de la Recherche Scientifique (CNRS).

[1] P. J. Chirik, K. Wieghardt, *Science* **2010**, *327*, 794–795.
[2] K. Jørgensen, *Coord. Chem. Rev.* **1966**, *1*, 164–178.
[3] S. K. Szilagyi, B. S. Lim, T. Glaser, R. H. Holm, B. Hedman, K. O. Hodgson, E. I. Solomon, *J. Am. Chem. Soc.* **2003**, *125*, 9158–9169.
[4] a) M. D. Ward, J. A. McCleverty, *J. Chem. Soc., Dalton Trans.* **2002**, 275–288; b) P. Chaudhuri, C. N. Verdani, E. Bill, E. Bothe, T. Weyhermüller, K. Wieghardt, *J. Am. Chem. Soc.* **2001**, *123*, 2213–2223; c) C. G. Pierpont, *Coord. Chem. Rev.* **2001**, *216–217*, 99–125; d) W. Kaim, *Inorg. Chem.* **2011**, *50*, 9752–9765.
[5] R. H. Crabtree, *The Organometallic Chemistry of the Transition Metals*, 5th ed., John Wiley & Sons, Hoboken NJ, **2009**.
[6] For selected reviews, see: a) C. Bolm, J. Legros, J. Le Paih, L. Zani, *Chem. Rev.* **2004**, *104*, 6217–6254; b) A. Fürstner, R. Martin, *Chem. Lett.* **2005**, *34*, 624–629; c) B. Plietker (Ed.), *Iron Catalysis in Organic Chemistry: Reactions and Applications*, Wiley-VCH, Weinheim, **2008**; d) A. Correa, O. García Mancheño, C. Bolm, *Chem. Soc. Rev.* **2008**, *37*, 1108–1117; e) S. Enthaler, K. Junge, M. Beller, *Angew. Chem.* **2008**, *120*, 3363–3367; *Angew. Chem. Int. Ed.* **2008**, *47*, 3317–3321; f) B. D. Sherry, A. Fürstner, *Acc. Chem. Res.* **2008**, *41*, 1500–1511; g) W. M. Czaplik, M. Mayer, J. Cvengros, A. Jacobi von Wangelin, *ChemSusChem* **2009**, *2*, 396–417; h) E. Nakamura, N. Yoshikai, *J. Org. Chem.* **2010**, *75*, 6061–6067. For a review on iron-catalyzed C–H activation, see: i) C.-L. Sun, B.-J. Li, Z.-J. Shi, *Chem. Rev.* **2011**, *111*, 1293–1314.
[7] For research highlights, see: a) O. García Mancheño, *Angew. Chem.* **2011**, *123*, 2264–2266; *Angew. Chem. Int. Ed.* **2011**, *50*, 2216–2218; b) G. Bauer, K. A. Kirchner, *Angew. Chem.* **2011**, *123*, 5918–5920; *Angew. Chem. Int. Ed.* **2011**, *50*, 5798–5800; c) A. Fürstner, *Angew. Chem.* **2009**, *121*, 1390–1393; *Angew. Chem. Int. Ed.* **2009**, *48*, 1364–1367.
[8] a) D. Zhu, I. Thapa, I. Korobkov, S. Gambarotta, P. H. Budzelaar, *Inorg. Chem.* **2011**, *50*, 9879–9887; b) A. M. Tondreau, C. Milsmann, A. D. Patrick, H. M. Hoyt, E. Lobkovsky, K. Wieghardt, P. J. Chirik, *J. Am. Chem. Soc.* **2010**, *132*, 15046–15059 and references cited therein.
[9] a) D. Herebian, E. Bothe, F. Neese, T. Weyhermüller, K. Wieghardt, *J. Am. Chem. Soc.* **2003**, *125*, 9116–9128; b) R. Hübner, S. Weber, S. Strobel, B. Sarkar, S. Zalis, W. Kaim, *Organometallics* **2011**, *30*, 1414–1418; c) C. R. Hess, T. Weyhermüller, E. Bill, K. Wieghardt, *Inorg. Chem.* **2010**, *49*, 5686–5700 and references cited therein; d) S. Ye, T. Tuttle, E. Bill, L. Simkhovich, Z. Gross, W. Thiel, F. Neese, *Chem. Eur. J.* **2008**, *14*, 10839–10851 and references cited therein; e) E. Evangelio, M.-L. Bonnet, M. Cabaças, M. Nakano, J.-P. Sutter, A. Dei, V. Robert, D. Ruiz-Molina, *Chem. Eur. J.* **2010**, *16*, 6666–6677.
[10] B. L. Small, M. Brookhart, A. M. A. Bennett, *J. Am. Chem. Soc.* **1998**, *120*, 4049–4050.
[11] G. J. P. Britovsek, V. C. Gibson, B. S. Kimberley, P. J. Maddox, S. J. McTavish, G. A. Solan, A. J. P. White, D. J. Williams, *Chem. Commun.* **1998**, 849–850.
[12] V. C. Gibson, C. Redshaw, G. A. Solan, *Chem. Rev.* **2007**, *107*, 1745–1776.
[13] V. C. Gibson, S. K. Spitzmesser, *Chem. Rev.* **2003**, *103*, 283–315.
[14] V. C. Gibson, G. A. Solan, *Top. Organomet. Chem.* **2011**, 1–52.
[15] For a recent review see ref.[8a]
[16] A. M. A. Bennett, EI Du Pont de Nemours and Co, USA, PCT Int. Appl. WO 9827124, **1998**.
[17] G. J. P. Britovsek, M. Bruce, V. C. Gibson, B. S. Kimberley, P. J. Maddox, S. Mastroianni, S. J. McTavish, C. Redshaw, G. A. Solan, S. Strömberg, A. J. P. White, D. J. Williams, *J. Am. Chem. Soc.* **1999**, *121*, 8728–8740.
[18] G. J. P. Britovsek, S. Mastroianni, G. A. Solan, S. P. D. Baugh, C. Redshaw, V. C. Gibson, A. J. P. White, D. J. Williams, M. R. J. Elsegood, *Chem. Eur. J.* **2000**, *6*, 2221–2231.
[19] B. L. Small, M. Brookhart, *J. Am. Chem. Soc.* **1998**, *120*, 7143–7144.
[20] M. W. Bouwkamp, E. Lobkovsky, P. J. Chirik, *J. Am. Chem. Soc.* **2005**, *127*, 9660–9661.
[21] J. Scott, S. Gambarotta, I. Korobkov, P. H. M. Budzelaar, *J. Am. Chem. Soc.* **2005**, *127*, 13019–13029.
[22] R. Poli, *Eur. J. Inorg. Chem.* **2011**, 1513–1530.
[23] a) V. L. Cruz, J. Ramos, J. Martinez-Salazar, S. Gutiérrez-Oliva, A. Toro-Labbé, *Organometallics* **2009**, *28*, 5889–5895; b) J. Martínez, V. Cruz, J. Ramos, S. Gutiérrez-Oliva, J. Martínez-Salazar, A. Toro-Labbé, *J. Phys. Chem. C* **2008**, *112*, 5023–5028; c) For some spectroscopic evidence, see also: G. J. P. Britovsek, G. K. B. Clentsmith, V. C. Gibson, D. M. L. Goodgame, S. J. McTavish, Q. A. Pankhurst, *Catal. Commun.* **2002**, *3*, 207–211.
[24] Throughout the microreview, DFT calculations will be used in order to check the redox character of the ligand. It has been shown in the literature that DFT calculations are pertinent in that field and compare well with multi-reference calculations. For examples, see: a) H. Chen, J. Song, W. Lai, W. Wu, S. Shaik, *J. Chem. Theory Comput.* **2010**, *6*, 940–953; b) A. Altun, D. Kumar, F. Neese, W. Thiel, *J. Phys. Chem. A* **2008**, *112*, 12904–12910.
[25] a) L. Deng, P. Margl, T. Ziegler, *J. Am. Chem. Soc.* **1999**, *121*, 6479–6487; b) D. V. Khoroshun, D. G. Musaev, T. Vreven, K. Morokuma, *Organometallics* **2001**, *20*, 2007–2026.
[26] R. Raucoules, T. de Bruin, P. Raybaud, C. Adamo, *Organometallics* **2009**, *28*, 5358–5367.
[27] R. Raucoules, T. de Bruin, C. Adamo, P. Raybaud, *Organometallics* **2011**, *30*, 3911–3914.
[28] J. Scott, S. Gambarotta, I. Korobkov, P. H. M. Budzelaar, *J. Am. Chem. Soc.* **2005**, *127*, 13019–13029.
[29] H. F. Haarman, F. R. Bregman, P. W. N. M. van Leeuwen, K. Vrieze, *Organometallics* **1997**, *16*, 979–985.
[30] a) B. de Bruin, E. Bill, E. Bothe, T. Weyhermüller, K. Wieghardt, *Inorg. Chem.* **2000**, *39*, 2936–2947; For related studies on bis(imino)pyridine iron complexes, see also: b) S. C. Bart, K. Chlopek, E. Bill, M. W. Bouwkamp, E. Lobkovsky, F. Neese, K. Wieghardt, P. J. Chirik, *J. Am. Chem. Soc.* **2006**, *128*, 13901–13912.
[31] S. Blanchard, E. Bill, T. Weyehermüller, F. Neese, E. Bothe, K. Wieghardt, *Inorg. Chem.* **2005**, *44*, 3636–3656 and references cited therein.
[32] D. Enright, S. Gambarotta, G. P. A. Yap, P. H. M. Budzelaar, *Angew. Chem.* **2002**, *114*, 4029–4032; *Angew. Chem. Int. Ed.* **2002**, *41*, 3873–3876.
[33] S. Blanchard, E. Bill, T. Weyehermüller, K. Wieghardt, *Inorg. Chem.* **2004**, *43*, 2324–2329.
[34] S. Shaik, S. P. de Visser, F. Ogliaro, H. Schwarz, D. Schröder, *Curr. Opin. Chem. Biol.* **2002**, *6*, 556–567.
[35] a) D. Schröder, S. Shaik, H. Schwarz, *Acc. Chem. Res.* **2000**, *33*, 139–145; b) S. Shaik, H. Hirao, D. Kumar, *Acc. Chem. Res.* **2007**, *40*, 532–542.
[36] F. Ogliaro, S. P. de Visser, J. T. Groves, S. Shaik, *Angew. Chem.* **2001**, *113*, 2958–2962; *Angew. Chem. Int. Ed.* **2001**, *40*, 2874–2878.
[37] A. Fürstner, K. Majima, R. Martín, H. Krause, E. Kattnig, R. Goddard, C. W. Lehmann, *J. Am. Chem. Soc.* **2008**, *130*, 1992–2004.

 © 2012 Wiley-VCH Verlag GmbH & Co. KGaA, Weinheim

[38] C. H. Macgillavry, G. D. Rieck (Eds.), *International Tables for X-ray Crystallography*, *Physical and Chemical Tables Vol. III*, **1968**, Kynoch Press, Birmingham, England, p. 276.
[39] R. A. Brown, A. Houlton, R. M. G. Roberts, J. Silver, E. Slade, *J. Chem. Soc., Dalton Trans.* **1993**, 1519–1523.
[40] F. Varret, J. P. Mariot, J. R. Hamon, D. Astruc, *Hyp. Int.* **1988**, *39*, 67–81.
[41] a) D. Herebian, K. Wieghardt, F. Neese, *J. Am. Chem. Soc.* **2003**, *125*, 10997–11005; b) H. Chun, E. Bill, T. Weyhermüller, K. Wieghardt, *Inorg. Chem.* **2003**, *42*, 5612–5620.
[42] M. W. Bouwkamp, A. C. Bowman, E. Lobkovsky, P. J. Chirik, *J. Am. Chem. Soc.* **2006**, *128*, 13340–13341.
[43] S. C. Bart, E. Lobkovsky, P. J. Chirik, *J. Am. Chem. Soc.* **2004**, *126*, 13794–13807.
[44] A. M. Archer, M. W. Bouwkamp, M.-P. Cortez, E. Lobkovsky, P. J. Chirik, *Organometallics* **2006**, *25*, 4269–4278.
[45] S. K. Russell, E. Lobkovsky, P. J. Chirik, *J. Am. Chem. Soc.* **2011**, *133*, 8858–8861.
[46] K. T. Sylvester, P. J. Chirik, *J. Am. Chem. Soc.* **2009**, *131*, 8772–8774.
[47] B. Moreau, J. Y. Wu, T. Ritter, *Org. Lett.* **2009**, *11*, 337–339.
[48] C.-L. Sun, B.-J. Li, Z.-J. Shi, *Chem. Rev.* **2011**, *111*, 1293–1314.
[49] a) J. Norinder, A. Matsumoto, N. Yoshikai, E. Nakamura, *J. Am. Chem. Soc.* **2008**, *130*, 5858–5859; b) N. Yoshikai, A. Matsumoto, J. Norinder, E. Nakamura, *Angew. Chem.* **2009**, *121*, 2969–2972; *Angew. Chem. Int. Ed.* **2009**, *48*, 2925–2928.
[50] For a review article, see: E. Nakamura, N. Yoshikai, *J. Org. Chem.* **2010**, *75*, 6061–6067.
[51] A. Matsumoto, L. Ilies, E. Nakamura, *J. Am. Chem. Soc.* **2011**, *133*, 6557–6559.
[52] J. Y. Wu, B. Moreau, T. Ritter, *J. Am. Chem. Soc.* **2009**, *131*, 12915–12917.
[53] C. C. Lu, E. Bill, T. Weyehermüller, E. Bothe, K. Wieghardt, *J. Am. Chem. Soc.* **2008**, *130*, 3181–3197.
[54] A. M. Tondreau, J. M. Darmon, B. M. Wile, S. K. Floyd, E. Lobkovsky, P. J. Chirik, *Organometallics* **2009**, *28*, 3928–3940.
[55] J. Y. Wu, B. N. Stanzl, T. Ritter, *J. Am. Chem. Soc.* **2010**, *132*, 13214–13216.
[56] E. Derat, S. Cohen, S. Shaik, A. Altun, W. Thiel, *J. Am. Chem. Soc.* **2005**, *127*, 13611–13621.

Received: September 15, 2011
Published Online: December 15, 2011

 © 2012 Wiley-VCH Verlag GmbH & Co. KGaA, Weinheim

DOI: 10.1002/ejic.201100995

Ligand Redox Non-Innocence in Transition-Metal σ-Alkynyl and Related Complexes

Phil A. Schauer[a] and Paul J. Low*[a]

Keywords: Redox chemistry / Radical reactions / Ligand effects / Alkyne ligands / Ruthenium

Transition-metal σ-alkynyl complexes are valuable functional materials that have found application as sructural units in the assembly of polymetallic arrays and large molecular structures, reagents for the transfer, oligomerisation or functionalisation of alkynes, magnetic or optical materials and putative components for use in a future molecular-based electronics platform. Many σ-alkynyl complexes are redox-active, undergoing facile oxidation (reduction) at moderate potentials to generate radical cations (anions) in which the charge and spin density can be tuned from being largely metal-centred to alkynyl ligand-centred by variation of the nature of the metal, supporting ligands and alkynyl substituents. This review summarises the diverse chemical behaviour of metal-supported σ-alkynyl radicals, and some selected closely related systems, which can often be rationalised in terms of the distribution of electron-spin density over the metal–alkynyl scaffold.

1. Introduction

The redox reactions of 18-electron organometallic complexes are often described in terms of formal metal electron counts, with one-electron oxidation or reduction leading to 17- or 19-electron radical species, respectively. In addition, many common reaction mechanisms (e.g., oxidative addition, reductive elimination) are described in terms of formal two-electron redox state changes at a metal centre. The capacity for metal complexes to accommodate such a variable number of electrons has led to interest in these systems as electron reservoirs[1,2] and mono- or multi-electron redox reagents,[3,4] and accounts for the wide-spread application of metal complexes in the catalytic transformations of organic substrates through oxidative or reductive coupling processes.[5–7] Electrochemical activation of metal complexes to promote chemical reactions is also known, but less widely employed as a tool in synthetic chemistry.[8] However, descriptions of redox reactions in terms of a change in the population of metal-centred orbitals are now recognised as being overly simplistic, particularly for those complexes featuring π-donor or -acceptor ligands in which the frontier orbitals that support the unpaired electron have appreciable metal–ligand to ligand character.[9] Thus, in the broadest possible terms, the redox chemistry of transition-metal (organometallic) σ-alkynyl systems $\{L_nM\}$–C≡CR can be interpreted in terms of either changes in the metal oxidation state or the redox ligand non-innocence of the alkynyl ligand (Figure 1). Of course, these descriptions of metal versus ligand redox character are the extremes, and in reality many systems occupy positions across the middle ground of this continuum of electronic structures with electron spin density being distributed to varying degrees over

[a] Department of Chemistry, Durham University, South Rd, Durham, DH1 3LE, UK

Phil A. Schauer (left) obtained his B. Sc. (Hons.) and Ph. D. from the University of Western Australia in 2009 under the supervision of George A. Koutsantonis, investigating the synthesis of heterocycle-functionalised group-VIII allenylidene and σ-alkynyl complexes. On completion of his thesis he spent a year working as a research associate with George A. Koutsantonis and Mark A. Spackman, performing experimental charge-density studies of crown-ether clathrates. In 2010 he joined the group of Paul J. Low at Durham University as a PDRA where he continues to develop his interests in the synthesis and redox properties of organometallic complexes.

Paul J. Low (right) obtained his PhD from the University of Adelaide (1997) with Michael I. Bruce where he began studies of the synthesis and reactions of metal complexes bearing carbon-rich ligands. After postdoctoral work at the Steacie Institute for Molecular Sciences (1997–1999) with Arthur J. Carty he moved to Durham University to take up a Lectureship in Inorganic Chemistry. He was promoted to Reader in 2006 and Professor in 2010. The Low group at Durham follows a research program of considerable breadth and collaborative effort in which spectroscopic tools are chosen and matched with chemical synthesis, molecular structure determination, computational chemistry and surface science to provide an insight into the physical properties of organometallic and organic molecular materials.

© 2012 Wiley-VCH Verlag GmbH & Co. KGaA, Weinheim

the metal and alkynyl moiety. Even within a family of closely structurally related complexes, the relative metal versus alkynyl ligand contributions to the stabilisation of the unpaired electron can be tuned by substituent effects, R,[10–18] as well as the symmetry of the metal d orbitals imposed by the supporting ligands, L_n,[19–21] and the number of electrons available.[22,23]

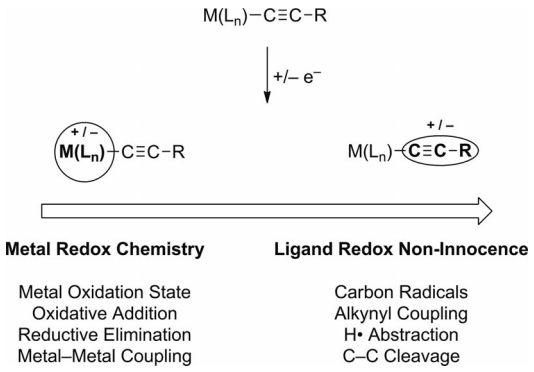

Figure 1. Schematic depiction of potential reactions resulting from redox reactions of transition-metal σ-alkynyl complexes.

In general, the descriptions of the radical products formed from redox reactions of closed-shell precursors requires an additional degree of care as the effects of structural reorganisation (e.g., change in ligand hapticity or other variation in ligand bonding mode) and electronic relaxation in response to a change in the oxidation state of the molecule can lead to reordering of the critical molecular orbitals in the frontier region before and after electron transfer. The strong M–C σ bond usually prevents significant redox-induced structural rearrangement and orbital reordering, which makes comparisons of electronic structure between the closed- and open-shell forms relatively simple and aids rationalisation of the redox-induced chemical transformations of σ-alkynyl complexes that form the subject of this review. However, examples of orbital reorganisation following oxidation are known for σ-alkynyl complexes, and therefore it is prudent to explicitly consider the electronic structure of both partners in a redox pair before describing a redox reaction in terms of metal- or ligand-centred processes.[24]

Previous reviews have addressed various aspects of the redox chemistry of organometallic complexes,[25] including the electronic structures and chemical reactions of 17-electron metal-centred radicals,[26] the ligand-centred reactions of organometallic radicals,[27–29] including the reduction chemistry of unsaturated ligands such as carbenes,[30] and the redox chemistry of complexes bearing vinylidene and higher cumulene ligands.[31] We have been drawn to the chemistry of σ-alkynyl complexes because the π-donor character of the σ-alkynyl ligand, coupled with moderate π-accepting behaviour,[32,33] provides scope for the involvement of the ligand in higher-lying molecular orbitals. In turn, the involvement of the alkynyl π system in stabilising the unpaired electron (or hole) can be conveniently assessed through the variation in the ν(C≡C) frequency as a function of molecular oxidation state.[15,20] Alkynyl complexes therefore offer a platform for the construction of open-shell systems in which the unpaired electron can be tuned across the spectrum of metal-localised to ligand-localised radicals. This variable electronic character, together with the approximately cylindrical distribution of π electron density along the C≡C axis, has also sparked immense interest in the electronic character (mixed valence or otherwise) of radicals derived from bimetallic complexes with alkynyl-bridging ligands.[34] Transition-metal σ-alkynyl complexes have also found application as building blocks for the assembly of larger molecular structures and polymetallic complexes, and as functional materials with redox-switchable magnetic,[35] optical and non-linear optical response.[36,37] In this contribution we survey the nature of the redox processes associated with metal σ-alkynyl complexes and selected closely related systems, with particular emphasis on the chemical consequences of the change in molecular redox state.

2. Metal-Localised Redox Chemistry

Two-electron changes in the formal redox state of the metal centre in σ-alkynyl complexes are critical to many mechanistic interpretations of metal-complex-mediated or -catalysed alkynyl coupling reactions, many of which have found application in synthetically useful procedures.[38] Many aspects of this two-electron redox chemistry have been thoroughly reviewed from the view point of applications in synthetic organic chemistry,[7,39,40] whilst examples of formal two-electron oxidative coupling reactions of alkynyl ligands that take place on polymetallic scaffolds to give diynes and polyynes, including the formation of polyynes that are retained within the metal coordination sphere of mono- and polymetallic systems, have been reviewed elsewhere.[41] In this section we will briefly summarise aspects of this chemistry from the point of view of formal redox state changes at the metal centre as a prelude to discussions of the reactivity derived from the redox non-innocent character of alkynyl ligands that follow.

Some of the oldest examples of metal-mediated C–C coupling reactions of alkynyl moieties, such as the Glaser reaction[42] and its variants (Eglinton, Hay, Cadiot and Chodkiewicz),[43–47] involve a copper-based redox cycle, although precise mechanistic details of these useful alkyne coupling reactions are still a topic of debate. Nevertheless, the Glaser and related reactions are firmly established as key synthetic methodologies for the preparation of 1,3-diynes from terminal alkynes.[47] In the parent (Glaser) reaction, a Cu^{I} alkynyl complex $\{Cu(C{\equiv}CR)\}_n$ is treated with an oxidant, such as molecular oxygen, K_2MnO_4, $K_4Fe(CN)_6$, I_2 or even Cu^{II}, in the presence of base to afford the corresponding 1,3-diyne, RC≡CC≡CR. Closely related reactions that employ stoichiometric $Cu(OAc)_2$ (Eglinton reaction) or catalytic Cu^{I} (Hay reaction) are also known, the latter in particular being a convenient laboratory preparation of 1,3-diynes in good yields.[48] [CAUTION: A report

 © 2012 Wiley-VCH Verlag GmbH & Co. KGaA, Weinheim

has described a serious explosion during the preparation of 1,4-bis(trimethylsilyl)buta-1,3-diyne by the Hay procedure ($CuCl/TMEDA/O_2$), thought due to static discharge igniting the acetone/trimethylsilylacetylene reaction mixture. The precautionary warnings in the *Organic Syntheses* descriptions must be heeded and care taken to eliminate all sources of ignition during reactions involving acetylenes in oxygen atmospheres].[49]

Early mechanistic suggestions for the Glaser reaction implicate Cu^{II} as the oxidant and discount radical mechanisms.[50] More recent DFT calculations concerning the Hay reaction have implicated a bimetallic intermediate with a $[Cu_2(\mu\text{-}O_2)]^{2+}$ core (**1b**; Scheme 1), formed from the reaction of the Cu^{I}–TMEDA/alkyne complex (**1a**) with O_2, which implies a formal oxidation of Cu^{I} to Cu^{III}. Rearrangement via mononuclear **1c** followed by reductive elimination of the diyne gives two mononuclear Cu^{II} centres (**1d**). Complex **1d** enters into a second cycle of alkyne/acetylide addition, dimerisation and reductive elimination to give a second molecule of the diyne and restore the catalyst to the Cu^{II} state (**1d**).[51] This bimetallic process, which shuffles the copper between the $Cu^{I/III}$ states with an oxygen-derived aqua/hydroxy co-ligand, accounts for many of the otherwise disconcerting aspects of descriptions of the Hay process that are based on a simple mono-metallic Cu^{I} centre and O_2 as an innocent oxidant. Recent variants to the Glaser, Hay and Eglinton procedures include the use of catalytic $CuCl_2$/DBU (a combination that favours disproportionation to Cu^{I}),[52] $CuCl_2/NEt_3$[53] and a system catalytic in $Cu(OAc)_2$ in the presence of piperidine.[54] A variety of other metals have also been developed as catalyst systems, including systems based on Ti[55] and Co.[56]

Other examples of alkyne coupling reactions mediated by changes in the metal oxidation state include the Sonogashira reaction[57,58] and the interception of the Pd^{II}/Pd^{0} cycle as a route to the facile formation of diynes,[59–61] which can be extended to a palladium-catalysed version of the Cadiot–Chodkiewicz (hetero) cross-coupling reaction of terminal and halo alkynes.[62] It has been noted that in the palladium-mediated homocoupling of alkynes, the kinetic profile of the reaction (zero order in alkyne) is consistent with the $Pd^{0/II}$ reoxidation step being rate determining.[59] Cu^{II} is known to accelerate the oxidation of Pd^{0} to Pd^{II} by oxygen, which prompted Marder and Fairlamb to suggest a dual role of the copper species in aiding both alkynyl ligand transmetallation to Pd^{II} and the reoxidation of Pd^{0} (Scheme 2).[60] Similar observations of the efficacy of mixed Pd/Cu catalysts in alkyne homocoupling have been reported elsewhere.[63–69] Other mixed-metal catalyst systems for the oxidative homo- and heterocoupling of alkynes have been reported recently, including $[Fe(acac)_3]/[Cu(acac)_2]$[70] and an unusual Cu/Ni system in which Cu plays a role as a templating group for the assembly of the active nickel bis(alkynyl) moiety (Scheme 3),[71] $NiCl_2$/CuI has also been shown to be an effective catalyst for the cross-coupling of alkynes to give substituted 1,3-diynes in a modification of

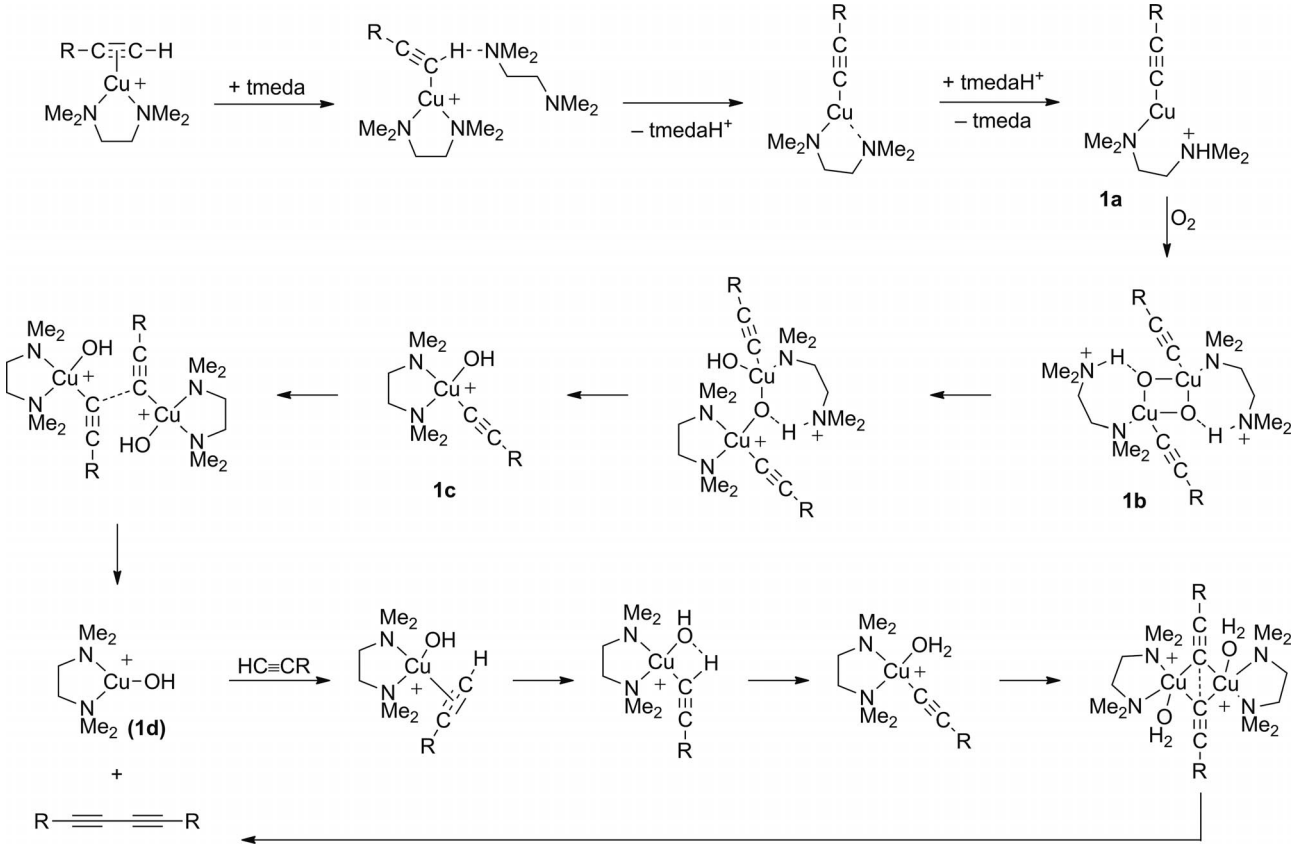

Scheme 1. Key mechanistic steps in the Glaser reaction, as determined by DFT studies.[51]

 © 2012 Wiley-VCH Verlag GmbH & Co. KGaA, Weinheim

the Hay process, which can also be tuned to give acceptable yields of hetero-cross-coupled products.[72] Mixed Pd^{II}/Au^{I} catalysts to effect the cross-coupling of aryl iodides with terminal alkynes have been described by Laguna and co-workers, although the rates of reaction are slower than with a copper(I) co-catalyst,[73] with further complications arising from the use of 2 equiv. of Au^{I} to regenerate Pd^{II} from Pd^{0}.[74] Pre-formed Au^{I} alkynyl complexes can be used to introduce alkynyl fragments into the $Pd^{II/0}$ cycle, although in toluene the reaction conditions are quite forcing (130 °C, 16–24 h).[75]

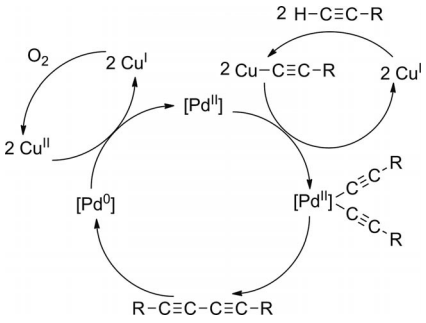

Scheme 2. Role of $Cu^{I/II}$ in aiding both the transmetallation and reoxidation of $Pd^{0/II}$ in alkyne homocoupling.

Examples of potentially useful trimetallic systems in which gold alkynyls or mono- or bis-gold diyn(di)yls are cross-coupled with aryl or alkynyl halides or halo-carbynes by the Sonogashira Pd/Cu catalyst system have recently been described.[76–78] In this case, the gold serves as a transmetallation agent, and the use of a pre-formed Au^{I} complex permits the transfer of the alkynyl or diynediyl species to Pd^{II} under mild conditions.[79] In this manner, differentially substituted 1,3-diynes can be prepared by the sequential cross-coupling of each Au-alkynyl moiety in $Ph_3PAuC{\equiv}CC{\equiv}CAuPPh_3$ (Scheme 4); similar Au-mediated transmetallation chemistry has been used in conjunction with Pd/Cu cycles in the synthesis of metal complexes featuring polyyn(di)yl ligands of considerable length.[80–83] In these cases, the Au^{I} reagent is redox innocent, serving to mediate the introduction of the alkynyl moiety to the Pd/Cu catalyst system, the $Pd^{II/0}$ redox cycle being the critical factor. Recently, examples in which an unusual $Au^{I/III}$ redox couple is used to mediate alkynyl cross-coupling chemistry have been reported, with an external oxidant being neces-

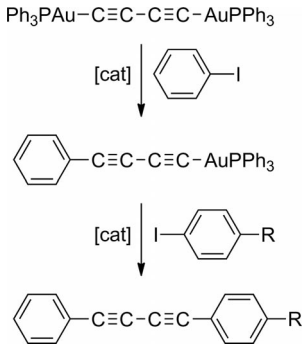

Scheme 4. Au^{I}-mediated sequential cross-coupling reaction to form asymmetric 1,3-diynyl products {[cat] = $[PdCl_2(PPh_3)_2/CuI]$}.

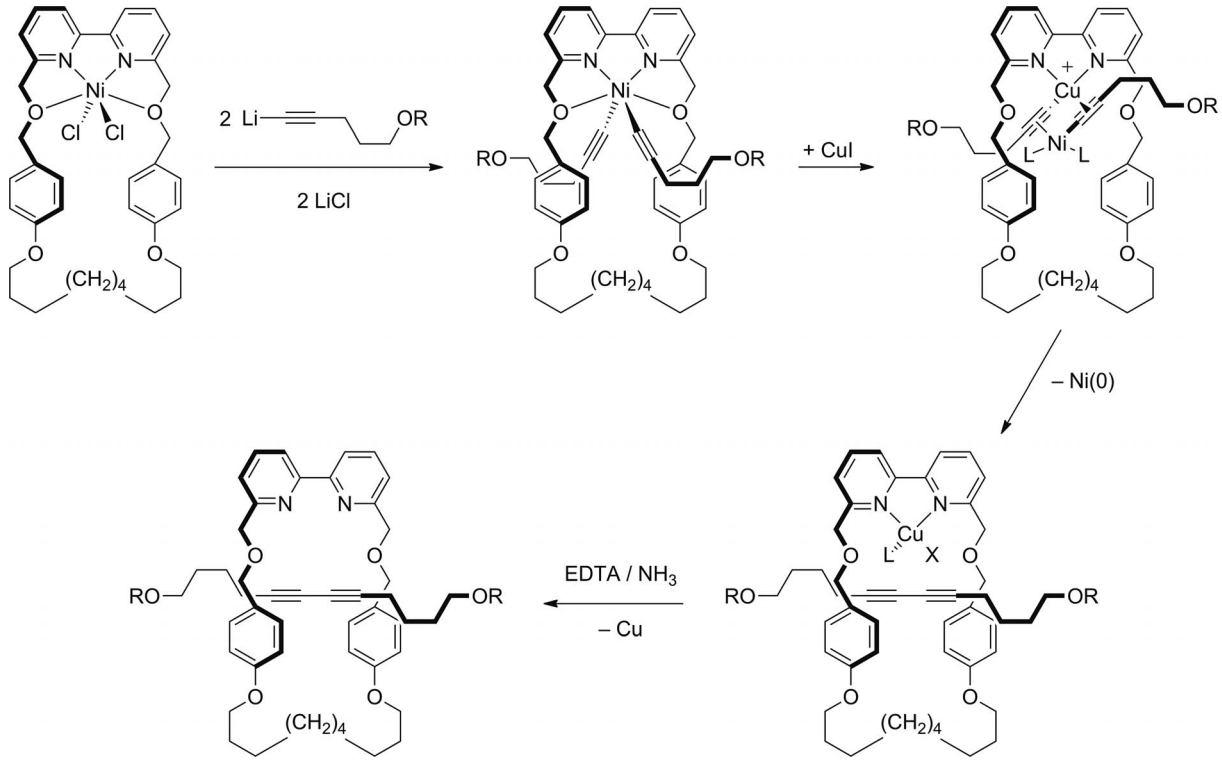

Scheme 3. An unusual Cu-templated/Ni-catalysed alkyne cross-coupling reaction (L = thf, dme).

 © 2012 Wiley-VCH Verlag GmbH & Co. KGaA, Weinheim

sary to complete the cycle by regenerating an active Au^{III} species from the Au^{I} formed together with the coupling product by the key reductive elimination step.[84,85]

One-electron metal-centred redox chemistry of alkynyl complexes is also known, although the reaction pathways are distinct from the two-electron oxidative addition/reductive elimination steps that govern the alkynyl coupling processes noted above. In cases in which one-electron transfer leads to metal-centred radicals, particularly those in which the metal centre is afforded minimal steric protection, the formation of new metal–metal bonds rather than carbon–carbon bonds can be observed. For example, the one-electron oxidation of Li[W(C≡CR)(CO)(NO)Cp] (R = Ph, *t*Bu, $SiMe_3$; **2**, Scheme 5) with $[FeCp_2]BF_4$ at low temperature leads to the formation of bimetallic μ-σ,π-alkynyl complexes **4**, presumably via the M–M coupled intermediate **3** and subsequent loss of the carbonyl ligands.[86] The validity of **3** as the intermediate is affirmed by the notable absence of any products corresponding to an M–C_β or C_β–C_β coupled product, which would point towards more substantial delocalisation of the electron spin density on the alkynyl ligand.

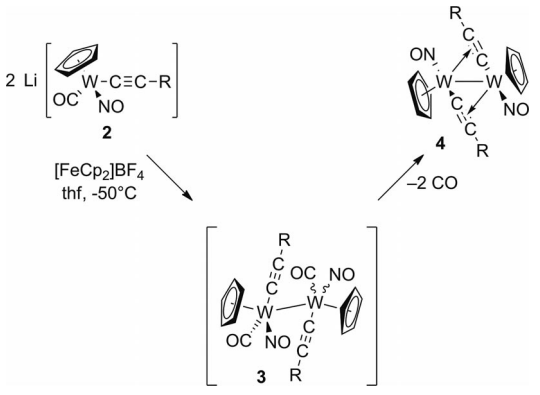

Scheme 5. M–M coupling on one-electron oxidation of the tungsten σ-alkynyl complexes **2** (R = Ph, *t*Bu, $SiMe_3$).

In contrast, thermolysis of [Mo(C≡CR)$(CO)_3$Cp] (**5**) affords the μ-η^2-diyne complex [{Mo$(CO)_2$Cp}$_2$(μ-η^2-$RC_2C{\equiv}CR$)] (**6**, R = $SiMe_3$, Ph, C_6H_4F-4); cross-over experiments with mixtures of the R = Ph and R = C_6H_4F-4 mononuclear precursors give mixtures of both homocoupled products together with both isomers of the cross-coupled product.[87,88] These reactions involve the formal reduction of the two metal centres from Mo^{II} in **5** to Mo^{I} in the bimetallic product **6**, with concomitant oxidative coupling of the two alkynyl ligands to a 1,3-diyne (Scheme 6). Analogous chemistry with [Cr(C≡CPh)$(CO)_3$Cp] is also known,[87] although the product diynyl complex is thermally sensitive. In the case of [W(C≡C$SiMe_3$)$(CO)_3$Cp], thermolysis in the presence of {W$(CO)_3$Cp}$_2$ gave the C–C coupled product [{$W_2(CO)_4Cp_2$}$_2$(μ-η^2:μ-η^2-$Me_3SiC_2C_2SiMe_3$)]. Under more extreme conditions, the reaction proceeds to give metal carbides and small amounts of metal(0).[89] Clearly, the supporting ligand sets in the intermediates described in Schemes 5 and 6 [(NO) + e^- vs. $(CO)_2$] play a decisive role in determining the reactions along the M–M coupling route versus M–M/C–C pathways. Similar metal-reduction/alkynyl ligand oxidative-coupling electron redistribution reactions that result in the formation of the free 1,3-diyne are known to occur following the thermolysis of [Fe(C≡C$SiMe_3$)$(CO)_2$Cp] or [{Fe$(CO)_2$Cp}(μ-η^1,η^2-(C_2SiMe_3){$Co_2(CO)_6$}})] to give [$Fe_2(CO)_4Cp_2$] and either $Me_3SiC{\equiv}CC{\equiv}CSiMe_3$ or [{$Co_2(CO)_6$}$_2$(μ-η^2,η^2-$Me_3SiC_2C_2SiMe_3$)], respectively.[90]

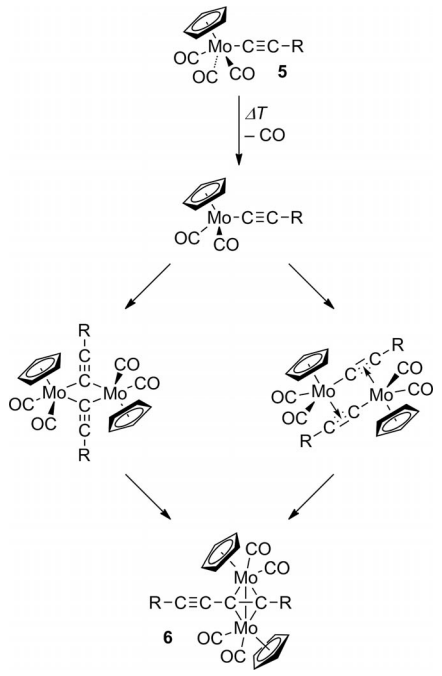

Scheme 6. Thermolysis of molybdenum(II) σ-alkynyl complexes.

Quite remarkably, the alkynyl and diynyl ligands in the tungsten complexes [W(C≡CR)$(CO)_3$Cp*] (R = Ph, CH_2OMe, *n*Pr),[91] [W(C≡CC≡CH)$(CO)_3$Cp*] and [{W$(CO)_3$Cp*}$_2$(μ-C≡CC≡C)][92] are sufficiently stable to survive treatment with H_2O_2/H_2SO_4 to give the oxo-peroxo derivatives [W(C≡CR)(O)(O_2)Cp*], which subsequently react with PPh_3 to undergo oxygen abstraction and yield the corresponding bis(oxo) derivatives (Scheme 7). This chemical oxidation from W^{II} to W^{VI} is accompanied by an increased decoupling of the metal and alkynyl orbitals; as a consequence, the HOMO in these systems is essentially alkynyl-centred and well-removed from the low-lying W^{VI} d orbitals.[93]

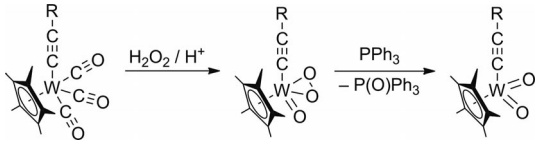

Scheme 7. Oxidation and subsequent oxygen abstraction to form bis(oxo)tungsten(VI) σ-alkynyl complexes.

 © 2012 Wiley-VCH Verlag GmbH & Co. KGaA, Weinheim

3. Ligand Redox Non-Innocence and Subsequent Chemistry

Ligand redox non-innocence in alkynyl complexes has been evidenced in a wide variety of studies, ranging from the direct spectroscopic demonstration of radical character in the alkynyl ligand following a redox reaction in cases in which the redox product is sufficiently stable to be observed, to the identification of products arising from chemical reactions following initial, ligand-based electrochemical processes (i.e. electrochemical–chemical (EC) processes). These latter chemical reactions of ligand-based radicals can in turn be considered either as "nuisances" responsible for the chemical irreversibility of electrochemical processes or as useful tools in synthetic strategies.

3.1. Chemical Reactions of π-Alkyne-Based Radicals

In an early example of redox non-innocence in a metal alkyne complex, one-electron oxidation of the anion derived from the deprotonation of $[Co_2(\mu\text{-}Me_3SiC_2H)(CO)_6]$ (estimated to have an oxidation potential of +0.58 V versus SCE in thf) gave $[\{Co_2(CO)_6\}(\mu\text{-}Me_3SiC_2C{\equiv}CSiMe_3)]$ and $[\{Co_2(CO)_6\}_2(\mu\text{-}Me_3SiC_2C_2SiMe_3)]$.[94] Similar oxidative coupling of "$\{Co_2(CO)_6\}_2(\mu\text{-}\eta^2,\eta^2\text{-}Me_3SiC_2C_2Li)$" gave $[\{Co_2(CO)_6\}_3(\mu\text{-}\eta^2,\eta^2,\eta^2\text{-}Me_3SiC_2C_2C{\equiv}CC_2SiMe_3)]$ in low yield. In both cases, extrusion of a Co_2 fragment appears driven by steric factors. The reaction of $[M(C{\equiv}CPh)(PPh_3)]$ (M = Ag, Au) or $[Hg(C{\equiv}CPh)_2]$ with $[Co_2(CO)_8]$ is thought to give initially the expected alkyne complex $[\{Co_2(CO)_6\}\{\mu\text{-}PhC_2ML\}]$ (L = PPh_3, C≡CPh), which converts by an unspecified mechanism into the C–C oxidatively coupled product $[\{Co_2(CO)_6\}_2(\mu\text{-}PhC_2C_2Ph)]$.[95] Similarly, reactions of 1-iodo-2-ferrocenylacetylene (FcC≡CI) with excess $[Co_2(CO)_8]$ give $[\{Co_2(CO)_6\}_2(\mu\text{-}FcC_2C_2Fc)]$, presumably accompanied by the formation of I_2.[96] Further examples of the chemistry involving the coupling of σ-alkynyl ligands with concomitant aggregation of metal fragments have been comprehensively reviewed elsewhere.[41]

3.2. Chemical Reactions of σ-Alkynyl-Based Radicals and Closely Related Systems

One of the most elementary reactions of an organic radical, Y˙, is the abstraction of a hydrogen atom from the reaction environment to give a closed-shell hydrocarbon Y–H. Even in the case of metal alkynyl complexes, $[M(C{\equiv}CR)L_n]$, in which there is substantial evidence of "metal-centred" radical character in oxidised derivatives, similar hydrogen-abstraction processes are often found to occur, especially at room temperature, to give the analogous vinylidene $[M\{{=}C{=}C(H)R\}L_n]^+$, with clear evidence of a degree of radical character at the alkynyl C_β carbon (Scheme 8). This hydrogen-abstraction pathway, leading to the conversion of an alkynyl radical into a vinylidene, is in competition with C_β–C_β homocoupling, which is also a common reaction for organic radicals, affording in the case of alkynyl derivatives a bis(vinylidene).[29,31]

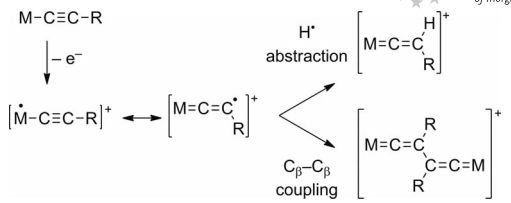

Scheme 8. General schematic of radical-coupling reactions observed upon oxidation of 18-electron σ-alkynyl complexes.

A meticulous study of the oxidation of *trans*-$[Ru\{C{\equiv}CC(H)R_2\}Cl(dppe)_2]$ (**7-R**) and the isotopologues *trans*-$[Ru\{C{\equiv}CC(D)R_2\}Cl(dppe)_2]$ (**7D-R**, R = H, Me, Ph) has revealed some of the mechanistic factors affecting the reactivity of alkynyl complex radicals, specifically regarding the nature of hydrogen abstraction from the environment.[97] The oxidation of *trans*-$[Ru\{C{\equiv}CC(H)Ph_2\}Cl(dppe)_2]$ (**7-Ph**) with $[FeCp_2]PF_6$ rapidly affords a 1:1 mixture of the vinylidene (**8-Ph**) and allenylidene (**9-Ph**) complexes (Scheme 9). In contrast, the oxidation of *trans*-$[Ru\{C{\equiv}CC(H)Me_2\}Cl(dppe)_2]$ (**7-Me**) with $[FeCp_2]PF_6$ affords only a slow and minimal conversion into the corresponding vinylidene complex **8-Me**. The reaction of **7-Me** with $[FeCp_2]PF_6$ followed by the addition of $[CoCp_2]$ after 1 hour [for which $E°$(cobaltocene) is sufficient to reduce the redox-generated alkynyl radical cation, although not the derived vinylidene complexes] yields a 95:5 mixture of **7-Me** and **8-Me**.

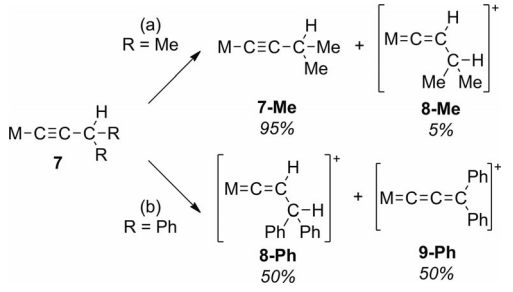

Scheme 9. Redox chemistry of the C_γ-unsaturated σ-alkynyl complexes {M = *trans*-$[RuCl(dppe)_2]$; (a) $[FeCp_2]PF_6$, 1 h; $[CoCp_2]$; (b) $[FeCp_2]PF_6$}.

To further understand the different products observed, identical reactions were performed with the isotopologues *trans*-$[Ru\{C{\equiv}CC(D)R_2\}Cl(dppe)_2]$ (**7D**). The oxidation of *trans*-$[Ru\{C{\equiv}CC(D)Ph_2\}Cl(dppe)_2]$ (**7D-Ph**) yields a 1:1 mixture of the allenylidene **9-Ph** and the doubly deuteriated vinylidene **8DD-Ph**, which implies an intermolecular reaction of the oxidised cation. The reaction of **7D-Me** or **7D-H** with $[FeCp_2]PF_6$ followed by $[CoCp_2]$ again yields a mixture of the starting alkynyl **7D** in addition to a small percentage of the mono-deuteriated vinylidene **8HD**, which clearly implies a mechanism different to that observed in the phenyl-functionalised derivative. These results are interpreted according to Scheme 10, in which the redox-generated cationic radical $[\mathbf{7D\text{-}Ph}]^{\cdot+}$ undergoes intermolecular proton transfer to the neutral complex **7D-Ph** to form the vinylidene **8DD-Ph**, concomitantly forming the stable neu-

 © 2012 Wiley-VCH Verlag GmbH & Co. KGaA, Weinheim

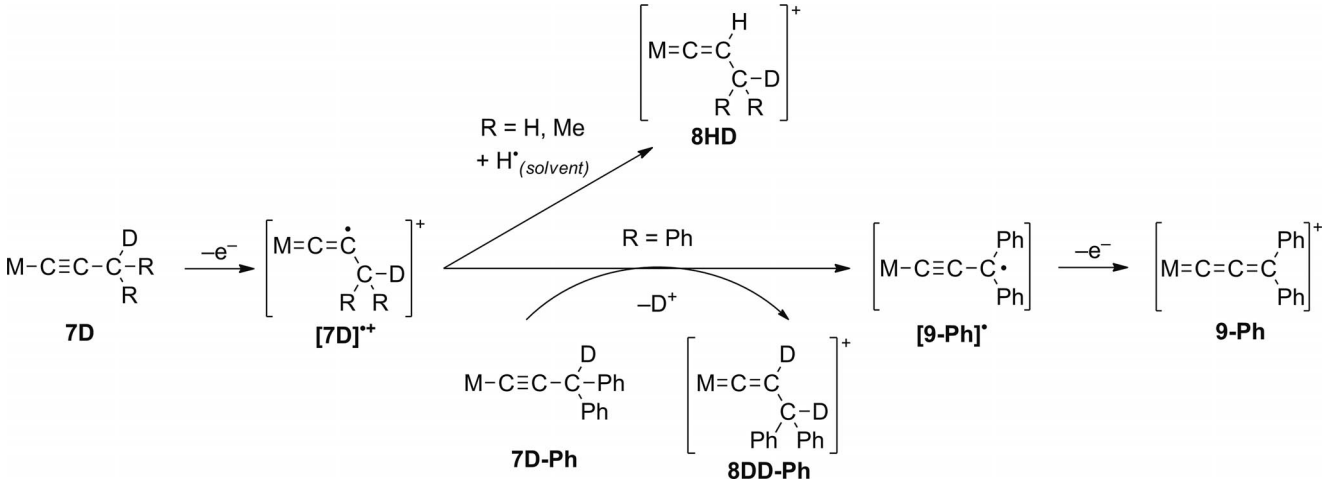

Scheme 10. Various products resulting from the one- and two-electron oxidation of deuteriated ruthenium complexes {[M] = *trans*-[RuCl(dppe)$_2$]}.

tral radical [**9-Ph**]$^{\bullet}$, which is further oxidised to the allenylidene **9-Ph**. The neutral radical [**9-Ph**]$^{\bullet}$ is stabilised by spin delocalisation on to the phenyl rings, whereas in the methylated derivative such spin delocalisation is not possible and therefore the radical cation [**7D-Me**]$^{\bullet+}$ is stabilised relative to [**9-Me**]$^{\bullet}$, although nevertheless [**7D-Me**]$^{\bullet+}$ is a sufficiently reactive radical cation to abstract hydrogen from the reaction medium to form the vinylidene complex **8HD-Me**. Interestingly, these results are also supported by the inverse reaction, that is, the reduction of an allenylidene complex in which the reaction of *trans*-[Ru(=C=C=CR$_2$)Cl(dppe)$_2$]-PF$_6$ (R = Me, Ph) with [CoCp$_2$] and subsequent trapping of the radical intermediate with Ph$_3$SnH yields the C$_\gamma$-substituted alkynyl analogue *trans*-[Ru{C≡CC(H)R$_2$}-Cl(dppe)$_2$].[98] The oxidation of [Ru{C≡CC(H)-Ph$_2$}(=C=C=CPh$_2$)(dppe)$_2$]$^+$ with Ce^{IV} in the presence of KB(C$_6$F$_5$)$_4$ also served as the first synthetically facile means to accessing a bis(allenylidene)ruthenium complex.[99]

Vinylidene complexes M(C=CR$_2$)L$_n$ are also redox-active in their own right, with examples of both reduction and oxidation being known. The reduction of vinylidene complexes is favoured at the C$_\alpha$ carbene carbon, even in the presence of strongly electron-withdrawing substituents on the C$_\beta$R$_2$ fragment,[100] giving rise to C-localised radicals that can have significant chemical stability due to the steric protection afforded by the L$_n$M fragment. In addition to these steric considerations, the chemistry of oxidised derivatives of vinylidene complexes is directed by the various resonance forms of the resulting radical, which can be stabilised by the supporting metal fragment. For example, deprotonation of the carbyne complex [Mo(≡CCH$_2$*t*Bu){P(OMe)$_3$}$_2$Cp] (**10**) yields the anionic vinylidene [Mo{C=C(H)*t*Bu}{P(OMe)$_3$}Cp]$^-$ (**11a**), which may also be represented by a carbyne form (**11b**). Subsequent oxidation of **11** by [FeCp$_2$]BF$_4$ or CuI results in the formation of the bis(carbyne) complex **12**, which was isolated as both the

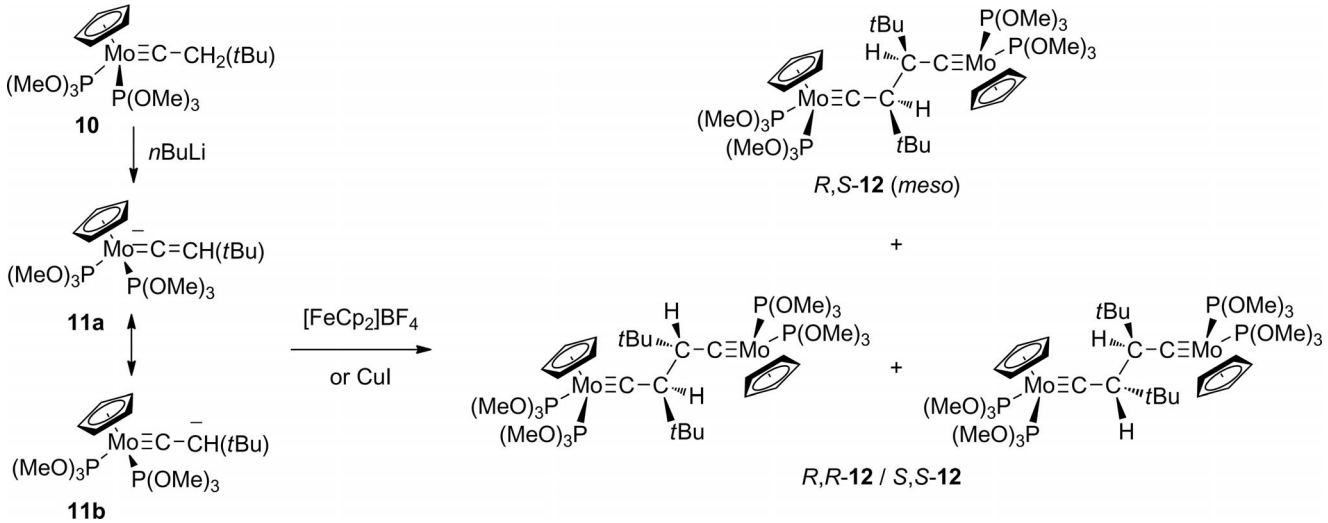

Scheme 11. C$_\beta$–C$_\beta$ coupling resulting from the oxidation of the anionic molybdenum complex **11**.

 © 2012 Wiley-VCH Verlag GmbH & Co. KGaA, Weinheim

meso compound and the diastereomeric pair (Scheme 11).[101]

A particularly well-explored aspect of C–C coupling reactions in redox-generated organometallic radicals relates to the oxidation chemistry of the manganese vinylidene complexes depicted in Scheme 12.[102,103] The reaction of the vinylidene complex **13** with $[FeCp_2]PF_6$ at room temperature affords varying mixtures of the bis(carbyne) complexes **14** and **17**. The reaction proceeds by the initial oxidation of the vinylidene to give the radical cation $[\mathbf{13}]^{\bullet+}$, which may then undergo immediate C_β–C_β coupling to afford complex **14**. This process results in almost quantitative conversion of the mononuclear vinylidene **13** into the bis(carbyne) **14** for complexes with R = H or Me. In those cases in which the terminal vinylidene substituent is more readily able to stabilise the vinylidene radical cation $[\mathbf{13}]^{\bullet+}$, the kinetics of the reaction are decreased to such an extent that an alternate reaction pathway becomes favourable. In those cases in which accumulation of the vinylidene radical is possible, a proton-transfer reaction with the parent vinylidene **13** results in the formation of carbyne **15** and alkynyl radical cation **16**, the latter undergoing C_β–C_β coupling to afford the alternate bis(carbyne) complex **17**. The role of the terminal vinylidene substituent in determining the susceptibility to dimerisation and the formation of complexes **14** has been explored by DFT calculations, which support the experimentally observed trend of R = H > Me > Ph ≈ C_6H_4Me > Si(*t*Bu)Me_2. Of note is the fact that the reactions of complexes **14** with $[Co(Cp^*)_2]$ often result in quantitative conversion back to the vinylidene **13**, this redox reversibility again following the DFT-determined trends described above and leading to the description of such systems as electron reservoirs.

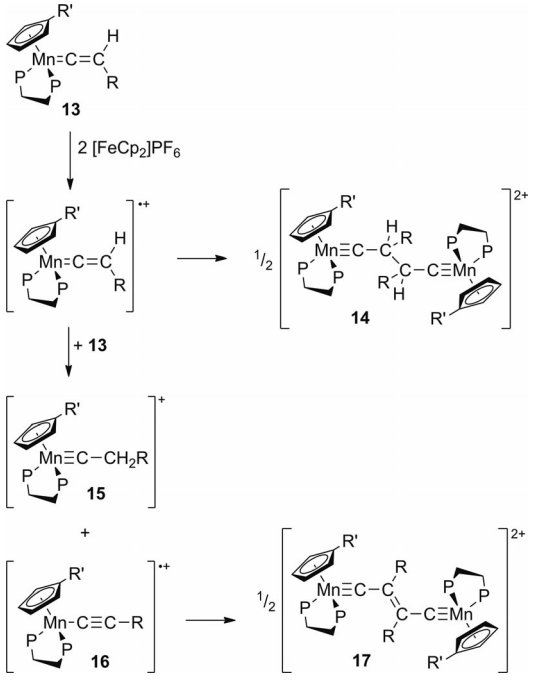

Scheme 12. Oxidation of Mn^I vinylidene complexes, resulting in the formation of mono- and bimetallic carbyne complexes ($\widehat{PP}$ = dmpe, depe; R′ = H, Me; R = H, Ph, C_6H_4Me-4, C_4H_3S-3; not all combinations).

The carbonyl complexes $[Mn\{C{=}C(H)Ph\}(CO)(L)Cp']$ (Cp′ = Cp, L = CO, PPh_3; Cp′ = Cp*, L = CO) behave similarly. In the case of the dicarbonyl complex $[Mn\{C{=}C(H)Ph\}(CO)_2Cp]$, the oxidation and subsequent loss of H· results in the formation of the 16-electron alkynyl radical cation $[Mn(C{\equiv}CPh)(CO)_2Cp']^+$. Coupling in the usual C_β–C_β fashion gives the bis(carbyne) $[Cp'(CO)_2Mn{\equiv}C–C(Ph){=}C(Ph)–C{\equiv}Mn(CO)_2Cp']^{2+}$, which in turn can be reversibly reduced to the neutral bis(vinylidene).[104] The oxidative dehydrodimerisation of the more electron-rich systems featuring L = PPh_3 or Cp′ = Cp* supporting ligands proceeds by a sequence of oxidation and C_β–C_β coupling to give a species closely related to **14** with subsequent proton loss resulting in the formation of a neutral bis(vinylidene) $[Cp'(CO)(L)Mn{=}C{=}C(Ph)–C(Ph){=}CMn(CO)(L)Cp']$.[105] In turn, the neutral bis(vinylidene) can be reversibly oxidised by two electrons to give a dication, best formulated as a bis(carbyne) similar to **17**. The reactivity of the μ-C_4Ph_2 ligand can be switched by these redox processes, with the neutral bis(vinylidene) system being inert towards oxygen nucleophiles (H_2O, OH^-) whereas the dicationic bis(carbyne) is readily converted into furan derivatives upon reaction with H_2O or OH^-.[106]

In an interesting counterpoint, reduction of the group 6 alkynyl complexes $[M(C{\equiv}CPh)(CO)_3Cp']$ either chemically (Na/K, M = Cr, Cp′ = Cp) or electrochemically (M = Cr, Cp′ = Cp; M = Mo, W, Cp′ = Cp*) also affords bis(carbyne) complexes $[Cp'(CO)_2M{\equiv}C–C(Ph){=}C(Ph)–C{\equiv}M(CO)_2Cp']$, albeit in very low yields for the Mo and W examples, and is thought to occur by the sequence of reduction, CO elimination, C_β–C_β coupling and oxidation shown in Scheme 13.[107,108] The bis(carbyne) product undergoes two reversible reduction processes, separated by around 140 mV, although the electronic characteristics of the intermediate mono-anion have not been investigated in detail.

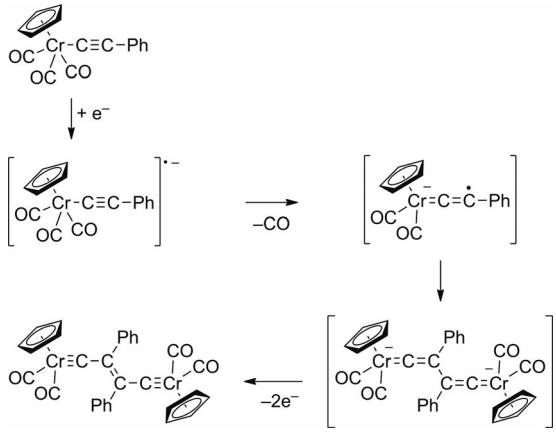

Scheme 13. Reductive coupling of chromium(II) σ-alkynyl to afford the alkenyl bis(carbyne).

 © 2012 Wiley-VCH Verlag GmbH & Co. KGaA, Weinheim

Depending on the nature of the L_nM fragment, the oxidation of a vinylidene may also result in the loss of a proton, thereby yielding an alkynyl radical; similar chemistry has been shown to take place following oxidation of the metal-substituted butatrienylidene [Cp*(dppe)Fe{C=C=C=C(H)}Fe(CO)$_2$Cp*]$^+$. Although H$^\cdot$ abstraction may regenerate the parent vinylidene, the alkynyl radical is also susceptible to C_β–C_β coupling reactions, which result in the formation of bis(vinylidene) products. This chemistry was first noted by Iyer and Selegue following treatment of [Fe{C=C(H)R}(dppe)Cp]BF_4 with iodosobenzene (R = Me) or Cu(OAc)$_2$ (R = Me, Ph) at room temperature.[109] Crystallisation of the resulting reaction mixture afforded [{Fe(dppe)Cp}$_2${μ-C=C(R)–C(R)=C}][BF_4]$_2$ in good yield (R = Me, 77%; Ph, unspecified). Early attempts to convert the related alkynyl complexes [Fe(C≡CR)(dppe)Cp] into the bis(vinylidene) by chemical (Cu^{II} or Ag^I,[109] and later ferrocenium[110]) or anodic oxidation[109] were unsuccessful, although it was ultimately demonstrated that accumulation of alkynyl radical cations by chemical oxidation at low temperatures can lead to more effective C–C coupling.[111] Alkynyl radical coupling to form bis(vinylidene) species generally occurs in competition with the hydrogen-abstraction pathway, and the relative extent of dimerisation versus hydrogen abstraction is subject to thermodynamic and/or kinetic (steric) factors.[112]

These competing pathways of oxidation, hydrogen atom abstraction and C_β–C_β coupling are clearly illustrated in the behaviour of complexes [Mo(C≡CR)(dppe)(η^7-C_7H_7)] (**18**, R = Ph, *n*Bu, *t*Bu) described by Whiteley and co-workers. Chemical oxidation ([$FeCp_2$]PF_6) of the *n*-butyl derivative affords the 17-electron radical **19-*n*Bu** as only a transient species prior to the rapid formation of the dimeric product **20-*n*Bu** (Scheme 14). In contrast, the radical cation **19-Ph** has been isolated and structurally characterised, although prolonged stirring in tetrahydrofuran affords the dimerised product **20-Ph**. The sterically demanding analogue **19-*t*Bu** does not dimerise, but instead affords the cationic vinylidene **21** upon prolonged stirring.[113,114] The lack of dimerisation exhibited in the *tert*-butyl-functionalised derivative is logically attributable to steric hindrance at the C_β atom of the alkynyl radical, whereas the slow reaction is a consequence of the significant d_{z^2} character of the β-LUSO) (lowest unoccupied spin orbital) in [Mo(C≡CC_6H_5)(dppe)(η^7-C_7H_7)]$^+$, which offers a poor symmetry match with the alkynyl π orbitals and thereby limits the concentration of spin density on the alkynyl moiety (see below).[20]

Similar observations have been made for the series of complexes [Fe(C≡CR)(dppe)Cp*]; the C≡CH acetylide complex dimerises on low-temperature oxidation[112] whereas the *tert*-butyl, phenyl and a range of other substituted arylalkynyl complexes form stable, isolable radical cations.[11,13,14,16,17,115–119] Very recently this work has been extended by Paul and co-workers to demonstrations of the substantial accumulation of spin density at the ligand γ atom in isolable radicals [Fe(L)(dppe)Cp*]$^+$ (L = N_3, NCS), which bodes well for the use of such complexes as metalloligands in the assembly of larger, redox-active polymetallic complexes.[120]

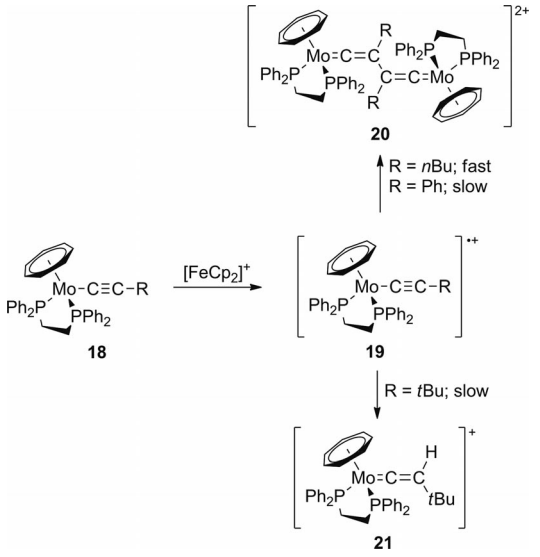

Scheme 14. Differing reactivities of the radical cations **19** depending upon the terminal alkynyl substituent.

The reactions of analogous complexes [M(C≡CR)(PP)Cp] with potential oxidising agents such as tropylium [M = Fe, Ru, Os; R = Ph, PP = (PPh_3)$_2$, dppm, dppe; not all combinations],[121,122] diazobenzene [M = Ru, R = Ph, PP = (PPh_3)$_2$, dppe][121] or halogens [R = Ph, PP = (PPh_3)$_2$][123,124] gave products resulting from the electrophilic addition to C_β rather than one-electron oxidation. However, the treatment of the parent acetylide complex [Ru(C≡CH)(PPh_3)$_2$Cp] with [C_7H_7]$^+$ or MeI gave green solutions thought to contain the coupled product [{Ru(PPh_3)$_2$Cp}$_2${μ-C=C(H)–C(H)=C}]$^{2+}$ on the basis of mass spectrometric data.[125] The more facile coupling of the ethynyl complex is consistent with the steric factors described for the [Mo(dppe)(η^7-C_7H_7)] and [Fe(dppe)Cp*] systems above.

The reaction of [Ru(C≡CPh){P(OMe$_3$)}$_2$Cp] with [Cu(NCMe)$_4$]PF_6 in methanol gave the π complex [Ru(C≡CPh){P(OMe)$_3$}$_2$Cp]$_2$$CuPF_6$ together with small amounts of a complex formulated as the bis(vinylidene) [(Ru{P(OMe)$_3$}$_2$Cp)$_2${μ-C=C(Ph)–C(Ph)=C}]$^{2+}$ arising from the oxidation of either the alkynyl complex or traces of the vinylidene contained in the alkynyl precursor.[126] More control over the coordination versus oxidation pathways could be achieved in reactions with Ag^I, given the sensitivity of the $Ag^{I/0}$ couple to solvation factors.[3] Thus, the 1:2 reaction of $AgPF_6$ with [Ru(C≡CPh)(PPh_3)$_2$Cp] (**22**) in toluene at 0 °C gave yellow, π-coordinated **23** (Scheme 15).[127] However, when the reaction was conducted with 1:1 stoichiometry in toluene/CH_2Cl_2, Ag^I serves as an oxidant, leading to the formation of a bimetallic complex initially formulated as **24** in high yield (82%).[127] However, very recent results suggest that the coupled products derived from phenylethynylene radicals may have an alternative structure.[128] Cyclic voltammetry

 © 2012 Wiley-VCH Verlag GmbH & Co. KGaA, Weinheim

experiments show that [Ru(C≡CPh)(PPh$_3$)$_2$Cp] undergoes two anodic redox processes, the first poorly chemically reversible and the second essentially irreversible under standard conditions, with variations in scan rate, temperature and alkynyl substituents pointing towards an EC mechanism dominating the first redox event and thereby inhibiting chemical reversibility.[18] Bruce et al. have reported a careful study of the products formed from the oxidation of [Ru(C≡CPh)(PPh$_3$)$_2$Cp] and [Ru(C≡CC$_6$H$_4$Me-4)(PPh$_3$)$_2$Cp], which evidences the accumulation of radical character in the arylalkynyl ligand.[128] Treatment of **22** with a slightly sub-stoichiometric quantity of [FeCp$_2$]PF$_6$ resulted in the formation of the highly reactive radical cation [Ru(C≡CPh)(PPh$_3$)$_2$Cp]$^{\cdot+}$, which, rather than coupling in the usual C$_\beta$–C$_\beta$ fashion, presumably on steric grounds, coupled through C$_\beta$ of one radical and the *para*-phenyl carbon of the alkynyl substituent in another. The proton liberated on re-aromatisation of the phenylene ring is transferred to the basic acetylide moiety to give an unusual bis(vinylidene) product (**25**; Scheme 16). Deprotonation of this vinylidene ligand proceeds as expected, yielding the alkynyl-vinylidene complex **26**, and addition of acid regenerates **25** in a reversible process. Clearly, the alkynyl radical [Ru(C≡CPh)(PPh$_3$)$_2$Cp]$^{\cdot+}$ exhibits concentrations of spin density at both C$_\beta$ and the *para* position of the arylalkynyl ligand, an assertion in keeping with DFT calculations of the spin-density distribution (C$_\beta$ +0.27, C$_{para}$ +0.13). When the *para* position was blocked, as in [Ru(C≡CC$_6$H$_4$Me-4)(PPh$_3$)$_2$Cp], intermolecular coupling took place between C$_\beta$ and the cyclopentadienyl ring, with the liberated proton being transferred to the remaining alkynyl moiety to yield a bis(vinylidene) complex (**27**; Scheme 16). Although deprotonation gave the alkynyl-vinylidene **28**, complex **27** was prone to oxidative decomposition (or hydrolysis) to the carbonyl **29** (see below).

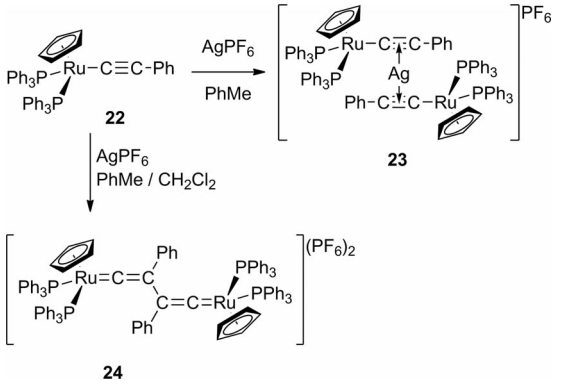

Scheme 15. Solvent-dependent redox reactivity of Ag^{I} with the ruthenium alkynyl complex.

Nevertheless, the oxidative coupling of terminal alkynyl complexes [M(C≡CH)L$_n$] is now recognised as a viable synthetic strategy for the assembly of bis(vinylidene) complexes [{L$_n$M}$_2${μ-C=C(H)–C(H)=C}]$^{2+}$, which can in turn be deprotonated to give butadiynediyl compounds as an alternative to Glaser/Hay coupling reactions,[42,45,129] transmetallation reactions with dilithio-butadiynediyl reagents[130] or copper diyn(di)yls formed in situ[131–133] and desilylation/

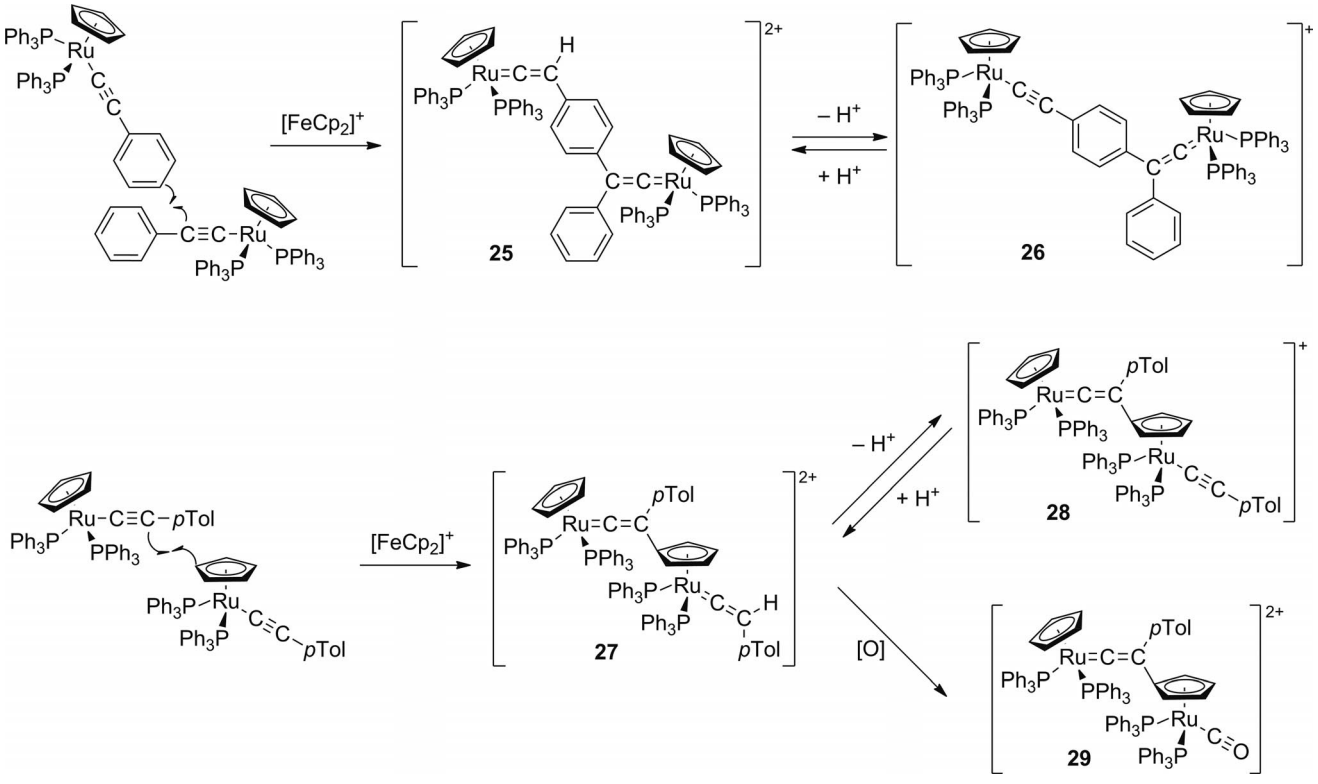

Scheme 16. Different bimetallic products isolated from ferrocenium oxidation of [Ru(C≡CPh)(PPh$_3$)$_2$Cp] and [Ru(C≡CC$_6$H$_4$Me-4)(PPh$_3$)$_2$Cp].

 © 2012 Wiley-VCH Verlag GmbH & Co. KGaA, Weinheim

metallation protocols.[134] The complexes [M(C≡CH)(dppe)(L)] (L = Cp*, M = Fe, Ru, Os; L = η^7-C_7H_7, M = Mo) and [Ru(C≡CH)(dppm)Cp*] all react with 1 equiv. of $[FeCp_2]PF_6$ at –78 °C to yield the bimetallic bis(vinylidene), which is then readily deprotonated to form the bimetallic butadiynediyl complexes [{M(dppX)(L)}$_2$(1,4-μ-C≡C–C≡C)] (Scheme 17).[112,135–138]

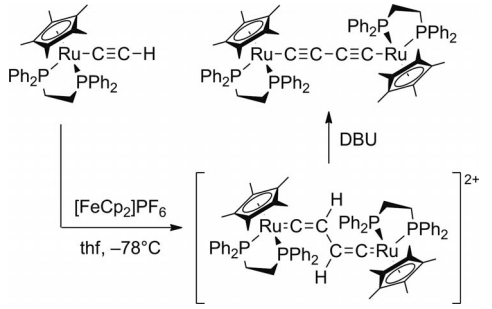

Scheme 17. Oxidative coupling and subsequent deprotonation to yield bimetallic μ-1,3-diyne-1,4-diyl complexes.

Steric factors at the metal centre, rather than at the alkynyl termini, also play a significant role in determining the reactivities of alkynyl radical cations in coupling reactions, as illustrated by the complexes [Nb(η^5-$C_5H_4SiMe_3$)$_2$(C≡CPh)(L)] (**30**, L = CO, PMe_2Ph; Scheme 18).[139] Oxidation of **30-CO** in dichloromethane at –30 °C rapidly results in the formation of the vinylidene complex **32-CO** (or the isotopologue [Nb(η^5-$C_5H_4SiMe_3$)$_2${=C=C(D)Ph}(CO)]$^+$ in [D_2]dichloromethane) by hydrogen abstraction, whereas oxidation of the sterically hindered phosphane analogue readily allows the isolation of the stable radical cation [**31-PMePh$_2$**][BPh_4]. After several weeks at room temperature in dichloromethane, this complex also converts into the vinylidene derivative **32-PMePh$_2$**. Also of note is a significant solvent effect;[140] the carbonyl-derived radical cation **31-CO** rapidly dimerises in tetrahydrofuran solution to form the bimetallic bis(vinylidene) **33**, whereas no analogous reaction was observed for the phosphane-ligated derivative under a variety of reaction conditions (nor for the related carbonyl derivative [Nb(η^5-$C_5H_4SiMe_3$)$_2$(C≡C*t*Bu)(CO)]$^{\cdot+}$).

In contrast to the C–C coupling chemistry exhibited by the parent alkynyl radical cation [Fe(C≡CH)(dppe)Cp*]$^{\cdot+}$, more sterically congested iron alkynyl complexes [Fe(C≡CC_6H_4R)(dppe)Cp*]$^+$, with the exception of the NMe_2 derivative, are generally amenable to isolation and crystallisation and offer Mossbauer signatures consistent with descriptions based on formal Fe^{III} oxidation states.[11] The analogous arylalkynyl ruthenium systems [Ru(C≡CC_6H_4R)(PP)Cp′]$^+$ [(PP)Cp′ = (PPh_3)$_2$Cp, (dppe)Cp*][10,18] and related *trans*-[RuCl(C≡CC_6H_4R)(dppe)$_2$]$^{+}$[12] exhibit more spin density on the alkynyl ligand (see below) and are generally far more chemically active, resisting attempts at crystallisation, often "decomposing" by either hydrogen abstraction to vinylidene complexes or C≡C cleavage reactions to give carbonyl complexes. Indeed, for systems in which the alkynyl ligand supports even a modest amount of radical character, decomposition to the analogous metal carbonyl is commonly observed during attempts to prepare and isolate radicals derived from ruthenium σ-alkynyl complexes.[12,19,97,141,142]

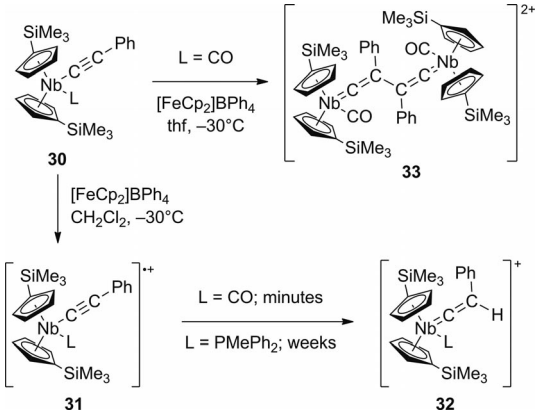

Scheme 18. Solvent- and ligand-dependent redox reactivity of niobocenyl alkynyl complexes.

As noted above, the formation of vinylidene complexes by hydrogen abstraction is a commonly observed reaction of alkynyl radical cations. In turn, vinylidene complexes are known to hydrolyse to give the metal carbonyl complex,[122,143] whereas reaction of, for example, [Ru{C=C(H)Ph}L(PPh_3)Cp]$^+$ (L = CO, PPh_3) with dioxygen gives [Ru(CO)L(PPh_3)Cp]$^+$ and benzaldehyde (L = CO) or benzoic acid (L = PPh_3);[144] other examples of the oxidation of vinylidenes to carbonyls under ambient conditions are also known.[136,145–147] Therefore the intermediacy of vinylidenes cannot be excluded in the conversion of alkynyl radical cations into carbonyls. However, these reactions are generally slow and a growing body of evidence points to more direct hydrolysis mechanisms that may occur on faster timescales. By way of example, the oxidation of *trans*-[Ru(C≡CMe)Cl(dppe)$_2$] by $[FeCp_2]PF_6$ in CH_2Cl_2 results in the formation of a thermally stable radical cation *trans*-[Ru(C≡CMe)Cl(dppe)$_2$]$^{\cdot+}$, which slowly forms the vinylidene *trans*-[Ru{C=C(H)Me}Cl(dppe)$_2$]$^+$ by the abstraction of H$^{\cdot}$. The reaction mixture is partially hydrolysed by residual water to give *trans*-[Ru(CO)Cl(dppe)$_2$]$^+$, but at a rate faster than the hydrolysis of the vinylidene, which strongly implies the formation of the carbonyl complex by hydrolysis of the alkynyl radical.[97] Likewise, mixtures of *trans*-[Ru(CO)Cl(dppe)$_2$]$^+$ and *trans*-[Ru{C=C(H)$C_6H_4NO_2$-4}Cl(dppe)$_2$]$^+$ have been obtained from the NO^+-mediated oxidation of *trans*-[Ru(C≡C$C_6H_4NO_2$-4)Cl(dppe)$_2$].[12]

Perhaps the most comprehensive study of this process has been conducted by Paul and Lapinte and co-workers, who explored the mechanism of formation of [Fe(CO)(dppe)Cp*]$^+$ from [Fe(C≡C$C_6H_4NMe_2$-4)(dppe)Cp*]$^+$.[148] Although solutions of [Fe(C≡C$C_6H_4NMe_2$-4)(dppe)Cp*]PF_6 ([**34**]PF_6) in CH_2Cl_2 are relatively stable under argon, when exposed to dry oxygen, **34** converts slowly (ca. 90% over 36 h) into the carbonyl **35**, accompanied by the formation of 4,4′-bis(dimethylamino)bibenzoyl (**36**). The reaction is first order in both the alkynyl radical and

 © 2012 Wiley-VCH Verlag GmbH & Co. KGaA, Weinheim

oxygen concentrations, obeying a rate law of general form $-d[\mathbf{34}]/dt = k[\mathbf{34}][O_2]$, with $k_{app} = 4 \times 10^{-3}$ M min^{-1}. There was no significant acceleration in the rate of carbonyl formation upon introduction of water, although higher cumulenylidenes are known to be extremely sensitive to reaction with traces of water or other nucleophiles.[149] These results indicate that both the H· abstraction/vinylidene and direct alkynyl radical hydrolysis pathways are substantially slower than the reaction of **34** with O_2 as a route to the formation of **35**. Indeed, NMR monitoring of the reaction failed to identify a vinylidene intermediate. The rate of reaction with O_2 is sensitive to the nature of the alkynyl ligand substituent, with the nitro-substituted complex [Fe(C≡CC$_6$H$_4$NO$_2$-4)(dppe)Cp*]PF$_6$ exhibiting a k_{app} of 2.1×10^{-5} M min^{-1}, consistent with the decreased spin density located on the alkynyl ligand (see below). A mechanism involving the attack of molecular oxygen on the alkynyl radical has been proposed (Scheme 19), although the formation of an initial Fe^{IV} superoxo species cannot be unambiguously ruled out. However, it is clear that the combination of steric protection of the metal centre and C$_\beta$ by the Cp* and dppe ligands, together with the limited accumulation of radical character on the alkynyl ligand brought about by the iron centre (see below), limits both radical coupling and hydrogen atom abstraction pathways, promoting the relatively clean, albeit slow, conversion of **34** into the carbonyl complex **35**.

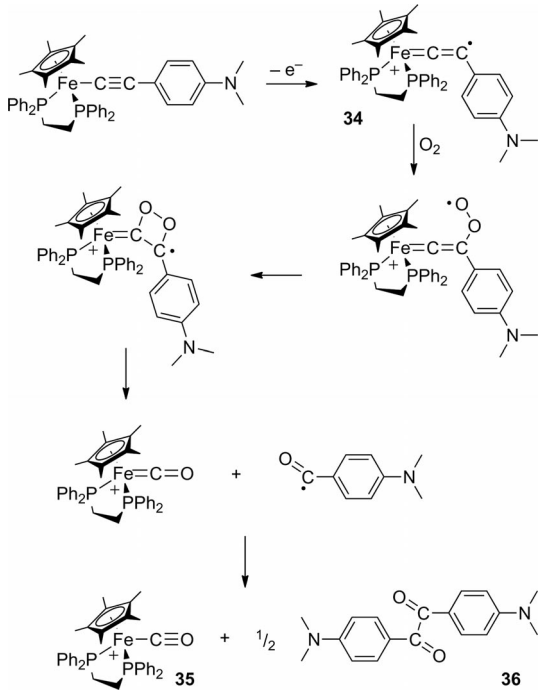

Scheme 19. Postulated mechanism for the O_2-induced "decomposition" of the alkynyl radical cation.

A likely related reaction has been employed in the conversion of alkynyl fragments connected to the apical carbon of Co$_3$C clusters of general form [Co$_3$(μ$_3$-CC≡CR)(CO)$_7$(dppm)] into acyl groups and CO. Thus, the reaction of [Co$_3$(μ$_3$-CC≡CR)(CO)$_7$(dppm)] with [FeCp$_2$]PF$_6$ and O_2 gave [Co$_3${μ$_3$-C(=O)R}(CO)$_7$(dppm)] clusters as the isolated products in moderate yield. A possible mechanism involving the metathesis of O_2 with the C≡C radical to give an intermediate β-diketone is proposed (Scheme 20).[150]

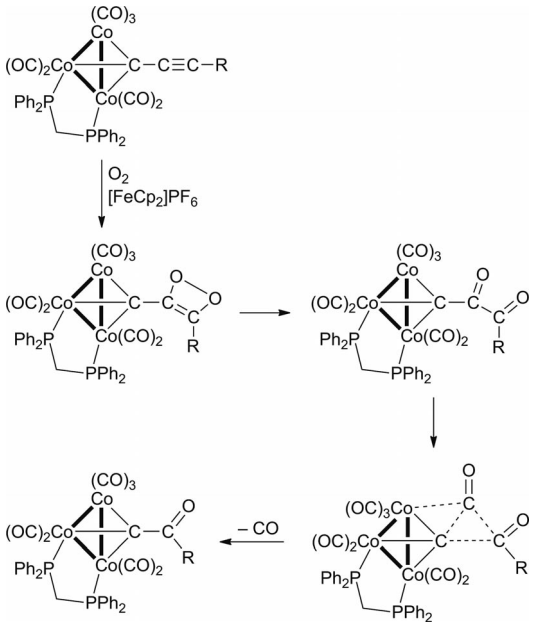

Scheme 20. Postulated mechanism by which an acyl ligand is formed via a β-diketonate intermediate on oxidative reaction of a μ$_3$-alkynyl complex with O_2.

The cationic derivatives [Ru{C≡C(C=CH$_2$)NR$_2$R′}Cl(dppm)$_2$]$^+$ (Scheme 21) reported by Winter and Hornung exhibit significantly different redox behaviour to that of the neutral Ru^{II} complexes discussed above.[151] The cyclic voltammograms of these cationic ammonium complexes are, generally, typified by a pseudo-reversible oxidation couple in addition to two closely spaced, chemically irreversible reduction processes. Observations from EPR and UV/Vis/NIR/IR spectroelectrochemical experiments are consistent with a Ru^{II}/Ru^{III} redox process defining the oxidation couple, in contrast to the ligand-centred oxidation behaviour of most ruthenium alkynyl complexes (see above), although readily understandable on account of the electron-withdrawing character of the ammonium substituent. In contrast, the appearance of a reduction process is in keeping with substantial cumulenic character in the ligand, consistent with square-wave and cyclic voltammetry experiments which demonstrate the irreversible release of a tertiary amine fragment from the complex upon electrochemical reduction. Unfortunately, as a consequence of the high cathodic potential of the reduction process, it was not possible to conclusively validate the number of electrons involved in the reduction or the exact fate of the organometallic fragment. In light of the electrochemical behaviour, specifically with respect to the inversion of the ligand/metal HOMO/LUMO character, these cationic ammonium alkynyl complexes very closely resemble related amino-allenylidene complexes.[152]

 © 2012 Wiley-VCH Verlag GmbH & Co. KGaA, Weinheim

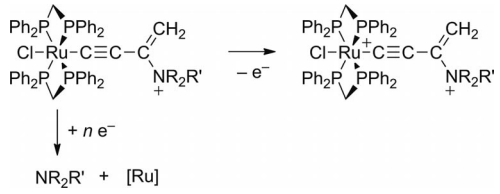

Scheme 21. Redox chemistry of an unusual/novel cationic alkynyl complex [NR_2R' = NEt_3, $N(nPr)_3$, quinuclidine, *N*-ethylmorpholine, Me_3-tacn, NMe_2Bz, $NMe_2(CH_2C_6H_4OMe\text{-}3)$, dmap].

4. Polyynyl Derivatives

In complexes bearing polyynyl ligands it is evident that it should be possible to observe not only C_β–C_β coupling of the oxidised radical, but in fact coupling reactions at any (all) even-numbered carbon atoms. Theoretical treatments on the series of complexes $[Ru\{(C{\equiv}C)_nPh\}(PH_3)_2Cp]^{\cdot+}$ (n = 1–6)[153] indicate that the redox-generated radical remains strongly delocalised across the alkynyl ligand with increasing alkynyl chain length, with a decreasing contribution of the metal-based orbitals with increasing chain length. Few reactions exploiting the redox non-innocence of the polyynyl chain have been reported in the literature, yet nevertheless they deserve comment. The complex *trans*-$[Ru(C{\equiv}CC{\equiv}CR)Cl(dppe)_2]$ (**37**, R = H or $SiMe_3$) reacts with a 0.5 mol equiv. of $[FeCp_2]PF_6$ at room temperature to yield the bimetallic cation $[\{RuCl(dppe)_2\}_2(1,8\text{-}\mu\text{-}C_8H_3)]$ (**38**; Scheme 22).[154] The bimetallic complex is presumably formed by a [2 + 2] C_γ–C_δ cycloaddition reaction between the radical cation and a neutral molecule to form a cyclic radical cation, which subsequently abstracts hydrogen from the solvent medium to yield the cation **38**.

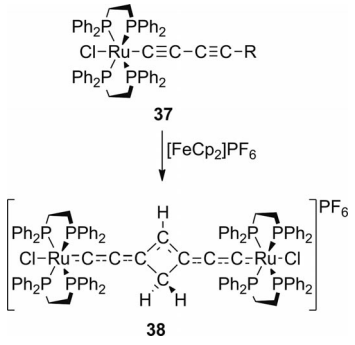

Scheme 22. C_γ–C_δ cycloaddition resulting from oxidation of **37** (R = H, $SiMe_3$).

The delicate interplay between the reactivity of the oxidised complex and both the metal head group and terminal alkynyl substituent is illustrated in the series of complexes $[Mo(C{\equiv}CC{\equiv}CR)(\widehat{LL})(\eta^7\text{-}C_7H_7)]$ ($\widehat{LL}$ = bpy, R = $SiMe_3$; $\widehat{LL}$ = dppe, R = H, $SiMe_3$).[155] The complex $[Mo(C{\equiv}CC{\equiv}CSiMe_3)(bpy)(\eta^7\text{-}C_7H_7)]$ is oxidised by $[FeCp_2]PF_6$ to form a stable, isolable radical cation, with EPR spectroscopic experiments consistent with a metal-centred radical analogous to related $[Mo(X)(bpy)(\eta^7\text{-}C_7H_7)]^{\cdot+}$ complexes. Substitution of the bipyridine ligand for a diphosphane (**39**) and oxidation under identical conditions yields the C_β–C_β coupled bis(alkynylvinylidene) **40** (Scheme 23), with no evidence of the C_δ–Si bond scission observed for the ruthenium analogue discussed above. The product of oxidation for the desilylated derivative $[Mo(C{\equiv}CC{\equiv}CH)(dppe)(\eta^7\text{-}C_7H_7)]$ was not readily isolated and, although EPR spectroscopic experiments were consistent with a radical delocalised across the diynyl ligand, additional spectroscopic data did not support the formation of a coupled product in this case.

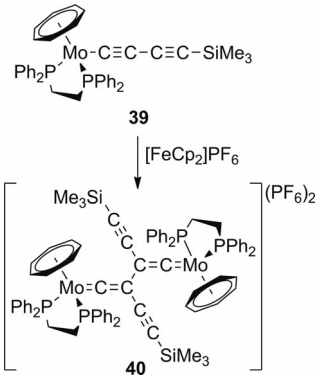

Scheme 23. C_β–C_β coupling resulting from the oxidation of **39**.

The d^0 titanocenyl analogue of **37** and **39**, $[Ti(\eta^5\text{-}C_5H_4SiMe_3)_2(C{\equiv}CC{\equiv}CSiMe_3)_2]$, did not exhibit any anodic redox activity (chemically or voltammetrically).[156] In contrast, the analogous complexes **41**, bearing a metallocenyl functionality on the butadiynyl ligands, are oxidised by 2 equiv. of $AgPF_6$ to yield the free titanocenyl derivative **43** and the intramolecularly coupled polyynediyl metallocenes **42** (Scheme 24).[157] The ruthenocenyl-substituted complexes are slower to dimerise than the ferrocenyl derivatives, consistent with decreased spin delocalisation through the polyynyl chain in the latter case. The role of the titanocenyl moiety in this C_α–C_α radical coupling reaction is highlighted by the fact that $[Fc\text{–}(C{\equiv}C)_2\text{–}Me]$ reacts with $AgPF_6$ under identical conditions to afford the stable, crystalline product $[Fc\text{–}(C{\equiv}C)_2\text{–}Me]PF_6$, readily described as a ferrocenyl-centred cation. Overall, the oxidation of these titanocenyl derivatives is comparable to a "traditional" reductive elimination, although unique in the fact that the electron source to generate the carbon radical is the pendant metallocene rather than the M–C_α σ bond.

The difference in reactivity described in the examples above is attributable largely to the metal head groups and their relative ability to stabilise the diynyl radical in the cationic complex. Substitution of methyl for "$[TiCp'_2X]$" in $[Fc\text{–}(C{\equiv}C)_2\text{–}Me]$ presumably results in increased accumulation of spin density in the polyynyl chain at C_α (C_δ with respect to the ferrocenyl moiety) and a subsequent radical coupling reaction assisted by the templating effect of the titanocenyl moiety. Not only is the titanocenyl moiety less electron-releasing than the ruthenium and molybdenum examples, there is also significantly less steric "protection" of

 © 2012 Wiley-VCH Verlag GmbH & Co. KGaA, Weinheim

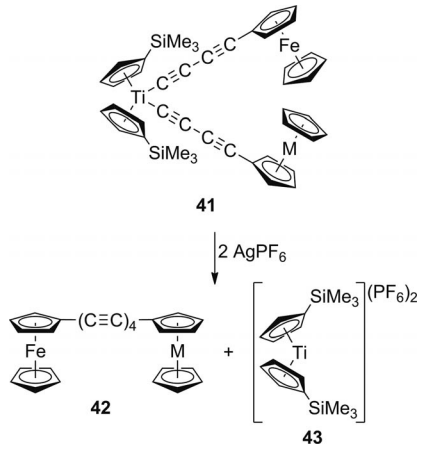

Scheme 24. Redox-induced C_α–C_α coupling in a titanocenyl system (M = Fe, Ru).

the C_α site. The "[Mo(bpy)(η^7-C_7H_7)]" moiety results in a radical that is largely metal-centred whereas the C_β reactivity exhibited by the "[Mo(dppe)(η^7-C_7H_7)]" moiety indicates moderate spin delocalisation on to the diynyl ligand. More extensive delocalisation on to the ligand is exemplified by the "[RuCl(dppe)$_2$]" moiety for which the reactivity of the ligand is at C_δ, the most remote site from the metal centre. Notably this difference in reactivity may also be attributable to the different steric environments of the metal centres, with the C_β atom "less accessible" in the case of the bis(diphosphane)ruthenium complex. However, the concurrent desilylation of the radical-cation intermediate, not observed in the molybdenum analogue, supports a significantly greater radical delocalisation on to the diynyl ligand in the ruthenium complex and consequently points towards an electronic basis for the difference in reactivity exhibited by the oxidised complexes. The greater contribution of electronic factors over and above steric considerations is further highlighted by the two reactions of [Ru(=C=C=C=C=CPh$_2$)Cl(dppe)$_2$]PF$_6$ (**44**; Scheme 25).[98] The reaction of **44** with hydride yields the neutral allenyl-alkynyl complex **45** as a result of nucleophilic addition at C_γ, whereas reduction to the neutral radical with $CoCp_2$ in the presence of a hydrogen source yields the pentadiynyl complex **46** by C–H radical coupling at the terminal carbon atom. Assuming identical steric environments in both reactions, the preferential C_γ or C_ε reaction is ready evidence for a significant rearrangement of the electronic structure throughout the C_5Ph_2 ligand between the cationic and reduced cumulenic forms.

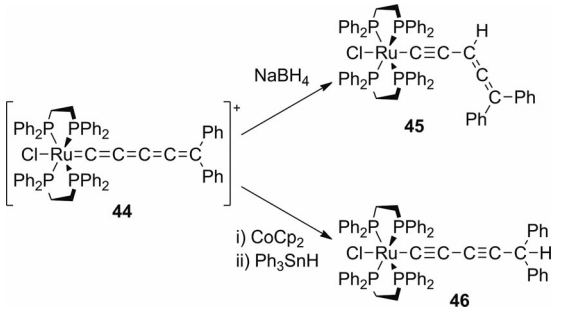

Scheme 25. Selected reactions of the pentatetraenylidene complex.

4.1. Chemical Reactions of σ-Alkynyl Complexes with "Redox-Active" Ligand Substituents

In addition to the complexes discussed above, particular attention is warranted for those complexes bearing ligand functionalities that may explicitly be considered "redox-active". Careful selection/matching of the metal head group and redox-active moiety can consequently allow for the specific design of complexes in which either of the electrophores dominates the properties of the redox-generated species. For example, complexes functionalised with tetrathiafulvalenyl[158–160] or (metallated) pyridyl[117,142,161–165] derivatives exhibit minimal electronic coupling between the two moieties, with the redox-active functionality generally dominating the redox-generated state. However, moderation of the spin density or charge distribution in such systems has most notably and extensively been explored through functionalisation with a ferrocenyl moiety.[166–186] In the most fundamental illustration of this premise one may consider the complex [Ru(C≡CFc)(PPh$_3$)$_2$Cp]$^{\cdot+}$ (Scheme 26).[187,188] Whereas the phenylethynylene complex [Ru(C≡CPh)(PPh$_3$)$_2$Cp]$^{\cdot+}$ is highly unstable and rapidly undergoes various intermolecular reactions, the ferrocenylethynylene complex is remarkably stable under ambient conditions to the point that [Ru(C≡CFc)(PPh$_3$)$_2$Cp]PF$_6$ (**48**) has been characterised by a single-crystal X-ray structural determination. The solid-state structure, in combination with NMR, Mössbauer, UV/Vis/NIR and IR spectroscopic data, indicate that the radical cation is best represented by a delocalised structure, with neither an alkynyl nor cumulenylidene structure dominating the geometric and electronic character. Chemical oxidation of [Ru(C≡CFc)(dppf)Cp] and [Ru(C≡CFc)(PPh$_3$)$_2$Cp*] also yields stable, isolable radical cations with spectroscopic features similarly consistent with the above observations. Chemical oxidation of the dppe-ligated congeners of these two complexes yielded only unstable, impure mixtures of oxidised material,[187] although low-temperature spectroelectrochemical experiments were able to satisfactorily characterise the oxidation products to be consistent with the above descriptions.[188] The underlying causes of the relative instability of the dppe-ligated complexes were not readily apparent from the experimental data, although the source of the difference is presumably electronic in nature.

A series of substituted ruthenocenyl derivatives ably demonstrate the influence of both electronic and steric factors on the redox reactivity of metallocenyl-functionalised alkynyl complexes (Scheme 27). The oxidation of [Ru(C≡CRc)(PPh$_3$)$_2$Cp] (**49**) with $AgBF_4$ or *p*-BQ/$BF_3{\cdot}OEt_2$ (*p*-BQ = *p*-benzoquinone) yields a diamagnetic 16-electron dication [**49**]$^{2+}$, for which spectroscopic parameters are consistent with a cumulenylidene/fulvalenyl struc-

 © 2012 Wiley-VCH Verlag GmbH & Co. KGaA, Weinheim

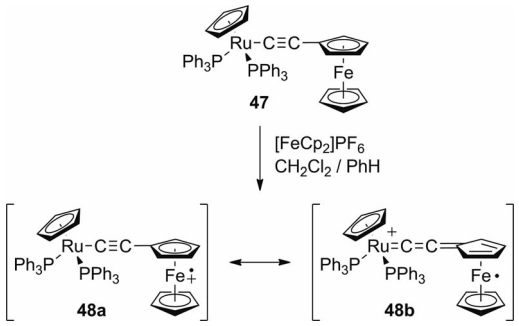

Scheme 26. Formation of the stable ruthenium/ferrocenyl radical cation.

tural description, although full characterisation was precluded by the inherent instability of the complex.[189] Permethylation of either cyclopentadienyl ring of the ruthenocenyl moiety results in the observation of markedly different reactivity of the oxidised complexes. The oxidation of **50** with excess *p*-BQ/BF_3·OEt_2 yields the 16-electron dication $[\mathbf{50}]^{2+}$, with the spectroscopic data comparable to that obtained for $[\mathbf{49}]^{2+}$ above, although with markedly increased stability. A single-crystal X-ray structural determination of the two-electron-oxidised dppe-ligated congener of **50** gives rise to a cumulenylidene/fulvalenyl structure, in which the ruthenocenyl ruthenium atom is bound in a novel η^6 fashion to the C_5Me_4 ring and the C_β cumulenic atom of a bent C_3 chain bridging to the Ru(dppe)Cp fragment.[190] In contrast, on permethylation of the alternate cyclopentadienyl ring, one- and two-electron oxidation of **51** yields the vinylidene cations $[\mathbf{51}]^+$ and $[\mathbf{51}]^{2+}$, respectively. In contrast to a solvent-donated hydrogen-abstraction mechanism in the case of $[\mathbf{51}]^+$, selective deuteriation experiments are consistent with an intramolecular hydrogen abstraction in the formation of the dicationic vinylidene $[\mathbf{51}]^{2+}$.[189]

The photochromic properties of the dithienylethene (DTE) derivatives in complexes **52**–**54** in Scheme 28 are maintained on incorporation into the bimetallic organometallic framework; by selective irradiation the DTE moiety may undergo a reversible intramolecular ring-closing (opening) reaction at the α-thienyl position. However, in addition to the photochromic switching behaviour exhibited by organic DTE derivatives, some metallated analogues are also susceptible to electrochromic switching behaviour. Two-electron oxidation of [**52-O**] with $[FeCp_2]PF_6$ results in the formation of a dicationic diradical intermediate that undergoes photochromic ring-closing on UV irradiation (in addition to significant decomposition), and subsequent two-electron reduction with $[CoCp_2]$ yields the ring-closed isomer [**52-C**].[191] The reverse reaction, the conversion of [**52-C**] into [**52-O**], is more facile, with isomerism of the oxidised $[\mathbf{52\text{-}C}]^{2+}$ state induced either thermally or by visible-light irradiation. Oxidation of the ruthenium analogue [**53-O**] results in spontaneous ring-closing to yield $[\mathbf{53\text{-}C}]^{2+}$, which is similarly reduced to form neutral [**53-C**].[192] In this instance the cumulenic dication $[\mathbf{53\text{-}C}]^{2+}$ is so stable that the retro-conversion of [**53-C**] into [**53-O**] was not possible. In contrast, extension of the alkynyl-ruthenium path in complex **54** allows fully reversible electrochemical interconversion between the isomers.[193] Electronic structure calculations performed on the model systems of $[\mathbf{52\text{-}O}]^{n+}$ and $[\mathbf{53\text{-}O}]^{n+}$ (n = 0, 2) indicate that the different susceptibility to isomerisation of the oxidised complexes is again attributable to the localisation of spin density: the ruthenium complex is calculated to have more than twice as much spin density localised on the conjugated ligand as the iron analogue, and thus the α–α thienyl coupling to form the closed isomer is a favourable process. This behaviour is consistent with that of the simpler alkynyl complexes [M(C≡CPh)(dppe)Cp*], which on oxidation can be described in terms of an essentially chemically stable M^{III} species (M = Fe) or a much more reactive phenylethynylene radical (M = Ru; see above). Extension of this notion to the ruthenium-phenylenediynyl derivative **54** yields the plausible conclusion that the spin density at the relevant α-thienyl atoms of the DTE moiety is intermediate between that observed in **52** and **53** as a consequence of the larger delocalised π system, and thus the

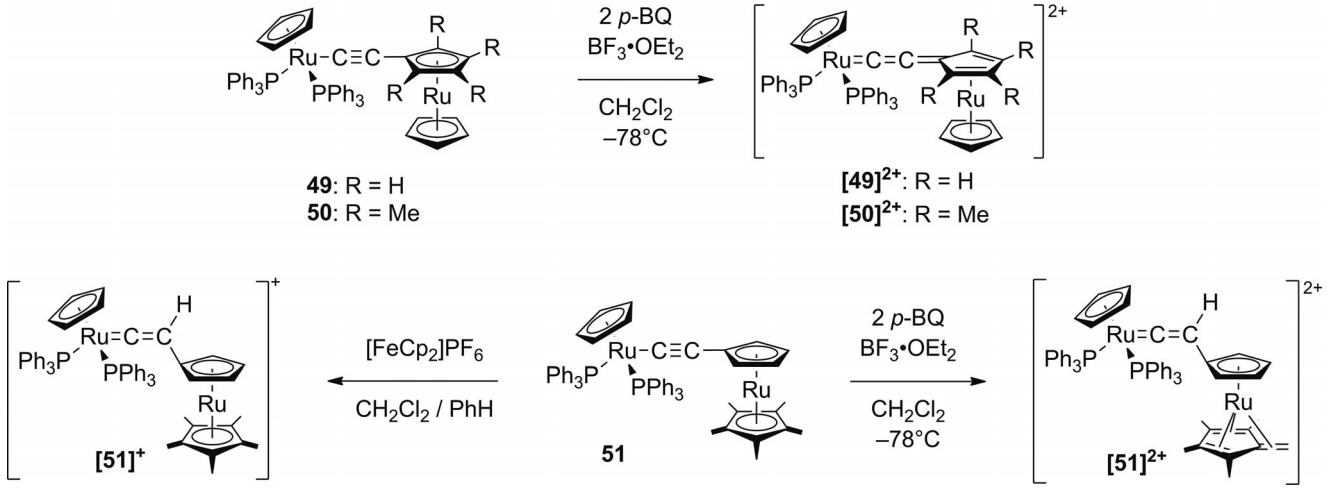

Scheme 27. Various oxidation pathways of the ruthenocenyl-substituted complexes (R = H, Me; *p*-BQ = *p*-benzoquinone).

 © 2012 Wiley-VCH Verlag GmbH & Co. KGaA, Weinheim

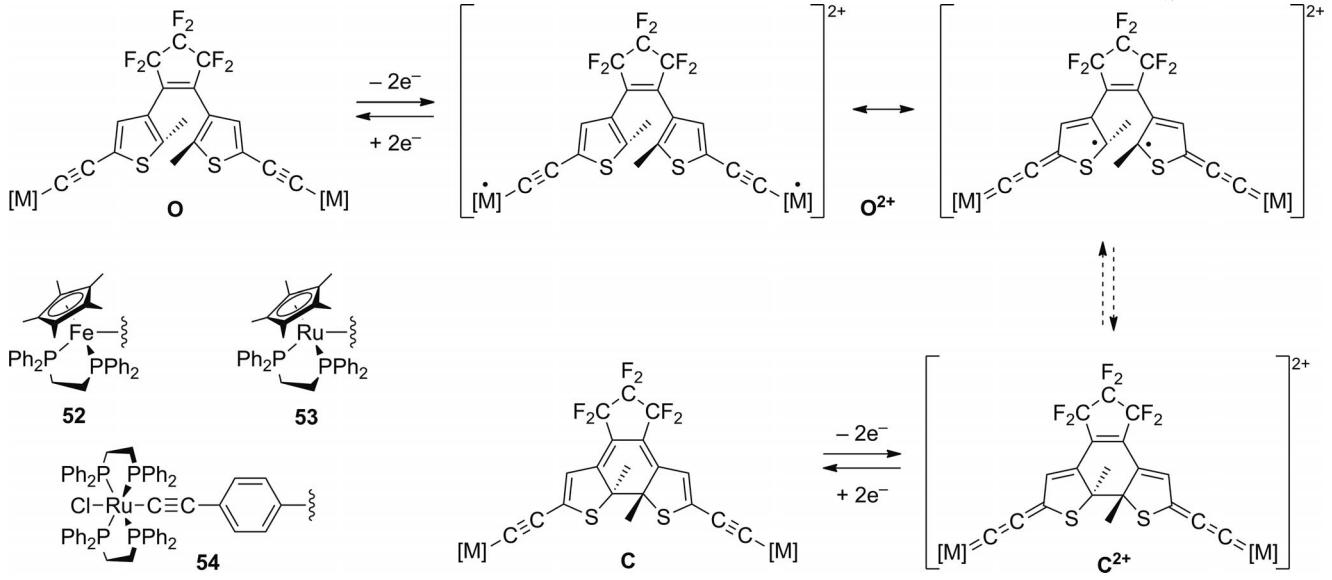

Scheme 28. Electrochromic behaviour observed in the DTE derivatives [**52**]–[**54**].

relative stability of the closed form over the open form is not as significant, thereby rendering the isomerisation reversible.

The thienyl moiety is inherently susceptible to oxidative coupling reactions, particularly at the α position, resulting in the formation of dimeric, oligomeric or polymeric products dependant upon additional substituents on the thienyl ring and the specific reaction conditions. Such oxidative coupling reactions have been observed in organometallic complexes incorporating the thienyl moiety, as illustrated by the series of complexes [FcC≡C(2,5-thienyl)$_m$H] (m = 1–3) (Figure 2).[194] The cyclic voltammograms of the complexes exhibit two anodic redox processes: an initial ferrocenyl-based oxidation followed by irreversible oxidation of the thienyl moiety. Repeated electrochemical cycling at potentials sufficient to oxidise the thienyl moiety of the bi- and terthienyl complexes results in the deposition of conducting films that exhibit properties consistent with dimerisation of the parent complex. However, as the films formed by this electrochemical process are not particularly stable, it was not possible to completely characterise the electrogenerated products. Analogous electrochemical oxidative oligo- and polymerisation has also been postulated for the related bis-alkynyl complexes [Ru{C≡C(2,5-thienyl)$_n$H}$_2$(dppe)$_2$] (n = 2, 3)[195] and the allenylidene complexes [Ru(=C=C=CR$_2$)Cl($\widehat{PP}$)$_2$]$^+$ [$\widehat{PP}$ = dppm, dppe; R$_2$ = (α-thienyl)$_2$, cyclopentadithiophene] and [Ru{=C=C=C(α-thienyl)$_2$}(dppe)Cp]PF$_6$ (Figure 2).[196]

One particularly interesting example of a structural rearrangement induced by redox reactions is depicted in Scheme 29. The isomer **55a** is thermally stable under ambient conditions and does not undergo haptotropic rearrangement to **55b**. However, upon oxidation and subsequent re-reduction, isomeric mixtures of **55a**/**55b** are isolated. The isomerisation process appears cumulative, whereby subjecting **55a** to two successive oxidation/reduction cycles doubles the **a**/**b** ratio from 94:6 to 88:12. The exact nature and underlying factors affecting the rearrangement are not immediately evident.[197]

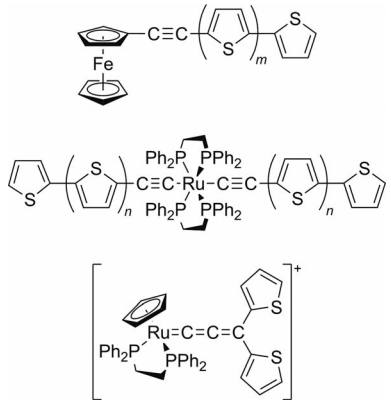

Figure 2. Thienyl-functionalised organometallic complexes exhibiting evidence of electro-polymerisation.

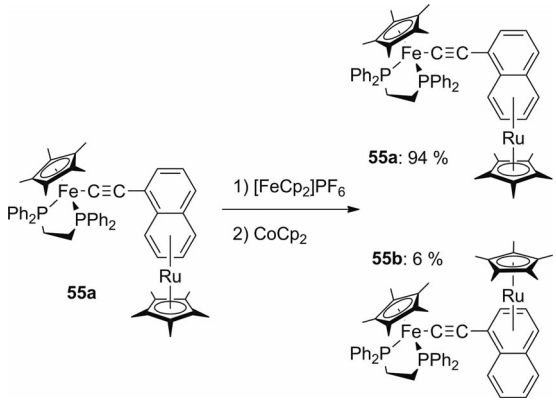

Scheme 29. Haptotropic rearrangement of **55** on oxidation and re-reduction.

 © 2012 Wiley-VCH Verlag GmbH & Co. KGaA, Weinheim

4.2. Electronic Basis for Ligand Redox Non-Innocence in σ-Alkynyl Complexes

Electronic structure calculations have been used to rationalise some of the more recent observations concerning the redox non-innocent character of σ-alkynyl and polyynyl ligands, particularly for complexes based on piano-stool fragments [M(L_2)Cp′] [M = Fe, L_2 = (dppe), Cp′ = Cp*;[13,14,17] M = Ru, L_2 = (PPh_3)$_2$, dppe, Cp′ = Cp, Cp*],[10,18,32,128,153] [Mo(CO)L_2Cp′] [L_2 = (PMe_3)$_2$, dppe; Cp′ = Cp, Cp*],[198] [M(dppe)(η^7-C_7H_7)] [M = Mo,[20,21] W[19]] and the octahedral moiety *trans*-[RuCl(dppe)$_2$].[12,32] Many aspects of the computational rationalisation of ligand non-innocence have recently been reviewed by Costuas and Rigaut,[34] and so only key points will be emphasised here. The Ru(L_2)Cp′-based complexes provide a convenient starting point for descriptions of the electronic structure of σ-alkynyl complexes, with numerous detailed studies and different computational treatments leading to essentially the same qualitative picture.[10,18,128,153] In brief, the strongest interaction between the ruthenium and alkynyl fragments occurs between the alkynyl HOMO, a σ-type lone-pair orbital at C_α and the d_{z^2} orbital on ruthenium. This interaction forms a strong bonding/anti-bonding pair, of which only the bonding combination is occupied, and results in the formal Ru–C single bond. The lowest- and highest-energy ruthenium orbitals, $d_{x^2-y^2}$ and d_{xy}, respectively, do not have the appropriate symmetry to interact with the alkynyl fragment and thus remain largely non-bonding. Finally, the d_{xz} and d_{yz} orbitals combine with a pair of C(pπ) orbitals of the alkynyl fragment to form a filled bonding and anti-bonding set, the anti-bonding set becoming the two highest-occupied molecular orbitals (Figure 3).[32,153] Thus, the orthogonal HOMO and [HOMO − 1] are an admixture of the alkynyl π system and ruthenium d orbitals, whereas the LUMO and [LUMO + 1] are predominantly metal or alkynyl π* in character depending on the nature of the alkynyl substituent and the level of theory employed in the calculations. In general, the ligand π* character of the LUMO is enhanced by larger aromatic substituents, such as 9-anthracenyl,[18] elongated conjugated alkynyl ligands, such as polyynyl[153] and oligo(phenylene-ethynylene)[141] derivatives, or phenylene rings bearing strong electron-withdrawing groups. Note that in the case of arylalkynyl (C≡CAr) complexes, the composition and energy of the occupied frontier orbitals across the Ru–C≡C–Ar fragment are sensitive to the orientation of the phenyl group with respect to the {Ru(PPh_3)$_2$Cp} fragment, and that the contribution of the arylalkynyl ligand to these critical occupied orbitals can also be tuned by the introduction of electron-donating or -withdrawing moieties,[32,153] or by varying the size or conjugation length of the aromatic substituent.[14,141,153]

On oxidation the complex exhibits a net decrease in alkynyl π-bonding character, shifting towards the partial evolution of cumulenic character on the basis of geometric parameters and frequency calculations. The frontier orbitals of the cation remain largely similar to the neutral complex, with the α-HOSO (highest occupied spin orbital) and β-LUSO displaying significant Ru(d) and alkynyl(π) character. In the case of [Ru(C≡CPh)(dppe)Cp*]/[Ru(C≡CPh)(PPh_3)$_2$Cp], computed spin densities at various levels of theory and from different model systems situate the unpaired spin at approximately 40:30:25% across the Ru/C≡C/Ph moieties with the C_β atom of the ethynylene moiety and the carbon *para* to the ethynylene moiety accepting the major contributions in the last two cases.[18,128,153] Low-temperature EPR experiments[10] imply the radical to be largely metal-centred, exhibiting a single rhombic signal devoid of any hyperfine splitting, although the kinetic instability of the radical on warming to room temperature, in addition to the reactivity described above, lend some weight to the calculated distribution across the phenylethynylene moiety. The electronic structures of *trans*-[Ru(C≡CC_6H_4R)Cl(dppe)$_2$] complexes are similar, with the HOMOs distributed over the Ru–C≡C–C_6H_4R moiety, the precise weightings of which are sensitive to both the orientation of the aryl ring and the nature of the R substituent.[12,32] The significant concentration of spin density on the alkynyl C_β carbon and C_{ortho} and C_{para} phenylene ring carbons is consistent with the C_β–C_β coupling observed in the case of sterically unstrained Ru–alkynyl complexes, affording bis(vinylidene) complexes[125,135] and variation in the position of coupling following oxidation of [Ru(C≡CPh)(PPh_3)$_2$Cp] and [Ru(C≡CC_6H_4Me-4)(PPh_3)$_2$-Cp].[128]

Again, by using the {RuL_2Cp} fragment as a tool for discussion, as the σ-alkynyl ligand is extended the polyynyl ligand becomes increasingly heavily weighted in both the HOMO of the closed-shell complexes and the semi-occupied orbital of the one-electron-oxidised derivatives.[153] The spin density is distributed along the polyynyl chain, but particularly concentrated on C_β, C_δ and so on. This proposal is supported by the observation of C_γ–C_δ coupling reactions following the oxidation of *trans*-[Ru(C≡CC≡CSiMe_3)Cl(dppe)$_2$] to give the C_8H_3-bridged species **38** (Scheme 22).[34,154]

In contrast, the iron complexes [Fe(C≡CR)(dppe)Cp*], although offering largely the same qualitative metal–alkynyl interactions as noted for ruthenium analogues,[160] exhibit more metal character in the frontier orbitals, a feature reflected in the generally greater environmental stability of the analogous Fe^{III} complexes [Fe(C≡CC_6H_4R)(dppe)-Cp*]$^+$[13,14,16,17] and related systems.[11] In turn, this sensitivity of the metal/alkynyl ligand contribution to the alkynyl ligand substituent is consistent with the facile formation of [Fe(CO)(dppe)Cp*]$^+$ from [Fe(C≡CC_6H_4NMe_2-4)(dppe)-Cp*] upon oxidation (see above). The sensitivity of the distribution of radical character between the metal, C≡C and substituent groups is further illustrated by the rather extensive delocalisation of charge in the radical cation [Fe(C≡CTTFMe_3)(dppe)Cp*]$^+$, which features the strongly electron-donating TTF moiety.[160]

The composition of the frontier orbitals is also sensitive to the nature of the supporting ligands. A combination of photoelectron spectroscopy and Fenske–Hall calculations

 © 2012 Wiley-VCH Verlag GmbH & Co. KGaA, Weinheim

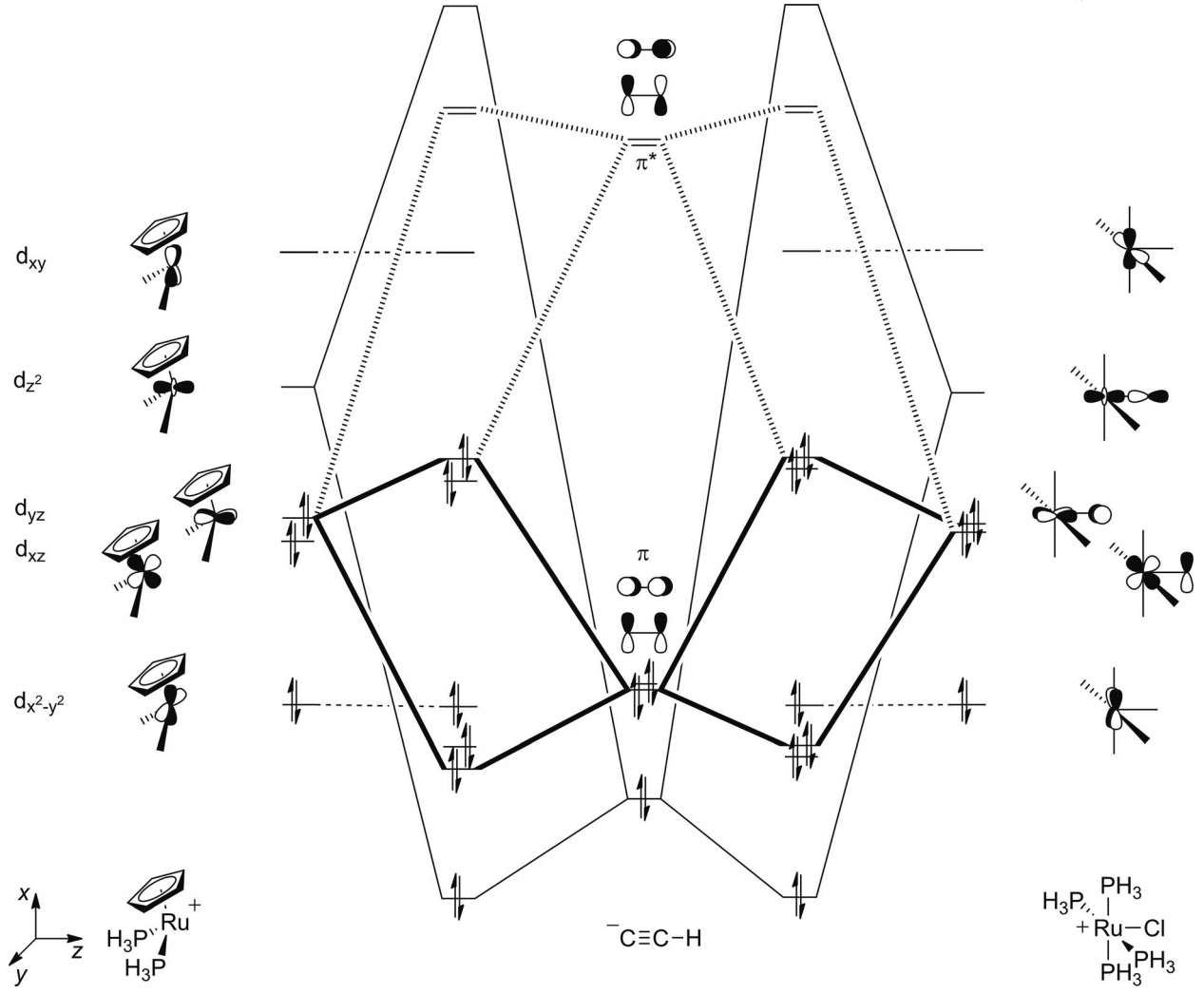

Figure 3. MO diagram for select ruthenium acetylide complexes.

have shown a significant mixing of the metal and alkynyl π orbitals in [Fe(C≡CR)(CO)$_2$Cp] (R = H, *t*Bu, Ph) systems, brought about by the lowering of the metal d orbitals by the ancillary carbonyl ligands. Substitution of Cp for the more electron-donating Cp* decreases the d–π interaction.[199] Extension of the alkynyl ligand to butadiynyl (C≡CC≡CH) also serves to enhance the ligand character in [Fe(C≡CC≡CH)(CO)$_2$Cp] by better matching of the lower-lying butadiynyl π system with the [Fe(CO)$_2$Cp] metal-based orbitals.[200] The ordering of the critical metal orbitals can also be influenced by the nature of the supporting ligands, as illustrated by the rather more metal-localised frontier orbitals associated with [M(C≡CR)(dppe)(η^7-C_7H_7)]$^{n+}$ (n = 0, 1; M = Mo, W) complexes.[19–21] The C_7H_7 ring promotes strong π and δ interactions with four of the five metal d orbitals, with d_{z^2} being somewhat destabilised by repulsive interactions with the C_7H_7 a_1-type orbital (Figure 4). As a consequence, the interactions between the group 6 metal centre and the alkynyl ligand in the frontier orbital region are rather restricted due to the poor spatial overlap of the high-lying d_{z^2} and the alkynyl π system, as evidenced by the small shifts in the ν(C≡C) frequency as a function of molecular oxidation state. Nevertheless, sufficient spin density is associated with the alkynyl ligand in [M(C≡CR)(dppe)(η^7-C_7H_7)]$^+$ systems to give rise to hyperfine couplings with the alkynyl substituent R in both alkynyl[19–21,201] and polyynyl[155] systems, as well as C_β–C_β coupling processes in the least sterically encumbered derivatives.[113,138,155]

In the case of four-legged piano-stool structures such as *trans*-[Mo(C≡CR)(CO)(PMe$_3$)$_2$Cp′] and *cis*-[Mo(C≡CR)-(CO)(dppe)Cp′] (Cp′ = Cp, Cp*; Figure 5), there are important differences in the nature of the frontier orbitals brought about by the position of the carbonyl ligand and the requirement of the system to maximise back-bonding and minimise the overall energy. These orbital characteristics are preserved on one-electron oxidation and account for the different degree to which the metal centre and alkynyl ligand support the unpaired electron.[198] In the case of the *trans* system, the four-legged piano stool structure favours π-bonding interactions between the metal (d_{yz}, d_{xz}) and the e_1 orbitals of the Cp ligand, whereas strong back-bonding interactions between the carbonyl ligand and the remaining d orbital of π-type symmetry (d_{xy}) leads to d_{z^2}

 © 2012 Wiley-VCH Verlag GmbH & Co. KGaA, Weinheim

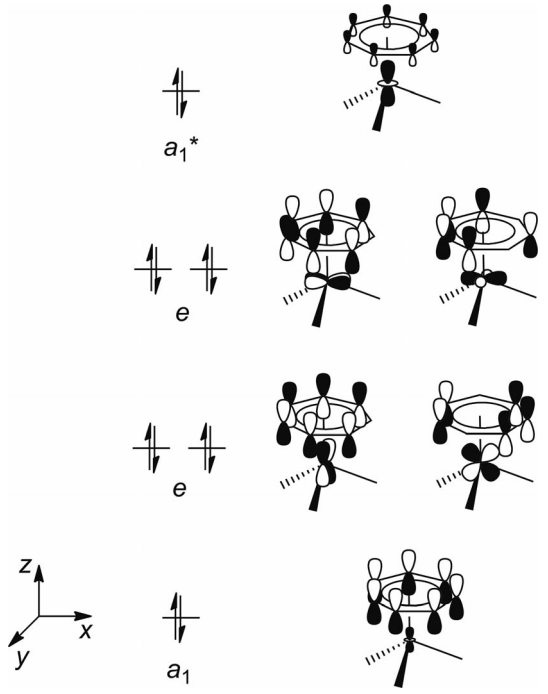

Figure 4. Schematic representation of the orbital interactions and ordering in the {Mo(η^7-C_7H_7)L_3} fragment, highlighting the d_{z^2} character of the highest-occupied molecular orbital.

character in the HOMO in this case. Consequently, *trans*-[Mo(C≡CR)(CO)(PMe_3)$_2$Cp′] complexes display similar metal-localised redox chemistry as the {Mo(C≡CR)(dppe)(η^7-C_7H_7)} systems, albeit for subtly different reasons. The electronic structures of the *cis* complexes can be considered as a perturbation of that described for the *trans* case. Keeping a common coordinate system (*z*-oriented towards the centroid of the Cp ligand) for ease of discussion, the HOMO is d_{xy}-alkynyl π in character, unconstrained by either symmetry or competition from the strongly electron-withdrawing CO ligand. The lowering of symmetry from pseudo-C_{4v} towards C_{2v} permits a significant degree of rehybridisation of d_{z^2} and $d_{x^2-y^2}$, which hampers a simple description, but the key feature is the stabilisation of the resulting "on-axis" components by interaction with the carbonyl and alkynyl ligands. The consequence of greater alkynyl character in supporting the unpaired electron on oxidation is evidenced not only by computational studies of the precursor closed-shell derivatives (*trans*-[Mo(C≡CPh)(CO)(PH_3)$_2$Cp]: 59% Mo, 16% CO, 12% C_β; *cis*-[Mo(C≡CPh)(CO)(dHpe)Cp]: 34% Mo, 4% CO, 51% C≡CPh), but also by the relative magnitudes of the shifts in the ν(CO) and ν(C≡C) frequencies on oxidation [*trans*-[Mo(C≡CR)(CO)(PMe_3)$_2$Cp*]$^{0/+}$ $\Delta\nu$(CO) ≈ +155 cm^{-1}, $\Delta\nu$(C≡C) ≈ –10 cm^{-1}; *cis*-[Mo(C≡CR)(CO)(dppe)Cp*]$^{0/+}$

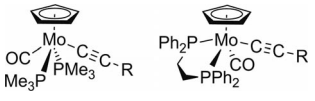

Figure 5. *trans*-[Mo(C≡CR)(CO)(PMe_3)$_2$Cp′] and *cis*-[Mo(C≡CR)(CO)(dppe)Cp′], illustrated for the case Cp′ = Cp.

$\Delta\nu$(CO) ≈ +140 cm^{-1}, $\Delta\nu$(C≡C) ≈ –50 cm^{-1}] as well as EPR data.[198]

5. Conclusions

The radicals derived from the one-electron oxidation or reduction of metal σ-alkynyl complexes exhibit tuneable electronic structures with the unpaired electron localised across the extremes of largely metal-centred to largely alkynyl-ligand-centred by variation of the metal, supporting ligands and alkynyl ligand substituent. The systems that display ligand redox non-innocence give a range of chemical reactions, which have principally been exploited as tools for the preparation of larger or more diverse ligand systems through C–C bond-forming reactions and hydrogen atom abstraction. In addition to providing routes to new ligand structures, the capacity for ligand redox non-innocence in metal σ-alkynyl complexes presents a particular challenge for the description of the results of electrochemical measurements alone in terms of metal-centred processes. All told, the chemical transformations of the alkynyl ligand upon redox reaction serve to emphasise the need for a combination of spectroscopic methods, usually supported by computational studies, to be employed to determine the electronic structure in metal σ-alkynyl complexes.

Acknowledgments

The colleagues and friends whose names appear in the reference list are thanked for many fruitful and instructive discussions concerning the redox properties of σ-alkynyl complexes over many years. We thank the Engineering and Physical Science Research Council (EPSRC) for funding our work through the award of a Leadership Fellowship to P. J. L.

[1] D. Astruc, *Chem. Asian J.* **2011**, *6*, 1679–1687.
[2] D. Astruc, *New J. Chem.* **2009**, *33*, 1191–1206.
[3] N. G. Connelly, W. Geiger, *Chem. Rev.* **1996**, *96*, 877–910.
[4] D. Astruc, *New J. Chem.* **2011**, *35*, 764–772.
[5] F. Diedrich, P. J. Stang, R. R. Tykwinski (Eds.), *Acetylene Chemistry: Chemistry, Biology and Materials Chemistry*, Wiley-VCH, Weinheim, Germany, **2004**.
[6] P. J. Stang, F. Diedrich (Eds.), *Modern Acetylene Chemistry*, Wiley-VCH, Weinheim, Germany, **1995**.
[7] A. de Meijere, F. Diedrich (Eds.), *Metal-Catalyzed Cross-Coupling Reactions*, Wiley-VCH, Weinheim, Germany, **2004**.
[8] T. V. Magdesieva, K. P. Butin, *Russ. Chem. Rev.* **2002**, *71*, 223–238.
[9] R. Poli, *Chem. Rev.* **1996**, *96*, 2135–2204.
[10] F. Paul, B. G. Ellis, M. I. Bruce, L. Toupet, T. Roisnel, K. Costuas, J.-F. Halet, C. Lapinte, *Organometallics* **2006**, *25*, 649–665.
[11] F. Paul, F. Malvolti, G. da Costa, S. Le Stang, F. Justaud, G. Argouarch, A. Bondon, S. Sinbandhit, K. Costuas, L. Toupet, C. Lapinte, *Organometallics* **2010**, *29*, 2491–2502.
[12] N. Gauthier, N. Tchouar, F. Justaud, G. Argouarch, M. P. Cifuentes, L. Toupet, D. Touchard, J.-F. Halet, S. Rigaut, M. G. Humphrey, K. Costuas, F. Paul, *Organometallics* **2009**, *28*, 2253–2266.
[13] F. Paul, G. da Costa, A. Bondon, N. Gauthier, S. Sinbandhit, L. Toupet, K. Costuas, J.-F. Halet, C. Lapinte, *Organometallics* **2007**, *26*, 874–896.

 © 2012 Wiley-VCH Verlag GmbH & Co. KGaA, Weinheim

[14] F. Paul, L. Toupet, J.-Y. Thépot, K. Costuas, J.-F. Halet, C. Lapinte, *Organometallics* **2005**, *24*, 5464–5478.
[15] F. Paul, J.-Y. Mevellec, C. Lapinte, *J. Chem. Soc., Dalton Trans.* **2002**, 1783–1790.
[16] R. Denis, L. Toupet, F. Paul, C. Lapinte, *Organometallics* **2000**, *19*, 4240–4251.
[17] K. Costuas, F. Paul, L. Toupet, J.-F. Halet, C. Lapinte, *Organometallics* **2004**, *23*, 2053–2068.
[18] M. A. Fox, R. L. Roberts, W. M. Khairul, F. Hartl, P. J. Low, *J. Organomet. Chem.* **2007**, *692*, 3277–3290.
[19] H. N. Lancashire, N. J. Brown, L. Carthy, D. Collison, E. C. Fitzgerald, R. Edge, M. Helliwell, M. Holden, P. J. Low, J. J. W. McDouall, M. W. Whiteley, *Dalton Trans.* **2011**, *40*, 1267–1278.
[20] N. J. Brown, D. Collison, R. Edge, E. C. Fitzgerald, M. Helliwell, J. A. K. Howard, H. N. Lancashire, P. J. Low, J. J. W. McDouall, J. Raftery, C. A. Smith, D. S. Yufit, M. W. Whiteley, *Organometallics* **2010**, *29*, 1261–1276.
[21] E. Carter, D. Collison, R. Edge, E. C. Fitzgerald, H. N. Lancashire, D. M. Murphy, J. J. W. McDouall, J. Sharples, M. W. Whiteley, *Dalton Trans.* **2010**, *39*, 11424–11434.
[22] G. Frapper, M. Kertesz, *Inorg. Chem.* **1993**, *32*, 732–740.
[23] N. Re, A. Sgamellotti, C. Floriani, *J. Chem. Soc., Dalton Trans.* **1998**, 2521–2529.
[24] S. Záliš, R. F. Winter, W. Kaim, *Coord. Chem. Rev.* **2010**, *254*, 1383–1396.
[25] W. E. Geiger, *Organometallics* **2007**, *26*, 5738–5765.
[26] M. C. Baird, *Chem. Rev.* **1988**, *88*, 1217–1227.
[27] K. Torraca, L. McElwee-White, *Coord. Chem. Rev.* **2000**, *206*, 469–491.
[28] G. G. Melikyan, in: *Frontiers in Organometallic Chemistry* (Ed.: M. A. Cato), Nova Science Publishers, New York, **2006**, pp. 155–190.
[29] N. A. Ustynyuk, O. V. Gusev, L. N. Novikova, M. G. Peterleitner, L. I. Denisovich, T. A. Peganova, O. V. Semeikin, D. A. Valyaev, *J. Solid State Electrochem.* **2007**, *11*, 1621–1634.
[30] M. A. Sierra, M. Gómez-Gallego, R. Martínez-Álvarez, *Chem. Eur. J.* **2007**, *13*, 736–744.
[31] D. A. Valyaev, O. V. Semeikin, N. A. Ustynyuk, *Coord. Chem. Rev.* **2004**, *248*, 1679–1692.
[32] J. E. McGrady, T. Lovell, R. Stranger, M. G. Humphrey, *Organometallics* **1997**, *16*, 4004–4011.
[33] C. D. Delfs, R. Stranger, M. G. Humphrey, A. M. McDonagh, *J. Organomet. Chem.* **2000**, *607*, 208–212.
[34] K. Costuas, S. Rigaut, *Dalton Trans.* **2011**, *40*, 5643–5658.
[35] C. Lapinte, *J. Organomet. Chem.* **2008**, *693*, 793–801.
[36] K. A. Green, M. P. Cifuentes, M. Samoc, M. G. Humphrey, *Coord. Chem. Rev.* **2011**, *255*, 2025–2038.
[37] K. A. Green, M. P. Cifuentes, M. Samoc, M. G. Humphrey, *Coord. Chem. Rev.* **2011**, *255*, 2530–2541.
[38] C. Liu, H. Zhang, W. Shi, A. Lei, *Chem. Rev.* **2011**, *111*, 1780–1824.
[39] I. P. Beletskaya, A. V. Cheprakov, *Coord. Chem. Rev.* **2004**, *248*, 2337–2364.
[40] K. C. Nicolaou, P. G. Bulger, D. Sarlah, *Angew. Chem.* **2005**, *117*, 4516; *Angew. Chem. Int. Ed.* **2005**, *44*, 4442–4489.
[41] P. J. Low, M. I. Bruce, *Adv. Organomet. Chem.* **2001**, *48*, 71–288.
[42] C. Glaser, *Ber. Dtsch. Chem. Ges.* **1869**, *2*, 422–424.
[43] G. Eglinton, A. R. Galbraith, *J. Chem. Soc.* **1959**, 889–896.
[44] G. Eglinton, W. McRae, in: *Advances in Organic Chemistry* (Eds.: R. A. Raphael, E. C. Taylor, H. Wynberg), Wiley, New York, **1963**, p. 225.
[45] A. S. Hay, *J. Org. Chem.* **1962**, *27*, 3320–3321.
[46] P. Cadiot, W. Chodkiewicz, in: *Chemistry of Acetylenes* (Ed.: H. G. Viehe), Marcel Dekker, New York, **1969**, pp. 597–647.
[47] L. Brandsma, in: *Synthesis of Acetylenes, Allenes and Cumulenes: Methods and Techniques*, Elsevier, Oxford, **2004**, pp. 281–291.
[48] G. E. Jones, D. A. Kendrick, A. B. Holmes, *Org. Synth.* **1987**, *65*, 52.
[49] D. F. Perepichka, S. Jeeva, *Chem. Eng. News* **2010**, *88*, 2.
[50] F. Bohlmann, H. Schönowsky, E. Inhoffen, G. Grau, *Chem. Ber.* **1964**, *97*, 794–800.
[51] L. Fomina, B. Vazquez, E. Tkatchouk, S. Fomine, *Tetrahedron* **2002**, *58*, 6741–6747.
[52] R. Balamurugan, N. Naveen, S. Manojveer, M. V. Nama, *Aust. J. Chem.* **2011**, *64*, 567–575.
[53] D. Wang, J. Li, N. Li, T. Gao, S. Hou, B. Chen, *Green Chem.* **2010**, *12*, 45–48.
[54] K. Balaraman, V. Kesavan, *Synthesis* **2010**, 3461–3466.
[55] P. Bharathi, M. Periasamy, *Organometallics* **2000**, *19*, 5511–5513.
[56] M. Krafft, C. Hirosawa, N. Dalal, C. Ramsey, A. Stiegman, *Tetrahedron Lett.* **2001**, *42*, 7733–7736.
[57] K. Sonogashira, *J. Organomet. Chem.* **2002**, *653*, 46–49.
[58] R. Chinchilla, C. Nájera, *Chem. Rev.* **2007**, *107*, 874–922.
[59] P. Nguyen, Z. Yuan, L. Agocs, G. Lesley, T. B. Marder, *Inorg. Chim. Acta* **1994**, *220*, 289–296.
[60] A. S. Batsanov, J. C. Collings, I. J. S. Fairlamb, J. Holland, J. A. K. Howard, Z. Lin, T. B. Marder, A. Parsons, R. M. Ward, J. Zhu, *J. Org. Chem.* **2005**, *70*, 703–706.
[61] E. Merkul, D. Urselmann, T. J. J. Mueller, *Eur. J. Org. Chem.* **2011**, 238–242.
[62] C. Amatore, E. Blart, J. P. Genét, A. Jutand, S. Lemaire-Audoire, M. Savignac, *J. Org. Chem.* **1995**, *60*, 6829–6839.
[63] A. Lei, M. Srivastava, X. Zhang, *J. Org. Chem.* **2002**, *67*, 1969–1971.
[64] S.-N. Chen, W.-Y. Wu, F.-Y. Tsai, *Green Chem.* **2009**, *11*, 269–274.
[65] J.-H. Li, Y. Liang, Y. Xie, *J. Org. Chem.* **2005**, *70*, 4393–4396.
[66] J.-H. Li, Y. Liang, X. Zhang, *Tetrahedron* **2005**, *61*, 1903–1907.
[67] M. Shi, H.-X. Qian, *Appl. Organomet. Chem.* **2006**, *20*, 771–774.
[68] J. Yan, J. Wu, H. Jin, *J. Organomet. Chem.* **2007**, *692*, 3636–3639.
[69] Q. Liu, D. J. Burton, *Tetrahedron Lett.* **1997**, *38*, 4371–4374.
[70] X. Meng, C. Li, B. Han, T. Wang, B. Chen, *Tetrahedron* **2010**, *66*, 4029–4031.
[71] J. D. Crowley, S. M. Goldup, N. D. Gowans, D. A. Leigh, V. E. Ronaldson, A. M. Z. Slawin, *J. Am. Chem. Soc.* **2010**, *132*, 6243–6248.
[72] W. Yin, C. He, M. Chen, H. Zhang, A. Lei, *Org. Lett.* **2009**, *11*, 709–712.
[73] L. A. Jones, S. Sanz, M. Laguna, *Catal. Today* **2007**, *122*, 403–406.
[74] D. Weber, M. R. Gagné, *Chem. Commun.* **2011**, *47*, 5172–5174.
[75] T. Lauterbach, M. Livendahl, A. Rosellón, P. Espinet, A. M. Echavarren, *Org. Lett.* **2010**, *12*, 3006–3009.
[76] A. S. K. Hashmi, R. Döpp, C. Lothschuetz, M. Rudolph, D. Riedel, F. Rominger, *Adv. Synth. Catal.* **2010**, *352*, 1307–1314.
[77] A. S. K. Hashmi, C. Lothschuetz, R. Döpp, M. Rudolph, T. D. Ramamurthi, F. Rominger, *Angew. Chem.* **2009**, *121*, 8392; *Angew. Chem. Int. Ed.* **2009**, *48*, 8243–8246.
[78] W. M. Khairul, M. A. Fox, N. N. Zaitseva, M. Gaudio, D. S. Yufit, B. W. Skelton, A. H. White, J. A. K. Howard, M. I. Bruce, P. J. Low, *Dalton Trans.* **2009**, 610–620.
[79] W. Y. Man, S. Bock, N. N. Zaitseva, M. I. Bruce, P. J. Low, *J. Organomet. Chem.* **2011**, *696*, 2172–2176.
[80] M. I. Bruce, M. E. Smith, N. N. Zaitseva, B. W. Skelton, A. H. White, *J. Organomet. Chem.* **2003**, *670*, 170–177.
[81] A. B. Antonova, M. I. Bruce, B. Ellis, M. Gaudio, P. A. Humphrey, M. Jevric, G. Melino, B. K. Nicholson, G. J. Perkins, B. W. Skelton, B. Stapleton, A. H. White, N. N. Zaitseva, *Chem. Commun.* **2004**, 960–961.
[82] M. I. Bruce, N. N. Zaitseva, B. K. Nicholson, B. W. Skelton, A. H. White, *J. Organomet. Chem.* **2008**, *693*, 2887–2897.
[83] M. I. Bruce, B. K. Nicholson, N. N. Zaitseva, *C. R. Chim.* **2009**, *12*, 1280–1286.
[84] H. A. Wegner, S. Ahles, M. Neuburger, *Chem. Eur. J.* **2008**, *14*, 11310–11313.

 © 2012 Wiley-VCH Verlag GmbH & Co. KGaA, Weinheim

[85] T. de Haro, C. Nevado, *J. Am. Chem. Soc.* **2010**, *132*, 1512–1513.
[86] J. Ipaktschi, F. Munz, *Eur. J. Inorg. Chem.* **2006**, 2078–2082.
[87] N. A. Ustynyuk, V. N. Vinogradova, V. N. Korneva, D. N. Kravtsov, V. G. Andrianov, Y. T. Struchkov, *J. Organomet. Chem.* **1984**, *277*, 285–296.
[88] H. Lang, S. Blau, G. Rheinwald, L. Zsolnai, *J. Organomet. Chem.* **1995**, *494*, 65–73.
[89] H. Lang, S. Blau, G. Rheinwald, G. Wildermuth, *J. Organomet. Chem.* **1995**, *489*, C17–C21.
[90] H. Lang, S. Blau, G. Rheinwald, *J. Organomet. Chem.* **1995**, *492*, 81–85.
[91] C.-W. Shiu, C.-J. Su, C.-W. Pin, Y. Chi, P. S.-M. Peng, G.-H. Lee, *J. Organomet. Chem.* **1997**, *545*, 151–156.
[92] R. L. Roberts, H. Puschmann, J. A. K. Howard, J. Yamamoto, A. J. Carty, P. J. Low, *Dalton Trans.* **2003**, 1099–1105.
[93] Y. F. Cheng, D. L. Phillips, G. He, C.-M. Che, Y. Chi, *Chem. Phys. Lett.* **2001**, *338*, 308–316.
[94] P. Magnus, D. P. Becker, *J. Chem. Soc., Chem. Commun.* **1985**, 640–642.
[95] B. F. G. Johnson, J. Lewis, P. R. Raithby, D. A. Wilkinson, *J. Organomet. Chem.* **1991**, *408*, C9–C12.
[96] M. I. Bruce, B. W. Skelton, M. E. Smith, A. H. White, *Aust. J. Chem.* **1999**, *52*, 431–435.
[97] S. Rigaut, F. Monnier, F. Mousset, D. Touchard, P. H. Dixneuf, *Organometallics* **2002**, *21*, 2654–2661.
[98] S. Rigaut, O. Maury, D. Touchard, P. H. Dixneuf, *Chem. Commun.* **2001**, 373–374.
[99] S. Rigaut, K. Costuas, D. Touchard, J.-Y. Saillard, S. Golhen, P. H. Dixneuf, *J. Am. Chem. Soc.* **2004**, *126*, 4072–4073.
[100] N. J. Brown, P. K. Eckert, M. A. Fox, D. S. Yufit, J. A. K. Howard, P. J. Low, *Dalton Trans.* **2008**, 433–436.
[101] R. G. Beevor, M. J. Freeman, M. Green, C. E. Morton, A. G. Orpen, *J. Chem. Soc., Chem. Commun.* **1985**, 68–70.
[102] K. Venkatesan, O. Blacque, T. Fox, M. Alfonso, H. W. Schmalle, S. Kheradmandan, H. Berke, *Organometallics* **2005**, *24*, 920–932.
[103] K. Venkatesan, O. Blacque, H. Berke, *Organometallics* **2006**, *25*, 5190–5200.
[104] L. N. Novikova, M. G. Peterleitner, K. A. Sevumyan, O. V. Semeikin, D. A. Valyaev, N. A. Ustynyuk, V. N. Khrustalev, L. N. Kuleshova, M. Y. Antipin, *J. Organomet. Chem.* **2001**, *631*, 47–53.
[105] L. N. Novikova, M. G. Peterleitner, K. A. Sevumyan, O. V. Semeikin, D. A. Valyaev, N. A. Ustynyuk, *Appl. Organomet. Chem.* **2002**, *16*, 530–536.
[106] D. A. Valyaev, M. G. Peterleitner, L. I. Leont'eva, L. N. Novikova, O. V. Semeikin, V. N. Khrustalev, M. Y. Antipin, N. A. Ustynyuk, B. W. Skelton, A. H. White, *Organometallics* **2003**, *22*, 5491–5497.
[107] N. A. Ustynyuk, V. N. Vinogradova, V. G. Andrianov, Y. T. Struchkov, *J. Organomet. Chem.* **1984**, *268*, 73–78.
[108] L. I. Denisovich, T. Filatova, M. G. Peterleitner, N. A. Ustynyuk, V. N. Vinogradova, L. I. Leont'eva, *Russ. Chem. Bull. Int Ed.* **1998**, *47*, 1901–1904.
[109] R. S. Iyer, J. P. Selegue, *J. Am. Chem. Soc.* **1987**, *109*, 910–911.
[110] C. Bitcon, M. W. Whiteley, *J. Organomet. Chem.* **1987**, *336*, 385–392.
[111] N. Le Narvor, C. Lapinte, *J. Chem. Soc., Chem. Commun.* **1993**, 357–359.
[112] N. Le Narvor, L. Toupet, C. Lapinte, *J. Am. Chem. Soc.* **1995**, *117*, 7129–7138.
[113] R. L. Beddoes, C. Bitcon, A. Ricalton, M. W. Whiteley, *J. Organomet. Chem.* **1989**, *367*, C21–C24.
[114] R. L. Beddoes, C. Bitcon, R. W. Grime, A. Ricalton, M. W. Whiteley, *J. Chem. Soc., Dalton Trans.* **1995**, 2873–2883.
[115] N. G. Connelly, M. P. Gamasa, J. Gimeno, C. Lapinte, E. Lastra, J. P. Maher, N. Le Narvor, A. L. Rieger, P. H. Rieger, *J. Chem. Soc., Dalton Trans.* **1993**, 2575–2578.
[116] F. Coat, M.-A. Guillevic, L. Toupet, F. Paul, C. Lapinte, *Organometallics* **1997**, *16*, 5988–5998.
[117] S. Ibn Ghazala, N. Gauthier, F. Paul, L. Toupet, C. Lapinte, *Organometallics* **2007**, *26*, 2308–2317.
[118] F. de Montigny, G. Argouarch, T. Roisnel, L. Toupet, C. Lapinte, S. C.-F. Lam, C.-H. Tao, V. W.-W. Yam, *Organometallics* **2008**, *27*, 1912–1923.
[119] P. Hamon, F. Justaud, O. Cador, P. Hapiot, S. Rigaut, L. Toupet, L. Ouahab, H. Stueger, J.-R. Hamon, C. Lapinte, *J. Am. Chem. Soc.* **2008**, *130*, 17372–17383.
[120] F. Malvolti, A. Trujillo, O. Cador, F. Gendron, K. Costuas, J.-F. Halet, A. Bondon, L. Toupet, Y. Molard, S. Cordier, F. Paul, *Inorg. Chim. Acta* **2011**, *374*, 288–301.
[121] M. I. Bruce, C. Dean, D. N. Duffy, M. G. Humphrey, G. A. Koutsantonis, *J. Organomet. Chem.* **1985**, *295*, C40–C44.
[122] M. I. Bruce, M. G. Humphrey, G. A. Koutsantonis, M. J. Liddell, *J. Organomet. Chem.* **1987**, *326*, 247–256.
[123] M. I. Bruce, M. G. Humphrey, G. A. Koutsantonis, B. K. Nicholson, *J. Organomet. Chem.* **1985**, *296*, C47–C50.
[124] M. I. Bruce, G. A. Koutsantonis, M. J. Liddell, B. K. Nicholson, *J. Organomet. Chem.* **1987**, *320*, 217–227.
[125] M. I. Bruce, G. A. Koutsantonis, *Aust. J. Chem.* **1991**, *44*, 207–217.
[126] M. I. Bruce, M. P. Cifuentes, M. R. Snow, E. R. T. Tiekink, *J. Organomet. Chem.* **1989**, *359*, 379–399.
[127] M. I. Bruce, G. A. Koutsantonis, M. J. Liddell, E. R. T. Tiekink, *J. Organomet. Chem.* **1991**, *420*, 253–269.
[128] M. I. Bruce, A. Burgun, F. Gendron, G. Grelaud, J.-F. Halet, B. W. Skelton, *Organometallics* **2011**, *30*, 2861–2868.
[129] M. Brady, W. Weng, Y. Zhou, W. Jeffery, *J. Am. Chem. Soc.* **1997**, *119*, 775–788.
[130] A. Wong, P. C. W. Kang, C. D. Tagge, D. R. Leon, *Organometallics* **1990**, *9*, 1992–1994.
[131] M. I. Bruce, K. Costuas, J.-F. Halet, B. C. Hall, P. J. Low, B. K. Nicholson, B. W. Skelton, A. H. White, *J. Chem. Soc., Dalton Trans.* **2002**, 383–398.
[132] M. I. Bruce, M. Ke, P. J. Low, B. W. Skelton, A. H. White, *Organometallics* **1998**, *17*, 3539–3549.
[133] M. I. Bruce, M. Ke, P. J. Low, *Chem. Commun.* **1996**, 2405–2406.
[134] M. I. Bruce, B. C. Hall, B. D. Kelly, P. J. Low, B. W. Skelton, A. H. White, *J. Chem. Soc., Dalton Trans.* **1999**, 3719–3728.
[135] M. I. Bruce, B. G. Ellis, P. J. Low, B. W. Skelton, A. H. White, *Organometallics* **2003**, *22*, 3184–3198.
[136] M. I. Bruce, B. G. Ellis, B. W. Skelton, A. H. White, *J. Organomet. Chem.* **2005**, *690*, 792–801.
[137] M. I. Bruce, K. Costuas, T. Davin, J.-F. Halet, K. A. Kramarczuk, P. J. Low, B. K. Nicholson, G. J. Perkins, R. L. Roberts, B. W. Skelton, M. E. Smith, A. H. White, *Dalton Trans.* **2007**, 5387–5399.
[138] E. C. Fitzgerald, N. J. Brown, R. Edge, M. Helliwell, H. N. Roberts, F. Tuna, A. Beeby, D. Collison, P. J. Low, M. W. Whiteley, *Organometallics* **2011**, in press; DOI: 10.1021/om200712m.
[139] A. Antiñolo, C. García-Yebra, M. Fajardo, I. del Hierro, C. López-Mardomingo, I. López-Solera, A. Otera, Y. Pérez, S. Prashar, *J. Organomet. Chem.* **2003**, *670*, 123–131.
[140] G. Litwinienko, A. L. J. Beckwith, K. U. Ingold, *Chem. Soc. Rev.* **2011**, *40*, 2157–2163.
[141] W. M. Khairul, M. A. Fox, P. A. Schauer, D. Albesa-Jove, D. S. Yufit, J. A. K. Howard, P. J. Low, *Inorg. Chim. Acta* **2011**, *374*, 461–471.
[142] E. Di Piazza, L. Norel, K. Costuas, A. Bourdolle, O. Maury, S. Rigaut, *J. Am. Chem. Soc.* **2011**, *133*, 6174–6176.
[143] M. I. Bruce, M. G. Humphrey, M. J. Liddell, *J. Organomet. Chem.* **1987**, *321*, 91–102.
[144] M. I. Bruce, A. G. Swincer, R. C. Wallis, *J. Organomet. Chem.* **1979**, *171*, C5–C8.
[145] M. I. Bruce, A. G. Swincer, *Adv. Organomet. Chem.* **1983**, *22*, 59–128.

 © 2012 Wiley-VCH Verlag GmbH & Co. KGaA, Weinheim

[146] M. I. Bruce, M. G. Humphrey, *Aust. J. Chem.* **1989**, *42*, 1067–1075.
[147] R. Le Lagadec, E. Roman, L. Toupet, U. Müller, P. H. Dixneuf, *Organometallics* **1994**, *13*, 5030–5039.
[148] F. Paul, L. Toupet, T. Roisnel, P. Hamon, C. Lapinte, *C. R. Chim.* **2005**, *8*, 1174–1185.
[149] M. I. Bruce, P. Hinterding, P. J. Low, B. W. Skelton, A. H. White, *J. Chem. Soc., Dalton Trans.* **1998**, 467–474.
[150] M. I. Bruce, P. A. Humphrey, N. N. Zaitseva, B. K. Nicholson, B. W. Skelton, A. H. White, *Dalton Trans.* **2010**, *39*, 8801–8811.
[151] R. F. Winter, F. M. Hornung, *Organometallics* **1999**, *18*, 4005–4014.
[152] R. F. Winter, K. W. Klinkhammer, S. Záliš, *Organometallics* **2001**, *20*, 1317–1333.
[153] O. F. Koentjoro, R. Rousseau, P. J. Low, *Organometallics* **2001**, *20*, 4502–4509.
[154] S. Rigaut, L. Le Pichon, D. Touchard, P. H. Dixneuf, J.-C. Daran, *Chem. Commun.* **2001**, 1206–1207.
[155] N. J. Brown, D. Collison, R. Edge, E. C. Fitzgerald, P. J. Low, M. Helliwell, Y. T. Ta, M. W. Whiteley, *Chem. Commun.* **2010**, *46*, 2253–2255.
[156] Y. Hayashi, M. Osawa, K. Kobayashi, Y. Wakatsuki, *Chem. Commun.* **1996**, 1617–1618.
[157] Y. Hayashi, M. Osawa, Y. Wakatsuki, *J. Organomet. Chem.* **1997**, *542*, 241–246.
[158] A. Vacher, F. Barrière, T. Roisnel, D. Lorcy, *Chem. Commun.* **2009**, 7200–7202.
[159] A. Vacher, F. Barrière, T. Roisnel, L. Piekara-Sady, D. Lorcy, *Organometallics* **2011**, *30*, 3570–3578.
[160] A. Miyazaki, Y. Ogyu, F. Justaud, L. Ouahab, T. Cauchy, J.-F. Halet, C. Lapinte, *Organometallics* **2010**, *29*, 4628–4638.
[161] R. Packheiser, P. Ecorchard, B. Walfort, H. Lang, *J. Organomet. Chem.* **2008**, *693*, 933–946.
[162] G. A. Koutsantonis, G. I. Jenkins, P. A. Schauer, B. Szczepaniak, B. W. Skelton, C. Tan, A. H. White, *Organometallics* **2009**, *28*, 2195–2205.
[163] C.-Y. Wong, G. Tong, C.-M. Che, N. Zhu, *Angew. Chem.* **2006**, *118*, 2760; *Angew. Chem. Int. Ed.* **2006**, *45*, 2694–2698.
[164] O. Pelerin, C. Olivier, T. Roisnel, D. Touchard, S. Rigaut, *J. Organomet. Chem.* **2008**, *693*, 2153–2158.
[165] M. P. Cifuentes, M. G. Humphrey, G. A. Koutsantonis, N. A. Lengkeek, S. Petrie, V. Sanford, P. A. Schauer, B. W. Skelton, R. Stranger, A. H. White, *Organometallics* **2008**, *27*, 1716–1726.
[166] E. O. Fischer, M. Schluge, J. O. Besenhard, P. Friedrich, G. Huttner, F. R. Kreißl, *Chem. Ber.* **1978**, *111*, 3530–3541.
[167] M. Sato, Y. Hayashi, S. Kumakura, N. Shimizu, M. Katada, S. Kawata, *Organometallics* **1996**, *15*, 721–728.
[168] M. I. Bruce, P. A. Humphrey, M. Jevric, G. J. Perkins, B. W. Skelton, A. H. White, *J. Organomet. Chem.* **2007**, *692*, 1748–1756.
[169] M. I. Bruce, M. E. Smith, B. W. Skelton, A. H. White, *J. Organomet. Chem.* **2001**, *637*, 484–499.
[170] M. I. Bruce, P. A. Humphrey, M. Jevric, B. W. Skelton, A. H. White, *J. Organomet. Chem.* **2007**, *692*, 2564–2574.
[171] P. Butler, J. F. Gallagher, A. R. Manning, H. Mueller-Bunz, C. J. McAdam, J. Simpson, B. H. Robinson, *J. Organomet. Chem.* **2005**, *690*, 4545–4556.
[172] J. H. K. Yip, J. Wu, K.-Y. Wong, K. Yeung, J. J. Vittal, *Organometallics* **2002**, *21*, 1612–1621.
[173] J. H. K. Yip, J. Wu, K.-Y. Wong, K. P. Ho, C. Pun, J. J. Vittal, *Organometallics* **2002**, *21*, 5292–5300.
[174] J. F. Berry, F. A. Cotton, C. A. Murillo, *Organometallics* **2004**, *23*, 2503–2506.
[175] G. Xu, R. J. Crutchley, M. C. DeRosa, Q. Pan, H. Zhang, X. Wang, T. Ren, *J. Am. Chem. Soc.* **2005**, *127*, 13354–13363.
[176] Y. Zhu, O. Clot, M. O. Wolf, G. Yap, *J. Am. Chem. Soc.* **1998**, *120*, 1812–1821.
[177] M. C. B. Colbert, J. Lewis, N. Long, P. R. Raithby, A. J. P. White, D. J. Williams, *J. Chem. Soc., Dalton Trans.* **1997**, 99–104.
[178] N. D. Jones, M. O. Wolf, D. M. Giaquinta, *Organometallics* **1997**, *16*, 1352–1354.
[179] Á. Díez, J. Fernández, E. Lalinde, M. T. Moreno, S. Sánchez, *Dalton Trans.* **2008**, 4926–4936.
[180] S. S. Kumar, N. D. Reddy, H. W. Roesky, D. Vidovic, J. Magull, R. F. Winter, *Organometallics* **2003**, *22*, 3348–3350.
[181] N. Szesni, M. Drexler, J. Maurer, R. F. Winter, F. de Montigny, C. Lapinte, S. Steffens, J. Heck, B. Weibert, H. Fischer, *Organometallics* **2006**, *25*, 5774–5787.
[182] R. F. Winter, S. Záliš, *Coord. Chem. Rev.* **2004**, *248*, 1565–1583.
[183] R. F. Winter, *Chem. Commun.* **1998**, 2209–2210.
[184] S. Hartmann, R. F. Winter, T. Scheiring, M. Wanner, *J. Organomet. Chem.* **2001**, *637*, 240–250.
[185] S. Hartmann, R. F. Winter, B. M. Brunner, B. Sarkar, A. Knodler, I. Hartenbach, *Eur. J. Inorg. Chem.* **2003**, 876–891.
[186] L. T. Byrne, G. A. Koutsantonis, V. Sanford, J. P. Selegue, P. A. Schauer, R. S. Iyer, *Organometallics* **2010**, *29*, 1199–1209.
[187] M. Sato, H. Shintate, Y. Kawata, M. Sekino, M. Katada, S. Kawata, *Organometallics* **1994**, *13*, 1956–1962.
[188] M. I. Bruce, P. J. Low, F. Hartl, P. A. Humphrey, F. de Montigny, M. Jevric, C. Lapinte, G. J. Perkins, R. L. Roberts, B. W. Skelton, A. H. White, *Organometallics* **2005**, *24*, 5241–5255.
[189] M. Sato, Y. Kawata, H. Shintate, Y. Habata, S. Akabori, K. Unoura, *Organometallics* **1997**, *16*, 1693–1701.
[190] M. Sato, A. Iwai, M. Watanabe, *Organometallics* **1999**, *18*, 3208–3219.
[191] Y. Tanaka, A. Inagaki, M. Akita, *Chem. Commun.* **2007**, 1169–1171.
[192] Y. Tanaka, T. Ishisaka, A. Inagaki, T. Koike, C. Lapinte, M. Akita, *Chem. Eur. J.* **2010**, *16*, 4762–4776.
[193] K. A. Green, M. P. Cifuentes, T. C. Corkery, M. Samoc, M. G. Humphrey, *Angew. Chem.* **2009**, *121*, 8007; *Angew. Chem. Int. Ed.* **2009**, *48*, 7867–7870.
[194] Y. Zhu, M. O. Wolf, *J. Am. Chem. Soc.* **2000**, *122*, 10121–10125.
[195] Y. Zhu, D. B. Millet, M. O. Wolf, S. J. Rettig, *Organometallics* **1999**, *18*, 1930–1938.
[196] G. A. Koutsantonis, P. A. Schauer, B. W. Skelton, *Organometallics* **2011**, *30*, 2680–2689.
[197] J. A. Shaw-Taberlet, S. Sinbandhit, T. Roisnel, J.-R. Hamon, C. Lapinte, *Organometallics* **2006**, *25*, 5311–5325.
[198] H. N. Roberts née Lancashire, N. J. Brown, R. Edge, R. Lewin, D. Collison, P. J. Low, M. W. Whiteley, *Organometallics* **2011**, *30*, 3763–3778.
[199] D. L. Lichtenberger, S. K. Renshaw, R. M. Bullock, *J. Am. Chem. Soc.* **1993**, *115*, 3276–3285.
[200] D. L. Lichtenberger, S. K. Renshaw, A. Wong, C. D. Tagge, *Organometallics* **1993**, *12*, 3522–3526.
[201] G. M. Aston, S. Badriya, R. D. Farley, R. W. Grime, S. J. Ledger, F. E. Mabbs, E. J. L. McInnes, H. W. Morris, A. Ricalton, C. C. Rowlands, K. Wagner, M. W. Whiteley, *J. Chem. Soc., Dalton Trans.* **1999**, 4379–4388.

Received: September 19, 2011
Published Online: December 13, 2011

 © 2012 Wiley-VCH Verlag GmbH & Co. KGaA, Weinheim

DOI: 10.1002/ejic.201100880

Cooperative Aliphatic PNP Amido Pincer Ligands – Versatile Building Blocks for Coordination Chemistry and Catalysis

Sven Schneider,*[a] Jenni Meiners,[a] and Bjorn Askevold[a]

Keywords: Cooperative catalysis / Pincer complexes / N ligands / Homogeneous catalysis / C–H activation

In this review, the coordination chemistry of electron-rich metal complexes with the simple aliphatic, anionic diphosphanylamido ligand $\{N(CH_2CH_2PR_2)_2\}^-$ is covered and compared with other commonly used, anionic PEP (E = C, N) pincer ligands. The strong π-basicity of this ligand enables both the stabilization of electronically and coordinatively highly unsaturated complexes and their use as cooperating ligands in bifunctional stoichiometric bond activation reactions and catalysis. Versatile ligand backbone dehydrogenation gives access to related enamido and dienamido ligands $\{(R_2PCHCH)N(CH_2CH_2PR_2)\}^-$ and $\{N(CHCHPR_2)_2\}^-$, respectively. This oxidative functionalization enables fine-tuning of the ligand donor properties and thereby of the structural features, electronic structure, and reactivity of the respective complexes, which is discussed for several examples.

1. Introduction

"Pincer ligands" are tridentate ligands that coordinate to a metal center in a meridional fashion.[1] For many pincer ligand frameworks, bulky substituents are easily introduced to sterically protect vacant coordination sites and allow for reactivity control by rational ligand design. Consequently, pincer complexes have found widespread use for several applications, such as catalysis, sensing, or metal-centered bond activation.[1,2] Electronic effects that arise from pincer modifications, particularly at the central ligand framework in *trans*-position with respect to the substrate binding site, offer further synthetic strategies for catalysis and bond activation reactions. As an example, variation of electron-donating/withdrawing substituents X on the aryl backbone of "archetypal" PCP pincer ligand $\{p\text{-X-}C_6H_2\text{-}2,6\text{-}(CH_2PR_2)_2\}^-$ was shown to have a strong influence on the thermodynamics of the oxidative addition of E–H (E = H, C) to a d^8 metal center, attributable to M–C_{PCP} π-MO interactions.[3] Alternatively, rigid, anionic pincer ligands with a central amido unit derived from diarylamines (Figure 1, $\{L_A{}^R\}^-$) or from pyridine-based chelates upon benzylic deprotonation (Figure 1, $\{L_B{}^R\}^-$) have recently attracted considerable attention. The latter were extensively utilized for novel dehydrogenative coupling reactions of polar functional groups as metal–ligand cooperative catalysts based on reversible amide/pyridine de-/aromatization.[1,4–6]

In comparison, despite seminal work from Fryzuk's group using a disilylamido PNP ligand (Figure 1, $\{L_C{}^R\}^-$) in combination with d^6 and d^8 metal ions, aliphatic amido pincer ligands were neglected for some time.[7] Amido ligands with C–H bonds in the α-position are generally prone to β-hydride elimination giving rise to imine formation.[8] Hence, the expected lower thermal stabilities and more complex reactivity patterns from ligand chemical non-innocence might have impeded the use of alkylamido ligands to some extent. However, chelating amido ligands exhibit higher barriers for imine extrusion as compared to terminal amides. Particularly, the great success of "bifunctional catalysis" for the hydrogenation of polar multiple bonds sparked great interest in flexible, chelating ligands that can facilitate H_2 heterolysis by the stabilization of both amido and amino intermediates, which occur during ionic hydrogenation.[9]

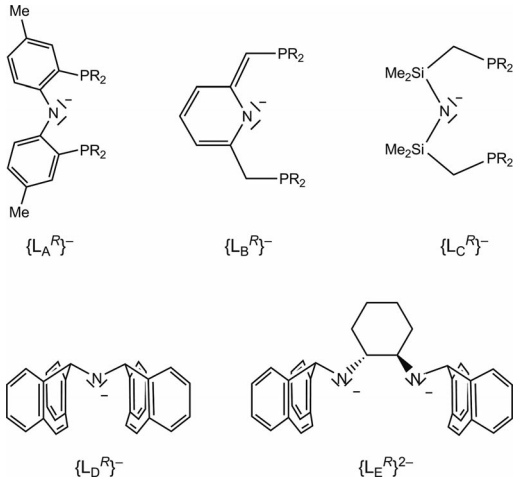

Figure 1. Amido pincer ligands structurally related to the aliphatic PNP ligands discussed here.

[a] Department Chemie und Pharmazie, Friedrich-Alexander-Universität Erlangen-Nürnberg,
Egerlandstr. 1, 91058 Erlangen, Germany
E-mail: sven.schneider@chemie.uni-erlangen.de

© 2012 Wiley-VCH Verlag GmbH & Co. KGaA, Weinheim

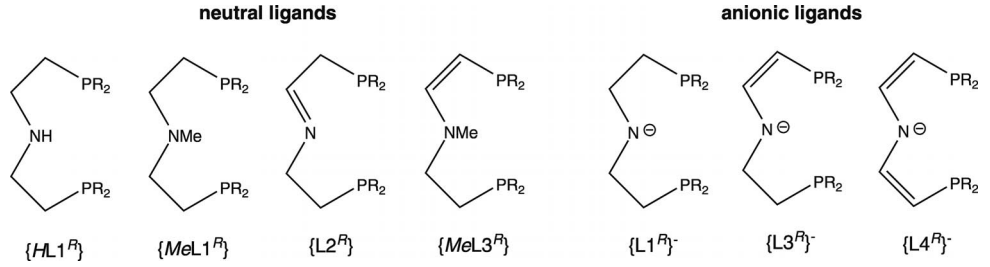

Figure 2. Neutral and anionic ligands derived from parent $HN(CH_2CH_2PR_2)_2$.

This review covers the recent work with aliphatic, anionic PNP ligands, particularly ethylene bridged ligand $N(CH_2CH_2PR_2)_2^-$ ($\{L1^R\}^-$), and related ligands derived by simple ligand backbone functionalization (Figure 2). These oxidative ligand modifications are discussed in combination with their impact on donor properties and electronic structure and reactivity of the respective complexes. After a concise introduction into the bonding and reactivity of amido ligands coordinated to electron-rich transition metal centers (section 1.1), the properties of PNP amido, enamido, and dienamido ligands are compared with those of other common pincer ligands (section 2). Finally, their use for the stabilization of unusual, electronically unsaturated complexes (section 3) and for metal–ligand cooperative bond activation and catalysis (section 4) are discussed.

1.1. Electron-Rich Transition Metal Amides: Bonding, Electronic Structure, and Reactivity

Covalently bound π-donating ligands, such as amido ligand (NR_2^-), are frequently used to stabilize complexes of electron-poor (early) transition metals in high oxidation states.[10] In contrast, until more recently electron-rich (late) transition metal complexes in low oxidation states (d^6–d^{10}) with these ligands were comparatively rare.[11] However, the participation of late transition metal amido complexes in catalytic transformations, such as C–N cross coupling reactions,[12] has stimulated several studies on M–NR_2 bonding. Pearson's hard and soft acid and base (HSAB) theory predicts weak bonding of hard, π-donating amido ligands with electron-rich metal centers.[13] Nevertheless, Bercaw and coworkers demonstrated a linear relationship of M–R (M = Ru^{II}, Pt^{II}; R = alkyl, aryl, acetylide, hydride, alkoxide, and amide) bond dissociation energies (BDEs) with the corresponding H–R BDEs.[14] On the other hand, comparison of metal amido hydrogenolysis along the transition series ($L_nM–NR_2 + H_2 \leftrightarrows L_nM–H + HNR_2$) provides some qualitative information with respect to relative M–N_{amido} bond energetics:[15] While d^6 and d^8 anilido complexes $[Cp^*Ru(NHPh)(PMe_3)_2]$ or $[PtH(NHPh)(PEt_3)_2]$ readily react with H_2 to give the corresponding hydride complex and

Sven Schneider studied chemistry at the Technische Universität Darmstadt (Diploma 1999 with Prof. H.-J. Klein) and received a Ph.D. from Humboldt Universität Berlin (2003) working on group 6 amido complexes under the supervision of Prof. A. C. Filippou. He subsequently joined the group of Prof. T. J. Marks at Northwestern University for postdoctoral studies dedicated to single-source precursors for copper chalcogenide materials. In 2006, he started his independent career at the Technische Universität München as an Emmy-Noether group leader, and in 2010 he received his current position as W2 (associate) professor for inorganic chemistry at the Universität Erlangen-Nürnberg. His research interests include organometallic chemistry and homogeneous catalysis, particularly as directed towards small molecule activation, (de-) hydrogenation, and inorganic materials synthesis.

Jenni Meiners studied chemistry at Humboldt Universität Berlin and obtained her Diploma (M.Sc.) in 2007 in the group of Prof. P. W. Roesky (Freie Universität Berlin). She joined the group of Sven Schneider at the Technische Universität München in 2008. Currently she is finishing her Ph.D. at the Universität Erlangen-Nürnberg, working on the coordination chemistry of iridium amido complexes and C–H functionalization reactions.

Bjorn Askevold studied chemistry at the Technische Universität München in 2008 and obtained an M.Sc. under the supervision of Prof. J. Eppinger. In 2009 he joined the group of Sven Schneider at TU München as a Ph.D. student to work on low-coordinated iridium and ruthenium PNP complexes. He is currently finishing his Ph.D. Thesis at the Universität Erlangen-Nürnberg.

 © 2012 Wiley-VCH Verlag GmbH & Co. KGaA, Weinheim

free amine, $[Cp^*_2Zr(H)_2]$ exhibits reverse reactivity and releases H_2 with NH_2Ph.[14,16] This reactivity is in line with calculated relative BDEs $\{BDE_{M-H} - BDE_{M-N}$: 151 kJ mol^{-1} $[Cp^*Ru(PMe_3)_2]$; 121 kJ mol^{-1} $[PtH(PEt_3)_2]$; 4 kJ mol^{-1} $(Cp^*_2ZrH)\}$. These results can be rationalized on the basis of M–N bonding: High anionic charge density on the nitrogen atom is expected as a result of polar metal–amido σ-bonding.[17] If vacant metal orbitals for N→M π-donation are available, the charge will be effectively delocalized, strengthening the M–N bond as in the case of d^0 complex $[Cp^*_2Zr(NHPh)(H)]$.[18] For metal centers without empty d orbitals of suitable symmetry and energy, for example, octahedral d^6 or square-planar d^8 complexes, no net M–N π-bond results from the M–N π-interaction.[19]

This lack of charge delocalization results in high basicity and nucleophilicity of the amido ligand, exemplified by C–N coupling with *C*-electrophiles.[20,21] Proton transfer to the amido ligand upon H_2 heterolysis was first demonstrated by Fryzuk and co-workers for d^6 and d^8 complexes with disilylamido pincer ligand $\{L_C{}^R\}^-$.[22] This reaction was later recognized as key step for "bifunctional" (also denoted "metal–ligand cooperative" or "Noyori–Morris type" catalysis or initially as "N–H effect") hydrogenation catalysis and was therefore extensively studied.[9] Other than H_2, weakly acidic sp, sp^2, and sp^3 C–H bonds were also shown to add across $M–N_{amido}$ bonds.[21a,23]

However, cooperativity of amido ligands is not restricted to acid–base chemistry. A mainly *N*-centered HOMO suggests potential ligand redox non-innocence for amido radical complexes or, in terms of a simple Lewis formalism, a description as aminyl (*N*-radical) rather than amido (metalloradical) complex (Figure 3).[24] The electronic structure of amido radical complexes is of relevance for catalysis, for example, oxidative dehydrogenation of amines, which is particularly well promoted by metals of the iron triad.[25] The oxidation of alcohols to aldehydes catalyzed by the oxidoreductase enzyme galactose oxidase provides a related example in nature.[26] In the active site, the copper phenoxide moiety undergoes both metal- and ligand-centered one-electron redox steps to accomplish the overall two-electron redox reaction.

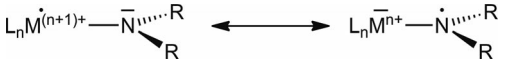

Figure 3. Canonic Lewis structures for open-shell amido complexes.

para-Aryl C–C-coupling was reported in early studies as a consequence of platinum(II) anilide oxidation, pointing towards ligand-centered radical reactivity.[27] EPR spectroscopic characterization revealed some metal-to-ligand spin transfer for radical complex $[Cp^*Mn(CO)_2\{N(H)C_6H_4\text{-}4\text{-}NMe_2\}]$ ($Cp^* = \eta^5\text{-}C_5Me_5$).[28] Wieghardt and co-workers isolated the first examples that could be unequivocally assigned to persistent anilino radical complexes (Figure 4, **A**).[29] In recent years, several other aminyl complexes were spectroscopically characterized or isolated (Figure 4).[21d,30–34] For example, spectroscopic and quantum chemical examination of radical complex $[NiCl\{L_A{}^{iPr}\}]^+$ (Figure 4, **B**) indicates considerable spin-density delocalization into the diarlyamido PNP pincer ligand and, in turn, nickel(II) as the most appropriate assignment for the metal oxidation state.[31] Besides the relevance of transient aminyl complexes as possible intermediates in oxidation catalysis, more persistent aminyl complexes might allow for the utilization of amido non-innocence in metal–ligand cooperative catalysis.[35] As a rare example, Grützmacher and co-workers presented the use of an iridium amido complex as catalyst for the oxidation of alcohols with benzoquinone (Scheme 1). The authors proposed a mechanism with an intermediate aminyl radical complex as the crucial intermediate, undergoing C–H hydrogen abstraction from the substrate ligand.[36]

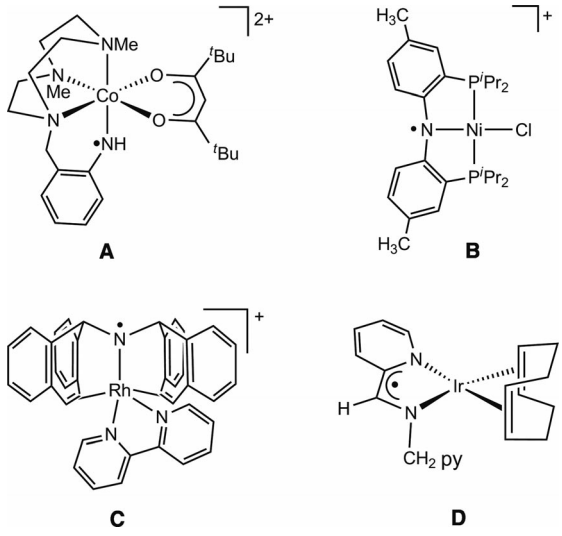

Figure 4. Representative examples for radical complexes with predominant aminyl character (py = 2-pyridyl).

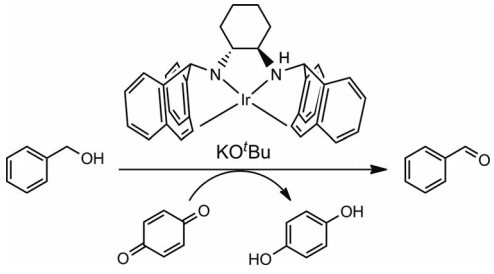

Scheme 1. Oxidative dehydrogenation of alcohols catalyzed by an iridium amido complex.

2. 16 Valence Electron (16 VE) Amido, Enamido, and Dienamido Complexes: Probing Properties and Reactivity

2.1. Synthesis of Amine Ligands *H*L1^R

Nucleophilic substitution of *N*,*N*-bis(2-chloroethyl)-amine[37] provides versatile access to amine ligands $HN(CH_2CH_2PR_2)_2$ (*H*L1^R, Figure 2) with a wide variety of

 © 2012 Wiley-VCH Verlag GmbH & Co. KGaA, Weinheim

aromatic and aliphatic substituents at the phosphane moiety. The synthesis of diphenylphosphanyl derivative HL1^{Ph} was reported by reaction of $HN(CH_2CH_2X)_2$ (X = Cl, Br) with $KPPh_2$ or, more conveniently, from hydrochloride $[H_2N(CH_2CH_2Cl)_2]Cl$ with diphenylphosphane and excess KO*t*Bu (Scheme 2).[38,39] This route also affords aryl phosphanes HL1^{R} [R = mesityl, *p*-tolyl, C_6H_3-3,5-$(CF_3)_2$].[40] The primary phosphane ligand HL1^{H} is similarly obtained in high yield from $[H_2N(CH_2CH_2Cl)_2]Cl$ and PH_3 under basic conditions (KOH/DMSO).[41] Initial attempts to synthesize dialkylphosphanyl ligands HL1^{Me} and HL1^{Et} from $HN(CH_2CH_2Cl)_2$ and $NaPMe_2$ in liquid ammonia or from $[H_2N(CH_2CH_2Cl)_2]Cl$ and $LiPEt_2$ in THF, respectively, suffered from moderate to poor yields.[42] Synthesis of ligands with bulkier dialkylphosphanyl substituents failed by this route. The low yield is attributed to the formation of aziridines $(CH_2CH_2N)CH_2CH_2PR_2$ as side products.[43] This base-promoted nucleophilic cyclization can be avoided by silyl-protection of the amine. Deprotection of the product is easily achieved by heating to reflux in H_2O or treatment with KF or $[n Bu_4N]F$ in MeOH.[43,44,45] This pathway affords a wide range of dialkylphosphanyl ligands HL1^{R} (R = Me, Et, *i*Pr, *t*Bu, 1-adamantyl, cyclohexyl) with good yields (Scheme 2).[43,46,47] Particular mention should be made of the possibility to introduce very bulky groups, such as P*t*Bu$_2$ or PAd$_2$, which was not reported for the popular diarylamido pincer ligands (Figure 1, {HL$_A$}).

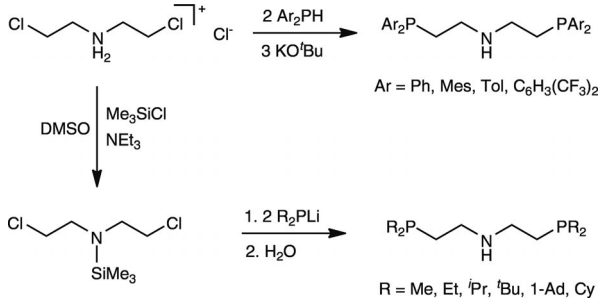

Scheme 2. Synthesis of PNP amine ligands HL1^{R} (1-Ad = 1-adamantyl, Cy = cyclohexyl, Mes = mesityl, Tol = *p*-tolyl).

Chiral, nonracemic derivatives were also reported. Bis{2-[(2*S*,5*S*)-2,5-dimethyl-phospholanoethyl]}amine (HL1$^{S,S–Me2Phospholane}$) can be synthesized by reaction of (2*S*,5*S*)-2,5-dimethyl-1-phenylphospholyllithium with $Me_3SiN(CH_2CH_2Cl)_2$ (Scheme 3).[45] Another pathway towards chiral phospholane ligands is provided by deprotonation of the *N*-protected primary phosphane $Me_3SiN(CH_2CH_4PH_2)_2$ with *n*BuLi and subsequent reaction with chiral, cyclic 2*S*,4*S*-2,4-pentanediol sulfate or 2*S*,5*S*-2,5-hexanediol sulfate (Scheme 3).[46a] Axially chiral binaphthyl ligand (HL1^{Binaph}) is obtained by *P*-lithiation of enantiomerically pure 4-chloro-4,5-dihydro-3*H*-4-phosphacyclohepta[2,1-*c*;1′,2′-*e*]phosphepine,[48] subsequent reaction with $Me_3SiN(CH_2CH_2Cl)_2$, and *N*-deprotection (Scheme 3).[46a]

2.2. Square-Planar 16 VE Amine and Amido Complexes: Synthesis, Stability, and N–H Acidity

Reaction of $[IrCl(COE)_2]_2$ (COE = cyclooctene) with HL1$^{i\mathrm{Pr}}$ in 2-propanol affords iridium(III) complex $[Ir(H)_2Cl\{H\mathrm{L1}^{i\mathrm{Pr}}\}]$.[46a] Use of THF as solvent provides access to a wide range of stable, square-planar d^8 amine complexes, $[IrL\{H\mathrm{L1}^{i\mathrm{Pr}}\}]^+$ (L = CO, COE, C_2H_4, C_3H_6, PMe_3) (Scheme 4).[49] However, exchange of chloride with a weakly coordinating counteranion is crucial. In nonprotic solvents, the chloride anion of $[Ir(COE)\{H\mathrm{L1}^{i\mathrm{Pr}}\}]Cl$ is hydrogen-bonded to the N–H proton, which is evidenced by a strong downfield shift in the ^{1}H NMR spectrum, accompanied by decomposition towards an equimolar mixture of amide $[Ir(COE)\{\mathrm{L1}^{i\mathrm{Pr}}\}]$ and iridium(III) complex $[Ir(Cl)_2H\{H\mathrm{L1}^{i\mathrm{Pr}}\}]$ and minor amounts of cyclooctenyl complex $[IrCl(C_8H_{13})H\{H\mathrm{L1}^{i\mathrm{Pr}}\}]$ (Scheme 5). Kinetic examinations indicate that the amido complex results from HCl elimination, which oxidatively adds to the initial cyclooctene complex. Intramolecular, vinylic C–H activation and subsequent trapping by chloride is kinetically competitive with this reaction.[50] In comparison, $[Ir(COE)\{H\mathrm{L1}^{t\mathrm{Bu}}\}]Cl$ and $[IrCl(C_8H_{13})H\{H\mathrm{L1}^{t\mathrm{Bu}}\}]$ form a strongly solvent-dependent equilibrium.[51] The increased steric bulk favors the vinyl

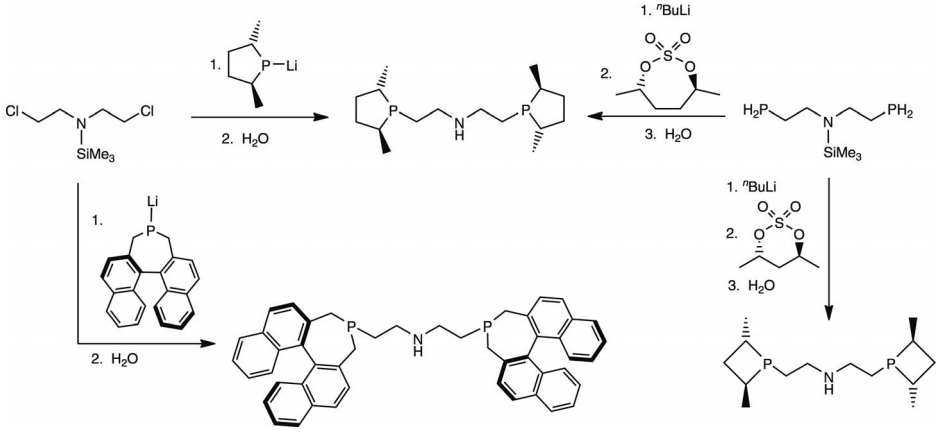

Scheme 3. Synthesis of chiral PNP ligands HL1^{R}.

 © 2012 Wiley-VCH Verlag GmbH & Co. KGaA, Weinheim

hydride over the olefin isomer, slows down C–H oxidative addition/reductive elimination, and renders chloride trapping of iridium(III) reversible.

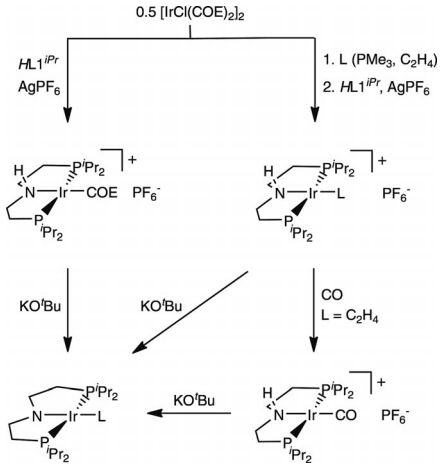

Scheme 4. Synthesis of iridium(I) PNP amine and amido complexes.

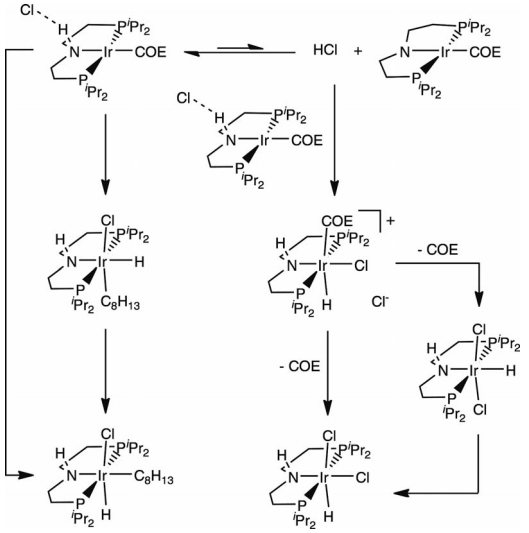

Scheme 5. Decomposition of [Ir(COE){*H*L1$^{i\mathrm{Pr}}$}]Cl in nonprotic solvents.

Deprotonation of [IrL{*H*L1$^{i\mathrm{Pr}}$}] provides access to iridium(I) amido complexes [IrL{L1$^{i\mathrm{Pr}}$}] (L = CO, COE, C_2H_4, PMe_3), which are thermally relatively robust towards β-H elimination (Scheme 4).[49,52] Likewise, palladium(II) PNP amido complexes [PdX{L1$^{i\mathrm{Pr}}$}] (X = Cl, Me, Ph) and [PdL{L1$^{i\mathrm{Pr}}$}]PF_6 (L = PMe_3, CN*t*Bu) were synthesized.[53] The large hypsochromic shift ($\Delta\nu$ = 68 cm^{-1}, Table 1) of the [Ir(CO){L1$^{i\mathrm{Pr}}$}] C–O stretching vibration and the large [Ir(olefin){L1$^{i\mathrm{Pr}}$}] olefin ^{13}C NMR spectroscopic high-field shifts ($\Delta\delta^{\mathrm{C2H4}}$ = 22.1 ppm; $\Delta\delta^{\mathrm{COE}}$ = 20.8 ppm) upon deprotonation of the respective amine complexes indicate a very electron-rich Ir{L1^{R}} fragment. In turn, the ligand *trans* to the nitrogen atom has a profound effect on the amine pK_a value, which varies over more than 7 orders of magnitude (in dmso) within the series L = CO [14.9(3)], COE [16.0(4)], PMe_3 [22.0(1)].[52] In comparison, the value for the olefin complex is close to that of the square-planar *cis*-diamine-diolefin–Rh$^{\mathrm{I}}$ complex [Rh{H_2L_E}]$^+$ (pK_a^{dmso} = 15.7) but considerably less acidic than the corresponding Ir$^{\mathrm{I}}$ complex [Ir{H_2L_E}]$^+$ (pK_a^{dmso} = 10.5).[36,54] However, the pK_a trend within the [IrL{*H*L1$^{i\mathrm{Pr}}$}]$^+$ series can be rationalized with a N→Ir→L *push-pull*-interaction that stabilizes the N–Ir π* orbital (HOMO) if *trans*-ligand L is a π-acceptor ligand,

Table 1. Comparison of M(CO){PEP} (E = N, C) CO stretching vibrations. Complexes with ligands derived from *H*L1^{R} are shown in bold italic typeface.

Complex	ν_{CO} [cm^{-1}]	Ref.
[Ir(CO){HL1^{iPr}}]PF$_6$	***1976***[a]	[49]
[Ir(CO){$C_5H_3N(CH_2PtBu_2)_2$}]PF_6	1962[b]	[61]
[Ir(CO){$C_6H_3(OPtBu_2)_2$}]	1949[c]	[62]
[Ir(CO)Cl(PiPr$_3$)$_2$]	1939[a]	[63]
[Ir(CO)(L4^{tBu})]	***1937***[a]	[69]
[Ir(CO){$NC_5H_3(CHPtBu_2)(CH_2PtBu_2)$}]	1932[b]	[64]
[Ir(CO){L$_C^{i\mathrm{Pr}}$}]	1930[d]	[7c]
[Ir(CO){L$_A^{i\mathrm{Pr}}$}]	1930[d]	[65]
[Ir(CO){$C_6H_3(CH_2PiPr_2)_2$}]	1928[e]	[3]
[Ir(CO){$CpFeC_5H_2(CH_2PiPr_2)_2$}]	1926[f]	[66]
[Ir(CO){$C_7H_4(CHPtBu_2)(CH_2PtBu_2)$}]	1919[g]	[67]
[Ir(CO)(L1^{iPr})]	***1908***[a]	[49]
[Ir(CO){$C_7H_5(CH_2PtBu_2)_2$}]	1905[g]	[68]
[RuCl(CO)(L4^{tBu})]	***1916***[a]	[69]
[RuCl(CO){$CpFeC_5H_2(CH_2PtBu_2)_2$}]	1914[h]	[70]
[RuCl(CO){$C_6H_3(CH_2PtBu_2)_2$}]	1909[a]	[71]
[RuCl(CO)(L3^{tBu})]	***1896***[a]	[69]
[RuCl(CO)(L1^{tBu})]	***1888***[a]	[69]
[RuCl(CO){$CH(CH_2CH_2PtBu_2)_2$}]	1887[a]	[72]

[a] Sample preparation: Nujol mull. [b] Sample preparation: Neat film. [c] Pentane solution. [d] THF solution. [e] Cyclooctane solution. [f] Hexane solution. [g] KBr pellet. [h] CH_2Cl_2 solution.

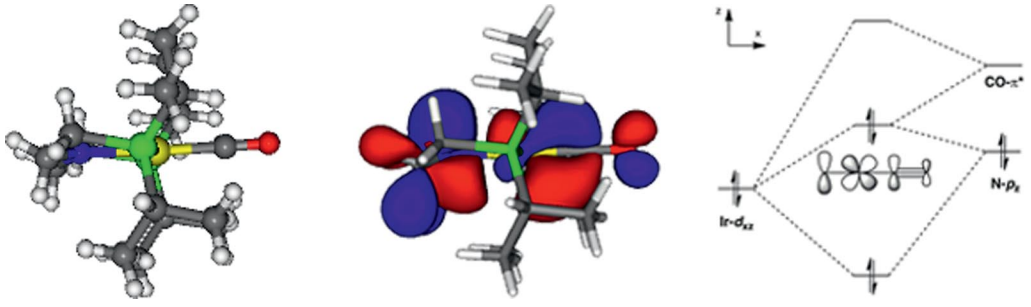

Figure 5. Molecular structure of [Ir(CO){L1$^{i\mathrm{Pr}}$}] from X-ray diffraction (left), DFT-computed HOMO (center), and qualitative representation of the N–Ir–CO orbital π-interaction (right).

 © 2012 Wiley-VCH Verlag GmbH & Co. KGaA, Weinheim

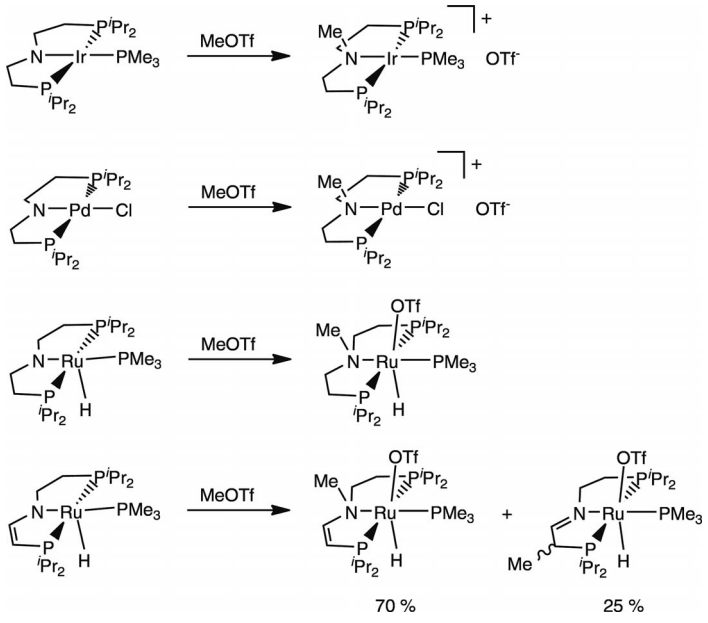

Scheme 6. Reactions of amido and enamido complexes with MeOTf.

such as CO or olefins (Figure 5). The same bonding situation was found for iridium(I) olefin amido complex [Ir(COD){κ²-bpa}] {COD = cyclooctadiene; bpa = $N(CH_2C_5H_4N)_2$}.[33b] High nucleophilicity of the amido group towards *C*-nucleophiles is also observed. [Ir(PMe_3)-{L1$^{i\mathrm{Pr}}$}] and [PdCl{L1$^{i\mathrm{Pr}}$}] are selectively attacked by MeOTf at the nitrogen atom (Scheme 6), and an iridium(III) methyl complex was not observed.[52,53]

2.3. Functionalization of the Pincer Backbone: Fine-Tuning N→M Donation

2.3.1. Amido, Enamido, and Dienamido Pincer Ligands: Comparison of Donor Properties

Dehydrogenation of the chelate backbone bridges towards enamido and dienamido ligands {L3^R}$^-$ and {L4^R}$^-$ (Figure 2) provides another approach to fine-tune electronic properties and reactivity. These enamido ligands are related to chelating (2-phosphanyl)vinylalcoholates, which are used in the Shell Higher Olefin Process (SHOP).[55] In analogy, Braunstein and co-workers prepared the enamido nickel(II) complexes [Ni(Ph)L{N(Ph)-CPhCHPPh$_2$}] (L = PMe_3, PMe_2Ph, $PMePh_2$) by P–Ph oxidative addition of an α-iminophosphorus ylide to [Ni(COD)$_2$] (Scheme 7).[56] However, deprotonation of coordinated or free imine ligands at the C–H-acidic α-position represents a more general approach to phosphanylenamido ligands.[57,58] For example, Morris recently reported the synthesis of dienamido PNNP iron(II) complexes by deprotonation of the corresponding imines (Scheme 7).[59] Both catalyze transfer hydrogenation of ketones with comparable rates, suggesting that ligand backbone proton transfer reactions might be involved in a metal–ligand cooperative hydrogenation mechanism. Deprotonation of bis(2-picolyl)-amido ligands coordinated to rhodium(I) and iridium(I) affords "dearomatized" vinylenediamido complexes [M(COD){RNC(H)C_5H_4N}]$^-$ (M = Rh, Ir; COD = cyclooctadiene; R = $CH_2C_5H_4N$) (Scheme 7).[33b,60]

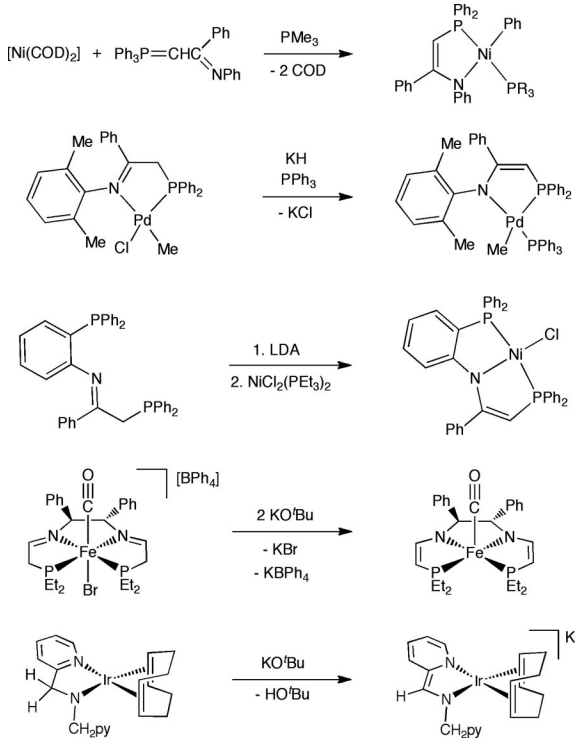

Scheme 7. Syntheses of chelating enamido complexes.

Synthetic access to free ligands {L3^R}$^-$ and {L4^R}$^-$ has not been reported yet. Their metal complexes are obtained by starting from coordinated amine, imine, or amido precursors and following several routes, which are discussed

 © 2012 Wiley-VCH Verlag GmbH & Co. KGaA, Weinheim

in the subsequent sections. However, comparison of parent amido complexes carrying $\{L1^R\}^-$ with related enamido and dienamido complexes formally derived from it ($\{L3^R\}^-$ and $\{L4^R\}^-$) and with complexes of other popular PEP (E = N, C) pincer ligands is informative at this point to understand reactivity trends. CO stretching vibrations (ν_{CO}) can serve as a probe in trying to scale the electronic effects of backbone dehydrogenation. Table 1 shows representative examples of square-planar $[Ir^I(CO)\{PEP\}]$ and five-coordinate $[Ru^{II}Cl(CO)\{PEP\}]$ complexes (E = N, C), all carrying bulky dialkylphosphane ($PiPr_2$ or $PtBu_2$) substituents but different pincer backbones.[73] Amine and amido complexes $[Ir(CO)\{HL1^{iPr}\}]^+$ (ν_{CO} = 1976 cm^{-1}) and $[Ir(CO)\{L1^{iPr}\}]$ (ν_{CO} = 1908 cm^{-1}) represent the upper and lower ends of a wide range of CO stretching vibrations found for cationic and neutral $[Ir^I(CO)\{PEP\}]^{+/0}$ pincer complexes. On the other hand, fully dehydrogenated pincer complex $[Ir(CO)\{L4^{tBu}\}]$ (Scheme 11) exhibits an intermediate ν_{CO} (1937 cm^{-1}).[69] This observation suggests reduced N→Ir electron donation upon oxidative ligand backbone functionalization, owing to stabilization of the *N*-lone-pair by *C*(p)–*N*(p) overlap, that is, the vinyl substituents acting as π-acceptors. These qualitative considerations are further reflected within the series $[RuCl(CO)\{L1^{tBu}\}]$ (ν_{CO} = 1888 cm^{-1}), $[RuCl(CO)\{L3^{tBu}\}]$ (ν_{CO} = 1896 cm^{-1}), and $[RuCl(CO)\{L4^{tBu}\}]$ (ν_{CO} = 1916 cm^{-1}), which can be prepared by reaction of CO with the respective four-coordinate complexes.[69] As for the square-planar Ir^I platform, the five-coordinate Ru^{II} complexes span a range of about 30 cm^{-1}, indicating comparable electronic effects for the different metals and coordination geometries upon backbone dehydrogenation. $[RuCl(CO)\{L1^{tBu}\}]$ and $[RuCl(CO)\{CH(CH_2CH_2PtBu_2)_2\}]$ exhibit almost identical ν_{CO}. Hence, weaker E→Ru (E = N, C) σ-donation of the amido relative to the alkyl ligand is offset by N→Ru π-donation. Other frequently used anionic pincer ligands, such as the aryl pincer $\{C_6H_3(CH_2PiPr_2)_2\}^-$, diarylamido pincer $\{L_A\}^-$, disilylamido pincer $\{L_C\}^-$, or pyridine-based "dearomatized" pincer $\{L_B\}^-$, fall within a relatively narrow range between $\{L3\}^-$ and $\{L4\}^-$ with respect to their donor properties, as judged by their CO stretching vibrations.

2.3.2. 16 VE Amido Versus Enamido Complexes: Consequences for Structure and Reactivity

The molecular structure and reactivity of $[RuH(PMe_3)\{L1^{iPr}\}]$, as compared with $[RuH(PMe_3)\{L3^{iPr}\}]$, provides further information. The enamido complex is quantitatively obtained from $[RuCl_2(PMe_3)\{HL1^{iPr}\}]$ with excess KO*t*Bu (Scheme 8).[74] Decomposition of the tentative amido intermediate $[RuCl(PMe_3)\{L1^{iPr}\}]$ by β-hydride migration and backbone deprotonation of the resulting imine provides a reasonable mechanism.[75] $[RuH(PMe_3)\{L3^{iPr}\}]$ adds two equivalents of H_2 to give amine complex $[Ru(H)_2(PMe_3)\{HL1^{iPr}\}]$ (Scheme 15). This reaction is fully reversible, but elimination of the first equivalent is considerably faster (see below), rendering amido complex $[RuH(PMe_3)\{L1^{iPr}\}]$ easily isolable.

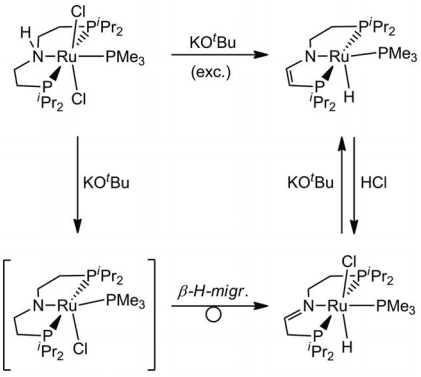

Scheme 8. Proposed mechanism of synthesis of enamido complex $[Ru(H)PMe_3\{L3^{iPr}\}]$.

The molecular structures of both $[RuH(PMe_3)\{L1^{iPr}\}]$ (X-ray) and $[RuH(PMe_3)\{L3^{iPr}\}]$ (DFT) can be described by starting from trigonal-bipyramidal (TBPY) geometry, with N, H, and PMe_3 in equatorial positions, but with different modes of distortion from ideal TBPY.[74] For $[RuH(PMe_3)\{L1^{iPr}\}]$, the strongly compressed H–Ru–PMe_3 angle [76.0(7)°] and widened H–Ru–N [124.8(7)°] and N–Ru–PMe_3 [159.12(3)°] angles indicate a "Y-shaped" distortion from TBPY coordination. This geometry is typically found for five-coordinate d^6 complexes with a strong π-donor ligand to avoid repulsive filled–filled N(p)–M(d) π-interactions and instead maintain stabilizing N→M π-bonding with the coordinatively unsaturated metal center (Figure 6).[76,77] In contrast, $[RuH(PMe_3)\{L3^{iPr}\}]$ (H–Ru–PMe_3: 84.6°; H–Ru–N: 102.5°; N–Ru–PMe_3: 172.6°) exhibits stronger resemblance of "T-shaped" distortion from TBPY [i.e. square-pyramidal (SQPY) geometry], suggesting again

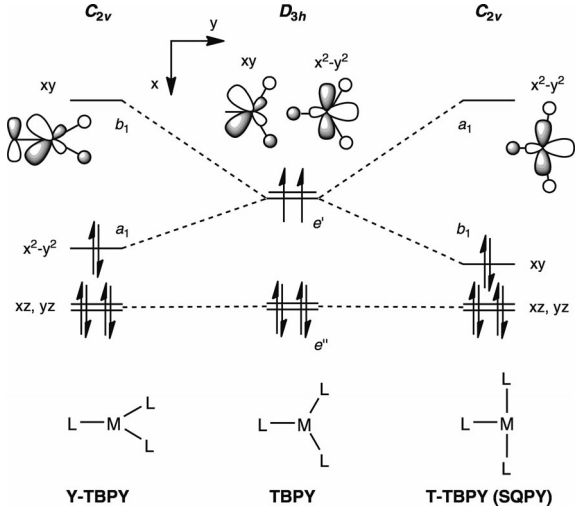

Figure 6. Qualitative valence d-orbital splitting in a TBPY (D_{3h}) ligand field (center) with d^6 occupation (d_{z^2} LUMO omitted) and lifted degeneracy of the *e*′-orbitals upon Y-shaped (left) and T-shaped (right) distortion, respectively. The respective LUMOs indicate the suitability in the Y-TBPY case for π-bonding with a π-donor ligand (axial ligands omitted for clarity).

 © 2012 Wiley-VCH Verlag GmbH & Co. KGaA, Weinheim

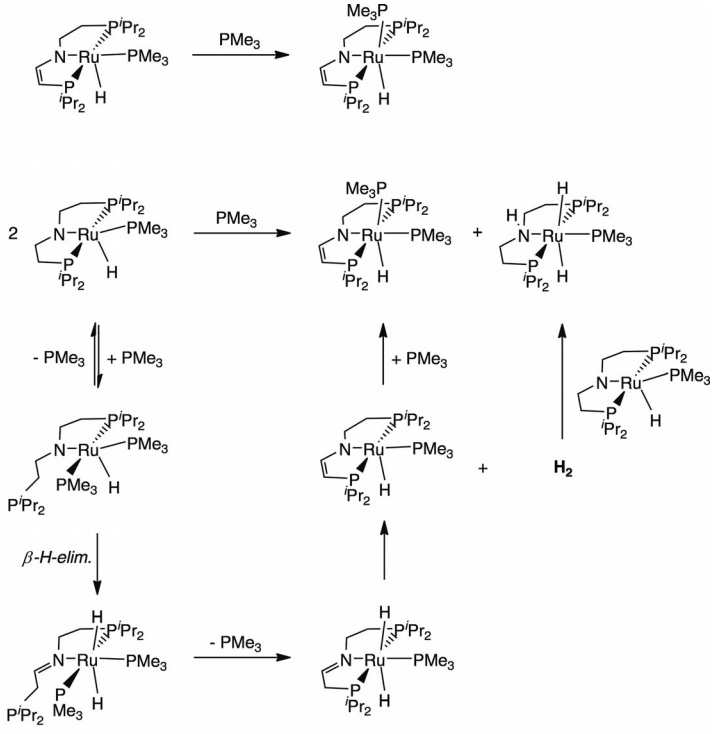

Scheme 9. Reactions of enamide [RuH(PMe$_3$){L3$^{i\mathrm{Pr}}$}] (top) and amide [RuH(PMe$_3$){L1$^{i\mathrm{Pr}}$}] (bottom) with PMe$_3$ and proposed mechanism for the latter.

attenuated π-donation by the enamido nitrogen atom. This interpretation is further supported by comparison of the Ru–N Wiberg bond indices for [RuH(PMe$_3$){L1$^{i\mathrm{Pr}}$}] (0.50) and [RuH(PMe$_3$){L3$^{i\mathrm{Pr}}$}] (0.37), indicating a lower degree of covalent bonding for the latter.

Hence, the ruthenium center in the enamido complex exhibits a higher degree of electronic unsaturation, which is reflected in its reactivity with nucleophiles. [RuH(PMe$_3$){L3$^{i\mathrm{Pr}}$}] shows Lewis acid reactivity, typical for SQPY Ru^{II} complexes, exemplified by the formation of octahedral [RuH(PMe$_3$)$_2${L3$^{i\mathrm{Pr}}$}] with PMe$_3$ (Scheme 9).[75] In contrast, [RuH(PMe$_3$){L1$^{i\mathrm{Pr}}$}] does not form an isolable six-coordinate amido complex. Upon addition of PMe$_3$, broadening of all signals in the ^{31}P NMR spectrum indicates rapid ligand exchange. Furthermore, slow ligand disproportionation towards amine [Ru(H)$_2$(PMe$_3$){*H*L1$^{i\mathrm{Pr}}$}] and enamide [RuH(PMe$_3$)$_2${L3$^{i\mathrm{Pr}}$}] is observed, which is attributed to the mechanism in Scheme 9. The instability of proposed imine intermediate [Ru(H)$_2$(PMe$_3$){L2$^{i\mathrm{Pr}}$}] towards H$_2$ elimination was confirmed by DFT computations (Scheme 15). The reactivity towards electrophiles was also examined. With MeOTf, [Ru(H)(PMe$_3$){L1$^{i\mathrm{Pr}}$}] forms the expected tertiary amine complex [Ru(H)OTf(PMe$_3$){*Me*L1$^{i\mathrm{Pr}}$}] selectively. [Ru(H)(PMe$_3$){L3$^{i\mathrm{Pr}}$}] exhibits reactivity with both nucleophilic positions on the ligand backbone, resulting in a mixture of enamine [Ru(H)OTf(PMe$_3$){*Me*L3$^{i\mathrm{Pr}}$}] and the products from backbone *C*-methylation to a minor extent (Scheme 6).

3. 15 and 14 VE Complexes: Control of Electronic Structure by Pincer Variation

3.1. Oxidation of 16 VE Dialkylamido Complexes: Formation of Unstable Radicals

The d^8 amido complexes [IrL{L1$^{i\mathrm{Pr}}$}] (L = CO, COE, PMe$_3$) and [PdCl{L1$^{i\mathrm{Pr}}$}] in THF exhibit irreversible oxidation waves in the cyclic voltammograms (THF) at scan speeds up to 1 V s^{-1}, suggesting rapid chemical degradation of initially formed radical cations on the experimental timescale.[52] As for the pK_a values of the conjugate acids (see above), the oxidation potentials of the series [IrL{L1$^{i\mathrm{Pr}}$}] are highly dependent on the ligand in the *trans*-position to the nitrogen atom (L = CO: –0.39 V, COE: –0.49 V, PMe$_3$: –1.09 V vs. Fc/Fc$^+$). Chemical oxidation of [IrPMe$_3${L1$^{i\mathrm{Pr}}$}] and [PdPh{L1$^{i\mathrm{Pr}}$}] with AgPF$_6$ gives amine complexes [IrPMe$_3${*H*L1$^{i\mathrm{Pr}}$}]$^+$ or [PdPh{*H*L1$^{i\mathrm{Pr}}$}]$^+$ in around 90% or 80% yield, respectively, and a minor amount of the corresponding imines [IrPMe$_3${L2$^{i\mathrm{Pr}}$}]PF$_6$ and [PdPh{L2$^{i\mathrm{Pr}}$}]-PF$_6$.[52,53] Deuterium labeling in case of Pd supports initial formation of radical cation [PdPh{L1$^{i\mathrm{Pr}}$}]$^{+\cdot}$, which undergoes competitive hydrogen abstraction from the solvent (THF) and ligand backbone disproportionation (Scheme 10). Hence, the reactivity indicates "redox noninnocent" behavior of the dialkylamido ligand. Accordingly, DFT computations (B3LYP/6-311+G**) for [IrCO{L1$^{i\mathrm{Pr}}$}]$^+$ indicate about 63% of the Mullikan spin

 © 2012 Wiley-VCH Verlag GmbH & Co. KGaA, Weinheim

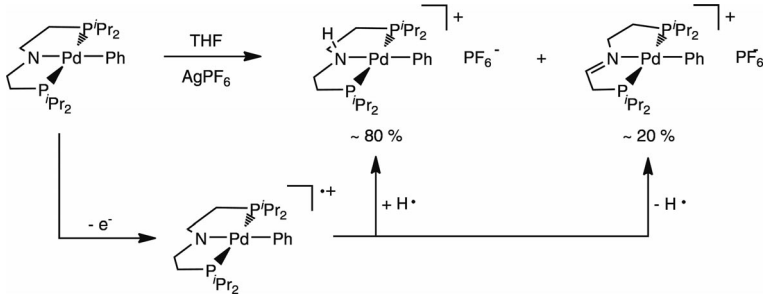

Scheme 10. Chemical oxidation of amido complex [PdPh{L1^{iPr}}] and proposed mechanism via aminyl radical complex [PdPh{L1^{iPr}}]$^{+\cdot}$.

density to be located on the nitrogen atom, and the SOMO of [IrCO{L1^{iPr}}]$^{+}$ (Figure 7) represents the N(p)–Ir(d_{xz}) π*-orbital resulting from removal of an electron from the HOMO of parent [IrCO{L1^{iPr}}] (Figure 5).

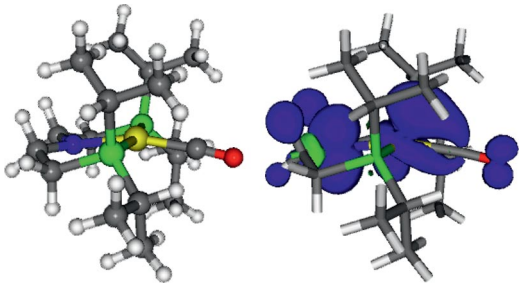

Figure 7. DFT-computed molecular structure of [Ir(CO)(L1^{iPr})]$^{+\cdot}$ (left) and spin density (right).

3.2. Ligand Modification: Stabilization of Square-Planar 15 VE Complexes

The decomposition mechanism of PNP dialkylamido iridium and palladium radical complexes suggests a simple synthetic strategy for the isolation of persistent open-shell complexes.[78] Replacement of the backbone ethylene with vinylene bridges (Figure 2), prevents putative aminoyl ligand disproportionation towards amine and imine complexes. In fact, in contrast to transient [IrPMe$_3$\{L1^{iPr}\}]$^{+\cdot}$ (see above), disilylamido complex [IrCl\{L$_C$^{tBu}\}] was isolated and characterized by EPR spectroscopy.[79] Furthermore, this modification should also stabilize a 15 VE radical complex electronically by delocalization of the *N*-lone-pair. Hence, the SOMO of enamido and dienamido radical complexes should exhibit less N(p) character as compared with an analogous dialkylamido radical complex, providing further stabilization with respect to possible ligand-centered radical decomposition reactions.[80] Oxidation of amine [IrH(C_8H_{13})Cl\{*H*L1^{tBu}\}] with benzoquinone gives dienamido complex [IrCl\{L4^{tBu}\}] in good yield (Scheme 11).[81] As for [IrCl\{L$_C$^{tBu}\}], the large anisotropy of the *g* values is in agreement with predominant d^7 metalloradical character. DFT computations confirmed 67% spin density to be located at the Ir metal. Isolable, monomeric d^7 complexes of iridium are relatively rare compared with cobalt (and to some extend rhodium).[79,82]

3.3. Fine-Tuning of N→M Donation: Low-Spin Versus Intermediate-Spin Square-Planar 14 VE Complexes

Ligand field considerations for square-planar complexes ($D4_h$) with strong-field ligands predict splitting of the d-orbital manifold into three nonbonding orbitals (d_{xy}, d_{xz} and d_{yz}), weakly antibonding d_{z^2} orbital (stabilized by valence s-orbital mixing), and a high-lying, strongly antibonding $d_{x^2-y^2}$ orbital. Hence, for d^6 ions, an intermediate-spin (S = 1) electronic configuration is expected (Figure 8A).[83] Iron(II) porphyrinato and bis(dithiolato) complexes provide well-examined examples.[84,85] In contrast, four-coordinate 14 VE complexes of the platinum metals are usually found in a sawhorse (*cis*-divacant octahedral) conformation with electronic low-spin (S = 0) configuration and stabilizing C–H agostic interactions at the vacant coordination sites.[86] DFT computations also suggested an intermediate-spin electronic ground state for square-planar alkyl PCP pincer complex [RuCl\{HC($CH_2NHPtBu_2$)$_2$\}].[87] This species was postulated as a transient intermediate in the equilibrium formed by the closed-shell α- and β-hydrogen elimination products (Scheme 12). The high reaction rate of hydrido

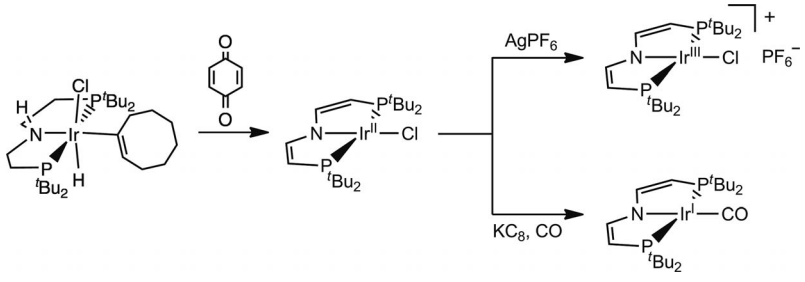

Scheme 11. Synthesis of iridium(I), iridium(II), and iridium(III) dienamido complexes.

 © 2012 Wiley-VCH Verlag GmbH & Co. KGaA, Weinheim

alkylidene and olefin isomer interconversion was attributed to two-state reactivity[88] via triplet intermediate [RuCl{HC($CH_2NHPtBu_2$)$_2$}].

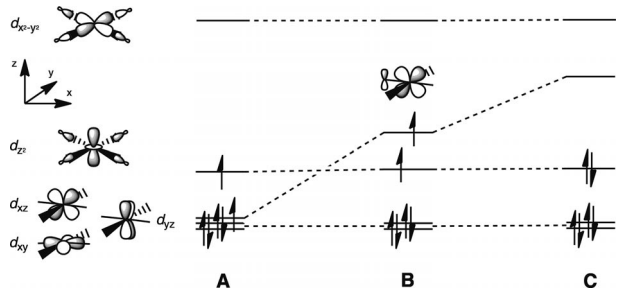

Figure 8. Valence d-orbital splitting in square-planar coordination for a d^6 ion with pure σ-donor ligands (**A**) and one weak (B) or strong (C) single-faced, perpendicular π-donor, respectively.

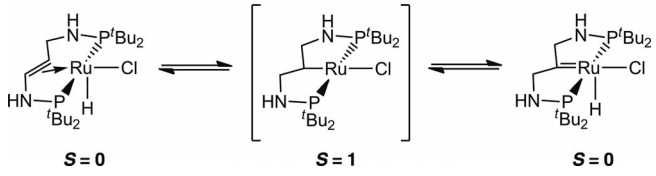

Scheme 12. Equilibrium of [Ru(H)Cl{PtBu$_2$NHCH=CHCH$_2$NHPtBu$_2$}] and [Ru(H)Cl{C($CH_2NHPtBu_2$)$_2$}] attributed to two-state reactivity via triplet intermediate [RuCl{CH($CH_2NHPtBu_2$)$_2$}].

The introduction of one perpendicular single-faced π-donor, such as an amido ligand, further perturbs the valence orbital splitting by lifting the d_{xz}/d_{yz} degeneracy. If the π-donor is located along the *x*-axis, the d_{xz} orbital will be considerably destabilized, subject to the extent of N→M π-donation (Figure 8, B/C). Hence, two electronic configurations can arise: An intermediate-spin (S = 1) state having a singly occupied N–M π*-orbital [$(xy,yz,z^2)^5(xz)^1(x^2–y^2)^0$; Figure 8, B] or a low-spin configuration (S = 0) in which this orbital is vacant [$(xy,yz,z^2)^6(xz)^0(x^2–y^2)^0$, Figure 8, C]. Therefore, N→M π-bonding should directly influence the singlet–triplet gap, eventually favoring a low-spin over intermediate-spin ground state if the spin pairing energy is overcompensated.

3.3.1. [IrCl($L4^{tBu}$)]$^+$ and [RuCl($L1^{tBu}$)]: Square-Planar d^6 Low-Spin Complexes

Electrochemical characterization of [IrCl{L4$^{t\mathrm{Bu}}$}] indicates reversible oxidation at $E_{1/2}$ = +0.02 V (vs. $FeCp_2/FeCp_2^+$).[81] Accordingly, diamagnetic d^6 complex [IrCl{L4$^{t\mathrm{Bu}}$}]PF_6 can be synthesized upon chemical oxidation with $AgPF_6$, as a unique example for a square-planar Ir^{III} complex (Scheme 11). DFT calculations confirm that the singlet state is more stable by more than 4 kcal mol^{-1} (ZORA-B3LYP/TZVP), which is attributable to strong N→Ir π-donation. This complex is isoelectronic with Shaw's "classic" carbene complex [IrCl{=C(CH_2CH_2PtBu)$_2$}].[89] Square-planar Ru^{II} complex [RuCl{L1$^{t\mathrm{Bu}}$}] is obtained by HCl elimination from [$RuCl_2${HL1$^{t\mathrm{Bu}}$}] (Scheme 13).[90] Like [IrCl{L4$^{t\mathrm{Bu}}$}]$^+$, [RuCl{L1$^{t\mathrm{Bu}}$}] is diamagnetic, as evidenced by sharp NMR spectroscopic signals. DFT computations suggested a small singlet–triplet gap. The short Ru–N bond derived by single-crystal X-ray diffraction [1.890(2) Å] is in agreement with the DFT-optimized structure for the singlet state (1.90 Å) and considerably shorter than that computed for the triplet state (1.99 Å). This structural feature is particularly indicative for the spin state, since the N–M π*-orbital is vacant in the singlet state (Figure 8, C) but singly occupied in the triplet state (B). Furthermore, the NMR spectra (^{1}H and ^{31}P) exhibit some unusual chemical shifts with strong temperature dependence. Population of an energetically low-lying triplet state was proposed as explanation, and the thermodynamic parameters were estimated by fitting of the NMR spectroscopic data (ΔH = 10.6 ± 0.3 kJ mol^{-1}; ΔS = 4.2 ± 0.8 J mol^{-1} K^{-1}).[90]

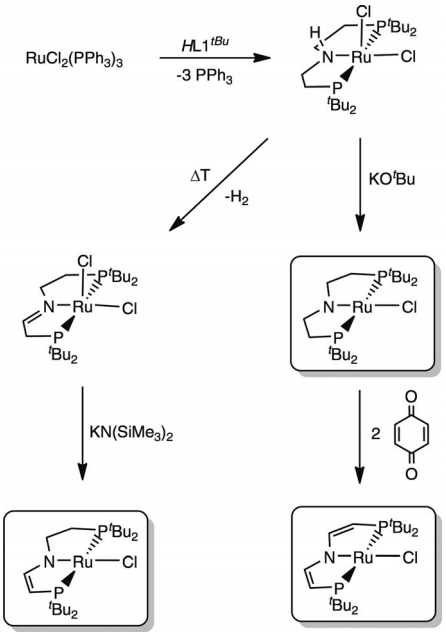

Scheme 13. Synthesis of square-planar Ru^{II} amido, enamido, and dienamido complexes.

3.3.2. [RuCl{$L_C{}^{tBu}$}], [RuCl{L3^{tBu}}], and [RuCl{L4^{tBu}}]: In Favor of Intermediate Spin

In contrast, Caulton's disilylamido complex [RuCl{$L_C{}^{t\mathrm{Bu}}$}] exhibits strongly paramagnetically shifted signals in the ^{1}H NMR spectrum, and no ^{31}P NMR signal was detected.[91] At 298 K, the magnetic susceptibility is in agreement with two unpaired electrons ($\chi_M T$ = 1.03), and the triplet state was calculated to be favored by 10 kcal mol^{-1}.[92] However, at low temperatures, $\chi_M T$ drops to near zero, indicating a nonmagnetic ground state.[91] These results were rationalized with a spin triplet ground state which is further split into the nonmagnetic | S = 1, M_S

 © 2012 Wiley-VCH Verlag GmbH & Co. KGaA, Weinheim

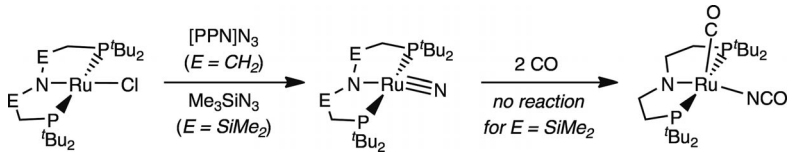

Scheme 14. Synthesis of square-planar ruthenium(IV) nitrido complexes and their reactivity with CO.

$= 0\rangle$ microstate placed below $|S = 1, M_S = \pm 1\rangle$ owing to zero-field-splitting (ZFS).[93] The magnetic data fitting gave a large axial ZFS parameter ($D = +273\ cm^{-1}$). The intermediate-spin ground state, also observed for [RuX{$L_C{}^{t\mathrm{Bu}}$}] (X = F, OTf), [OsI{$L_C{}^{t\mathrm{Bu}}$}], and hydrolysis product [Ru(OSiMe$_2$CH$_2$P*t*Bu$_2$)$_2$], are highly unusual for second- and third-row transition metal complexes.[92,94] The magnetic properties are reminiscent of those of Ru^{II}/Ru^{II} paddlewheel complexes [$Ru_2(O_2CR)_4$] (R = CH_3, Ph) which exhibit two unpaired electrons but are essentially nonmagnetic at low temperatures as a result of a $\sigma^2\pi^4\delta^2\delta^{*2}\pi^{*2}$ electronic triplet configuration of the $Ru_2{}^{4+}$ core and a large ZFS.[95]

Direct comparison of [RuCl{$L1^{t\mathrm{Bu}}$}] and [RuCl{$L_C{}^{t\mathrm{Bu}}$}] suggests that the different electronic structure might be attributed to stronger N→M π-donation by the dialkyl with respect to the disilylamido ligand. In terms of donor properties, enamido and dienamido ligands scale closer to disilylamides (see above). Therefore, the corresponding square-planar Ru^{II} complexes [RuCl{$L3^{t\mathrm{Bu}}$}] and [RuCl{$L4^{t\mathrm{Bu}}$}] were prepared to probe this qualitative picture (Scheme 13).[69] Both complexes exhibit two unpaired electrons at room temperature, as judged by SQUID magnetometry and NMR spectroscopic data. In analogy to [RuCl{$L_C{}^{t\mathrm{Bu}}$}], $\chi_M T$ drops to near zero at low temperatures. Fitting of the magnetic data to a model with $S = 1$ gave large axial ZFS parameters at around $+380\ cm^{-1}$ ([RuCl{$L3^{t\mathrm{Bu}}$}]) and $+230\ cm^{-1}$ ([RuCl{$L4^{t\mathrm{Bu}}$}]), as found for [RuCl{$L_C{}^{t\mathrm{Bu}}$}] ($D = +273\ cm^{-1}$). To exclude a gradual spin transition as an alternative explanation for the magnetic data, the molecular structure of [RuCl{$L4^{t\mathrm{Bu}}$}] was derived by single-crystal X-ray diffraction over a wide temperature range (30–200 K). Both the Ru–N distance [1.994(2) Å] and the N–Ru–Cl angle (180.0°) are invariant. DFT computations confirmed that both structural parameters should be sensitive indicators for the spin multiplicity ($\Delta_{Ru-N} = 0.07$ Å; $\Delta_{N-Ru-Cl} = 15.2°$).

Hence, the bulky ligands {$L1^{t\mathrm{Bu}}$}$^-$, {$L3^{t\mathrm{Bu}}$}$^-$, and {$L4^{t\mathrm{Bu}}$}$^-$ enable the isolation of square-planar 15 and 14 VE Ir^{II}, Ir^{III}, and Ru^{II} complexes. In case of Ru^{II}, the ligand variation allows for control of the electronic structure, attributed to modified N→M π-donation. As pointed out by Caulton and co-workers, other factors such as pincer ligand conformational variations, certainly affect M–N π-bonding, as well, and therefore the generally small singlet–triplet gap for this class of compounds.[92] As for [IrCl{$L4^{t\mathrm{Bu}}$}]$^+$, the supposedly weakest π-donor within the series {$L1^R$}$^-$/{$L3^R$}$^-$/{$L4^R$}$^-$ is able to cause spin pairing, which is probably an effect of the charge and generally stronger d-orbital splitting compared with that of Ru^{II} compounds.

3.4. M(PNP) Complexes as Platforms for Late Transition Metal Nitrides

The coordinatively and electronically highly unsaturated 14 VE complexes should be suitable platforms for the stabilization of multiply bonded ligands. Accordingly, diamagnetic Ru^{IV} nitrides [RuN{$L_C{}^{t\mathrm{Bu}}$}] and [RuN{$L1^{t\mathrm{Bu}}$}] are isolated in high yield from the corresponding chloride complexes by salt metathesis with azides and N_2 elimination (Scheme 14).[96,97] Terminal nitrido complexes with d^n-electron counts $n > 2$ are exceedingly rare.[98] At variance with more common Ru^{VI} nitrides,[99] [RuN{$L_C{}^{t\mathrm{Bu}}$}] exhibits a nucleophilic nitrido ligand, exemplified by methylation with MeOTf and lack of reactivity with phosphanes.[100] However, while [RuN{$L_C{}^{t\mathrm{Bu}}$}] does not react with CO, selective nitride–CO coupling was observed for [RuN{$L1^{t\mathrm{Bu}}$}] (Scheme 14).[97] Nitride hydrogenolysis with H_2 was also examined and will be discussed in section 4.3. The mechanism of N–CO coupling was not reported, but [RuN{$L_C{}^{t\mathrm{Bu}}$}] does not react with the π-acid CO,[101] possibly because of the weaker nucleophilicity of its nitride ligand. As a consequence of the mutual *trans*-configuration of two strong π-donors (nitride and amide), both nitrido complexes exhibit molecular structures with considerable deviation from planarity by N–Ru–N angle bending. Weaker Ru≡N bonding in case of [RuN{$L1^{t\mathrm{Bu}}$}] is indicated by the comparatively low stretching vibration ($\nu_{Ru\equiv N} = 976\ cm^{-1}$; [RuN{$L_C{}^{t\mathrm{Bu}}$}]: $1030\ cm^{-1}$).[102]

4. Metal–Ligand Cooperativity: Hydrogenation and Dehydrogenation Catalysis

4.1. Cooperative H_2 Activation

The twofold H_2 elimination/addition equilibrium of amine, amido, and enamido complexes [Ru(H)$_2$PMe$_3$-{*H*L1$^{i\mathrm{Pr}}$}], [Ru(H)PMe$_3$-{L1$^{i\mathrm{Pr}}$}], and [Ru(H)PMe$_3$-{L3$^{i\mathrm{Pr}}$}] was investigated by kinetic examinations and DFT computations for the PMe_2 truncated model (Scheme 15).[75] H_2 elimination from amine complex [Ru(H)$_2$PMe$_3$-{*H*L1$^{i\mathrm{Pr}}$}] (Scheme 15, left branch) proceeds by proton transfer from the amine group to the *syn*-coplanar hydride ligand to give a dihydrogen complex (omitted in Scheme 15) with a moderate barrier ($\Delta G^{\ddagger} = 18.3\ kcal\,mol^{-1}$ for the PMe_2 model), which loses H_2 in almost barrierless fashion. The reverse, H_2 heterolysis by amido complexes, was well examined experimentally and computationally for several related systems in the context of hydrogenase model reactivity and metal–ligand cooperative hydrogenation of ketones.[9,103]

 © 2012 Wiley-VCH Verlag GmbH & Co. KGaA, Weinheim

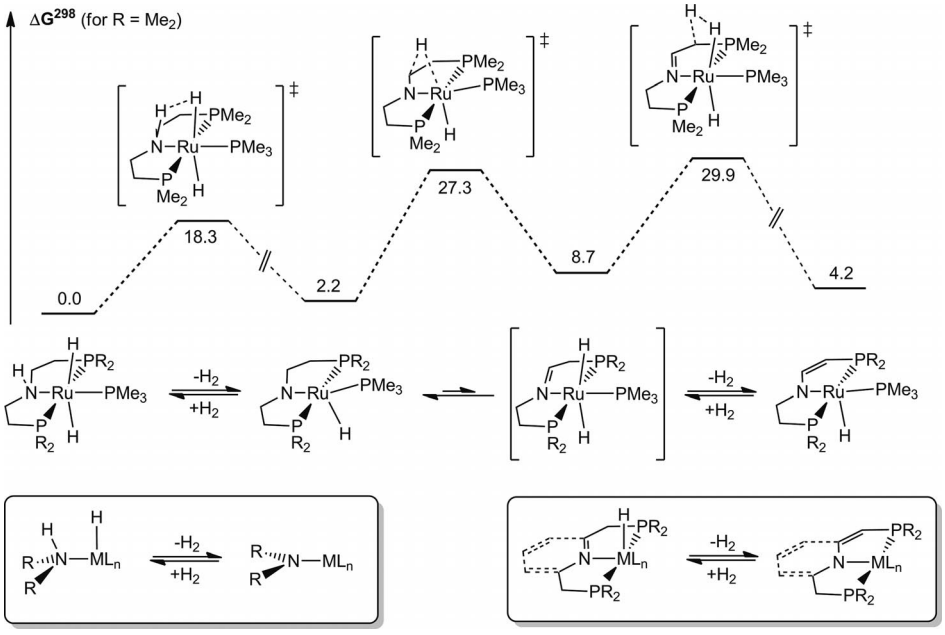

Scheme 15. Center: H_2 addition/elimination equilibrium of [Ru(H)$_2$PMe$_3${*H*L1^{iPr}}], [Ru(H)PMe$_3${L1^{iPr}}], and [Ru(H)PMe$_3${L3^{iPr}}] and proposed intermediate [Ru(H)$_2$PMe$_3${L2^{iPr}}] (H_2 complex intermediates omitted). Top: Computed energies for the PMe_2 truncated model (kcal mol^{-1}). Bottom: Analogies with catalysts of the Noyori (left) and Milstein (right) type.

On the right branch of the equilibrium reaction, that is, elimination of H_2 from the ligand backbone, considerably higher barriers were obtained from computations and H/D exchange kinetics (Scheme 15).[75] The putative imine intermediate [Ru(H)$_2$PMe$_3${L2^{iPr}}] was not detected spectroscopically. Accordingly, the calculations predict that it is unstable towards both H_2 elimination and migrative imine insertion. Dihydrogen complex [Ru(H)$_2$(H)PMe$_3${L3^{iPr}}] (omitted in Scheme 15) was located as an intermediate on the H_2-elimination path, losing H_2 in almost barrierless fashion. The computations indicate that C–H proton transfer from the ligand backbone to the hydride ligand is kinetically feasible without dissociation of one of the pincer "arms". However, predissociation might considerably lower the barrier for amide β-H elimination, which could account for the more rapid disproportionation of [Ru(H)PMe$_3$-{L1^{iPr}}] in the presence of PMe_3 (see above). The equilibrium $L_nM(H)\{L2^R\} \leftrightarrows L_nM\{L3^R\} + H_2$ provides an aliphatic analogue of Milstein's pyridine- and acridine-based PNP pincer catalysts, which operate upon reversible ligand backbone aromatization/dearomatization (Scheme 15).[6]

Several studies for related "Noyori–Morris type" metal–ligand cooperative catalysts suggest that Brønsted acids catalyze the H_2 heterolysis step.[104] For [Ru(H)$_2$PMe$_3$-{*H*L1^{iPr}}], proton exchange rates with H_2O were studied by ^{1}H-EXSY NMR spectroscopy.[105] The examinations indicate stereoselective H^+/H^- exchange of water with the hydride ligand that is *syn*-coplanar with the N–H proton. This observation is in line with a water-catalyzed proton shuttle mechanism for H_2 heterolysis upon hydrogen bonding with the secondary amine (Scheme 16). Accordingly, tertiary amine complex [Ru(H)$_2$PMe$_3${*Me*L1^{iPr}}] shows considerably slower and unselective H^+/H^- exchange of both hydride ligands with H_2O. DFT computations confirm the proposed mechanism, indicating that water catalysis reduces the kinetic barrier for H_2 heterolysis by around 8 kcal mol^{-1} for the PMe_2 truncated model (Scheme 16). Similarly, computations for proton transfer ("dearomatization") from the ligand backbone to a hydride ligand in [Ir(H)$_2$Ph{NC$_5$H$_3$(CH$_2$PMe$_2$)$_2$}] indicate water catalysis, as well.[106]

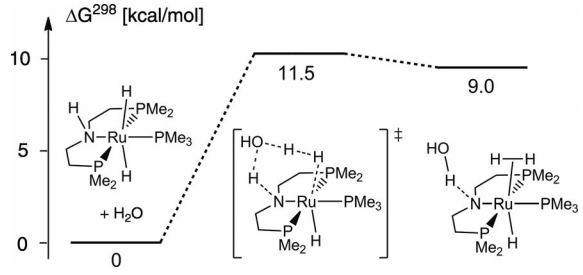

Scheme 16. DFT-computed water-catalyzed H_2 heterolysis.

4.2. Outer-Sphere Hydrogenation and Dehydrocoupling of Organic Substrates

Early studies reported on olefin hydrogenation with [RhCl{*H*L1^{Ph}}] and [IrCl{*H*L1^{Ph}}] as precatalysts.[107,108] However, the observation of the "N–H effect" by Noyori and co-workers sparked interest in these ligands for metal–ligand cooperative ("bifunctional") catalysis.[9] As a rare example, iridium(III) complex [Ir(H)$_2$Cl{*H*L1^{iPr}}] catalyzes both the hydrogenation of a wide range of aldehydes and ketones and the transfer hydrogenation of ketones and imines at mild reaction conditions upon activation with

 © 2012 Wiley-VCH Verlag GmbH & Co. KGaA, Weinheim

base (Scheme 17).[46b,109] Chemoselective direct hydrogenation of the carbonyl group is observed for benzylideneacetone, while transfer hydrogenation results in the saturated alcohol.

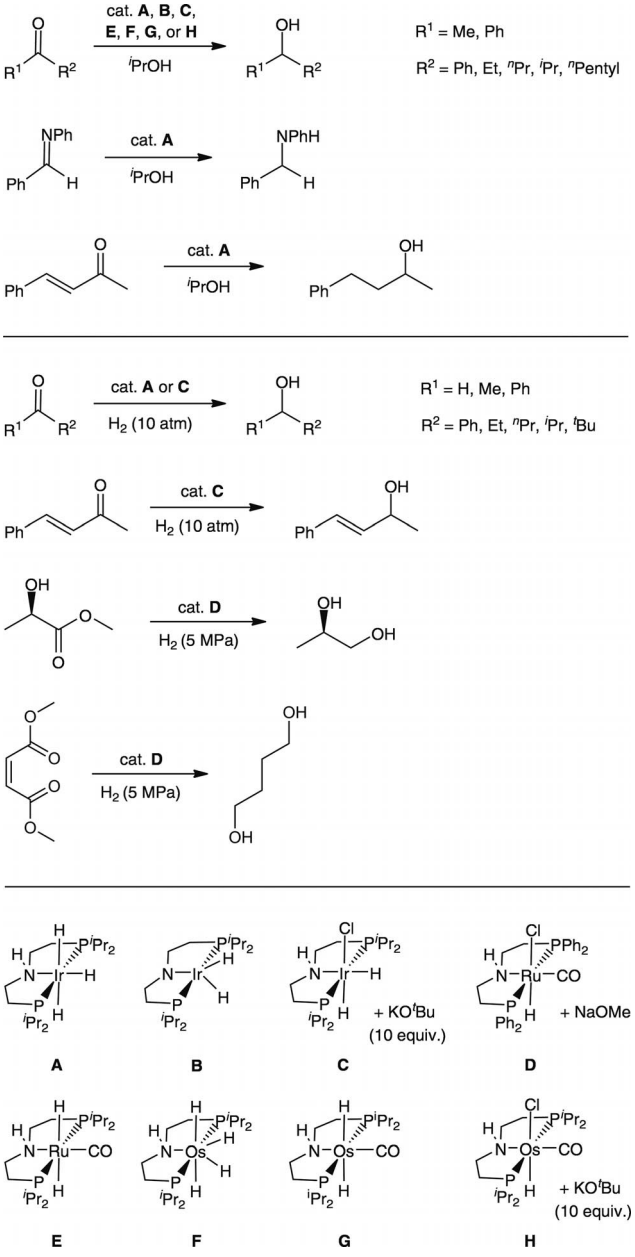

Scheme 17. Transfer hydrogenation and direct hydrogenation of carbonyl and carboxyl groups catalyzed by $HL1^R$ complexes.

Amine and amido complexes $[Ir(H)_3\{HL1^{iPr}\}]$ and $[Ir(H)_2\{L1^{iPr}\}]$ catalyze the reaction with comparable rates without base activation. Therefore, a metal–ligand cooperative "Noyori–Morris type" mechanism, with concerted H^+/H^- transfer to the substrate was proposed for hydrogenation and transfer hydrogenation (Scheme 18), and DFT computations confirmed this suggestion.[110] Ruthenium and osmium catalysts with ligand $HL1^R$ (R = *i*Pr, Ph) were also reported as excellent bifunctional catalysts for transfer hydrogenation of ketones[111] and for direct hydrogenation of esters to alcohols (Scheme 17).[40] α-Hydroxy esters and β-boc-amino esters are hydrogenated with retention of the configuration. Despite the availability of chiral PNP ligands, asymmetric hydrogenation has not been reported yet.

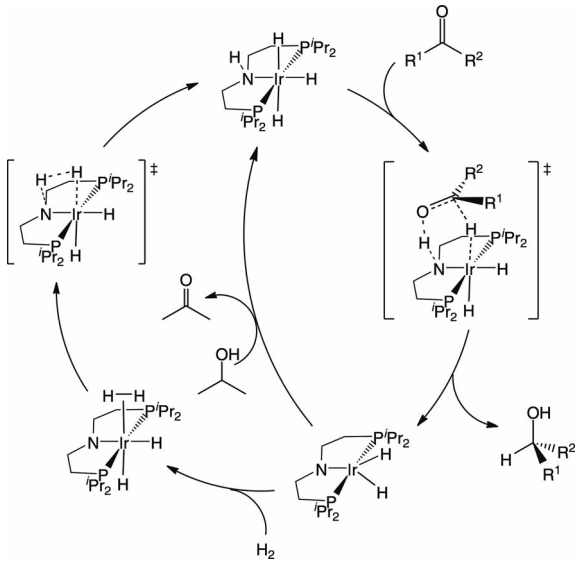

Scheme 18. Proposed catalytic cycles for transfer hydrogenation (inner cycle) and direct hydrogenation (outer cycle) of ketones with $[Ir(H)_3\{HL1^{iPr}\}]$.

Microscopic reversibility suggests that these catalysts could be suitable for acceptorless dehydrocoupling and reactions using the "borrowing hydrogen" methodology, as well.[112] Beller and co-workers reported the highly efficient (TON > 40000; $TOF_{max} > 14000\ h^{-1}$) release of H_2 and acetone from neat 2-propanol at very mild conditions (90 °C) with $[RuH_2(CO)(PPh_3)_3]/HL1^{iPr}$ (4.0 ppm loading) in the absence of base. Interestingly, the addition of base (e.g. NaO*i*Pr) results in considerably smaller TOF and the dehydrogenation of the PNP-ligand backbone in the presence of base (see above) provides a possible explanation.[113]

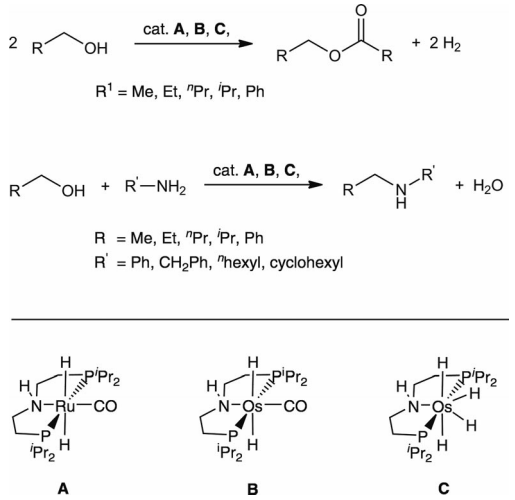

Scheme 19. Dehydrogenative coupling reactions with ruthenium and osmium PNP complexes.

 © 2012 Wiley-VCH Verlag GmbH & Co. KGaA, Weinheim

Ruthenium and osmium complexes with ligand HL1$^{i\mathrm{Pr}}$ were also used for dehydrocoupling of primary alcohols to symmetric esters and for amine alkylation with alcohols, and they exhibited high turnover numbers (Scheme 19).[111] The latter reaction was reported for [Ir(H)$_2$Cl{HL1$^{i\mathrm{Pr}}$}]/base as precatalyst, as well.[114]

4.3. De-/Hydrogenation of Inorganic Substrates: CO_2, Azide, and Borane-Amines

The d^6 complexes [Re(H)$_2$NO{HL1$^{i\mathrm{Pr}}$}] and [Ir(H)$_3$-{HL1$^{i\mathrm{Pr}}$}] rapidly insert CO_2 into a metal–hydride bond to form the formate complexes [Re(O$_2$CH)NO(H){HL1$^{i\mathrm{Pr}}$}] and [Ir(O$_2$CH)(H)$_2${HL1$^{i\mathrm{Pr}}$}], respectively.[115,116] The latter catalyzes the hydrogenation of CO_2 to formate in basic, aqueous solution with high activity (Scheme 20). In analogy to "Noyori–Morris type" ketone hydrogenation, an outer-sphere hydrogen transfer mechanism to the substrate was proposed and was supported by DFT computations.

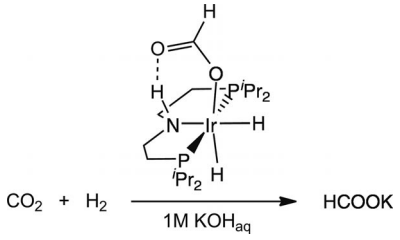

Scheme 20. Hydrogenation of CO_2 in aqueous solution catalyzed by [Ir(O$_2$CH)(H)$_2${HL1$^{i\mathrm{Pr}}$}].

Nitrido complexes could serve as model compounds to examine ammonia formation en route to a highly desirable homogeneous catalyst for N_2 hydrogenation at ambient conditions. However, only a few examples were reported that show reactivity towards H_2.[117] Otherwise, terminal nitrides are surprisingly inert towards H_2,[118] including [RuN{L$_C$$^{t\mathrm{Bu}}$}].[100] In contrast, nitrido complex [RuN{L1$^{t\mathrm{Bu}}$}] reacts with H_2 at relatively mild conditions (1 bar, 50 °C).[97] Unprecedented formation of ammonia and polyhydride [RuH$_4${HL1$^{t\mathrm{Bu}}$}] is observed in high yield (Scheme 21). Preliminary mechanistic examination is in agreement with initial, rate-determining heterolytic hydrogen splitting across the Ru–amido bond followed by stepwise proton transfer reactions to the nitride via imido, amido, and ammine intermediates. Hence, the role of the PNP pincer ligand is twofold: weakening Ru–N bonding to the *trans*-nitrido ligand (see above) and acceleration of the reaction by metal–ligand cooperative H_2 activation. Recycling of the ruthenium product by protonolysis followed by reaction with azide and base with high yields was also demonstrated, giving an overall synthetic cycle for catalytic hydrogenation of azide to NH_3 (Scheme 21).

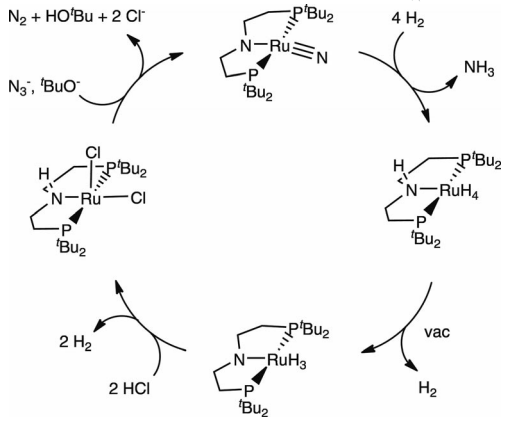

Scheme 21. Synthetic cycle for the hydrogenation of azide to ammonia.

In recent years, the dehydrogenation of borane–amine adducts has attracted considerable interest for chemical hydrogen storage and the synthesis of novel inorganic polymers and B–N ceramics.[119,120] Both [Ru(H)PMe$_3${L1$^{i\mathrm{Pr}}$}] and [Ru(H)$_2$PMe$_3${HL1$^{i\mathrm{Pr}}$}] catalyze the release of H_2 (1 equiv.) from H_3N–BH_3 (AB) solutions with high activities (TOF $\approx 20\ s^{-1}$) and turnover numbers (TON > 3000) without base at room temperature (Scheme 22).[74] According to ^{11}B-MQ-MAS spectra of the AB dehydrocoupling product, linear polyaminoboranes H_3N–[H_2B–H_2N]$_n$–BH_3 are formed.[121] Dehydrocoupling of MeH_2N–BH_3 towards linear, high-molecular-mass poly-*N*-methylaminoborane MeH_2N–[H_2B–MeHN]$_n$–BH_3 and of Me_2HN–BH_3 towards aminoborane dimer [Me_2N–BH_2]$_2$ were reported, as well.[122,123] The related catalyst [RuCl$_2$(H$_2$NCH$_2$CH$_2$-PtBu$_2$)$_2$] (with 10 equiv. KOtBu) was also used for dehydrogenation of borane–amine adducts.[124,125] On the basis of DFT computations, Fagnou proposed for this catalyst a metal–ligand cooperative ("Noyori–Morris type") mechanism with concerted H^+/H^- transfer from the substrate to a catalyst amido species and subsequent, turnover-limiting H_2 elimination from the amine complex. In fact, for H_3N–BH_3 dehydrocoupling catalyzed by [Ru(H)PMe$_3${L1$^{i\mathrm{Pr}}$}], high kinetic isotope effects upon deuteriation of the substrate both at the *N*- and at the *B*-termini were reported, as expected for such a mechanism.[74] However, the experimen-

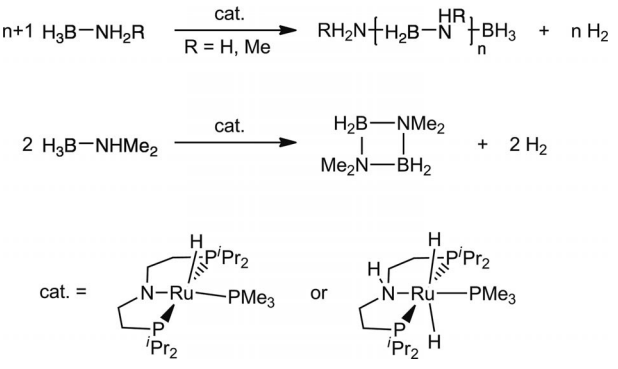

Scheme 22. Dehydrocoupling of borane–amine adducts catalyzed by [Ru(H)PMe$_3${HL1$^{i\mathrm{Pr}}$}] and [Ru(H)$_2$PMe$_3${HL1$^{i\mathrm{Pr}}$}].

 © 2012 Wiley-VCH Verlag GmbH & Co. KGaA, Weinheim

tal rate law is first-order in substrate, indicating a different rate-determining step for this catalyst. Iridium(III) complexes $[Ir(Cl)_2H\{HL1^{tBu}\}]$ and $[Ir(C_8H_{13})HCl\{HL1^{tBu}\}]$ were also reported to be efficient catalysts for the hydrolysis of ammonia borane in *i*PrOH/H_2O solution, mediating the rapid release of almost 3 equiv. H_2 (ca. 9 wt.-%).[126]

Conclusions

The present review emphasizes the remarkable versatility of the chelating amido, imine, enamido, and dienamido ligands derived from ethylene-bridged amine $HN(CH_2CH_2PR_3)_2$ by deprotonation or oxidative backbone functionalization. The parent amine, arguably one of the simplest PEP (E = C, N) pincer ligand platforms, is synthetically easily accessible with a wide range of available substituents including very bulky and some chiral examples. Most importantly, backbone dehydrogenation allows for electronic fine-tuning of the ligand donor properties, giving rise to a relatively wide range as compared with many other popular pincer ligand platforms.

The strong π-basicity of the dialkylamide $\{L1^R\}^-$ accounts for the main properties, such as ligand centered nucleophilicity. Hence, these ligands are ideal building blocks for metal–ligand cooperative (Noyori–Morris type) stoichiometric bond activation reactions and catalysis, exemplified by several efficient hydrogenation and dehydrocoupling reactions of organic and inorganic substrates. In addition to the bifunctional reactivity of the amido moiety, the easily obtained enamido ligand $\{L3^R\}^-$ represents an aliphatic analogue of another ligand class, Milstein's "dearomatized" PNP ligands, which is successfully applied in hydrogenation and dehydrocoupling catalysis. In addition to nitrogen-centered basic reactivity, the π-basicity also affects the electronic structure of coordinatively and electronically unsaturated complexes. Strong N(p)→M(d) π-donation by the dialkylamido ligand results in considerable nitrogen contribution to the HOMO of square-planar 16 VE complexes. Consequently, 1-electron oxidation of such iridium(I) and palladium(II) amides gives unstable radical complexes with predominant aminyl character. In turn, d^6 dialkylamides in this geometry are strongly stabilized by N→M π-donation. The d-orbital needed for π-bonding is vacant in the electronic low-spin configuration found for $[RuCl\{L1^{tBu}\}]$ and $[IrCl\{L4^{tBu}\}]^+$, which can therefore be described as 16 VE complexes. In case of ruthenium(II), the use of weaker π-donating ligands, $\{L_C\}^-$, $\{L3\}^-$, or $\{L4\}^-$, enables the control of the ground state spin multiplicity. Hence, it will be an interesting goal for future developments to assess whether the relatively unusual and to some extent adjustable electronic structure of these compounds will translate into unusual reactivity.

Acknowledgment

S. S. thanks the Deuthsche Forschungsgemeinschaft for an Emmy-Noether grant (SCHN950/2-1) and the IDK Nanocat for funding. B. A. is grateful to the TUM graduate school for support.

[1] D. Morales-Morales, C. M. Jensen (Eds.), *The Chemistry of Pincer Compounds*, Elsevier, Amsterdam, **2007**.

[2] a) M. Albrecht, G. van Koten, *Angew. Chem.* **2001**, *113*, 3866–3898; *Angew. Chem. Int. Ed.* **2001**, *40*, 3750–3781; b) M. E. Van der Boom, D. Milstein, *Chem. Rev.* **2003**, *103*, 1759–1792; c) W. Leis, H. A. Mayer, W. C. Kaska, *Coord. Chem. Rev.* **2008**, *252*, 1787–1797; d) J. Choi, A. H. R. McArthur, M. Brookhart, A. S. Goldman, *Chem. Rev.* **2011**, *111*, 1761–1779.

[3] K. Krogh-Jespersen, M. Czerw, K. Zhu, B. Singh, M. Kanzelberger, N. Darji, P. D. Achord, K. B. Renkema, A. S. Goldman, *J. Am. Chem. Soc.* **2002**, *124*, 10797–10809.

[4] L.-C. Liang, *Coord. Chem. Rev.* **2006**, *250*, 1152–1177.

[5] a) O. V. Ozerov, C. Guo, V. A. Papkov, B. M. Foxman, *J. Am. Chem. Soc.* **2004**, *126*, 4792–4793; b) L. Fan, L. Yang, C. Guo, B. M. Foxman, O. V. Ozerov, *Organometallics* **2004**, *23*, 4778–4787; c) W. Weng, C. Guo, C. Muora, L. Yang, B. M. Foxman, O. V. Ozerov, *Organometallics* **2005**, *24*, 3487–3499; d) L. Fan, O. V. Ozerov, *Chem. Commun.* **2005**, 4450–4452; e) L. Fan, S. Parkin, O. V. Ozerov, *J. Am. Chem. Soc.* **2005**, *127*, 16772–16773.

[6] a) J. I. van der Vlugt, J. N. H. Reek, *Angew. Chem.* **2009**, *121*, 8990–9004; *Angew. Chem. Int. Ed.* **2009**, *48*, 8832–8846; b) D. Milstein, *Top. Catal.* **2010**, *53*, 915–923; c) C. Gunanathan, D. Milstein, *Acc. Chem. Res.* **2011**, *44*, 588–602.

[7] a) M. D. Fryzuk, P. A. McNeil, *J. Am. Chem. Soc.* **1981**, *103*, 3592–3593; b) M. D. Fryzuk, P. A. McNeil, *Organometallics* **1983**, *2*, 355–356; c) M. D. Fryzuk, P. A. McNeil, S. J. Rettig, *Organometallics* **1986**, *5*, 2469–2476.

[8] Representative examples: a) S. E. Diamond, F. Mares, *J. Organomet. Chem.* **1977**, *142*, C55–C57; b) J. M. Mayer, C. J. Curtis, J. E. Bercaw, *J. Am. Chem. Soc.* **1983**, *105*, 2651–2660; c) J. F. Hartwig, S. Richards, D. Barañano, F. Paul, *J. Am. Chem. Soc.* **1996**, *118*, 3626–3633; d) J. F. Hartwig, *J. Am. Chem. Soc.* **1996**, *118*, 7010–7011; e) S. Wagaw, R. A. Rennels, S. L. Buchwald, *J. Am. Chem. Soc.* **1997**, *119*, 8451–8458; f) J. Zhao, H. Hesslink, J. F. Hartwig, *J. Am. Chem. Soc.* **2001**, *123*, 7220–7227; g) P. Zhao, J. F. Hartwig, *J. Am. Chem. Soc.* **2005**, *127*, 12066–12073; h) I. Matas, J. Campora, P. Palma, E. Alvarez, *Organometallics* **2009**, *28*, 6515–6523.

[9] a) R. Noyori, T. Okhuma, *Angew. Chem.* **2001**, *113*, 40–75; *Angew. Chem. Int. Ed.* **2001**, *40*, 40–73; b) S. E. Clapham, A. Hadzovic, R. H. Morris, *Coord. Chem. Rev.* **2004**, *248*, 2201–2237; c) K. Muñiz, *Angew. Chem.* **2005**, *117*, 6780–6785; *Angew. Chem. Int. Ed.* **2005**, *44*, 6622–6627; d) H. Grützmacher, *Angew. Chem.* **2008**, *120*, 1838–1842; *Angew. Chem. Int. Ed.* **2008**, *47*, 1814–1818; e) J. S. M. Samec, J.-E. Bäckvall, P. G. Andersson, P. Brandt, *Chem. Soc. Rev.* **2006**, *35*, 237–248; f) T. Ikariya, A. J. Blacker, *Acc. Chem. Res.* **2007**, *40*, 1300–1308; g) M. Ito, T. Ikariya, *Chem. Commun.* **2007**, 5134–5142.

[10] a) R. Kempe, *Angew. Chem.* **2000**, *112*, 478–504; *Angew. Chem. Int. Ed.* **2000**, *39*, 468–493; b) M. Lappert, P. Power, A. Protchenko, A. Seeber in *Metal Amide Chemistry*, Wiley, Chichester, **2009**.

[11] a) H. E. Bryndza, W. Tam, *Chem. Rev.* **1988**, *88*, 1163–1188; b) M. D. Fryzuk, C. D. Montgomery, *Coord. Chem. Rev.* **1989**, *95*, 1–40; c) D. M. Roundhill, *Chem. Rev.* **1992**, *92*, 1–27; d) R. G. Bergman, *Polyhedron* **1995**, *14*, 3227–3237; e) J. R. Fulton, A. W. Holland, D. J. Fox, R. G. Bergman, *Acc. Chem. Res.* **2002**, *35*, 44–56; f) T. B. Gunnoe, *Eur. J. Inorg. Chem.* **2007**, 1185–1203.

[12] a) J. F. Hartwig, *Acc. Chem. Res.* **1998**, *31*, 852–860; b) J. F. Hartwig, *Synlett* **2006**, 1283–1294; c) J. F. Hartwig, *Nature* **2008**, *455*, 314–322.

[13] R. G. Pearson, *J. Am. Chem. Soc.* **1963**, *85*, 3533–3539.

[14] H. E. Bryndza, L. K. Fong, R. A. Paciello, W. Tam, J. E. Bercaw, *J. Am. Chem. Soc.* **1987**, *109*, 1444–1456.

[15] For an excellent discussion, see ref.[11f]

 © 2012 Wiley-VCH Verlag GmbH & Co. KGaA, Weinheim

[16] a) G. L. Hillhouse, J. E. Bercaw, *J. Am. Chem. Soc.* **1984**, *106*, 5472–5478; b) R. L. Cowan, W. C. Trogler, *J. Am. Chem. Soc.* **1989**, *111*, 4750–4761.

[17] P. L. Holland, R. A. Andersen, R. G. Bergman, *Commun. Inorg. Chem.* **1999**, *21*, 115–129.

[18] L. A. Goj, E. D. Blue, S. A. Delp, T. B. Gunnoe, T. R. Cundari, A. W. Pierpont, J. L. Petersen, P. D. Boyle, *Inorg. Chem.* **2006**, *45*, 9032–9045.

[19] K. G. Caulton, *New J. Chem.* **1994**, *18*, 25–41.

[20] S. Park, A. L. Rheingold, D. M. Roundhill, *Organometallics* **1991**, *10*, 615–623.

[21] a) J. R. Fulton, M. W. Bouwkamp, R. G. Bergman, *J. Am. Chem. Soc.* **2000**, *122*, 8799–8800; b) T. Büttner, F. Breher, H. Grützmacher, *Chem. Commun.* **2004**, 2820–2821; c) P. Maire, F. Breher, H. Schönberg, H. Grützmacher, *Organometallics* **2005**, *24*, 3207–3218; d) T. Büttner, J. Geier, G. Frison, J. Harmer, C. Calle, A. Schweiger, H. Schönberg, H. Grützmacher, *Science* **2005**, *307*, 235–238.

[22] a) M. D. Fryzuk, P. A. McNeil, *Organometallics* **1983**, *2*, 682–684; b) M. D. Fryzuk, P. A. McNeil, S. J. Rettig, *Organometallics* **1985**, *4*, 1145–1147; c) M. D. Fryzuk, P. A. McNeil, S. J. Rettig, *J. Am. Chem. Soc.* **1987**, *109*, 2803–2812.

[23] a) D. Rais, R. G. Bergman, *Chem. Eur. J.* **2004**, *10*, 3970–3978; b) D. Conner, K. N. Jayaprakash, T. R. Cundari, T. B. Gunnoe, *Organometallics* **2004**, *23*, 2724–2733; c) A. N. Walstrom, L. A. Watson, M. Pink, K. G. Caulton, *Organometallics* **2004**, *23*, 4814–4816; d) Y. Feng, M. Lail, N. A. Foley, T. B. Gunnoe, K. A. Barakat, T. R. Cundari, J. L. Petersen, *J. Am. Chem. Soc.* **2006**, *128*, 7982–7994.

[24] Selected reviews and comments on non-innocent ligands: a) K. Ray, T. Petrenko, K. Wieghardt, F. Neese, *Dalton Trans.* **2007**, 1552–1566; b) R. G. Hicks, *Angew. Chem.* **2008**, *120*, 7503–7505; *Angew. Chem. Int. Ed.* **2008**, *47*, 7393–7395; W. Kaim, *Science* **2005**, *307*, 216–217; c) W. Kaim, *Inorg. Chem.* **2011**, *50*, 9752–9765.

[25] F. R. Keene, *Coord. Chem. Rev.* **1999**, *187*, 121–149.

[26] L. Que Jr., W. B. Tolman, *Nature* **2008**, *455*, 333–340.

[27] a) N. W. Alcock, R. D. O'Sullivan, A. W. Parkins, *J. Chem. Soc., Chem. Commun.* **1980**, 1216–1218; b) R. D. O'Sullivan, A. W. Parkins, N. W. Alcock, *J. Chem. Soc., Dalton Trans.* **1986**, 571–575.

[28] R. Gross, W. Kaim, *Inorg. Chem.* **1987**, *26*, 3596–3600.

[29] F. N. Penkert, T. Weyhermüller, E. Bill, P. Hildebrandt, S. Lecomte, K. Wieghardt, *J. Am. Chem. Soc.* **2000**, *122*, 9663–9673.

[30] a) P. Maire, M. Königsmann, A. Sreekanth, J. Harmer, A. Schweiger, H. Grützmacher, *J. Am. Chem. Soc.* **2006**, *128*, 6578–6580; b) N. Donati, D. Stein, T. Büttner, H. Schönberg, J. Harmer, S. Anadaram, H. Grützmacher, *Eur. J. Inorg. Chem.* **2008**, 4691–4703.

[31] Y. Miyazato, T. Wada, J. T. Muckerman, E. Fujita, K. Tanaka, *Angew. Chem.* **2007**, *119*, 5830–5832; *Angew. Chem. Int. Ed.* **2007**, *46*, 5728–5730.

[32] D. Adhikari, S. Mossin, F. Basuli, J. C. Huffmann, R. K. Szilagyi, K. Meyer, D. J. Mindiola, *J. Am. Chem. Soc.* **2008**, *130*, 3676–3682.

[33] a) C. Tejel, M. A. Ciriano, M. Pilar del Rio, D. G. H. Hetterscheid, N. Tsichlis i Spithas, J. M. N. Smits, B. de Bruin, *Chem. Eur. J.* **2008**, *14*, 10932–10936; b) C. Tejel, M. P. del Rio, M. A. Ciriano, E. J. Reijerse, F. Hartl, S. Zalis, D. G. H. Hetterscheid, N. Tsichlis i Spithas, B. de Bruin, *Chem. Eur. J.* **2009**, *15*, 11878–11889.

[34] N. P. Mankad, W. E. Antholine, R. K. Szilagyi, J. C. Peters, *J. Am. Chem. Soc.* **2009**, *131*, 3878–3880.

[35] a) P. J. Chirik, K. Wieghardt, *Science* **2010**, *327*, 794–795; b) W. I. Dzik, J. I. van der Vlugt, J. N. H. Reek, B. de Bruin, *Angew. Chem.* **2011**, *123*, 3416–3418; *Angew. Chem. Int. Ed.* **2011**, *50*, 3356–3358.

[36] M. Königsmann, N. Donati, D. Stein, H. Schönberg, J. Harmer, A. Sreekanth, H. Grützmacher, *Angew. Chem.* **2007**, *119*, 3637–3640; *Angew. Chem. Int. Ed.* **2007**, *46*, 3567–3570.

[37] Free amine $HN(CH_2CH_2Cl)_2$ and its hydrochloride salt are carcinogenic and should be handled with care. The related compounds $RN(CH_2CH_2Cl)_2$ (R = Me, Et, CH_2CH_2Cl) were produced as chemical warfare agents ("nitrogen mustards") and used as antitumor drugs. Their cytotoxicity relies on the formation of aziridinium salts upon intramolecular electrophilic substitution. Ring opening by nucelobases results in irreversible DNA damage by interstrand cross-linking: S. M. Rink, M. J. Solomon, M. J. Taylor, S. B. Rajur, L. W. McLaughlin, P. B. Hopkins, *J. Am. Chem. Soc.* **1993**, *115*, 2551–2557.

[38] a) L. Sacconi, R. Morassi, *J. Chem. Soc. A* **1968**, 2997–3002; b) M. M. T. Khan, E. R. Rao, *Polyhedron* **1987**, *6*, 1727–1735.

[39] a) M. E. Wilson, R. G. Nuzzo, G. E. Whitesides, *J. Am. Chem. Soc.* **1978**, *100*, 2269–2270; b) R. G. Nuzzo, S. L. Haynie, M. E. Wilson, G. M. Whitesides, *J. Org. Chem.* **1981**, *14*, 2861–2867.

[40] W. Kuriyama, T. Matsumoto, Y. Ino, O. Ogata (Takasago Int.), WO 2011048727, **2011**.

[41] A. Heßler, S. Kucken, O. Stelzer, W. S. Sheldrick, *J. Organomet. Chem.* **1998**, *553*, 39–52.

[42] A. A. Danopoulos, P. G. Edwards, *Polyhedron* **1989**, *8*, 1339–1344.

[43] A. A. Danopoulos, A. R. Wills, P. G. Edwards, *Polyhedron* **1990**, *9*, 2413–2418.

[44] B. Askevold, S. Schneider, unpublished.

[45] a) M. J. Burk, J. E. Feaster, R. L. Harlow, *Tetrahedron: Asymmetry* **1991**, *2*, 569–592; b) M. J. Burk (Du Pont), WO 92/19630, **1992**.

[46] a) K. Abdur-Rashid, US 20050107638, **2005**; b) Z. E. Clarke, P. T. Maragh, T. P. Dasgupta, D. G. Gusev, A. J. Lough, K. Abdur-Rashid, *Organometallics* **2006**, *25*, 4113–4117; c) K. Abdur-Rashid, T. Graham, C.-W. Tsang, X. Chen, R. Guo, W. Jia, D. Amoroso, C. Sui-Seng (Kanata Chem. Tech.), WO 2008/141439, **2008**.

[47] J. Meiners, A. Friedrich, E. Herdtweck, S. Schneider, *Organometallics* **2009**, *28*, 6331–6338.

[48] a) Y. Chi, X. Zhang, *Tetrahedron Lett.* **2002**, *43*, 4849–4852; b) H. Klein, R. Jackstell, K.-D. Wiese, C. Borgmann, M. Beller, *Angew. Chem.* **2001**, *113*, 3505–3508; *Angew. Chem. Int. Ed.* **2001**, *40*, 3408–3411.

[49] A. Friedrich, R. Ghosh, R. Kolb, E. Herdtweck, S. Schneider, *Organometallics* **2009**, *28*, 708–718.

[50] Selected examples for vinylic COE C–H oxidative addition: a) M. J. Fernandez, M. J. Rodriguez, L. A. Oro, F. J. Lahoz, *J. Chem. Soc., Dalton Trans.* **1989**, 2073–2076; b) D. Hermann, M. Gandelman, H. Rozenberg, L. J. W. Shimon, D. Milstein, *Organometallics* **2002**, *21*, 812–818; c) M. Iimura, D. R. Evans, T. C. Flood, *Organometallics* **2003**, *22*, 5370–5373.

[51] J. Meiners, A. Friedrich, E. Herdtweck, S. Schneider, *Organometallics* **2009**, *28*, 6331–6338.

[52] B. Askevold, A. Friedrich, M. R. Buchner, S. Schneider, in preparation.

[53] A. N. Marziale, E. Herdtweck, J. Eppinger, S. Schneider, *Inorg. Chem.* **2009**, *48*, 3699–3709.

[54] P. Maire, F. Breher, H. Grützmacher, *Angew. Chem.* **2005**, *117*, 6483–6487; *Angew. Chem. Int. Ed.* **2005**, *44*, 6325–6329.

[55] W. Keim, *Angew. Chem.* **1990**, *102*, 251–260; *Angew. Chem. Int. Ed. Engl.* **1990**, *29*, 235–244.

[56] P. Braunstein, J. Pietsch, Y. Chauvin, S. Mercer, L. Saussine, A. DeCian, J. J. Fischer, *J. Chem. Soc., Dalton Trans.* **1996**, 3571–3574.

[57] a) K. S. Coleman, M. L. H. Green, S. I. Pascu, N. H. Rees, A. R. Cowley, L. H. Rees, *J. Chem. Soc., Dalton Trans.* **2001**, 3384–3395; b) S. Pascu, G. D. W. Anderson, M. L. H. Green, J. C. Green, N. H. Rees, A. R. Cowley, *Inorg. Chim. Acta* **2006**, *359*, 3677–3692.

[58] Z.-X. Wang, L. Wang, *Chem. Commun.* **2007**, 2423–2425.

[59] a) P. O. Lagaditis, A. J. Lough, R. H. Morris, *Inorg. Chem.* **2010**, *49*, 10057–10066; b) P. O. Lagaditis, A. J. Lough, R. H. Morris, *J. Am. Chem. Soc.* **2011**, *133*, 9662–9665.

 © 2012 Wiley-VCH Verlag GmbH & Co. KGaA, Weinheim

[60] C. Tejel, M. Pilar del Río, L. Asensio, F. J. van den Bruele, M. A. Ciriano, N. Tsichlis i Spithas, D. G. H. Hetterscheid, B. de Bruin, *Inorg. Chem.* **2011**, *50*, 7524–7534.
[61] S. M. Kloeck, M. Heinekey, K. I. Goldberg, *Organometallics* **2006**, *25*, 3007–3011.
[62] I. Göttker-Schnetmann, P. S. White, M. Brookhart, *Organometallics* **2004**, *23*, 1766–1776.
[63] R. Meij, D. J. Stufkens, K. Vrieze, W. van Gerresheim, C. H. Stam, *J. Organomet. Chem.* **1979**, *164*, 353–370.
[64] L. Schwartsburd, M. A. Iron, L. Konstantinovski, Y. Diskin-Posner, G. Leitus, L. J. W. Shimon, D. Milstein, *Organometallics* **2010**, *29*, 3817–3827.
[65] M. T. Whithead, R. H. Grubbs, *J. Am. Chem. Soc.* **2008**, *130*, 5874–5875.
[66] S. A. Kulkin, A. M. Sheloumov, F. M. Dolgushin, M. G. Ezernitskaya, A. S. Peregudov, P. V. Petrovskii, A. A. Koridze, *Organometallics* **2006**, *25*, 5466–5476.
[67] A. M. Winter, K. Eichele, H.-G. Mack, W. C. Kaska, H. A. Mayer, *Organometallics* **2005**, *24*, 1837–1844.
[68] A. M. Winter, K. Eichele, H.-G. Mack, W. C. Kaska, H. A. Mayer, *Dalton Trans.* **2008**, 527–532.
[69] B. Askevold, M. Khusniyarov, E. Herdtweck, F. Heinemann, S. Schneider, in preparation.
[70] A. M. Sheloumov, F. M. Dolgushin, M. V. Kondrashov, P. V. Petrovskii, K. A. Barbakadze, O. I. Lekashvili, A. A. Koridze, *Russ. Chem. Bull. Int. Ed.* **2007**, *56*, 1757–1764.
[71] D. G. Gusev, M. Madott, F. M. Dolgushin, K. A. Lyssenko, M. Y. Antipin, *Organometallics* **2000**, *19*, 1734–1739.
[72] D. G. Gusev, A. J. Lough, *Organometallics* **2002**, *21*, 5091–5099.
[73] All ruthenium complexes in Table 1 exhibit square-pyramidal molecular structures with CO in the apical position.
[74] M. Käß, A. Friedrich, M. Drees, S. Schneider, *Angew. Chem.* **2009**, *121*, 922–924; *Angew. Chem. Int. Ed.* **2009**, *48*, 905–907.
[75] A. Friedrich, M. Drees, M. Käß, E. Herdtweck, S. Schneider, *Inorg. Chem.* **2010**, *49*, 5482–5494.
[76] a) D. L. Thorn, R. Hoffmann, *New J. Chem.* **1979**, *3*, 39–45; b) J. F. Riehl, Y. Jean, O. Eisenstein, M. Pélessier, *Organometallics* **1992**, *11*, 729–737.
[77] a) H. Werner, A. Höhn, M. Dziallas, *Angew. Chem.* **1986**, *98*, 1112–1112; *Angew. Chem. Int. Ed. Engl.* **1986**, *25*, 1090–1092; b) M. D. Fryzuk, P. A. McNeil, R. G. Ball, *J. Am. Chem. Soc.* **1986**, *108*, 6414–6416.
[78] Selected reviews on open-shell platinum metal complexes: a) K. K. Pandey, *Coord. Chem. Rev.* **1992**, *121*, 1–42; b) D. G. DeWit, *Coord. Chem. Rev.* **1996**, *147*, 209–246; c) B. de Bruin, D. G. Hetterscheid, A. J. J. Koekkoek, H. Grützmacher, *Prog. Inorg. Chem.* **2007**, *55*, 247–354.
[79] N. P. Tsvetkov, M. F. Laird, H. Fan, M. Pink, K. G. Caulton, *Chem. Commun.* **2009**, 4578–4580.
[80] B. de Bruin, D. G. H. Hetterscheid, *Eur. J. Inorg. Chem.* **2007**, 211–230.
[81] J. Meiners, M. G. Scheibel, M.-H. Lemée-Cailleau, S. A. Mason, M. B. Boeddinghaus, T. F. Fässler, E. Herdtweck, M. M. Khusniyarov, S. Schneider, *Angew. Chem.* **2011**, *123*, 8334–8337; *Angew. Chem. Int. Ed.* **2011**, *50*, 8184–8187.
[82] a) M. P. García, M. V. Jimenez, L. A. Oro, F. J. Lahoz, P. J. Alonso, *Angew. Chem.* **1992**, *104*, 1512–1514; *Angew. Chem. Int. Ed. Engl.* **1992**, *31*, 1527–1529; b) A. B. Danopoulos, G. Wilkinson, B. Hussain-Bates, M. B. Hursthouse, *J. Chem. Soc., Dalton Trans.* **1992**, 3165–3170; c) H. Zhai, A. Bunn, B. Wayland, *Chem. Commun.* **2001**, 1294–1295; d) B. de Bruin, T. P. J. Peters, S. Thewissen, A. N. J. Blok, J. B. M. Wilting, R. de Gelder, J. M. M. Smits, A. W. Gal, *Angew. Chem.* **2002**, *114*, 2239–2242; *Angew. Chem. Int. Ed.* **2002**, *41*, 2135–2138; e) A. S. Ionkin, W. J. Marshall, *Organometallics* **2004**, *23*, 6031–6041; f) D. G. H. Hetterscheid, J. Kaiser, E. Reijerse, T. P. J. Peters, S. Thewissen, A. N. J. Blok, J. M. M. Smits, R. de Gelder, B. de Bruin, *J. Am. Chem. Soc.* **2005**, *127*, 1895–1905; g) W. I. Dzik, L. F. Arruga, M. A. Siegler, A. L. Spek, J. N. H. Reek, B. de Bruin, *Organometallics* **2011**, *30*, 1902–1913.
[83] S. Alvarez, J. Cirera, *Angew. Chem.* **2006**, *118*, 3078–3087; *Angew. Chem. Int. Ed.* **2006**, *45*, 3012–3020.
[84] a) B. W. Dale, R. J. P. Williams, C. E. Johnson, T. L. Thorp, *J. Chem. Phys.* **1968**, *49*, 3441–3444; b) H. Goff, G. N. La Mar, C. A. Reed, *J. Am. Chem. Soc.* **1977**, *99*, 3641–3646.
[85] K. Ray, A. Begum, T. Weyhermüller, S. Piligkos, J. van Slageren, F. Neese, K. Wieghardt, *J. Am. Chem. Soc.* **2005**, *127*, 4403–4415.
[86] a) G. Ujaque, A. C. Cooper, F. Maseras, O. Eisenstein, K. G. Caulton, *J. Am. Chem. Soc.* **1998**, *120*, 361–365; b) W. Baratta, E. Herdtweck, P. Rigo, *Angew. Chem.* **1999**, *111*, 1733–1735; *Angew. Chem. Int. Ed.* **1999**, *38*, 1629–1631; c) J. P. Lee, Z. Ke, M. A. Ramirez, T. B. Gunnoe, T. R. Cundari, P. D. Boyle, J. L. Petersen, *Organometallics* **2009**, *28*, 1758.
[87] V. F. Kuznetsov, K. Abdur-Rashid, A. J. Lough, D. G. Gusev, *J. Am. Chem. Soc.* **2006**, *128*, 14388–14396.
[88] a) D. Schröder, S. Shaik, H. Schwarz, *Acc. Chem. Res.* **2000**, *33*, 139–145; b) R. Poli, J. N. Harvey, *Chem. Soc. Rev.* **2003**, *32*, 1–8.
[89] D. Empsall, E. M. Hyde, R. Markham, W. S. McDonald, M. C. Norton, B. L. Shaw, W. Weeks, *J. Chem. Soc., Chem. Commun.* **1977**, 589–590.
[90] B. Askevold, M. M. Khusniyarov, E. Herdtweck, K. Meyer, S. Schneider, *Angew. Chem.* **2010**, *122*, 7728–7731; *Angew. Chem. Int. Ed.* **2010**, *49*, 7566–7569.
[91] L. A. Watson, O. V. Ozerov, M. Pink, K. G. Caulton, *J. Am. Chem. Soc.* **2003**, *125*, 8426–8427.
[92] X. Yang, A. Walstrom, N. Tsvetkov, M. Pink, K. G. Caulton, *Inorg. Chem.* **2007**, *46*, 4612–4616.
[93] R. Boca, *Coord. Chem. Rev.* **2004**, *248*, 757–815.
[94] a) A. Walstrom, M. Pink, N. P. Tsvetkov, H. Fan, M. Ingleson, K. G. Caulton, *J. Am. Chem. Soc.* **2005**, *127*, 16780–16781; b) A. Walstrom, M. Pink, K. G. Caulton, *Inorg. Chem.* **2006**, *45*, 5617–5620; c) N. Tsvetkov, M. Pink, H. Fan, J.-H. Lee, K. G. Caulton, *Eur. J. Inorg. Chem.* **2010**, 4790–4800.
[95] F. A. Cotton, V. M. Miskowski, B. Zhong, *J. Am. Chem. Soc.* **1989**, *111*, 6177–6182.
[96] A. Walstrom, M. Pink, X. Yang, J. Tomaszewski, M.-H. Baik, K. G. Caulton, *J. Am. Chem. Soc.* **2005**, *127*, 5330–5331.
[97] B. Askevold, J. T. Nieto, S. Tussupbayev, M. Diefenbach, E. Herdtweck, M. C. Holthausen, S. Schneider, *Nature Chem.* **2011**, *3*, 532–537.
[98] a) T. A. Betley, J. C. Peters, *J. Am. Chem. Soc.* **2004**, *126*, 6252–6254; b) C. Vogel, F. W. Heinemann, J. Sutter, C. Anthon, K. Meyer, *Angew. Chem.* **2008**, *120*, 2721–2724; *Angew. Chem. Int. Ed.* **2008**, *47*, 2681–2684; c) J. J. Scepaniak, M. D. Fulton, R. P. Bontchev, E. N. Duesler, M. L. Kirk, J. M. Smith, *J. Am. Chem. Soc.* **2008**, *130*, 10515–10517; d) J. J. Scepaniak, J. A. Young, R. P. Bontchev, J. M. Smith, *Angew. Chem.* **2009**, *121*, 3204–3206; *Angew. Chem. Int. Ed.* **2009**, *48*, 3158–3160; e) J. Schöffel, A. Y. Rogachev, S. DeBeer George, P. Burger, *Angew. Chem.* **2009**, *121*, 4828–4832; *Angew. Chem. Int. Ed.* **2009**, *48*, 4734–4738; f) C. C. H. Atienza, A. C. Bowman, E. Lobkovsky, P. J. Chrik, *J. Am. Chem. Soc.* **2010**, *132*, 16343–16345; g) J. J. Scepaniak, C. S. Vogel, M. M. Khusniyarov, F. W. Heinemann, K. Meyer, J. M. Smith, *Science* **2011**, *331*, 1049–1052.
[99] R. A. Eikey, M. M. Abu-Omar, *Coord. Chem. Rev.* **2003**, *243*, 83–124.
[100] A. Walstrom, H. Fan, M. Pink, K. G. Caulton, *Inorg. Chim. Acta* **2010**, *363*, 633–636.
[101] C. Lee, W. Yang, R. G. Parr, *THEOCHEM* **1988**, *163*, 305–313.
[102] J. F. Berry, *Comments Inorg. Chem.* **2009**, *30*, 28–66.
[103] a) G. J. Kubas, *Chem. Rev.* **2007**, *107*, 4152–4205; b) J. C. Gordon, G. J. Kubas, *Organometallics* **2010**, *29*, 4682–4701.
[104] a) R. Hartmann, P. Chen, *Angew. Chem.* **2001**, *113*, 3693–3697; *Angew. Chem. Int. Ed.* **2001**, *40*, 3581–3585; b) M. Ito, M. Hirakawa, K. Murata, T. Ikariya, *Organometallics* **2001**,

 © 2012 Wiley-VCH Verlag GmbH & Co. KGaA, Weinheim

20, 379–381; c) V. Rautenstrauch, X. Hoang-Cong, R. Churland, K. Abdur-Rashid, R. H. Morris, *Chem. Eur. J.* **2003**, *9*, 4954–4967; d) C. Hedberg, K. Källström, P. I. Arvidsson, P. Brandt, P. G. Andersson, *J. Am. Chem. Soc.* **2005**, *127*, 15083–15090; e) W. Baratta, K. Siega, P. Rigo, *Chem. Eur. J.* **2007**, *13*, 7479–7486; f) A. Hadzovic, D. Song, C. M. MacLaughlin, R. H. Morris, *Organometallics* **2007**, *26*, 5987–5999.

[105] A. Friedrich, M. Drees, J. Schmedt auf der Günne, S. Schneider, *J. Am. Chem. Soc.* **2009**, *131*, 17552–17553.

[106] M. A. Iron, E. Ben-Ari, R. Cohen, D. Milstein, *Dalton Trans.* **2009**, 9433–9439.

[107] a) M. M. T. Khan, B. T. Khan, S. Nazeeruddin, K. Nazeeruddin, *J. Mol. Catal.* **1984**, *26*, 207–217; b) M. M. T. Khan, B. T. Khan, S. Begum, *J. Mol. Catal.* **1986**, *34*, 9–18; c) M. M. T. Khan, B. T. Khan, S. Begum, S. M. Ali, *J. Mol. Catal.* **1986**, *34*, 283–291; d) M. M. T. Khan, E. R. Rao, M. R. H. Siddiqui, B. T. Khan, S. Begum, S. M. Ali, J. Reddy, *J. Mol. Catal.* **1988**, *45*, 35–50.

[108] Tertiary amine ligands *R*L1^{Ph} (R ≠ H) were also used, e.g in chemoselective hydrogenation of α,β-unsaturated ketones, asymmetric hydrogenation, and transfer hydrogenation, but are not subject of this review: a) C. Bianchini, E. Farnetti, M. Graziani, G. Nardin, A. Vacca, F. Zanobini, *J. Am. Chem. Soc.* **1990**, *112*, 9190–9197; b) C. Bianchini, E. Farnetti, L. Glendenning, M. Graziani, G. Nardin, M. Peruzzini, E. Rocchini, F. Zanobini, *Organometallics* **1995**, *14*, 1489–1502; c) C. Bianchini, L. Glendenning, F. Zanobini, E. Farnetti, M. Graziani, E. Nagy, *J. Mol. Catal. A* **1998**, *132*, 13–19; d) M. S. Rahman, P. D. Prince, J. W. Steed, K. K. M. Hii, *Organometallics* **2002**, *21*, 4927–4933.

[109] X. Chen, W. Jia, R. Guo, T. W. Graham, M. A. Gullons, K. Abdur-Rashid, *Dalton Trans.* **2009**, 1407–1410.

[110] S. Bi, Q. Xie, X. Zhao, Y. Zhao, X. Kong, *J. Organomet. Chem.* **2008**, *693*, 633–638.

[111] a) M. Bertoli, A. Choualeb, A. J. Lough, B. Moore, D. Spasyuk, D. G. Gusev, *Organometallics* **2011**, *30*, 3479–3482; b) M. Bertoli, A. Choualeb, D. G. Gusev, A. J. Lough, Q. Major, B. Moore, *Dalton Trans.* **2011**, *40*, 8941–8949.

[112] a) M. H. S. A. Hamid, P. A. Slatford, J. M. J. Williams, *Adv. Synth. Catal.* **2007**, *349*, 1555–1575; b) A. Friedrich, S. Schneider, *ChemCatChem* **2009**, *1*, 72–73; c) T. D. Nixon, M. K. Whittlesey, J. M. J. Williams, *Dalton Trans.* **2009**, 753–762; d) A. J. A. Watson, J. M. J. Williams, *Science* **2010**, *329*, 635–636; e) G. E. Dobereiner, R. H. Crabtree, *Chem. Rev.* **2010**, *110*, 681–703; f) G. Guillena, D. J. Ramón, M. Yus, *Chem. Rev.* **2010**, *110*, 1611–1641; g) J. Choi, A. H. R. McArthur, M. Brookhart, A. S. Goldman, *Chem. Rev.* **2011**, *111*, 1761–1779.

[113] M. Nielsen, A. Kammer, D. Cozzula, H. Junge, S. Gladiali, M. Beller, *Angew. Chem.* **2011**, *123*, 9767–9771; *Angew. Chem. Int. Ed.* **2011**, *50*, 9593–9597.

[114] N. Andrushko, V. Andrusjko, P. Roose, K. Moonen, A. Börner, *ChemCatChem* **2010**, *2*, 640–643.

[115] T. J. Schmeier, G. E. Dobereiner, R. H. Crabtree, N. Hazari, *J. Am. Chem. Soc.* **2011**, *133*, 9274–9277.

[116] A. Choualeb, A. J. Lough, D. G. Gusev, *Organometallics* **2007**, *26*, 3509–3515.

[117] a) S. D. Brown, M. P. Mehn, J. C. Peters, *J. Am. Chem. Soc.* **2005**, *127*, 13146–13147; b) J. Schöffel, A. Y. Rogachev, S. DeBeer George, P. Burger, *Angew. Chem.* **2009**, *121*, 4828–4832; *Angew. Chem. Int. Ed.* **2009**, *48*, 4734–4738.

[118] M. P. Shaver, M. D. Fryzuk, *Adv. Synth. Catal.* **2003**, *345*, 1061–1076.

[119] a) F. H. Stephens, V. Pons, R. T. Baker, *Dalton Trans.* **2007**, 2613–2626; b) C. W. Hamilton, R. T. Baker, A. Staubitz, I. Manners, *Chem. Soc. Rev.* **2009**, *38*, 279–293; c) N. C. Smythe, J. C. Gordon, *Eur. J. Inorg. Chem.* **2010**, 509–521; d) A. Staubitz, A. P. M. Robertson, I. Manners, *Chem. Rev.* **2010**, *110*, 4079–4124.

[120] a) T. J. Clark, K. Lee, I. Manners, *Chem. Eur. J.* **2006**, *12*, 8634–8648; b) A. Staubitz, A. P. M. Robertson, M. E. Sloan, I. Manners, *Chem. Rev.* **2010**, *110*, 4023–4078.

[121] A. Friedrich, PhD Thesis, Technische Universität München, **2010**.

[122] A. Staubitz, M. E. Sloan, A. P. M. Robertson, A. Friedrich, S. Schneider, P. J. Gates, J. Schmedt auf der Günne, I. Manners, *J. Am. Chem. Soc.* **2010**, *132*, 13332–13345.

[123] A. Friedrich, M. Drees, S. Schneider, *Chem. Eur. J.* **2009**, *15*, 10339–10342.

[124] N. Blaquiere, S. Diallo-Garcia, S. I. Gorelsky, D. A. Black, K. Fagnou, *J. Am. Chem. Soc.* **2008**, *130*, 14034–14035.

[125] S. S. Mal, F. H. Stephens, R. T. Baker, *Chem. Commun.* **2011**, *47*, 2922–2924.

[126] T. W. Graham, C.-W. Tsang, X. Chen, R. Guo, W. Jia, S.-M. Lu, C. Sui-Seng, C. B. Ewart, A. Lough, D. Amoroso, K. Abdur-Rashid, *Angew. Chem.* **2010**, *122*, 8890–8893; *Angew. Chem. Int. Ed.* **2010**, *49*, 8708–8711.

Received: August 23, 2011
Published Online: November 22, 2011

 © 2012 Wiley-VCH Verlag GmbH & Co. KGaA, Weinheim

DOI: 10.1002/ejic.201101023

Ligand Effect on Cobalt(II)-Catalyzed Asymmetric Cyclopropanation with Diazosulfones – Approaching High Stereoselectivity through Modular Design of D_2-Symmetric Chiral Porphyrins

Shifa Zhu,[a,b] Xin Cui,[a] and X. Peter Zhang*[a]

Keywords: Cyclopropanation / Chiral porphyrins / Cobalt / Ligand effects / Asymmetric catalysis

A significant ligand effect study has been summarized for asymmetric cyclopropanation with diazosulfones catalyzed by Co^{II} complexes of a series of D_2-symmetric chiral porphyrins. The structure of the ligands was shown to play an important role in both the reactivity and the stereoselectivity of the reactions. Fine-tuning of the porphyrin ligand environments led to the development of an efficient Co^{II}-based catalytic system for cyclopropanation of styrene with diazosulfones in high diastereoselectivity and enantioselectivity.

Introduction

Cyclopropanes, a unique class of saturated carbocyclic compounds with highly strained three-membered-ring structures, serve as valuable building blocks in many organic transformations.[1] Asymmetric cyclopropanation of alkenes with diazo reagents catalyzed by transition metal complexes represents a fundamental transformation with great practical importance.[1,2] During the past decades, complexes of a variety of transition metals,[1,2] including Cu,[3] Rh,[4] Ru,[5] and Co,[6] have been reported as efficient catalysts for asymmetric cyclopropanation reactions. While the majority of metal-catalyzed asymmetric cyclopropanation reactions employ diazocarbonyls as carbene sources, it has been recently demonstrated that diazosulfones, an-

[a] Department of Chemistry, University of South Florida, Tampa, Florida 33620-5250, USA
Fax: +1-813-974-3203
E-mail: xpzhang@usf.edu
[b] School of Chemistry and Chemical Engineering, South China University of Technology, Guangzhou 510640, China

Supporting information for this article is available on the WWW under http://dx.doi.org/10.1002/ejic.201101023.

Shifa Zhu was born in Jiangxi Province, China in 1978. He received his bachelor's degree from Hunan University in 2001. Prof. Zhu obtained his Ph.D. from Shanghai Institute of Organic Chemistry, Chinese Academy of Sciences (SIOC) in 2006, under the supervision of Prof. Shizheng Zhu. After two years of postdoctoral training with Professor Peter Zhang from 2007 to 2008 at the University of South Florida, he returned to China and joined the South China University of Technology (SCUT) as an associate professor in 2009 and started his independent research. His current research interest involves the design and synthesis of new chiral catalysts and their application in asymmetric synthesis. He was the recipient of the New Century Excellent Talents in University award of the Ministry of Education, China (2010).

Xin Cui received his Ph.D. degree in chemistry from the University of Science and Technology of China (USTC) in 2008, where he carried out research work on phosphane-free Pd-catalyzed cross-coupling reactions and synthesis of heterocyclic compounds under the supervision of Professor Qingxiang Guo. Since 2008, he has been working with Professor Peter Zhang at the University of South Florida as a postdoc. His research is mainly devoted to asymmetric cyclopropenation reactions, synthesis of heterocyclic compounds, and C–H functionalization by Co^{II}-based metalloradical catalysis.

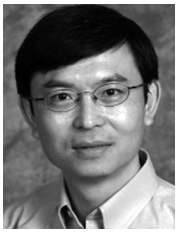

Peter Zhang received his Ph.D. degree in chemistry from the University of Pennsylvania in 1996, where he carried out research work on a Rh^{II}-based system for the activation of methane and carbon monoxide under the direction of Professor Bradford Wayland. He then undertook postdoctoral work at the Massachusetts Institute of Technology (MIT) as a National Institutes of Health (NIH) Postdoctoral Fellow during the period of 1996–2001, first with Professor Stephen Lippard on the construction of functional models for methane monooxygenase (MMO) and then with Professor Stephen Buchwald on the synthesis of polyanilines (PANIs) by Pd-catalyzed amination. Dr. Zhang began his independent career as Assistant Professor of Chemistry at the University of Tennessee in 2001. He joined the University of South Florida as Associate Professor of Chemistry in 2006 and was promoted to Professor of Chemistry in 2010. Dr. Zhang's research and education activity were recognized with several awards, including the NSF CAREER Award in 2006.

© 2012 Wiley-VCH Verlag GmbH & Co. KGaA, Weinheim

other class of known diazo reagents, could stereoselectively cyclopropanate a wide range of olefins (Scheme 1).[6c] Except a Cu-based intramolecular version of asymmetric cyclopropanation with diazosulfones reported previously by Nakada and co-workers,[7–10] this Co^{II}-based catalytic system still represents the only example of metal-catalyzed asymmetric intermolecular cyclopropanation reactions with this broad class of diazo reagents. Given that the resulting cyclopropyl sulfones have found a variety of applications,[7–12] the development of this catalytic transformation would still be highly attractive.

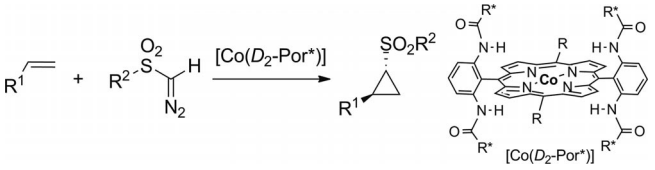

Scheme 1. Cyclopropanation with diazosulfones catalyzed by Co^{II} complexes of D_2-symmetric chiral porphyrins.

Structurally well-defined cobalt(II) complexes of D_2-symmetric chiral porphyrins [Co(D_2-Por*)] have emerged as a new class of effective catalysts for asymmetric cyclopropanation.[6,13] The Co^{II}-based metalloradical cyclopropanation (MRC) has been shown to possess a unique reactivity profile and can achieve highly stereoselective cyclopropanation of both aromatic and aliphatic olefins with varied electronic properties, including electron-rich and electron-poor olefins.[6,14] As important as the metal center, the surrounding chiral porphyrin ligands can influence the electronic and steric properties of the catalysts systematically or in a dramatic manner, offering a vast tunability of the catalytic system for controlling reactivity and stereoselectivity.[6,15] Through modular construction of chiral porphyrins through palladium-catalyzed multiple amidation reactions of bromoporphyrin synthons with chiral amides,[6f] a "toolbox" of growing numbers of [Co(D_2-Por*)] catalysts with varied chiral (R*) and nonchiral (R) substituents (Scheme 1) has been constructed and applied for various asymmetric catalytic processes.[6,13,15] A detailed study of ligand effects from this catalyst "toolbox" will establish the ligand–reactivity relationship that should lead to not only the identification of more efficient catalysts for existing transformations, but also the design of a new generation of catalysts with broad chemistry. Herein we present a microreview on a detailed ligand effect for the [Co(D_2-Por*)]-catalyzed asymmetric cyclopropanation of styrene with diazosulfones. Specifically, ligand–reactivity and ligand–selectivity relationships are described in this overview.

Ligand Effect in Co^{II}-Catalyzed Asymmetric Cyclopropanation of Styrene with N_2CHTs

Under practical conditions (room temperature without slow addition),[6,14] catalyzed by 1 mol-% of [Co(D_2-Por*)], styrene was cyclopropanated with tosyldiazomethane in dichloromethane at room temperature for 24 h. Major diastereomer *trans*-cyclopropyl sulfone **1** was isolated, and its enantiomeric excess was measured by chiral HPLC. A number of chiral [Co(D_2-Por*)] complexes have been applied as the catalysts for this reaction. The structures of the catalysts have been systematically tuned by varying chiral building blocks R* and nonchiral groups R (Scheme 1).

Initially, a series of porphyrins [Co(ChenP)] bearing an (*S*)-2,2-dimethylcyclopropanecarboxamido group (ChenAmido), which has been previously shown to be highly effective for various cyclopropanation reactions, were chosen as the catalysts. (Table 1).[6] While two relatively less sterically hindered catalysts, Co(ChenP1)[6f] and Co(ChenP2),[6f] resulted in the desired product with moderate yields, Co(ChenP3),[6f] with 3,5-di-*tert*-butylphenyl groups, gave the product in 91% yield, albeit in poor enantioselectivity.[6c] It is believed that the bowl-shaped ligand ChenP3 provided a more appropriate environment for the MRC, which has been shown to involve highly sensitive radical intermediates.[14] Further increasing the steric hindrance of the catalysts led to the usage of Co(ChenP4)[6f] and Co(ChenP5).[6f] Although lower yields were obtained, presumably due to the overcrowded metal center, 2,6-MeO groups facilitated chiral induction dramatically, and a 56% *ee* was obtained.[6c] In contrast to the flexible nature of the MeO group in Co(ChenP5), the use of a highly rigid anthryl group as nonchiral partners (R) in catalyst Co(ChenP6)[6f] resulted in very low activity toward this reaction, and the product was detected only in trace quantities.

Table 1. Asymmetric cyclopropanation of styrene with N_2CHTs catalyzed by Co(ChenP).[a]

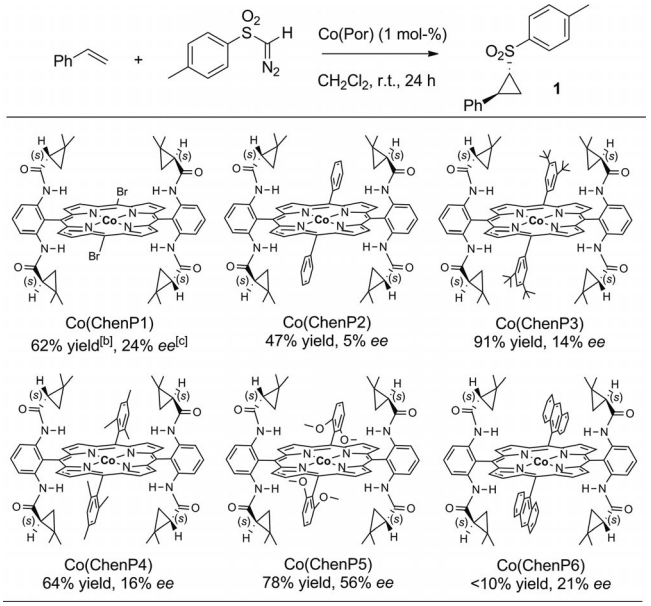

[a] Performed in CH_2Cl_2 at room temp. for 24 h with 1 mol-% [Co(Por)] under N_2 with 1.0 equiv. of styrene and 1.2 equiv. of N_2CHTs; [styrene] = 0.25 M. [b] Isolated yields of *trans* isomer. [c] The *ee* value was determined by chiral HPLC.

In addition to Co(ChenP), an (*S*)-2-methoxypropanamido group (RuppelAmido), readily derived from lactic acid, was employed as the chiral arms in the catalysts Co-

 © 2012 Wiley-VCH Verlag GmbH & Co. KGaA, Weinheim

(RuppelP) (Table 2). The nonchiral partners (R) were also systematically tuned in the Co(RuppelP)-catalyzed reaction. While Co(RuppelP1)[6f] and Co(RuppelP2)[6f] might be expected to be ineffective for the reaction because of the openness of the structure, we were somewhat surprised by the inferior performance of the 3,5-di-*tert*-butylphenyl version Co(RuppelP3)[6] with only 60% yield.[6c] Subsequent screening with Co(RuppelP5)[6] demonstrated again that 2,6-dimethoxyphenyl groups constructed just the proper environment for this cyclopropanation, giving 99% yield with 61% *ee*.[6c] Interestingly, even a structurally similar Co(RuppelP6)[6f] with ethoxy groups resulted in a dramatically decreased yield of only 48% with 47% *ee*.

Table 2. Asymmetric cyclopropanation of styrene with N_2CHTs catalyzed by Co(RuppelP).[a]

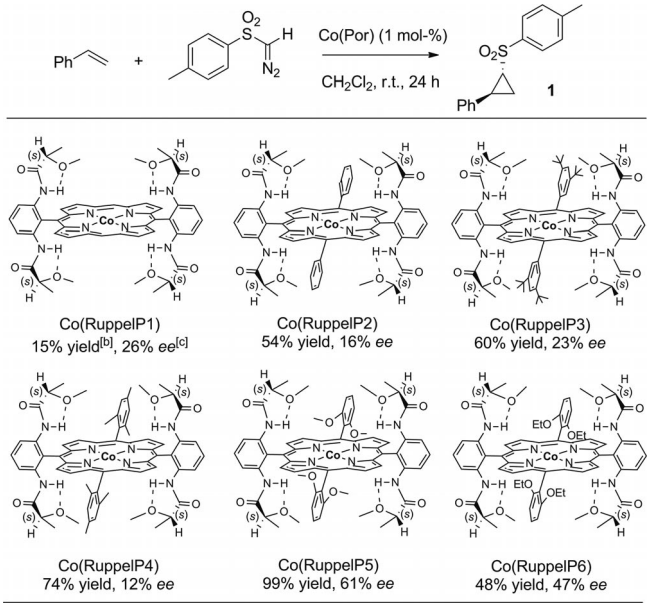

[a] Performed in CH_2Cl_2 at room temp. for 24 h with 1 mol-% [Co(Por)] under N_2 with 1.0 equiv. of styrene and 1.2 equiv. of N_2CHTs; [styrene] = 0.25 M. [b] Isolated yields of *trans* isomer. [c] The *ee* value was determined by chiral HPLC.

Co^{II}-Catalyzed Cyclopropanation with Different Diazosulfones

Cyclopropanation reactions with varied diazosulfones catalyzed by Co(RuppelP5) were studied (Table 3). Reactions with phenylsulfonyldiazo reagents with different substituted groups at the 4-position (Me, MeO, and NO_2) gave the corresponding cyclopropanes in good to excellent yields. It was shown that reagents with the electron-withdrawing group (NO_2) gave a lower *ee* than those with electron-donating groups (MeO and Me). Increasing the steric hindrance of the diazo compounds resulted in a decrease in enantioselectivities. Therefore, in view of the combination of both yield and enantioselectivity, $TsCHN_2$ gave the most satisfactory results.

Table 3. Asymmetric cyclopropanation of styrene with diazosulfones catalyzed by Co(RuppelP5).[a]

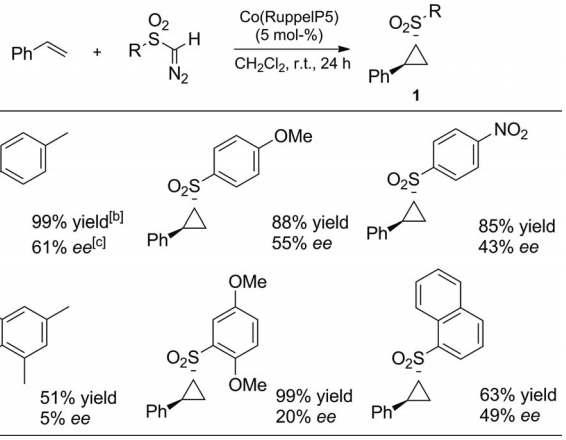

[a] Performed in CH_2Cl_2 at room temp. for 24 h with 5 mol-% [Co(Por)] under N_2 with 1.0 equiv. of styrene and 1.2 equiv. of diazo; [styrene] = 0.25 M. [b] Isolated yields of *trans* isomer. [c] The *ee* value was determined by chiral HPLC.

Rigidification of the Chiral Environment of the Ligand through Intramolecular Hydrogen Bonding

In difference to (*S*)-2,2-dimethylcyclopropanecarboxamido groups in Co(ChenP), catalysts Co(RuppelP) bearing oxygen atoms possess intramolecular O···H–N hydrogen bonding interactions, which are believed to provide more rigid chiral environments for better chiral induction of the reaction. The experimentally observed higher *ee* values for Co(RuppelP) systems relative to those with Co(ChenP) are consistent with this hypothesis. The aziridine-2-carboxamido group (GaoAmido) bearing a second chiral center on the side chain of the aziridine ring turned out to be an interesting chiral building block for the catalysts for several reasons. First, the aziridine unit possesses a rigid three-membered-ring structure. Second, it allows a potential intramolecular N···H–N hydrogen-bonding interaction. Together, these two attributes enable a more rigid bicyclic-ring-based system for chiral induction. Lastly, the extra chiral center might lead to enhanced chiral induction. Two catalysts of this type, Co(GaoP1)[6f] and Co(GaoP2),[6f] have been successfully synthesized and applied in catalytic cyclopropanation with tosyldiazomethane. Catalytic reactions with Co(GaoP1) and Co(GaoP2), however, gave the desired cyclopropane products in only moderate yields and with poor enantioselectivity. The observed results are presumably due to the large steric hindrance of the chirality-dense amido group despite the quite open nonchiral parts (Table 4).

For a more suitable chiral environment, a (*S*)-2-tetrahydrofurancarboxamido (ZhuAmido) group was introduced to construct Co(ZhuP)[6c] (Table 4). The combined incorporation of cyclic structures and intramolecular O···H–N hydrogen bonding interactions also ensured a highly rigid bicyclic-ring-based chiral environment. In contrast to Co(GaoP), more openness was provided by the ZhuAmido group. Given the fact that the 2,6-dimeth-

 © 2012 Wiley-VCH Verlag GmbH & Co. KGaA, Weinheim

Table 4. Asymmetric cyclopropanation of styrene with N_2CHTs catalyzed by Co(GaoP) and Co(ZhuP).[a]

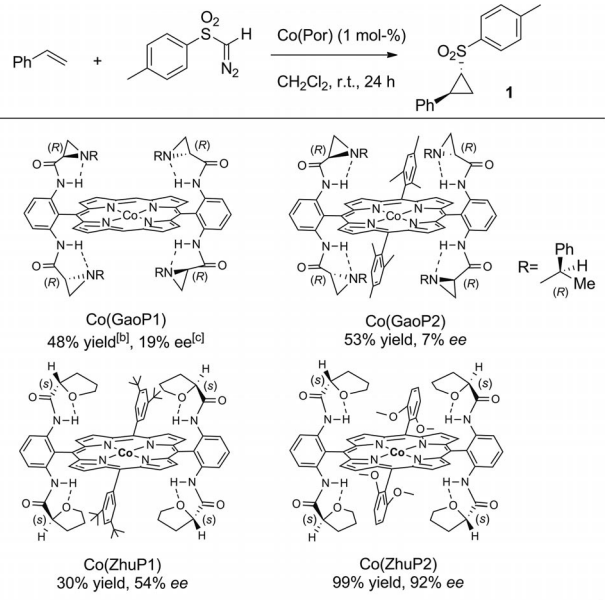

[a] Performed in CH_2Cl_2 at room temp. for 24 h with 1 mol-% [Co(Por)] under N_2 with 1.0 equiv. of styrene and 1.2 equiv. of N_2CHTs; [styrene] = 0.25 M. [b] Isolated yields of *trans* isomer. [c] The *ee* value was determined by chiral HPLC.

oxyphenyl group as the nonchiral part typically provided the highest *ee* value, Co(ZhuP2), which is Co(2,6-DiMeO-ZhuPhyrin), has been synthesized and proven to be a highly active catalyst for Co^{II}-catalyzed cyclopropanation with tosyldiazomethane, producing the desired product **1** in 99% yield and 92% *ee*.[6c] However, the Co(ZhuP1) group, with 3,5-di-*tert*-butylphenyl as the nonchiral part, gave only a poor yield (30%) and a moderate *ee* (54%). With Co(ZhuP2) as the catalyst, styrene could also be cyclopropanated by both 4-methoxybenzenesulfonyldiazomethane and 4-nitrobenzenesulfonyldiazomethane in excellent yields and enantioselectivities (Table 5).[6c]

Table 5. Asymmetric cyclopropanation of styrene with diazosulfones catalyzed by Co(ZhuP2).[a]

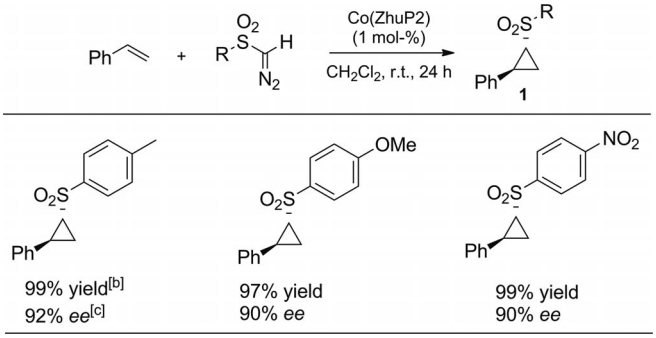

[a] Performed in CH_2Cl_2 at room temp. for 24 h with 1 mol-% [Co(Por)] under N_2 with 1.0 equiv. of styrene and 1.2 equiv. of diazosulfones; [styrene] = 0.25 M. [b] Isolated yields of *trans* isomer. [c] The *ee* value was determined by chiral HPLC.

Conclusions

Co^{II} complexes of D_2-symmetric chiral porphyrins have been demonstrated as efficient catalysts for asymmetric cyclopropanation with diazosulfones. Systematic studies of the ligand effect indicated that the structures of porphyrin ligands played an important role in controlling both reactivity and stereoselectivity of the reactions. Rigidification of the porphyrin ligand environment has been found to significantly enhance the asymmetric induction of the catalytic process. Co(2,6-DiMeO-ZhuPhyrin) has proved to be a general catalyst to enable the formation of enantiomerically enriched cyclopropyl sulfones from the reactions of a wide range of diazosulfones with alkenes. Despite the progress, asymmetric catalytic systems that are capable of more challenging substrates such as sterically hindered diazosulfones and acceptor/acceptor diazosulfones remain to be developed in future and would be attractive future directions because of the potential utilities of the corresponding products. In addition to further elucidating the ligand–reaction relationship for cyclopropanation with diazosulfones, our detailed studies of the ligand effect may provide guidance for the development of cyclopropanation reactions with varied diazosulfones and other stereoselective transformations.

Supporting Information (see footnote on the first page of this article): Details of instrumentation, general procedure for the cyclopropanation of styrene, and characterization data.

Acknowledgments

We are grateful for financial support by the National Science Foundation (CAREER Award: CHE-0711024).

[1] a) C. A. Carson, M. A. Kerr, *Chem. Soc. Rev.* **2009**, *38*, 3051–3060; b) A. Reichelt, S. F. Martin, *Acc. Chem. Res.* **2006**, *39*, 433–442; c) M. Yu, B. L. Pagenkopf, *Tetrahedron* **2005**, *61*, 321–347; d) H. U. Reissig, R. Zimmer, *Chem. Rev.* **2003**, *103*, 1151–1196; e) J. Pietruszka, *Chem. Rev.* **2003**, *103*, 1051–1070; f) L. A. Wessjohann, W. Brandt, T. Thiemann, *Chem. Rev.* **2003**, *103*, 1625–1647; g) W. A. Donaldson, *Tetrahedron* **2001**, *57*, 8589–8627; h) J. Salaun, *Chem. Rev.* **1989**, *89*, 1247–1270.

[2] a) H. Pellissier, *Tetrahedron* **2008**, *64*, 7041–7095; b) H. Lebel, J. F. Marcoux, C. Molinaro, A. B. Charette, *Chem. Rev.* **2003**, *103*, 977–1050; c) H. M. L. Davies, E. Antoulinakis, *Org. React.* **2001**, *57*, 1–326; d) M. P. Doyle, D. C. Forbes, *Chem. Rev.* **1998**, *98*, 911–935; e) A. Padwa, K. E. Krumpe, *Tetrahedron* **1992**, *48*, 5385–5453.

[3] a) H. Fritschi, U. Leutenegger, A. Pfaltz, *Angew. Chem.* **1986**, *98*, 1028; *Angew. Chem. Int. Ed. Engl.* **1986**, *25*, 1005–1006; b) D. A. Evans, K. A. Woerpel, M. M. Hinman, M. M. Faul, *J. Am. Chem. Soc.* **1991**, *113*, 726–728; c) M. M. C. Lo, G. C. Fu, *J. Am. Chem. Soc.* **1998**, *120*, 10270–10271.

[4] a) V. N. G. Lindsay, W. Lin, A. B. Charette, *J. Am. Chem. Soc.* **2009**, *131*, 16383–16385; b) D. Marcoux, S. Azzi, A. B. Charette, *J. Am. Chem. Soc.* **2009**, *131*, 6970–6972; c) D. Marcoux, A. B. Charette, *Angew. Chem.* **2008**, *120*, 10309; *Angew. Chem. Int. Ed.* **2008**, *47*, 10155–10158; d) J. R. Denton, K. Cheng, H. M. L. Davies, *Chem. Commun.* **2008**, 1238–1240; e) J. L. Maxwell, S. Omalley, K. C. Brown, T. Kodadek, *Organometallics* **1992**, *11*, 645–652; f) M. P. Doyle, W. R. Winchester, J. A. A. Hoorn, V. Lynch, S. H. Simonsen, R. Ghosh, *J. Am. Chem. Soc.* **1993**, *115*, 9968–9978; g) H. M. L. Davies, P. R.

 © 2012 Wiley-VCH Verlag GmbH & Co. KGaA, Weinheim

Bruzinski, D. H. Lake, N. Kong, M. J. Fall, *J. Am. Chem. Soc.* **1996**, *118*, 6897–6907.

[5] a) H. Nishiyama, Y. Itoh, H. Matsumoto, S. B. Park, K. Itoh, *J. Am. Chem. Soc.* **1994**, *116*, 2223–2224; b) C. M. Che, J. S. Huang, F. W. Lee, Y. Li, T. S. Lai, H. L. Kwong, P. F. Teng, W. S. Lee, W. C. Lo, S. M. Peng, Z. Y. Zhou, *J. Am. Chem. Soc.* **2001**, *123*, 4119–4129.

[6] a) S. F. Zhu, X. Xu, J. A. Perman, X. P. Zhang, *J. Am. Chem. Soc.* **2010**, *132*, 12796–12799; b) S. Fantauzzi, E. Gallo, E. Rose, N. Raoul, A. Caselli, S. Issa, F. Ragaini, S. Cenini, *Organometallics* **2008**, *27*, 6143–6151; c) S. F. Zhu, J. V. Ruppel, H. J. Lu, L. Wojtas, X. P. Zhang, *J. Am. Chem. Soc.* **2008**, *130*, 5042–5043; d) S. Zhu, J. A. Perman, X. P. Zhang, *Angew. Chem.* **2008**, *120*, 8588; *Angew. Chem. Int. Ed.* **2008**, *47*, 8460–8463; e) Y. Chen, J. V. Ruppel, X. P. Zhang, *J. Am. Chem. Soc.* **2007**, *129*, 12074–12075; f) Y. Chen, K. B. Fields, X. P. Zhang, *J. Am. Chem. Soc.* **2004**, *126*, 14718–14719.

[7] a) M. Honma, T. Sawada, Y. Fujisawa, M. Utsugi, H. Watanabe, A. Umino, T. Matsumura, T. Hagihara, M. Takano, M. Nakada, *J. Am. Chem. Soc.* **2003**, *125*, 2860–2861; b) T. Sawada, M. Nakada, *Adv. Synth. Catal.* **2005**, *347*, 1527–1532; c) H. Takeda, M. Nakada, *Tetrahedron: Asymmetry* **2006**, *17*, 2896–2906.

[8] For a Rh-based earlier attempt of intramolecular asymmetric cyclopropanation, see: M. Kennedy, M. A. McKervey, A. R. Maguire, G. H. P. Roos, *J. Chem. Soc., Chem. Commun.* **1990**, 361–362.

[9] For a Cu-catalyzed asymmetric intermolecular cyclopropanation with α-diazo-sulfonate esters, see: T. Ye, C. Y. Zhou, *New J. Chem.* **2005**, *29*, 1159–1163.

[10] For an Rh-catalyzed asymmetric cyclopropenation of acetylenes with tosyldiazomethane, see: R. A. Weatherhead-Kloster, E. J. Corey, *Org. Lett.* **2006**, *8*, 171–174.

[11] For select examples of other approaches for the syntheses and applications of optically active cyclopropyl sulfones, see: a) J. L. G. Ruano, S. A. A. de Diego, M. R. Martin, E. Torrente, A. M. M. Castro, *Org. Lett.* **2004**, *6*, 4945–4948; b) A. M. Bernard, A. Frongia, P. P. Piras, F. Secci, M. Spiga, *Org. Lett.* **2005**, *7*, 4565–4568; c) W. H. Midura, J. A. Krysiak, M. Cypryk, M. Mikolajczyk, M. W. Wieczorek, A. D. Filipczak, *Eur. J. Org. Chem.* **2005**, 653–662; d) I. Das, T. K. Pal, T. Pathak, *J. Org. Chem.* **2007**, *72*, 9181–9189.

[12] For an interesting synthesis of cyclopropyl sulfones by Rh-catalyzed intramolecular 1,3 C–H carbene insertion, see: W. F. Shi, B. Zhang, J. Zhang, B. G. Liu, S. W. Zhang, J. B. Wang, *Org. Lett.* **2005**, *7*, 3103–3106.

[13] M. P. Doyle, *Angew. Chem.* **2009**, *121*, 864; *Angew. Chem. Int. Ed.* **2009**, *48*, 850–852.

[14] For mechanistic studies on Co^{II} porphyrin-catalyzed cyclopropanation, see: a) W. I. Dzik, X. Xu, X. P. Zhang, J. N. H. Reek, B. de Bruin, *J. Am. Chem. Soc.* **2010**, *132*, 10891–10902; b) H. J. Lu, W. I. Dzik, X. Xu, L. Wojtas, B. de Bruin, X. P. Zhang, *J. Am. Chem. Soc.* **2011**, *133*, 8518–8521.

[15] a) X. Cui, X. Xu, H. J. Lu, S. F. Zhu, L. Wojtas, X. P. Zhang, *J. Am. Chem. Soc.* **2011**, *133*, 3304–3307; b) X. Xu, H. J. Lu, J. V. Ruppel, X. Cui, S. L. de Mesa, L. Wojtas, X. P. Zhang, *J. Am. Chem. Soc.* **2011**, *133*, 15292–15295.

Received: September 26, 2011
Published Online: December 23, 2011

 © 2012 Wiley-VCH Verlag GmbH & Co. KGaA, Weinheim

DOI: 10.1002/ejic.201100623

Systematics and Future Projections Concerning Redox-Noninnocent Amide/Imine Ligands

Kenneth G. Caulton*[a]

Keywords: Redox-noninnocent ligands / N ligands / Conjugation / Pincer ligands

An analysis of the conjugative possibilities of dienes carrying two terminal heteroatom donors shows some generalizations of these as possible redox-active (redox "noninnocent") ligands. If the two E=C functionalities (E = O,S, NR, CHR) are connected by an odd number of sp^2-hybridized atoms, full conjugation between the two terminal E donors is not possible, a situation which is found both in 2,6-bis(imino)pyridine (BIMPY) and beta-diketiminate ligands; the character of their redox noninnocence is thus altered, compared to 1,4-diheterodienes. Some insight into the BIMPY ligand comes from the analog where one imino arm is absent. The traditional stereochemical relationships which govern conjugation in arenes are analyzed for their implications for different bis(imino)pyridine isomers, and also for 2,6-dipyrimidyl- and dipyridazinyl-pyridines, as generalizations of the classic terpyridyl ligands. Factors which favor oxidized vs. reduced ligand forms are discussed.

Introduction

Coordination chemists have a tradition to work with *models* of reality, and one of these is that a complex ion can be divided into subunits which have a well-defined charge, hence the concept of metal ion separated from ligand. When this is *not* based on the objective well-defined structural characteristic of connectivity {e.g. the [$(Cp)_2M(\eta^n$-$C_4H_6)$] isomers, Scheme 1} but rather simply on charge, the concept can encounter challenges. In contrast to classical ligands like halides or water or ammonia, when the metal-free ligand has instead two or more distinctly different charge states, ligand composition alone does not identify its charge (i.e. redox) state. This led, already decades ago in the hands of Christian Klixbull Jorgensen,[1] to coining the term "noninnocent" for such ligands. For example, cyclic C_8H_8 might be cyclooctatetraene, or its dianion in $U(C_8H_8)_2$. In this article, we make some observations about redox-noninnocent ligands,[2–4] with special focus on multifunctional cases where that distinction is not immediately and unambiguously evident, and generally requires deeper experimental and computational examination on a case-by-case basis. Indeed the field has become so rich with noninnocent ligands that this is an essential time to try to organize, to categorize, to compare and contrast, and to seek some systematic and perhaps predictive principles. Relevant examples are not limited to very recent and unusual ligands. Indeed the classical N_2O_2 salen ligand (salicylaldehyde ethylenediimine) has been called[5] a "pro-radical" and its redox activity discussed. Other newly developed ones have also been reported,[6–8] although others involve net change at benzylic C atoms.[9,10] The methods developed for identification of the actual oxidation level of a ligand in a metal complex have been actively reviewed, and will not be repeated here.[11–13]

Scheme 1.

Care is required with regard to the use of the term "noninnocent," since some authors use it to refer to cases where bond making or breaking to a ligand, not redox change, is involved.[14–17]

[a] Department of Chemistry, Indiana University,
800 East Kirkwood Avenue, Bloomington, Indiana 47405, USA
Fax: +1-812-855-0985
E-mail: caulton@indiana.edu

Kenneth G. Caulton is professor of chemistry teaching at Indiana University, Bloomington Indiana, and researching in the areas of transition metal reactivity and homogeneous catalysis. Ligands of special interest include hydrides, nitrosyls, and carbenes, all with highly unsaturated complexes that yield rapid rates. His current work with redox-active ligands continues his interest in activation by photolysis and redox change, leading to radical complexes.

 © 2012 Wiley-VCH Verlag GmbH & Co. KGaA, Weinheim

Discussion

Redox-active ligands are often conjugated dienes, where the terminal atoms are heteroatoms capable of binding to metals; redox activity then derives from progressive addition of electrons to the diene LUMO. These ligands are often attached to *ortho*-phenylene moieties, hence catecholates, semiquinone, quinone, or monoiminoquinone, diimine, dithioquinones, etc. (Scheme 2) In short, they are diheterodienes where the carbon atoms at the diene 2 and 3 positions can bond together either by single or double bonds. It is the purpose of this comment to point out how traditional principles of conjugation apply to these, and thus to integrate a larger variety of ligands with regard to their redox noninnocence, and to make different species more systematically understandable. While all of this discussion will be illustrated using Lewis structures, a molecular orbital analysis would lead to the same conclusions. In what follows, we shall illustrate using two-electron changes, but the principles and conclusions apply equally well to the one-electron altered radical oxidation level also.

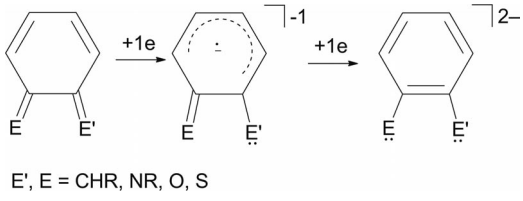

Scheme 2.

Of special interest are examples where two nitrogens are the coordinating donors (Scheme 3). These focus on imines in various states of separation by intervening sp^2 centers, but can also be involved in competing conjugated systems. As one generalizes the redox activity discussed here, it is useful to remember that E=O and NR, being the most electronegative examples, are easiest to achieve the fully reduced bis(amide) or enediolate state,[18] and we will illustrate principles and trends with these heterocenters, which can then be generalized. *ortho*-Iminopyridines (IMPY, Scheme 3) were originally sampled as ligands for olefin polymerization catalysis, without any recognition of their redox potential.[19,20] However, there has been growing recognition that certain of the examples in Scheme 3 can be redox-active,[21] and others probably await exploitation in this regard. For example, the *ortho*-iminopyridines have been shown to be richly redox-active.[11,12] The *ortho*-iminopyridyl ligand allows formation of unusual species like $M(L)_2^-$ where M is Co or Zn and also $Zn(L)_2^+$.

Iminopyridine ligands, IMPY, are also interesting for learning whether or not having one imino appended to an aromatic system makes reduction (where aromaticity is interrupted) more energetically costly. Monoiminopyridine ligands also serve as a useful comparison standard for the BIMPY ligands (Scheme 3), which look superficially like the result of simply *adding* a second imino functionality (see below); does "additivity" actually pertain then? Is BIMPY

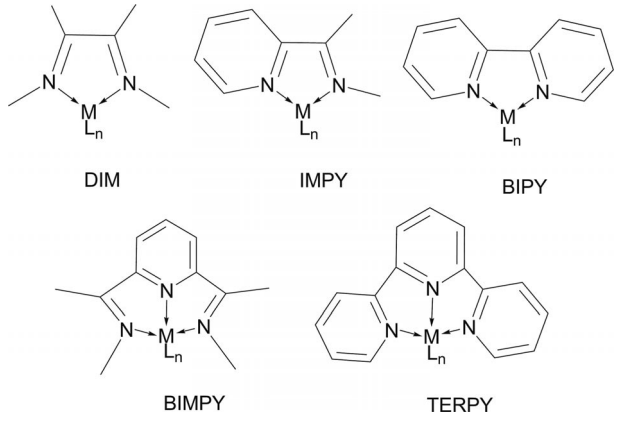

Scheme 3.

simply a more easily reduced *ortho*-iminopyridyl? Or is it the reverse?

The ability of the above bidentate ligands to support different oxidation levels relates to their conjugation and thus their LUMOs, beginning from the heterodiene oxidation level. While these three oxidation levels are often named by their arene equivalents (quinone, catecholate), the six membered ring is not essential to their noninnocence, and merely confers special stability to one oxidation level, the fully reduced form of the diene, where the six-membered ring is aromatic (Scheme 4). Making the diene part of a six-membered ring thus merely alters redox potentials, but makes no fundamental change.

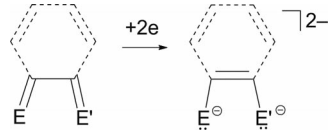

Scheme 4.

Another example of clever utilization of this idea is the positioning of two imino groups on an acenaphthalene framework[22] at left in Scheme 5. Here, this remains fundamentally a 1,4-diazadiene.

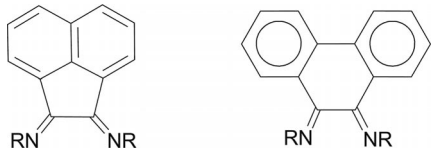

Scheme 5.

The diiminophenanthrene ligand[23] (at right in Scheme 5) is different from the diiminoacenaphthalene since the phenanthrene, with greater delocalization in the reduced state, favors the diamide state, while the acenaphthalene, because of its odd number of ring atoms, does not conjugate with the naphthalene subunit. The diiminoacenaphthalene thus has an isolated heterodiene, with less stabilization of the diamide state; its diheterodiene is thus less easily reduced.

 © 2012 Wiley-VCH Verlag GmbH & Co. KGaA, Weinheim

Evaluating these redox couples in terms of their redox level (i.e. the number of double bonds) is a very useful way to quickly establish whether a given species will *function* as an oxidant or a reductant. Moreover, the preferred metal oxidation state in a species $M(E/C/C/E)_2$ can *sometimes* be anticipated by asking if the metal can most readily be in oxidation state 0, or +2 or +4; which oxidation state is most consistent with the known chemistry of that metal? On the other hand, if the metal has a demonstrated special preference for oxidation state +1 or +3, then this ligand set can also accommodate that with *mixed* ligand redox levels M(diimine)(semiquinone) or M(semiquinone)(catecholate), respectively.

An application[24] of these ideas of metal dominating the redox preference of the ligand is $Cr_2(RNCHCHNR)_2$, which could contain Cr_2^0, Cr_2^{2+} or Cr_2^{4+}. Structural data (both short C/C and Cr/Cr distances) indicate that this contains enediamide, hence two Cr^{II}. The latter is apparently favored since the d^4 configuration at each divalent metal permits formation of a quadruple metal/metal bond. This assembly might be sketched (Scheme 6) as a naphthalene analog where the central atoms are linked by a quadruple bond.

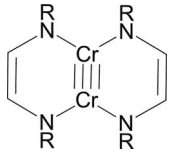

Scheme 6.

Another indication of the power of this reasoning is available simply for 1,2,4,5-tetrazine itself. Reaction of Cp_2Ti(alkyne), as a source of Ti^{II}, with $C_2N_4H_2$ gives the product Cp_2Ti(tetrazine) in which bond lengths within the $C_2N_4H_2$ ligand shows its reduction to the monoanion. The molecule is actually a tetramer, where the nitrogen *para* to that bonded to Ti^{III} donates to a second Ti^{III}, but with a Ti/N bond length longer by 0.10 Å. The C_2N_4 ring is boat shaped, consistent with the ring containing two remaining C=N bonds, like a 1,4-cyclohexadiene.[25]

The impact of this reasoning is also demonstrated by a recent study[26] of diazabutadiene complexes of monovalent Rh and Ir: [(DAB)M(CN*t*Bu)Cl]. These react with H_2 to give dihydrides, and with O_2 to give η^2 peroxide products, both containing M^{III}. While the authors discuss possible redox activity of their ligands, it is clear that, starting from the *diimine* oxidation level, one cannot oxidize the ligand further, so the site of oxidation can only be the metal. Redox activity at their ligand is only a possibility if reductive reagents are employed. For example, oxalate, $C_2O_4^{2-}$, might react to deliver two electrons and eliminate 2 CO_2, and then the reduction might not be purely at metal (yielding M^{-I}) but take diimine ligand towards enediamide.

The identification of the actual oxidation level based on experimental and computational methods has been thoroughly developed over the decades.[2,13] What happens if there are two such heterodiene moieties in a single ligand?

ortho-Bis(imino)pyridyl Ligands

The very popular bis iminopyridine ligand class BIMPY have been authoritatively identified as redox-active,[27–37] but some features have not been fully rationalized in comparison to the 1,4-heteroatom dienes. A two-electron reduced imine is an electron donating group, which can then conjugate with the other imine, which, being in a higher oxidation state, is an electron withdrawing group. These constitute a "push/pull" pair. While three different oxidation levels have been identified for the BIMPY ligand class, we wish to point out that these are *distinct* from the 1,4-diimines. If the singly and double reduced forms are sketched by Lewis structures, it is seen that each confers amide anion character to one (singly reduced) or two (dianions) nitrogens (Scheme 7, a), but these two nitrogens are never *both* (simultaneously) two pendant imine nitrogens, but always one pendant imine and also the pyridyl nitrogen. While this improves ligand nucleophilicity towards the metal, these never make a dianion where both anions are on the pendant nitrogens (Scheme 7, a).[38]

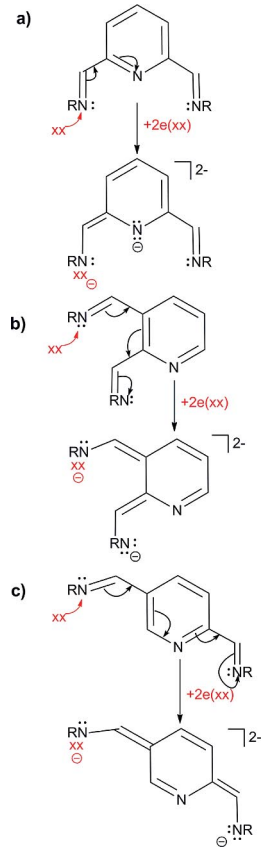

Scheme 7.

Thus, two 1,4-diazadienes "fused" at the central nitrogen as in BIMPY are not simultaneously conjugated, but only alternatively so. While *either* pendant nitrogen gains nucleophilicity, there is no viable resonance form where pyridyl nitrogen remains neutral and both pendant nitrogens become amides. Said otherwise, this can make either 1,4-diazadiene, contained within BIMPY, anionic, but never the 1,7

 © 2012 Wiley-VCH Verlag GmbH & Co. KGaA, Weinheim

N atoms both anionic. This is because conjugation relates heteroatoms separated by an *even* number of atoms, not only by four. This is evident by considering alternative BIMPY isomers (Scheme 7, b and c). BIMPY, the 2,6 isomer, has been analyzed above. Let us consider now the 2,3-diimino isomer. As shown in Scheme 7 (b), these conjugate compatibly. In the 2,5 isomer (Scheme 7, c) the same is true: all three oxidation levels are accessible at what is predicted to be reasonable energies, due to conjugative stabilization. In contrast, the 2,6 isomer BIMPY analyzed above is left in a diradical state (see below) if both pendant arms are made anionic, hence this form is distinctly destabilized. In the pyridyl analog (the pyridyl nitrogen plays no *crucial* role in this analysis of arene substituent conjugation, so isolobal replacement of this nitrogen by CH changes nothing in our argument), the underlying principle is that conjugation is possible between mutually *ortho* and *para* functionalities, but not between *meta* functionalities; in this case, however, it is the *meta* example that is most appealing for a pincer ligand application, but precisely this isomer *interferes* with inter-substituent conjugation. In other words, two *ortho* imines comprise a 1,6-diazahexatriene (Scheme 7, a) and two *para* imines comprise a 1,8-diazaoctatetraene (Scheme 7, b). *meta* Imines form an odd member chain, hence are not fully conjugated. Since terpyridyl is a generalization of BIMPY, it also suffers this limited degree of delocalization upon reduction, whereas 2,2′-bipyridyl (see below) is free of this problem.

The *ortho*/*para* vs. *meta* rule which applies to the BIMPY pincer can be immediately recognized as failing the conjugative principle since the number of sp^2 centers connecting the two imine functionalities in Scheme 7 (a) is either one (through the pyridyl nitrogen) or three (around the other direction of the pyridyl ring). The only bis-terminal amide resonance form has diradical character (Scheme 8, which is written alternatively,[37] with the radical centers at the two pendant C atoms).

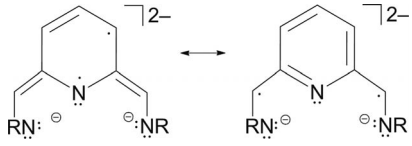

Scheme 8.

Beta-Diketiminate Ligands

How can we generalize these *ortho*/*para* vs. *meta* observations to other diimine ligands? Conjugation is possible when there is an *even* number of sp^2-hybridized atoms linking the two imine functionalities. One case that violates this is the beta diketiminate ligand class, commonly called nacnac ligands.[39] Here the two imine HC=NR functionalities are linked by only one sp^2 carbon, and thus these do not both conjugate in their doubly reduced form. The present analysis of resonance contributors (Scheme 9), drawn initially to show the presence of two imine functionalities, shows that **A** is inferior due to accumulated negative charge at the less electronegative (carbon) atom, and **B** is better. Two-electron reduction yields **C**, where both electronegative atoms have become anionic, but finally a carbanion cannot be avoided. The lack of conjugation when the heteroatoms are positioned 1,5 inhibits resonance delocalization, and is predicted to make beta-diketiminates *poorer* than 1,4-diheterodienes as electron storage sites. Not impossible, but merely inferior!

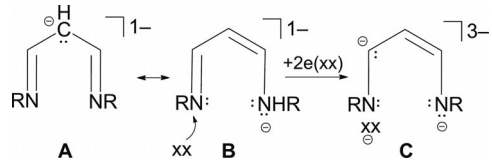

Scheme 9.

Beta-diketiminates have been analyzed[40] in the context of redox activity, with the result that the term "hidden noninnocence" is proposed, due to the bond *length* changes not significantly reflecting their oxidation level. For beta-diketiminates (**B**), the LUMO is nonbonding between any two *adjacent* ligand atoms, so that population of this orbital (i.e. reduction of the ligand) will not significantly change bond lengths; this ligand type "hides" its noninnocence.[40] The nodal pattern of nacnac is the origin of this difference.

One can test this assertion in the following interesting context. {(HC(CMeNAr)$_2$}Al has been synthesized and described[41] as a remarkable example of monovalent aluminum. If we assert that this is in fact the trianionic redox isomer of the beta diketiminate ligand, then the comparison in Scheme 9 shows that the biggest difference as the chelate goes from –1 to –3 charge is at the ring C/N bonds, which decrease from bond order 1.5 to 1.0. In fact, while the measured C/N distance in {(HC(CMeNAr)$_2$}Al, 1.341(3) Å, is longer than a large number of authentic (Nacnac)AlX$_2$ structures, the bond lengthening is only about 0.01 Å, hence only about 2 esd's, and *not* persuasive of the assertion that the two coordinate aluminum species has charge distribution {(HC(CMeNAr)$_2^{3-}$}Al^{III}.

It is useful to recognize that dipyrromethenes[42,43] (Scheme 10) are redox-active examples of beta diketiminates, and of course porphyrins are merely more expansively delocalized examples of dipyrromethenes. The breadth of application of this analysis is thus considerable.

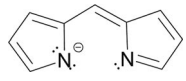

Scheme 10.

Additional Observations on 1,4-Diazadienes

For ligand applications, the 1,4-positioning of donor functionalities seems most appropriate, and thus it is diheterobutadiene positioning that is most suitable for eliciting redox-active noninnocence (i.e. thermodynamic ease of

 © 2012 Wiley-VCH Verlag GmbH & Co. KGaA, Weinheim

reduction). Once many such examples are recognized as having this common feature, the difference between them will be more one of quantitative redox potential and less a confusing collection of apparently unrelated ligands. Hopefully, this recognition will help to systemize a broad variety of noninnocent ligands, even when they represent fused examples of 1,4-diheteroatom cases. Relevant examples are shown in Scheme 3, and can even be generalized to azoles, etc. Viewed in this way, the ubiquitous 2,2′-bipyridyl ligand[44–46] may be visualized (Scheme 11), upon reduction, very analogously, as another 1,4-diazadiene. Redox noninnocence is evident in remarkable molecules[47–49] like $Si(bipy)_2Cl_2$ and $Ru(bipy)_3^0$, as well as recent uranium containing examples. Incorporation of nitrogen into an arene (e.g. bipy) stabilizes the oxidized (imine) redox levels by their aromaticity, but such incorporation is not *essential* to the redox noninnocence. Note that this selective stabilization of the higher (imine) oxidation level is opposite to that when the redox-active substituents are *appended* to a single arene ring (cf. the diiminophenanthrene of Scheme 5). Such recognition of these opposite effects of ancillary moieties allows rational tuning of redox performance for targeted goals.

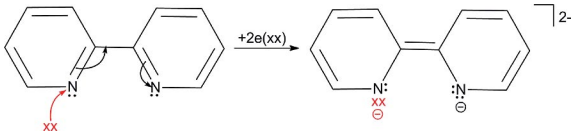

Scheme 11.

This thinking also makes it clear, when a ligand like BIMPY is reacted with a zerovalent metal source, that oxidation of the metal by the ligand is a viable outcome, not to be viewed with surprise. This is especially true with BIMPY, since it contains not two, but three imine oxidizing functionalities. Note that many of the earliest synthetic forays with quinones[2] used binary metal carbonyls, $M_n(CO)_p$, as the metal source, hence oxidation of the metal is a very natural result. For this reason, Ni(cyclooctadiene)$_2$ and Ru(cyclooctatriene)(cyclooctadiene) are similarly attractive synthetic reagents.

When changing the redox state of a ligand between diamide and heterodiene involves changing the *hybridization* of some constituent backbone atoms, redox change demands full removal of substituents (bond disruption). For example, this is the case when ethylene diamide is oxidized to diazadiene (Scheme 12). This contrasts to when the backbone atom is already sp^2-hybridized in the reduced ligand form (Scheme 4), where no such substituent removal is required. In the former case, proton-coupled electron transfer can be the mechanism (facilitated by the Brønsted acidity of the oxidized C–H species), but even if this has a relatively

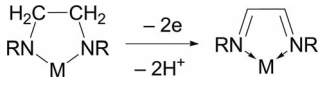

Scheme 12.

low barrier, it involves bond breaking that slows the process *compared to* the simple flow of only electrons which happens in the ene diamide case. The simple electron flow does not require that the ligand backbone be part of an aromatic ring, but this may be facilitated, both kinetically and thermodynamically, if it is.

Anticipating Incompatible Ligand and Reactivity Conditions

Certain ideas here are elementary but effective. Simply calling imines "oxidized" helps anticipate a reactive environment where the ligand will be vulnerable to degradation. For example, recognition of this oxidation level characterization makes it immediately clear that BIMPY ligands are a poor choice for use under nucleophilic (e.g. carbanion) environments, since the imine oxidation level is analogous to the ketone oxidation level in being subject to nucleophilic attack (Scheme 13); this leads to the demise of a number of olefin polymerization catalysis efforts.[50]

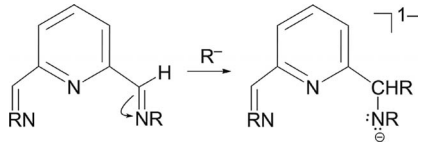

Scheme 13.

Because the principles discussed here apply also to the widely used pybox (Scheme 14), that ligand class (a BIMPY analog) must be recognized for its potential noninnocence. Moreover, by its imine oxidation level, it is suitable for oxidizing and electrophilic reaction conditions, but is not for electron rich, reducing or nucleophilic situations.[51]

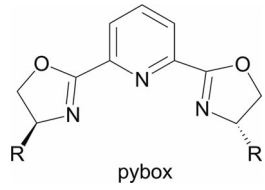

Scheme 14.

Many of the topics raised here involve merely the basic principles of orbital conjugation, but their application to polyimine ligands and their analogs (Scheme 2, various E) is informative. For example, the dihydride complex of a diimine may be vulnerable to isomerization to the redox alternative shown in Scheme 15.

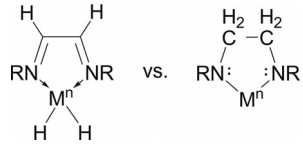

Scheme 15.

 © 2012 Wiley-VCH Verlag GmbH & Co. KGaA, Weinheim

Other Ligands: Into the Future

The above ideas guide recognition of other opportunities for noninnocent ligand development. Already very productive is the previously discussed (Scheme 5) 1,2-bis(imino)acenaphthalene ligand, a straightforward case of a 1,4-diazadiene, but with the assistance of an aromatic moiety fused to the 2,3-diene positions. If larger ring sizes are envisioned for metal/ligand complexes, then 1,6-diazatrienes as well as a 1,8-diazatetraene of various architectures can be sketched (Scheme 16).

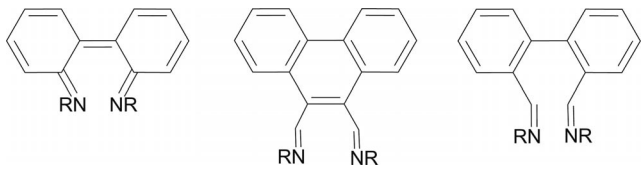

Scheme 16.

Increased Ligand Nitrogen Content

Isolobal substitution of *further* CH by N in terpy illustrates several points.[52–57] In the bis pyrimidyl example shown in Scheme 17, drawn, before reduction, to resemble BIMPY, there are again the same alternative locations of the anionic nitrogens as for BIMPY, but also the one where the "outside" nitrogen N^b can carry the anionic charge (not productive when it functions as a tridentate ligand); *both* N^a and N^b bear a 1,4 relationship with the pyridyl nitrogen, hence conjugate with it. In contrast (Scheme 18), when the pendant arms carry two nitrogens in adjacent positions (pyridazine), there is no significant difference from BIMPY itself, since only N^a can share the negative charge with the pyridyl nitrogen. N^b cannot be in conjugation with the pyridyl nitrogen since they bear a 1,5 relationship. Notice that all of these in Scheme 17 have the two N atoms separated by an even number of sp^2 atoms, and all but one of these is a 1,4-diazadiene.

Although these polynitrogen ligands are anticipated to be increasingly readily reduced, even terpyridyl has been demonstrated several times to be subject to reduction, in molecules like (terpy)Ni(CH_3)[58] and (terpy)PtCl.[59]

Consideration of elementary principles from heterocyclic chemistry helps understand some trends in susceptibility to two-electron reduction of these diimines (Scheme 19). For example, two-electron reduction of pyridine puts anionic charge at the *ortho* and *para* sites, which means that $(CH)_4N_2$ isomers will be most easily reduced if the N atoms

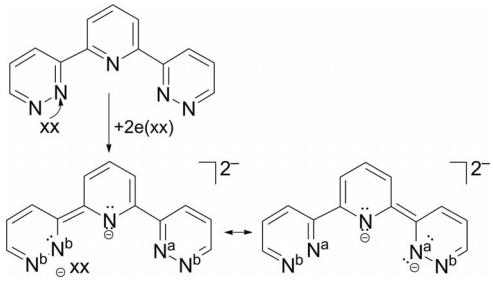

Scheme 18.

are in positions 1,2 (pyridazines) or 1,4 (pyrazines), where the formal negative charge can be carried by the more electronegative nitrogen.

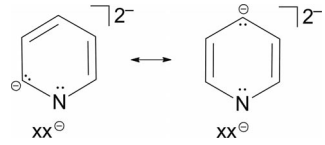

Scheme 19.

The ready reduction of nitrogen-rich arenes leads to the suggestion that perhaps the Creutz–Taube ion (pyrazine)$[Ru(NH_3)_5]_2^{5+}$ might contain some contribution of the electronic state with two Ru^{III} and one pyrazine radical anion, in addition to the normally assumed neutral pyrazine and Ru_2^{5+} pair.

If we generalize to two fused rings, resonance forms for quinoline dianion show (Scheme 20) that a second nitrogen at locations 2 or 4 or 5 or 7 will best accommodate the negative charge in the dianion. Thus, the 1,8-naphthyridine ligand (Scheme 21), which is good for bridging two metals

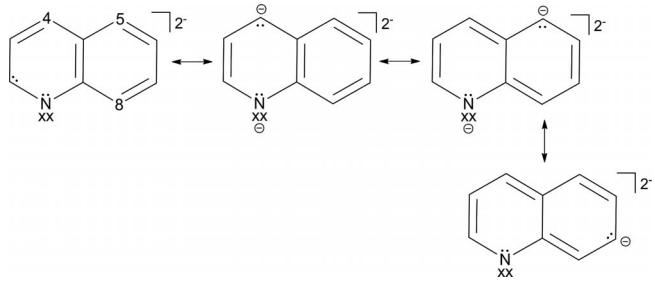

Scheme 20.

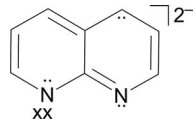

Scheme 21.

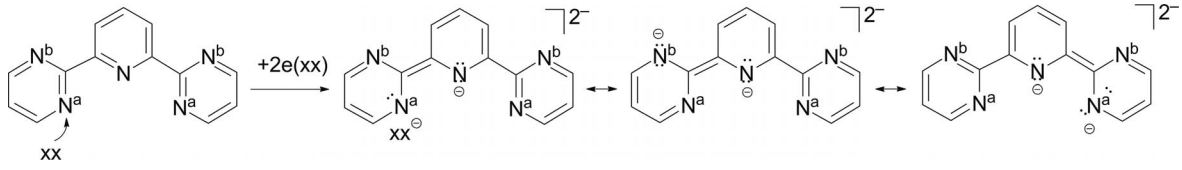

Scheme 17.

 © 2012 Wiley-VCH Verlag GmbH & Co. KGaA, Weinheim

as a neutral, is not as readily susceptible for two-electron reduction as the other $C_8H_6N_2$ isomers. These ideas therefore assist in choosing bridging ligands which have enhanced capacity to store electrons.

Likewise unsuitable for two-electron reduction (Scheme 22) are the very popular amidinates, $XC(NR)_2^{-1}$, including guanidinates (X = NR_2), since there is only one sp^2 center separating the two NR functionalities.[60] Reduction of these by two electrons demands carbanion character in the resulting trianion, hence is energetically unfavorable. The DBU-derived bicyclic guanidinate ligand (Scheme 23, monoanionic), while it is strongly electron-donating to an attached metal, is likewise not a ready subject for being additionally reduced, and thus not redox-active.[61]

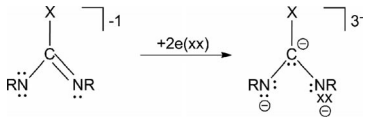

Scheme 22.

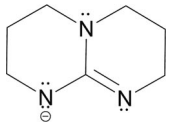

Scheme 23.

Conclusions

Hopefully the systematics, the warnings and the generalizations discussed here will stimulate others to develop new ligand types, and to avoid utilization of "suicidal" combinations of ligands with hostile reactive environments, and thus to advance both fundamental and applied directions for this field of redox noninnocent ligands.

Broadened examples of redox-active ligands are being envisioned[62–64] where a redox-active moiety is attached remotely to a ligand, with the expectation that intramolecular electron transfer can still be facile over 6–8 Å.[65,66] Another long recognized and extremely simple moiety with multiple redox states is MCCM (dianion, acetylide, or tetraanion, ethylene tetraide). Likewise, as bridging N_2 is increasingly explored,[67] the unit MNNM can have N_2 not only neutral, but also –1, –2, –3 and –4 charges.

Since multiple states characterize redox-active groups, future applications in magnetism (bistable switching) can be envisioned,[68] as can applications as ATRP catalysts, where redox potentials are of central importance.

Crabtree has pointed out[69] an increasing number of clever examples where addition of an electrophile to a nucleophilic ligand atom remote from the metal creates a new metal complex with greatly altered reactivity. In the cases at hand (Schemes 17 and 18), such electrophilic derivatization at remote N^b will make the ligand much more easily reducible. This is an idea that deserves to be exploited. Recall that quaternization of a nitrogen converts 4,4′-bipyridine into a good oxidizing agent: paraquat (Scheme 24).

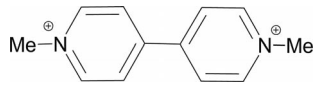

Scheme 24.

For alternative electronic structures like M^{n+}(semiquinone)$_2$ or M^{n+1}(semiquinone)(catecholate), the ideas presented here cannot discriminate open shell triplet from singlet ground states, but can alert us to where such alternatives demand consideration. Relative energies of these electron distribution and spin alternatives are currently best done by computational methods.[70,71]

The recent appearance of a phosphorus analog of BIMPY suggests that new developments with this $C_5NH_3(CH{=}PAr)_2$ analog will appear.[72] Heterodienes incorporating two phosphorus (instead of nitrogen) show electrochemical reduction potentials *less* negative than those of their nitrogen analogs: bipy vs. the P analogs.[73] Since this is not what is predicted by electronegativity, it must be that the poorer C/P overlap leaves the LUMO of the C/P neutral at a lower energy.[74] While this is discussed, in these references, in terms of back donation, that term is synonymous with redox transfer between metal and ligand. It thus appears that the ideas discussed here will continue to have some utility, as new diheterodiene ligands are developed.

There is a recent increase of recognition that it is possible to establish radical character, and also radical reactivity, at carbene ligands, so this ligand can join other radical ligands like NO for enhancing reactivity beyond simply bond making/breaking at the *metal*.[75–79]

Utilization of redox noninnocence for reactivity purposes currently occupies many researchers.[80–95] One fundamental question is does the location of spin density within a molecule influence its bond making/breaking chemical reactivity?

Acknowledgments

This work was supported in part by the U.S. National Science Foundation (NSF). The author's research group members are also thanked for input during the organization of the ideas presented here.

Dedicated to Wolfgang Kaim and Karl Wieghardt, who have unearthed such a multitude of redox-active ligands, and unconventional electronic states, that this effort to categorize becomes necessary.

[1] C. K. Jorgensen, *Oxidation Numbers and Oxidation States*, Springer Publishing, New York, **1969**.
[2] C. G. Pierpont, C. W. Lange, *Prog. Inorg. Chem.* **1994**, *41*, 331–442.
[3] D. N. Hendrickson, C. G. Pierpont, *Top. Curr. Chem.* **2004**, *234*, 63–95.

 © 2012 Wiley-VCH Verlag GmbH & Co. KGaA, Weinheim

[4] C. G. Pierpont, R. M. Buchanan, *Coord. Chem. Rev.* **1981**, *38*, 45–87.
[5] O. Rotthaus, O. Jarjayes, F. Thomas, C. Philouze, C. P. Del Valle, E. Saint-Aman, J.-L. Pierre, *Chem. Eur. J.* **2006**, *12*, 2293–2302.
[6] D. Adhikari, S. Mossin, F. Basuli, J. C. Huffman, R. K. Szilagyi, K. Meyer, D. J. Mindiola, *J. Am. Chem. Soc.* **2008**, *130*, 3676–3682.
[7] J. I. van der Vlugt, E. A. Pidko, D. Vogt, M. Lutz, A. L. Spek, *Inorg. Chem.* **2009**, *48*, 7513–7515.
[8] T. Buettner, J. Geier, G. Frison, J. Harmer, C. Calle, A. Schweiger, H. Schoenberg, H. Gruetzmacher, *Science* **2005**, *307*, 235–238.
[9] A. T. Radosevich, J. G. Melnick, S. A. Stoian, D. Bacciu, C.-H. Chen, B. M. Foxman, O. V. Ozerov, D. G. Nocera, *Inorg. Chem.* **2009**, *48*, 9214–9221.
[10] J. I. van der Vlugt, J. N. H. Reek, *Angew. Chem. Int. Ed.* **2009**, *48*, 8832–8846.
[11] C. C. Lu, T. Weyhermuller, E. Bill, K. Wieghardt, *Inorg. Chem.* **2009**, *48*, 6055–6064.
[12] M. van Gastel, C. Lu Connie, K. Wieghardt, W. Lubitz, *Inorg. Chem.* **2009**, *48*, 2626–2632.
[13] K. Ray, T. Petrenko, K. Wieghardt, F. Neese, *Dalton Trans.* **2007**, 1552–1566.
[14] G. S. Day, B. Pan, D. L. Kellenberger, B. M. Foxman, C. M. Thomas, *Chem. Commun.* **2011**, *47*, 3634–3636.
[15] D. Aguilar, F. Aznarez, R. Bielsa, L. R. Falvello, R. Navarro, E. P. Urriolabeitia, *Organometallics* **2007**, *26*, 6397–6402.
[16] M. Said, M. Thornton-Pett, D. L. Hughes, M. Bochmann, *Inorg. Chim. Acta* **2007**, *360*, 1354–1363.
[17] T. Steinke, B. K. Shaw, H. Jong, B. O. Patrick, M. D. Fryzuk, J. C. Green, *J. Am. Chem. Soc.* **2009**, *131*, 10461–10466.
[18] G. H. Spikes, C. Milsmann, E. Bill, T. Weyhermuller, K. Wieghardt, *Inorg. Chem.* **2008**, *47*, 11745–11754.
[19] D. Reardon, F. Conan, S. Gambarotta, G. Yap, Q. Wang, *J. Am. Chem. Soc.* **1999**, *121*, 9318–9325.
[20] V. C. Gibson, S. K. Spitzmesser, *Chem. Rev.* **2003**, *103*, 283–315.
[21] H. Sugiyama, G. Aharonian, S. Gambarotta, G. P. A. Yap, P. H. M. Budzelaar, *J. Am. Chem. Soc.* **2002**, *124*, 12268–12274.
[22] I. L. Fedushkin, V. M. Makarov, V. G. Sokolov, G. K. Fukin, *Dalton Trans.* **2009**, 8047–8053.
[23] D. W. Shaffer, S. A. Ryken, R. A. Zarkesh, A. F. Heyduk, *Inorg. Chem.* **2011**, *50*, 13–21.
[24] K. A. Kreisel, G. P. A. Yap, O. Dmitrenko, C. R. Landis, K. H. Theopold, *J. Am. Chem. Soc.* **2007**, *129*, 14162–14163.
[25] S. Kraft, E. Hanuschek, R. Beckhaus, D. Haase, W. Saak, *Chem. Eur. J.* **2005**, *11*, 969–978.
[26] A. Penner, T. Braun, *Eur. J. Inorg. Chem.* **2011**, 2579–2587.
[27] S. C. Bart, K. Chlopek, E. Bill, M. W. Bouwkamp, E. Lobkovsky, F. Neese, K. Wieghardt, P. J. Chirik, *J. Am. Chem. Soc.* **2006**, *128*, 13901–13912.
[28] D. Zhu, I. Thapa, I. Korobkov, S. Gambarotta, P. H. M. Budzelaar, *Inorg. Chem.* **2011**, *50*, 9879–9887.
[29] D. Zhu, P. H. M. Budzelaar, *Organometallics* **2008**, *27*, 2699–2705.
[30] J. Scott, I. Vidyaratne, I. Korobkov, S. Gambarotta, P. H. M. Budzelaar, *Inorg. Chem.* **2008**, *47*, 896–911.
[31] I. Vidyaratne, J. Scott, S. Gambarotta, P. H. M. Budzelaar, *Inorg. Chem.* **2007**, *46*, 7040–7049.
[32] Q. Knijnenburg, S. Gambarotta, P. H. M. Budzelaar, *Dalton Trans.* **2006**, 5442–5448.
[33] J. Scott, S. Gambarotta, I. Korobkov, Q. Knijnenburg, B. de Bruin, P. H. M. Budzelaar, *J. Am. Chem. Soc.* **2005**, *127*, 17204–17206.
[34] T. M. Kooistra, D. G. H. Hetterscheid, E. Schwartz, Q. Knijnenburg, P. H. M. Budzelaar, A. W. Gal, *Inorg. Chim. Acta* **2004**, *357*, 2945–2952.
[35] Q. Knijnenburg, D. Hetterscheid, T. M. Kooistra, P. H. M. Budzelaar, *Eur. J. Inorg. Chem.* **2004**, 1204–1211.
[36] L. E. N. Allan, E. D. Cross, T. W. Francis-Pranger, M. E. Hanhan, M. R. Jones, J. K. Pearson, M. R. Perry, T. Storr, M. P. Shaver, *Macromolecules* **2011**, *44*, 4072–4081.
[37] P. J. Chirik, K. Wieghardt, *Science* **2010**, *327*, 794–795.
[38] Reduction is the redox direction of interest here since the structure of BIMPY starts the discussion from the imine oxidation level. Because the N atoms are at their highest oxidation level, imine, they can only be reduced.
[39] L. Bourget-Merle, M. F. Lappert, J. R. Severn, *Chem. Rev.* **2002**, *102*, 3031–3066.
[40] M. M. Khusniyarov, E. Bill, T. Weyhermueller, E. Bothe, K. Wieghardt, *Angew. Chem. Int. Ed.* **2011**, *50*, 1652–1655, S1652/1651-S1652/1610.
[41] C. Cui, H. W. Roesky, H.-G. Schmidt, M. Noltemeyer, H. Hao, F. Cimpoesu, *Angew. Chem.* **2000**, *112*, 4444; *Angew. Chem. Int. Ed.* **2000**, *39*, 4274–4276.
[42] E. R. King, T. A. Betley, *Inorg. Chem.* **2009**, *48*, 2361–2363.
[43] S. M. Cohen, S. R. Halper, *Inorg. Chim. Acta* **2002**, *341*, 12–16.
[44] S. J. Kraft, P. E. Fanwick, S. C. Bart, *Inorg. Chem.* **2010**, *49*, 1103–1110.
[45] C. H. Booth, D. Kazhdan, E. L. Werkema, M. D. Walter, W. W. Lukens, E. D. Bauer, Y.-J. Hu, L. Maron, O. Eisenstein, M. Head-Gordon, R. A. Andersen, *J. Am. Chem. Soc.* **2010**, *132*, 17537–17549.
[46] M. Schultz, J. M. Boncella, D. J. Berg, T. D. Tilley, R. A. Andersen, *Organometallics* **2002**, *21*, 460–472.
[47] S. Pyo, E. Perez-Cordero, S. G. Bott, L. Echegoyen, *Inorg. Chem.* **1999**, *38*, 3337–3343.
[48] E. E. Perez-Cordero, C. Campana, L. Echegoyen, *Angew. Chem.* **1997**, *109*, 85; *Angew. Chem. Int. Ed. Engl.* **1997**, *36*, 137–140.
[49] P. M. Broudy, A. D. Berry, B. B. Wayland, A. G. MacDiarmid, *J. Am. Chem. Soc.* **1972**, *94*, 7577–7579.
[50] J. Scott, S. Gambarotta, I. Korobkov, P. H. M. Budzelaar, *J. Am. Chem. Soc.* **2005**, *127*, 13019–13029.
[51] A. B. Kazi, G. D. Jones, D. A. Vicic, *Organometallics* **2005**, *24*, 6051–6054.
[52] R. Huebner, S. Weber, S. Strobel, B. Sarkar, S. Zalis, W. Kaim, *Organometallics* **2011**, *30*, 1414–1418.
[53] W. Kaim, B. Schwederski, *Coord. Chem. Rev.* **2010**, *254*, 1580–1588.
[54] W. Kaim, G. K. Lahiri, *Angew. Chem.* **2007**, *119*, 1808; *Angew. Chem. Int. Ed.* **2007**, *46*, 1778–1796.
[55] W. Kaim, B. Sarkar, *Coord. Chem. Rev.* **2007**, *251*, 484–594.
[56] W. Kaim, *Coord. Chem. Rev.* **2002**, *230*, 127–139.
[57] W. Kaim, A. Klein, M. Gloeckle, *Acc. Chem. Res.* **2000**, *33*, 755–763.
[58] G. D. Jones, J. L. Martin, C. McFarland, O. R. Allen, R. E. Hall, A. D. Haley, R. J. Brandon, T. Kanovalova, P. J. Desrochers, P. Pulay, D. A. Vicic, *J. Am. Chem. Soc.* **2006**, *128*, 13175–13183.
[59] M. G. Hill, J. A. Bailey, V. M. Miskowski, H. B. Gray, *Inorg. Chem.* **1996**, *35*, 4585–4590.
[60] P. P. Fontaine, B. L. Yonke, P. Y. Zavalij, L. R. Sita, *J. Am. Chem. Soc.* **2010**, *132*, 12273–12285.
[61] F. A. Cotton, J. C. Durivage, N. E. Gruhn, D. L. Lichtenberger, C. A. Murillo, L. O. Van Dorn, C. C. Wilkinson, *J. Phys. Chem. B* **2006**, *110*, 19793–19798.
[62] W. Kaim, B. Schwederski, *Pure Appl. Chem.* **2004**, *76*, 351–364.
[63] W. Kaim, M. Moscherosch, *Coord. Chem. Rev.* **1994**, *129*, 157–193.
[64] W. Kaim, *Coord. Chem. Rev.* **1987**, *76*, 187–235.
[65] L. T. Dulatas, S. N. Brown, E. Ojomo, B. C. Noll, M. J. Cavo, P. B. Holt, M. M. Wopperer, *Inorg. Chem.* **2009**, *48*, 10789–10799.
[66] D. Lionetti, A. J. Medvecz, V. Ugrinova, M. Quiroz-Guzman, B. C. Noll, S. N. Brown, *Inorg. Chem.* **2010**, *49*, 4687–4697.
[67] M. Fang, D. S. Lee, J. W. Ziller, R. J. Doedens, J. E. Bates, F. Furche, W. J. Evans, *J. Am. Chem. Soc.* **2011**, *133*, 3784–3787.

 © 2012 Wiley-VCH Verlag GmbH & Co. KGaA, Weinheim

[68] S. Wanniarachchi, B. J. Liddle, J. Toussaint, S. V. Lindeman, B. Bennett, J. R. Gardinier, *Dalton Trans.* **2010**, *39*, 3167–3169.
[69] R. H. Crabtree, *New J. Chem.* **2011**, *35*, 18–23.
[70] N. Guihery, V. Robert, F. Neese, *J. Phys. Chem. A* **2008**, *112*, 12975–12979.
[71] M. M. Conradie, J. Conradie, A. Ghosh, *J. Inorg. Biochem.* **2006**, *100*, 620–626.
[72] Y. Nakajima, Y. Nakao, S. Sakaki, Y. Tamada, T. Ono, F. Ozawa, *J. Am. Chem. Soc.* **2010**, *132*, 9934–9936.
[73] P. Le Floch, *Coord. Chem. Rev.* **2006**, *250*, 627–681.
[74] A. Hayashi, M. Okazaki, F. Ozawa, R. Tanaka, *Organometallics* **2007**, *26*, 5246–5249.
[75] W. I. Dzik, J. I. van der Vlugt, J. N. H. Reek, B. de Bruin, *Angew. Chem. Int. Ed.* **2011**, *50*, 3356–3358.
[76] W. I. Dzik, X. Xu, X. P. Zhang, J. N. H. Reek, B. de Bruin, *J. Am. Chem. Soc.* **2010**, *132*, 10891–10902.
[77] F. F. Puschmann, H. Grutzmacher, B. de Bruin, *J. Am. Chem. Soc.* **2010**, *132*, 73–75.
[78] W. I. Dzik, X. P. Zhang, B. de Bruin, *Inorg. Chem.* **2011**, *50*, 9896–9903.
[79] G. K. Lahiri, W. Kaim, *Dalton Trans.* **2010**, *39*, 4471–4478.
[80] C. J. Rolle III, K. I. Hardcastle, J. D. Soper, *Inorg. Chem.* **2008**, *47*, 1892–1894.
[81] A. L. Smith, L. A. Clapp, K. I. Hardcastle, J. D. Soper, *Polyhedron* **2010**, *29*, 164–169.
[82] C. A. Lippert, J. D. Soper, *Inorg. Chem.* **2010**, *49*, 3682–3684.
[83] C. A. Grapperhaus, K. Ouch, M. S. Mashuta, *J. Am. Chem. Soc.* **2009**, *131*, 64–65.
[84] K. J. Blackmore, M. B. Sly, M. R. Haneline, J. W. Ziller, A. F. Heyduk, *Inorg. Chem.* **2008**, *47*, 10522–10532.
[85] R. A. Zarkesh, J. W. Ziller, A. F. Heyduk, *Angew. Chem.* **2008**, *120*, 4793; *Angew. Chem. Int. Ed.* **2008**, *47*, 4715–4718.
[86] N. A. Ketterer, H. Fan, K. J. Blackmore, X. Yang, J. W. Ziller, M.-H. Baik, A. F. Heyduk, *J. Am. Chem. Soc.* **2008**, *130*, 4364–4374.
[87] A. L. Smith, K. I. Hardcastle, J. D. Soper, *J. Am. Chem. Soc.* **2010**, *132*, 14358–14360.
[88] K. J. Blackmore, J. W. Ziller, A. F. Heyduk, *Inorg. Chem.* **2005**, *44*, 5559–5561.
[89] J. T. Muckerman, D. E. Polyansky, T. Wada, K. Tanaka, E. Fujita, *Inorg. Chem.* **2008**, *47*, 1787–1802.
[90] C. Mukherjee, T. Weyhermueller, E. Bothe, P. Chaudhuri, *Inorg. Chem.* **2008**, *47*, 2740–2746.
[91] R. Celenligil-Cetin, P. Paraskevopoulou, R. Dinda, R. J. Staples, E. Sinn, N. P. Rath, P. Stavropoulos, *Inorg. Chem.* **2008**, *47*, 1165–1172.
[92] C. Mukherjee, T. Weyhermueller, E. Bothe, E. Rentschler, P. Chaudhuri, *Inorg. Chem.* **2007**, *46*, 9895–9905.
[93] J. L. Boyer, J. Rochford, M.-K. Tsai, J. T. Muckerman, E. Fujita, *Coord. Chem. Rev.* **2010**, *254*, 309–330.
[94] C. Stanciu, M. E. Jones, P. E. Fanwick, M. M. Abu-Omar, *J. Am. Chem. Soc.* **2007**, *129*, 12400–12401.
[95] M. R. Ringenberg, M. J. Nilges, T. B. Rauchfuss, S. R. Wilson, *Organometallics* **2010**, *29*, 1956–1965.

Received: June 20, 2011
Published Online: November 14, 2011

 © 2012 Wiley-VCH Verlag GmbH & Co. KGaA, Weinheim

DOI: 10.1002/ejic.201101072

Metal–Ligand Electron Transfer in 4d and 5d Group 9 Transition Metal Complexes with Pyridine, Diimine Ligands

Daniel Sieh,[a] Mandy Schlimm,[a] Lars Andernach,[a] Friedrich Angersbach,[a] Stefan Nückel,[a] Julia Schöffel,[a] Nevena Šušnjar,[a] and Peter Burger*[a]

Dedicated to Heinz Berke on the occasion of his 65th birthday

Keywords: Charge transfer / NMR spectroscopy / Density functional calculations / Rhodium / Iridium

Our recent results of the chemistry of group 9 Rh and Ir metal complexes bearing the ubiquitous pyridine, diimine (PDI) terdentate nitrogen donor are reviewed. Examples reflecting the special nature of the PDI ligand include a facile C–H activation process and the stabilization of a very rare late transition metal iridium nitrido compound, (PDI)Ir≡N, and its direct hydrogenation to the corresponding amido complex according to (PDI)Ir≡N + H_2 → (PDI)Ir–NH_2. The amount of electron transfer to the PDI ligands in (PDI)Rh,Ir–R,X complexes encompassing a variety of R,X ligands with weak/strong σ- and π-donors/acceptors was analyzed in terms of the innocence of the PDI ligand. With this regard, a combination of DFT methods, X-ray-crystallographic data, and, in particular, ^{13}C NMR spectroscopy was employed for a series of square-planar Rh and Ir complexes including a large number of new representatives. Their syntheses, spectroscopic characterization, and X-ray crystal structures are reported.

Introduction

The synthetic access and study of late transition metal complexes with metal–ligand multiple bonds is at the center of our research with a particular emphasis on systems with terminal metal oxygen (M=O) or nitrogen units (M≡N). Holm[1] and Mayer[2] had previously rationalized a high reactivity for this type of complexes for the most common coordination geometries with an electron configuration d^n with $n \geq 6$, which is due to 4e⁻, 2-orbital π-repulsion between filled metal d_π orbitals and p_π orbitals of the strong oxo and nitrido donors. It is therefore not surprising that, despite many attempts by several groups, complexes of this type are still rare[3,4] and only recently have Hill,[5] Milstein[6] (M=O), and our group (M≡N)[7] reported on isolated and fully characterized examples. Although the steric demand of the employed ligands and other ligand substitution effects play an important role, as demonstrated for the nitrido compounds shown in Figure 1,[7–8] here we will consider exclusively the electronic impact of the ligand on the reactivity and electronic structure of the complexes.

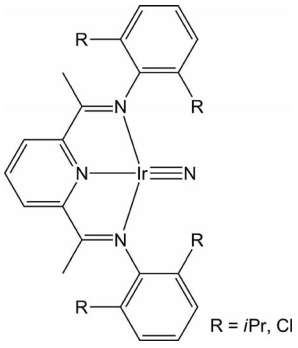

Figure 1. Late transition metal iridium nitrido complexes.

Herein, we will focus on specific issues of ligand design including non-innocence to enhance the stability of this type of complexes. After a short survey of our contributions to this field, we will describe a new method to evaluate the amount of electron transfer from the metal center to the ligand.

Survey

To relieve d_π–p_π repulsive interactions between the metal center and the O or N π-donor in metal oxo or nitrido complexes, a 4e⁻, 3-orbital scenario with a bonding, nonbonding, and antibonding orbital, as in the allyl anion,

[a] Institut für Anorganische und Angewandte Chemie, Universität Hamburg, Martin-Luther-King-Platz 6, 20146 Hamburg, Germany
Fax: +49-040 42838 6097
E-mail: burger@chemie.uni-hamburg.de

Supporting information for this article is available on the WWW under http://dx.doi.org/10.1002/ejic.201101072.

WILEY ONLINE LIBRARY
© 2012 Wiley-VCH Verlag GmbH & Co. KGaA, Weinheim

$C_3H_5^-$, was envisaged. This required an additional ligand with a (strong) π-acceptor property to install a push–pull situation. Furthermore, we considered chelating (terdentate) ligands with nitrogen donors (1) to cope with the strong *trans* influence of the π-donors, thus avoiding potential ligand loss, and (2) due to the higher resistance of nitrogen toward N–O bond formation. The latter situation is frequently encountered for phosphane ligands leading to phosphane oxides with concomitant decay of the initial metal oxo systems.[6b]

Daniel Sieh studied chemistry at the University Hamburg and graduated with a Diploma in 2008 in the Burger group, where he continued to work on his PhD project, which he is currently finalizing. Apart from his synthetic contributions to this microreview he solved and refined most of the X-ray crystal structures reported here.

Mandy Schlimm studied chemistry at the University of Hamburg and joined the Burger group for her Diploma Thesis, which was awarded in 2011. She has a PhD fellowship of the Graduate School "C_1-chemistry for resource and energy management" and is pursuing her PhD Thesis in the Burger labs.

Lars Andernach studied chemistry at the University of Hamburg and received his Diploma Thesis in 2011, with work in the Burger labs. He recently moved to the University of Mainz to join the group of Till Opatz as a PhD student.

Friedrich Angersbach studied chemistry at the University of Giessen and received his Diploma at the University of Kiel in a combined project with Siegfried Schindler and Felix Tuczek. He joined the Burger group as PhD student at the University of Hamburg in 2009.

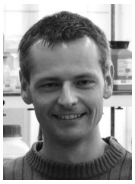

Stefan Nückel studied chemistry at the University Erlangen. After his Diploma in Lutz Dahlenburg's group, he moved to the Burger labs at the University of Zürich in 1999, where he obtained his PhD in 2002. He is presently working in industry with RC Tritec AG in Switzerland.

Julia Schöffel studied chemistry at the University of Jena, where she received her Diploma in 2004 in the group of Sven Rau. She moved to Hamburg in 2005 to work in the Burger group and obtained her PhD in 2008. She was a DFG postdoctoral fellow at UC San Diego in Clifford Kubiak's group from 2009 to 2010 and took a position in industry with Continental AG in Hannover in 2010.

Nevena Šušnjar studied chemistry at the University of Belgrade, where she graduated with a Diploma in 2001 in the group of Sofija Sovilj. She joined the Burger research group 2002 in Zürich and moved with him to the University of Hamburg, where she obtained her PhD in 2006. After a postdoctoral stay at the Technical University Dortmund with Peter Eilbracht she joined Synthomer Ltd. and is currently working in industry at NH Scientific in Rotterdam.

Peter Burger studied chemistry at the University of Konstanz and received his Diploma and PhD degrees in 1987 and 1991, respectively, working with Hans-Herbert Brintzinger on the synthesis, dynamics, and structural analysis of ansa-metallocenes. In 1991 he joined Bob Bergman's group at UC California Berkeley as a DFG-funded postdoctoral fellow establishing cationic Ir^{III} complexes as highly active C–H activation systems. In 1993 he started his independent career as Oberassistent working on his Habilitation at the University of Zürich in the group of Heinz Berke, where he also received his venia legendi in inorganic chemistry. In 2002 he accepted a call for a professorship at the University of Hamburg. He is deputy chair of the Graduate School "C_1-chemistry for resource and energy management" and chairman of the very recently funded Graduate School "Key Technologies for Sustainable Energy Systems in Smart Grids". His research interests are: Inorganic synthesis (molecules!), quantum-chemical high throughput/computational & C_1-chemistry, theoretical and experimental electronic structure elucidation, reaction mechanisms, energy research.

 © 2012 Wiley-VCH Verlag GmbH & Co. KGaA, Weinheim

Thus, complexes with phenyl, diimine pincer ligands (**PhDI**) were initially envisaged.

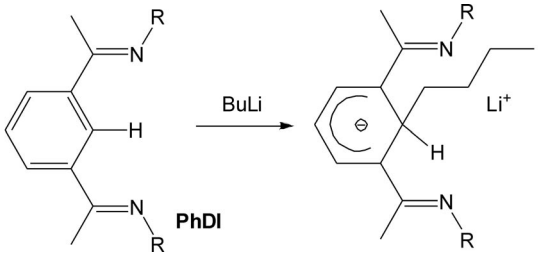

Due to problems with the C–H activation step of the central C–H bond required for metal complexation, we soon switched over to the pyridine, diimine system (PDI).[9] Nevertheless, the electrochemistry of **PhDI** and its formation of stable Meisenheimer complexes upon (nucleophilic) addition of butyllithium to the phenyl ring in **PhDI** clearly established the electron-deficient character of the aromatic system.[10] For pyridine congeners of **PhDI** even more pronounced electron acceptor properties were therefore anticipated, that is, ideally suited for the accommodation of a metal oxo/nitrido unit. Nearly coincidental with our findings for the **PhDI** phenyl system, the pyridine, diimine ligand experienced a renaissance initiated by the independent discovery of cobalt- and iron-based olefin polymerization catalysts by the groups of Gibson[11] and Brookhart.[12] It should be noted in passing that Brookhart et al. showed that the analogous cationic d^8-configured PDI Rh systems are not catalytically active for ethylene polymerization.[13]

Shortly after the latter report by the Brookhart group, we provided evidence for the desired push–pull interaction through the rotational barrier in the iridium methoxido complex presented in Figure 2.[14]

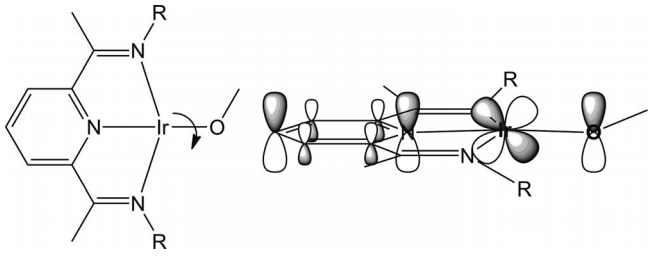

Figure 2. Push–pull interaction in an iridium methoxido complex.

In this 4e⁻, 3-orbital interaction, the filled d_{xz} and p_π orbitals of the Ir center and the sp^2-hybridized oxygen atom of the methoxido group and an additional π*-acceptor orbital are involved; the latter is essentially localized on the pyridine unit. Overlapping timewise with our report, Wieghardt, Budzelaar, and de Bruin were the first to discuss the non-innocent character of the PDI ligand system.[15] They also provided geometrical diagnostic criteria to evaluate the degree of electron transfer from the metal center to the PDI ligand. The latter are based on deviations of the bond lengths found in the free ligand from the corresponding bond lengths of the formal double bond of the C=N imine unit and the exocyclic C–C single bond to the pyridine group (vide infra). This method was refined later and confirmed by several groups.[16,17]

It should be clearly noted that the non-innocent state represents the extreme limit of the *complete* transfer of one or more electrons from the metal center, thereby formally reducing the ligand and leading to a concomitant formal oxidization of the metal center. In this regard, the transfer of up to three electrons to the ligand is discussed/established for the PDI ligand based on DFT calculations and experimental methods, for example, Mössbauer,[17,18] EPR,[19] or XAS[7] spectroscopy and magnetometry.[19b] Besides potential problems in establishing the degree of electron transfer from structural parameters (cf. below), there are obviously intermediate cases, where less than one electron is transferred. While this renders the assignment of the oxidation states of the metal centers delicate, the situation becomes even more complicated when another non-innocent ligand is attached to the metal center. Herein, we will discuss two recent cases incorporating an additional nitrosyl (NO) and nitrido ligand, and we will also introduce a new method based on ^{13}C NMR spectroscopy to evaluate the extent of electron transfer to the PDI ligand. Before we report on these details, we will briefly mention a specific propensity of the PDI ligand, which is only weakly recognized to the best of our knowledge. We traced/realized this special feature of the terdentate N-donor in the course of our investigation of the facile C–H activation in benzene by a (PDI)Ir methyl complex, which yields methane and the corresponding phenyl compound according to C_6H_6 + [(PDI)Ir]–CH_3 → [(PDI)Ir]–C_6H_5 + CH_4 within 2 hours at 40 °C.[20]

This feature can easily be recognized by inspection of the X-ray crystal structures of virtually all 4d and 5d PDI transition metal complexes and is highlighted below in Figure 3. In contrast to pincer ligands with –CH_2NMe_2 or –CH_2PR_2/–OPR_2 ligand arms, the imine's double bond is too short to reach a perfect square-planar geometry with an angle of 180° between the *trans*-positioned imine N-donors. We noted typical values of 156° for planar, four-coordinate Rh and Ir 4d and 5d complexes, which are hence best termed pseudo-square-planar. Smaller N_{imine}–M–N_{imine} bond angles of 153° were observed in the aforementioned methyl compound and as low as 148° in a nitrido complex. Figure 3 readily illustrates that this positioning of the π* orbitals localized on the imine units allows π-(back) donation from the d_{xz} orbital, which would be a nonbonding interaction in a perfect square-planar geometry, where the

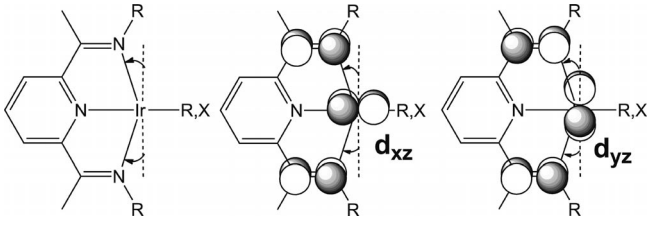

Figure 3. Consequence of the pseudo-square-planar geometry in PDI complexes (see text for an explanation).

 © 2012 Wiley-VCH Verlag GmbH & Co. KGaA, Weinheim

ligand orbital would be placed in the nodal plane. Although this "back-bending" of the imine ligand slightly reduces overlap with the d_{yz} orbital, increased metal–ligand π-overlap is observed overall (Figure 3). This particular feature leads to a very shallow potential for the out-of-plane bending of the fourth ligand (Figure 3).

At a value of 90° for the out-of-plane bending angle, the typical orbital set of the d^8-configured C_{2v} ML_4 fragment is obtained (Figure 4),[21] which readily explains the observed facile C–H activation processes. Furthermore, the formation of five-coordinate square pyramidal complexes can be understood. We will report on hydrido and phenyl iridium compounds of this type with additional ethylene and η^2-silane ligands soon.

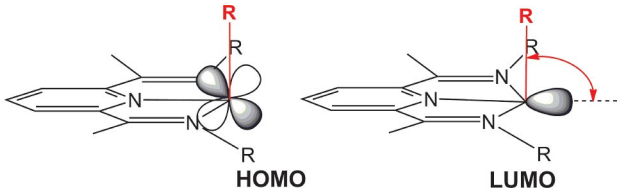

Figure 4. Frontier orbitals in distorted d_8-configured metal complexes. Only contributions from the metal center are shown.

Along with the discussion of the innocence versus non-innocence of the PDI ligand, we report on the syntheses of starting materials that proved to be highly useful for our chemistry. Their ^{13}C NMR spectroscopic data and X-ray crystal structures served as data points to probe for the amount of electron transfer to the PDI ligand in these complexes.

The a_2 and b_2 π-acceptor orbitals of the PDI ligand shown below have been previously identified as a source of its non-innocence, and they take up electrons from the metal centers.[15a,17,16]

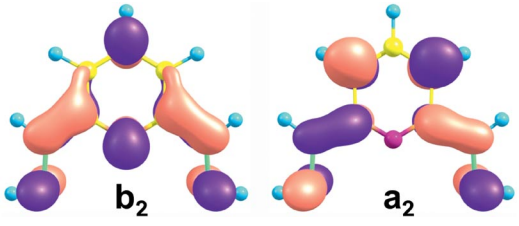

Their orbital energies are very close, thus readily explaining why the reduced PDI^{2-} dianion has a triplet ground state. Broken symmetry DFT and CASSCF calculations revealed that the corresponding singlet state is only a few kcal/mol higher in energy, however.[17] In most systems previously studied, the reduced PDI^{2-} ligand adheres to its triplet state in the metal complexes and couples antiferromagnetically to the (high-spin) metal centers.[17,15a,16,22] This type of biradical metal–ligand interaction also holds for most of the singly reduced PDI ligands (PDI^{1-}) and is in sharp contrast to the Rh and Ir complexes described herein, for which a typical back-donation scenario is observed. This different type of metal–ligand interactions is best shown by the illustration below, which was adapted from a publication of Budzelaar et al.[15a]

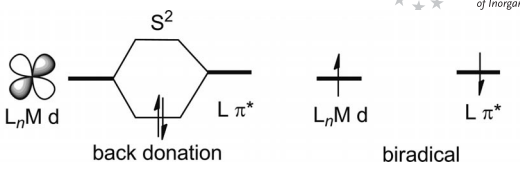

Since most of the previous studies of PDI complexes employed 3d metal centers, this situation might have been expected considering the following two points: Firstly, back-donation requires substantial overlap (S^2) between the d orbitals of the transition metal centers and the π* orbital of the ligand. For the more contracted 3d orbitals, the overlap is reduced. Larger $d\pi_{metal}$–π^*_{ligand} overlap is anticipated for the larger and more diffuse 4d and 5d orbitals, which are hence better situated for back-donation. Secondly, contrary to their 3d congeners, 4d and 5d transition metal centers or fragments (L_nM) usually have a preference for lower spin states, thus overruling the weak preference for the $S = 1$ state in the reduced PDI^{2-} ligand. In any case, there is a continuous transition between the limiting back-donation and biradical scenarios.[23]

We had our first encounter with the (potential) non-innocence of the PDI ligand in the course of the investigation of the nitrido and the corresponding amido and nitrosyl complexes **1**–**3** shown in Scheme 1.[7] It deserves special mention that all three compounds are diamagnetic.

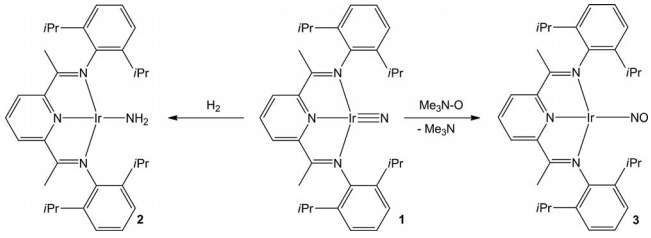

Scheme 1. Reactions of the terminal nitrido complex **1**.

NO complex **3** is formed by attack of the trimethylamine N-oxide nucleophile at the Ir–N moiety, thus supporting our view of an electrophilic nitrido unit. For the discussion of the electronic structures of the nitrido and nitrosyl complexes **1** and **3**, a comparison with the properties and bonding situation of metal carbyne (CR) compounds is instrumental. The carbyne ligand usually forms strong metal–carbon triple bonds and adheres to the well-known dichotomy of nucleophilic Schrock- and electrophilic Fischer-type carbynes with corresponding CR^{3-} and CR^{+} units, respectively.[2b,24] This is accompanied by a change of the oxidation state of the metal center by 4 units from +III (Schrock) to –I (Fischer). The carbyne unit might therefore be also considered as a non-innocent ligand; this terminology is not in common use, however. It should be noted that Fischer-type carbyne ligands are anticipated for late transition metals systems.[25] On the basis of the aforementioned nucleophilic attack at the isoelectronic nitrido unit, description as a positively charged Fischer-type "N^+" ligand would

 © 2012 Wiley-VCH Verlag GmbH & Co. KGaA, Weinheim

seem adequate for the nitrido unit. This is in conflict with the common perception of the nitrido moiety as a Schrock-type, albeit nucleophilic(!), N^{3-} ligand.

For the consecutive analysis, let us first consider the PDI ligand as innocent, which leaves either a d^{10}-configured Ir^{-I} system for a Fischer-type N^+ ligand or an iridium(III) d^6 complex with a Schrock-type N^{3-} unit. There is a related situation for the nitrosyl ligand, for which NO^+ and NO^- (and NO^{3-}) binding modes are established, which results in formal d^{10}- and d^8-configured Ir^{-I} and Ir^{+I} metal centers, respectively. Now switching on electron transfer to the PDI ligand, further possibilities arise, which are summarized in Table 1.

Table 1. Electronic configurations of the ligands and Ir center in (PDI)IrL complexes (L = N,NO).

Entry	L = NO,N configuration	PDI configuration	Ir: oxidation state, configuration
1	NO^+	PDI^0	Ir(-I), d^{10}
2	NO^+	PDI^{2-}	Ir^{I}, d^8
3	NO^-	PDI^0	Ir^{I}, d^8
4	NO^-	PDI^{2-}	Ir^{I}, d^6
5	N^+	PDI^0	Ir(-I), d^{10}
6	N^+	PDI^{2-}	Ir^{I}, d^8
7	N^-	PDI^0	Ir^{I}, d^8
8	N^-	PDI^{2-}	Ir^{III}, d^6
9	N^{3-}	PDI^0	Ir^{III}, d^6
10	N^{3-}	PDI^{2-}	Ir^{V}, d^4

Even without considering the less common even oxidation states II and IV for the Ir center, inspection of Table 1 reveals the variety of the possible oxidation states for the Ir centers in these complexes, reaching from Ir^V to Ir^{-I}. This shows the complicated situation for the assignment of the electronic configurations in these systems, and experimental support to address this issue was therefore urgently sought. Mössbauer spectroscopy, which was highly instrumental for previous studies on PDI complexes of iron, was therefore initially considered. Since Mössbauer discovered the effect for iridium,[26] it is somehow ironical to note that this technique is rather inadequate for complexes of this particular element due to short lifetimes and concomitant broad linewidths. We have therefore turned to X-ray photoelectron (XPS) and absorption spectroscopy for the study of the nitrosyl (XPS) and nitrido (XPS & XAS) compounds. The corresponding square-planar PDI chlorido and amido complexes, [Cl(PDI)Ir] (not shown) and [(NH_2)(PDI)Ir] (**2**) served as references for (formal) d^8-configured Ir^I metal centers in these measurements.[7] The recorded XPS ionization energies of +62 eV for the $4f_{7/2}$ component were identical for the nitrosyl and chlorido complexes, while a value of 63.1 eV for the nitrido compound suggested a higher oxidation state. Usually, raising the oxidation state by 1 unit is accompanied by an increase of the binding energy by 1 eV, while the values remain essentially unchanged for the same oxidation state in closely related compounds[27,28] Therefore Ir^I oxidation states were proposed for the NO and chlorido complexes, while a tervalent Ir^{III} center was considered for the nitrido system, although there is only a difference of 1.1 eV for the binding energies. The XAS spectra recorded for the L_1-edge of the nitrido and amido complexes **1** and **2** were also consistent with this view, since an increase of 1.5 eV was observed for the rising position of the L_1-edge in going from the amido complex to nitrido compound **1**. Considering a typical shift of +1 eV per unit of oxidation state,[29] these findings supported the proposed Ir^{III} oxidation state in nitrido complex **1**.

According to the book keeping in Table 1, this left entries 2, 3, and 8, 9, respectively, for the electronic structures of the nitrosyl and nitrido iridium compounds **3** and **1**. Depending on the state of innocence of the PDI ligand, this would require either a NO^+ and NO^- ligand for nitrosyl complex **3** and a N^{3-} or N^- moiety for nitrido system **1**. While NO^+/NO^- ligands are well established, the consideration of a formal "N^-" ligand is much less obvious.[30] We will first analyze the electronic structure in nitrosyl complex **3**, which will be followed by a brief discussion of nitrido compound **1**. Finally, we will put our findings into the general context of electron transfer in these Ir systems.

NO Ligand

The assessment of the electronic structure of a M–NO unit in metal nitrosyl complexes is not a simple task.[28,31,32,33] While IR and ^{15}N NMR spectroscopic data are helpful to distinguish between the linear and bent binding modes of the NO ligand, the assignment of its formal charge, for example $NO^+/NO^-/NO^{3-}$, is not unambiguously possible.[28] Problems with the assignment of formal oxidation states in metal nitrosyl complexes can be circumvented in an elegant way using the Enemark and Feltham $\{MNO\}^n$ notation.[31] Here n denotes the number contributed from the d electrons, an additional electron stems from the NO ligand. For the nitrosyl complexes with a neutral PDI ligand a $\{MNO\}^{10}$ notation is obtained [$(d^9\text{-}Ir^0)$ + $1e^-$ $(NO^{\cdot})$], while $\{MNO\}^8$ denotes the situation for a doubly reduced PDI^{2-} ligand [d^7-Ir(+2) + $1e^-$ $(NO^{\cdot})$]. While this notation masks the oxidation state of the metal center, it proves helpful for comparison with other NO complexes.

The linear binding mode of the M–NO unit observed in the X-ray crystal structure of the nitrosyl ligand might be taken as a first hint for a positively charged NO^+ ligand, although this older criteria is clearly outdated.[28,31,33,34,35] Currently, charges of +1, –1, and –3 for the linear and –1 and –3 for the bent M–NO binding modes are considered.[32] Note that, for the sake of argument, the triply negatively charged ligand has not been included in the previous discussion. The electronic situation ($M{\equiv}N^+{-}O^-$) would nevertheless be identical to the N^{3-} ligand (entries 9 and 10 in Table 1).

The short N–O bond length of 1.119(5) Å in **3** was remarkable and was between the bond lengths observed for free NO^+ (1.06 Å) and NO^- (1.26 Å) ($NO^{\cdot}$ 1.15 Å); suggesting substantial multiple bond character.[33] This also holds for the Ir–$N_{nitrosyl}$ bond length of 1.752(5) Å, which was approximately 0.2 Å shorter than the Ir–N_{amido} bond length

 © 2012 Wiley-VCH Verlag GmbH & Co. KGaA, Weinheim

for the corresponding bond to the amido ligand (Ir–NH_2) in **2** and closer to the Ir–$N_{nitrido}$ bond length of 1.646(9) Å found in nitrido complex **1**. Of particular interest, however, was the bond length of the exocyclic C–C bond of the pyridine ring of 1.391(6) Å. This was considerably shorter than any of the corresponding values of all systems described herein, which display an average bond length of 1.44 Å (vide infra). Furthermore, DFT calculations revealed the occupation of the aforementioned PDI-based b_2 orbital (HOMO), shown below,

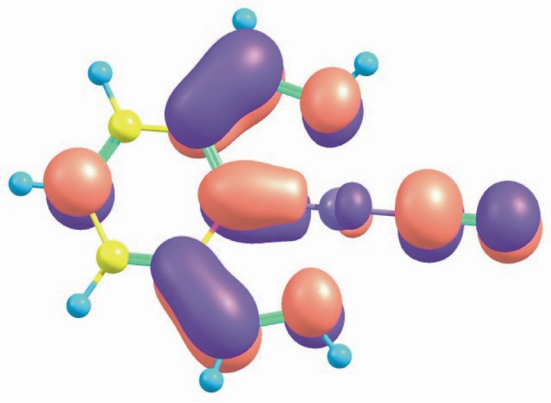

which is mostly localized on the PDI ligand (72%) and has further contributions from the π* orbital (20%) of the NO ligand according to Mulliken population analysis (see Table 2).

Table 2. Orbital occupation according to Mulliken population analysis.

Model compound	Occupation b_2 orbital	Occupation a_2 orbital	Mulliken population analysis PBIS(b_2)/Ir(d_{xz})/R,X(b_2)
$(PDI)Ir(CO)^+$	0	0	–
(PDI)Ir–Cl	2	0	45:37:18
(PDI)Ir–H	2	0	37:63/–
(PDI)Ir–NH_2	2	0	56:23:21
(PDI)Ir–NO	2	0	72:8:20
(PDI)Ir–N	2	0	67:15:18

Note that there is only negligible participation of the iridium d_{xz} orbital (8%), revealing that 2 electrons are transferred from the metal to a ligand-centered orbital. This leads to a formal increase of the oxidation state of the iridium center by 2 units (d^7). The participation of this PDI-inherited b_2 orbital in the occupied orbitals does not suffice as a general criterion to judge on its non-innocence, however, as will be discussed in detail below.

IR spectroscopy is usually an excellent tool to evaluate the amount of electron transfer to/from the NO ligand, since a bond order of 3 is expected for a linear NO^+ ligand and lower bond orders of 1–2 in its reduced state. The observed IR ν(NO) absorption at 1759 cm^{-1} was unambiguously confirmed by the band at 1712 cm^{-1} for the ^{15}N-isotopologue [(PDI)Ir(^{15}NO)] and is in the typical range of linear M–NO units (1600–1950 cm^{-1}). The ν(NO) stretching frequency was at the lower limit of the previously established range for complexes with a formal NO^+ ligand, for which the ν(NO) bands for free NO^+, NO, and NO^- at 2377, 1878, and 1470 cm^{-1} represent benchmark values.[36] In agreement with the X-ray crystal structure, the observed ^{15}N NMR chemical shift of δ = 569 ppm for the NO ligand lies in the established range 280–580 ppm for linear M–NO units. Unfortunately, the ^{15}N NMR spectroscopic data provide only little information with regard to the electron count within the NO moiety (NO^+/NO^-, NO^{3-}).[28,32,31]

These data can be summed up as follows: (1) Two electrons are transferred from the d_{xz} orbital to ligand-centered orbitals. Based on the long bond length of the exocyclic C–C bond of the pyridine unit in combination with the Mulliken population analysis, we suggest that these electrons are exclusively transferred to the PDI ligand, rendering it doubly reduced, PDI^{2-}. (2) This leaves a d^7-configured metal center, which achieves its d^8-electron configuration by the transfer of one e^- from the nitrosyl ligand to yield a formal NO^+ unit. This is consistent with the short N–O bond length and the IR vibrational data. In conclusion, the electronic structure of nitrosyl complex **3** is best described by: (PDI^{2-})(NO^+)(d^8-Ir).

Nitrido Complex 1

Without going into details, it shall be briefly mentioned that we went through a similar analysis for the nitrido complex, which included up to [14,14] multireference CASSCF and consecutive MCQDPT2 calculations.[7] Since this continued study is not fully completed and will be reported in a forthcoming paper, we will focus on specific details related to the ^{13}C NMR spectral analysis of the PDI–metal interaction. As in the case of the NO complex, the PDI-inherited b_2 orbital is filled in the nitrido complex. It displays a contribution of 67% from the PDI ligand, rendering it essentially a doubly reduced PDI^{2-} ligand (Table 2). Considering the proposed Ir^{III} oxidation state of the additional XPS and XAS measurements for this complex, this would require a singly negatively charged "N^{-}" ligand. The latter assignment is also consistent with results from the population analysis for the Ir≡N triple bond. In total, a (PDI^{2-})(N^-)(d^6-Ir) electronic structure can be conveyed from these data. In addition to the aforementioned electrophilic reactivity of the Ir–N unit, we have further evidence, which points more to an ambiphilic character of the Ir–N unit, fully consistent with a "N^-" ligand. This is (1) the calculated high proton affinity[7] and (2) experimental evidence of its nucleophilic character observed in the Si–H activation of silanes.[8b] Note that any of this assignment is highly delicate and may not reflect the true nature of this complex. As previously pointed out by Budzelaar et al., the PDI ligand is highly flexible in delivering and providing electrons along a reaction path. With that regard, an electronic structure according to (PDI^0)(N^+)(d^8-Ir) may be built up, thus reflecting a higher electrophilic nature of the M–N unit.

In the course of the study of the nitrosyl and nitrido complex, further (experimental) diagnostic criteria for the assessment of the electronic structures of the PDI com-

 © 2012 Wiley-VCH Verlag GmbH & Co. KGaA, Weinheim

plexes were sought. Since most of the square-planar Rh and Ir compounds are diamagnetic, the analysis of NMR spectroscopic data was considered. We focused on ^{13}C NMR spectroscopic data, because of their small dependence on solvent and anisotropy effects. It should be mentioned in passing that Budzelaar et al. has briefly looked into the correlation of ^{1}H NMR spectroscopic data for different cobalt PDI systems.[19a] Also, the assessment of σ-donor and π-acceptor properties of the PDI and related ligands by his group deserves a special mention.[23] The result of our systematic study will be presented below. In the next section, we will firstly report on the unpublished reference molecules, which were employed for this analysis. Along with the description of their syntheses and specific properties, X-ray crystal structures of some representatives will be shown.

Syntheses and X-ray Crystal Structures[37]

The syntheses of novel square-planar complexes along with their starting materials and relevant related compounds are summarized in Scheme 2. Several complexes utilized in this study were previously published.[7–8,14,13,20] This is indicated in the short survey for all compounds below, where specific details and properties for each class of compound and the availability of X-ray crystal structures are also compiled. The detailed syntheses of the new compounds together with their IR and NMR spectroscopic characterization, elemental analysis, and crystallographic data are found in the Supporting Information. The assignment of the ^{13}C NMR resonances of all compounds is based on the careful analysis of DEPT and ^{13}C–^{1}H correlated HSQC and HMBC spectra.

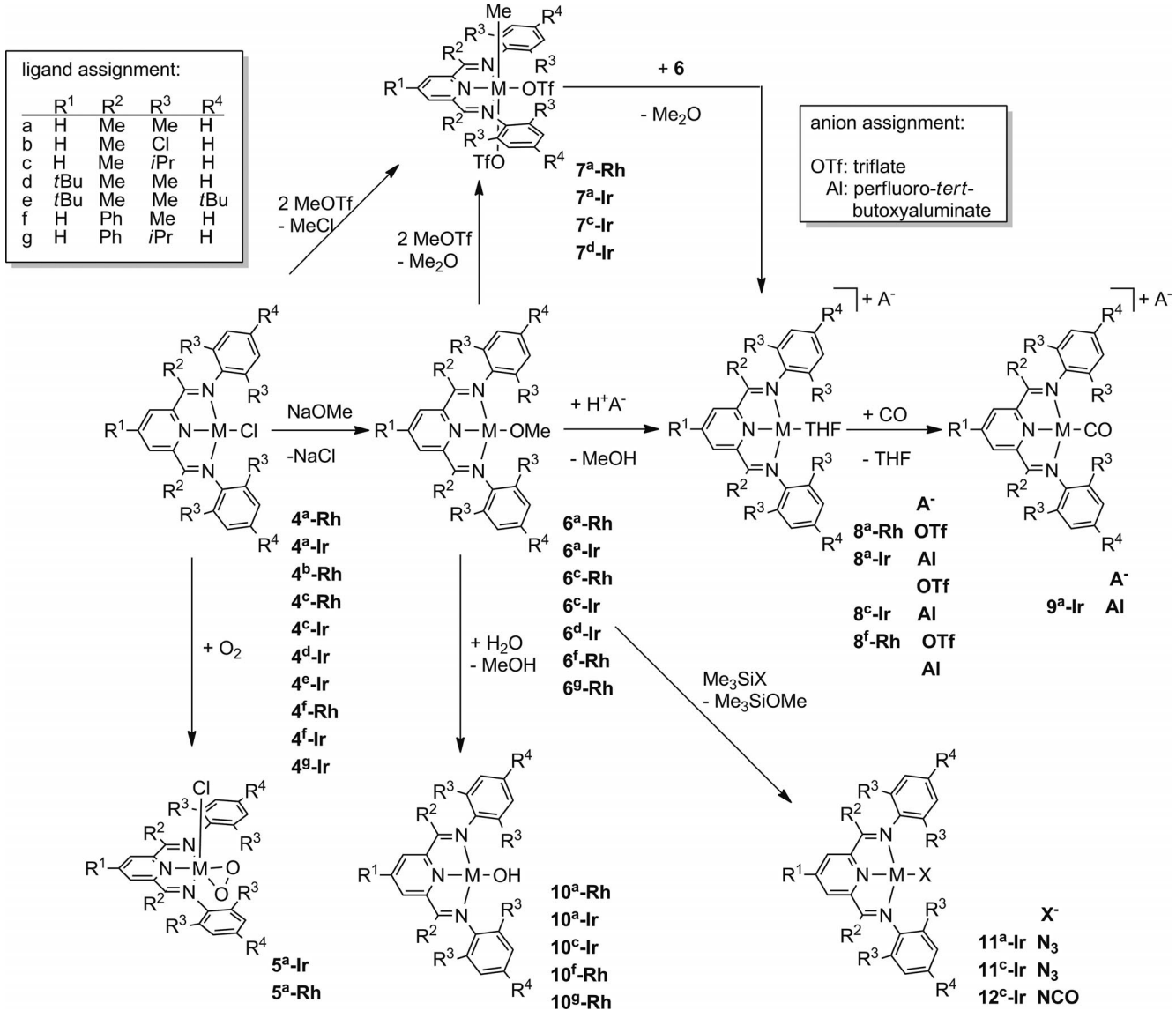

Scheme 2. Syntheses of the Rh and Ir complexes.

 © 2012 Wiley-VCH Verlag GmbH & Co. KGaA, Weinheim

Chlorido Complexes 4

The chlorido complexes **4** are our central starting materials for all compounds described herein. They were synthesized by reaction of the respective ligand with the dimeric $[M(C_2H_4)_2Cl]_2$ (M = Rh,[38] Ir[39]) complexes.[13–14,40] The previously unpublished complexes **4^{d}-Ir**, **4^{e}-Ir**, **4^{f}-Rh/Ir**, and **4^{g}-Rh** were characterized by standard spectroscopic methods and also X-ray structure analysis, when suitable crystals could be obtained. Figure 5 shows the molecular structure of complex **4^{f}-Rh**; selected bond lengths and angles are given in the figure caption.

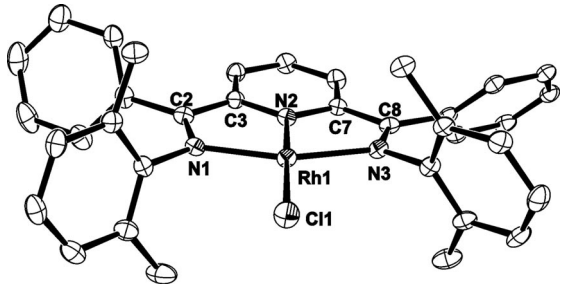

Figure 5. ORTEP representation of **4^{f}-Rh** with anisotropic displacement parameters shown at the 50% probability level. Hydrogen atoms and the co-crystallized toluene molecule are omitted for clarity. Selected bond lengths [Å] and angles [°] with esd values in parentheses: Rh1–N1 2.034(2), Rh1–N2 1.8970(19), Rh1–N3 2.037(2), Rh1–Cl1 2.3332(6), N1–C2 1.319(3), C2–C3 1.460(3), N3–C8 1.321(3), C7–C8 1.463(3), N1–Rh1–N3 158.55(8), N2–Rh1–Cl1 179.64(6), N1–Rh1–N2 79.46(8), N1–Rh1–Cl1 100.44(6), N2–Rh1–N3 79.22(8), N3–Rh1–Cl1 100.89(6).

All chlorido complexes **4** studied so far by us exhibit a pseudo-square-planar geometry, evidenced by the sum of angles around the Rh or Ir center of essentially 360°. The ^{1}H and ^{13}C NMR spectroscopic data are consistent with C_{2v} symmetry in these complexes.

Chlorido Peroxido Complexes 5

Exposure of chlorido complexes **4^{a}-Rh/Ir** to pure O_2 or air leads to addition of dioxygen with formation of chlorido peroxido complexes, which has also been noticed by Vrieze et al. for analogous Rh complexes.[40] This reaction was used for the syntheses of peroxido complexes **5^{a}-Rh** and **5^{a}-Ir** by reaction of **4^{a}-Rh** and **4^{a}-Ir** with dioxygen. Inspection of the NMR spectroscopic data revealed the loss of C_{2v} symmetry, indicated by two diastereotopic aromatic methyl groups. This is also reflected in the crystal structure of complex **5^{a}-Ir** (Figure 6). The chlorido ligand occupies an apical position. The plane spanned by the dioxygen ligand and the metal center is perpendicular to the PDI ligand plane, leading to C_s symmetry in complexes **5^{a}-Rh/Ir**. The bonding mode of the O_2 ligand was further proved by the presence of strong IR stretching vibrations at 887 cm^{-1} (**5^{a}-Rh**) and 846 cm^{-1} (**5^{a}-Ir**), which is in the expected range for η^2-bound O_2 ligands.[41,42]

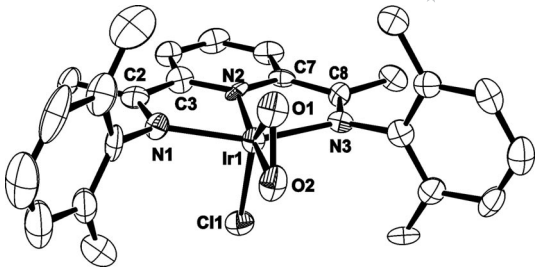

Figure 6. ORTEP representation of **5^{a}-Ir** with anisotropic displacement parameters shown at the 50% probability level. Hydrogen atoms and the co-crystallized solvent molecules are omitted for clarity. Selected bond lengths [Å] and angles [°] with esd values in parentheses: Ir1–N1 2.067(6), Ir1–N2 1.933(6), Ir1–N3 2.054(6), Ir1–O1 2.009(5), Ir1–O2 2.025(5), Ir1–Cl1 2.379(2), N1–C2 1.306(10), C2–C3 1.477(11), N3–C8 1.311(9), C7–C8 1.449(11), O1–O2 1.471(8), N1–Ir1–N3 155.9(2), N2–Ir1–O2 170.4(2), N1–Ir1–N2 79.1(2), N1–Ir1–O2 99.2(2), N2–Ir1–N3 78.2(2), N3–Ir1–O2 101.7(2), N2–Ir1–O1 127.7(2), N2–Ir1–Cl1 85.02(17), Cl1–Ir1–O2 104.55(19), Cl1–Ir1–O1 147.31(17).

Methoxido Complexes 6

Reaction of chlorido complexes **4** with NaOMe leads to conversion to the corresponding methoxido complexes **6**,[14] of which **6^{c}-Rh**, **6^{d}-Ir**, **6^{f}-Rh**, and **6^{g}-Rh** represent previously unpublished examples. The ^{1}H NMR resonances for the OCH_3 ligand were found in a range between 3.7 and 4.7 ppm for the Rh complexes and are generally shifted downfield for the analogous Ir congeners (4.9–5.5 ppm). The crystal structures obtained for the new methoxido complexes revealed C_s symmetry. As previously observed (cf. Figure 2), the methoxido ligand is oriented in the plane of the PDI ligand. The molecular structure of complex **6^{d}-Ir** is shown in Figure 7; selected bond lengths and angles are given in the figure caption.

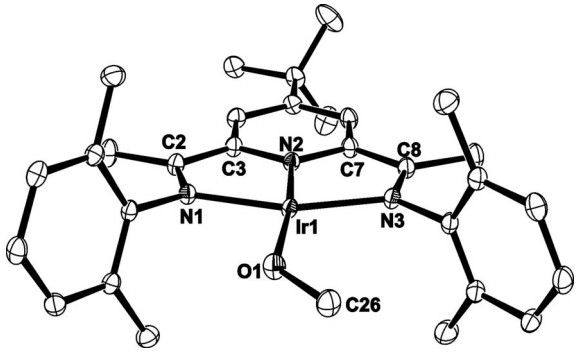

Figure 7. ORTEP representation of **6^{d}-Ir** with anisotropic displacement parameters shown at the 50% probability level. Hydrogen atoms and the co-crystallized THF molecules are omitted for clarity. Selected bond lengths [Å] and angles [°] with esd values in parentheses: Ir1–N1 2.0255(16), Ir1–N2 1.8884(16), Ir1–N3 2.0185(16), Ir1–O1 1.9639(14), N1–C2 1.331(2), C2–C3 1.440(3), N3–C8 1.329(3), C7–C8 1.441(3), O1–C26 1.398(2), N1–Ir1–N3 157.89(7), N2–Ir1–O1 172.27(6), N1–Ir1–N2 79.37(7), N1–Ir1–O1 93.75(6), N2–Ir1–N3 78.69(7), N3–Ir1–O1 108.32(6), Ir1–O1–C26 128.15(13).

 © 2012 Wiley-VCH Verlag GmbH & Co. KGaA, Weinheim

This is in contrast to the collected ^{1}H and ^{13}C NMR spectroscopic data, which point out to C_{2v} symmetrical methoxido complexes, indicated by only one resonance for the aromatic methyl (R^3 = Me) or *i*Pr methine (R^3 = *i*Pr) protons. We explained this observation by the rotation of the methoxido ligand around the N_{py}–Ir–O bond, which is fast on the NMR time scale (cf. Figure 2).

Cationic Complexes 7 and 8

As previously published by us and others,[13–14] chlorido **4** and methoxido complexes **6** can be converted into the corresponding distorted octahedral methyl bis(triflato) complexes **7** by reaction with MeOTf. Single-crystal X-ray structure analysis for new complexes **7^c-Ir** and **7^d-Ir** showed two triflate ligands in the *cis* position to each other with the methyl ligand in the apical position, which leads to an overall C_s symmetry for complexes **7**. The molecular structure of the representative **7^d-Ir** is shown in Figure 8; selected bond lengths and angles are given in the figure caption.

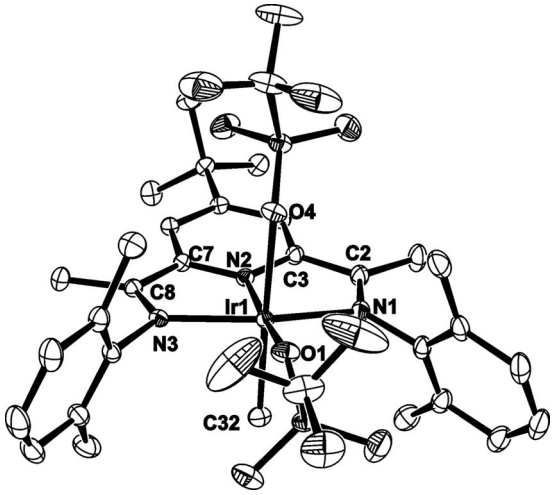

Figure 8. ORTEP representation of **7^d-Ir** with anisotropic displacement parameters shown at the 50% probability level. Hydrogen atoms are omitted for clarity. Selected bond lengths [Å] and angles [°] with esd values in parentheses: Ir1–N1 2.0734(12), Ir1–N2 1.9109(11), Ir1–N3 2.0628(11), Ir1–O1 2.1095(10), Ir1–O4 2.2471(10), Ir1–C32 2.0516(14), N1–C2 1.3098(19), C2–C3 1.473(2), N3–C8 1.3084(17), C7–C8 1.4766(19), N1–Ir1–N3 158.83(5), N2–Ir1–O1 169.73(4), N1–Ir1–N2 79.22(5), N1–Ir1–O1 103.49(5), N2–Ir1–N3 80.03(5), N3–Ir1–O1 97.68(4), C32–Ir1–O4 175.58(5), N2–Ir1–O4 88.53(4), N2–Ir1–C32 95.88(5), O1–Ir1–C32 94.06(5), O1–Ir1–O4 81.56(4).

This is in accordance with the NMR spectroscopic data collected for these complexes where two resonances were observed for the aromatic methyl (R^3 = Me) or *i*Pr methine (R^3 = *i*Pr) protons and carbon atoms, respectively. In case of the less sterically hindered (R^3 = Me) methyl bis(triflato) complexes, the reaction of tervalent Rh^{III} and Ir^{III} complexes **7** with their corresponding pseudo-square-planar methoxido complexes **6** leads to the formation of two equivalents of cationic complexes **8** with concomitant release of dimethyl ether. The ^{19}F NMR and IR spectra did not allow to unambiguously establish the binding mode of the triflate group, that is, whether ionic or coordinated to the metal center. Single-crystal X-ray structural analysis for complexes **8^a-Rh**, **8^a-Ir**, and **8^f-Rh** proved that the triflate group is not coordinated to the metal centers and a THF molecule occupies the fourth coordination site in pseudo-square-planar cationic complexes **8**. Figure 9 shows one of the two independent molecules of the asymmetric unit of the molecular structure of complex **8^f-Rh**; selected bond lengths and angles for this molecule are given in the figure caption.

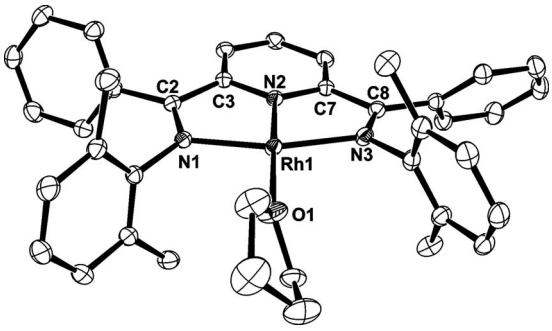

Figure 9. ORTEP representation of one of the two independent molecules of **8^f-Rh** with anisotropic displacement parameters shown at the 50% probability level. Hydrogen atoms, anions, and the co-crystallized THF molecules are omitted for clarity. Selected bond lengths [Å] and angles [°] with esd values in parentheses: Rh1–N1 2.0311(14), Rh1–N2 1.8805(14), Rh1–N3 2.0281(14), Rh1–O1 2.0812(13), N1–C2 1.312(2), C2–C3 1.465(2), N3–C8 1.313(2), C7–C8 1.473(2), N1–Rh1–N3 159.72(6), N2–Rh1–O1 175.46(6), N1–Rh1–N2 80.03(6), N1–Rh1–O1 100.07(6), N2–Rh1–N3 79.70(6), N3–Rh1–O1 100.06(6).

For complexes with the sterically more demanding *i*Pr groups in the 2- and 6-positions of the aryl rings (R^3), no reaction was observed between methyl bis(triflato) complex **7^c-Ir** and methoxido complex **6^c-Ir**. Therefore, we established a different route for the preparation of cationic square-planar complexes **8** by reaction of methoxido complexes **6** with Brønsted acids {HOTf or $[H(Et_2O)][Al(pftb)_4]$}.

Cationic Carbonyl Complex 9^a-Ir

The π-accepting carbonyl ligand was introduced by reaction of cationic complex **8^a-Ir** with carbon monoxide. Cationic CO complex **9^a-Ir** was characterized by NMR and IR spectroscopy as well as elemental analysis and single-crystal X-ray structure determination. The ^{13}C NMR resonance for the CO ligand was found at δ = 181.5 ppm in $[D_8]$THF and was proved by ^{13}C isotopic labeling. The IR spectrum (KBr) of complex **9^a-Ir** exhibits a strong stretching vibration at 2002 cm^{-1}, which is redshifted by 46 cm^{-1} to 1956 cm^{-1} for the ^{13}C-isotopically labeled complex. This is in accordance with comparable square-planar cationic Ir CO complexes,[43] indicating only marginal π-back-bonding to the CO ligand. The pseudo-square-planar geometry of complex **9^a-Ir** was unambiguously established by single-crystal X-ray structural analysis (Figure 10), revealing a sum of angles around the Ir center of 360°. The determined

 © 2012 Wiley-VCH Verlag GmbH & Co. KGaA, Weinheim

C–O bond length in the CO ligand of 1.152(7) Å in the solid state is also an indication of marginal π-back-bonding from the metal center to the CO ligand.

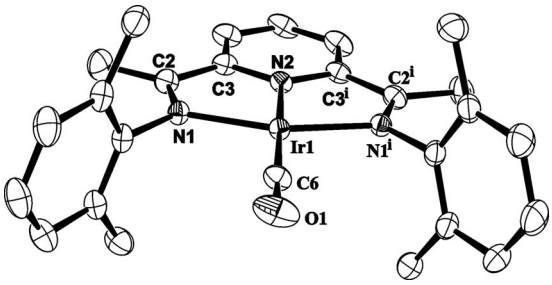

Figure 10. ORTEP representation of **9[a]-Ir** with anisotropic displacement parameters shown at the 50% probability level. Hydrogen atoms and the anion are omitted for clarity. Selected bond lengths [Å] and angles [°] with esd values in parentheses: Ir1–N1 2.022(2), Ir1–N2 1.980(2), Ir1–C6 1.848(3), C6–O1 1.147(4), N1–C2 1.308(3), C2–C3 1.480(4), N1–Ir1–N1^{i} 157.08(11), N2–Ir1–C6 180.000(1), N1–Ir1–N2 78.54(6), N1–Ir1–C6 101.46(6), Ir1–C6–O1 180.000(1). The Ir center and the atoms of the carbonyl group (C6, O1) are located on a crystallographic twofold rotational axis.

Hydroxido Complexes 10

Hydroxido complexes **10** were obtained through hydrolysis of the corresponding methoxido complexes **6** with degassed water. The reaction was clearly indicated by the absence of the distinctive methoxido ^{1}H and ^{13}C NMR resonances. There is a significant downfield shift of the resonances for the hydroxido protons in iridium hydroxido complexes **10-Ir**. The latter were detected at δ = 8.3 and 7.9 ppm in **10[a]-Ir** and **10[c]-Ir**, respectively. On the contrary, the ^{1}H NMR shifts of the OH groups in Rh complexes **10[a]-Rh**, **10[f]-Rh**, and **10[g]-Rh** are observed in the range 1.8 and 2.6 ppm. For both Rh and Ir, a dependence of the ^{1}H NMR resonance on the concentration of the complex could be observed. This strong discrepancy between analogous Rh and Ir complexes has already been noticed by us for the corresponding Rh and Ir methyl complexes with ^{1}H NMR resonances at 2.2 (Rh) and 6.9 (Ir) ppm.[14] Except for complex **10[a]-Ir**, single crystals suitable for X-ray structure determination could be obtained. The molecular structure of the representative **10[g]-Rh** is shown in Figure 11; selected bond lengths and angles are given in the figure caption.

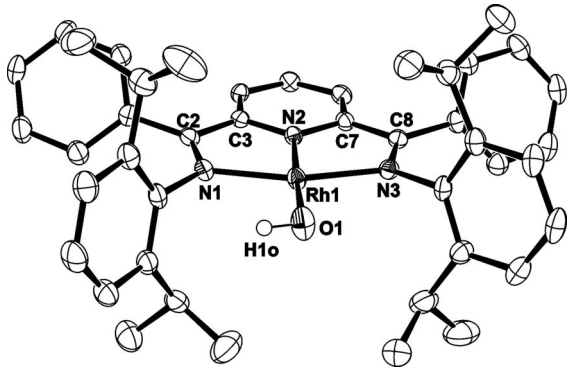

Figure 11. ORTEP representation of **10[g]-Rh** with anisotropic displacement parameters shown at the 50% probability level. Carbon-bound hydrogen atoms and the co-crystallized toluene molecules are omitted for clarity. Selected bond lengths [Å] and angles [°] with esd values in parentheses: Rh1–N1 2.013(2), Rh1–N2 1.880(2), Rh1–N3 2.040(2), Rh1–O1 1.965(2), N1–C2 1.321(4), C2–C3 1.458(4), N3–C8 1.317(3), C7–C8 1.456(4), N1–Rh1–N3 159.28(10), N2–Rh1–O1 176.22(9), N1–Rh1–N2 79.25(9), N1–Rh1–O1 102.21(9), N2–Rh1–N3 80.04(9), N3–Rh1–O1 98.43(9).

For Rh complexes **10[a]-Rh** and **10[g]-Rh**, the single crystals were of sufficient quality to locate the hydroxido H atom in the Fourier electron density maps: it lies in the PDI plane and was refined isotropically.

Azido 11 and Isocyanato 12 Complexes

In analogy to the published azido complexes, **11[a]-Ir**[8b] and **11[c]-Ir**,[7] isocyanato complex **12[c]-Ir** was obtained by metathesis of the OMe ligand in complex **6[c]-Ir** with Me_3Si-NCO. The IR spectrum (KBr) of complex **12[c]-Ir** exhibits a strong absorption band at 2224 cm^{-1}, which is characteristic for the asymmetric stretching vibration of terminal bound and μ-1,3-bridged NCO complexes.[44] Single-crystal X-ray structure determination revealed a pseudo-square-planar Ir complex with a terminally bound isocyanato ligand, which is arranged in nearly linear fashion (Figure 12).

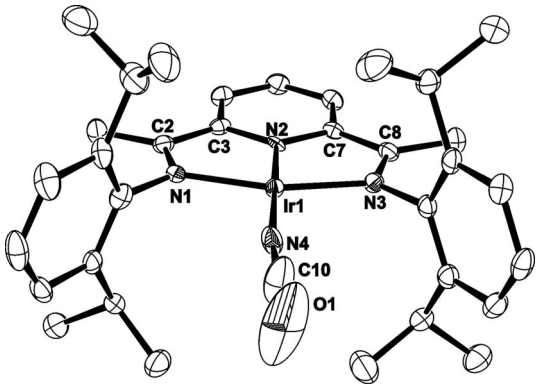

Figure 12. ORTEP representation of **12[c]-Ir** with anisotropic displacement parameters shown at the 50% probability level. Hydrogen atoms are omitted for clarity. Selected bond lengths [Å] and angles [°] with esd values in parentheses: Ir1–N1 2.012(4), Ir1–N2 1.899(4), Ir1–N3 2.010(4), Ir1–N4 2.004(4), N4–C10 1.162(7), C10–O1 1.188(8), N1–C2 1.317(6), C2–C3 1.459(7), N3–C8 1.336(6), C7–C8 1.450(6), N1–Ir1–N3 159.06(15), N2–Ir1–N4 179.68(17), N1–Ir1–N2 79.70(15), N1–Ir1–N4 99.99(16), N2–Ir1–N3 79.38(15), N3–Ir1–N4 100.93(16), Ir1–N4–C10 169.8(5), N4–C10–O1 177.6(8).

Correlation of ^{13}C NMR Spectroscopic Data with Electronic Properties

Before we go into details of the analysis, the following point deserves a special mention. As anticipated, only a small dependence of the ^{13}C NMR shifts on the solvent was observed; in general the individual chemical shifts were within a 1–2 ppm range for all solvents, that is, [D_6]benzene, [D_8]toluene, [D_8]THF, [D_2]dichloromethane. Nevertheless,

 © 2012 Wiley-VCH Verlag GmbH & Co. KGaA, Weinheim

[D_8]THF NMR spectroscopic data, when available, were used for this study. The inspection of the ^{13}C NMR spectroscopic data of the series shown below with a four-coordinate pseudo-square-planar geometry revealed a strong dependence of the ^{13}C NMR shifts of the PDI imine carbon atom (C=N) on the substituents R,X of the metal center covering a huge range of 146–180 ppm for the available iridium system.

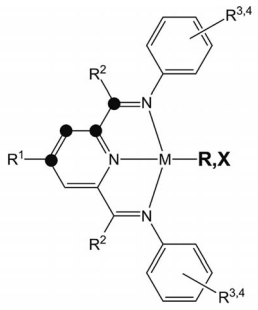

R,X = NO, N, NH_2, OH, OMe, Me, Ph, Cl, NCO, N_3. $(THF)^+$, $(CO)^+$

An excellent correlation of the ^{13}C NMR shift for the imine carbon atom with Hammett's σ_{para} parameter of the R,X group[45] was observed and is shown in Figure 13.

For the analogous Rh system, a similar correlation was observed. The range of approximately 6 ppm for the chemical shifts of the imine carbon atoms in the rhodium complexes with different R,X groups at our disposal [σ_{para}: –0.26(OMe) to 0.23(Cl)] is, however, smaller than the value of approximately 15 ppm for the analogous Ir systems. Since a larger database was available for the iridium complexes, we will focus on the complexes of the higher homologue in the following discussion.

While the ^{13}C NMR resonances of the *meta* pyridine carbon atoms remain essentially unchanged for different R,X groups, the chemical shifts of the *ortho* and *para* pyridine carbon atoms also correlate with the σ_{para} Hammett constants. The corresponding correlation coefficients of 0.83 and 0.82, respectively, are inferior, however. Also note that the CO and THF compounds, and in particular the nitrosyl and nitrido complexes (vide infra), were not included in these correlations because the Hammett constants were not available. An additional analysis of the ^{13}C NMR spectroscopic data revealed that the substitution pattern of the N-aryl groups, for example, 2,6-dichloro or -dialkyl groups, has only little influence on the ^{13}C NMR spectroscopic data. This is not surprising, considering that the planes between the aryl rings of the N-imine substituent and the PDI ligand are almost perpendicular in all X-ray crystal structures studied so far. Therefore, only a smaller inductive rather than a mesomeric interaction between these two parts of the ligand system is anticipated. Although we have so far only limited data for two different substituents of the imine carbon atom, that is, phenyl and methyl groups, it seems that the ^{13}C NMR resonances of the central PDI framework are not affected strongly by this ligand variation.

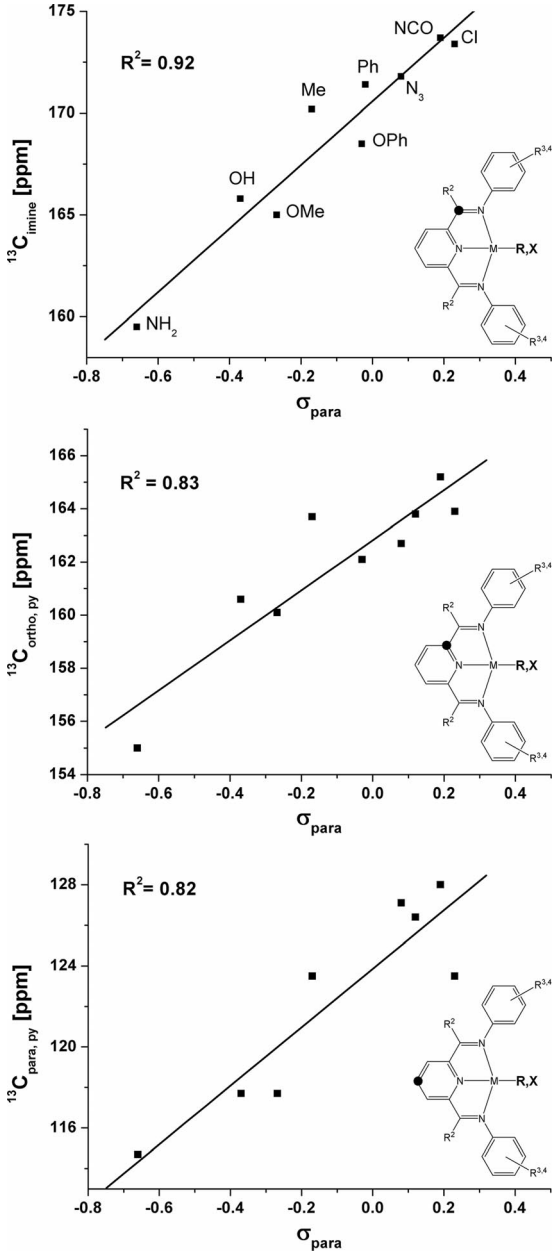

Figure 13. Dependence of the ^{13}C NMR shifts on the Hammett parameter σ_{para}. In the inset graphics of the molecules, the dot indicates the position of the carbon atom used for the plot.

These data clearly established a strong correlation of the ^{13}C NMR spectroscopic data with the electronic parameters of the complexes. As might be expected, stronger electron-withdrawing groups lead to downfield shifts of the ^{13}C NMR resonances. Further insights into this interdependence was obtained from the correlation of the ^{13}C NMR shift of the imine carbon atom with the corresponding experimental bond lengths of the imine C=N ($r_{CN,imine}$) and the exocyclic C–C bonds of the pyridine unit ($r_{CC,py}$) from X-ray crystal structure analyses (Figure 14). The other R,X groups, for which no Hammett parameters were available, could also be included in this correlation analysis. Note that

 © 2012 Wiley-VCH Verlag GmbH & Co. KGaA, Weinheim

the values for the ^{13}C NMR shifts and the bond lengths were both averaged when data for more than one representative for an R,X group were available.

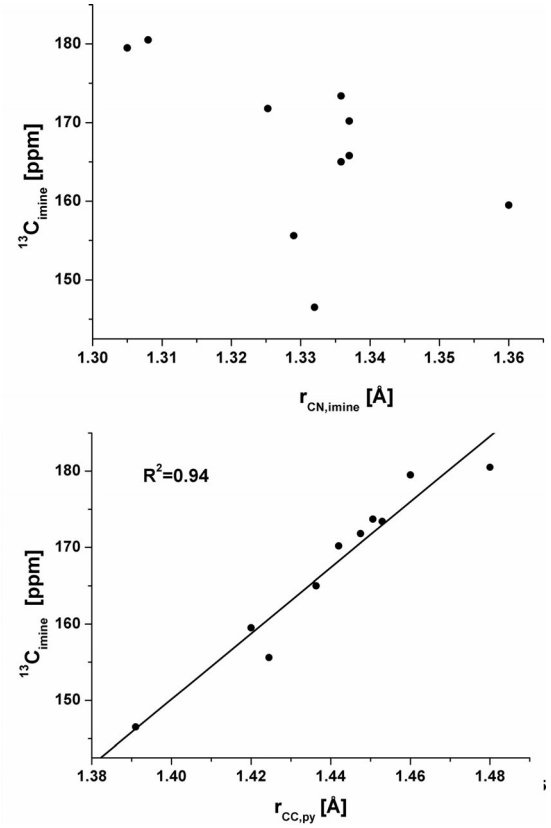

Figure 14. Plot of the ^{13}C NMR shifts of the imine carbon atom versus experimental bond lengths of the imine C–N bond (top) and the exocyclic C–C bond of the pyridine unit (bottom).

While the correlation with the C–N bond lengths, $r_{CN.imine}$, was poor, the plot of the ^{13}C NMR resonance against the exocyclic C–C bond of the pyridine unit displayed an excellent linear relationship (Figure 14, bottom). It should be noted that non-averaged data did not give a better correlation for the ^{13}C NMR shifts with $r_{CN.imine}$. We suspected that this poor correlation arose from the (available) quality of the experimental C–N bond lengths (vide infra). We therefore turned to an analogous analysis, for which DFT-calculated bond lengths were employed. The latter were derived for the small iridium model complexes shown below, in which the substituents of the imine group were replaced by hydrogen atoms.

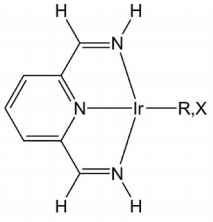

R,X = NO, N, NH_2, OH, OMe, Me,Ph
Cl, NCO, N_3. $(THF)^+$, $(CO)^+$

Considering the negligible influence of the PDI substituents on the ^{13}C NMR spectroscopic data (vide supra), this approach seemed granted. As will be shown below, it allowed to access the energy hypersurface for geometrical changes within the PDI ligand framework (vide infra) with reasonable effort.

For the calculated bond lengths, there is now a good linear relationship for the ^{13}C NMR resonances of the imine carbon atom (Figure 15, top). Note that the Mayer bond orders rather than distances are utilized in Figure 15 for better comparison with the further analysis of the ^{13}C

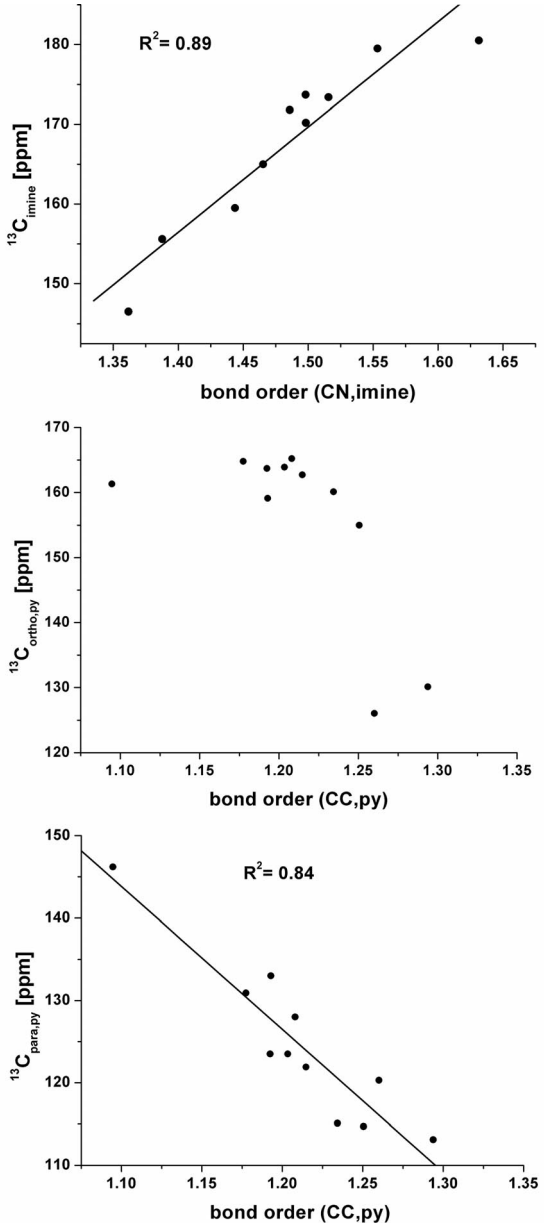

Figure 15. Correlation of experimental ^{13}C NMR shifts of the PDI ligand with calculated Mayer bond orders [traces: top, imine group; middle, pyridine 2,6-positions (*ortho*); bottom, 4-position (*para*)]. Linear regression coefficients R^2 are given, where deemed appropriate.

 © 2012 Wiley-VCH Verlag GmbH & Co. KGaA, Weinheim

NMR spectroscopic data. This approach is granted, since there is good linear relationship between the calculated values for the C–N and C–C bond orders and their distances ($r_{CN,imine}$, $r_{CC,py}$). A reasonable correlation coefficient (R^2 = 0.84) is also observed for the linear dependence of the ^{13}C NMR shifts for the pyridine carbon atoms in the *para*-positions on the calculated imine and pyridine C–N and C–C bond orders (Figure 15, bottom).

On the contrary, there appeared to be *no* (linear) correlation between the ^{13}C NMR resonance of the *ortho* carbon atoms of the pyridine ring with the bond order of the exocyclic pyridine C–C bond (Figure 15, middle). The ^{13}C NMR shifts for all but two compounds fall in the narrow range 155–160 ppm. For the remaining two complexes, that is, nitrido and nitrosyl compound **1** and **3**, the corresponding ^{13}C NMR resonances are shifted to higher field by approximately 30 ppm and are located at 126 and 131 ppm, respectively. Since the careful reinvestigation of our HSQC and HMBC data for nitrido and nitrosyl complexes **1** and **3** confirmed our previous NMR spectroscopic assignments, we had to provide a rationale for the unique position of these strongly high-field-shifted *ortho* pyridine ^{13}C NMR resonances. Initially, we wondered whether we had discovered experimental NMR spectroscopic evidence for the non-innocence of the PDI ligand in the NO and nitrido complexes.

To address this point, we calculated the ^{13}C NMR resonances for the model systems shown above with the BP86 density functional using either ZORA or Douglas-Kroll-Hess (DKH2) scalar relativistic corrections and employing either the IGLO[46] or GIAO[47] treatment. The large all-electron ZORA/DKH-optimized SARC (def2-TZVPP based) basis set was used for the Ir center,[48] while the NMR-optimized IGLO-III basis sets were utilized for the residual lighter atoms (H, C, N, O, Cl). The plot of the experimental versus calculated ^{13}C NMR shifts for the ZORA (IGLO) data are shown in Figure 16. Considering that only a small model system was employed in the calculations and solvent effects were ignored, the match between the experimental and theoretical data is adequate.

The good agreement of the experimental and calculated ^{13}C NMR resonances (R^2 = 0.92) for the pyridine *ortho* carbon atoms is particularly noteworthy (Figure 16, middle). We have therefore attempted to investigate the ^{13}C NMR shifts of the *ortho* pyridine (and other) carbon atoms in more detail by natural chemical shielding analysis (NCS) within the framework of NBO theory.[49] While this proved to be complicated because of the highly delocalized electronic structure of the PDI iridium complexes, the individual MO contributions to the shielding tensor of the *ortho* pyridine carbon atoms provided the necessary hints. A comparison of the data for all differently substituted model complexes revealed an exclusive (additional) feature for the NO and nitrido complexes, that is, significant MO contributions to the σ_{zz} component of the shielding tensor. The involved MOs correspond to the HOMOs in these two complexes (Figure 17); the relevant orbitals of the excited state for the application of Cornwell's orbital rotation model[50]

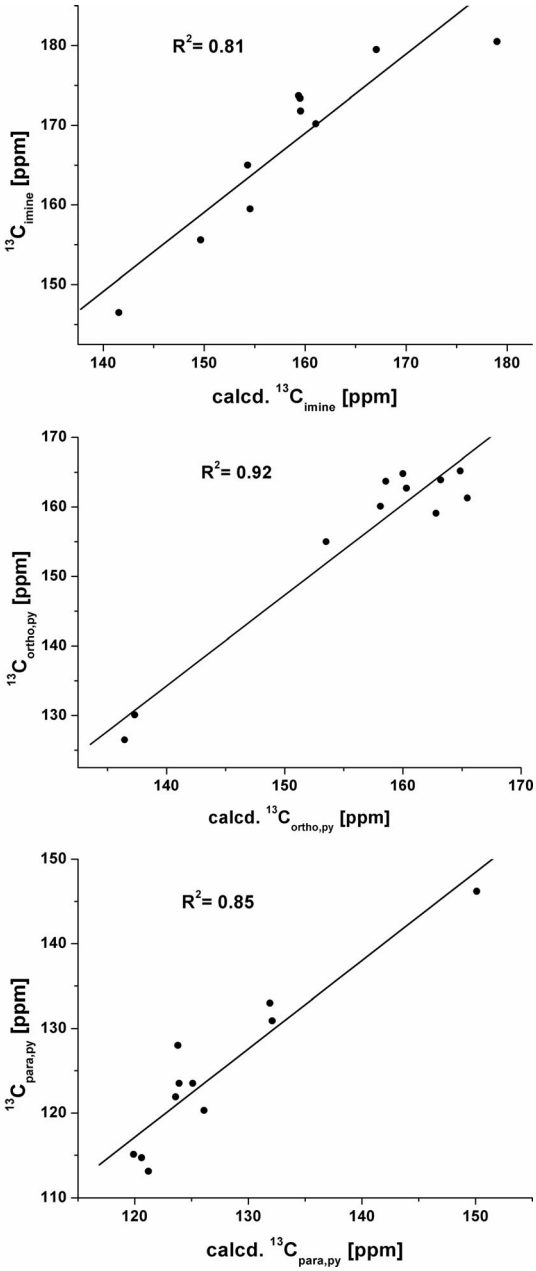

Figure 16. Plots of the experimental (ordinate) against calculated (abscissa) ^{13}C NMR shifts in the PDI ligand of the model compounds [top: imine group; middle, pyridine 2,6-positions (*ortho*); bottom, 4-position (*para*)].

are readily identified as the LUMOs in these complexes (Figure 17).

The orbital energies of the Kohn–Sham orbitals (BP86 functional) corresponding to the LUMOs in **1** and **3** are only about 1.1 eV above the position of the HOMOs. A large contribution to the chemical shift is therefore expected, considering the inverse relationship of the contribution of the energy gap, ΔE, to the chemical shielding tensor: $\sigma \approx 1/\Delta E$.[51] The energy gap ΔE corresponds to the excitation energy for the one-electron magnetic dipole transition $b_2 \rightarrow b_1$.

 © 2012 Wiley-VCH Verlag GmbH & Co. KGaA, Weinheim

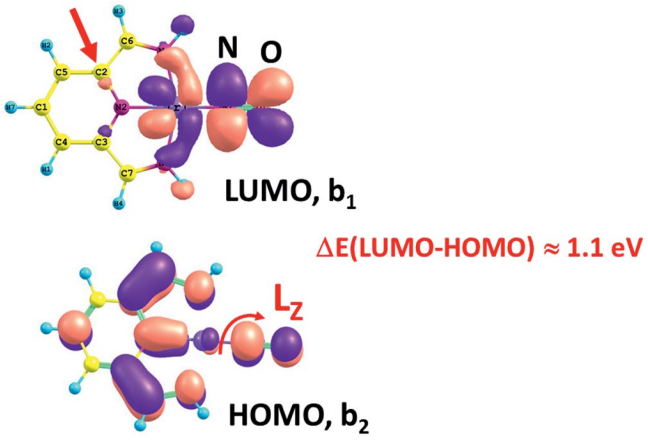

Figure 17. Additional contribution to the ^{13}C NMR shielding tensor for PDI complexes with metal–ligand multiple bond character. The involved orbitals for the model complex of nitrosyl compound **3** are shown.

The HOMO of nitrido and nitrosyl complexes **1** and **3** is readily recognized as the aforementioned b_2 orbital involved in electron transfer with additional contributions from the remaining fourth ligand. The LUMO displays b_1 symmetry for both the nitrido and the nitrosyl complexes, **1**, **3**, and corresponds to the π*-antibonding orbital of the metal–ligand multiple M–N(O) bond. One of the factors determining the magnitude of the local magnetic field contributing to the shielding tensor is the integral $<\Psi_{LUMO}|L_z|\Psi_{HOMO}>$. The latter is nonzero, which can easily be seen from its totally symmetrical direct product $a_1 = b_1(LUMO) \times a_2(L_z) \times b_2$ (HOMO). The action of L_z can be visualized as a 90-degree rotation of the HOMO about the *z* axis. While the orbitals b_1 and b_2 are orthogonal, the 90°-rotated b_2 orbital readily overlaps with the b_1 orbital in the *yz*-plane of the molecules, therefore contributing strongly to the shielding tensor. From this analysis, it becomes clear that only complexes with unoccupied low-lying orbitals of b_1 symmetry display this additional contribution to the NMR shielding tensor. This is the case for complexes with multiple bonds, which provide π*-antibonding orbitals in the molecular plane. This view was confirmed by calculations for the model carbyne complex, that is, (PDI)Ir≡CH, which also displays a significant high-field shift of the *ortho*-pyridine ^{13}C NMR resonance (δ =136.7 ppm, see Supporting Information).

For the cationic carbonyl complex, (PDI)Ir–CO^+, a similar situation might be anticipated. However, both the experimental and calculated ^{13}C NMR shifts of 161.3 and 165.5 ppm, respectively, for the *ortho* pyridine carbon atoms provide strong arguments against this view. The analysis of the shielding tensor indeed showed the absence of such a contribution. This was readily conceived upon inspection of the frontier orbitals. In contrast to nitrosyl and nitrido compounds, the necessary b_2 symmetrical orbital is *unoccupied* in the carbonyl complex. It can therefore not contribute in the sense of the aforementioned mechanism.

In the course of this investigation, the frontier orbitals of all complexes were inspected for occupations of the PDI-ligand-based a_2 and b_2 orbitals. The result is compiled in Table 2.

The orbital of a_2 symmetry was found for all molecules in the low energetic LUMO range. This is contrary to the b_2 symmetrical orbital, which is filled for *all molecules but the carbonyl and THF complexes*. The contributions to the b_2 orbital from the PDI ligand, the Ir center, and the residual R,X group was analyzed by Mulliken population analysis. The values of 67 and 72% for the contributions of the PDI ligand in the nitrido and nitrosyl model compounds, respectively, were in full agreement with our line of arguments to ascribe a non-innocent character (PDI^{2-}) to the ligand in these complexes. The assignment was also a facile task in the hydrido model compound, where the Mulliken population analysis revealed a significantly larger contribution for the Ir center (63%), and hence an innocent PDI ligand. Nevertheless, the issue became complicated for the chlorido and amido model compounds (X = Cl, R = NH_2). For both systems, the PDI ligands contributed more strongly to the b_2 orbital than the metal center. While the situation for the chlorido complex is almost balanced [45% (PDI), 37% (Ir)], the situation is more straightforward for the amido complex. For this (PDI)Ir–NH_2 model complex, Mulliken population analysis clearly speaks in favor of a non-innocent ligand. It deserves special mention that we noted only a negligible dependence of these values for the latter complex on either basis set (def2-TZVPP vs. def2-SVP) of the DFT functional (BP86, PBE, B3LYP), crediting the aforementioned values of the Mulliken population analysis. One can certainly argue about the reliability of the Mulliken population analysis;[52] it cannot be denied, however, that the observed trend of the experimental ^{13}C NMR spectroscopic data is reflected. We are nevertheless somehow reluctant to make a full cut based on the Mulliken population analysis for the chlorido and amido model complexes, since this would require the assignment of formal d^6 configurations to the Ir^{III} metal centers in these complexes.[53] We have therefore intended to include additional diagnostic criteria discussed in the next section for our final judgment. As discussed previously by several authors, the occupation of the b_2 orbital, which is antibonding and bonding with regard to the imine C=N and the exocyclic C–C pyridine units, respectively, leads to a decrease and increase of the corresponding bond orders, viz. longer and shorter bonds.[15a,16,17,54] This is clearly reflected in the DFT-calculated C_{imine}–N_{imine} and C_{imine}–$C_{pyridine}$ bond lengths and Mayer bond orders. As Pople and Karplus showed, the effect of increased charge on ^{13}C NMR resonances can also be expressed in terms of the corresponding Mayer bond orders of the involved carbon atoms.[55] This readily explains the observed excellent correlation of the electronic parameters of the Ir–R,X unit measured by the Hammett σ_{para} parameter with the ^{13}C NMR resonances. Within the series of the same transition metal, the ^{13}C NMR resonance can be directly used as a measure for the amount of back-donation from the metal center. Due the

 © 2012 Wiley-VCH Verlag GmbH & Co. KGaA, Weinheim

larger variation of the chemical shifts and to avoid additional contributions to the shielding tensors, it is advisable to employ the ^{13}C NMR resonance of the imine group for this probe. Finally, it should be concluded that the electron transfer from the metal centers (Ir–R,X fragments) to the PDI ligand displays a smooth transition, that is, there is no discontinuity for systems that might be anticipated to contain non-innocent PDl ligands, for example, nitrosyl and nitrido compounds **1** and **3**.

X-ray Crystallography

Previously, the metric parameters of the imine C=N and exocyclic C–C bonds of the pyridine unit in the PDI ligand were used with success to establish its non/innocence.[15a,16–17] We have therefore also attempted to correlate the experimentally determined C_{imine}–$C_{pyridine}$ and C_{imine}–N_{imine} bond lengths with the Hammett parameter σ_{para}. The experimental data were averaged for the series of iridium systems independent of the substitution pattern of the PDI ligand and are compiled in Table 3.

Table 3. Averaged X-ray crystallographically determined C–N and C–C bond lengths in (PDI)Ir ligand complexes. (For typical esd values, see section "Syntheses and X-ray Crystal Structures").

Ligand R,X in (PDI)Ir–R,X complexes	$r_{CC,py}$ [Å]	$r_{CN,imine}$ [Å]
$(CO)^+$	1.480	1.308
$(THF)^+$	1.460	1.305
NCO	1.456	1.327
N_3	1.448	1.325
Cl	1.453	1.336
Me	1.442	1.337
OMe	1.430	1.338
OH	1.436	1.337
NH_2	1.420	1.360
N	1.425	1.329
NO	1.391	1.332

The plot of the experimental bond lengths for the exocyclic C–C bond of the pyridine unit against σ_{para} displays an excellent linear relationship with a correlation coefficient R^2 = 0.98 (Figure 18). As expected, longer C–C bonds are found for more strongly electron-withdrawing groups ($> \sigma_{para}$).

An analogous plot for the imine C–N bond length against σ_{para}, on the other hand (not shown), revealed only a very poor correlation, comparable to the plot of the ^{13}C NMR spectroscopic data against the imine C–N bond length (Figure 14 top). Although the correlation for the exocyclic C–C bond length of the pyridine ring provided such an excellent result, we still had some doubts about the reliability of this type of analysis. Firstly, we looked into the correlation of the experimental and calculated bond lengths of these two bonds (Figure 19).

As expected, the correlation for the imine C–N bond was poor, while a linear relationship with a modest correlation coefficient, R^2 = 0.84, was observed for the C–C bond. In both cases, the experimental trend was reproduced. In this

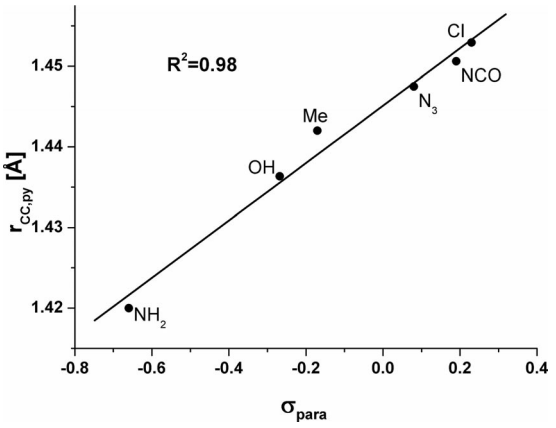

Figure 18. Dependence of the experimentally determined exocyclic C–C bond lengths of the pyridine unit on the Hammett constant σ_{para}.

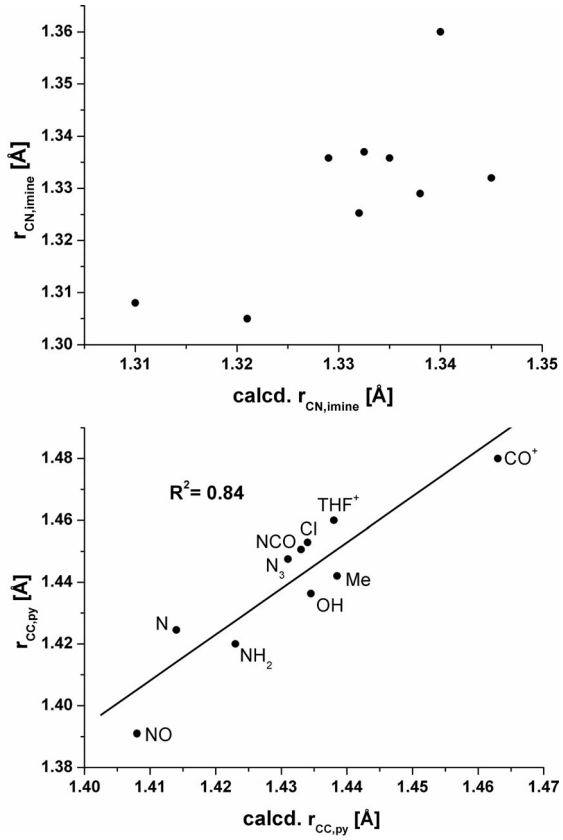

Figure 19. Correlation of the experimentally determined (ordinate) and calculated (abscissa) C–N and C–C bond lengths of the imine unit (top) and the exocyclic bond of the pyridine group in the model complexes (bottom).

context, we also analyzed the interdependence of the calculated C–N and C–C bond lengths in the imine unit and the exocyclic C–C bond of the pyridine group (Figure 20).

The inspection of Figure 20 reveals a good linear correlation with R^2 = 0.94. Note that the data of the free model ligand fits well on the slope for the model compounds: the correlation coefficient is only slightly reduced (R^2 = 0.91)

 © 2012 Wiley-VCH Verlag GmbH & Co. KGaA, Weinheim

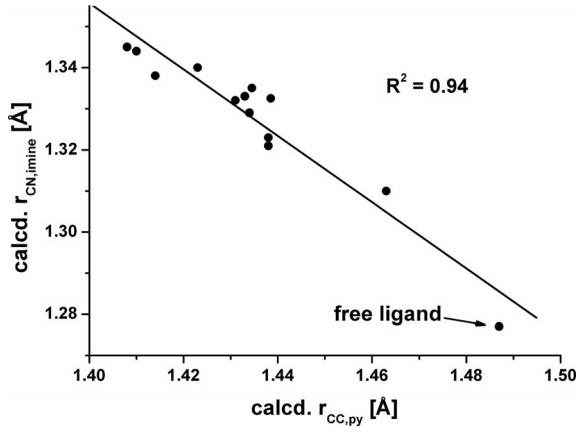

Figure 20. Plot of calculated C–N and C–C bond lengths in the imine unit and the exocyclic C–C bond of the pyridine group of the model complexes. The data of the free ligand are not included in the linear regression.

when the data of the free model ligand are included. On the basis of these results, we were therefore confident that we could learn more about the reliability of the X-ray crystallographic data from the calculations of the energetic hypersurfaces for the small model systems shown above for the two bonding parameters $r_{Cimine–Nimine}$ and $r_{Cimine–Cpy}$. The C_{2v} symmetry observed in the optimized geometries of all model systems was maintained in these calculations, which might introduce small errors for the evaluation of the energies for the distorted structures. The results for a variety of systems ranging from strong π-donors/acceptors to stronger/weaker σ-donors are presented in Figure 21.

The contour plots of the energetic hypersurfaces revealed shallow minima for all model systems.[56] Within 0.5 and 1 kcal/mol of the minima, bond length changes of approximately ±0.02 and ±0.04 Å, respectively, are within reach for all systems, and crystal packing effects might therefore easily overrule the small preference for the combination of $r_{CN,imine}$ and $r_{CC–Cpy}$. Considering (1) the typical precision of X-ray diffraction experiments for C–C bond lengths of 0.01 Å[57] and (2) the small dispersion of only 0.05 Å of the vertical plot of the bond lengths against the Hammett parameters σ_{para} (Figure 18), it is therefore surprising that such a good correlation was obtained. This result nevertheless explains the poor correlation of the experimental bond lengths of the imine bond with the calculated bond lengths (Figure 19, top) and also the experimental ^{13}C NMR shifts (Figure 14, top). Similar observations were previously made for the C–O bond lengths in metal carbonyl complexes, where large dispersions of the ν(CO) bands in the IR spectra were accompanied only by small (erroneous) bond length changes.[58] We therefore recommend the use of the imine ^{13}C NMR resonances as a more reliable probe for electron transfer to the PDI ligand, even though it is only applicable for diamagnetic compounds and requires a small series of complexes.

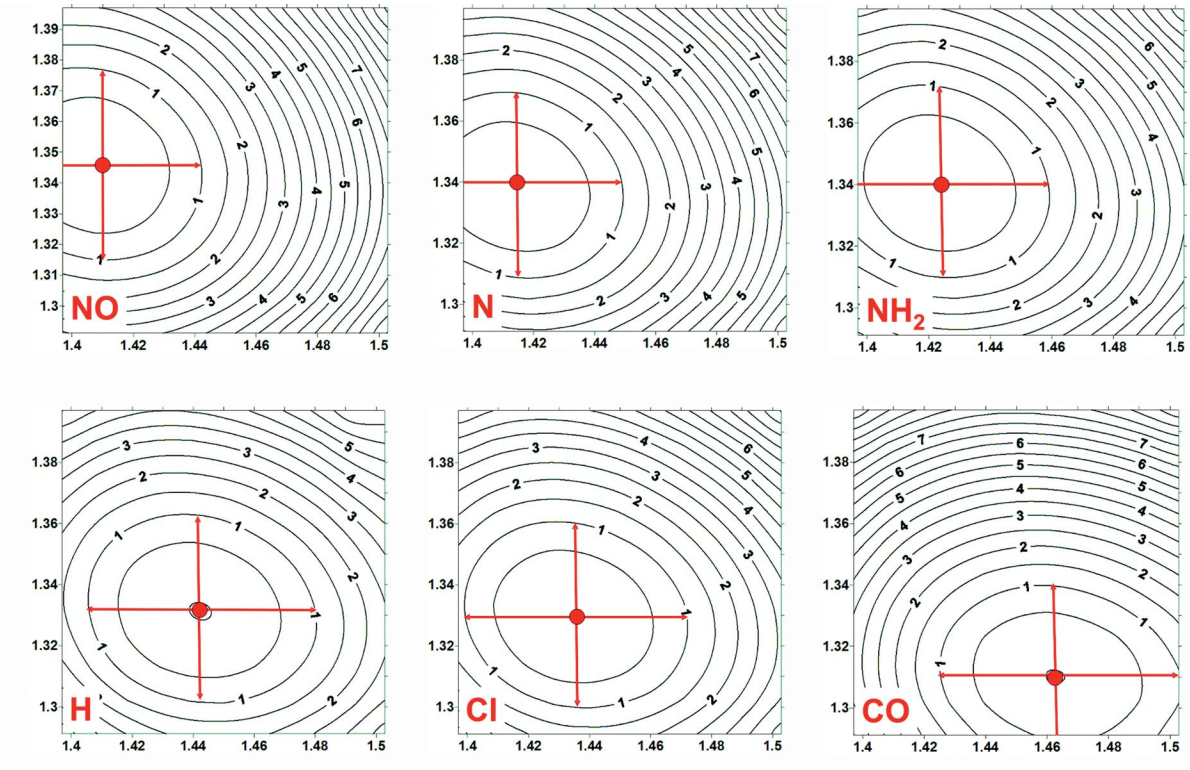

Figure 21. Contour diagrams for the dependence of the total energy [kcal/mol] on $r_{cc,py}$ and $r_{CN,imine}$ in the model systems (PDI)Ir–L. The ligand L, the minima (circle), and the 1 kcal/mol energetic range are also shown in the hypersurface plots.

 © 2012 Wiley-VCH Verlag GmbH & Co. KGaA, Weinheim

Complexes with Coordination Numbers 5 and 6

Finally, we shall briefly inspect the metric parameters of the PDI ligand in systems in which the metal centers can be safely assigned to the tervalent oxidation state. This includes the five-coordinate peroxido chlorido iridium complex **5** shown in Figure 6, for which related examples with alkyl-substituted imine groups were previously reported by Vrieze et al.[40] Furthermore, the octahedral rhodium and iridium(III) methyl, bis(triflato) complexes **7-Rh**,**Ir** presented in Figure 8 were inspected, for which an example was also reported by Brookhart et al.[13] Considering the strongly electron-withdrawing OTf ligand, the latter molecules represent interesting benchmarks for systems with reduced back-donation to the PDI ligand. For complexes with coordination numbers CN = 5, 6 and the square-planar complexes discussed above, comparison of the essential metal–ligand bonding parameters $r_{M–Nimine}$, $r_{M–Npy}$ revealed that the bond angle α remains essentially unchanged with values of approximately 155 ± 2°.

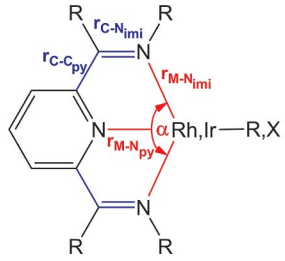

This also holds for the metal–ligand N-bond to the pyridine unit with typical bond lengths $r_{M–Npy}$ of approximately 1.90 ± 0.02 Å except for the square-planar complexes, which display a significant *trans* influence. This is the case for the methyl and nitrido iridium compounds, where $r_{M–Npy}$ amounts to 1.94 and 2.00 Å. The only notable difference is observed for the bond lengths $r_{M–Nimine}$ for the metal–imine bond. The averaged bond length $r_{M–Nimine}$ of 2.08 Å in the five- and six-coordinate complexes is considerably longer than the corresponding averaged bond length of 2.02 Å in the square-planar systems, which are nearly invariant with respect to the nature of the fourth ligand. This observation is at first glance counterintuitive, considering the more contracted tervalent metal centers (smaller ion/covalent radius) in the complexes with the higher coordination numbers. Since typically longer metal–ligand bond lengths are observed in complexes with higher coordination numbers, it is unclear whether the latter term dominates, or whether the elongated bond lengths reflect the reduced back-donation in these complexes relative to the square-planar compounds discussed above (cf. also Figure 3).

The averaged $r_{CN,imine}$ and $r_{CC,py}$ bond lengths of the imine unit and the exocyclic C–C bond of the pyridine unit amount to 1.31 and 1.48 Å, respectively, suggesting only negligible electron transfer to the imine unit in compounds **5** and **7**. There is, in fact, additional evidence for electron-deficient metal centers in these complexes. As previously noted, the size of the ^1J(C,H) coupling constant of a methyl group correlates well with the electrophilicity of the carbon atom. The observed values of up to 142 Hz for the ^1J(C,H) coupling constants for the methyl group in metal systems **7**[59] are positioned between those for methanol [^1J(C,H) = 141 Hz] and methyl iodide [^1J(C,H) = 151 Hz],[51] revealing that the tervalent PDI metal fragment is quite electron-withdrawing.

Conclusions

If a lesson is to be learnt from our study, then it is perhaps the most obvious. As the world is, in general, neither black nor white, the PDI ligand is usually neither completely innocent nor "guilty". With that we could end our conclusion; however, we will attempt to be more elaborate in our verdict. Support for this statement could be readily provided by the smooth transition of the ^{13}C NMR shifts of the PDI ligand, which display a linear relationship with the electron density of the respective carbon atoms viz. the σ_{para} Hammett parameter. With this regard, the amount of the electron transfer to the PDI ligand is best evaluated from the ^{13}C NMR shift of the carbon atom of the imine group. There are certain extremes, however, which define the borderlines, that is, nitrosyl complex **3** and its structurally closely related cationic iridium carbonyl congener **9**. These compounds differ by two electrons, of which a significant extent is transferred in nitrosyl compound **3** to the PDI ligand, which becomes $PDI^{2–}$. These two are safe bets for innocent and non-innocent cases **3** and **9**, respectively. Things start to get really complicated for nitrido complex **1** and also for the corresponding amido compound **2**. Even the experimental XPS and XAS measurements may not be of great assistance for the assignment of their oxidation states, since both methods are reference-based. These measurements for the closely related (PDI)Ir–L compounds clearly indicated the same oxidation state for L = Cl and NO, NH_2 and a higher oxidation state for nitrido complex **1** (L = N). On the basis of these data, the metal centers in the group of the first three metal complexes were assigned to the Ir^{I} oxidation state and Ir^{III} in nitrido complex **1**. Considering the close position of the ^{13}C NMR resonances of the imine carbon atoms in nitrido and amido complexes **1** and **2** and the Mulliken population analysis of **2**, however, one might also argue that the PDI ligand is non-innocent and hence the iridium center in the amido complex **2** would be tervalent Ir^{III}. Consecutively, this would render the metal center in nitrido compound **1** d^4-configured, that is, Ir^{V}, which might be admittedly closer to the chemical intuition with a $(PDI^{2–})Ir(N^{3–})$ electronic structure. The reaction of **1** with nucleophiles and the unprecedented reactivity of the Ir–N unit with H_2 might be considered as hints against this view. However, one must be aware that ground-state (thermodynamic) arguments are mixed here with kinetic considerations, that is, the electrophilicity. We highly appreciate the great achievements of expert research groups working on the issues of innocence versus non-innocence. Nevertheless and without wanting to be disrespectful, we want to conclude that we will presumably refrain in the fu-

 © 2012 Wiley-VCH Verlag GmbH & Co. KGaA, Weinheim

ture from delicate assignments of oxidation states in these compounds. We will rather study the propensity of these molecules by means of physical organic analysis and "enjoy" the high reactivity of these molecules, for which they were intentionally constructed.

Supporting Information (see footnote on the first page of this article): The complete description of the syntheses of the new compounds, together with their IR and NMR spectroscopic characterization, elemental analysis, crystallographic data, and refinement, as well as details of the DFT calculations, is reported.

Acknowledgments

We are indebted to the Swiss National Science Foundation and the Deutsche Forschungsgemeinschaft for their generous financial support over the years. Discussions with Marc Prosenc and the continuous assistance of Ulrich Behrens with the refinement of difficult X-ray data are gratefully acknowledged. They will be missed in the Department. Finally, we would like to thank all undergraduates, who contributed to this work during their practice lab in our group.

[1] R. H. Holm, *Chem. Rev.* **1987**, *87*, 1401–1449.
[2] a) J. M. Mayer, *Comments Inorg. Chem.* **1988**, *8*, 125–135; b) W. A. Nugent, J. M. Mayer, *Metal Ligand Multiple Bonds*, Wiley, New York, **1988**.
[3] a) P. R. Sharp, *Comments Inorg. Chem.* **1999**, *21*, 85–114; b) P. R. Sharp, *J. Chem. Soc., Dalton Trans.* **2000**, 2647–2657.
[4] J. Berry, *Comments Inorg. Chem.* **2009**, *30*, 28–66 and references specified therein.
[5] a) T. M. Anderson, R. Cao, E. Slonkina, B. Hedman, K. O. Hodgson, K. I. Hardcastle, W. A. Neiwert, S. Wu, M. L. Kirk, S. Knottenbelt, E. C. Depperman, B. Keita, L. Nadjo, D. G. Musaev, K. Morokuma, C. L. Hill, *J. Am. Chem. Soc.* **2005**, *127*, 11948–11949; b) T. M. Anderson, W. A. Neiwert, M. L. Kirk, P. M. B. Piccoli, A. J. Schultz, T. F. Koetzle, D. G. Musaev, K. Morokuma, R. Cao, C. L. Hill, *Science* **2004**, *306*, 2074–2077; c) R. Cao, T. M. Anderson, P. M. B. Piccoli, A. J. Schultz, T. F. Koetzle, Y. V. Geletii, E. Slonkina, B. Hedman, K. O. Hodgson, K. I. Hardcastle, X. Fang, M. L. Kirk, S. Knottenbelt, P. Körgerler, D. G. Musaev, K. Morokuma, M. Takahashi, C. L. Hill, *J. Am. Chem. Soc.* **2007**, *129*, 11118–11133.
[6] a) I. Efremenko, E. Poverenov, J. M. L. Martin, D. Milstein, *J. Am. Chem. Soc.* **2010**, *132*, 14886–14900; b) E. Poverenov, I. Efremenko, A. I. Frenkel, Y. Ben-David, L. J. W. Shimon, G. Leitus, L. Konstantinovski, J. M. L. Martin, D. Milstein, *Nature* **2008**, *455*, 1093–1096. So far no X-ray crystal structure has been reported for this oxo complex.
[7] J. Schöffel, A. Y. Rogachev, S. DeBeer George, P. Burger, *Angew. Chem.* **2009**, *121*, 4828; *Angew. Chem. Int. Ed.* **2009**, *48*, 4734–4738.
[8] a) J. Schöffel, N. Šušnjar, S. Nückel, D. Sieh, P. Burger, *Eur. J. Inorg. Chem.* **2010**, 4911–4915; b) D. Sieh, J. Schöffel, P. Burger, *Dalton Trans.* **2011**, *40*, 9512–9524.
[9] V. C. Gibson, C. Redshaw, G. A. Solan, *Chem. Rev.* **2007**, *107*, 1745–1776.
[10] S. Nückel, P. Burger, *Organometallics* **2000**, *19*, 3305–3311.
[11] G. J. P. Britovsek, M. Bruce, V. C. Gibson, B. S. Kimberley, P. J. Maddox, S. Mastroianni, S. J. McTavish, C. Redshaw, G. A. Solan, S. Strömberg, A. J. P. White, D. J. Williams, *J. Am. Chem. Soc.* **1999**, *121*, 8728–8740.
[12] B. L. Small, M. Brookhart, A. M. A. Bennett, *J. Am. Chem. Soc.* **1998**, *120*, 4049–4050.
[13] E. L. Dias, M. Brookhart, P. S. White, *Organometallics* **2000**, *19*, 4995–5004.
[14] S. Nückel, P. Burger, *Organometallics* **2001**, *20*, 4345–4359.
[15] a) P. H. M. Budzelaar, B. de Bruin, A. W. Gal, K. Wieghardt, J. H. van Lenthe, *Inorg. Chem.* **2001**, *40*, 4649–4655; b) B. de Bruin, E. Bill, E. Bothe, T. Weyhermüller, K. Wieghardt, *Inorg. Chem.* **2000**, *39*, 2936–2947.
[16] Q. Knijnenburg, S. Gambarotta, P. H. M. Budzelaar, *Dalton Trans.* **2006**, 5442–5448.
[17] S. C. Bart, K. Chłopek, E. Bill, M. W. Bouwkamp, E. Lobkovsky, F. Neese, K. Wieghardt, P. J. Chirik, *J. Am. Chem. Soc.* **2006**, *128*, 13901–13912.
[18] S. K. Russell, J. M. Darmon, E. Lobkovsky, P. J. Chirik, *Inorg. Chem.* **2010**, *49*, 2782–2792.
[19] a) Q. Knijnenburg, D. G. H. Hetterscheid, T. M. Kooistra, P. H. M. Budzelaar, *Eur. J. Inorg. Chem.* **2004**, 1204–1211; b) A. C. Bowman, C. Milsmann, E. Bill, E. Lobkovsky, T. Weyhermüller, K. Wieghardt, P. J. Chirik, *Inorg. Chem.* **2010**, *49*, 6110–6123.
[20] S. Nückel, P. Burger, *Angew. Chem.* **2003**, *115*, 1670; *Angew. Chem. Int. Ed.* **2003**, *42*, 1632–1636.
[21] T. A. Albright, J. K. Burdett, M. H. Whangbo, *Orbital Interactions in Chemistry*, Wiley, New York, Chichester, **1985**.
[22] D. Zhu, I. Thapa, I. Korobkov, S. Gambarotta, P. H. M. Budzelaar, *Inorg. Chem.* **2011**, *50*, 9879–9887.
[23] D. Zhu, P. H. M. Budzelaar, *Organometallics* **2008**, *27*, 2699–2705.
[24] S. F. Vyboishchikov, G. Frenking, *Chem. Eur. J.* **1998**, *4*, 1439–1448.
[25] H. F. Luecke, R. G. Bergman, *J. Am. Chem. Soc.* **1998**, *120*, 11008–11009.
[26] R. Mössbauer, *Z. Phys.* **1958**, *151*, 124–143.
[27] G. J. Leigh, W. Bremser, *J. Chem. Soc., Dalton Trans.* **1972**, 1216–1219.
[28] G.-B. Richter-Addo, P. W. Legzdins, *Metal Nitrosyls*, Oxford University Press, Oxford, **1992**.
[29] J. L. DuBois, P. Mukherjee, T. D. P. Stack, B. Hedman, E. I. Solomon, K. O. Hodgson, *J. Am. Chem. Soc.* **2000**, *122*, 5775.
[30] J. Bendix, K. Meyer, T. Weyhermüller, E. Bill, N. Metzler-Nolte, K. Wieghardt, *Inorg. Chem.* **1998**, *37*, 1767–1117.
[31] J. H. Enemark, R. D. Feltham, *Coord. Chem. Rev.* **1974**, *13*, 339–406.
[32] V. K. Landryand, K. Pang, S. M. Quan, G. Parkin, *Dalton Trans.* **2007**, *8*, 820–824.
[33] J. A. McCleverty, *Chem. Rev.* **2004**, *104*, 403–418.
[34] X.-Y. Yi, T. C. H. Lam, Y.-K. Sau, Q. F. Zhang, I. Williams, W.-H. Leung, *Inorg. Chem.* **2007**, *46*, 7193–7198.
[35] D. S. Williams, T. J. Meyer, P. S. White, *J. Am. Chem. Soc.* **1995**, *117*, 823–824.
[36] Y. Chen, F.-T. Lin, R. E. Shepherd, *Inorg. Chem.* **1999**, *38*, 973–998.
[37] CCDC-845993 (for **4^{c}-Ir**), -845002 (for **4^{f}-Rh**), -845001 (for **4^{f}-Ir**), -845780 (for **4^{g}-Rh**), -845997 (for **5^{a}-Ir**), -713138 (for **6^{c}-Ir**), -845781 (for **6^{d}-Ir**), -845782 (for **7^{c}-Ir**), -845003 (for **7^{d}-Ir**), -845995 (for **8^{a}-Rh^{OTf}**), -845994 (for **8^{a}-Ir^{OTf}**), -845004 (for **8^{c}-Ir^{Al}**), -845783 (for **8^{f}-Rh^{OTf}**), -845005 (for **9^{a}-Ir**), -845996 (for **10^{a}-Rh**), -845784 (for **10^{c}-Ir**), -845785 (for **10^{g}-Rh**), -845787 (for **11^{a}-Ir**), and 845786 (**12^{c}-Ir**) contain the supplementary crystallographic data for this paper. These data can be obtained free of charge from The Cambridge Crystallographic Data Centre via www.ccdc.cam.ac.uk/data_request/cif.
[38] R. R. Cramer, J. A. McCleverty, J. Bray, *Inorg. Synth.* **1990**, *28*, 86–88.
[39] M. A. Arthurs, J. Bickerton, S. R. Stobart, J. Wang, *Organometallics* **1998**, *17*, 2743–2750.
[40] H. F. Haarman, F. R. Bregman, P. W. N. M. van Leeuwen, K. Vrieze, *Organometallics* **1997**, *16*, 979–985.
[41] L. Vaska, *Acc. Chem. Res.* **1976**, *9*, 175–183.
[42] H. A. O. Hill, D. G. Tew in *Comprehensive Coordination Chemistry Vol. 2* (Eds.: G. Wilkinson, R. D. Gillard, J. A. McCleverty), Pergamon Press, Oxford, **1987**, pp. 315–333.

 © 2012 Wiley-VCH Verlag GmbH & Co. KGaA, Weinheim

[43] J. Díez, M. P. Gamasa, J. Gimeno, P. Paredes, *Organometallics* **2005**, *24*, 1799–1802.
[44] a) W. Beck, W.-P. Fehlhammer, P. Pöllmann, H. Schächl, *Chem. Ber.* **1969**, *102*, 1976–1987; b) K. Nakamoto, *Infrared and Raman Spectra of Inorganic and Coordination Compounds B*, 5th ed., John Wiley & Sons, New York, **1997**.
[45] C. Hansch, A. Leo, R. W. Taft, *Chem. Rev.* **1991**, *91*, 165–195.
[46] M. Schindler, W. Kutzelnigg, *J. Chem. Phys.* **1982**, *76*, 1919–1933.
[47] M. Kaupp, M. Bühl, V. Malkin, *Calculation of NMR and EPR Parameters*, Wiley-VCH, Weinheim, **2004**.
[48] D. A. Pantazis, X.-Y. Chen, C. R. Landis, F. Neese, *J. Chem. Theory Comput.* **2004**, *4*, 908–919.
[49] J. Bohmann, F. Weinhold, T. Farrar, *J. Chem. Phys.* **1997**, *107*, 1173–1184.
[50] C. D. Cornwell, *J. Chem. Phys.* **1966**, *44*, 874–880.
[51] H.-O. Kalinowski, S. Berger, S. Braun, *^{13}C-NMR-Spektroskopie*, Thieme, Stuttgart, **1984**.
[52] F. Jensen, *Introduction to Computational Chemistry*, John Wiley & Sons, West Sussex, **2007**.
[53] The transfer of only one electron from the metal center to the PDI ligand (PDI^{1-}) was left out in the discussion. This would lead to a d^7-configured iridium(II) center, which ought to couple antiferromagnetically to the doublet state of PDI^{1-} to adhere to the observed diamagnetism in **2** (as in all these complexes). A related line of arguments holds for the transfer of three electrons to the PDI ligand. We have clearly ruled out such a scenario for nitrido complex **1** by broken symmetry DFT and multireference calculations and might pursue this type of analysis for amido compound **2** in the near future.
[54] A. Bowman, C. Milsmann, C. C. H. Atienza, L. Lobkovsky, K. Wieghardt, P. J. Chirik, *J. Am. Chem. Soc.* **2010**, *132*, 1676–1684.
[55] M. Karplus, J. A. Pople, *J. Chem. Phys.* **1963**, *38*, 2803–2807.
[56] We have also calculated hypersurfaces for the dependence of the ^{13}C NMR resonances of the imine carbon atoms on these two bond lengths. These plots are provided in the Supporting Information.
[57] F. H. Allen, O. Kennard, D. G. Watson, L. Brammer, A. G. Orpen, R. Taylor, *J. Chem. Soc. Perkin Trans. 2* **1987**, S1–S19.
[58] C. Elschenbroich, A. Salzer, *Organometallics 2nd edition*, Wiley-VCH Weinheim, New York, **1982**.
[59] S. Nückel, Dissertation, University of Zürich, **2002**.

Received: October 7, 2011
Published Online: January 5, 2012

 © 2012 Wiley-VCH Verlag GmbH & Co. KGaA, Weinheim

DOI: 10.1002/ejic.201101352

Unexpected Formation of a Cobalt(III) Phenoxazinylate Electron Reservoir

Frank D. Lesh,[a] Richard L. Lord,*[a] Mary Jane Heeg,[a] H. Bernhard Schlegel,[a] and Cláudio N. Verani*[a]

Keywords: Coordination chemistry / Redox-active ligands / Cobalt / Electrochemistry / Density functional calculations

The redox-active ligand *N*,*N*′-bis(3,5-di-*tert*-butyl-2-hydroxyphenyl)-1,2-phenylenediamine (H_4L), known for supporting catalytic processes with both late and early transition metals, unexpectedly undergoes an unusual and thus far unobserved cyclization. Upon equimolar treatment of a cobalt(II) salt in the presence of Et_3N under aerobic conditions, a ligand rearrangement occurs to afford an unprecedented phenoxazinyl radical moiety (L′). The resulting bisligated Co complex, thoroughly characterized structurally and electronically and analyzed by multiple experimental and computational approaches, is presented. It is shown to traverse oxidation states from 2+ to 3–, spanning a thermodynamic window of approximately 2 V.

Introduction

There is considerable interest in the development and characterization of redox-active ligands with finely tuned potentials that act as electron reservoirs during catalytic processes.[1] Among an ever growing group of such redox-active ligands, the species *N*,*N*′-bis(3,5-di-*tert*-butyl-2-hydroxyphenyl)-1,2-diamine (H_4L) has received substantial attention.[2–5] Coordination compounds with this ligand demonstrate catalytic behavior in pseudo-octahedral complexes with early transition metals and square-planar complexes with late transition metals. Such metal complexes mediate reductive bond formation[3–5] and bioinspired aerobic oxidation,[2] respectively, partially due to five ligand-based discrete oxidation levels. When complexed to metals, the most commonly observed ligand oxidation state is 2– ($H_4L \rightarrow L^{2-} + 4H^+ + 2e^-$, Scheme 1 left), which can be written with both closed shell[2] and diradical electron configurations (only one shown). To the best of our knowledge, however, similar adducts with middle 3d metals (Mn, Fe, Co) have not received similar attention, despite the intriguing combination of this ligand with redox-rich metals.[1,6–8] Towards this goal, we report here an unprecedented ligand transformation of L^{2-} whereby one of the phenolate/phenoxyl arms has cyclized to form a mixed phenolate/phenoxazinyl radical species, which we denote L'^{2-} ($L^{2-} \rightarrow L'^{2-} + H^+ + e^-$, Scheme 1 right).

Phenoxazines, found in nature as potent chromophores,[9–11] demonstrate efficient electron transfer and high luminescence quantum yields required for organic light-emitting diodes and dye-sensitized solar cells.[12] Pierpont et al. observed a related transformation involving cyclization of a Schiff base biquinone ligand to confer a phenoxazinylate radical anion.[13,14] Defining a ligand shorthand for this new ligand is complicated by the fact that the bridging amide can conjugate with both arms. In the past, there has been reference to imino and diimino catecholate/semiquinonate redox behavior when it was straightforward to group this nitrogen atom with a single arm of the ligand, phenolate or phenoxazinylate, respectively. We prefer to discuss the ligand as three fragments (Scheme 1, right): (i) the phenolate (PhO^-, left box), (ii) the bridging amide (N^-, overlap between boxes), and (iii) the phenoxazinyl radical (Phz˙, right box). Thus, L'^{2-} is abbreviated PhO^-–N^-–Phz˙. While this description is inherently too localized a description, it emphasizes correctly whether the phenoxazinyl or the phenolate arm is the major contributor to a given redox process.[15] Herein, we describe the synthesis and characterization of the species $[Co(L')_2]^0$ along with its rich redox chemistry.

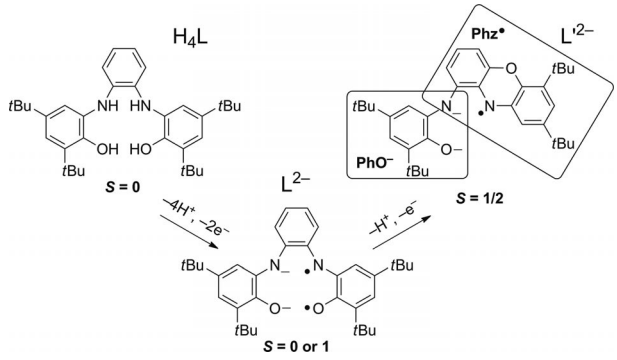

Scheme 1.

[a] Department of Chemistry, Wayne State University
5101 Cass Avenue, Detroit, MI 48202, USA
E-mail: cnverani@chem.wayne.edu
rllord@chem.wayne.edu

Supporting information for this article is available on the WWW under http://dx.doi.org/10.1002/ejic.201101352.

 © 2012 Wiley-VCH Verlag GmbH & Co. KGaA, Weinheim

Results and Discussion

Condensation of 3,5-di-*tert*-butylcatechol and *o*-phenylenediamine (2:1) together with Et_3N in *n*-heptane generates H_4L after four days of stirring at ambient temperature under aerobic conditions.[2,4] Equimolar treatment of H_4L with anhydrous $CoCl_2$ in the presence of Et_3N under aerobic conditions in acetonitrile afforded a microcrystalline precipitate of $[Co(L')_2]^0$. This stoichiometry does not seem to be affected by 1:1 vs. 2:1 H_4L/Co^{II} loadings or by the equivalents of added base (see Supporting Information). Dark green crystals suitable for X-ray analysis were obtained by slow evaporation from a CH_2Cl_2/CH_3CN mixture (1:1), and the unanticipated bisligated structure, in which each ligand is coordinated in a [O–N–N′] (O1–N1–N2/O3–N3–N4) meridional fashion, is presented in Figure 1. It is tempting to assign this neutral species as $[Co^{II}(L'^{1-})_2]^0$ on the basis of the fairly similar bond lengths within each of the two ligands (see Supporting Information); however, averaged metal–ligand bond lengths of 1.896 ± 0.004, 1.882 ± 0.006, and 1.955 ± 0.002 Å for Co–O, Co–N, and Co–N′, respectively, strongly imply a low-spin cobalt(III) ($^{LS}Co^{III}$) metal center.[16–18]

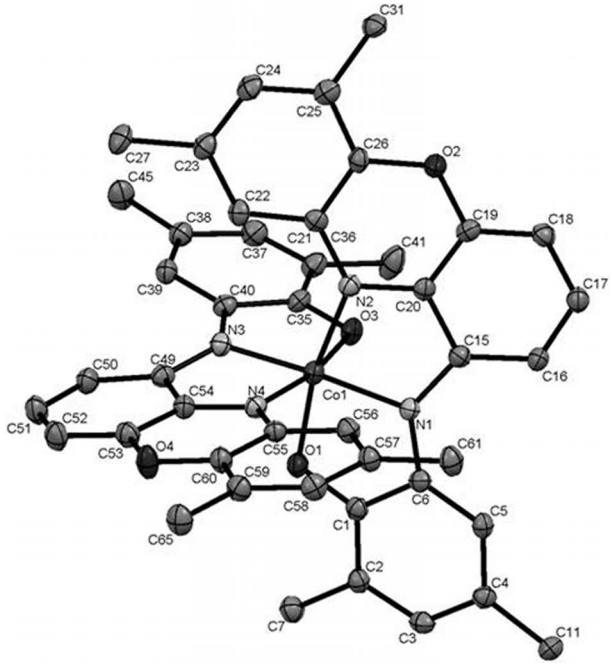

Figure 1. ORTEP diagram for $[Co(L')_2]\cdot 2MeCN$ showing 50% probability of the thermal ellipsoids. Solvent and hydrogen atoms are excluded, and the *t*Bu groups are truncated to the central quaternary carbon for clarity. Selected bond lengths (in Å) and angles (in °): Co1–N1 1.876(2), Co1–N3 1.887(2), Co1–O1 1.892(2), Co1–O3 1.899(2), Co1–N2 1.953(2), Co1–N4 1.956(2); N2–Co1–N3 104.83(8), N2–Co1–N4 92.64(8), O1–Co1–N3 86.55(7), O1–Co1–O3 91.35(7), O1–Co1–N1 84.80(7), O1–Co1–N4 89.33(7).

The formation of phenoxazinyl rings is known to occur in a basic, oxidizing medium for some aminocatechols.[19] It is noteworthy that we have observed this ligand transformation in the presence of cobalt, but not manganese or iron ions, under similar basic, oxidizing conditions.[20] One plausible difference between these metals is that the Co^{II} ion is capable of reducing dioxygen to superoxide.[21] Anaerobic mixing of H_4L and the cobalt salt affords the uncyclized metal–ligand adduct in a 2:1 ratio $[Co^{II}(HL)_2]^0$, similar to the manganese species, as suggested by ESI mass spectrometric methods (see Supporting Information). Pursuit of mechanistic details and the possible role of superoxide are ongoing, but these are beyond the scope of this communication.

In order to understand the oxidation and spin states of the metal ion and ligands in the $[Co^{III}(L')_2]$ species, we investigated multiple electronic structures with density functional theory (DFT) calculations.[22] Two low-energy structures were identified, which are best described as a $^{LS}Co^{III}$ species with one unpaired electron, $S = 1/2$ (see Supporting Information for structural details and comparison to X-ray structure). One has ligands in different oxidation states, 2– and 1–, while the other is symmetric and has formal charges of 1.5– for each ligand. We present the former, because it does not invoke fractional electron charges, but it is important to note that these species are isoenergetic, which suggests that multiple resonance forms are accessible. A corresponding orbital analysis[23] of this localized species suggests that one ligand is in the $PhO^-–N^-–Phz^{\cdot}$ oxidation state with an unpaired α electron (Figure 2 top), while the other ligand is in the $PhO^{\cdot}–N^-–Phz^{\cdot}$ oxidation state with two antiferromagnetically (AF) coupled radicals (Figure 2 bottom). The overlap of the antiferromagnetically coupled orbitals is 0.8, which is quite large and may suggest a closed-shell description. However, all attempts to compute a structure with a closed-shell, localized 1– ligand collapsed to the delocalized structure with fractional ligand charges. The EPR-derived *g* value of 2.0 is consistent with the assignment of an organic radical, and despite the known shortcomings for predicting spin states of transition metal complexes a priori, DFT seems to capture correctly the physicochemical properties of $[^{LS}Co^{III}(PhO^-–N^-–Phz^{\cdot})(PhO^{\cdot}–N^-–Phz^{\cdot})]^0$.[24,25]

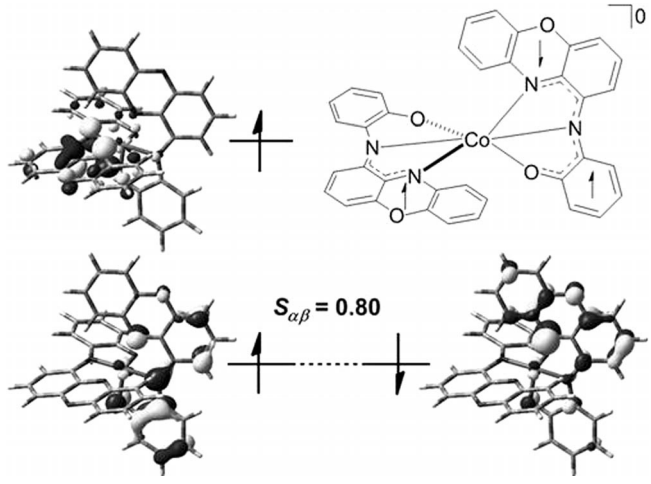

Figure 2. Contour plots (0.05 au) for the singly occupied (top) and AF coupled (bottom) orbitals resulting from the corresponding orbital analysis. $S_{\alpha\beta}$ is the overlap integral for the AF coupled corresponding orbitals.

 © 2012 Wiley-VCH Verlag GmbH & Co. KGaA, Weinheim

The unpaired electrons in the PhO^{-}–N^{-}–$Phz^{\cdot}$ and $PhO^{\cdot}$–N^{-}–$Phz^{\cdot}$ ligands should demonstrate diagnostic intra- or interligand charge-transfer bands, and we therefore measured the absorption spectrum to probe further the electronic structure.

The UV/Vis spectrum of [$^{LS}Co^{III}$(PhO^{-}–N^{-}–$Phz^{\cdot}$)($PhO^{\cdot}$–N^{-}–$Phz^{\cdot}$)] was collected in CH_2Cl_2 (see Figure 3). Prominent σ→π* and π→π* transition bands positioned at 271 nm (88770 $L\,mol^{-1}\,cm^{-1}$) are succeeded by less intense shoulders at 387 and 474 nm (16630 and 9660 $L\,mol^{-1}\,cm^{-1}$). Just beyond the visible region is a broad, low-energy band centered at 871 nm (9690 $L\,mol^{-1}\,cm^{-1}$). TD-DFT calculations corroborate the existence of a broad absorption feature around 1000 nm with an intensity of approximately 10000 $L\,mol^{-1}\,cm^{-1}$, which comprises transitions mostly corresponding to intra- and interligand charge transfers.[26] This assignment is consistent with earlier reports containing single and multiple phenoxazinylates[11,27–28] and with our hypothesis of one or more ligand-based radicals.

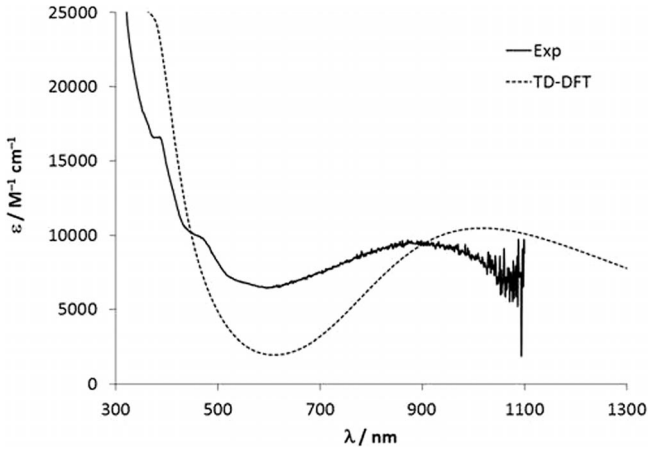

Figure 3. Experimental (solid) and simulated (dashed) UV/Vis absorption spectra of [$^{LS}Co^{III}$(PhO^{-}–N^{-}–$Phz^{\cdot}$)($PhO^{\cdot}$–N^{-}–$Phz^{\cdot}$)$_2$]^0 in CH_2Cl_2.

Because the ligand can accommodate multiple oxidation levels in the ground state of the cobalt(III) complex, we investigated the redox behavior of [$^{LS}Co^{III}$(PhO^{-}–N^{-}–$Phz^{\cdot}$)($PhO^{\cdot}$–N^{-}–$Phz^{\cdot}$)] by cyclic voltammetric methods in CH_2Cl_2 with TBA(tetra-*n*-butylammonium)PF_6 as supporting electrolyte. As Figure 4 demonstrates, five quasireversible electrochemical responses are observed between 800 and –1300 mV vs. Fc^{+}/Fc as the internal reference. The two redox couples at –1090 and –870 mV correspond to PhO^{-}–N^{-}–$Phz^{\cdot}$/PhO^{-}–N^{-}–Phz^{-}[27–29] and are consistent with the fact that the phenoxazinylate is more electron-rich than the phenolate in the fully reduced PhO^{-}–N^{-}–Phz^{-} state. The first two cathodic processes are followed at more positive potentials (–500 and –260 mV) by phenolate oxidation, $PhO^{\cdot}$–N^{-}–$Phz^{\cdot}$/PhO^{-}–N^{-}–$Phz^{\cdot}$.[30–32] This description supports qualitatively the proposed electronic structure, which has two phenoxazinyl-based radicals and one phenoxyl-based radical. The redox process at 370 mV is presumably the formal oxidation of the amide ($PhO^{\cdot}$–$N^{\cdot}$–$Phz^{\cdot}$/$PhO^{\cdot}$–N^{-}–$Phz^{\cdot}$), though the remaining charge may be quite delocalized. One further oxidation is observed at 650 mV, though this process is highly irreversible and seems to correspond to the transfer of more than one electron. If correct, this scheme suggests that the [$^{LS}Co^{III}$(PhO^{-}–N^{-}–$Phz^{\cdot}$)-($PhO^{\cdot}$–N^{-}–$Phz^{\cdot}$)] complex can access oxidation states ranging from 2+ to 3– with no metal-based redox events. We are currently pursuing a detailed experimental and computational characterization of the intermediate oxidation states within this redox series, aiming to compare them to the redox behavior of the manganese species with uncyclized ligands, [$Mn(HL)_2$].

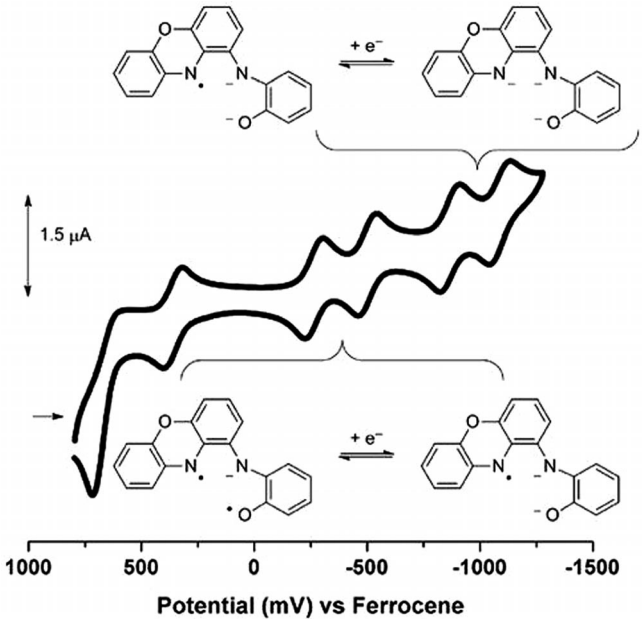

Figure 4. CV trace in CH_2Cl_2, with 0.1 M $TBAPF_6$, and 1.0×10^{-3} M [$^{LS}Co^{III}$(PhO^{-}–N^{-}–$Phz^{\cdot}$)($PhO^{\cdot}$–N^{-}–$Phz^{\cdot}$)], 150 $mV\,s^{-1}$; mV vs. Fc^{+}/Fc. Insets are representations of the cathodic ligand redox events; only one resonance structure is shown for each.

Conclusions

In summary, we report a serendipitous functionalization of the redox-active ligand H_4L in the presence of a cobalt(II) salt, affording the new mixed phenoxazinylate/phenoxylate ligand L′. Multiple oxidation levels were accessible within this ligand when templated to a $^{LS}Co^{III}$ metal center in a 2:1 ratio, which DFT describes as [$^{LS}Co^{III}$(L'^{1-})(L'^{2-})]. We anticipate the rich redox chemistry exhibited by this bisligated complex, with five reversible, one-electron responses, to be an important electron reservoir motif towards our ultimate goal of multimetallic catalytic assemblies.

Experimental Section

H_4L was prepared as described by Chaudhuri et al.,[2] by incorporating the purification steps recommended by Heyduk and coworkers,[4] in approximately 50% overall yield.

 © 2012 Wiley-VCH Verlag GmbH & Co. KGaA, Weinheim

Anhydrous $CoCl_2$ (0.130 g, 1 mmol) and Et_3N (0.2 mL) were added to a solution of H_4L (0.517 g, 1 mmol) in CH_3CN (25 mL), and the resultant mixture was heated at reflux for 1 h followed by stirring at ambient temperature for 4 h while exposed to air. A dark brown microcrystalline solid was collected by filtration and washed with CH_3CN. Yield: 40%. $C_{68}H_{86}CoN_4O_4$ (1082.4): calcd. C 75.18, H 8.35, N 5.16; found C 74.90, H 8.05, N 5.10. IR (KBr): $\tilde{\nu}$ = 2955, 2906, 2869 (νC–H, *t*Bu), 1528, 1479, 1457 (νC–O/νC–N, Phz/PhO) cm^{-1}. UV/Vis (CH_2Cl_2, 1.0×10^{-3} M): λ (ε, $L\,mol^{-1}\,cm^{-1}$) = 271 (88770); 387 sh (16630), 474 sh (9660), 871 (9690). ESI^+-MS (CH_2Cl_2): *m*/*z* (%) = 1082.61 (100%) $[M + H]^+$.

Supporting Information (see footnote on the first page of this article): Materials and methods, syntheses, ORTEP drawings for $[Co(L'^{1-})(L'^{2-})]$, $[Mn(HL)_2]$, and [Fe(L)Cl], EPR spectrum for $[Co(L'^{1-})(L'^{2-})]$, computational details (spin densities for doublets, Cartesian coordinates, frequencies, and energetics for computed structures, TD-DFT assignments).

Acknowledgments

This research was made possible by the Division of Chemical Sciences, Geosciences, and Biosciences, Office of Basic Energy Sciences of the U.S. Department of Energy (DOE-BES) through the Single-Investigator and Small-Group Research (SISGR) – Solar Energy Program Grant DE-FG02-09ER16120 to C. N. V. and H. B. S., including financial support for F. D. L. and R. L. L. The Wayne State Grid is gratefully acknowledged for supercomputing resources.

[1] W. I. Dzik, J. I. van der Vlugt, J. N. H. Reek, B. de Bruin, *Angew. Chem. Int. Ed.* **2011**, *50*, 3356–3358.
[2] P. Chaudhuri, M. Hess, J. Müller, K. Hildenbrand, E. Bill, T. Weyhermüller, K. Wieghardt, *J. Am. Chem. Soc.* **1999**, *121*, 9599–9610.
[3] K. J. Blackmore, N. Lal, J. W. Ziller, A. F. Heyduk, *J. Am. Chem. Soc.* **2008**, *130*, 2728–2730.
[4] K. J. Blackmore, N. Lal, J. W. Ziller, A. F. Heyduk, *Eur. J. Inorg. Chem.* **2009**, *6*, 735–743.
[5] A. L. Zelikoff, J. Kopilov, I. Goldberg, G. W. Coates, M. Kol, *Chem. Commun.* **2009**, 6804–6806.
[6] P. J. Chirik, K. Wieghardt, *Science* **2010**, *327*, 794–795.
[7] A. L. Smith, K. I. Hardcastle, J. D. Soper, *J. Am. Chem. Soc.* **2010**, *132*, 14358–14360.
[8] E. P. Ivakhnenko, A. G. Starikov, V. I. Minkin, K. A. Lyssenko, M. Y. Antipin, V. I. Simakov, V. I. Korobov, G. S. Borodkin, P. A. Knyazev, *Inorg. Chem.* **2011**, *50*, 7022–7032.
[9] D. Gegiou, J. R. Huber, K. J. Weiss, *J. Am. Chem. Soc.* **1970**, *92*, 5058–5062.
[10] C. E. Barry, P. G. Nayar, T. P. Begley, *J. Am. Chem. Soc.* **1988**, *110*, 3333–3334.
[11] C. Mukherjee, T. Weyhermüller, E. Bothe, E. Rentschler, P. Chaudhuri, *Inorg. Chem.* **2007**, *46*, 9895–9905.
[12] K. M. Karlsson, X. Jiang, S. K. Eriksson, E. Gabrielsson, H. Rensmo, A. Hagfeldt, L. Sun, *Chem. Eur. J.* **2011**, *17*, 6415–6424.
[13] L. A. DeLearie, R. C. Haltiwanger, C. G. Pierpont, *Inorg. Chem.* **1989**, *28*, 644–650.
[14] C. L. Simpson, S. R. Boone, C. G. Pierpont, *Inorg. Chem.* **1989**, *28*, 4379–4385.
[15] See Supporting Information for a scheme outlining all oxidation states of L′ in terms of PhO, N, and Phz.
[16] J. C. Jeffery, E. Schatz, M. D. Ward, *J. Chem. Soc., Dalton Trans.* **1992**, 1921–1927.
[17] C. N. Verani, S. Gallert, E. Bill, T. Weyhermüller, K. Wieghardt, P. Chaudhuri, *Chem. Commun.* **1999**, 1747–1748.
[18] R. Shakya, C. Imbert, H. P. Hratchian, M. Lanznaster, M. J. Heeg, B. R. McGarvey, M. Allard, H. B. Schlegel, C. N. Verani, *Dalton Trans.* **2006**, 2517–2525.
[19] H. B. Stegmann, K. Scheffler, *Chem. Ber.* **1968**, *101*, 262–271.
[20] Monoligated Fe and bisligated Mn complexes of uncyclized H_4L have been synthesized and characterized structurally. ORTEP diagrams for each may be found in the Supporting Information.
[21] D. H. Busch, N. W. Alcock, *Chem. Rev.* **1994**, *94*, 585–623.
[22] Calculations at the B3LYP/6-31G(d,p) level of theory were conducted on a model where *t*Bu groups have been replaced by H for computational efficiency. See Supporting Information for full details.
[23] F. Neese, *J. Phys. Chem. Solids* **2004**, *65*, 781–785.
[24] H. Paulsen, A. X. Trautwein in *Spin Crossover in Transition Metal Compounds*, Springer-Verlag, Berlin, **2004**, vol. 235, pp. 197.
[25] R. L. Lord, F. A. Schultz, M.-H. Baik, *J. Am. Chem. Soc.* **2009**, *131*, 6189–6197.
[26] TD-B3LYP/6-311+G(d,p)//B3LYP/6-31G(d,p) with IEF-PCM/CH_2Cl_2. See Supporting Information for transition assignments. An error of 130 nm seems large, but this is only 0.2 eV on an energy scale and consistent with the accuracy of the methodology.
[27] A. M. Whalen, S. Bhattacharya, C. G. Pierpont, *Inorg. Chem.* **1994**, *33*, 347–353.
[28] G. Speier, A. M. Whalen, J. Csihony, C. G. Pierpont, *Inorg. Chem.* **1995**, *34*, 1355–1360.
[29] S. Bhattacharya, C. G. Pierpont, *Inorg. Chem.* **1992**, *31*, 2020–2029.
[30] P. Chaudhuri, C. N. Verani, E. Bill, E. Bothe, T. Weyhermüller, K. Wieghardt, *J. Am. Chem. Soc.* **2001**, *123*, 2213–2223.
[31] K. S. Min, T. Weyhermüller, K. Wieghardt, *Dalton Trans.* **2004**, 178–186.
[32] S. Mukherjee, T. Weyhermüller, E. Bill, K. Wieghardt, P. Chaudhuri, *Inorg. Chem.* **2005**, *44*, 7099–7108.

Received: December 2, 2011
Published Online: December 20, 2011

 © 2012 Wiley-VCH Verlag GmbH & Co. KGaA, Weinheim

DOI: 10.1002/ejic.201100798

A Redox-Active Ligand as a Reservoir for Protons and Electrons: O_2 Reduction at Zirconium(IV)

Feng Lu,[a] Ryan A. Zarkesh,[a] and Alan F. Heyduk*[a]

Keywords: Redox-active ligands / Zirconium / Oxygen reduction / Redox chemistry / Structure elucidation

The [ONO] ligand {$(ONO^{cat})^{3-}$ = bis(3,5-di-*tert*-butyl-2-phenoxy)amide} can be installed onto zirconium(IV) in two different protonation states. The reaction of $(ONO^{cat})^{3-}$ with $ZrCl_4$ afforded the octahedral complex $(ONO^{cat})ZrCl(THF)_2$ (**1**). This complex, characterized in the solid state by single-crystal X-ray diffraction and in solution by NMR, UV/Vis, and IR spectroscopy, is assigned as a zirconium(IV) complex coordinated to the fully reduced form of the [ONO] redox-active ligand. When $(ONO^{cat})H_3$ was doubly deprotonated and treated with $ZrCl_4$, the complex $(ONHO)ZrCl_2(THF)$ (**2**) was isolated, in which one ligand proton remains on the [ONO] ligand. Exposure of **2** to dry O_2 resulted in a four-electron, two-proton reaction to form the bis(hydroxo) complex $[(ONO^{q})ZrCl_2(\mu\text{-}OH)]_2$ (**3**), which shows that the [ONO] ligand platform can serve as both an electron and proton reservoir in small-molecule reactions.

Introduction

The activation of O_2 by transition-metal complexes is of continuing interest for its relevance to both synthetic and biological systems.[1–6] Most studies of O_2 activation employ mid- and late transition metals owing to the existence of multiple metal oxidation states to facilitate the reduction of O_2 to superoxo, peroxo, hydroxo, or oxo ligands. In the case of early transition-metal coordination complexes, the metal ion is most often found in its maximal oxidation state, which confers a d^0 electron configuration to the metal and renders it incapable of reducing O_2. Zirconium(IV) complexes with halide, alkoxide, and amide ligands are stable in an atmosphere of dry air, though organometallic complexes do react with O_2, which results in oxidation of the alkyl ligands to the corresponding alkoxide ligands.[7–10] A notable exception to this trend is the reaction of the zirconium bis(enediamide) complex $[Zr\{(2,6\text{-}C_6H_3iPr_2)NCHCHN(2,6\text{-}C_6H_3iPr_2)\}_2]$ with O_2 to form a bis(peroxide) complex.[11] In this example, the metal center stays in the zirconium(IV) oxidation state throughout the reaction, while each ligand is oxidized by two electrons. The ligands change from the ene(diamide) form in the reactant to the diimine form in the product. Thus, in the reaction the ligands serve as an electron reservoir to help effect multielectron reactivity at a non-redox-active metal. Similar reactions with redox-active ligands have been elucidated for oxidative addition,[12–14] reductive elimination,[15] and nitrene transfer[16,17] reactivity at d^0 complexes of the group 4 and 5 metals. In this report, we extend this approach beyond the utilization of the ligands as just electron reservoirs to develop a redox-active ligand that serves as both an electron and proton reservoir for O_2 reduction.

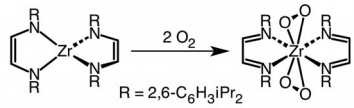

Results and Discussion

The [ONO] ligand {$(ONO^{cat})^{3-}$ = bis(3,5-di-*tert*-butyl-2-phenoxy)amide} is a well-established redox-active ligand capable of accessing multiple oxidation states when coordinated to a metal ion (Scheme 1).[18] Deprotonation of $(ONO^{cat})H_3$ with 3 equiv. *n*BuLi affords the trianionic form of the ligand, $(ONO^{cat})^{3-}$. Previous work in our laboratory has shown that $(ONO^{cat})^{3-}$ readily binds to early transition metals, adopting a *mer* coordination geometry.[19,20] Treatment of cold, ethereal solutions of freshly generated $(ONO^{cat})^{3-}$ with $ZrCl_4$ resulted in a color change to yellow and the formation of $[(ONO^{cat})ZrCl(THF)_2]$ (**1**), which was isolated as a yellow solid in 74% yield (Scheme 2).

Complex **1** was characterized in the solid state and in solution as an octahedral zirconium(IV) complex. Single crystals of **1** were deposited from solutions of the complex in a mixture of toluene and pentane chilled to –35 °C. Crystals of complex **1** belong to the tetragonal space group $P4_3$. Two toluene solvent molecules are also contained in the asymmetric unit. The structure of **1** is shown in Figure 1, and selected metrical parameters are provided in Table 1. The zirconium complex is a six-coordinate, C_{2v} structure in which the $(ONO^{cat})^{3-}$ ligand adopts the expected meridio-

[a] Department of Chemistry, University of California,
1102 Natural Sciences 2, Irvine, California 92697-2025, USA
Fax: +1-949-824-8571
E-mail: aheyduk@uci.edu

Supporting information for this article is available on the WWW under http://dx.doi.org/10.1002/ejic.201100798 or from the author.

 © 2012 Wiley-VCH Verlag GmbH & Co. KGaA, Weinheim

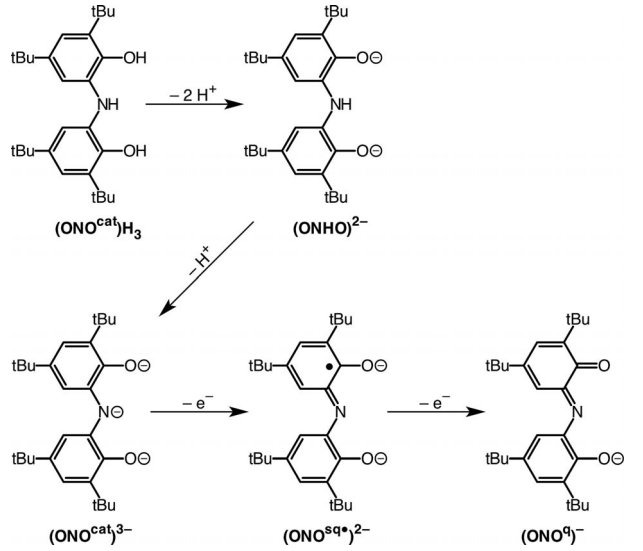

Scheme 1. Protonation and oxidation states of the [ONO] ligand platform.

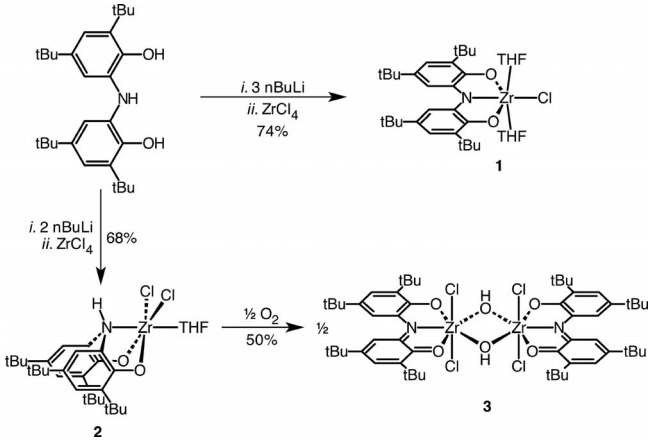

Scheme 2. Synthesis of zirconium complexes **1**, **2**, and **3**.

nal coordination geometry. The chloride ligand is *trans* to the [ONO] nitrogen atom, which leaves two *trans* coordination sites for the THF ligands. The two O–Zr–N bond angles are acute at 74° owing to the small bite angle of the [ONO] ligand. The C–O and C–N distances of 1.37 and 1.40 Å, respectively, within the [ONO] ligand are consistent with single bonds; C–C bond lengths within the six-membered rings fall in the range 1.38–1.41 Å, consistent with an aromatic ring. These ligand metrics are indicative of the fully reduced catecholate form of the ligand.[19] Similarly, the solution characterization of **1** is consistent with the solid-state structure and the assignment of the metal center to the zirconium(IV) oxidation state. The ^{1}H NMR spectrum of **1** is consistent with a C_{2v} symmetry and shows two *tert*-butyl proton resonances (1.50 and 1.68 ppm) and two aromatic proton resonances (7.01 and 7.80 ppm) attributable to the [ONO] ligand. The resonances for the coordinated THF molecules appear as broad singlets at δ = 0.93 and 3.97 ppm. The pale yellow color of **1** is reflected in the UV/Vis spectrum of the complex, which has absorption bands in the near UV region at 328 and 383 nm (Figure 2).

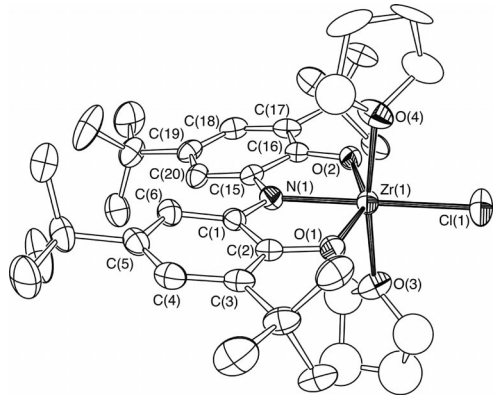

Figure 1. ORTEP diagram of [(ONO^{cat})ZrCl(THF)$_2$] (**1**). Ellipsoids are drawn at 50% probability. Hydrogen atoms, one orientation of the disordered THF ligands, and solvent toluene molecules are omitted for clarity.

Table 1. Selected bond lengths [Å] for [(ONO^{cat})ZrCl(THF)$_2$] (**1**) and [(ONO^{q})ZrCl$_2$(μ-OH)]$_2$ (**3**).

(ONO^{cat})ZrCl(THF)$_2$ (**1**)[a]		[(ONO^{q})ZrCl$_2$(μ-OH)]$_2$ (**3**)	
–	–	Zr–OH	2.1289(8)
Zr–O(1)	1.996(2)	Zr–O(1)	2.1238(9)
Zr–N(1)	2.148(2)	Zr–N(1)	2.3616(15)
Zr–Cl(1)	2.4856(9)	Zr–Cl(1)	2.4490(4)
Zr–O(THF)	2.201(3)	–	–
N(1)–C(1)	1.400(4)	N(1)–C(1)	1.3475(14)
O(1)–C(2)	1.373(4)	O(1)–C(2)	1.2860(16)
C(1)–C(2)	1.410(4)	C(1)–C(2)	1.4532(18)
C(2)–C(3)	1.391(4)	C(2)–C(3)	1.4316(18)
C(3)–C(4)	1.402(5)	C(3)–C(4)	1.3738(19)
C(4)–C(5)	1.381(5)	C(4)–C(5)	1.434(2)
C(5)–C(6)	1.401(4)	C(5)–C(6)	1.359(2)
C(6)–C(1)	1.393(4)	C(6)–C(1)	1.4233(17)

[a] Bond lengths for one half of the molecule are shown. Bond lengths for the other unique half of the molecule are similar but not identical.

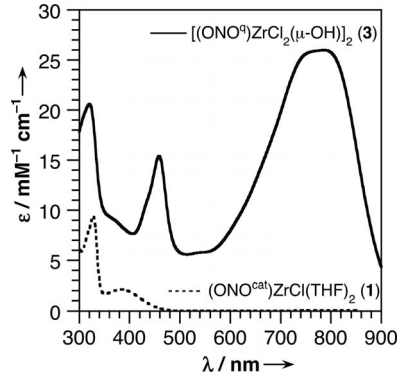

Figure 2. UV/Vis absorption spectra of [(ONO^{cat})ZrCl(THF)$_2$] (**1**) and [(ONO^{q})ZrCl$_2$(μ-OH)]$_2$ (**3**) dissolved in toluene at 298 K.

Another method for inserting zirconium into the [ONO] ligand platform was by partial deprotonation of the ligand. Because of the disparate pK_as of N–H and O–H protons in [ONO^{cat}]H$_3$, the ligand could be selectively deprotonated by using only 2 equiv. *n*BuLi to afford the dianionic form of the ligand, [ONHO]$^{2–}$, in which one proton remains on

 © 2012 Wiley-VCH Verlag GmbH & Co. KGaA, Weinheim

the nitrogen atom (Scheme 1). Treatment of this species, generated in situ, with $ZrCl_4$ afforded the new product $(ONHO)ZrCl_2(THF)$ (**2**) as an off-white solid in 68% yield. The IR spectrum of **2** shows an N–H stretch at 3106 cm^{-1}, and the diagnostic feature in the ^1H NMR spectrum of **2** is a broad singlet observed at δ = 5.82 ppm for the N–H proton. Again, two *tert*-butyl resonances and two aromatic proton resonances are observed in the ^1H NMR spectrum, which indicate mirror plane symmetry in the complex, consistent with the structure depicted in Scheme 2 in which the $(ONHO)^{2-}$ ligand is folded along the N–Zr bond to give an overall C_s-symmetric structure.[21,22]

Exposure of solutions of **2** to air resulted in a rapid color change from pale yellow to forest green, consistent with oxidation of the [ONO] ligand. When a suspension of **2** in benzene was treated with one equivalent of dry O_2, the solid dissolved to produce a forest green solution. The product, $[(ONO^q)ZrCl_2(\mu\text{-}OH)]_2$ (**3**), was isolated in 50% yield after removal of the solvent and extraction with a mixture of toluene and pentane.

Single-crystal X-ray diffraction experiments on **3** reveal a dimeric structure with two bridging hydroxide ligands. Complex **3** co-crystallizes with benzene in the orthorhombic space group *Fddd*. An ORTEP diagram of **3** is shown in Figure 3, and selected bond lengths are given in Table 1. The structure of **3** is an edge-sharing dimer with two bridging hydroxide ligands. The hydroxy protons are located in the Fourier difference map, and their presence is confirmed by an IR stretch at 3305 cm^{-1} (KBr). Each metal center is pentagonal bipyramidal, and both [ONO] ligands occupy the same plane as the bridging hydroxide ligands. As expected for bridging hydroxide ligands, the Zr–O bond length is long (2.13 Å), though the Zr–Cl distance of 2.45 Å is contracted slightly relative to the Zr–Cl distance in **1**. Notably, the Zr–O and Zr–N distances between the metal center and the [ONO] ligand are elongated significantly relative to those in **1**. The C–O and C–N distances within the [ONO] ligand are contracted to 1.29 and 1.35 Å, respectively, and the C–C bond lengths within the six-membered ring show the alternating pattern associated with a cyclohexadiene ring rather than an arene.[23] Accordingly, the ligand oxidation state in **3** can be assigned as $[ONO^q]^-$.

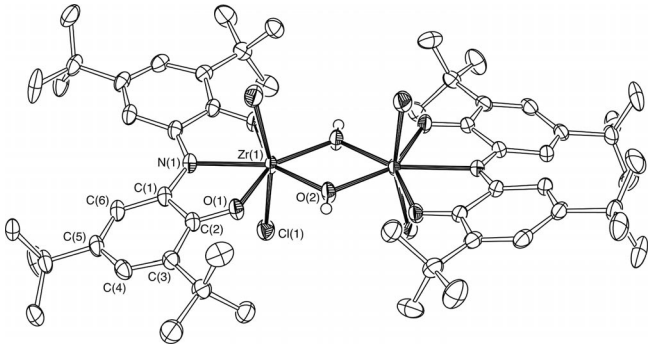

Figure 3. ORTEP diagram of $[(ONO^q)ZrCl_2(\mu^2\text{-}OH)]_2$ (**3**). Ellipsoids are drawn at 50% probability and hydrogen atoms are omitted for clarity.

The ligand oxidation state in **3** manifests striking UV/Vis absorption features, as shown in Figure 2. A strong set of absorption bands centered at 773 nm (ε = 25500 M^{-1} cm^{-1}) is consistent with the presence of the oxidized $[ONO^q]^-$ ligand. These absorptions are significantly more intense than the low-energy absorption observed for the complex $[ONO^q]TaCl_4$ (λ_{max} = 804 nm; ε = 5600 M^{-1} cm^{-1}).[19] In the case of the tantalum complex, the band is assigned primarily as an intraligand charge-transfer (ILCT) absorption. In the case of **3**, these low-energy features may include ligand-to-ligand charge-transfer (LLCT) components in addition to ILCT components.[24,25] The intensity of such LLCT transitions should be enhanced given the coplanar arrangement of the donor and acceptor groups.

Conclusions

The [ONO] ligand platform is capable of serving as both an electron and proton donor in the reduction of O_2 at a zirconium(IV) coordination complex. Coordination of the singly protonated ligand derivative, $(ONHO)^{2-}$, to zirconium(IV) produces a redox-active ligand complex with an active proton that can be delivered in a small molecule reaction. The reduction of O_2 by **2** is an overall four-electron, two-proton reaction that may be broadly classified as a multielectron, proton-coupled electron-transfer (PCET) process.[2,26,27] The product, $[(ONO^q)ZrCl_2(\mu\text{-}OH)]_2$ (**3**), is a hydroxide-bridged dimer with strong absorption bands in the UV/Vis spectrum, which suggests a high degree of charge-transfer character in the complex. Future studies will be aimed at developing the spectroscopy of this charge-transfer complex and the mechanism of its formation.

Experimental Section

General Considerations: The complexes described below are air and moisture sensitive, which necessitated that manipulations be carried out under an inert atmosphere of argon or nitrogen gas by using standard Schlenk, vacuum-line, and glovebox techniques. Ambient temperature in the glovebox is 27 °C. Hydrocarbon solvents were sparged with nitrogen and then deoxygenated and dried by passage through Q5 and activated alumina columns, respectively. Ethereal and halogenated solvents were sparged with nitrogen and then dried by passage through two activated alumina columns. The starting materials $ZrCl_4$ and *n*BuLi in hexanes was purchased from Alfa-Aesar and used as received. $(ONO^{cat})H_3$ was synthesized according to published procedures.[19]

Physical Methods: NMR spectra were collected on a Bruker Avance 500 MHz spectrometer in dry, degassed C_6D_6. ^1H NMR spectra were referenced to TMS by using the residual proteo impurities of the solvent. ^{13}C NMR spectra were referenced to TMS by using the natural-abundance ^{13}C impurities of the solvent. All chemical shifts are reported by using the standard δ notation in parts per million; positive chemical shifts are to a higher frequency of the given reference. Infrared spectra were recorded as KBr pellets with a Perkin–Elmer Spectrum One FTIR spectrophotometer. Electronic absorption spectra were recorded with a Perkin–Elmer Lambda 800 UV/Vis spectrophotometer by using 1-cm quartz cuvettes. APCI-MS data was collected on a Waters LCT Premier mass spectrometer.

 © 2012 Wiley-VCH Verlag GmbH & Co. KGaA, Weinheim

[(ONO^{cat})ZrCl(THF)$_2$] (1): Deprotonation of (ONO^{cat})H$_3$ (623 mg, 1.47 mmol) with *n*BuLi (1.52 mL/2.89 M in hexanes, 4.39 mmol, 3 equiv.) in a mixture of diethyl ether and THF was followed up with the addition of $ZrCl_4$ (342 mg, 1.47 mmol). The mixture was stirred for 12 h at ambient temperature to form a yellowish-brown suspension. The solvent was removed under reduced pressure, and the residue was extracted with diethyl ether and filtered through Celite. The filtrate was evaporated to dryness and triturated and washed with cold pentane to give the product as a bright yellow solid. Yield: 750 mg, 74%. ^{1}H NMR: δ = 7.77 (d, J = 2 Hz, 2 H, aryl-H), 6.98 (d, J = 2 Hz, 2 H, aryl-H), 3.95 (br. s, 8 H, THF), 1.65 (s, 18 H, *t*Bu), 1.46 (s, 18 H, *t*Bu), 0.90 (br. s, 8 H, THF) ppm. ^{13}C NMR: δ = 156.10 (aryl-C), 146.25 (aryl-C), 142.29 (aryl-C), 131.91 (aryl-C), 113.02 (aryl-C), 108.44 (aryl-C), 73.87 (THF), 34.69 [*C*(CH$_3$)$_3$], 32.01 [*C*(CH$_3$)$_3$], 29.97 [C(*C*H$_3$)$_3$], 24.77 [C(*C*H$_3$)$_3$], 22.38 (THF) ppm. IR: $\tilde{\nu}$ = 465, 492, 544, 625, 640, 653, 744, 767, 858, 914, 1012, 1046, 1204, 1275, 1302, 1342, 1358, 1389, 1434, 1480, 1557, 2954 cm^{-1}. UV/Vis (toluene): λ_{max}/nm (ε/M^{-1} cm^{-1}) = 282 (14200), 328 (9470), 383 (2100).

[(ONHO)ZrCl$_2$(THF)] (2): A solution of *n*BuLi in hexanes (0.39 mL/2.65 M, 1.04 mmol) was added dropwise to a cold diethyl ether solution of (ONO^{cat})H$_3$ (223 mg, 0.52 mmol). The mixture was stirred at ambient temperature for 30 min before a suspension of $ZrCl_4$ (127 mg, 0.55 mmol) in pentane/THF (3:1) was added. The mixture was stirred for 8 h to afford a yellow suspension that was taken to dryness under reduced pressure. The residue was extracted with diethyl ether and filtered through Celite. The filtration was evaporated under reduced pressure, triturated, and washed with cold pentane to give a pale yellow solid. Yield: 210 mg, 62%. ^{1}H NMR: δ = 7.28 (s, 2 H, aryl-H), 7.08 (s, 2 H, aryl-H), 5.81 (br. s, 1 H, NH), 3.95 (br. s, 4 H, THF), 1.46 (s, 18 H, *t*Bu), 1.25 (s, 18 H, *t*Bu), 1.11 (br. s, 4 H, THF) ppm. ^{13}C NMR: δ = 156.90 (aryl-C), 139.75 (aryl-C), 137.24 (aryl-C), 135.11 (aryl-C), 122.79 (aryl-C), 120.23 (aryl-C), 73.01 (THF), 35.02 [*C*(CH$_3$)$_3$], 34.08 [*C*(CH$_3$)$_3$], 31.43 [C(*C*H$_3$)$_3$], 29.50 [C(*C*H$_3$)$_3$], 24.81 (THF) ppm. IR: $\tilde{\nu}$ = 489, 553, 601, 655, 696, 755, 778, 813, 839, 878, 914, 983, 1015, 1130, 1165, 1203, 1240, 1261, 1302, 1362, 1392, 1414, 1481, 1568, 2961, 3106 cm^{-1}.

[(ONO^q)ZrCl$_2$(μ^2-OH)]$_2$ (3): Dry O_2 gas (7 mL, 0.3 mmol) was injected into to the headspace of a flask containing [(ONHO)ZrCl$_2$(py)] (200 mg, 0.3 mmol) dissolved in frozen benzene. As the solution thawed, the color immediately changed from pale yellow to dark green. After stirring for 8 h at ambient temperature, the solution was taken to dryness under reduced pressure and the residue was extracted with a mixture of toluene and pentane. The extracted solution was filtered through Celite and evaporated to afford a dark green solid. Yield: 90 mg, 50%. Single crystals of the product were deposited from a benzene solution stored at ambient temperature. ^{1}H NMR: δ = 7.38 (dd, J = 20 Hz, 4 H, aryl-H), 7.35 (dd, J = 20 Hz, 2 H, aryl-H), 1.65 (s, 18 H, *t*Bu), 1.14 (s, 18 H, *t*Bu), 1.11 (s, 18 H, *t*Bu), 1.04 (s, 18 H, *t*Bu) ppm. ^{13}C NMR: δ = 187.39 (aryl-C), 177.28 (aryl-C), 151.07 (aryl-C), 147.46 (aryl-C), 143.93 (aryl-C), 143.39 (aryl-C), 141.63 (aryl-C), 140.14 (aryl-C), 136.17 (aryl-C), 133.64 (aryl-C), 118.16 (aryl-C), 116.72 (aryl-C), 35.69 [*C*(CH$_3$)$_3$], 35.10 [*C*(CH$_3$)$_3$], 34.55 [*C*(CH$_3$)$_3$], 34.11 [*C*(CH$_3$)$_3$], 30.29 [C(*C*H$_3$)$_3$], 29.33 [C(*C*H$_3$)$_3$], 29.15 [C(*C*H$_3$)$_3$], 29.01 [C(*C*H$_3$)$_3$] ppm. IR: $\tilde{\nu}$ = 501, 512, 529, 596, 629, 641, 660, 733, 798, 857, 900, 950, 1000, 1022, 1093, 1197, 1260, 1320, 1362, 1393, 1481, 1542, 2960, 3305 cm^{-1}. UV/Vis (toluene): λ_{max}/nm (ε/M^{-1} cm^{-1}) = 330 (20100), 460 (15100), 773 (25500).

Supporting Information (see footnote on the first page of this article): Crystallographic data for **1** and **3** and complete ^{1}H and ^{13}C NMR spectra for **1**–**3** are available. CCDC-837089 (**1**) & 837090 (**3**) contain the complete supplementary crystallographic data for this paper. These data can be obtained free of charge from The Cambridge Crystallographic Data Centre via www.ccdc.cam.ac.uk/data_request/cif.

Acknowledgments

This work was funded by the National Science Foundation (NSF)-CAREER program (CHE-0645685). A. F. H. is a Camille-Dreyfus Teacher-Scholar.

[1] A. S. Borovik, *Acc. Chem. Res.* **2005**, *38*, 54–61.
[2] J. Rosenthal, D. G. Nocera, *Acc. Chem. Res.* **2007**, *40*, 543–53.
[3] S. S. Stahl, *Angew. Chem.* **2004**, *116*, 3480; *Angew. Chem. Int. Ed.* **2004**, *43*, 3400–20.
[4] S. S. Stahl, J. A. Labinger, J. E. Bercaw, *Angew. Chem.* **1998**, *110*, 2298; *Angew. Chem. Int. Ed.* **1998**, *37*, 2180–2192.
[5] M. Costas, M. P. Mehn, M. P. Jensen, L. Que, *Chem. Rev.* **2004**, *104*, 939–86.
[6] E. Y. Tshuva, S. J. Lippard, *Chem. Rev.* **2004**, *104*, 987–1012.
[7] J. A. Labinger, D. W. Hart, W. E. Seibert III, J. Schwartz, *J. Am. Chem. Soc.* **1975**, *97*, 3851–3852.
[8] T. V. Lubben, P. T. Wolczanski, *J. Am. Chem. Soc.* **1987**, *109*, 424–435.
[9] T. D. Tilley, *Organometallics* **1985**, *4*, 1452–1457.
[10] S. J. Kim, D. W. Choi, Y. J. Lee, B. H. Chae, J. Ko, S. O. Kang, *Organometallics* **2004**, *23*, 559–567.
[11] C. Stanciu, M. E. Jones, P. E. Fanwick, M. M. Abu-Omar, *J. Am. Chem. Soc.* **2007**, *129*, 12400–12401.
[12] K. J. Blackmore, J. W. Ziller, A. F. Heyduk, *Inorg. Chem.* **2005**, *44*, 5559–61.
[13] K. J. Blackmore, M. B. Sly, M. R. Haneline, J. W. Ziller, A. F. Heyduk, *Inorg. Chem.* **2008**, *47*, 10522–32.
[14] N. A. Ketterer, H. Fan, K. J. Blackmore, X. Yang, J. W. Ziller, M. H. Baik, A. F. Heyduk, *J. Am. Chem. Soc.* **2008**, *130*, 4364–74.
[15] M. R. Haneline, A. F. Heyduk, *J. Am. Chem. Soc.* **2006**, *128*, 8410–8411.
[16] A. I. Nguyen, R. A. Zarkesh, D. C. Lacy, M. K. Thorson, A. F. Heyduk, *Chem. Sci.* **2011**, *2*, 166–169.
[17] A. I. Nguyen, K. J. Blackmore, S. M. Carter, R. A. Zarkesh, A. F. Heyduk, *J. Am. Chem. Soc.* **2009**, *131*, 3307–3316.
[18] P. Chaudhuri, M. Hess, K. Hildenbrand, E. Bill, T. Weyhermueller, K. Wieghardt, *Inorg. Chem.* **1999**, *38*, 2781–2790.
[19] R. A. Zarkesh, J. W. Ziller, A. F. Heyduk, *Angew. Chem.* **2008**, *120*, 4793; *Angew. Chem. Int. Ed.* **2008**, *47*, 4715–4718.
[20] R. A. Zarkesh, A. F. Heyduk, *Organometallics* **2009**, *28*, 6629–6631.
[21] A. I. Poddelsky, N. V. Somov, Y. A. Kurskii, V. K. Cherkasov, G. A. Abakumov, *J. Organomet. Chem.* **2008**, *693*, 3451–3455.
[22] A. I. Poddelsky, N. N. Vavilina, N. V. Somov, V. K. Cherkasov, G. A. Abakumov, *J. Organomet. Chem.* **2009**, *694*, 3462–3469.
[23] S. Bhattacharya, P. Gupta, F. Basuli, C. G. Pierpont, *Inorg. Chem.* **2002**, *41*, 5810–5816.
[24] W. Paw, S. D. Cummings, M. A. Mansour, W. B. Connick, D. K. Geiger, R. Eisenberg, *Coord. Chem. Rev.* **1998**, *171*, 125–150.
[25] S. D. Cummings, R. Eisenberg, *J. Am. Chem. Soc.* **1996**, *118*, 1949–1960.
[26] J. J. Warren, T. A. Tronic, J. M. Mayer, *Chem. Rev.* **2010**, *110*, 6961–7001.
[27] J. M. Mayer, *Acc. Chem. Res.* **2011**, *44*, 36–46.

Received: July 30, 2011
Published Online: October 10, 2011

 © 2012 Wiley-VCH Verlag GmbH & Co. KGaA, Weinheim

DOI: 10.1002/ejic.201101100

Electrochemical Reductive Deprotonation of an Imidazole Ligand in a Bipyridine Tricarbonyl Rhenium(I) Complex

Qiang Zeng,[a] Mahdi Messaoudani,[b] Antonín Vlček Jr.,*[b] and František Hartl*[a]

Keywords: Rhenium / Imidazole / N ligands / Heterocycles / Electrochemistry

The reduction pathway of *fac*-[Re^{I}(imH)$(CO)_3$(bpy)]$^+$ was studied in situ by UV/Vis/NIR–IR spectroelectrochemistry with an OTTLE cell. The complex underwent 1e$^-$ reduction of the 2,2′-bipyridine (bpy) ligand and intramolecular electron transfer, which resulted in the conversion of the axial imidazole (imH) ligand to 3-imidazolate (3-im$^-$). This step was followed by two bpy-based 1e$^-$ reductions to ultimately produce five-coordinate [Re$(CO)_3$(bpy)]$^-$ and free 3-im$^-$. The identity of the reduction product *fac*-[Re(3-im$^-$)$(CO)_3$(bpy)] has been proven by partial chemical deprotonation of the parent complex followed by IR spectroelectrochemistry. This is the first time that the reductive electrochemical conversion of metal-coordinated imidazole to terminal 3-imidazolate has been observed.

Introduction

The redox activity, photophysical properties and synthetic flexibility of rhenium(I) carbonyl–diimine (*N*,*N*) complexes make them useful sensitizers of electron transfer and energy transfer processes.[1,2] Thus, these materials have attracted significant attention for applications as catalysts in the electrochemical and photochemical reduction of CO_2,[3,4] as luminescent labels in biomolecules[5] and as redox probes to investigate long-range electron transfer in proteins[6] and in synthetic donor–bridge–acceptor dyads.[7] Proteins, such as *Pseudomonas aeruginosa azurins*, allow redox-active Re metallolabels to be attached in defined positions at their surface through the histidine side chains, which provides an ideal system to investigate relaxation dynamics and long-range electron transfer reactions (tunneling) between the Cu^{I} center and the distant, electronically excited [Re(imidazole)$(CO)_3$(*N*,*N*)]$^+$ chromophore.

In a different context, various imidazolato-bridged transition metal complexes (frequently Mn^{II}, Ni^{II}, Cu^{II} and Zn^{II}) have been studied in part as mimics of active sites in metalloproteins.[8] Preparation of mononuclear precursors by deprotonation of the monodentate imidazole ligand thus becomes a crucial step in the synthesis of the binuclear complexes with the metalloligand approach. Pérez and coworkers[9] have reported the first successful deprotonation of terminal imidazole in organometallic complexes, which include [Re^{I}(imH)$(CO)_3$(bpy)]$^+$, in tetrahydrofuran (THF) at –78 °C by $KN(SiMe_3)_2$, which avoided the formation of oligo- and polymeric species.

Reduction of [Re^{I}(imH)$(CO)_3$(*N*,*N*)]$^+$ complexes is a highly topical research subject, which is relevant to the development of Re-based protein and supramolecular photocatalytic systems, in which the Re chromophore is photochemically reduced, as well as a perspective route to new complexes of the strongly donating im$^-$ ligand and their polymers. [Re(imH)$(CO)_3$(phen)]$^+$ (phen = 1,10-phenanthroline) has been studied by cyclic voltammetry in MeCN and has been reported[6a] to undergo a fully reversible electrochemical reduction with no evidence of any accompanying reactions or molecular transformations. Similarly, the quasireversible reduction of several [Re(histidine)$(CO)_3$(*N*,*N*)]$^+$ complexes and [Re(imH)$(CO)_3$(bpy-$(COO)_2$)]$^-$ have been observed in aqueous solutions.[10] Herein, we communicate the first electrochemical reduction of bpy in [Re(imH)$(CO)_3$(bpy)]$^+$, which induces rapid deprotonation of the imidazole ligand at room temperature. UV/Vis/NIR–IR spectroelectrochemistry was employed as a convenient tool to identify and assign the carbonyl species formed along the reduction pathway on the timescale of a few seconds to minutes.

Results and Discussion

Cyclic Voltammetry

The cyclic voltammogram of [Re(imH)$(CO)_3$(bpy)]$^+$ in THF/TBAH (TBAH = Bu_4NPF_6) at 293 K shows a reversible one-electron reduction R_1 at $E_{1/2}$ = –1.64 V vs. Fc/Fc$^+$, which is followed by an irreversible cathodic step R_2 at $E_{p,c}$ = –2.24 V (Figure 1). This potential range is common for this family of Re cationic complexes.[3c,11,12a] Compared to

[a] Department of Chemistry, University of Reading, Whiteknights, Reading RG6 6AD, United Kingdom
Fax: +44-118-378-6331
E-mail: f.hartl@reading.ac.uk
[b] Queen Mary University of London, School of Biological and Chemical Sciences,
Mile End Road, London E1 4NS, United Kingdom
E-mail: a.vlcek@qmul.ac.uk
Supporting information for this article is available on the WWW under http://dx.doi.org/10.1002/ejic.201101100.

 © 2012 Wiley-VCH Verlag GmbH & Co. KGaA, Weinheim

$[Re(MeCN)(CO)_3(bpy)]^+$ ($E_{1/2}$ = –1.58 V),[3c] the slight shift to more negative potential reflects the stronger donor nature of the imidazole ligand. By analogy with other Re^I carbonyl–diimine complexes,[12] the first reduction of $[Re(imH)(CO)_3(bpy)]^+$ (R_1) is assumed to be localized on the bpy ligand to generate the radical $[Re^I(imH)(CO)_3(bpy^{\cdot-})]$. The second cathodic step (R_2) is attributed to the formation of five-coordinate $[Re(CO)_3(bpy)]^-$. Thus, in line with the previous report on $[Re(imH)(CO)_3(phen)]^+$,[6a] the cyclic voltammogram of $[Re(imH)(CO)_3(bpy)]^+$ does not indicate any secondary reactivity of the imidazole ligand after the initial 1e⁻ reduction.

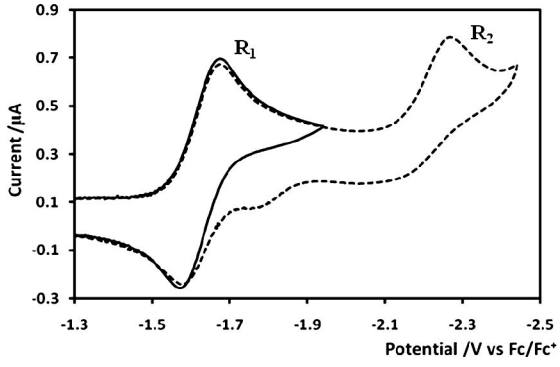

Figure 1. The cathodic cyclic voltammetric response of 10^{-3} M $[Re(imH)(CO)_3(bpy)]^+$ at a freshly polished Pt microdisc working electrode. Conditions: 293 K, THF/10^{-1} M TBAH; scan rate: 100 mV s^{-1}.

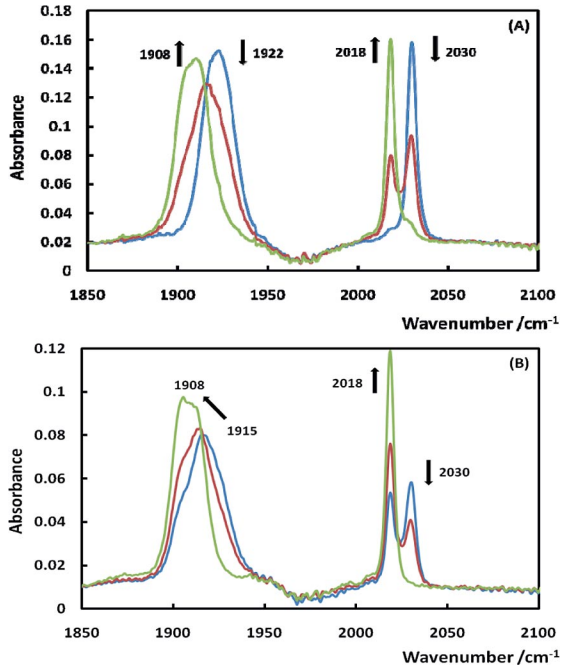

Figure 2. (A) IR spectral changes recorded at room temperature in the course of the electrochemical reductive deprotonation of $[Re(imH)(CO)_3(bpy)]^+$ in THF/TBAH at –1.70 V. (B) Electrochemical conversion of $[Re(imH)(CO)_3(bpy)]^+$ to $[Re(3\text{-}im^-)(CO)_3(bpy)]$ at the same cathodic potential conducted in a solution of $[Re(imH)(CO)_3(bpy)]^+$ and $[Re(3\text{-}im^-)(CO)_3(bpy)]$ prepared by partial deprotonation. The first IR spectrum (blue line) was recorded without the applied reduction potential.

IR Spectroelectrochemistry

In THF/TBAH, $[Re(imH)(CO)_3(bpy)]^+$ exhibits two ν(CO) bands at 2030 and 1922(br) cm^{-1} in its IR spectrum, which is in line with the local C_{3v} symmetry. Monitoring its 1e⁻ reduction at 293–253 K with IR spectroscopy revealed smooth conversion to another tricarbonyl complex, which absorbed at 2018 and 1908(br) cm^{-1} (Figure 2A). This low-energy ν(CO) shift by 12 and 14 cm^{-1} is much smaller than the expected values of 22–30 cm^{-1}[12a] for the primary radical $[Re(imH)(CO)_3(bpy^{\cdot-})]$. On the other hand, the product of the ν(CO) wavenumbers is close to those of the neutral complexes $[ReCl(CO)_3(bpy)]$[12a] and, in particular, $[Re(3\text{-}im^-)(CO)_3(bpy)]$ (2017, 1911 and 1904 cm^{-1}), which contains the chemically deprotonated 3-imidazolato (3-im⁻) ligand reported by Pérez et al.[9] These data point to electrochemical imH→3-im⁻ conversion that accompanies the reduction of the bpy ligand. It is surprising that 1e⁻-reduced $[Re(imH)(CO)_3(bpy^{\cdot-})]$ was not detected by IR spectroelectrochemistry even at 253 K.

To confirm the product assignment, the imidazole ligand in $[Re(imH)(CO)_3(bpy)]^+$ was partly deprotonated with $KN(SiMe_3)_2$ (2:1 molar ratio)[9] and the resulting mixture of $[Re(imH)(CO)_3(bpy)]^+$ and $[Re(3\text{-}im^-)(CO)_3(bpy)]$ in THF/TBAH was transferred into the optically transparent thin-layer electrode (OTTLE) cell. Cathodic IR spectroelectrochemistry (Figure 2B) shows conversion of the remaining $[Re(imH)(CO)_3(bpy)]^+$ to $[Re(3\text{-}im^-)(CO)_3(bpy)]$ [ν(CO) bands at 2018 and 1908(br) cm^{-1}]; the IR bands of the electrochemical product and chemically generated $[Re(3\text{-}im^-)(CO)_3(bpy)]$ are coincident.

A thin-layer cyclic voltammogram recorded in the course of the electrochemical reduction of $[Re(imH)(CO)_3(bpy)]^+$ in the OTTLE cell (scan rate = 2 mV s^{-1}) documents its irreversible nature. In contrast to the conventional cyclic voltammogram (Figure 1), the first cathodic wave lacks the anodic counterwave due to the reoxidation of $[Re(imH)(CO)_3(bpy^{\cdot-})]$. Instead, a new reversible redox couple is observed at ca. 190 mV more negative potential, i.e. at around $E_{1/2}$ = –1.85 V. The corresponding spectroelectrochemical reduction revealed the formation of a stable product characterized by ν(CO) bands at 1995 and 1878(br) cm^{-1} (Figure 3 and S1) whose assignment as $[Re(3\text{-}im^-)(CO)_3(bpy^{\cdot-})]^-$ is strongly supported by a comparison[3c] with $[Re(Cl)(CO)_3(bpy^{\cdot-})]^-$, which is formed at $E_{1/2}$ = –1.86 V and shows similar ν(CO) absorbances (1996, 1883 and 1868 cm^{-1}).

The subsequent cathodic step observed in the thin-layer cyclic voltammogram at ca. 600 mV more negative potential from the preceding wave is due to the conversion of $[Re(3\text{-}im^-)(CO)_3(bpy^{\cdot-})]^-$ to the known[12a] five-coordinate anion $[Re(CO)_3(bpy)]^-$ [ν(CO) at 1948 and 1843 cm^{-1}; Figure S2]. The dissociation of the axial 3-im⁻ ligand (Scheme 1) is not surprising given the strongly π-delocalized bonding in the ultimate reduction product.[13]

 © 2012 Wiley-VCH Verlag GmbH & Co. KGaA, Weinheim

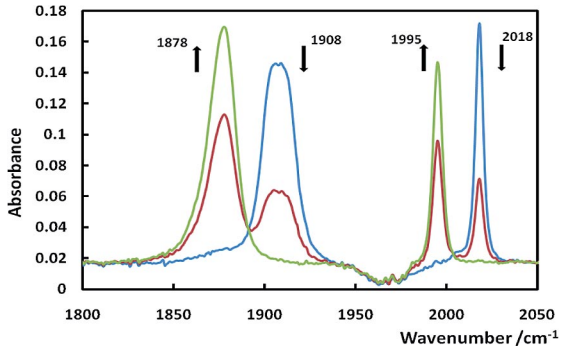

Figure 3. Reversible IR spectral changes in the ν(CO) region that accompany the 1e⁻ reduction of [Re(3-im⁻)(CO)$_3$(bpy)] to [Re(3-im⁻)(CO)$_3$(bpy•⁻)]⁻ between –1.80 and –1.95 V in THF/TBAH at room temperature.

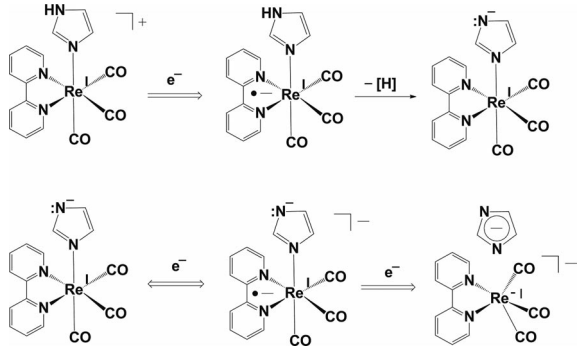

Scheme 1. The reduction pathway of [Re(imH)(CO)$_3$(bpy)]$^+$, which involves the conversion of imidazole to the terminal 3-imidazolato ligand.

The experimental IR spectroelectrochemical data revealed that the 1e⁻ reduction of [Re(imH)(CO)$_3$(bpy)]$^+$ induces deprotonation of the imidazole ligand. Frontier molecular orbital (MO) analysis based on DFT calculations[6d,14] shows that the lowest unoccupied molecular orbital (LUMO) is almost exclusively localized on the bpy ligand. This is in line with the reversible cathodic wave in the cyclic voltammogram of [Re(imH)(CO)$_3$(bpy)]$^+$ recorded with a scan rate of 0.1 V s^{-1} (Figure 1). Therefore, the added electron first occupies the lowest π*(bpy) orbital that rises in energy and the electron density becomes partially delocalized over the imidazole ligand, which weakens the N–H bond. Subsequently, the im⁻ ligand is formed by concomitant electron transfer from bpy•⁻ and dissociation of the imidazole N–H bond (Scheme 1). The resulting neutral complex [Re(3-im⁻)(CO)$_3$(bpy)] is capable of reversible bpy-localized 1e⁻ reduction to produce [Re(3-im⁻)(CO)$_3$(bpy•⁻)]⁻, which undergoes further 1e⁻ reduction to give stable [Re(CO)$_3$(bpy)]⁻.

UV/Vis/NIR Spectroelectrochemistry

The mechanism outlined in Scheme 1 is further supported by UV/Vis/NIR spectra of the Re tricarbonyl–bpy complexes that occur along the reduction pathway (Figures 4 and S3). For the [Re(imH)(CO)$_3$(bpy)]$^+$ parent complex, the absorption band at around 350 nm belongs to Re/imidazole→bpy charge transfer (CT) transitions.[6d,15,16] The UV/Vis/NIR spectroelectrochemistry shows that the 1e⁻ reduction of this complex to [Re(3-im⁻)(CO)$_3$(bpy)] shifts the CT band to ca. 380 nm, which tails down to ca. 500 nm (Figure 4). This observation is in line with the deprotonation of the imidazole ligand, which increases the electron density at the Re center and shifts the Re/im⁻→bpy transition to a lower energy. The subsequent 1e⁻ reduction of [Re(3-im⁻)(CO)$_3$(bpy)] to [Re(3-im⁻)(CO)$_3$(bpy•⁻)]⁻ is accompanied by the appearance of new absorption bands at 390, 480 and 510 nm and a broad absorption in the NIR region (Figure 4), which are characteristic of π–π* transitions in the bpy•⁻ ligand.[11,16,17] Importantly, these features are completely absent in the spectra recorded during the initial cathodic step of [Re(imH)(CO)$_3$(bpy)]$^+$, which confirms the short lifetime of the primary reduction product, [Re(imH)(CO)$_3$(bpy•⁻)], under the conditions of thin-layer voltammetry in the OTTLE cell.

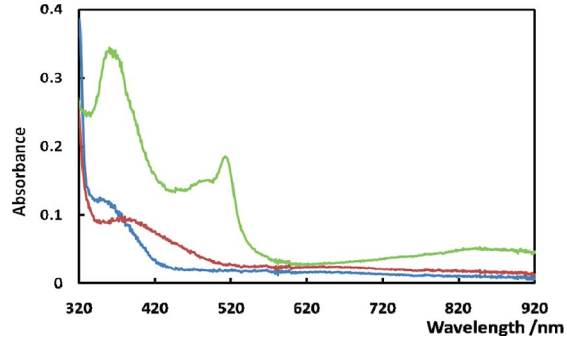

Figure 4. UV/Vis/NIR absorption spectra of parent [Re(imH)(CO)$_3$(bpy)]$^+$ (blue line), 1e⁻ reduced and deprotonated [Re(3-im⁻)(CO)$_3$(bpy)] (purple line) and [Re(3-im⁻)(CO)$_3$(bpy•⁻)]⁻ (green line). The reduced species were generated at –1.70 and –1.85 V, respectively, in THF/TBAH at 293 K in an OTTLE cell (see Scheme 1).

The final irreversible reduction of [Re(3-im⁻)(CO)$_3$(bpy•⁻)]⁻ produced a broad, intense absorption at 550 nm with shoulders at 630, 680 and 730 nm (Figure S3), which is characteristic of [Re(CO)$_3$(bpy)]⁻,[12a] and in agreement with the IR spectroscopic characterization and dissociation of the 3-imidazolato ligand (Scheme 1).

Conclusions

The reduction pathway of [Re(imH)(CO)$_3$(bpy)]$^+$ has been described using data obtained from conventional and thin-layer cyclic voltammetry and variable-temperature UV/Vis/NIR–IR spectroelectrochemistry in THF. The initial bpy-localized reduction triggers a rapid conversion of the axial imidazole to the terminal 3-imidazolato ligand. This smooth electrochemical reaction is unprecedented in the literature and adds to the few successful attempts to deprotonate the coordinated imidazole chemically, which is relevant to systems of major importance in biology.[18] The 3-imidazolato ligand remains coordinated after the subsequent bpy-localized 1e⁻ reduction of [Re(3-im⁻)(CO)$_3$(bpy)]

 © 2012 Wiley-VCH Verlag GmbH & Co. KGaA, Weinheim

to $[Re(3\text{-}im^{-})(CO)_3(bpy^{\bullet-})]^{-}$ but dissociates after further $1e^{-}$ reduction to produce $[Re(CO)_3(bpy)]^{-}$. The imidazole reactivity depends on the nature of the noninnocent α-diimine ligand, which will be shown in a forthcoming publication.

Experimental Section

$[Re(imH)(CO)_3(bpy)][OTf]$ was prepared by a literature procedure.[9] The reaction between $[Re(OTf)(CO)_3(bpy)]$ and imH in CH_2Cl_2 was monitored by IR spectroscopy to ensure complete conversion before the product was precipitated by hexane. The product purity was checked by ^1H NMR and IR spectroscopy. THF used in electrochemical and spectroelectrochemical measurements was freshly distilled from a sodium/benzophenone mixture under an atmosphere of dry nitrogen. TBAH (Aldrich) was recrystallized twice from absolute ethanol and dried overnight under vacuum at 80 °C before use. Ferrocene (BDH) was used as received. $KN(SiMe_3)_2$ (Aldrich) was obtained as a 5×10^{-1} M solution in toluene.

Conventional cyclic voltammetry was performed in an air-tight cell connected to a computer controlled EG&G PAR Model 283 potentiostat. The cell was equipped with a Pt microdisc (0.14 mm^2) working electrode, which was carefully polished with 25-micron diamond paste, a Pt coil auxiliary electrode and an Ag coil pseudoreference electrode. All redox potentials are reported against the ferrocene/ferrocenium (Fc/Fc^+) redox couple, which was used as the internal standard. IR and UV/Vis spectra were recorded with a Bruker Vertex 70v FTIR spectrometer and a Scinco S3100 diode array spectrophotometer, respectively. UV/Vis/NIR–IR spectroelectrochemical experiments at room temperature were conducted with an OTTLE cell[19] equipped with a Pt-minigrid working electrode and CaF_2 windows. The UV/Vis/NIR–IR spectroelectrochemical experiments in THF at 253 K were carried out with a cryostatted OTTLE cell.[20] Controlled-potential electrolyses in the OTTLE cells were carried out using a PA4 potentiostat (Laboratory Devices, Polná, Czech Republic). The concentrations of $[Re(imH)(CO)_3(bpy)]^+$ and TBAH used in these measurements were 1.5×10^{-3} and 3×10^{-1} mol dm^{-3}, respectively.

Supporting Information (see footnote on the first page of this article): IR spectra showing the $1e^-$ reoxidation and $1e^-$ reduction of $[Re(3\text{-}im^{-})(CO)_3(bpy^{\bullet-})]^{-}$; UV/Vis absorption spectrum of the ultimate reduction product, $[Re(CO)_3(bpy)]^{-}$.

Acknowledgments

The research was funded by Queen Mary University of London and the University of Reading.

[1] A. Vlček Jr., *Top. Organomet. Chem.* **2010**, *29*, 73.
[2] A. Kumar, S.-S. Sun, A. J. Lees, *Top. Organomet. Chem.* **2010**, *29*, 1.
[3] a) J. Hawecker, J.-M. Lehn, R. Ziessel, *J. Chem. Soc., Chem. Commun.* **1984**, 328; b) B. P. Sullivan, C. M. Bolinger, D. Conrad, W. J. Vining, T. J. Meyer, *J. Chem. Soc., Chem. Commun.* **1985**, 1414; c) F. P. A. Johnson, M. W. George, F. Hartl, J. J. Turner, *Organometallics* **1996**, *15*, 3374; d) J. M. Smieja, C. P. Kubiak, *Inorg. Chem.* **2010**, *49*, 9283.
[4] a) J. Hawecker, J.-M. Lehn, R. Ziessel, *J. Chem. Soc., Chem. Commun.* **1983**, 536; b) A. J. Morris, G. J. Meyer, E. Fujita, *Acc. Chem. Res.* **2009**, *42*, 7383; c) M. D. Doherty, D. C. Grills, J. T. Muckerman, D. E. Polyansky, E. Fujita, *Coord. Chem. Rev.* **2010**, *254*, 2472; d) H. Takeda, K. Koike, H. Inoue, O. Ishitani, *J. Am. Chem. Soc.* **2008**, *130*, 2023; e) H. Takeda, O. Ishitani, *Coord. Chem. Rev.* **2010**, *254*, 346.
[5] K. K.-W. Lo, M.-W. Louie, K. Y. Zhang, *Coord. Chem. Rev.* **2010**, *254*, 2603.
[6] a) W. B. Connick, A. J. Di Bilio, M. G. Hill, J. R. Winkler, H. B. Gray, *Inorg. Chim. Acta* **1995**, *240*, 169; b) A. J. Di Bilio, B. R. Crane, W. A. Wehbi, C. N. Kiser, M. M. Abu-Omar, R. M. Carlos, J. H. Richards, J. R. Winkler, H. B. Gray, *J. Am. Chem. Soc.* **2001**, *123*, 3181; c) A. M. Blanco-Rodríguez, M. Busby, K. Ronayne, M. Towrie, C. Grădinaru, J. Sudhamsu, J. Sýkora, M. Hof, S. Záliš, A. J. Di Bilio, B. R. Crane, H. B. Gray, A. Vlček Jr., *J. Am. Chem. Soc.* **2009**, *131*, 11788; d) A. El Nahhas, C. Consani, A. M. Blanco-Rodríguez, K. M. Lancaster, O. Braem, A. Cannizzo, M. Towrie, I. P. Clark, S. Záliš, M. Chergui, A. Vlček Jr., *Inorg. Chem.* **2011**, *50*, 2932; e) C. Shih, A. K. Museth, M. Abrahamsson, A. M. Blanco-Rodriguez, A. J. Di Bilio, J. Sudhamsu, B. R. Crane, K. L. Ronayne, M. Towrie, A. Vlček Jr., J. H. Richards, J. R. Winkler, H. B. Gray, *Science* **2008**, *320*, 1760; f) A. M. Blanco-Rodríguez, A. J. Di Bilio, C. Shih, A. K. Museth, I. P. Clark, M. Towrie, A. Cannizzo, J. Sudhamsu, B. R. Crane, J. Sýkora, J. R. Winkler, H. B. Gray, S. Záliš, A. Vlček Jr., *Chem. Eur. J.* **2011**, *17*, 5350.
[7] D. Hanss, M. E. Walther, O. S. Wenger, *Coord. Chem. Rev.* **2010**, *254*, 2584.
[8] E. Colacio, M. Ghazi, R. Kivekäs, M. Klinga, F. Lioret, J. M. Moreno, *Inorg. Chem.* **2000**, *39*, 2770.
[9] E. Gómez, M. A. Huertos, J. Pérez, L. Riera, A. Menéndez-Velázquez, *Inorg. Chem.* **2010**, *49*, 9527.
[10] R.-J. Lin, K.-S. Lin, I.-J. Chang, *Inorg. Chim. Acta* **1996**, *242*, 179.
[11] A. Vlček Jr., in *Electron Transfer in Chemistry* (Eds.: V. Balzani, D. Astruc), Wiley-VCH, Weinheim, **2001**, vol. 2, pp. 804–877.
[12] a) G. J. Stor, F. Hartl, J. W. M. van Outersterp, D. J. Stufkens, *Organometallics* **1995**, *14*, 1115; b) F. Paolucci, M. Marcaccio, C. Paradisi, S. Roffia, C. A. Bignozzi, C. Amatore, *J. Phys. Chem. B* **1998**, *102*, 4759.
[13] F. Hartl, P. Rosa, L. Ricard, P. Le Floch, S. Záliš, *Coord. Chem. Rev.* **2007**, *251*, 557.
[14] I. de Aguiar, S. D. Inglez, F. C. A. Lima, J. F. S. Daniel, B. R. McGarvey, A. C. Tedesco, R. M. Carlos, *Inorg. Chem.* **2008**, *47*, 11519.
[15] A. Cannizzo, A. M. Blanco-Rodríguez, A. Nahhas, J. Šebera, S. Záliš, A. Vlček Jr., M. Chergui, *J. Am. Chem. Soc.* **2008**, *130*, 8967.
[16] S. Záliš, C. Consani, A. El Nahhas, A. Cannizzo, M. Chergui, F. Hartl, A. Vlček Jr., *Inorg. Chim. Acta* **2011**, *374*, 578.
[17] a) M. Krejčík, A. A. Vlček, *J. Electroanal. Chem.* **1991**, *313*, 243; b) J. Víchová, F. Hartl, A. Vlček Jr., *J. Am. Chem. Soc.* **1992**, *114*, 10903.
[18] J. S. Swartz, M. A. Stanford, J. N. Moy, B. M. Hoffman, J. S. Valentine, *J. Am. Chem. Soc.* **1979**, *101*, 3396.
[19] M. Krejčík, M. Daněk, F. Hartl, *J. Electroanal. Chem.* **1991**, *317*, 179.
[20] a) T. Mahabiersing, H. Luyten, R. C. Nieuwendam, F. Hartl, *Collect. Czech. Chem. Commun.* **2003**, *68*, 1687; b) F. Hartl, H. Luyten, H. A. Nieuwenhuis, G. C. Schoemaker, *Appl. Spectrosc.* **1994**, *48*, 1522.

Received: October 11, 2011
Published Online: November 23, 2011

 © 2012 Wiley-VCH Verlag GmbH & Co. KGaA, Weinheim

DOI: 10.1002/ejic.201101016

Alkyne Addition to a Metal-Stabilized Thiyl Radical: Carbon–Sulfur Bond Formation between 1-Octyne and $[Ru(SP)_3]^+$

Kagna Ouch,[a] Mark S. Mashuta,[a] and Craig A. Grapperhaus*[a]

Keywords: Alkynes / C–S bond formation / Oxidation / Sulfur / Electrochemistry

The metal-stabilized thiyl radical complex $[Ru(SP)_3]^+$, [Ru-**1**]$^+$, {SP = 2-(diphenylphosphanyl)benzenethiolate} adds 1-octyne across the *cis*-sulfur sites to yield the *S*-alkylated dithiolene product [Ru-**1**·octyne]$^+$. The product complex exists as a pair of inseparable geometric isomers, which were characterized by X-ray crystallography, ^{31}P NMR spectroscopy, and cyclic voltammetry. By using electrochemical methods, the rate constant for 1-octyne addition was determined as $8.7 \times 10^3\ M^{-1}\,s^{-1}$.

Introduction

We have recently reported a series of studies on the addition of alkenes to the oxidized metal-thiolate complexes $[M(SP)_3]^+$ {M = Ru, Re; SP = 2-(diphenylphosphanyl)-benzenethiolate}.[1–4] Although formally in the +4 oxidation state, the complexes are regarded as metal-stabilized thiyl radicals because of the delocalization of spin density over the metal and sulfur donors, Scheme 1.[4] Two of the S ligands are optimally positioned for C–S bond forming reactions with alkenes, which generate diamagnetic Ru^{II}-dithioether complexes. The reaction is initiated by electrochemical (Scheme 2 top) or chemical (Scheme 2 middle) oxidation of [Ru-**1**]$^-$. Similar alkene additions are reported with other oxidized ruthenium thiolates[5] and oxidized metal-dithiolenes.[6–9] For [Ru-**1**]$^+$, the alkene addition rate constant varies from $4.3 \times 10^7\ M^{-1}\,s^{-1}$ to $2.9 \times 10^3\ M^{-1}\,s^{-1}$, and higher values are observed for "electron-rich" alkenes.[1] While alkene addition to [Ru-**1**]$^+$ is irreversible, equilibrium binding constants for ethylene to [Re-**1**]$^{n+}$ (n = 0, 1, 2) depend on the complex charge. Three distinct binding regimes with equilibrium constants over 20 orders of magnitude are accessible within a 240 mV potential window.[2]

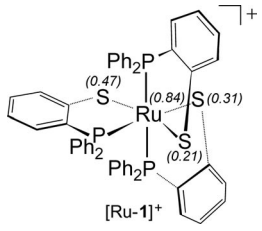

Scheme 1. Metal-coordinated thiyl radical complex [Ru-**1**]$^+$ with calculated spin density values (*italics*).[4]

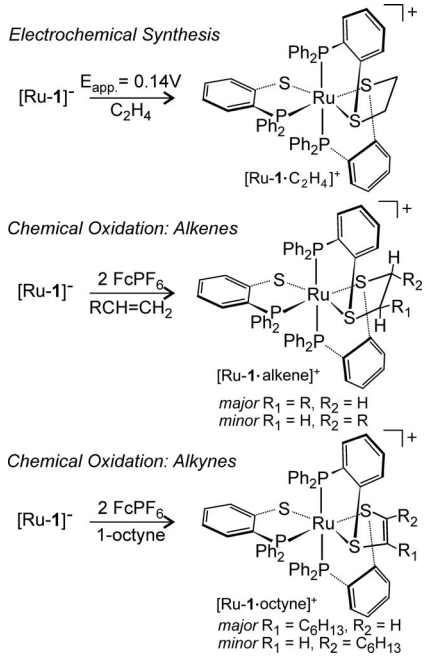

Scheme 2. Reactivity of [Ru-**1**]$^+$ with alkenes and alkynes.

Herein, we describe carbon–sulfur bond forming reactions between [Ru-**1**]$^+$ and 1-octyne (Scheme 2 bottom). Alkyne addition across the thiolate donors of neighboring SP chelates yields a new tetradentate, *S*-alkylated dithiolene ligand. The *intraligand* addition of alkynes across sulfur donors of Mo-tris(dithiolene)s was employed by the Fekl group to selectively displace a single dithiolene donor.[10] Similarly, Yan and co-workers detected a variety of metal-free alkyne disulfuration and hydrosulfuration products following alkyne addition to a dinuclear Co-thiolate.[11] Dis-

[a] Department of Chemistry, University of Louisville,
2320 South Brook Street, Louisville, KY 40292, USA
Fax: +1-502-852-8149
E-mail: grapperhaus@louisville.edu

Supporting information for this article is available on the WWW under http://dx.doi.org/10.1002/ejic.201101016.

 © 2012 Wiley-VCH Verlag GmbH & Co. KGaA, Weinheim

crete, isolable metal-coordinated alkyne addition products were also reported by Yan by using related dinuclear Ru-thiolates.[12,13] In that case, the formal oxidation states in the Ru precursor are +2 and +4, and alkyne addition occurs at the more oxidized center.

Results and Discussion

Oxidation of [Ru-**1**]$^-$ with ferrocenium hexafluorophosphate (2 equiv.) in the presence of 1-octyne yields the diamagnetic Ru(II) complex [Ru-**1**·octyne]PF_6 as a dark orange product. Recrystallization from THF/hexane gives pure [Ru-**1**·octyne]PF_6 as a yellow solid. The ESI-MS spectrum displays a parent peak at m/z = 1091.18, consistent with the theoretical value, m/z = 1091.37, for the desired complex, Figure S1.

Single crystals of [Ru-**1**·octyne]PF_6 for X-ray diffraction studies were obtained by evaporation of chlorobenzene/hexane mixtures. The asymmetric unit consists of co-crystallized mixtures of two geometric isomers (Scheme 2 bottom). Unlike the related alkene addition product [Ru-**1**·p-methylstyrene]PF_6, the isomers of [Ru-**1**·octyne]PF_6 could not be separated by crystallization or other methods.[1] Analyses of multiple crystals consistently reveal co-crystallized products. The isomers differ based on the relative position of the hexyl side chain, which can be located either at the R_1 (nearest S *trans* to S, major) or R_2 (nearest S *trans* to P, minor) position. An ORTEP[14] representation of the major [Ru-**1**·octyne]$^+$ isomer is provided in Figure 1.

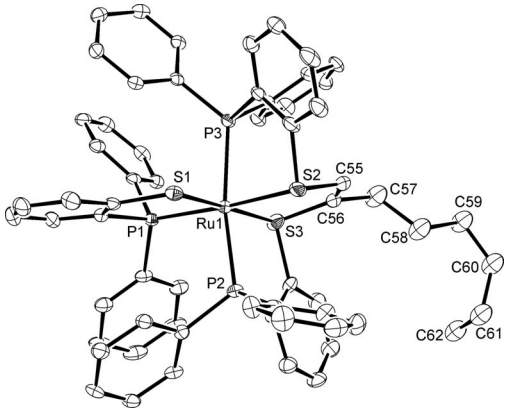

Figure 1. ORTEP[14] representation of [Ru-**1**·octyne]$^+$ showing a single isomer with the hexyl side chain (C57–C62) extending from C56. For clarity, the co-crystallized isomer with a hexyl side chain originating from C55 is not shown (see Supporting Information).

The [Ru-**1**·octyne]$^+$ complex contains a pseudo-octahedral Ru ion in a meridional P_3S_3 donor environment. The Ru–S and Ru–P bond lengths range from 2.3106(15) to 2.3890(14) Å and 2.3294(14) to 2.3823(14) Å, respectively, in accord with related structures, Table 1.[1,3,15] The alkynyl carbon atoms of 1-octyene provide a bridge, C55 and C56, between the *cis*-sulfur donors, S2 and S3. The S2–C55 and S3–C56 bond lengths of 1.798(8) and 1.796(7) Å, respectively, confirm covalent attachment of 1-octyne to the metal-stabilized thiyl radical core with values similar to those observed in alkene addition products such as [Ru-**1**·C_2H_4]$^+$. The S2–C55–C56–S3 torsion angle, 8.3(8)°, approaches zero as expected for an *S*-alkylated dithiolene chelate; in contrast to the torsion angle of –47.3(3)° for the dithioether fragment in [Ru-**1**·C_2H_4]$^+$. The C55–C56 bond length, 1.322(10) Å, matches the values of 1.312(9) and 1.394(10) Å reported by Yan in their alkyne addition products and is consistent with a C–C double bond.[12,13]

Table 1. Selected bond lengths [Å] and angles [°] of [Ru-**1**·octyne]$^+$, [Ru-**1**·C_2H_4]$^+$,[3] and [Ru-**1**]$^-$.[15]

	[Ru-**1**·octyne]$^+$	[Ru-**1**·C_2H_4]$^+$	[Ru-**1**]$^-$
Ru–S1	2.3890(14)	2.3856(9)	2.402(1)
Ru–S2	2.3663(15)	2.3749(9)	2.445(1)
Ru–S3	2.3106(15)	2.3365(9)	2.394(1)
Ru–P1	2.3294(14)	2.3290(9)	2.295(1)
Ru–P2	2.3422(14)	2.3965(10)	2.353(1)
Ru–P3	2.3823(14)	2.3648(9)	2.340(1)
S2–C55	1.798(8)	1.836(4)	
S3–C56	1.796(7)	1.843(4)	
C55-C56	1.322(10)	1.510(5)	
S2–Ru–S3	86.22(6)	87.71(3)	89.77(2)
Ru–S2–C55	103.1(3)	104.52(12)	
Ru–S3–C56	105.2(3)	103.59(12)	
S2–C55–C56–S3	8.3(8)	–47.3(3)	

The ^{31}P NMR of crystalline [Ru-**1**·octyne]$^+$ displays a pair of second-order spectra, Figure S2. The relative intensities, chemical shifts, and coupling constants for the major (60%) (δ_1 = 57.2, δ_2 = 42.8, δ_3 = 35.8 ppm; J_{12} = J_{13} = 31 and J_{23} = 313 Hz) and minor (40%) isomers (δ_1 = 57.2, δ_2 = 43.0, δ_3 = 36.2 ppm; J_{12} = J_{13} = 31 and J_{23} = 313 Hz) are similar to values previously reported for the two isomers of [Ru-**1**·p-methylstyrene]$^+$.[1] In that study, the isomer with the substituted carbon positioned nearest the S *trans* to S was identified as the major alkene addition product. This is consistent with the higher calculated spin densities[4] on the S *trans* to P (0.31) as compared to the S *trans* to S (0.21) and Tedder's Rules for radical alkene addition.[16] Given similar product ratios, we assign the major isomer of [Ru-**1**·octyne]$^+$ likewise.

The cyclic voltammogram of [Ru-**1**·octyne]$^+$ reveals a single, reversible redox event at +300 mV (vs. ferrocenium/ferrocene) [Figure 2 (top)] assigned to the $Ru^{III/II}$ couple. No other redox couples are observed, which indicates that both isomers have the same potential. Further, the $Ru^{II/I}$ couple lies outside the solvent window, which precludes the possibility of reduction promoted release of 1-octyne. As shown in Table 2, the redox couple is shifted by +1130 mV with respect to the $Ru^{III/II}$ couple in the thiolate precursor [Ru-**1**]$^-$.[17] Similar large shifts are observed for the related dithioether derivatives.[1,3,4,15]

The addition of 1-octyne to electrochemically generated [Ru-**1**]$^+$ was monitored by cyclic voltammetry. As shown in Figure 2 (bottom), the cyclic voltammogram of [Ru-**1**]$^-$ recorded in the presence of 1-octyne displays anodic peaks associated with the oxidation of [Ru-**1**]$^-$ to [Ru-**1**] at –830 mV and of [Ru-**1**] to [Ru-**1**]$^+$ at –60 mV. Following the second oxidation, 1-octyne rapidly adds to [Ru-**1**]$^+$ to yield [Ru-**1**·octyne]$^+$, as identified by its $Ru^{III/II}$ redox couple at

 © 2012 Wiley-VCH Verlag GmbH & Co. KGaA, Weinheim

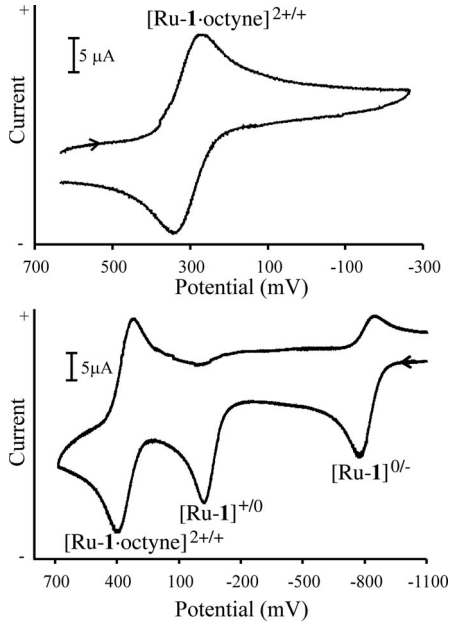

Figure 2. (top) Cyclic voltammogram of [Ru-**1**·octyne]$^+$ (1.0 mM in CH_3CN with 0.1 M TBAHFP) at a scan rate of 200 mV/s. (bottom) Cyclic voltammogram of [Ru-**1**]$^-$ (2.0 mM in CH_3CN with 0.1 M TBAHFP) in the presence of 1-octyne (200 mM) at a scan rate of 200 mV/s. Potentials are referenced vs. the ferrocenium/ferrocene couple.

Table 2. Electrochemical comparison of [Ru-**1**]$^-$, [Ru-**1**·octyne]$^+$, and [Ru-**1**·C_2H_4]$^+$.

Redox couple	$E_{1/2}$ (ΔE) / mV[a]	Formal oxidation states	Ref.
[Ru–1]$^{0/-}$	–830 (95)	$Ru^{III/II}$	[17]
[Ru-1·octyne]$^{2+/+}$	+300 (75)	$Ru^{III/II}$	this work
[Ru-**1**·C_2H_4]$^{2+/+}$	+285 (80)	$Ru^{III/II}$	[3]

[a] Potentials vs. ferrocenium/ferrocene reference. $\Delta E = E_{pc} - E_{pa}$ at a scan rate of 200 mV/s. Measurements were recorded in dry, degassed acetonitrile with 0.1 M tetrabutylammonium hexafluorophosphate as supporting electrolyte.

+300 mV. The rapid, irreversible binding of 1-octyne to [Ru-**1**]$^+$ is also evident by the decrease in cathodic current for the [Ru-**1**]$^{+/0}$ and [Ru-**1**]$^{+/0}$ couples.

The rate constant for 1-octyne addition to [Ru-**1**]$^+$ was evaluated by using methods previously described for alkene addition. A series of cyclic voltammograms were recorded over a range of scan rates, 100–1000 mV/s, for solutions containing [Ru-**1**]$^-$ and 1-octyne. The data were simultaneously fitted over all scan rates by using the Digisim software package[18] to determine a second-order rate constant of 8.7×10^3 $M^{-1}s^{-1}$ for the alkyne addition reaction. This value is two orders of magnitude lower than the corresponding alkene addition rate constant for 1-hexene to [Ru-**1**]$^+$, 7(2) $\times 10^5$ $M^{-1}s^{-1}$.[1] A 100–1000-fold decrease in rate constant is typical for electrophilic substitutions of comparable alkynes and alkenes. This corroborates our previous observation based on substituent effects of alkene addition to [Ru-**1**]$^+$ that our metal-stabilized thiyl radical complex is electrophilic.

Conclusions

The previously reported addition reaction of alkenes to the metal-stabilized thiyl radical [Ru-**1**]$^+$ has been extended to alkynes. By using similar chemical oxidation strategies, 1-octyne is efficiently added to [Ru-**1**]$^+$ to yield an *S*-alkylated dithiolene ligand that remains coordinated to the metal center. As with alkenes, the addition of alkyne to the Ru core is irreversible, which is attributable to the stability of the Ru^{II} oxidation state in a pseudo-octahedral environment. The rate constant for 1-octyne addition was found to be approximately 100 times lower than those of the corresponding alkenes, in line with the electrophilic character of our metal-stabilized thiyl radical. We are currently exploring the addition of other alkynes and related unsaturated compounds to establish the scope and limits of this reactivity.

Experimental Section

All reactions were performed under an inert nitrogen or argon atmosphere by using standard Schlenk techniques. Solvents were purified, dried, and freshly distilled and degassed immediately prior to use. The ruthenium thiolate precursors $HNEt_3$[Ru-**1**][19] and PPN[Ru-**1**][15] were prepared as described previously. All other chemicals were purchased from Aldrich and used as received. Elemental analyses were obtained from Midwest Microlab, LLC in Indianapolis, Indiana. Electrochemical measurements were performed with a PAR 273A potentiostat/galvanostat in dry, degassed acetonitrile with 0.1 M tetrabutylammonium hexafluorophosphate (TBAHFP) as supporting electrolyte. Additional details of the electrochemical measurements are described in the Supporting Information.

Crystallographic Studies: Crystals of [Ru-**1**·octyne]PF_6 adequate for X-ray diffraction studies were grown from chlorobenzene/hexane. $[Ru(C_{62}H_{55}P_3S_3)]^+[PF_6]^-$: yellow prism, monoclinic, space group $P2_1/n$, a = 12.0367(4), b = 24.2458(10) Å, c = 20.1572(9) Å, β = 98.291(3)°, V = 5821.2(7) Å^3, $r_{calcd.}$ = 1.409 g/cm^3, Z = 4. Data were collected on an Agilent Technologies/Oxford Diffraction Gemini CCD diffractometer at 100 K by using Mo-K_α radiation. For 8452 reflections, $I > 2\sigma(I)$ [R(int) 0.061], the final anisotropic full-matrix least-squares refinement on F^2 for 679 variables converged at $R1$ = 0.078 and $wR2$ = 0.133 with a GOF of 1.06. Full details of the data collection and structure refinement are provided in the Supporting Information. CCDC-844993 contains the supplementary crystallographic data for this paper. These data can be obtained free of charge from The Cambridge Crystallographic Data Centre via www.ccdc.cam.ac.uk/data_request/cif.

[Ru-1·octyne]PF_6: To a yellow solution of $HNEt_3$[Ru-**1**] (100 mg, 0.0935 mmol) in dry acetonitrile (40 mL) was added 1-octyne (1.38 mL, 9.35 mmol) by a syringe. The solution was cooled to 0 °C in an ice bath, and a blue solution of ferrocenium hexafluorophosphate (61.9 mg, 0.0187 mmol) in acetonitrile (30 mL) was slowly added by a cannula. The resulting solution was stirred overnight, during which time the solution gradually developed a dark orange color. The solvent was removed by rotary evaporation to yield an oily orange residue. The crude product was washed with an excess of hot water (≈300 mL) and diethyl ether (100 mL). The crude product was recrystallized from THF/hexane. Yield: 49 mg (0.040 mmol, 43%). X-ray quality crystals were obtained by slow evaporation of a 1:2 chlorobenzene/hexane mixture. $E_{1/2}$ ($Ru^{III/}$

 © 2012 Wiley-VCH Verlag GmbH & Co. KGaA, Weinheim

Ru^{II}) = +356 mV. +ESI-MS: calcd. for $C_{62}H_{56}P_3S_3Ru$ *m/z* (*Z* = 1) = 1091.37; found: 1091.18. $C_{62}H_{56}F_6P_4RuS_3$ (1236.26): calcd. C 60.23, H 4.57; found C 58.03, H 3.72. Electronic absorption: λ_{max} (ε [cm^{-1}], M^{-1}) = 305 (9527), 361 nm (shoulder). FTIR (KBr pellet): $\tilde{\nu}$ = 3052, 2929, 2852, 1434, 1086, 837, 559, 531 cm^{-1}.

Supporting Information (see footnote on the first page of this article): Details of X-ray diffraction and electrochemical methods, ESI-MS and ^{31}P NMR spectra, and cyclic voltammograms are presented.

Acknowledgments

Acknowledgments is made to the National Science Foundation (CHE-0749965). M. S. M. thanks the Department of Defense (W81XWH) from the Telemedicine and Advanced Technology Research Center of the US Army, the Department of Energy (DEFG02-08CH11538), and the Kentucky Research Challenge Trust Fund for the upgrade of our X-ray facilities.

[1] K. Ouch, M. S. Mashuta, C. A. Grapperhaus, *Inorg. Chem.* **2011**, *50*, 9904–9914.
[2] C. A. Grapperhaus, K. Ouch, M. S. Mashuta, *J. Am. Chem. Soc.* **2009**, *131*, 64–65.
[3] C. A. Grapperhaus, K. B. Venna, M. S. Mashuta, *Inorg. Chem.* **2007**, *46*, 8044–8050.
[4] C. A. Grapperhaus, P. M. Kozlowski, D. Kumar, H. N. Frye, K. B. Venna, S. Poturovic, *Angew. Chem.* **2007**, *119*, 4163; *Angew. Chem. Int. Ed.* **2007**, *46*, 4085–4088.
[5] R. Y. C. Shin, M. E. Teo, W. K. Leong, J. J. Vittal, J. H. K. Yip, L. Y. Goh, R. D. Webster, *Organometallics* **2005**, *24*, 1483–1494.
[6] M. J. Kerr, D. J. Harrison, A. J. Lough, U. Fekl, *Inorg. Chem.* **2009**, *48*, 9043–9045.
[7] D. J. Harrison, A. J. Lough, N. Nguyen, U. Fekl, *Angew. Chem.* **2007**, *119*, 7788; *Angew. Chem. Int. Ed.* **2007**, *46*, 7644–7647.
[8] D. J. Harrison, N. Nguyen, A. J. Lough, U. Fekl, *J. Am. Chem. Soc.* **2006**, *128*, 11026–11027.
[9] K. Wang, E. I. Stiefel, *Science* **2001**, *291*, 106–109.
[10] N. Nguyen, D. J. Harrison, A. J. Lough, A. G. De Crisci, U. Fekl, *Eur. J. Inorg. Chem.* **2010**, 3577–3585.
[11] H. D. Ye, B. H. Xu, M. S. Xie, Y. Z. Li, H. Yan, *Dalton Trans.* **2011**, *40*, 6541–6546.
[12] D. Wu, Y. Li, L. Han, Y. Li, H. Yan, *Inorg. Chem.* **2008**, *47*, 6524–6531.
[13] D.-H. Wu, C. Ji, Y.-Z. Li, H. Yan, *Organometallics* **2007**, *26*, 1560–1562.
[14] L. J. Farrugia, *J. Appl. Crystallogr.* **1997**, *30*, 565.
[15] C. A. Grapperhaus, S. Poturovic, M. S. Mashuta, *Inorg. Chem.* **2002**, *41*, 4309–4311.
[16] J. M. Tedder, *Angew. Chem.* **1982**, *94*, 433; *Angew. Chem. Int. Ed. Engl.* **1982**, *21*, 401–410.
[17] C. A. Grapperhaus, S. Poturovic, *Inorg. Chem.* **2004**, *43*, 3292–3298.
[18] *DigiSim* (3.03b), Bioanalytical Systems, Inc.: West Lafayette, IN, **2004**.
[19] J. Dilworth, Y. Zheng, S. Lu, Q. Wu, *Transition Met. Chem.* **1992**, *17*, 364–368.

Received: September 23, 2011
Published Online: Dezember 1, 2011

 © 2012 Wiley-VCH Verlag GmbH & Co. KGaA, Weinheim

DOI: 10.1002/ejic.201100787

A Reduced (β-Diketiminato)iron Complex with End-On and Side-On Nitriles: Strong Backbonding or Ligand Non-Innocence?

Ryan E. Cowley,[a] Gemma J. Christian,[b] William W. Brennessel,[a] Frank Neese,*[b,c] and Patrick L. Holland*[a]

Keywords: Nitriles / Iron / Density functional calculations / Pi interactions

Treatment of the iron(I) synthon $L^{Me}FeNNFeL^{Me}$ (L^{Me} = β-diketiminato ligand) with pivalonitrile gives a formally iron(I) complex $L^{Me}Fe(NC{t}Bu)_2$, which has one strongly bound side-on nitrile and one weakly bound end-on nitrile ligand. The side-on nitrile ligand has N–C–C bending and N–C weakening that suggests partial reduction of the nitrile group. The *S* = 3/2 ground state of this molecule can be described as either an iron(II) atom with a nitrile radical anion or an iron(I) atom that is strongly backbonding. DFT computations show that strong backbonding comes from a doubly occupied orbital, and that there is little ligand radical character. Therefore, the iron(I) formulation is the most appropriate. This study exemplifies how one-electron transfer to ligands and two-electron backbonding to ligands may be distinguished by using spectroscopically calibrated and validated computations.

Introduction

There is great interest in redox-active or "non-innocent" ligands, because these ligands can vary the number of electrons shared with the metal center.[1] In a number of examples, chemists have used the redox flexibility to bring about novel reactivity.[2] The chemistry community is still exploring the range of ligands that can display "non-innocent" behavior. We have found the formally iron(I) fragments $L^{tBu}Fe$ and $L^{Me}Fe$ to be very useful for exploring the chemistry of reduced iron with various ligands [L^{tBu} = 2,2,6,6-tetramethyl-3,5-bis(2,6-diisopropylphenylimido)-4-heptyl; L^{Me} = 2,4-bis(2,6-diisopropylphenylimido)-3-pentyl; L is used as the generic term for either of these β-diketiminate ligands]. As the dinitrogen complexes LFeNNFeL lose N_2 easily, they have been convenient synthons for formally iron(I) complexes of neutral ligands such as CO, CN*t*Bu, PPh_3, benzene, alkenes, and alkynes.[3,4]

In a number of cases, the formally iron(I) complexes of the LFe fragments have spin delocalization on the ligands. For example, spectroscopic and computational studies on $L^{Me}FeNNFeL^{Me}$ (**1**) showed that the sextet ground state of **1** was not $LFe^{I}(N_2^{0})Fe^{I}L$, but was best explained by the resonance form $LFe^{II}(N_2^{2-})Fe^{II}L$, in which one electron was transferred from each iron atom to the coordinated N_2 fragment to give triplet N_2^{2-}.[4,5] This behavior was also evident in a tetrazene (RNNNNR) complex of $L^{Me}Fe$, where the best electronic description was a tetrazene anion radical coordinated to iron(II).[6] In another case, we described the electronic structure of the alkyne complex $L^{tBu}Fe(PhCCH)$.[3c] There was substantial backbonding from the iron-based d_{xy} orbital to the alkyne π* orbital, with the alkyne ligand carrying a net charge of –0.8. Interestingly, the iron center in the alkyne complex held a charge of +1.1, implying that the net charge donation from iron(I) to the alkyne was compensated by a charge donation from the diketiminato ligand to the iron center.

Motivated by our interest in understanding the electronic structure of metal–ligand interactions in reduced iron complexes, we have now prepared a complex of pivalonitrile (NC*t*Bu) in order to investigate its electronic structure. Metal–nitrile complexes are ubiquitous in coordination chemistry,[7] and reduced metals such as nickel(0) have been shown to cleave C–CN bonds of nitriles,[8] demonstrating the utility of such compounds.

Results and Discussion

Addition of 4 equiv. of NC*t*Bu to a pentane solution of the dinitrogen complex **1** (Scheme 1) results in an immediate color change from dark red-orange to yellow-brown,

[a] Department of Chemistry, University of Rochester, Rochester, NY 14627, USA
E-mail: holland@chem.rochester.edu
[b] Lehrstuhl für Theoretische Chemie, Universität Bonn, Wegelerstraße 12, 53115 Bonn, Germany
[c] Max-Planck-Institute für Bioanorganische Chemie, Stiftstraße 34-36, 45470 Mülheim an der Ruhr, Germany
Supporting information for this article is available on the WWW under http://dx.doi.org/10.1002/ejic.201100787 or from the author.

 © 2012 Wiley-VCH Verlag GmbH & Co. KGaA, Weinheim

concomitant with gas evolution. The ^{1}H NMR spectrum (Figure 2 inset) of the product shows quantitative conversion to a new paramagnetic species **2**, which may be isolated in crystalline form in 54% yield. X-ray diffraction of a single crystal shows that the product is the bis(pivalonitrile) complex $L^{Me}Fe(NCtBu)_2$ (Figure 1). One nitrile ligand, which occupies the basal site in the pseudo-trigonal pyramid, is coordinated in a side-on (η^2) fashion, whereas the axial nitrile ligand is coordinated in the usual end-on (η^1) manner. Notably, **2** is the first structurally characterized mononuclear iron complex with side-on nitrile binding.[9] Side-on binding of nitriles has been seen in other electron-rich late-transistion-metal systems.[10] There is only one previous example of both end-on and side-on organonitrile ligands coordinated to the same metal atom.[10h]

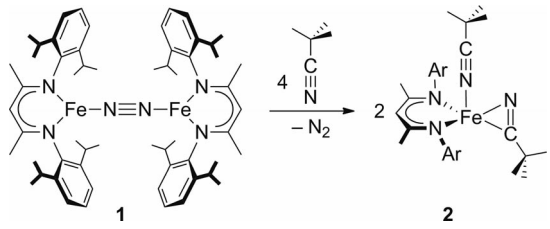

Scheme 1.

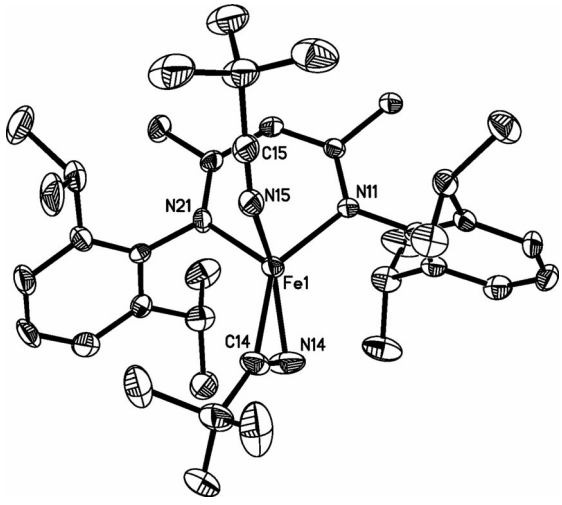

Figure 1. Molecular structure of $L^{Me}Fe(NCtBu)_2$ (**2**) with 50% probability thermal ellipsoids. Hydrogen atoms and minor components of the disorder are removed for clarity, and only one of the three unique molecules in the asymmetric unit is shown. Selected bond lengths [Å] and angles [°]: Fe1–N11 2.009(2), Fe1–N21 2.031(2), Fe1–N14 1.948(2), Fe1–C14 1.975(2), Fe1–N15 2.074(2), N14–C14 1.194(4), N15–C15 1.144(3); N11–Fe1–N21 94.01(8), N14–C14–C24 139.3(3), N15–C15–C25 177.3(3), Fe1–N15–C15 157.6(2).

The room-temperature magnetic moment of **2** of $4.1 \pm 0.2\ \mu_B$ is consistent with a quartet ($S = 3/2$) spin state (expected spin-only value $3.9\ \mu_B$). The quartet ground state is also evident from the X-band EPR spectrum recorded at 5 K (Figure 2), which shows a single rhombic signal with $g_{eff} = 5.58, 2.64, 1.72$. This spectrum may be readily simulated as an $S = 3/2$ species; however, there were multiple choices of D and g values that fit the spectrum equally well, so the particular choice of parameters used in Figure 2 is not unique.

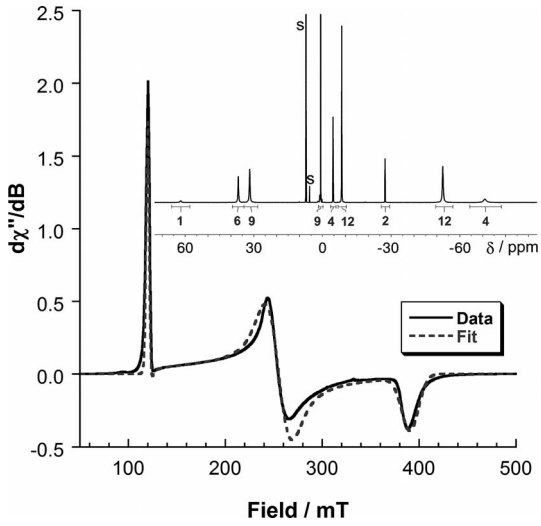

Figure 2. X-band EPR spectrum of $L^{Me}Fe(NCtBu)_2$ (**2**) recorded at 5.0 ± 0.1 K in frozen toluene solution (solid line). Parameters: microwave frequency 9.386 GHz, microwave power 1.0 mW, modulation amplitude 9.8 G, modulation frequency 100 kHz, time constant 98 ms. The dashed line represents a simulation with $S = 3/2$, $g_x = 2.62$, $g_y = 2.03$, $g_z = 2.33$, $D = 20\ cm^{-1}$, and $E/D = 0.33$. D and E are the axial and rhombic zero-field-splitting parameters, respectively. Inset: ^{1}H NMR spectrum of **2** in C_6D_6. Resonances for residual solvents are marked "s", and peak integrations are listed below the spectrum.

Interestingly, the chemical shifts in the ^{1}H NMR spectrum of **2** are dependent on the concentration of added [NC*t*Bu], indicating an NC*t*Bu-dependent equilibrium (see Supporting Information for spectra and fits). Fitting a plot of change in chemical shift ($\Delta\delta$) vs. $[NCtBu]_0$ yields an equilibrium binding constant of 0.70(4) M^{-1}. From the binding curve alone, it is not possible to distinguish whether this equilibrium involves reversible nitrile binding to the mono(nitrile) or to the bis(nitrile) species. However, the ^{1}H NMR spectrum recorded with 2.0 equiv. of NC*t*Bu per iron atom (Figure 2 inset) shows two inequivalent nine-proton resonances at $\delta = 32$ and $\delta = 0.78$ ppm corresponding to *t*Bu hydrogen atoms. The *t*Bu resonance located at $\delta = 0.78$ ppm is within 0.01 ppm of the resonance of free NC*t*Bu in the absence of **2**, suggesting that it is not bound to the paramagnetic metal center. Considering the very weak binding constant for NC*t*Bu, this observation is consistent with strong binding of 1 equiv. of NC*t*Bu (giving a single paramagnetically shifted *t*Bu signal) and weak bind-

 © 2012 Wiley-VCH Verlag GmbH & Co. KGaA, Weinheim

ing of the other (giving an unshifted signal). Thus, in dilute solution at 25 °C, complex **2** primarily exists as $L^{Me}Fe(NCtBu)$, and a second equivalent of NC*t*Bu binds weakly and exchanges rapidly on the NMR timescale. At the concentrations used in Figure 2 ($[Fe]_0$ = 21 mM, $[tBuCN]_0$ = 42.5 mM), a binding constant of 0.7 M^{-1} yields equilibrium concentrations of $[L^{Me}Fe(NCtBu)]_{eq}$ = 41.8 mM and $[L^{Me}Fe(NCtBu)_2]_{eq}$ = 1.2 mM. In other words, < 3% of the total iron atoms exist as $L^{Me}Fe(NCtBu)_2$ in C_6D_6 solution at room temperature. However, lowering of the temperature of the sample induces full binding of the nitrile to give the crystallographically characterized bis(nitrile) complex; accordingly, the low-temperature EPR spectrum in Figure 2 was unchanged by the addition of excess (> 100 equiv.) NC*t*Bu, indicating that the sample consists of only the bis(nitrile) complex at this temperature.

The Mössbauer spectrum of a solid sample of **2** (Figure 3) consists of a doublet with an isomer shift of δ = 0.72 mm/s and a quadrupole splitting of $|\Delta E_Q|$ = 1.87 mm/s. Interestingly, the isomer shift of complex **2** (δ = 0.72 mm/s) is significantly higher than that for the iron(I) complex $L^{tBu}Fe(PhCCH)$ [δ = 0.44(1) mm/s],[3c] but is close to those of pseudotetrahedral (diketiminato)iron(II) complexes[11] such as $L^{Me}Fe(N_4Ad_2)$ [N_4Ad_2 = 1,4-bis(1-adamantyl)-tetraazayl monoanion] (0.69 mm/s),[12] and $\{L^{Me}Fe\}_2(N_6Ad_2)$ [N_6Ad_2 = 1,6-bis(1-adamantyl)hexaazadiyl dianion] (0.75 mm/s).[6] This initially suggested a potential description of **2** as an iron(II) complex with a radical anion nitrile ligand.

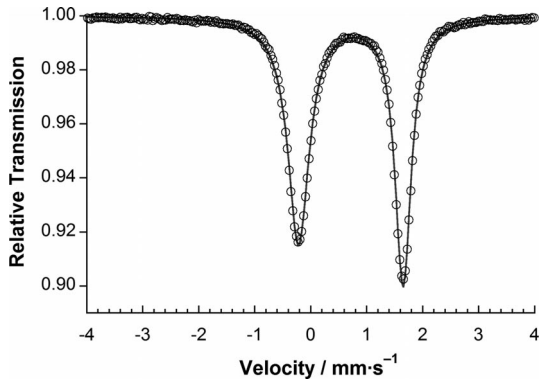

Figure 3. Zero-field Mössbauer spectrum of compound **2** recorded at 80 K. The data are the open circles, and the solid represents the fit to δ = 0.72 mm/s and $|\Delta E_Q|$ = 1.87 mm/s.

To investigate the electronic structure of **2** in more detail, we turned to DFT computations using ORCA.[13] The geometry of **2** was optimized with the B3LYP functional[14] with the ZORA-TZVP[15] basis set for Fe, N, and C and the ZORA-SVP[9] basis set for H. Relativistic corrections were treated by using the ZORA approximation.[16] Consistent with experiment, the quartet state was calculated to be the ground state, with the sextet and doublet spin states at least 60 kJ/mol higher in energy. The calculated Mössbauer parameters of δ = 0.73 mm/s and ΔE_Q = +1.71 mm/s match the experimental parameters well, suggesting that this theoretical model captures the electronic structure of the iron atom accurately.

The η^2-NC*t*Bu ligand has a calculated N–C bond length of 1.217 Å and an N–C–C bond angle of 139°. These match the crystallographically established values extremely well except for the N–C distance of 1.194(4) Å in the crystal structure; we attribute the discrepancy to a systematic error in the crystallographic structure due to libration of the nitrile N atom, which is evident in the refined thermal parameters of N14. Both the N–C distance and N–C–C angle are significantly different than those in free MeCN (1.167 Å, 180°), and the bending and C–N weakening suggest some metal donation into the C–N π* orbital. The N–C distance and N–C–C angle in **2** are much more similar to the corresponding values for singly reduced acetonitrile ($NCMe^{\cdot-}$), which has an N–C bond length of 1.231 Å and N–C–C angle of 139° (uncoordinated, gas phase). Hence, based on bond metrics, the computational results suggest close to a single reduction of the η^2-NC*t*Bu ligand.

This raises a key question: what is the nature of the side-on nitrile–iron interaction in **2**? There are two possibilities: (i) The NC*t*Bu ligand is reduced by a single electron (the "non-innocence" possibility), or (ii) a completely filled Fe d-orbital backbonds into the empty N–C π* orbital (the "backbonding" possibility). The data presented thus far are consistent with *both* possible scenarios. In each case, electron density is moved from the Fe atom to the NC*t*Bu ligand, which accounts for the Mössbauer isomer shift being more reminiscent of iron(II) than iron(I). Also, in each case, the N–C π* orbital would be at least partially occupied, which would decrease the N–C bond order and lengthen the bond.

The backbonding and non-innocence scenarios may be distinguished by evaluation of the frontier molecular orbitals from the spectroscopically validated computations (Figure 4). Importantly, the three singly occupied orbitals do not have significant ligand character. The d_{xz} orbital is involved in π bonding with the π* orbitals of the η^2-NC*t*Bu ligand, and the orbital is *doubly occupied*. This orbital has 52% d-character with the remaining contributions from the NC π* orbitals, indicating a strongly covalent interaction. An alternative ligand-radical solution and its corresponding broken symmetry solution can be found 70 kJ mol^{-1} higher in energy; however, this returns to the electronic structure described above upon geometry optimization. This behavior differs from the previous tetrazene complex of $L^{Me}Fe$, in which the broken-symmetry solution of the geometry-optimized complex placed a singly occupied MO on the $RNNNNR^{\cdot-}$ ligand in the lowest-energy state.[6] Thus, it is more appropriate to view the metal–ligand bond in **2** as highly covalent two-electron backbonding from the Fe d_{xz} orbital to the nitrile π* orbital, rather than a case of ligand redox non-innocence with radical character on the ligand.

 © 2012 Wiley-VCH Verlag GmbH & Co. KGaA, Weinheim

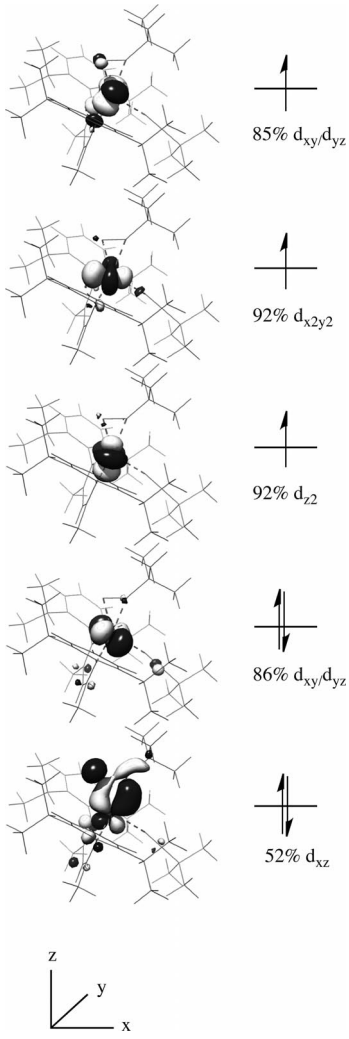

Figure 4. Frontier molecular orbitals for $L^{Me}Fe(NC\textit{t}Bu)_2$ (**2**) with their corresponding Fe d-orbital character. The two orbitals labeled d_{xy}/d_{yz} are linear combinations of d_{xy} and d_{yz}.

Conclusions

This study offers an interesting test of redox non-innocence: does transfer of electron density from a high-spin metal center to a coordinated ligand necessarily lead to spin density on the ligand? In this case, the spectroscopically calibrated computations indicate that the answer is no. Although the geometry of the coordinated nitrile is similar to that in the nitrile radical anion, and the Mössbauer isomer shift is suggestive of iron(II), the computations indicate that two-electron backbonding is the cause of the bending of the nitrile and weakening of the C–N bond. Backbonding is different than the usual definition of ligand "non-innocence," in which the ligand accepts spin density.[1] These results serve as a reminder that charge-sharing between the metal atom and ligand can occur through both one-electron and two-electron transfer, and highlight the important role of spectroscopically calibrated computations in distinguishing backbonding from non-innocence, especially when crystallography and spectroscopy do not make this distinction.

Supporting Information (see footnote on the first page of this article): Experimental and computational details, ^{1}H NMR binding curves.

Acknowledgments

The authors acknowledge funding from the National Science Foundation (CHE-0911314) and the University of Rochester (Elon Hooker Fellowship to R. E. C.). Microanalytical data were obtained at the CENTC Elemental Analysis Facility funded by the NSF (CHE-0650456). We thank Eckhard Bill and Bernd Mienert for providing the Mössbauer data.

[1] W. Kaim, *Inorg. Chem.* **2011**, DOI: 10.1021/ic2003832.
[2] a) K. Wang, E. I. Stiefel, *Science* **2001**, *291*, 106; b) D. J. Harrison, N. Nguyen, A. J. Lough, U. Fekl, *J. Am. Chem. Soc.* **2006**, *128*, 11026; c) M. R. Haneline, A. F. Heyduk, *J. Am. Chem. Soc.* **2006**, *128*, 8410; d) K. J. Blackmore, N. Lal, J. W. Ziller, A. F. Heyduk, *J. Am. Chem. Soc.* **2008**, *130*, 2728; e) D. Adhikari, S. Mossin, F. Basuli, J. C. Huffman, R. K. Szilagyi, K. Meyer, D. J. Mindiola, *J. Am. Chem. Soc.* **2008**, *130*, 3676; f) R. J. Trovitch, E. Lobkovsky, P. J. Chirik, *Inorg. Chem.* **2006**, *45*, 7252; g) M. W. Bouwkamp, A. C. Bowman, E. Lobkovsky, P. J. Chirik, *J. Am. Chem. Soc.* **2006**, *128*, 13340; h) C. Stanciu, M. E. Jones, P. E. Fanwick, M. M. Abu-Omar, *J. Am. Chem. Soc.* **2007**, *129*, 12400; i) F. F. Puschmann, H. Grützmacher, B. de Bruin, *J. Am. Chem. Soc.* **2010**, *132*, 73; j) A. L. Smith, K. I. Hardcastle, J. D. Soper, *J. Am. Chem. Soc.* **2010**, *132*, 14358; k) H. Lu, W. I. Dzik, X. Xu, L. Wojtas, B. de Bruin, X. P. Zhang, *J. Am. Chem. Soc.* **2011**, *133*, 8518.
[3] a) Y. Yu, A. R. Sadique, J. M. Smith, T. R. Dugan, R. E. Cowley, W. W. Brennessel, C. J. Flaschenriem, E. Bill, T. R. Cundari, P. L. Holland, *J. Am. Chem. Soc.* **2008**, *130*, 6624; b) Y. Yu, J. M. Smith, C. J. Flaschenriem, P. L. Holland, *Inorg. Chem.* **2006**, *45*, 5742; c) S. A. Stoian, Y. Yu, J. M. Smith, P. L. Holland, E. L. Bominaar, E. Münck, *Inorg. Chem.* **2005**, *44*, 4915; d) R. E. Cowley, N. A. Eckert, J. Elhaïk, P. L. Holland, *Chem. Commun.* **2009**, 1760.
[4] J. M. Smith, A. R. Sadique, T. R. Cundari, K. R. Rodgers, G. Lukat-Rodgers, R. J. Lachicotte, C. J. Flaschenriem, J. Vela, P. L. Holland, *J. Am. Chem. Soc.* **2006**, *128*, 756.
[5] S. A. Stoian, J. Vela, J. M. Smith, A. R. Sadique, P. L. Holland, E. Münck, E. L. Bominaar, *J. Am. Chem. Soc.* **2006**, *128*, 10181.
[6] R. E. Cowley, E. Bill, F. Neese, W. W. Brennessel, P. L. Holland, *Inorg. Chem.* **2009**, *48*, 4828.
[7] a) B. N. Storhoff, H. C. Lewis, *Coord. Chem. Rev.* **1977**, *23*, 1; b) R. A. Michelin, M. Mozzon, R. Bertani, *Coord. Chem. Rev.* **1996**, *147*, 299; c) A. J. L. Pombeiro, V. Y. Kukushkin, "Reactivity of Coordinated Nitriles," in *Comprehensive Coordination Chemistry II*, vol. 1 (Eds.: J. A. McCleverty, T. J. Meyer), Elsevier, Oxford, **2003**, pp. 639–660.
[8] For example: a) J. J. Garcia, W. D. Jones, *Organometallics* **2000**, *19*, 5544; b) J. J. Garcia, N. M. Brunkan, W. D. Jones, *J. Am. Chem. Soc.* **2002**, *124*, 9547; c) J. J. Garcia, A. Arévalo, N. M. Brunknan, W. D. Jones, *Organometallics* **2004**, *23*, 3997; d) G. Favero, A. Morvillo, A. Turco, *J. Organomet. Chem.* **1983**, *241*, 251.
[9] CSD version 5.32 (August 2011 update); F. H. Allen, *Acta Crystallogr., Sect. B* **2002**, *58*, 380.
[10] For example: a) M. H. Chisolm, K. Folting, J. C. Huffman, N. S. Marchant, *Polyhedron* **1984**, *3*, 1033; b) P. A. Chetcuti, C. B. Knobler, M. F. Hawthorne, *Organometallics* **1986**, *5*, 1913; c) T. C. Wright, G. Wilkinson, M. Motevalli, M. B.

 © 2012 Wiley-VCH Verlag GmbH & Co. KGaA, Weinheim

Hursthouse, *J. Chem. Soc., Dalton Trans.* **1986**, 2017; d) P. A. Chetcuti, C. B. Knobler, M. F. Hawthorne, *Organometallics* **1988**, *7*, 650; e) R. M. Bullock, C. E. L. Headford, K. M. Hennessy, S. E. Kegley, J. R. Norton, *J. Am. Chem. Soc.* **1989**, *111*, 3897; f) R. M. Bullock, C. E. L. Headford, S. E. Kegley, J. R. Norton, *J. Am. Chem. Soc.* **1985**, *107*, 727; g) D. Churchill, J. H. Shin, T. Hascall, J. M. Hahn, B. M. Bridgewater, G. Parkin, *Organometallics* **1999**, *18*, 2403; h) T. Komoru, T. Matsuo, H. Kawaguchi, K. Tatsumi, *J. Am. Chem. Soc.* **2003**, *125*, 2070; i) S. J. Anderson, F. J. Wells, G. Wilkinson, B. Hussain, M. B. Hursthouse, *Polyhedron* **1988**, *7*, 2615; J. Barrera, M. Sabat, W. D. Harman, *Organometallics* **1993**, *12*, 4381.

[11] Here we are comparing only the closest analogues, i.e., pseudo-tetrahedral complexes with nitrogen-based ligands.

[12] R. E. Cowley, J. Elhaïk, N. A. Eckert, W. W. Brennessel, E. Bill, P. L. Holland, *J. Am. Chem. Soc.* **2008**, *130*, 6074.

[13] F. Neese, *ORCA – an ab initio, Density Functional and Semiempirical Program Package*, 2.8 ed., Universität Bonn, Bonn, Germany, **2011**.

[14] a) A. D. Becke, *Phys. Rev. A* **1988**, *38*, 3098; b) J. P. Perdew, *Phys. Rev. B* **1986**, *33*, 8822; c) J. P. Perdew, *Phys. Rev. B* **1986**, *34*, 7406.

[15] a) D. A. Pantazis, X. Y. Chen, C. R. Landis, F. Neese, *J. Chem. Theory Comput.* **2008**, *4*, 908; b) F. Weigend, R. Ahlrichs, *Phys. Chem. Chem. Phys.* **2005**, *7*, 3297.

[16] a) E. van Lenthe, E. J. Baerends, J. G. Snijders, *J. Chem. Phys.* **1993**, *99*, 4597; b) E. van Lenthe, E. J. Baerends, J. G. Snijders, *J. Chem. Phys.* **1994**, *101*, 9783; c) E. van Lenthe, R. van Leeuwen, E. J. Baerends, J. G. Snijders, *Int. J. Quantum Chem.* **1996**, *57*, 281.

Received: July 27, 2011
Published Online: October 10, 2011

 © 2012 Wiley-VCH Verlag GmbH & Co. KGaA, Weinheim

DOI: 10.1002/ejic.201100780

Electronic Effects of Ligands on the Cobalt(II)–Porphyrin-Catalyzed Direct C–H Arylation of Benzene

Tek Long Chan,[a] Ching Tat To,[a] Bei-Sih Liao,[b] Shiuh-Tzung Liu,*[b] and Kin Shing Chan*[a]

Keywords: Electronic effects / Cobalt / C–H arylation / Rate-determining step / Ligand effects / Steric hindrance

The electronic effects of the porphyrin ligand on the cobalt(II)-porphyrin-catalyzed direct C–H arylation of benzene with 4-iodotoluene were explored. The investigation was facilitated by the easy preparation of various substituted porphyrin ligands. The reaction rates were found to be dependent on the electron richness of the cobalt(II)–porphyrins. Such effects are consistent with the electronic influences on the rate-determining aryl iodide bond cleavage.

Introduction

Utilization of ligands in homogeneous transition-metal-catalyzed reactions is essential. The ligands form transition-metal complexes with the inorganic metal salts, providing solubility and stability. However, the manner in which the ligands modify the reactivity of ligated metal centres through electronic effects is far more important to a reaction system. A demonstrative example is the successful oxidative addition of Pd complexes to strong C–Cl bonds of aryl chlorides with the use of electron-rich P*t*Bu$_3$ or PCy$_3$ ligands,[1] but it fails for the more commonly available PPh$_3$ ligand. The underlying principle involves the enhanced nucleophilicity of the Pd centre in the presence of very strong σ-donor ligands. Therefore, the Pd centre more readily attacks the σ* orbital of a C–Cl bond, facilitating the oxidative addition.[2] This shows that a suitable choice of ligand with varying electronic effects greatly facilitates the rate of the fundamental reaction step and makes reactions more facile.[3] The issue is particularly true when reaction pathways are ionic in nature or sensitive to electronic environments.

Therefore, finding the best ligand for a reaction system is crucial to optimization. Initial ligand screening is generally a random approach. Several readily available ligands are selected on the basis of their denticities, binding atoms, cone angles, hardness/softness or donor/acceptor properties. Although distinctive experimental results can be obtained, the commercially available ligands for preliminary studies may not be a final choice for maximum optimization when the scope of the reaction is broadened, such as the cross coupling of aryl chloride with C–Cl bond cleavage.[1] Moreover, a systematic evaluation of ligand electronic effects on the reaction will be a useful tool for mechanistic investigations.

The realization of ligand control can be accomplished by installing different substituents to tune the electronic factors, while keeping the steric environment minimally altered. Indeed, Busacca et al. discovered the ligand electronic dependence of stereoselectivity in asymmetric Heck reactions.[4] Very recently, Sanford et al. achieved the regioselective α-arylation of naphthalene through the systematic modulation of ligand substituent electronics.[5]

The macrocyclic porphyrin ligand is attractive for its thermal stability and easily tunable substituents at both the *meso* and β positions. Many porphyrin derivatives can be prepared from readily available aldehydes and pyrroles to meet the electronic requirements.[6] Therefore, the use of first-row transition-metal metalloporphyrins as catalysts, such as cobalt(II)–porphyrins, is attractive for the ease of ligand modulability and as a cheap metal source. Zhang et al. have extensively studied the chemistry of cobalt(II)–porphyrins on C–H amination,[7] cyclopropanation[8] and aziridination.[9] The studies revealed that the electronic factor of the porphyrin ligands is critical to the reaction outcome. Similarly, Sharghi et al. discovered that the electronics of cobalt(II)–porphyrins affect the reaction yields as well as the reaction rates in the thiocyanation of epoxides, because of the different formation constants for thiocyanate complexation.[10]

Aryl–aryl bond formations from two aromatics are of fundamental importance, and the search is always on for more user-friendly approaches.[11] Obtaining biaryls through direct C–H arylation is desirable.[12] Recently, we

[a] Department of Chemistry,
The Chinese University of Hong Kong, Shatin,
New Territories, Hong Kong, People's Republic of China
Fax: +852-26035057
E-mail: ksc@cuhk.edu.hk
[b] Department of Chemistry, National Taiwan University,
Taipei, Taiwan 106, Republic of China
Fax: +886-2-23636359
E-mail: stliu@ntu.edu.tw

 © 2012 Wiley-VCH Verlag GmbH & Co. KGaA, Weinheim

have reported the cobalt(II)–porphyrin-catalyzed direct C–H arylation of unactivated arenes with aryl halides.[13] In view of the easily tunable porphyrin ligands and thus its electronic effects on reaction systems, we report on the influences of electron-rich and -poor cobalt(II)–porphyrins on the direct C–H arylation of benzene. The axial ligand effects will also be discussed.

Results and Discussion

With the successful discovery of the direct C–H arylation of benzene with 4-iodotoluene catalyzed by $Co^{II}(t_{4\text{-}OMe}pp)$,[13] we further examined the porphyrin electronic effect by employing Co^{II}(tpp), Co^{II}(ttp), $Co^{II}(t_{4\text{-}Cl}pp)$, $Co^{II}(t_{4\text{-}CF3}pp)$ and Co^{II}(tmp) as the catalysts (Figure 1). These cobalt(II)–porphyrins were easily prepared by condensation of the corresponding substituted aldehydes with pyrrole, followed by metallation with $Co(OAc)_2{\cdot}4H_2O$.[14c] Electron-donating and -withdrawing *meso*-aryl substituents were installed with reference to Co^{II}(tpp).

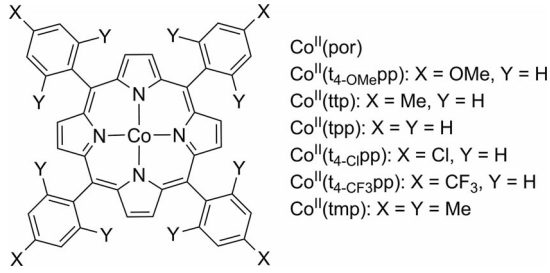

Figure 1. Structures of cobalt(II)–porphyrin complexes.

To our delight, we observed that the rate of direct C–H arylation increased with the electron richness of the Co^{II}(por) catalysts (Table 1). Electron-donating porphyrin $Co^{II}(t_{4\text{-}OMe}pp)$ resulted in the fastest C–H arylation in 2 h to give 79% of 4-methylbiphenyl (Table 1, Entry 1). A slightly longer reaction time was needed when less electron-rich Co^{II}(ttp) was used (Table 1, Entry 2). However, electron-poor cobalt(II)–porphyrins, such as $Co^{II}(t_{4\text{-}Cl}pp)$ and $Co^{II}(t_{4\text{-}CF3}pp)$, decreased the reaction rates significantly compared with other porphyrin ligands (Table 1, Entries 4 and 5). The poor solubility of $Co^{II}(t_{4\text{-}CF3}pp)$ in the reaction mixture also accounts for its lower performance. Interestingly, the reaction-rate enhancement was not observed when electron-rich and sterically hindered Co^{II}(tmp) was employed (Table 1, Entry 6). This is likely attributed to the offset of the electronic effect by bulky mesityl substituents. Meanwhile, reduction of 4-iodotoluene occurred in all cases as toluene was detected from the GC–MS analysis of the reaction mixtures. Therefore, cobalt(II)–porphyrins bearing electron-donating *meso*-aryl substituents increased the rate of direct C–H arylation of benzene.

Table 1. Electronic effects of porphyrins on the direct C–H arylation of benzene with 4-iodotoluene.

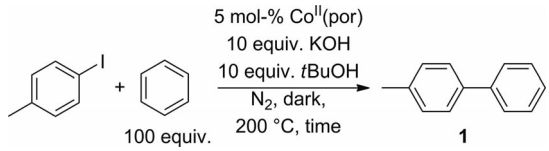

Entry	Co^{II}(por)	Time [h]	Yield of **1** [%][a]
1	$Co^{II}(t_{4\text{-}OMe}pp)$	2	79
2	Co^{II}(ttp)	3.5	88
3	Co^{II}(tpp)	4	70
4	$Co^{II}(t_{4\text{-}Cl}pp)$	8	78
5	$Co^{II}(t_{4\text{-}CF3}pp)$	20	66
6	Co^{II}(tmp)	4	84

[a] GC yield.

To obtain a quantitative comparison of the cobalt(II)–porphyrin electronic effect, the reactions of 4-iodotoluene with benzene catalyzed by various Co^{II}(por) complexes at 200 °C were monitored by withdrawing aliquots from the reaction mixtures for GC–MS analyses. The consumptions of 4-iodotoluene were plotted against reaction times. The plots fit well with a first-order exponential decay function (Figure 2) and confirmed the first-order dependence on 4-iodotoluene. The rate law can be expressed as rate $\propto k_{obs}$[4-iodotoluene]. The initial concentrations of benzene, Co^{II}(por) and 4-iodotoluene were 10.1 M, 5.07 mM and 101 mM, respectively.

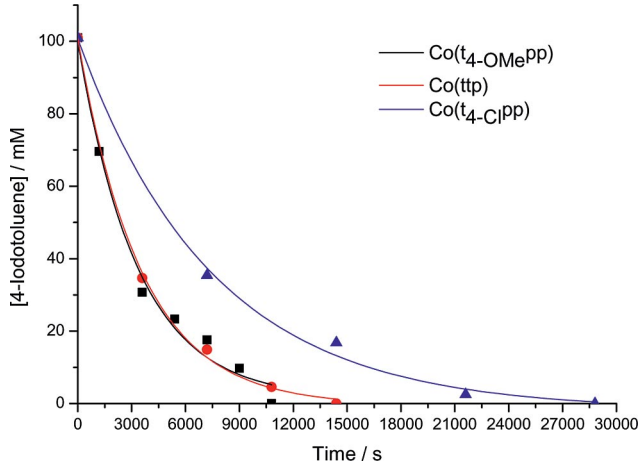

Figure 2. Reaction time profile of 4-iodotoluene.

The k_{obs} values for the $Co^{II}(t_{4\text{-}OMe}pp)$- Co^{II}(ttp)- and $Co^{II}(t_{4\text{-}Cl}pp)$-catalyzed direct C–H arylation were measured to be 2.1×10^{-4} s^{-1}, 2.0×10^{-4} s^{-1} and 9.2×10^{-5} s^{-1} at 200 °C, respectively (Table 2). Hence, the rate of consumption of 4-iodotoluene in the reaction with benzene catalyzed by Co^{II}(por) follows the order: $Co^{II}(t_{4\text{-}OMe}pp)$ > Co^{II}(ttp) > $Co^{II}(t_{4\text{-}Cl}pp)$.

Table 2. Observed rate constants of the Co^{II}(por)-catalyzed direct C–H arylation at 200 °C.

Entry	Co^{II}(por)	k_{obs} [s^{-1}]	Relative rate
1	$Co^{II}(t_{4\text{-}OMe}pp)$	2.1×10^{-4}	2.3
2	Co^{II}(ttp)	2.0×10^{-4}	2.2
3	$Co^{II}(t_{4\text{-}Cl}pp)$	9.2×10^{-5}	1.0

 © 2012 Wiley-VCH Verlag GmbH & Co. KGaA, Weinheim

We then examined the catalyst loading effects where 2.5, 5, 10 and 20 mol-% of $Co^{II}(t_{4\text{-}OMe}pp)$ catalyst was employed. Reducing the catalyst loading from 5 to 2.5 mol-% increased the reaction time without affecting the yield of **1** (Table 3, Entry 1). This is in line with the rate-determining formal iodine atom abstraction step with $Co^{II}(t_{4\text{-}OMe}pp)$, since the decreased concentration of $Co^{II}(t_{4\text{-}OMe}pp)$ reduces the rate of aryl radical generation.[13] However, when the catalyst loading was increased to 10 mol-%, the reaction was slower compared with that of 5 mol-% (Table 3, Entries 2 and 3), but there was a small increase in the reaction yield. This observation is interesting as the reaction rate did not increase with catalyst loading or attained saturation. Therefore, we then studied the catalytic arylation with 20 mol-% of $Co^{II}(t_{4\text{-}OMe}pp)$ loading. The catalysis required an unexpectedly long reaction time of 17 h, with only 41% of **1** formed. The low yield of **1** was accounted for by the possible formation of $Co^{III}(t_{4\text{-}OMe}pp)$(4-tolyl) from the trapping of the 4-tolyl radical with $Co^{II}(t_{4\text{-}OMe}pp)$ (Scheme 1).

Table 3. Catalyst loading effects on the direct C–H arylation of benzene with 4-iodotoluene.

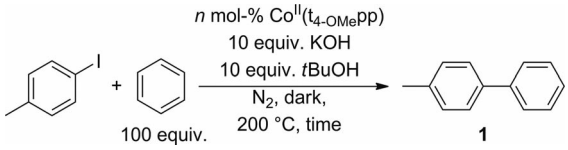

Entry	Catalyst loading [mol-%]	Time [h]	Yield of **1** [%][a]
1	2.5	4	77
2	5	2	79
3	10	4	81
4	20	17	41

[a] GC yield.

Scheme 1. Formation of $Co^{III}(t_{4\text{-}OMe}pp)$(4-tolyl) from $Co^{II}(t_{4\text{-}OMe}pp)$ and the 4-tolyl radical.

A higher catalyst loading should have resulted in faster 4-tolyl radical generation, a more rapid homolytic substitution of benzene and a faster catalytic direct C–H arylation.[13] However, instead of only being a catalyst for iodine atom abstraction, $Co^{II}(t_{4\text{-}OMe}pp)$ can also act as an aryl radical trap in the reaction mixture. Relatively high concentrations of 4-tolyl radical and $Co^{II}(t_{4\text{-}OMe}pp)$ combine to give $Co^{III}(t_{4\text{-}OMe}pp)$(4-tolyl) (Scheme 1) since the combination rate constants of various Co^{II} species with alkyl radicals are fast and some are close to diffusion-controlled.[15] Some examples of combination rate constants of Co^{II} complexes with alkyl radicals are illustrated in Scheme 2.[15] This process competes with the homolytic substitution for direct C–H arylation. Therefore, the rate of the 4-tolyl radical attack on benzene is reduced, leading to even slower reaction rates.

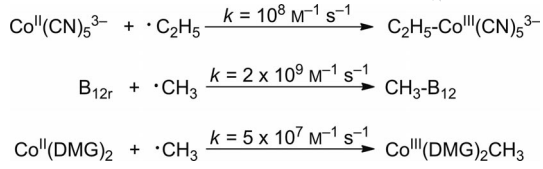

Scheme 2. Combination rate constants of some Co^{II} complexes with alkyl radicals. B_{12r} = cobalamin; $Co^{II}(DMG)_2$ = bis(dimethylglyoximato)cobalt(II).

In addition to the enhanced effect of the electron-donating porphyrin ligand on the rate of direct C–H arylation of benzene with 4-iodotoluene, the axial ligand effect was investigated. It has been reported that in the presence of σ-donor ligands, the energy level of the singly occupied d_{z^2} orbital of Co^{II}(por) rises, enriching the metalloradical character.[16] Pyridine and PPh_3 were thus added to form the more reactive LCo^{II}(por) (L = pyridine or PPh_3) in situ, hoping to facilitate the iodine atom abstraction step. However, both pyridine and PPh_3 were inefficient as longer reaction times were required (Table 4, Entries 2 and 5). The formation constant of the 1:1 adduct (py)$Co^{II}(t_{4\text{-}OMe}pp)$ at 200 °C was estimated to be 49.1 M^{-1},[17] indicating that about 87% of the added $Co^{II}(t_{4\text{-}OMe}pp)$ exists as (py)-$Co^{II}(t_{4\text{-}OMe}pp)$ in solution. The reduction of vacant sites on $Co^{II}(t_{4\text{-}OMe}pp)$ from two to one could account for the lower reactivity but is less reasonable. A rate enhancement should still have occurred. We favour the existence of a disproportionation equilibrium of axially ligated $Co^{II}(t_{4\text{-}OMe}pp)$ in the presence of L (L = OH^-, pyridine or PPh_3) to give $Co^{I}(t_{4\text{-}OMe}pp)^-$ and $L_nCo^{III}(t_{4\text{-}OMe}pp)^+$ (n = 1,2) at high temperatures (Scheme 3).[2b,18] This side reaction decreases the effective concentration of $Co^{II}(t_{4\text{-}OMe}pp)$ and, hence, the rate of iodine atom abstraction. Thus, the electronic effect of the porphyrin on the rate is unique.

Table 4. σ-Donor ligand effects on direct C–H arylation of benzene with 4-iodotoluene.

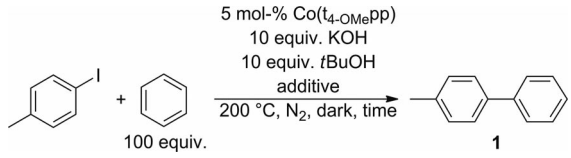

Entry	Additive	Loading [mol-%][a]	Time [h]	Yield of **1** [%][b]
1	none	–	2	79
2	pyridine	5	6	62
3	PPh_3	5	8	78
4	PPh_3	0.5	8	58
5	PPh_3	0.25	8	60

[a] With reference to 4-iodotoluene. [b] GC yield.

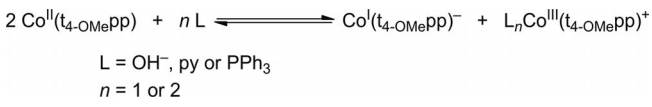

Scheme 3. Disproportionation of $Co^{II}(t_{4\text{-}OMe}pp)$ promoted by axial ligands.

 © 2012 Wiley-VCH Verlag GmbH & Co. KGaA, Weinheim

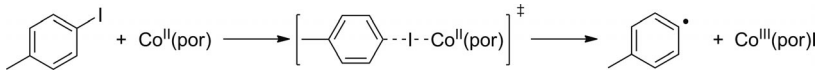

Scheme 4. Formal iodine atom abstraction as the rate-determining step.

From the above findings and the reaction mechanism proposed previously,[13] we conclude that the formal iodine atom abstraction is rate-determining (Scheme 4). The second-order rate constant for the formal iodine atom abstraction of 2-iodopyridine with $Co(CN)_5^{3-}$ at 25 °C is ca. 10^{-3} M^{-1} s^{-1}.[19] The nucleophilic radical nature of Co^{II}(por) is enhanced by electron-donating porphyrin ligands to facilitate the Ar–I bond cleavage.

Conclusions

The electronic effects of porphyrin ligands on the Co^{II}(por)-catalyzed direct C–H arylation are presented. The systematic modulation of ligand substituent electronics offers improved reactivity of economical first-row transition-metal catalysts. This provides another approach for reaction optimizations and mechanistic studies. Application of this concept to expand the scope of the ligand and substrate is ongoing.

Experimental Section

General: All reagents were purchased from commercial suppliers and used without further purification. Hexane for chromatography was distilled from anhydrous calcium chloride. Thin layer chromatography was performed on precoated silica gel 60 F254 plates. Silica gel (Merck, 230–400 mesh) was used for column chromatography in air. Melting points were measured with a Reichert apparatus. ^{1}H NMR spectra were recorded with a Bruker Avance III 400 (400 MHz) spectrometer. Spectra were referenced internally with tetramethylsilane (TMS; δ = 0.00 ppm) as the internal standard. Chemical shifts (δ) are reported in parts per million (ppm). Coupling constants (J) are reported in Hertz (Hz). GC–MS analyses were conducted with a GC–MS-QP2010 Plus system by using an Rtx-5MS column (30 m × 0.25 mm). Free-base porphyrins and corresponding cobalt(II)–porphyrins were prepared according to literature procedures.[14] All the reactions were carried out in the dark with Teflon-stoppered reaction tubes covered with aluminum foil. Unless otherwise stated, the reactions were duplicated, and the yields are the average yields. All the reactions were stopped once the starting materials were consumed to >95%.

General Procedure for the Various Co^{II}(por)-Catalyzed Direct C–H Arylations of Benzene with 4-Iodotoluene: $Co^{II}(t_{4\text{-}OMe}pp)$ (8.9 mg, 0.011 mmol), 4-iodotoluene (48.9 mg, 0.224 mmol), KOH (126 mg, 2.24 mmol), *t*BuOH (213 μL, 2.24 mmol) were added in benzene (2.0 mL, 22.4 mmol). The mixture was degassed during three freeze-pump-thaw cycles, flushed with N_2 and heated at 200 °C. After a GC–MS analysis of the reaction mixture to confirm complete consumption of 4-iodotoluene, the solvent was removed by rotary evaporation. The crude residue was purified by column chromatography (silica gel; 230–400 mesh) eluting with hexane to afford 4-methylbiphenyl (**1**). ^{1}H NMR (400 MHz, $CDCl_3$): δ = 2.39 (s, 3 H), 7.24 (d, J = 7.9 Hz, 2 H), 7.31 (t, J = 7.3 Hz, 1 H), 7.42 (t, J = 7.6 Hz, 2 H), 7.49 (d, J = 8.0 Hz, 2 H), 7.57 (d, J = 7.4 Hz, 2 H) ppm. M.p. 42.7–44.2 °C.[13] The same procedures were employed for the other Co^{II}(por) complexes.

General Procedure for the $Co^{II}(t_{4\text{-}OMe}pp)$-Catalyzed Direct C–H Arylation of Benzene with 4-Iodotoluene with Various Catalyst Loadings: $Co^{II}(t_{4\text{-}OMe}pp)$ (0.0055 mmol, 0.022 mmol and 0.044 mmol) was used in the same procedure as described above.

General Procedure for the $Co^{II}(t_{4\text{-}OMe}pp)$-Catalyzed Direct C–H Arylation of Benzene with 4-Iodotoluene with Various Additives: Pyridine (0.011 mmol) and PPh_3 were added. For 0.5 and 0.25 mol-% PPh_3, 0.56 mM and 0.28 mM standard solutions of PPh_3 (2 mL) in benzene were used as solvent, respectively.

Acknowledgments

We thank the Research Grants Council of Hong Kong (No. 400308), a Special Equipment Grant (SEG/ CUHK09) of the People's Republic of China, and the National Science Council (NSC-100-2113-M002-001-MY3) for financial support.

[1] G. C. Fu, *Acc. Chem. Res.* **2008**, *41*, 1555–1564.
[2] a) R. H. Crabtree in *The Organometallic Chemistry of the Transition Metals* 4th ed., John Wiley & Sons, Inc., Hoboken, New Jersey, **2005**, pp. 165–166; b) J. Halpern, *Acc. Chem. Res.* **1970**, *3*, 386–392; c) J. K. Stille, K. S. Y. Lau, *Acc. Chem. Res.* **1976**, *9*, 434–442.
[3] M. L. Clarke, J. J. R. Frew, *Organomet. Chem.* **2009**, *35*, 19–46.
[4] C. A. Busacca, D. Grossbach, R. C. So, E. M. O'Brien, E. M. Spinelli, *Org. Lett.* **2003**, *5*, 595–598.
[5] A. J. Hickman, M. S. Sanford, *ACS Catal.* **2011**, *1*, 170–174.
[6] K. M. Kadish, K. M. Smith, R. Guilard in *The Porphyrin Handbook* 1st Ed., Academic Press, San Diego, **2000**.
[7] a) J. D. Harden, J. V. Ruppel, G.-Y. Gao, X. P. Zhang, *Chem. Commun.* **2007**, 4644–4646; b) J. V. Ruppel, R. M. Kamble, X. P. Zhang, *Org. Lett.* **2007**, *9*, 4889–4892; c) V. Lyaskovskyy, A. I. O. Suarez, H. Lu, H. Jiang, X. P. Zhang, B. de Bruin, *J. Am. Chem. Soc.* **2011**, *133*, 12264–12273.
[8] a) L. Huang, Y. Chen, G.-Y. Gao, X. P. Zhang, *J. Org. Chem.* **2003**, *68*, 8179–8184; b) W. I. Dzik, X. Xu, X. P. Zhang, J. N. H. Reek, B. de Bruin, *J. Am. Chem. Soc.* **2010**, *132*, 10891–10902; c) H. Lu, W. I. Dzik, X. Xu, L. Wojtas, B. de Bruin, X. P. Zhang, *J. Am. Chem. Soc.* **2011**, *133*, 8518–8521.
[9] a) G.-Y. Gao, J. D. Harden, X. P. Zhang, *Org. Lett.* **2005**, *7*, 3191–3193; b) A. I. O. Suarez, H. Jiang, X. P. Zhang, B. de Bruin, *Dalton Trans.* **2011**, *40*, 5697–5705.
[10] H. Sharghi, A. H. Nejad, M. A. Nasseri, *New J. Chem.* **2004**, *28*, 946–951.
[11] G. P. McGlacken, L. M. Bateman, *Chem. Soc. Rev.* **2009**, *38*, 2447–2464.
[12] For first-row transition-metal catalyzed examples, see: a) H.-Q. Do, R. M. K. Khan, O. Daugulis, *J. Am. Chem. Soc.* **2008**, *130*, 15185–15192; b) F. Vallée, J. J. Mousseau, A. B. Charette, *J. Am. Chem. Soc.* **2010**, *132*, 1514–1516; c) W. Liu, H. Cao, A. Lei, *Angew. Chem.* **2010**, *122*, 2048; *Angew. Chem. Int. Ed.* **2010**, *49*, 2004–2008; d) G. Xie, T. Li, X. Qu, J. Mao, *J. Mol. Catal. A* **2011**, *340*, 48–52; e) W. Liu, H. Cao, J. Xin, L. Jin, A. Lei, *Chem. Eur. J.* **2011**, *17*, 3588–3592; f) H. Li, C.-L. Sun, M. Yu, D.-G. Yu, B.-J. Li, Z.-J. Shi, *Chem. Eur. J.* **2011**, *17*, 3593–3597; for transition-metal-free catalyzed examples, see: g)

 © 2012 Wiley-VCH Verlag GmbH & Co. KGaA, Weinheim

W. Liu, H. Cao, H. Zhang, K. H. Chung, C. He, H. Wang, F. Y. Kwong, A. Lei, *J. Am. Chem. Soc.* **2010**, *132*, 16737–16740; h) E. Shirakawa, K. Itoh, T. Higashino, T. Hayashi, *J. Am. Chem. Soc.* **2010**, *132*, 15537–15539; i) C.-L. Sun, H. Li, D.-G. Yu, M. Yu, X. Zhou, X.-Y. Lu, K. Huang, S.-F. Zheng, B.-J. Li, Z.-J. Shi, *Nat. Chem.* **2010**, *2*, 1044–1049; j) Y. Qiu, Y. Liu, K. Yang, W. Hong, Z. Li, Z. Wang, Z. Yao, S. Jiang, *Org. Lett.* **2011**, *13*, 3556–3559.

[13] C. T. To, T. L. Chan, B. Z. Li, Y. Y. Hui, T. Y. Kwok, S. Y. Lam, K. S. Chan, *Tetrahedron Lett.* **2011**, *52*, 1023–1026.

[14] a) A. D. Adler, F. R. Longo, J. D. Finarelli, J. Goldmacher, J. Assour, L. Korsakoff, *J. Org. Chem.* **1967**, *32*, 476; b) R. W. Wagner, D. Lawrence, J. S. Lindsey, *Tetrahedron Lett.* **1987**, *28*, 3069–3070; c) A. D. Adler, F. R. Longo, F. Kampas, J. Kim, *J. Inorg. Nucl. Chem.* **1970**, *32*, 2443–2445.

[15] a) J. Halpern, *Polyhedron* **1988**, *7*, 1483–1490; b) J. F. Endicott, G. F. Ferraudi, *J. Am. Chem. Soc.* **1977**, *99*, 243–245.

[16] B. B. Wayland, A. E. Sherry, A. G. Bunn, *J. Am. Chem. Soc.* **1993**, *115*, 7675–7684.

[17] F. A. Walker, *J. Am. Chem. Soc.* **1973**, *95*, 1150–1153. The formation constant was estimated by using $\Delta G = -RT\ln K$, assuming ΔG remained constant over the temperature range 298–473 K.

[18] a) D. Lexa, J. M. Savéant, J. Zickler, *J. Am. Chem. Soc.* **1980**, *102*, 2654–2663; b) V. Grass, D. Lexa, M. Momenteau, J. M. Savéant, *J. Am. Chem. Soc.* **1997**, *119*, 3536–3542; c) P. B. Chock, R. B. K. Dewar, J. Halpern, L.-Y. Wong, *J. Am. Chem. Soc.* **1969**, *91*, 82–84; d) B. B. Wayland, K. J. Balkus Jr., M. D. Farnos, *Organometallics* **1989**, *8*, 950–955; e) $Co^{I}(t_{4\text{-}OMe}pp)^{-}$, though more nucleophilic than $Co^{II}(t_{4\text{-}OMe}pp)$, probably precipitates in benzene rendering its poor reactivity.

[19] J. Halpern, J. P. Maher, *J. Am. Chem. Soc.* **1965**, *87*, 5361–5366.

Received: July 27, 2011
Published Online: November 10, 2011

 © 2012 Wiley-VCH Verlag GmbH & Co. KGaA, Weinheim

DOI: 10.1002/ejic.201101011

Protonation-Enhanced Lewis Acidity of Iridium Complexes Containing Noninnocent Amidophenolates

Mark R. Ringenberg[a] and Thomas B. Rauchfuss*[a]

Keywords: Protonation / Noninnocent ligand / Carbonylation / Amides / Phenoxide

The effect of protonation of metal complexes of noninnocent ligands is investigated. The anilidophenolate complexes $Cp^*Ir^tBA^{tBu}$ (**1**) and $Cp^*Ir^tBA^FPh$ (**2**) were examined [$H_2{}^tBA^{tBu}$ = 2-*tert*-butylamino-4,6-di-*tert*-butylphenol, $H_2{}^tBA^FPh$ = 2-(2-trifluoromethyl)amino-4,6-di-*tert*-butylphenol]. Protonation of **1** with HBF_4 gave the anilinophenolate [**1**H]$^+$. Crystallographic characterization of this complex revealed an elongatated Ir–N bond, but the Ir^{III} center remains pentacoordinate. The anilinophenolate hydride **1**H(H) was prepared by treatment of [**1**H]$^+$ with boron hydride reagents and with formic acid. X-ray crystallography confirmed the structure and revealed that the hydride and ammonium hydrons occupy sites on opposite sides of the $IrONC_6$ ring. Complex **2** is protonated only by strong acids, and the resulting derivative is unstable in the absence of ligands such as CO and PMe_3. Crystallographic characterization of [**2**(PMe_3)]$^+$ revealed that protonation occurs at O not N. The carbonylation of [**2**H]$^+$ reveals the intermediacy of kinetic adducts, which are proposed to be the anilino tautomer.

Introduction

The protonation of metal–amido complexes has attracted attention in recent years.[1] The equilibrium between 18e$^-$ amine and 16e$^-$ amido complexes is also mechanistically relevant to the substitution reactions of classical metal–ammine complexes, such as $[CoCl(NH_3)_5]^{2+}$, which involve intermediates of the type $[Co(NH_2)(NH_3)_4]^{2+}$.[2] More recently, the protonation of an amido group has been shown to strongly influence the nature of transfer hydrogenation (TH) catalysts. Some TH catalysts cannot activate H_2 but upon *N*-protonation, the resulting cationic amino complexes catalyze the direct hydrogenation of ketones and imines.[3]

We have been interested in the protonation of formally 16e$^-$ amido complexes, which leads to cationic 16e$^-$ metal–amine complexes, M–$NHR_2{}^+$. These unsaturated cations are good Lewis acids. This conversion, termed protonation-induced Lewis acidity (PI-LA), has been explored in the case of the conjugate acid–base pair Cp*IrH(TsDPEN-H)/[Cp*Ir(TsDPEN)]$^+$ (TsDPEN$^-$ = *N*-tosylamidodiphenylethyl-2-amine anion). *N*-Protonation breaks the π bonds between the NH center and Ir, but leaves the weaker π bonding between the anionic NTs group and Ir intact.[4] The enhanced Lewis acidity allows the activation of even non-basic substrates such as H_2.[5]

In related work, we have studied ligand oxidation to enhance the Lewis acidity of 16e$^-$ complexes that contain amido-based noninnocent ligands (NILs). We found that the oxidation of such complexes led to the dramatic enhancement of their Lewis acidity, which allowed the formation of a variety of adducts, e.g. with CO and tertiary phosphane ligands.[6] This process is termed oxidation-induced Lewis acidity (OI-LA, Scheme 1).

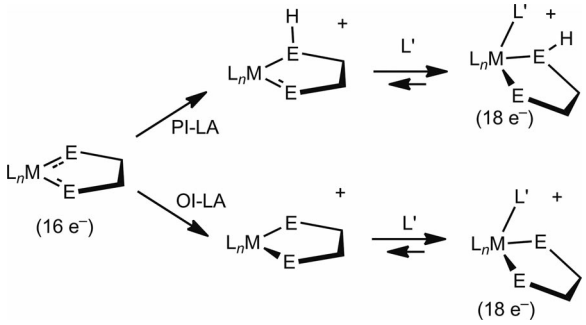

Scheme 1.

In order to further develop OI-LA and PI-LA, we have examined the cross-reaction, i.e. the protonation of complexes of NILs. Many NILs are based on dithiolene ligands,[7] but such complexes are often difficult to protonate. Anilido-based NILs should, however, be susceptible to protonation to give the corresponding anilino derivatives.[8] Indeed, Darensbourg et al. found that the protonation of a 16e$^-$ iron–amidothiophenolate complex induced the binding of CO.[9] Exploiting similar reactivity, we report on the acid–base properties of *N*-substituted Cp*Ir(3,5-di-*tert*-

[a] Department of Chemistry, University of Illinois,
600 S Mathews Ave., Urbana, IL 61801, USA
Fax: +1-217-244-3186
E-mail: rauchfuz@illinois.edu

Supporting information for this article is available on the WWW under http://dx.doi.org/10.1002/ejic.201101011.

WILEY ONLINE LIBRARY
© 2012 Wiley-VCH Verlag GmbH & Co. KGaA, Weinheim

butylamidophenolate) complexes. Two such derivatives were investigated, one derived from *tert*-butylamine (**1**) and the other derived from *o*-trifluoromethylaniline (**2**). Complexes **1** and **2** exhibit no measureable affinity for donor ligands such as MeCN, H_2, CO, or PMe_3.

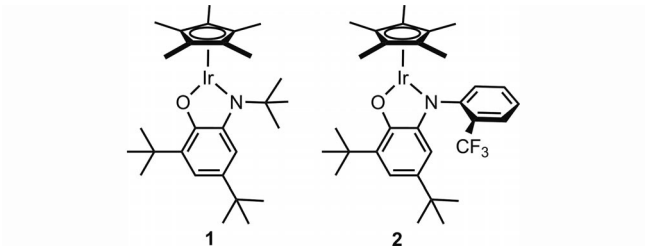

Results and Discussion

A solution of **1** in CH_2Cl_2 was quantitatively protonated by solutions of $HBF_4{\cdot}Et_2O$. The product, [**1**H]BF_4, was isolated as an analytically pure, brown solid. Solutions of [**1**H]BF_4 in CD_2Cl_2 decomposed at room temperature over the course of a day, but CD_2Cl_2 solutions of the related salt [**1**H]$BAr^F{}_4$ were found to be more stable. These observations suggest that the association of the anion results in degradation, which is consistent with the high Lewis acidity of the cationic complexes. Solutions of [**1**H]BF_4 in MeCN were found to be stable, and a solid was isolated as a bright yellow salt, which resists oxidation by air in contrast to [**1**H]BF_4. Measurements by UV/Vis, IR, and ^{1}H NMR spectroscopy indicate that MeCN forms an adduct with [**1**H]$^+$ (Figure 1). Concentration of these solutions produced [**1**H(MeCN)]BF_4.Using a series of standard bases and monitoring by UV/Vis spectroscopy, the p$K_a{}^{MeCN}$ of [**1**H(MeCN)]$^+$ was found to be 13.19 ± 0.20.[10]

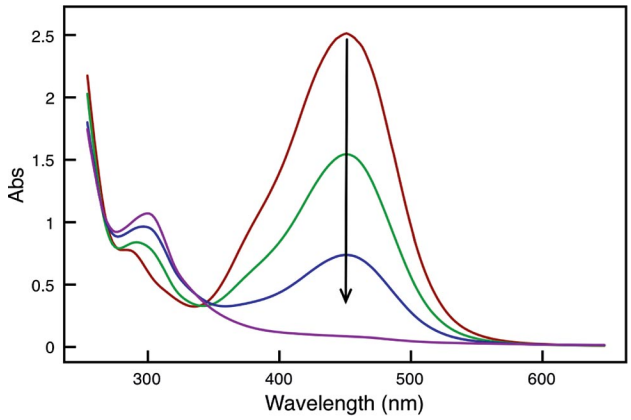

Figure 1. UV/Vis spectra of a 2.03×10^{-4} M solution of **1** (red) in MeCN treated with 0.37 (green), 0.75 (blue), and 1.11 (purple) equiv. of $HBF_4{\cdot}Et_2O$ in MeCN solution. Small deviations from isosbestic behavior are due to dilution by the titrated acid solution.

^{1}H and ^{19}F NMR spectra of [**1**H]BF_4 indicate the presence of a single diastereomer. The signal at δ = 7.49 ppm in the ^{1}H NMR spectrum with a width at half-height ($w_{1/2h}$) of 10 Hz, which remained invariant when the temperature of a CD_2Cl_2 solution was varied over the range 20 to –60 °C, is consistent with an N–H signal broadened by ^{14}N.[11]

The reaction of **1** with $HBF_4{\cdot}Et_2O$ was monitored in situ by ^{1}H NMR spectroscopy. After a few minutes of reaction time, two isomeric derivatives were observed in a 5:1 ratio. The major signal matched those of isolated [**1**H]BF_4. The minor product featured a broad signal at δ = 7.41 ppm, which sharpened upon cooling to –60 °C. After 2 h at room temperature, the mixture had fully converted into the major isomer. We propose that the minor isomer (δ = 7.41 ppm) arises from competitive *O*-protonation [Equation (1)].[11]

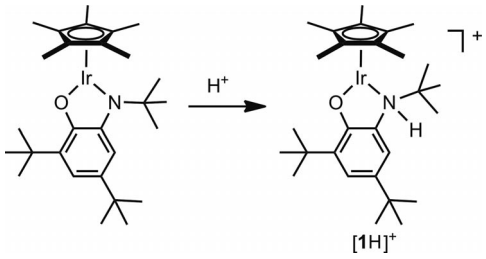

(1)

Despite its thermal instability, [**1**H]BF_4 was obtained as single crystals suitable for analysis by X-ray diffraction. The cation [**1**H]$^+$ exhibits a pentacoordinate iridium center with a pyramidalized nitrogen atom (Figure 2). The angle between the planes formed by the phenylene backbone, N atom, and O atom and the Cp* centroid is 60°. By contrast, the angles between the phenylene backbone and the Cp* planes for previously reported Cp*Ir(^{t}BA^{F}Ph) and the radical cation [Cp*Ir(^{t}BA^{F}Ph)]$BAr^F{}_4$ are 87.7 and 83.4°, respectively.[12] The geometry at the N atom is tetrahedral, unlike our previous examples of Cp*Ir–amidophenolates. A close contact of 2.937 Å exists between NH and one fluoride in BF_4^-, which is consistent with moderately strong hydrogen bonding.[13] The Ir–O bond length of 1.965(18) Å is essentially unchanged in comparison with neutral Cp*Ir–amidophenolates, e.g. **2**.[12] The Ir–N bond in [**1**H]BF_4 of 2.14(21) Å is elongated by ca. 10% vs. that in neutral **2**

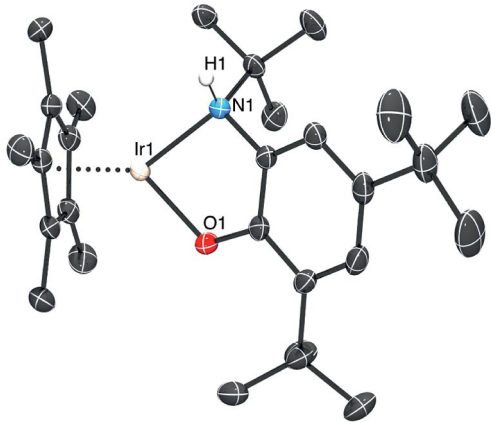

Figure 2. Molecular structure of [**1**H]BF_4. Hydrogen atoms (except for N*H*) are omitted for clarity, and thermal ellipsoids are shown at 50% probability.

 © 2012 Wiley-VCH Verlag GmbH & Co. KGaA, Weinheim

[1.99(8) Å]. The Ir–NR_2 bond lengths fall in the range 2.069 ± 0.048 Å.[14] The bond lengths within the amidophenolate ligand were unaltered by protonation with *d*(C–O) = 1.36(31) Å and *d*(N–C) = 1.46(32) Å, and the C–C bonds within the phenylene ring (1.39 Å) are similar to those in **2**.[12] The lack of bond alternation within the phenylene ring and the diamagnetic nature of [**1**H]BF_4 are consistent with an aromatic, not quinoidal,[12,15] phenylene backbone.

Synthesis and Properties of 1H(H)

Treatment of **1** with NH_3BH_3 resulted in the quantitative formation of the hydride **1**H(H) in about 10 min. The ^{1}H NMR spectrum of **1**H(H) exhibited a hydride signal at δ = –8.77 ppm. The same hydride was generated by treating solutions of [**1**H]$^+$ with $NaBH_4$, a reaction that surprisingly did not result in immediate deprotonation. Similarly, **1**H(H) was also prepared by treating a methanolic solution of **1** with $NaBH_4$, in which case the proton derives from the solvent.[4b] The complex **1**H(H) was also formed with formic acid by a reaction that cogenerated copious amounts of CO_2. Although **1**H(H) is formally the result of heterolytic addition of H_2 to **1**, no reaction was observed between **1** and H_2 (1 atm) over the course of a week.

Crystallographic analysis confirmed that **1**H(H) is pseudo-octahedral. The N–H bond and Ir–H bonds are mutually trans (Figure 3). The nitrogen center is more pyramidal than in [**1**H]BF_4, and the angle between the phenylene backbone and Cp* is 11.7°. A hydrogen bond of 2.52(6) Å exists between the noncoordinated MeCN and **1**H(H). A [D_3]MeCN solution of the crystals used for X-ray analysis featured a high-field ^{1}H NMR signal consistent with the hydride at δ = –8.77 ppm. A signal at δ = 5.45 ppm with a $w_{1/2h}$ value of 8 Hz is assigned to N–H. A solution of **1**H(H) in CD_2Cl_2 was unstable and degraded to a complex mixture within minutes.

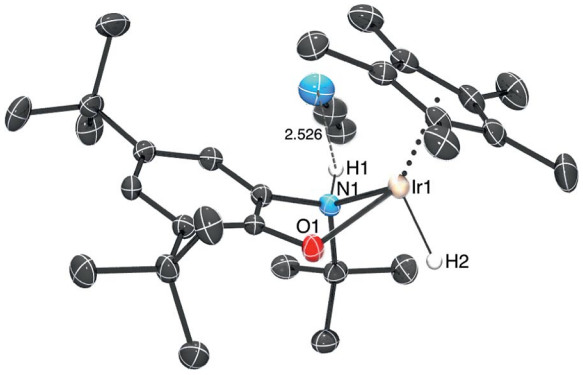

Figure 3. Molecular structure of **1**H(H)·MeCN. Thermal ellipsoids shown at 50% probability, and hydrogen atoms (except N*H* and Ir*H*) are omitted for clarity.

The similarity between **1** and the hydrogenation catalysts Cp*Ir(TsDPEN) and (cymene)Ru(TsDPEN)[3b,16,18] prompted us to investigate the preparation of **1**H(H) by hydrogenation. A CD_2Cl_2 solution of [**1**H]BF_4 rapidly (< 2 min) degraded under H_2 to the aminophenol and [$Cp^*_2Ir_2H_3$]$^+$.[17] Attempts to hydrogenate **1** in the presence of a catalytic amount of acid[18] also gave [$Cp^*_2Ir_2H_3$]$^+$ in proportion to the amount of added acid. These data suggest that [**1**H]$^+$ has a high affinity for H_2, and intramolecular hydrogenolysis of the Ir–N and Ir–O bonds is fast.

Binding of CO to [1H]$^+$

Unlike **1**, [**1**H]BF_4 formed adducts with Lewis bases. Addition of CO to a solution of [**1**H]BF_4 in CH_2Cl_2 solution was monitored in situ by IR and ^{1}H NMR spectroscopy. Two CO adducts formed initially (ν_{CO}: 2073 and 2041 cm^{-1}). These two bands initially appeared in the IR spectrum in nearly equal intensity, but over the course of a few minutes, the lower energy band at 2041 cm^{-1} became dominant (Figure 4). The same isomeric mixture and subsequent equilibration were observed when the reaction was monitored by ^{1}H NMR spectroscopy. Upon treatment with triethylamine, [**1**H(CO)]BF_4 reverted to **1**.

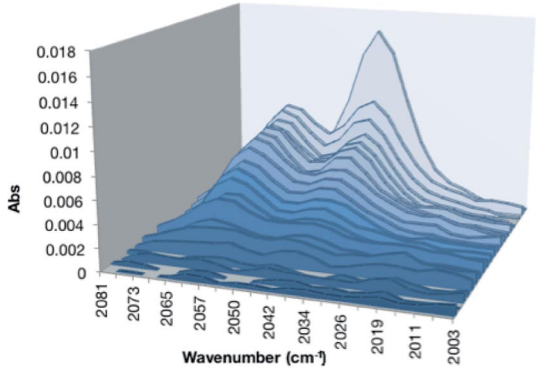

Figure 4. In situ IR spectra of the protonation of **1** with HBF_4·Et_2O in the presence of CO. Conditions: 298 K, CH_2Cl_2 solution. Data were collected for 600 s at 6 s intervals; shown are the first 120 s and the final spectrum.

Protonation of 2 and the Resulting Adducts

In contrast to the stability of [**1**H(NCMe)]$^+$, protonation of MeCN solutions of **2** was only achieved with strong acids such as $H(Et_2O)_2BAr^F_4$.[19] However, the products were unstable at room temperature. Adducts were only stable with stronger Lewis bases.

Addition of PMe_3 to a CD_2Cl_2 solution of [**2**H]$^+$ gave multiple products, which were assumed to be isomers, as indicated by ^{1}H, ^{19}F, and ^{31}P NMR spectroscopy. A single isomer of [**2**H(PMe_3)]BAr^F_4 was crystallized and was structurally characterized. In [**2**H(PMe_3)]$^+$ the added proton is located on O instead of N (Figure 5). The nitrogen center is planar, with the sum of the angles around the nitrogen atom of 359°. The angle between the planes of the phenylene backbone and the Cp* is 57.5°. The Ir–O bond length of 2.079(6) Å is 0.090 Å greater than that of the corresponding bond in **2**, consistent with an Ir–O(H)R bond.[14]

 © 2012 Wiley-VCH Verlag GmbH & Co. KGaA, Weinheim

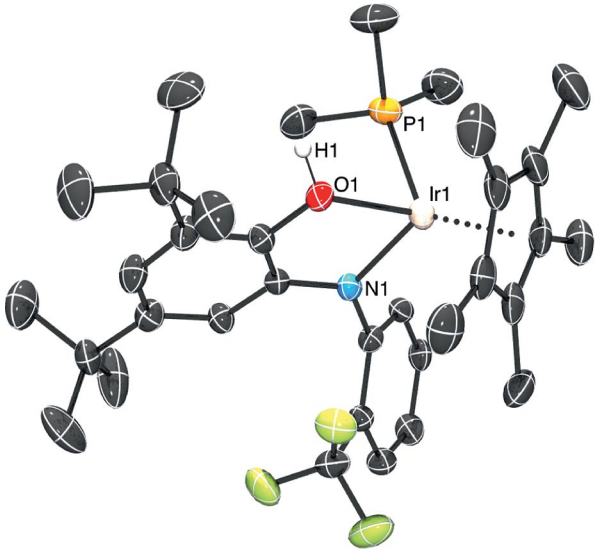

Figure 5. Molecular structure of [**2**H(PMe$_3$)]BAr$^F{}_4$. Hydrogen atoms (except for O*H*) and BAr$^F{}_4^-$ are omitted for clarity.

The carbonylation of [**2**H]$^+$ was also examined. ^{19}F and ^{1}H NMR spectra of the adduct [**2**H(CO)]BAr$^F{}_4$ consist of broad signals at room temperature, but they sharpen at –50 °C into two subspectra (see Supporting Information). The IR spectrum of [**2**H(CO)]$^+$ in CH_2Cl_2 solution displays ν_{CO} bands of roughly equal intensity at 2057 and at 2063 cm^{-1}. When the carbonylation was monitored by IR spectroscopy in situ, the pattern is similar to that for the carbonylation of [**1**H]$^+$. An isomer with a higher frequency was observed to form initially. At room temperature, the two isomers of [**2**H(CO)]$^+$ coexist with $K_{eq} \approx 0.7$.

Conclusions

In this paper we probed the protonation of complexes of noninnocent 2-amidophenolate ligands. The main findings are: (i) these species protonate, but the relevant pK_a values are highly sensitive to substituent effects, (ii) the protonated derivatives are good Lewis acids, and (iii) both *O*- and *N*-protonation is observed.

The anilido derivative **2** could only be protonated by H(Et$_2$O)$_2$BAr$^F{}_4$ in contrast with the far lower acidity of [**1**H]$^+$ with a pK_a near 13 (MeCN). The pK_a scale for MeCN solutions is larger than for water. For example, the pK_a^{MeCN} values of PhNH$_3^+$ and 4-O$_2$NC$_6$H$_4$NH$_3^+$ are 10.7 and 2.8, respectively.[10] By comparison, in water, the pK_a values are 4.87 and 1.[20] *o*-Aminophenolate complexes are precedented but rare.[21]

The treatment of **1** with NH$_3$BH$_3$ as well as other hydride-donor reagents gave an unusual example of a hydride complex that bears an aminophenolate ligand. In general, structurally characterized hydrides containing anionic N,O ligands are rare.[22] The nonreaction of **2** with NH$_3$BH$_3$ is consistent with the decreased basicity of this complex. Because **1**H(H) is *N*-protonated it does not exhibit redox behavior at mild potentials. In future studies, we hope to access metal hydrides that contain noninnocent ligands to test the effect of ligand-centered redox on the acidity of the M–H bond.[23]

Protonation of **1** and **2** can occur at either N or O. Furthermore, the *N*-protonated adducts can exist as two diastereomers depending on the relative stereochemistry of the R group with respect to the unidentate ligand. Prior to binding of the Lewis base, however, only two diastereoisomers are possible as the only stereogenic centers are on O or N. The clearest example of isomerism arising from *N*- vs. *O*-protonation is provided by the PMe$_3$ adduct of [**2**H]$^+$. Complexes of *O*-bonded phenols (vs. phenolates) are precedented[24] but not in the presence of an amido group. We suggest that the regiochemistry is strongly influenced by steric factors caused by the *N*-substituent, the Cp*Ir center, and the "sixth ligand". Hence, we observe the unusual *O*-protonated isomer for the largest ligand, PMe$_3$.

In the case of CO binding, two carbonyl bands were observed, which were distinguished by IR and NMR spectroscopy. For [**1**H(CO)]$^+$, a ν_{CO} band at 2073 cm^{-1} in the IR spectrum is associated with the kinetic product. We propose that the kinetic site of protonation is the sterically accessible phenolate. The lower energy band at 2041 cm^{-1}, which is associated with the thermodynamic more basic site, is assigned to the aminophenolate complex (Figure 6).

In summary, the protonation of the amidophenolate complexes was not as straightforward as the case for related complexes of TsDPEN. Our previous studies into the noninnocent behavior of **1** and **2** showed that they were effective at oxidizing H$_2$. This study provides a further example where an excess of protons in the presence of H$_2$ results in the rapid degredation of an amido complex to (Cp*Ir)$_2$H$_3^+$. The protonation also substantially increased the Lewis acidity of the metal. This study has given further insight into how these NIL complexes operate as H$_2$ oxidation catalysts.[6]

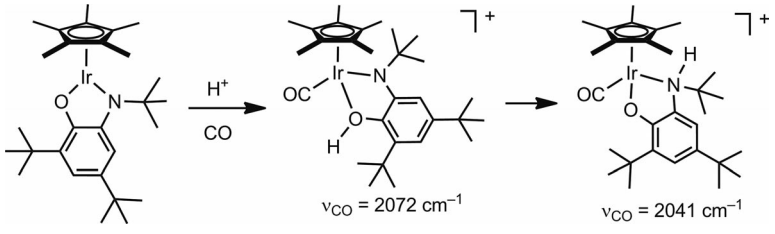

Figure 6. Isomers produced by protonation-induced carbonylation of **1**.

 © 2012 Wiley-VCH Verlag GmbH & Co. KGaA, Weinheim

Experimental Section

General: Materials and methods have been described previously.[6]

[Cp*IrH^{t}BA$^{r\mathrm{Bu}}$]BF$_4$ ([1H]BF$_4$): A solution of 51% HBF_4 in Et_2O (14 μL, 83 μmol) was added to a solution of **1** (50 mg, 83 μmol) in Et_2O (15 mL). The solution changed from orange to dark brown upon addition of the HBF_4, and a precipitate formed. After 1 h, the red-brown precipitate was isolated by filtration. The resulting solid was washed with Et_2O (approx. 10 mL) and hexanes (approx. 20 mL). The resulting brown powder was crystallized by dissolution in CH_2Cl_2 (1 mL) and layering with hexanes (7 mL). Yield: 42 mg (84%). ^{1}H NMR (CD_2Cl_2): δ = 1.23 (s, 9 H), 1.37 (s, 9 H), 1.42 (s, 9 H), 1.71 (s, 15 H), 7.05 (s, 1 H), 7.11 (s, 1 H), 7.42 (br.) ppm. $C_{29}H_{44}BF_4IrNO$: calcd. C 48.16, H 6.43, N 2.03; found C 47.17, H 6.40, N 2.58.

[Cp*IrH^{t}BA$^{r\mathrm{Bu}}$(NCMe)]BF$_4$ ([1H(MeCN)]BF$_4$): A solution of 51% HBF_4 in Et_2O (14 μL, 83 μmol) was added to a solution of **1** (50 mg, 83 μmol) in Et_2O (15 mL). The solution changed from orange to brown, and a solid precipitated. The precipitate was collected by filtration and washed with Et_2O (10 mL). The brown solid was extracted with MeCN (1 mL) to give a bright yellow solution. This solution was stirred for 1 h before Et_2O (10 mL) was added, which resulted in the formation of a bright yellow precipitate. The yellow solid was washed with Et_2O (10 mL) and hexanes (20 mL). Yield: 27 mg (44%). ^{1}H NMR (CD_2Cl_2): δ = 1.24 (s, 9 H), 1.38 (s, 9 H), 1.42 (s, 9 H), 1.69 (s, 15 H), 1.82 (s, 3 H), 7.05 (d, 1 H), 7.06 (d, 1 H), 7.13 (br., 1 H) ppm. UV/Vis (CH_2Cl_2): λ_{max} (ε) = 494 (1673) nm. $C_{30}H_{48}BF_4IrN_2O$: calcd. C 49.24, H 6.61, N 3.83; found C 47.37, H 6.46, N 3.77.

[Cp*IrH^{t}BA$^{r\mathrm{Bu}}$(CO)]BF$_4$ ([1H(CO)]BF$_4$): A solution of **1** (50 mg, 83 μmol) in CH_2Cl_2 (15 mL) was sparged with CO, and 51% HBF_4 in Et_2O (14 μL, 83 μmol) was added. The color of the reaction solution changed from orange to yellow upon protonation of the complex. The solution was concentrated to 1 mL under a stream of CO. Addition of Et_2O (10 mL) precipitated a dull orange solid, which was isolated by filtration and recrystallized by layering a CH_2Cl_2 solution (1 mL) with (Et_2O5 mL). Yield: 35 mg (58%). ^{1}H NMR (CD_3CN): δ = 1.25 (s, 9 H), 1.28 (s, 9 H), 1.34 (s, 9 H), 1.74 (s, 15 H), 5.87 (s, 1 H), 6.97 (d, 1 H), 7.00 (d, 1 H) ppm. IR (CH_2Cl_2): $\tilde{\nu}$ = 2072, 2041 (vs) cm^{-1}. $C_{29}H_{43}IrNO(CO)BF_4$: calcd. C 49.95, H 5.94, N 1.92; found C 50.55, H 6.01, N 2.33.

Cp*Ir(H^{t}BA$^{r\mathrm{Bu}}$)(H) ([1H(H)]): A solution of NH_3BH_3 (3.3 mg, 0.107 mmol) in MeCN (10 mL) was added to a solution of **1** (64.4 mg, 0.107 mmol) in MeCN (20 mL). Over the course of 2 h, the color of the reaction solution changed from deep orange to light yellow. The progress of the reaction was monitored by UV/Vis spectroscopy, following the diminution of the peak at 454 nm and the growth of the peak at 315 nm. MeCN was removed under reduced pressure, and the solids were extracted with the minimum amount of MeCN. Upon standing at –30 °C for 12 h, this solution yielded yellow crystals suitable for X-ray crystallography. Yield: 25 mg (41%). ^{1}H NMR (CD_3CN): δ = –8.83 (s, 1 H), 1.15 (s, 9 H), 1.23 (s, 9 H), 1.32 (s, 9 H), 1.62 (s, 15 H), 5.40 (br., 1 H), N-H 6.77 (d, 1 H), 6.85 (d, 1 H) ppm. $C_{29}H_{44}IrNO$: calcd. C 56.65, H 7.21, N 2.27; found C 56.23, H 7.25, N 3.28.

[Cp*IrH^{t}BA^F(CO)]BAr$^F_4$ ([2H(CO)]BAr$^F_4$): A solution of [**2**H(MeCN)]BAr$^F_4$ (24 mg, 0.015 mmol) in MeCN (5 mL) was sparged with CO gas for 5 min. The yellow solution became a dull orange during this process. The reaction solution was concentrated to yield an orange solid, which was dissolved in Et_2O (10 mL). Addition of pentane (10 mL) afforded a yellow solid, which was collected by filtration. IR: $\tilde{\nu}$ = 2057, 2063 cm^{-1}. $C_{63}H_{50}BF_{27}NO_2$·-2Et_2O: calcd. C 55.91, H 4.63, N 0.91; found C 55.14, H 4.61, N 1.52.

[Cp*Ir(H^{t}BA^F)(PMe$_3$)]BAr$^F_4$ ([2H(PMe$_3$)]BAr$^F_4$): A solution of [**2**H(MeCN)]BAr$^F_4$ (24 mg, 0.015 mmol) in MeCN (5 mL) was treated with PMe_3 (2 μL), which was added by syringe. After stirring for 10 min, the solution was diluted with Et_2O (20 mL) to precipitate a yellow solid. The solid was isolated by filtration and washed with pentane (10 mL). ^{31}P NMR: δ = –49, –56, –60 ppm. $C_{66}H_{61}BF_{27}IrNOP$·2Et_2O: calcd. C 49.95, H 4.59, N 0.79; found C 50.11, H 4.55, N1.21. A solution of [**2**H(PMe_3)]BAr$^F_4$ (20 mg) in CD_2Cl_2 (0.5 mL) was layered with pentane (2 mL) and cooled to –30 °C overnight to afford crystals suitable for X-ray crystallography.

pK_a Determination: A stock solution of [**1**H(MeCN)]BF$_4$ (4 mg, 0.547 μmol) in MeCN (20 mL) was prepared. The progress of the reaction was monitored by UV/Vis spectroscopy by the diminution of the peak at 454 nm and the growth of the peak at 315 nm upon titration with a solution of 2,6-lutidine (0.5 M).

X-ray Crystallography: CCDC-845989 (for [**1**H]BF$_4$), -845988 (for **1**H(H)·MeCN), -845987 (for [**2**H(PMe_3)]BAr$^F_4$) contain the supplementary crystallographic data for this paper. These data can be obtained free of charge from The Cambridge Crystallographic Data Centre via www.ccdc.cam.ac.uk/data_request/cif.

Supporting Information (see footnote on the first page of this article): ^{19}F and ^{1}H NMR spectra of [**2**H(CO)]BAr$^F_4$.

Acknowledgments

This research was supported by the U.S. Department of Energy. We thank Danielle Gray for assistance with the X-ray crystallography.

[1] J. R. Fulton, A. W. Holland, D. J. Fox, R. G. Bergman, *Acc. Chem. Res.* **2002**, *35*, 44–56.
[2] a) B. F. E. Curchod, F. P. Rotzinger, *Inorg. Chem.* **2011**, *50*, 8728–8740; b) W. G. Jackson, *Inorg. React. Mech.* **2002**, *4*, 1–30.
[3] a) S. E. Clapham, A. Hadzovic, R. H. Morris, *Coord. Chem. Rev.* **2004**, *248*, 2201–2237; b) K. Murata, T. Ikariya, R. Noyori, *J. Org. Chem.* **1999**, *64*, 2186–2187.
[4] a) Z. M. Heiden, B. J. Gorecki, T. B. Rauchfuss, *Organometallics* **2008**, *27*, 1542–1549; b) C. S. Letko, Z. M. Heiden, T. B. Rauchfuss, S. R. Wilson, *Inorg. Chem.* **2011**, *50*, 5558–5566.
[5] Z. M. Heiden, T. B. Rauchfuss, *J. Am. Chem. Soc.* **2006**, *128*, 13048–13049.
[6] M. R. Ringenberg, M. J. Nilges, T. B. Rauchfuss, S. R. Wilson, *Organometallics* **2009**, *28*, 1956–1965.
[7] W. Kaim, *Inorg. Chem.* **2011**, *50*, 9752–9765.
[8] S. Kokatam, T. Weyhermüller, E. Bothe, P. Chaudhuri, K. Wieghardt, *Inorg. Chem.* **2005**, *44*, 3709–3717.
[9] T. Liu, B. Li, C. V. Popescu, A. Bilko, L. M. Perez, M. B. Hall, M. Y. Darensbourg, *Chem. Eur. J.* **2010**, *16*, 3083–3089.
[10] K. Izutsu, *Acid-Base Dissociation Constants in Dipolar Aprotic Solvents*, Blackwell Scientific Publications, Oxford, UK,, **1990** vol. 35.
[11] G. A. E. Webb, K. E. Kamienska-Trela, *Nuclear Magnetic Resonance*, RSC, **2010**, vol. 39.
[12] M. R. Ringenberg, S. L. Kokatam, Z. M. Heiden, T. B. Rauchfuss, *J. Am. Chem. Soc.* **2008**, *130*, 788–789.
[13] J. Emsley, *Chem. Soc. Rev.* **1980**, *9*, 91–124.
[14] a) A. G. Orpen, L. Brammer, F. H. Allen, O. Kennard, D. G. Watson, R. Taylor, *J. Chem. Soc., Dalton Trans.* **1989**, S1–S83; b) F. Allen, *Acta Crystallogr., Sect. B* **2002**, *58*, 380–388; C. S. E. Harris, A. G. Orpen, I. J. Bruno, R. Taylor, *J. Chem. Inf. Model.* **2005**, *45*, 1727–1748.

 © 2012 Wiley-VCH Verlag GmbH & Co. KGaA, Weinheim

[15] a) C. G. Pierpont, R. M. Buchanan, *Coord. Chem. Rev.* **1981**, *38*, 45–87; b) C. G. Pierpont, C. Lange, *Prog. Inorg. Chem.* **1993**, *41*, 381–492.
[16] T. Ikariya, A. J. Blacker, *Acc. Chem. Res.* **2007**, *40*, 1300–1308.
[17] T. M. Gilbert, R. G. Bergman, *Organometallics* **1983**, *2*, 1458–1460.
[18] Z. M. Heiden, T. B. Rauchfuss, *J. Am. Chem. Soc.* **2009**, *131*, 3593–3600.
[19] I. Kaljurand, A. Kütt, L. Sooväli, T. Rodima, V. Mäemets, I. Leito, I. A. Koppel, *J. Org. Chem.* **2005**, *70*, 1019–1028.
[20] D. D. Perrin, *Dissociation Constants of Organic Bases in Aqueous Solution* (International Union of Pure and Applied Chemistry; Commission on Electroanalytical Chemistry), Butterworths, London, **1972**.
[21] H. Chun, P. Chaudhuri, T. Weyhermüller, K. Wieghardt, *Inorg. Chem.* **2002**, *41*, 790–795.
[22] a) C. P. Roy, L. A. Huff, N. A. Barker, M. A. G. Berg, J. S. Merola, *J. Organomet. Chem.* **2006**, *691*, 2270–2276; b) K. Severin, K. Sünkel, W. Beck, *Chem. Ber.* **1994**, *127*, 615–620.
[23] M. Tilset, *Comprehensive Organometallic Chemistry III* (Eds.: R. H. Crabtree, D. M. P. Mingos), Elsevier, Oxford, **2007**, pp. 279–305.
[24] a) G.-J. M. Meppelder, H.-T. Fan, T. P. Spaniol, J. Okuda, *Inorg. Chem.* **2009**, *48*, 7378–7388; b) L. D. Pachón, A. Golobiç, B. Kozlevçar, P. Gamez, H. Kooijman, A. L. Spek, J. Reedijk, *Inorg. Chim. Acta* **2004**, *357*, 3697–3702.

Received: September 22, 2011
Published Online: November 24, 2011

 © 2012 Wiley-VCH Verlag GmbH & Co. KGaA, Weinheim

DOI: 10.1002/ejic.201100811

Supramolecular Hydrogen-Bonding Tautomeric Sulfonamido–Phosphinamides: A Perfect P-Chirogenic Memory

Frederic W. Patureau,[a] Maxime A. Siegler,[b] Anthony L. Spek,[b] Albertus J. Sandee,[a] Sylvain Jugé,[c] Sarwar Aziz,[d] Albrecht Berkessel,[d] and Joost N. H. Reek*[a]

Keywords: Tautomerism / Rhodium / Hydrogenation / Phosphorus / Chirality

P-chirogenic, supramolecular hydrogen-bonding C_1-symmetrical sulfonamido–phosphinamides (METAMORPhos) have been successfully prepared. They were all found to possess a characteristic prototropic equilibrium between the P^{III} and the P^{V} tautomers that is slow on the NMR spectroscopic timescale. Despite the dynamic and reversible protonation of the P centre, the P-chirogenic information was found to be retained in the tautomerization process, even in a protic solvent environment. Several strategies to access the corresponding enantiopure compounds were investigated, such as diastereoselective crystallization, or enantioselective synthesis. It was possible to resolve such a class of chiral ligands with up to 99% *ee*, and apply them in the Rh-catalyzed asymmetric hydrogenation of alkenes. These ligands are interesting new building blocks in the area of acid/base-type noninnocent ligand catalysis.

Introduction

The field of organometallic chemistry and catalysis with noninnocent ligands is dominated by achiral ligand scaffolds, and in most examples the noninnocence involves redox chemistry of the particular ligand. Extension to chiral ligands for asymmetric conversions as well as other types of functional noninnocent behaviour of ligands is highly interesting. The field of supramolecular hydrogen-bonding ligand-mediated transition-metal catalysis typically involves such cooperative and noninnocent effects as the functional groups of the ligands may be reversibly deprotonated during the catalytic cycle, opening up novel mechanistic pathways for certain reactions. Also, simple reversible hydrogen-bond formation to a substrate, in addition to coordination to a transition metal, could be considered as a form of noninnocent behaviour of the ligand, moderating the activity and selectivity of the complex. The application of P-centred chirality in this field has been neglected so far. In general, the resolution and use of P-chirogenic phosphanes has remained marginal over the past five decades, although some interesting examples have shown their potential in asymmetric transition-metal catalysis.[1–3] Even more scarce are the examples of P^{III}-chirogenic phosphinites/phosphinamides,[4] partly because of the well-documented configurational instability of the P-chirogenic chlorophosphanes from which they are usually derived.[5] Despite this problem, the concept of P-chirogenic sulfonamido–phosphinamides appealed to us, as it represents a class of recently introduced hydrogen-bonding tautomeric ligands that have been successfully applied in the field of cooperative and supramolecular hydrogenation catalysis.[6] Sulfonamido–phosphinamides are a versatile class of ligands, which exist as a unique equilibrium between the P^{III} and the P^{V} tautomers that is shown on the NMR spectroscopic timescale in $CDCl_3$ (see ligand **1**, Figure 1), hence the name METAMORPhos.[6a]

The pivotal question in this enterprise is to determine whether the enantio-configuration of the chiral phosphorus centre is retained or not in the course of the tautomerization. Here we show that P-chirogenic sulfonamido–phosphinamides are configurationally stable despite the dynamic tautomeric equilibrium, even after prolonged exposure to protic solvents such as *i*PrOH. The synthesis of three chiral sulfonamido–phosphinamides has been achieved, with a resolution method on a P-chirogenic sulfonamido–phosphinamide that affords greater than 99% *ee*. A small study on the derived Rh complexes and the preliminary results in the Rh-catalyzed asymmetric hydrogenation of alkenes is presented.

[a] Van't Hoff Institute for Molecular Sciences,
Postbus 94720, 1090 GE Amsterdam, The Netherlands
Fax: +31-20-5255604
E-mail: J.N.H.Reek@uva.nl
[b] Bijvoet Center for Biomolecular Research, Crystal and Structural Chemistry, Utrecht University,
Padualaan 8, 3584CH Utrecht, The Netherlands
[c] Institut de Chimie Moléculaire de l'Université de Bourgogne (ICMUB) - UMR 5260,
Université de Bourgogne, UFR Sciences et Techniques,
9 avenue Alain Savary, BP 47870, 21078 Dijon, France
[d] Department of Chemistry, University of Cologne,
Greinstrasse 4, 50939 Köln, Germany
Supporting information for this article is available on the WWW under http://dx.doi.org/10.1002/ejic.201100811 or from the author.

© 2012 Wiley-VCH Verlag GmbH & Co. KGaA, Weinheim

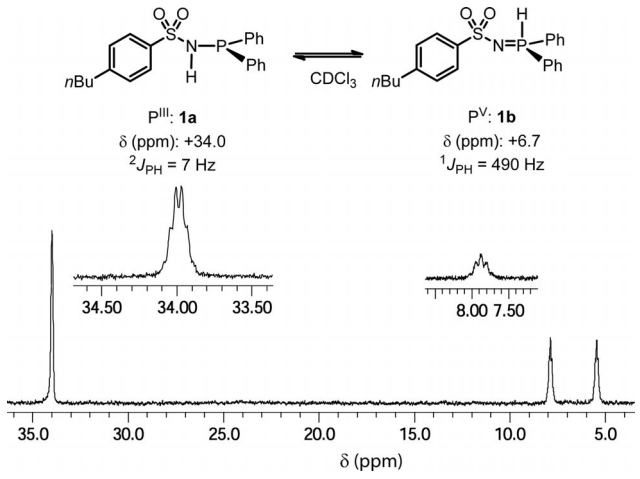

Figure 1. Tautomeric equilibrium of ligand **1** and ^{31}P NMR spectroscopy profile (202.3 MHz, 223 K) of a 12.6 mM solution in $CDCl_3$.

Results and Discussion

Ligand Synthesis

For the purpose of our study, the METAMORPhos racemic ligand *rac*-**2** was designed with a phenyl group and an anisyl group, as it is one of the easiest and cheapest P-chirogenic structures available (Scheme 1).[7] As in the case of ligand **1**, *rac*-**2** also exists as an equilibrium between the P^{III} and the P^{V} tautomers (**2a** and **2b**, respectively) that is slow on the NMR spectroscopic timescale in $CDCl_3$.[7] Ligand **3** was designed with an analogous electronic structure to ligand **2**, although with an extra chiral element based on C_2-chiral (*aR*)-2,2′-dimethoxy-1,1′-binaphthyl appending the P-chirogenic centre (Scheme 1).[7] While we anticipated resolving ligand *rac*-**2** by using "external" chiral agents, ligand **3** was to be resolved by diastereomer separation of (*aR*,*R*)-**3** and (*aR*,*S*)-**3** (using the enantiopure binaphthyl substituent). For comparison, ligand **4** was prepared, which does not need resolution, although chirality is incorporated in the two appending (*aR*)-2,2′-dimethoxy-1,1′-binaphthyl units. As expected, ligands **3** and **4** also exist as a tautomeric equilibrium between the P^{III} and P^{V} isomers that is slow on the NMR spectroscopic timescale in $CDCl_3$.[7]

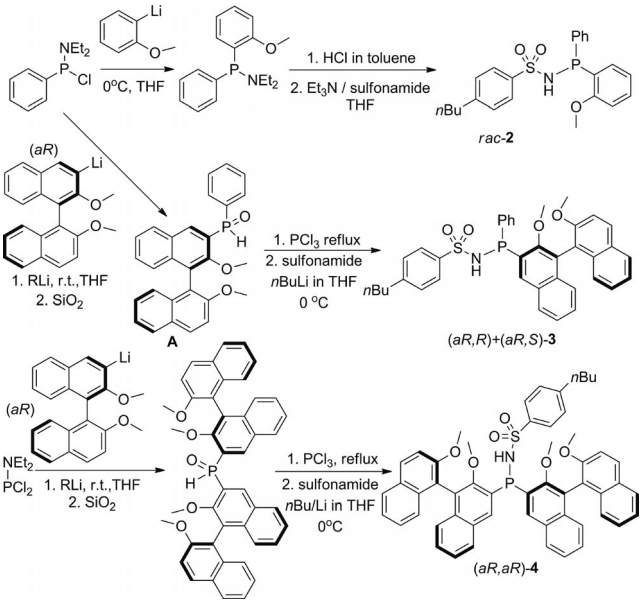

Scheme 1. Synthesis of chiral METAMORPhos ligands *rac*-**2**, (*aR*,*R*)-**3** + (*aR*,*S*)-**3** and (*aR*,*aR*)-**4**.

The first encouraging clue concerning the P-configurational stability of sulfonamido–phosphinamides came from the fact that ligand **3** was not obtained as a 50:50 diastereomeric mixture, but with an initial 12% diastereomeric excess (*de*) that did not change over time. This stereochemical stability was further confirmed by the separation obtained on chiral analytical HPLC (ODH and AD for ligand **2**, ODH for ligand **3**), even while using protic *i*PrOH as a cosolvent, a proton source that does not seem to affect the stability nor the chirality in the prototropic equilibrium.

Interestingly, ligand *rac*-**2** crystallizes as a hydrogen-bonded "head-to-tail" dimer of (*R*)-**2** with (*S*)-**2** (see X-ray structure in Figure 2). Likewise, crystallization of a diastereomeric mixture of (*aR*,*R*)-**3** + (*aR*,*S*)-**3** revealed that (*aR*,*R*)-**3** and (*aR*,*S*)-**3** also cocrystallize in a 1:1 ratio, in an analogous "head-to-tail" disposition in which the two diastereomers are strongly hydrogen bonded to one another

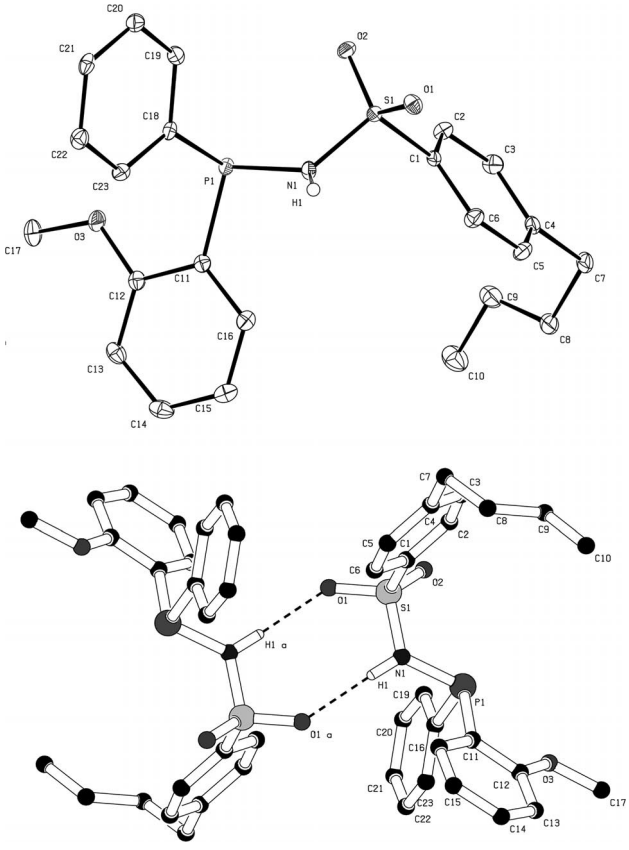

Figure 2. X-ray structure of ligand *rac*-**2** (ORTEP view), 30% probability level, protons omitted for clarity. Selected atomic distances [Å]: N1–P1 1.7321(15), N1–S1 1.6183(15), N1–H1 0.851(18), and the full dimeric hydrogen-bonded structure (beneath).

 © 2012 Wiley-VCH Verlag GmbH & Co. KGaA, Weinheim

(Figure 3). Interestingly, several distances vary significantly from one diastereomer to another. For example, N1A–S1A [*aR*,*R* diastereomer, 1.628(3) Å] is longer than N1B–SIB [a*R*,*S* diastereomer, 1.610(3) Å], and angle S1A–N1A–P1A [125.12(17)°] is larger than S1B–N1B–P1B [123.28(18)°, Figure 3]. The hydrogen-bonding behavior between (*aR*,*R*)-**3** and its diastereomer (*aR*,*S*)-**3** is clear from the short distances: O1B–H1A 2.10(3) and O1A–H1B 2.18(3) Å (Figure 3). Although it is usual for chiral compounds to cocrystallize both enantiomers in a 1:1 ratio, it is quite unusual to obtain crystals containing two different diastereomers, with a consequently very low symmetry level in the crystal. We therefore appreciate the beauty and rarity of such a structure, but it is clear that a diastereomeric separation through crystallization is probably not feasible. Unfortunately, and in spite of many attempts, the diastereomeric mixture (*aR*,*R*)-**3** + (*aR*,*S*)-**3** could not be separated by silica gel chromatography.

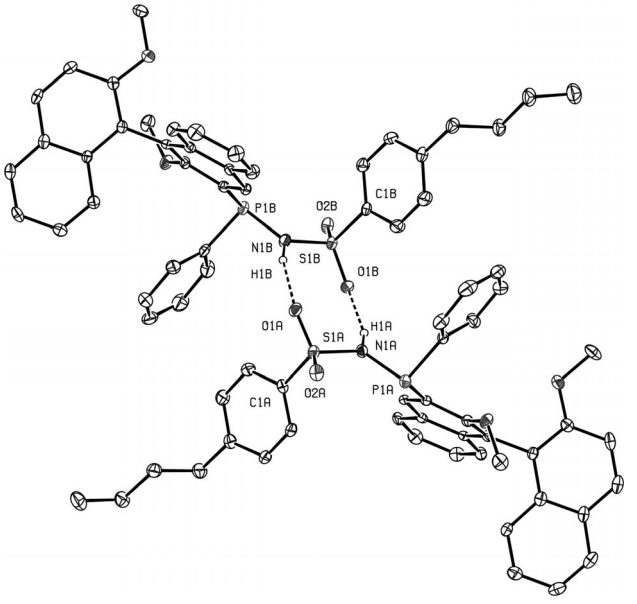

Figure 3. X-ray structure of ligand (*aR*,*R*)-**3** and (*aR*,*S*)-**3** (ORTEP view, 50% probability level, protons omitted for clarity). Selected atomic distances [Å]: N1A–P1A 1.728(3), N1B–P1B 1.735(3), N1A–S1A 1.628(3), N1B–S1B 1.610(3), N1A–H1A 0.84(3), N1B–H1B 0.84(3), O1B–H1A 2.10(3), O1A–H1B 2.18(3). Selected atomic angles [°]: S1A–N1A–P1A 125.12(17), S1B–N1B–P1B 123.28(18); selected atomic torsion angles [°]: H1–N1B–S1B–O1B +25(3), H1A–N1A–S1A-O1A –33(3).

We were fortunately more successful with ligand *rac*-**2**, which could be resolved using a chiral preparative HPLC system, eluting with *n*-hexane/*i*PrOH (75:25) at a flow of 100 mL min^{-1}, in cycles of 50 mg of starting material dissolved in 10 mL of injection volume. Fraction collection was monitored manually according to "real-time" UV detection. The first fraction was typically collected between 26.5 and 29.2 min from the injection, for a total of 37 min per run. Unfortunately, due to a heavy tailing of both enantiomers, only the first fraction was found enantiopure according to the post-run HPLC analysis of all fractions. All first fractions were therefore combined and the Hex/*i*PrOH solvents were evaporated. After a short filtration through silica gel in ethyl acetate, a white powder could be obtained and characterized as (–)-**2** (cumulated isolated yield: 7%).

A very simple experiment to accurately measure the enantiopurity of ligand (–)-**2** was devised. When *rac*-**2** was combined with the sulfonamido–phosphoramidite (*aR*)-[**5**][Et_3NH] and [Rh(acac)$(CO)_2$] (a typical catalyst precursor in hydroformylation, 1:1:1 respectively; acac = acetylacetonate) in CD_2Cl_2, a one-to-one mixture of square-planar (*aR*,*R*)-[Rh(**2c**)(**5**H)(CO)] and (*aR*,*S*)-[Rh(**2c**)(**5**H)(CO)] was formed by loss of [Et_3NH][acac], with distinctively different signals in the ^{1}H and the ^{31}P NMR spectra (Figure 4). When resolved (–)-**2** was combined with (*aR*)-[**5**][Et_3NH] and [Rh(acac)$(CO)_2$], only one set of signals was obtained in the ^{1}H and the ^{31}P NMR spectra, thereby indicating the formation of pure (*aR*,*R*)-[Rh(**2c**)(**5**H)(CO)] or (*aR*,*S*)-[Rh(**2c**)(**5**H)(CO)]. Although it is not yet determined of which absolute configuration (–)-**2** is, the ligand was isolated with more than 99% *ee*.[7]

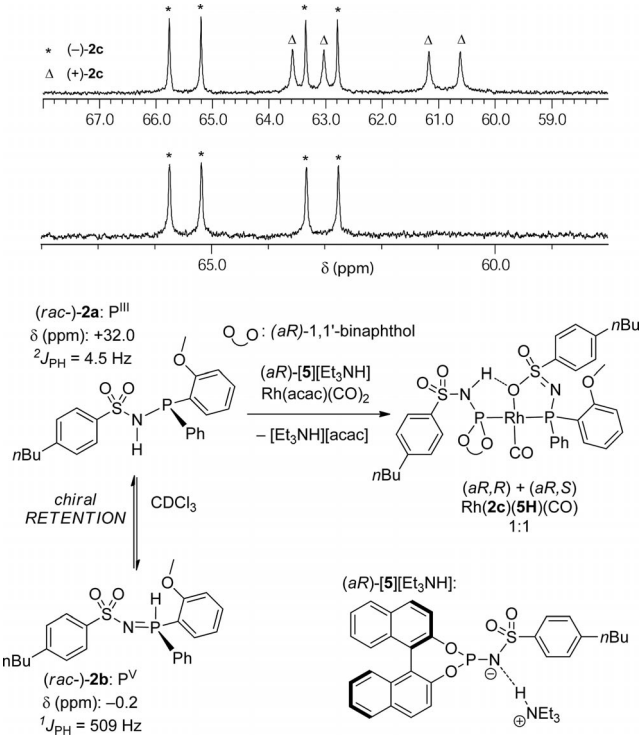

Figure 4. ^{31}P NMR (202.3 MHz, 298 K) spectroscopic profile of (*aR*,*R*)-[Rh(**2c**)(**5**H)(CO)] and (*aR*,*S*)-[Rh(**2c**)(**5**H)(CO)] (phosphinamide area half spectrum, top), and of diastereopure [Rh{(–)-**2c**}{(*aR*)-**5**H}(CO)] (beneath), both at 15.5 mM of [Rh] in CD_2Cl_2. δ = 64.28 [dd, $^1J_{P(-2),Rh}$ = 113 Hz, $^2J_{P(-2),P5}$ = 489 Hz, P of (–)-**2**], 62.10 [dd, $^1J_{P(+2),Rh}$ = 113 Hz, $^2J_{P(+2),P5}$ = 488 Hz, P of (+)-**2**] ppm.

An enantioselective synthesis of ligand **2** using (+)-ephedrine as chiral inductor was also attempted according to the methodology described by Jugé and co-workers.[3q] It is unclear why the condensation failed when using the described procedure with BuLi as a base. This could be attrib-

 © 2012 Wiley-VCH Verlag GmbH & Co. KGaA, Weinheim

uted to the low nucleophilicity and/or the steric hindrance of the lithium salt. However, using a soft base such as Et_3N did allow the reaction to proceed, but yielded only racemic product *rac*-**2** in the resulting crude product (Scheme 2). We assume that Et_3N increases the lability of the chloride anion, making the chiral chlorophosphane precursor less enantiostable under the reaction conditions.

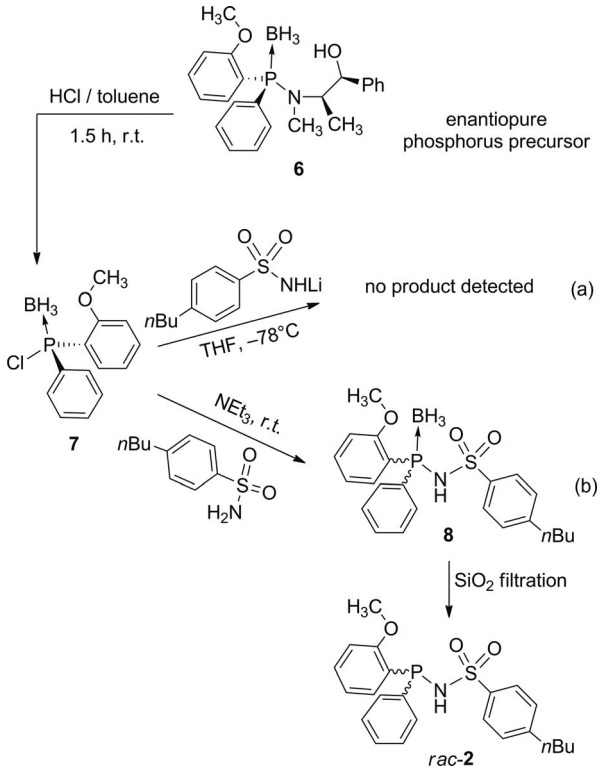

Scheme 2. Attempted enantioselective synthesis of P-chirogenic METAMORPhos ligand **2** using the methodology based on (+)-ephedrine.

Rh Complexation Studies

Preliminary complexation studies with $[Rh(nbd)_2BF_4]$ (a typical asymmetric hydrogenation catalyst precursor; nbd = norbornadiene) showed that ligand *rac*-**2** could furnish $[Rh(\mathbf{2a})_2(nbd)(BF_4)]$, analogously to $[Rh(\mathbf{1a})_2(nbd)(BF_4)]$. In contrast, ligand (*aR,aR*)-**4** was too bulky to form the analogous *cis*-coordinated complex, and formed the μ-(P–N–S=O) hemilabile $[Rh(\mathbf{4a})(nbd)(BF_4)]$, leaving the extra equivalent of ligand **4** uncoordinated. When using $[Rh(acac)(CO)_2]$, however, *trans*-coordinated complexes of the type [Rh(**La**)(**Lc**)(CO)] could be obtained by loss of acac–H (**L** = ligand **1**–**4**). The very broad NMR spectroscopy signals observed for [Rh(**4a**)(**4c**)(CO)] suggest steric congestion at the metal centre.[7] Pressurization with H_2 gas of $[Rh(\mathbf{1a})_2(nbd)(BF_4)]$ leads to $[Rh(\mathbf{1a})_2(BF_4)]$ by hydrogenation of the nbd, as indicated by NMR spectroscopy and mass spectrometry, in which case each ligand **1a** coordinates the square-planar cationic Rh^I centre in a hemi-labile μ-(P–N–S=O) fashion, a likely resting state for the hydrogenation reaction (Scheme 3).[7]

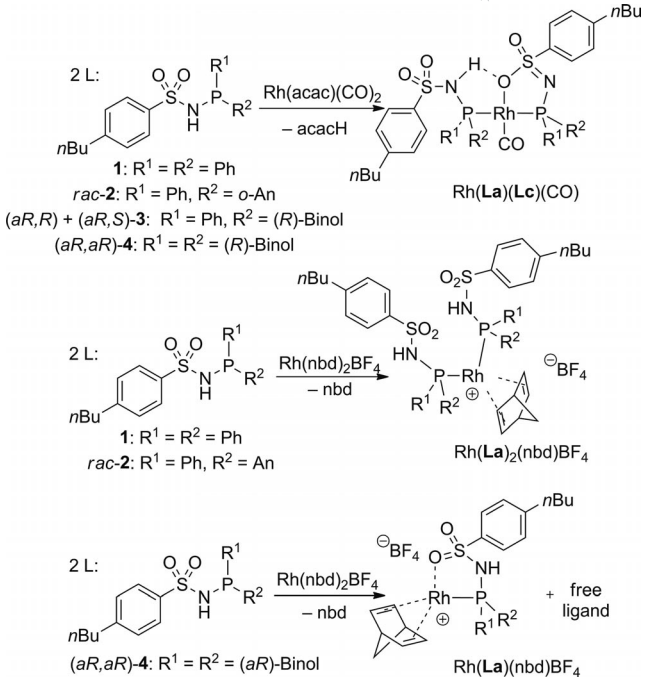

Scheme 3. Coordination modes of ligand **1**, *rac*-**2** and (*aR,aR*)-**4** to $[Rh(acac)(CO)_2]$ and $[Rh(nbd)_2BF_4]$.

Rh-Catalyzed Asymmetric Hydrogenation

Sulfonamido–phosphinamides are known to alter the mechanism of the Rh-catalyzed asymmetric hydrogenation reaction of alkenes through supramolecular hydrogen-bonding interactions and cooperative effects, which can be monitored through kinetic order measurements.[6a] Therefore, preliminary Rh-catalyzed asymmetric hydrogenation experiments were performed on methyl 2-acetamidoacrylate (MAA), based on enantiopure METAMORPhos (–)-**2** and, for comparison, enantiopure (*aR,aR*)-**4** {$[Rh(nbd)_2BF_4]$: 1 mol-% and 1 mM, ligand: 2.2 mol-%, CH_2Cl_2, 50 bar H_2, 298 K, 17 h}. Unfortunately only a very modest 25% *ee* could be obtained with ligand (–)-**2**, albeit with full conversion. The application of ligand (*aR,aR*)-**4** resulted in only traces of the hydrogenation product. We attribute this loss of activity to the sheer bulk of the ligand, which likely shields the active metal centre from the substrate, also with only one equivalent of ligand per Rh. Furthermore, full conversion could be obtained for the analogous substrate methyl 2-acetamido-3-phenylacrylate using (–)-**2** as the ligand, but the product was found to be racemic. With the trisubstituted cyclic substrate, *N*-(3,4-dihydronaphthalen-2-yl)acetamide, neither ligands (–)-**2** nor (*aR,aR*)-**4** led to any significant conversion (identical conditions). Elaborated screening is required to identify the substrate classes, which may lead to high activity and selectivity in the Rh-catalyzed asymmetric hydrogenation with P-chirogenic METAMORPhos ligands.

 © 2012 Wiley-VCH Verlag GmbH & Co. KGaA, Weinheim

Conclusion

In conclusion, it has been shown that sulfonamido–phosphinamides (METAMORPhos), which exist as an equilibrium between the P^{III} and the P^{V} tautomers that is slow on the NMR spectroscopic timescale in $CDCl_3$, could be made P-chirogenic and subsequently resolved. Specifically, the resolution of P-chirogenic sulfonamido–phosphinamide **2** was found possible with more than 99% *ee*; as far as we know, the first P-chirogenic enantiopure METAMORPhos ligand. The prototropic equilibrium, although involving the reversible protonation of the C_1-chiral phosphorus centre, does not lead to racemization. This means the prototropic equilibrium involves the protonation of systematically the same face of the phosphorus atom (chiral memory process), and that neither the P^{III} nor the P^{V} tautomers are susceptible to inversion, even under prolonged exposure to a protic solvent such as *i*PrOH. We expect that this discovery will have an impact on phosphorus-mediated asymmetric catalysis, especially that which involves cooperative or supramolecular hydrogen-bonding ligands.[6]

Experimental Section

General Procedures: All reactions were carried out in dry glassware under an argon or nitrogen atmosphere. Every solution addition or transfer was performed by means of syringes. All solvents were dried and distilled with standard procedures. NMR spectroscopy experiments were performed either on a Varian Inova500 spectrometer (^{1}H: 500 MHz, ^{31}P: 202.3 MHz, ^{13}C: 125.7 MHz) or on a Varian Mercury300 (^{1}H: 300.1 MHz, ^{19}F: 282.4 MHz). Chemical shifts are referenced to the solvent signal (δ = 7.26 ppm in ^{1}H and 77.0 ppm in ^{13}C NMR for $CDCl_3$). Chemical shifts in the ^{31}P NMR spectroscopic experiments are referenced from H_3PO_4 as an external standard. The ^{15}N NMR spectroscopic experiment was recorded using a (^{1}H,^{15}N) HMQC sequence on a Bruker DRX-300 operating a 30.42 MHz ^{15}N frequency.[8] The chemical shift is referenced to nitromethane = 0 ppm. Conversions and enantiomeric excess for the asymmetric hydrogenation reactions were determined by gas chromatography on a Focus CHIRALSIL DEX-CB and/or on a Ph Betadex FT. The chiral preparative HPLC system was CHIRALPAK AD, 5 cm inside diameter, 50 cm length, particle size 20 micron from Daicel Chemical Industries. Ligands **1** and **5** were prepared according to the literature.[6a] 4-Butylbenzenesulfonamide and (*R*)-2,2′-dimethoxy-1,1′-binaphthyl were always dried by co-evaporation in dry and distilled toluene before use.

METAMORPhos Ligand 1: See the ref.[6a] ^{31}P NMR (202.3 MHz, 12.6 mM in $CDCl_3$, 223 K): δ = 33.99 (d, $^2J_{P,H}$ = 7 Hz, tautomer **1a**), 6.66 (dm, $^1J_{P,H}$ = 490 Hz, tautomer **1b**) ppm. The tautomeric ratio **1a**/**1b** was found at 0.85 according to integrations. ^{1}H NMR (500 MHz, 1.7 mM in $CDCl_3$, 223 K): δ = 8.14 (d, $^1J_{P,H}$ = 490 Hz, PH of tautomer **1b**), 7.79–7.04 (aromatic region: tautomer **1a** and **1b**), 5.53 (d, $^2J_{H,P}$ = 7 Hz, NH of tautomer **1a**), 2.67 [t, ^3J = 7.5 Hz, (C_3H_7)–CH_2–Ar of tautomer **1a**], 2.53 [t, ^3J = 7.5 Hz, (C_3H_7)–CH_2–Ar of tautomer **1b**], 1.57 [m, (C_2H_5)–CH_2–CH_2–Ar of tautomer **1a**], 1.47 [m, (C_2H_5)–CH_2–CH_2–Ar of tautomer **1b**], 1.33–1.20 [m, CH_3–CH_2–(C_2H_4)–Ar, of tautomer **1a** and tautomer **1b**], 0.93–0.88 [m, CH_3–(C_3H_6)–Ar, of tautomer **1a** and tautomer **1b**] ppm. ^{13}C NMR (125.7 MHz, $CDCl_3$, 298 K): δ = 148.25 (s, C_{quat}), 138.81 (s, C_{quat}), 137.41 (d, $J_{C,P}$ = 12.7 Hz, C_{quat}), 133.48 (s, CH), 131.98 (CH), 131.89 (CH), 131.44 (CH), 131.27 (CH), 129.68 (s, CH), 129.22 (CH), 129.11 (CH), 129.01 (CH), 128.90 (CH), 128.62 (CH), 128.56 (CH), 128.25 (CH), 126.85 (s, CH), 126.42 (CH), 125.82 (s, CH), 35.47 [s, (C_3H_7)–CH_2–Ar], 33.21 [s, (C_2H_5)–CH_2–CH_2–Ar], 22.15 [s, CH_3–CH_2–(C_2H_4)–Ar], 13.86 [s, CH_3–(C_3H_6)–Ar] ppm. Note: in these concentrated conditions, most of the above-mentioned lines belong to major tautomer **1a**. (^{1}H,^{15}N)-HMQC NMR (30.42 MHz, 332 mM in $CDCl_3$, at natural abundance, 298 K): δ = –270.5 (dd, $^1J_{N,H}$ = 84 Hz, $^1J_{N,P}$ = 63 Hz, tautomer **1a**) ppm. MS (FAB$^+$): *m*/*z* calcd. for $C_{22}H_{25}NO_2PS^+$ [M + H]$^+$: 398.1344; found 398.1340.

Racemic METAMORPhos *rac*-2: 2-Bromoanisole (44 mmol) was dissolved in THF (15 mL) and was cooled to –78 °C. A solution of *n*BuLi (2.5 M in hexanes, 44 mmol) was added dropwise, and the solution was stirred at room temp. for 1 h. The resulting solution was added dropwise on a solution of racemic 1-chloro-*N*,*N*-diethyl-1-phenylphosphinamine (44 mmol in 400 mL of Et_2O, –78 °C) and left to stir back to room temp. The solvents were evaporated and the crude product was extracted with CH_2Cl_2/H_2O. The organic layers were dried on $MgSO_4$ and evaporated to give a very viscous light yellow oil: racemic *N*,*N*-diethyl-1-(2-methoxyphenyl)-1-phenylphosphinamine (93% isolated yield). The substance (8.3 mmol) was exposed to saturated HCl in toluene (80 mL) and stirred at room temp. for 1 h (conversion to the chlorophosphane was monitored by ^{31}P NMR spectroscopy). A third of the solution was then evaporated, hexanes (40 mL) were added and the resulting turbid solution was filtered. 4-Butylbenzenesulfonamide (8.3 mmol) was dissolved in THF (15 mL) and Et_3N (32.5 mmol). The previous chlorophosphane solution was added dropwise at room temp. and left to stir overnight. The solvents were evaporated and the product, racemic METAMORPhos *rac*-**2**, was purified by silica gel chromatography (toluene/ethyl acetate, 9:1). The product was isolated as a white powder in 34% isolated yield, characterized by X-ray crystallography (Figure 2). Crystallization method: slow diffusion of hexanes on top of a CH_2Cl_2 solution in a closed glass pipette (+4 °C). ^{31}P NMR (202.3 MHz, 8.9 mM in $CDCl_3$, 223 K): δ = +32.50 (br. d, $^2J_{P,H}$ = 5 Hz, 58% of the integration: tautomer **2a**), –2.16 (br. d, $^1J_{P,H}$ = 509 Hz, 42% of the integration, tautomer **2b**) ppm. ^{31}P{^{1}H} NMR (202.3 MHz, CD_2Cl_2, 298 K): δ = +31.79 (s, tautomer **2a**), –1.53 (s, tautomer **2b**) ppm. ^{1}H NMR (500 MHz, CD_2Cl_2, 298 K): δ = 8.26 (d, $^1J_{H,P}$ = 509 Hz, P–H of tautomer **2b**), 7.9–6.8 (dense aromatic signal range), 6.20 (d, $^2J_{H,P}$ = 5 Hz, NH of tautomer **2a**), 3.73 (small s, methoxy unit of tautomer **2b**), 3.56 (large s, methoxy unit of tautomer **2a**), 2.63 (t, ^3J = 8 Hz, CH_2–Ar of tautomer **2a**), 2.59 (t, ^3J = 8 Hz, CH_2–Ar of tautomer **2b**), 1.58 (m, CH_2–CH_2–Ar of **2a** and **2b**), 1.32 (m, CH_2–CH_2–CH_2–Ar of **2a** and **2b**), 0.93 (t, ^3J = 7.5 Hz, CH_3–C_3H_6–Ar of **2a** and **2b**) ppm. ^{13}C NMR (125.7 MHz, CD_2Cl_2, 298 K): δ = 161.29 (br. s, C_{quat}), 148.84 (s, C_{quat}), 139.65 (s, C_{quat}), 139.14 (d, $J_{C,P}$ = 11 Hz, C_{quat}), 136.20–126.19 (aromatic signal range, exclusively CH lines), 124.60 (d, $J_{C,P}$ = 17 Hz, C_{quat}), 122.03–111.78 (aromatic signal range, exclusively CH lines), 56.28 (very small s, methoxy unit of **2b**), 56.07 (s, methoxy unit of **2a**), 35.96 (s, CH_2–Ar of **2a**), 35.88 (very small s, CH_2–Ar of **2b**), 33.98 (very small s, CH_2–CH_2–Ar of **2b**), 33.82 (s, CH_2–CH_2–Ar of **2a**), 22.76 (s, CH_2–CH_2–CH_2–Ar, **2a** and **2b**), 14.21 (s, CH_3–C_3H_6–Ar, **2a** and **2b**) ppm. Note: under these concentrated conditions, the lines of tautomer **2b** are very small. For the C_{quat}, only the lines of **2a** are visible.

Resolution of Enantiopure METAMORPhos (–)-2: See main text. $[a]_D^{22}$ = –55.1 (*c* = 0.2, CH_2Cl_2).

Mixture (*aR*,*R*) + (*aR*,*S*)-3: Crystalline (*R*)-2,2′-dimethoxy-1,1′-binaphthyl (15.9 mmol) was slowly dissolved in THF (315 mL). A solution of *n*BuLi (2.5 M in hexanes, 16.7 mmol) was added drop-

 © 2012 Wiley-VCH Verlag GmbH & Co. KGaA, Weinheim

wise at room temp. and with strong stirring. The resulting dark brown solution was stirred at room temp. for 1 h. Racemic 1-chloro-*N*,*N*-diethyl-1-phenylphosphinamine (15.9 mmol in 140 mL of Et_2O) was added to it dropwise at room temp. The resulting solution was left to stir at room temp. for 1 h, and the solvents were evaporated. The crude product was extracted with CH_2Cl_2/H_2O, the organic layers were dried with $MgSO_4$ and the solvents were evaporated. The crude product was added to Et_2O (150 mL) yielding a white suspension that was filtered off. The organic layers were combined and solvents were evaporated to give a light yellow oil. The product was subjected to a silica gel purification in CH_2Cl_2, and then collected by flushing the silica gel with ethyl acetate. The resulting white crispy powder was identified as the corresponding P-chirogenic secondary phosphane derivative: compound **A** (Scheme 1); isolated yield: 25%. ^{31}P NMR (202.3 MHz, $CDCl_3$, 298 K): δ = +17.24 (br. d, $^1J_{P,H}$ = 499 Hz, major diastereomer), +16.86 (br. d, $^1J_{P,H}$ = 500 Hz, minor diastereomer) ppm. ^{1}H NMR (300 MHz, $CDCl_3$, 298 K): δ = 8.34 (d, $^1J_{H,P}$ = 500 Hz, PH of minor diastereomer), 8.33 (d, $^1J_{H,P}$ = 499 Hz, PH of major diastereomer), 8.56 (d, $^3J_{H,P}$ = 15 Hz, aromatic H of naphthyl unit *ortho* to P, minor diastereomer), 8.53 (d, $^3J_{H,P}$ = 16 Hz, aromatic H of naphthyl unit *ortho* to P, major diastereomer), 8.01–7.03 (aromatic region), 3.76 (s, methoxy unit of major diastereomer), 3.74 (s, methoxy unit of minor diastereomer), 3.05 (s, other methoxy unit of major diastereomer), 2.98 (s, other methoxy unit of minor diastereomer) ppm. According to the relative integration of the last two signals, the diastereomeric ratio is 64:36 (*de* = 28%). Compound **A** was dissolved in PCl_3 (15 mL) and heated at +100 °C for 2 h. The solution was then evaporated, and the crude product was dissolved in toluene (5 mL). The solution was again evaporated to a white foam. The product was finally dissolved in THF (25 mL). ^{31}P NMR (121.5 MHz, unlocked, 298 K): δ = +78.3 (s, first diastereomer), +77.3 (s, second diastereomer) ppm, the diastereomeric ratio is 1:1 (*de* = 0%). NMR spectroscopic yield: quantitative. 4-Butylbenzenesulfonamide (4.2 mmol) was dissolved in THF (50 mL) and a solution of *n*BuLi (2.5 M in hexanes, 4.2 mmol) was added dropwise at 0 °C under strong stirring. The resulting white suspension was stirred for 1 h and the previous solution was added dropwise at 0 °C, which led to an almost clear solution that was stirred at room temp. overnight. The solvents were evaporated, and the product was purified by silica gel chromatography (toluene/ethyl acetate 9:1). A white powder was obtained; isolated yield: 48%. Characterized by X-ray crystallography (Figure 3). Crystallization method: slow diffusion of hexanes on top of a CH_2Cl_2 solution in a closed glass pipette (+4 °C). ^{31}P NMR (202.3 MHz, $CDCl_3$, 298 K): δ = +33.75 (br. s, tautomer **3a**), +32.78 (s, tautomer **3a** of corresponding diastereomer), +0.03 (d, $^1J_{P,H} \approx$ 502 Hz, tautomer **3b** of the diastereomer at +33.75 ppm), –0.30 (d, $^1J_{P,H}$ = 502 Hz, tautomer **3b** of diastereomer at +32.78) ppm. Peak assignment was determined by ^{31}P NMR spectroscopic analysis of a diastereomerically enriched sample recovered from the mother solution of crystallization: lines at +33.75 and +0.03 ppm slightly but significantly decreased together relative to the two other lines and correspond therefore to the same diastereomer. The diastereomeric excess is therefore measured at *de* = 12% in the original batch, according to integrations. ^{31}P{^{1}H} NMR (202.3 MHz, CD_2Cl_2, 298 K): δ = +32.45 (s, **3a**), +31.12 (s, other diastereomer of **3a**), +0.35 (s, **3b**), +0.19 (s, other diastereomer of **3b**) ppm. ^{1}H NMR (500 MHz, CD_2Cl_2, 298 K): δ = 9.01–6.86 (aromatic area), 6.30 (d, $^2J_{H,P}$ = 6 Hz, NH of tautomer **3a**), 6.23 (d, $^2J_{H,P}$ = 5 Hz, NH of tautomer **3a** of corresponding diastereomer), 3.78 (s, methoxy unit of tautomer **3a**), 3.76 (s, methoxy unit of tautomer **3a**), 2.66 (very br. s, methoxy unit of tautomer **3a**), 2.62 (very br. s, methoxy unit of tautomer **3a**), 2.56 (br. m, C*H*$_2$–Ar signal range), 1.54–0.84 (broad alkyl signal range) ppm. Note: the signals of tautomer **3b** are small and broad. ^{13}C NMR (125.7 MHz, CD_2Cl_2, 298 K): δ = 157.14 (very br., C_{quat}), 155.59 (C_{quat}), 155.40 (C_{quat}), 149.08 (C_{quat}), 149.04 (C_{quat}), 139.91 (C_{quat}), 139.85 (C_{quat}), 139.66 (C_{quat}), 139.57 (C_{quat}), 135.98 (C_{quat}), 135.60–113.47 (dense aromatic signal range), 60.55 (br. s, methoxy unit, possibly 2 signals overlapping), 56.94 (s, methoxy unit), 56.60 (s, methoxy unit), 35.94 (s, *C*H$_2$–Ar), 33.71 (s, *C*H$_2$–CH$_2$–Ar), 22.79 (s, *C*H$_2$–CH$_2$–CH$_2$–Ar, first diastereomer of **3a**), 22.73 (s, *C*H$_2$–CH$_2$–CH$_2$–Ar, other diastereomer of **3a**), 14.20 (s, *C*H$_3$–C$_3$H$_6$–Ar, first diastereomer of **3a**), 14.14 (s, *C*H$_3$–C$_3$H$_6$–Ar, other diastereomer of **3a**) ppm. Note: in this case the lines of tautomer **3b** are too small to be accurately reported.

(*aR*,*aR*)-4: Crystalline (*R*)-2,2′-dimethoxy-1,1′-binaphthyl (28.6 mmol) was slowly dissolved in THF (250 mL). A solution of *n*BuLi (2.5 M in hexanes, 29.2 mmol) was added dropwise at room temp. and with strong stirring. The resulting dark brown solution was stirred at room temp. for 1 h. The solution was cooled to 0 °C and a solution of 1,1-dichloro-*N*,*N*-diethylphosphinamine in Et_2O (14.3 mmol in 150 mL) was added dropwise. The resulting clear solution was left to stir at room temp. overnight. The solvents were evaporated and the crude product was directly purified by silica gel chromatography in CH_2Cl_2. The product was then recovered by flushing the silica with ethyl acetate, and the solvent was evaporated to a white solid (the corresponding secondary phosphane oxide). Isolated yield: 25%. ^{31}P NMR (121.5 MHz, $CDCl_3$, 298 K): δ = +11.36 (dt, d: $^1J_{P,H}$ = 516 Hz, t: $^3J_{P,H}$ = 16 Hz) ppm. ^{1}H NMR (300 MHz, $CDCl_3$, 298 K): δ = 8.60 (d, $^1J_{H,P}$ = 516 Hz, P–*H*), 8.50 (d, $^3J_{H,P}$ = 16 Hz, aromatic H *ortho* to P), 8.45 (d, $^3J_{H,P}$ = 16 Hz, other aromatic H *ortho* to P, diastereotopic to the previous), 8.00–7.02 (aromatic area), 3.73 (s, methoxy unit), 3.67 (s, methoxy unit), 3.12 (s, methoxy unit), 3.07 (s, methoxy unit) ppm. The product (3.4 mmol) was dissolved in PCl_3 (40 mL) and heated at +100 °C for 1 h. The solution was then evaporated, and the crude product was dissolved in toluene (5 mL). The solution was again evaporated to a white foam. The product was then dissolved in THF (20 mL). ^{31}P NMR (121.7 MHz, unlocked, 298 K): δ = +74.57 (s) ppm. NMR spectroscopic yield: quantitative. 4-Butylbenzenesulfonamide (7.44 mmol) was dissolved in THF (100 mL) and a solution of *n*BuLi (2.5 M in hexanes, 7.44 mmol) was added dropwise at 0 °C under strong stirring. The resulting white suspension was stirred for 1 h and the previous solution was added dropwise, which led to an almost clear solution that was stirred at room temp. overnight. The solvents were evaporated, and the product was purified by silica gel chromatography in 100% CH_2Cl_2. A white powder was obtained; isolated yield: 53%. (Note: the large excess amount of activated sulfonamide is required because the previous chlorophosphane is less reactive due to steric congestion). HRMS (FAB$^+$): *m*/*z* calcd. for $C_{54}H_{49}NO_6PS^+$ [M + H]$^+$: 870.3018; found 870.3021. ^{31}P NMR (202.3 MHz, 13.4 mM in $CDCl_3$, 298 K): δ = +27.44 (dt, d: $^2J_{PNH}$ = 3 Hz, t: $^3J_{P,H}$ = 10 Hz, 83% of the integration, tautomer **4a**), –5.80 (dt, d: $^1J_{P,H}$ = 524 Hz, t: $^3J_{P,H}$ = 17 Hz, 17% of the integration, tautomer **4b**) ppm. ^{31}P{^{1}H} NMR (202.3 MHz, 13.4 mM in $CDCl_3$, 298 K): δ = +27.43 (s, tautomer **4a**), –5.80 (s, tautomer **4b**) ppm. ^{1}H NMR (500 MHz, 13.4 mM in $CDCl_3$, 298 K): δ = 8.71 (d, $^1J_{H,P}$ = 524 Hz, P–*H* of tautomer **4b**), 8.44 (d, $^3J_{H,P}$ = 17 Hz, aromatic H *ortho* to P, tautomer **4b**), 8.38 (d, $^3J_{H,P}$ = 17 Hz, H *ortho* to P, diastereotopic to the previous, **4b**), 8.20–6.81 (aromatic area), 6.70 (d, $^2J_{H,P}$ = 3 Hz, NH of tautomer **4a**), 3.74 (small s, methoxy unit of tautomer **4b**), 3.73 (large s, methoxy unit of tautomer **4a**), 3.63 (large s, methoxy unit of tautomer **4a**), 3.59 (small s, methoxy unit of tautomer **4b**), 3.03 (small s, methoxy

 © 2012 Wiley-VCH Verlag GmbH & Co. KGaA, Weinheim

unit of tautomer **4b**), 2.99 (small s, methoxy unit of tautomer **4b**), 2.74 (large s, methoxy unit of tautomer **4a**), 2.73 (large s, methoxy unit of tautomer **4a**), 2.52 (small t, ^3J = 8 Hz, CH_2–Ar of tautomer **4b**), 2.39 (≈t, ^3J = 8 Hz, CH_2–Ar of tautomer **4a**), 1.54–0.78 (alkyl region) ppm. ^{13}C NMR (125.7 MHz, 13.4 mM in $CDCl_3$, 298 K): δ = 156.86 (C_{quat}), 156.78 (C_{quat}), 156.67 (C_{quat}), 156.60 (C_{quat}), 154.93 (C_{quat}), 154.83 (C_{quat}), 147.86 (C_{quat}), 139.13 (C_{quat}), 134.93–123.54 (dense aromatic area, C_{quat} and CH), 118.51 (C_{quat}), 118.44 (C_{quat}), 113.70 (CH), 113.08 (CH), 60.71 (small s, CH_3–O of tautomer **4b**), 60.69 (small s, CH_3–O of tautomer **4b**), 60.39 (d, $^4J_{C,P}$ = 1 Hz, CH_3–O *ortho* to P of tautomer **4a**), 60.19 (d, $^4J_{C,P}$ = 1 Hz, CH_3–O *ortho* to P of tautomer **4a**, diastereotopic from previous), 56.38 (s, CH_3–O of tautomer **4a**), 56.34 [small s, CH_3–O of tautomer **4b** (the 4th methoxy of **4b** is overlapping)], 56.19 (s, CH_3–O of tautomer **4a**), 35.39 (small s, CH_2–Ar of tautomer **4b**), 35.30 (s, CH_2–Ar of tautomer **4a**), 33.23 (small s, CH_2–CH_2–Ar of tautomer **4b**), 32.90 (s, CH_2–CH_2–Ar of tautomer **4a**), 22.24 (small s, CH_2–C_2H_4–Ar of tautomer **4b**), 22.15 (s, CH_2–C_2H_4–Ar of tautomer **4a**), 13.87 (small s, CH_3–C_3H_6–Ar of tautomer **4b**), 13.77 (s, CH_3–C_3H_6–Ar of tautomer **4a**) ppm.

[Rh(2c)(5H)(CO)]: Racemic ligand *rac*-**2** or enantiopure ligand (–)-**2** (0.0078 mmol) was combined with ligand (*R*)-[**5**][Et_3NH] (0.0081 mmol) and [Rh(acac)$(CO)_2$] (0.0078 mmol) and subsequently dissolved in CD_2Cl_2 (0.5 mL). ^{31}P NMR (202.3 MHz, 15.5 mM in CD_2Cl_2, 298 K): δ = +149.14 [dd, $^1J_{P,Rh}$ = 195 Hz, $^2J_{P,P}$ = 489 Hz, P of (*R*)-**5**H associated with (+)-**2**], +148.69 [dd, $^1J_{P,Rh}$ = 196 Hz, $^2J_{P,P}$ = 488 Hz, P of (*R*)-**5**H associated with (–)-**2**], +64.28 [dd, $^1J_{P,Rh}$ = 113 Hz, $^2J_{P,P}$ = 489 Hz, P of (–)-**2** associated with (*R*)-**5**H], +62.10 [dd, $^1J_{P,Rh}$ = 113 Hz, $^2J_{P,P}$ = 488 Hz, P of (–)-**2** associated with (*R*)-**5**H] ppm. ^{1}H NMR (500 MHz, 15.5 mM in CD_2Cl_2, 298 K): δ = 15.55 (s, acidic H of [acac][Et_3NH]), 9.35 (very br. s, NH of **5**H), 8.05–6.79 (dense aromatic signal range), 5.56 (s, middle CH of [acac][Et_3NH]), 3.62 [s, methoxy unit of (–)-**2** associated with (*R*)-**5**H], 3.51 [s, methoxy unit of (+)-**2** associated with (*R*)-**5**H], 2.84–0.83 (alkyl region) ppm.

[Rh(1a)(1c)(CO)]: METAMORPhos ligand **1** (0.0350 mmol) and [Rh(acac)$(CO)_2$] (0.0174 mmol) were combined and dissolved in $CDCl_3$ (2.76 mL) leading to a clear yellow solution (6.3 mM of [Rh]). A sample of this solution (600 μL) was transferred to an NMR spectroscopy tube. ^{31}P{^{1}H} NMR (202.3 MHz, 13.5 mM in $CDCl_3$, 223 K): δ = 69.79 (dd, $^1J_{Pc,Rh}$ = 113.2 Hz, $^2J_{Pc,Pa}$ = 335.6 Hz, P of **1c**), 66.49 (dd, $^1J_{Pa,Rh}$ = 129.4 Hz, $^2J_{Pa,Pc}$ = 335.6 Hz, P of **1a**) ppm. ^{1}H NMR (500 MHz, 6.3 mM in $CDCl_3$, 223 K): δ = 7.86–7.32 (br. aromatic region), 7.14 (d, J = 8 Hz, Ar H), 6.83 (d, J = 8 Hz, Ar H), 6.77 (d, J = 8.5 Hz, Ar H), 6.73 (d, $^2J_{H,P}$ = 16 Hz, NH of **1a**), 5.58 (s, acac–H), 2.63 [t, ^3J = 8 Hz, (C_3H_7)–CH_2–Ar: **1a**], 2.50 [t, ^3J = 7.5 Hz, (C_3H_7)–CH_2–Ar: **1c**], 2.09 (s, acac–H), 1.56 [m, (C_2H_5)–CH_2–CH_2–Ar: **1a**], 1.47 [m, (C_2H_5)–CH_2–CH_2–Ar: **1c**], 1.34–1.24 [m, CH_3–CH_2–(C_2H_4)–Ar, **1a** and **1c**], 0.92–0.88 [m, CH_3–(C_3H_6)–Ar of both **1a** and **1c**] ppm.

[Rh(2a)(2c)(CO)]: Racemic ligand *rac*-**2** (0.0194 mmol) was added to [Rh(acac)$(CO)_2$] (0.0099 mmol) and dissolved in toluene (1 mL), and then evaporated. The process was repeated thrice (removal of acac–H) and the complex was finally dissolved in $CDCl_3$ (0.53 mL). ^{31}P NMR (202.3 MHz, 18.6 mM in $CDCl_3$, 223 K): δ = +67–60 ppm (very br. m, lines of **2a** and **2c**) ppm. No free ligand observed. From the tips of certain lines above the broad multiplet, one of the *trans* $^2J_{P,P}$ can be estimated at approximately 352 Hz, and one of the $^1J_{P,Rh}$ of **2a** can be estimated at approximately 119 Hz. ^{1}H NMR (500 MHz, 18.6 mM in $CDCl_3$, 223 K): δ = very broad spectrum: 8.20–6.74 (br. aromatic region), 6.53 (br. s, NH of **2a**), 3.58 (s, methoxy unit), 3.55 (s, methoxy unit), 3.50 (s, methoxy unit), 3.48 (s, methoxy unit), 2.68–0.84 (broad and crowded alkyl region). Note: the 4 methoxy groups are of approximately equal intensity at 298 K (the 2 diastereomeric complexes are in equal amounts), but one of the diastereomers seems to be favored at 223 K in a roughly 2:1 ratio according to the ^{1}H NMR spectroscopy integrations of the methoxy units. The structure of the complex was assigned by analogy with [Rh(**1a**)(**1c**)(CO)] (see above).[6a]

[Rh(3a)(3c)(CO)]: Diastereomeric mixture (*aR,R*) + (*aR,S*)-**3** (0.0388 mmol) was added to [Rh(acac)$(CO)_2$] (0.0194 mmol) and dissolved in CD_2Cl_2 (0.5 mL). ^{31}P{^{1}H} NMR (202.3 MHz, 39.9 mM in CD_2Cl_2, 298 K): δ = +71.10–57.47 (very br. m, lines of **3a** and **3c**) ppm. No free ligand was observed. ^{1}H NMR (500 MHz, 39.9 mM in CD_2Cl_2, 298 K): δ = +15.54 (s, H of free acac–H) ppm. The rest of the spectrum is extremely broad.

[Rh(4a)(4c)(CO)]: (*aR,aR*)-**4** (0.0194 mmol) was added to [Rh(acac)$(CO)_2$] (0.0097 mmol) and dissolved in CD_2Cl_2 (0.6 mL). ^{31}P{^{1}H} NMR (202.3 MHz, 16.1 mM in CD_2Cl_2, 298 K): δ = +80.49–48.41 (very br. m, lines of **4a** and **4c**) ppm. No free ligand was observed. ^{1}H NMR (500 MHz, 16.1 mM in CD_2Cl_2, 298 K): δ = +15.53 (s, H of free acac–H), 9.71–6.63 (very broad and dense aromatic region), 6.40 (br. s, possibly the NH of **4a**), 5.35 (s, acac–H), 3.75 (very br. s, methoxy area), 3.70 (very br. s, methoxy area), 3.45 (extremely br. s, methoxy area), 2.85 (very br. s, methoxy area), 2.70 (very br. s, methoxy area), 2.56 (very br. s, CH_2–Ar area), 2.39–0.76 (broad and dense alkyl area) ppm.

[Rh(1a)$_2$(nbd)(BF_4)]: Ligand **1** (0.0134 mmol) and [Rh(nbd)$_2BF_4$] (0.0067 mmol) were combined and dissolved in $CDCl_3$ (0.6 mL). ^{31}P{^{1}H} NMR (202.3 MHz, 11.1 mM in CD_2Cl_2, 298 K): δ = +60.46 (d, $^1J_{P,Rh}$ = 167 Hz) ppm. ^{1}H NMR (500 MHz, 11.1 mM in CD_2Cl_2, 298 K): δ = 7.84–7.04 (br. and dense aromatic region). 6.76 (very br. s, alkene H of free nbd, possibly overlapping with NH of **1a**), 4.74 (coordinated nbd), 4.71 (coordinated nbd), 4.39 (s, coordinated nbd), 3.79 (s, coordinated nbd), 3.58 (s, coordinated nbd), 2.66 (t, ^3J = 7.5 Hz, CH_2–Ar of **1a**), 1.98 (br. s, free nbd), 1.65–1.07 (alkyl region), 0.95 (t, ^3J = 7 Hz, CH_3–C_3H_6–Ar of **1a**) ppm.

[Rh(2a)$_2$(nbd)(BF_4)]: Ligand *rac*-**2** (0.0160 mmol) was added to [Rh(nbd)$_2BF_4$] (0.0080 mmol) and dissolved in CD_2Cl_2 (0.5 mL). ^{31}P{^{1}H} NMR (202.3 MHz, 16.1 mM in CD_2Cl_2, 298 K): δ = +59.84 {d, $^2J_{P,Rh}$ = 170 Hz, *rac*- or *meso*-[Rh(**2a**)$_2$(nbd)(BF_4)]}, +58.41 {d, $^2J_{P,Rh}$ = 169 Hz, *meso*- or *rac*-[Rh(**2a**)$_2$(nbd)(BF_4)]} ppm. The ratio between the former and the latter diastereomers is approximately 1.2:1, respectively, under these conditions. ^{1}H NMR (500 MHz, 16.1 mM in CD_2Cl_2, 298 K): δ = 7.86–6.78 (br. aromatic region), 6.41 (br. s, NH of *rac* or *meso* diastereomer), 6.34 (br. s, NH of *meso* or *rac* diastereomer), 4.52 (br. s), 4.41 (br. s), 3.86 (br. s), 3.64 (s, possibly CH_3–O, with overlapping), 3.63 (s, possibly CH_3–O, with overlapping), 3.61 (s, possibly CH_3–O, with overlapping), 2.71 (br. m, CH_2–Ar), 2.00–1.31 (alkyl region), 1.00 (t, ^3J = 7 Hz, CH_3–C_3H_6–Ar) ppm.

[Rh(4a)(nbd)(BF_4)]. Procedure A: Ligand (*aR,aR*)-**4** (0.0135 mmol) was added to [Rh(nbd)$_2BF_4$] (0.0067 mmol) and dissolved in CD_2Cl_2 (0.55 mL). ^{31}P{^{1}H} NMR (202.3 MHz, 12.1 mM in CD_2Cl_2, 298 K): δ = +79.77 (d, $^1J_{P,Rh}$ = 264 Hz, presumably a mono-coordinated species), +56.2 (very br. m, also a mono-coordinated species), +25.4 (very br. s, free ligand tautomer **4a**), –5.18 (s, free ligand tautomer **4b**) ppm.

Procedure B: Ligand (*aR,aR*)-**4** (0.0080 mmol) was added to [Rh(nbd)$_2BF_4$] (0.0080 mmol) and dissolved in CD_2Cl_2 (0.5 mL). ^{31}P{^{1}H} NMR (202.3 MHz, 16.1 mM in CD_2Cl_2, 298 K): δ = +67.24 {br. d, $^1J_{P,Rh}$ = 181 Hz, [Rh(**4a**)(nbd)(BF_4)]} ppm. ^{1}H

 © 2012 Wiley-VCH Verlag GmbH & Co. KGaA, Weinheim

NMR (500 MHz, 16.1 mM in CD_2Cl_2, 298 K): δ = 8.47–7.00 (dense aromatic region), 6.77 (d, $^2J_{H,P}$ = 8.5 Hz, NH of coordinated **4a**), 5.03 (very br. signal), 4.15 (br. s), 3.88–0.91 (dense alkyl region) ppm. Distinct signals: δ = 3.82 (s, CH_3–O), 3.73 (s, CH_3–O), 2.70 (t, ^3J = 8 Hz, CH_2–Ar), 2.61 (br. s, CH_3–O), 2.49 (br. s, CH_3–O) ppm.

Asymmetric Hydrogenation Experiments: Typically, a 15 mL pressure reactor containing a glass insert was subsequently charged, under inert conditions, with a solution of ligand (1 mL), a solution of $[Rh(nbd)_2BF_4]$ (0.5 mL), and a solution of the substrate (1 mL), all in dichloromethane at the needed concentrations. The solution was then exposed to 50 bar of H_2, and left to stir at room temperature (298 K) for 17 h (vortex-type stirring: 300 rpm). Conversions and enantioselectivities were determined by chiral GC.

CCDC-836862 (for **2**) and -836863 (for **3**) contain the supplementary crystallographic data for this paper. These data can be obtained free of charge from The Cambridge Crystallographic Data Centre via www.ccdc.cam.ac.uk/data_request/cif.

Supporting Information (see footnote on the first page of this article): ^{1}H, ^{31}P and ^{13}C NMR spectroscopic data.

Acknowledgments

Dr. Tatiana Besset and Dr. Mathieu Branca are acknowledged for discussions. The National Research School, Combination Catalysis Controlled by Chemical Design (NRSC Catalysis), BASF Nederland B.V., The Netherlands, and the Fonds der Chemischen Industrie are acknowledged for financial support. This work was also supported in part (A. L. S.) by the Council for the Chemical Sciences of The Netherlands Organization for Scientific Research (CW-NWO). Han Peeters is acknowledged for the mass spectrometry experiments, and Jan Meine Ernsting for the ^{15}N NMR spectroscopy characterization of ligand **1**.

[1] P. W. N. M. Van Leeuwen, in: *Homogeneous Catalysis, Understanding the Art*, Kluwer Academic Publishers, Dordrecht, The Netherlands, **2004**.

[2] For the popular C_2-chiral phosphorus ligands (not P-chirogenic) in asymmetric hydrogenation and the quadrant theory, see: a) *Handbook of Homogeneous Hydrogenation* (Eds.: J. G. de Vries, C. J. Elsevier), Wiley-VCH, **2007**; b) J. M. Brown, P. L. Evans, *Tetrahedron* **1988**, *44*, 4905.

[3] The applications involving P-chirogenic phosphanes that are C_1-symmetrical are especially scarce. For selected examples, see: a) W. Chen, W. Mbafor, S. M. Roberts, J. Whittall, *J. Am. Chem. Soc.* **2006**, *128*, 3922; b) R. Aznar, G. Muller, D. Sainz, M. Font-Bardia, X. Solans, *Organometallics* **2008**, *27*, 1967; c) I. V. Komarov, A. Spannenberg, J. Holz, A. Börner, *Chem. Commun.* **2003**, *17*, 2240; d) R. Romeo, L. A. Wozniak, C. Chatgilialoglu, *Tetrahedron Lett.* **2000**, *41*, 9899; e) S. R. Gilbertson, D. G. Genov, A. L. Rheingold, *Org. Lett.* **2000**, *2*, 2885; f) J. Albert, J. M. Cadena, S. Delgado, J. Granell, *J. Organomet. Chem.* **2000**, *603*, 235; g) M. Al-Masum, G. Kumaraswamy, T. Livinghouse, *J. Org. Chem.* **2000**, *65*, 4776; h) T. Watanabe, I. D. Gridnev, T. Imamoto, *Chirality* **2000**, *12*, 346; i) V. V. Dunina, L. G. Kuz'mina, M. Y. Rubina, Y. K. Grishin, Y. A. Veits, E. I. Kazakova, *Tetrahedron: Asymmetry* **1999**, *10*, 1483; j) P.-H. Leung, H. Lang, A. J. P. White, D. J. Williams, *Tetrahedron: Asymmetry* **1998**, *9*, 2961; k) B. Wolfe, T. Livinghouse, *J. Am. Chem. Soc.* **1998**, *120*, 5116; l) P.-H. Leung, S.-K. Loh, K. F. Mok, A. J. P. White, D. J. Williams, *Chem. Commun.* **1996**, *5*, 591; m) V. V. Dunina, E. B. Golovan', *Tetrahedron: Asymmetry* **1995**, *6*, 2747; n) Q. Jiang, H. Rüegger, L. M. Venanzi, *J. Organomet. Chem.* **1995**, *488*, 233; o) W. S. Knowles, M. J. Sabacky, B. D. Vineyard, *J. Chem. Soc., Chem. Commun.* **1972**, 10; p) J.-M. Camus, J. Andrieu, P. Richard, R. Poli, C. Darcel, S. Jugé, *Tetrahedron: Asymmetry* **2004**, *15*, 2061; q) C. Bauduin, D. Moulin, E. B. Kaloun, C. Darcel, S. Jugé, *J. Org. Chem.* **2003**, *68*, 4293; r) F. Chaux, S. Frynas, H. Laureano, C. Salomon, G. Morata, M.-L. Auclair, M. Stephan, R. Merdes, P. Richard, M.-J. Ondel-Eymin, J.-C. Henry, J. Bayardon, C. Darcel, S. Jugé, *C. R. Chim.* **2010**, *13*, 1213; s) J. J. Gammon, P. O'Brien, B. Kelly, *Org. Lett.* **2009**, *11*, 5022; t) Z.-C. Duan, X.-P. Hu, C. Zhang, Z. Zheng, *J. Org. Chem.* **2010**, *75*, 8319; u) J. Deng, Z.-C. Duan, J.-D. Huang, X.-P. Hu, D.-Y. Wang, S.-B. Yu, X.-F. Xu, Z. Zheng, *Org. Lett.* **2007**, *9*, 4825; v) W. Chen, S. M. Roberts, J. Whittall, A. Steiner, *Chem. Commun.* **2006**, 2916. For a review, see: w) A. Grabulosa, J. Granell, G. Muller, *Coord. Chem. Rev.* **2007**, *251*, 25.

[4] For examples of P-chirogenic phosphonites and phosphinamides, see: a) B. Pugin, M. Lotz, H. Landert, A. Wyss, R. Aardoom, B. Gschwend, A. Pfaltz, F. Spindler, PCT Int. Appl. **2009**, WO 2009065784 A1 20090528; b) B. Pugin, H. Landert, B. Gschwend, A. Pfaltz, F. Spindler, PCT Int. Appl. **2009**, WO 2009065783 A1 20090528; c) C. Darcel, D. Moulin, J.-C. Henry, M. Lagrelette, P. Richard, P. D. Harvey, S. Jugé, *Eur. J. Org. Chem.* **2007**, *13*, 2078; d) D. Moulin, C. Darcel, S. Jugé, *Tetrahedron: Asymmetry* **1999**, *10*, 4729.

[5] For a comprehensive study on the tendency of P-chirogenic chlorophosphanes to racemize, see: S. Humbel, C. Bertrand, C. Darcel, C. Bauduin, S. Jugé, *Inorg. Chem.* **2003**, *42*, 420.

[6] For our previous works concerning sulfonamido–phosphorus ligands, see: a) F. W. Patureau, M. Kuil, A. J. Sandee, J. N. H. Reek, *Angew. Chem.* **2008**, *120*, 3224; *Angew. Chem. Int. Ed.* **2008**, *47*, 3180. Highlight: b) H. Yamamoto, P. Li, *Synfacts* **2008**, *7*, 0721; c) F. W. Patureau, S. de Boer, M. Kuil, J. Meeuwissen, P.-A. R. Breuil, M. A. Siegler, A. L. Spek, A. J. Sandee, B. de Bruin, J. N. H. Reek, *J. Am. Chem. Soc.* **2009**, *131*, 6683. For a review about secondary interactions between chiral ligands and substrates, see: d) M. Sawamura, Y. Ito, *Chem. Rev.* **1992**, *92*, 857. For selected examples of hydrogen-bonding cooperative supramolecular ligands, see: e) P.-A. R. Breuil, F. W. Patureau, J. N. H. Reek, *Angew. Chem. Int. Ed.* **2009**, *48*, 3180; f) B. Breit, W. Seiche, *J. Am. Chem. Soc.* **2003**, *125*, 6608; g) M. Weis, C. Waloch, W. Seiche, B. Breit, *J. Am. Chem. Soc.* **2006**, *128*, 4188; h) C. Waloch, J. Wieland, M. Keller, B. Breit, *Angew. Chem.* **2007**, *119*, 3097; *Angew. Chem. Int. Ed.* **2007**, *46*, 3037; i) A. C. Laungani, B. Breit, *Chem. Commun.* **2008**, 844; j) M. N. Birkholz, N. V. Dubrovina, H. Jiao, D. Michalik, J. Holz, R. Paciello, B. Breit, A. Börner, *Chem. Eur. J.* **2007**, *13*, 5896; k) T. Šmejkal, B. Breit, *Angew. Chem.* **2008**, *120*, 4010; *Angew. Chem. Int. Ed.* **2008**, *47*, 3946; l) A. Börner, *Chirality* **2001**, *13*, 625; m) A. Börner, *Eur. J. Inorg. Chem.* **2001**, 327; n) J. Meeuwissen, M. Kuil, A. M. van der Burg, A. J. Sandee, J. N. H. Reek, *Chem. Eur. J.* **2009**, *15*, 10272; o) L. Diab, T. Šmejkal, J. Geier, B. Breit, *Angew. Chem.* **2009**, *121*, 8166; *Angew. Chem. Int. Ed.* **2009**, *48*, 8022; p) A. C. Laungani, M. Keller, J. M. Slattery, I. Krossing, B. Breit, *Chem. Eur. J.* **2009**, *15*, 10405; q) J. Meeuwissen, A. J. Sandee, B. de Bruin, M. A. Siegler, A. L. Spek, J. N. H. Reek, *Organometallics* **2010**, *29*, 2413; r) J. Meeuwissen, J. N. H. Reek, *Nature Chemistry* **2010**, *2*, 615; s) P. Dydio, W. I. Dzik, M. Lutz, B. de Bruin, J. N. H. Reek, *Angew. Chem. Int. Ed.* **2011**, *50*, 396; t) S. Carboni, C. Gennari, L. Pignataro, U. Piarulli, *Dalton Trans.* **2011**, *40*, 4355.

[7] See the Experimental Section.

[8] a) R. E. Hurd, B. K. John, *J. Magn. Reson.* **1991**, *91*, 648; b) J. Ruiz-Cabello, G. W. Vuister, C. T. W. Moonen, P. van Gelderen, J. S. Cohen, P. C. M. van Zijl, *J. Magn. Reson.* **1992**, *100*, 282; c) W. Wilker, D. Leibfritz, W. Kerssebaum, W. Bermel, *Magn. Reson. Chem.* **1993**, *31*, 287.

Received: August 1, 2011
Published Online: September 28, 2011

 © 2012 Wiley-VCH Verlag GmbH & Co. KGaA, Weinheim

DOI: 10.1002/ejic.201100800

Synthesis, Structures, and Transfer Hydrogenation Catalysis of Bifunctional Iridium Complexes Bearing a C–N Chelate Oxime Ligand

Megumi Watanabe,[a] Yohei Kashiwame,[a] Shigeki Kuwata,*[a] and Takao Ikariya*[a]

Dedicated to Prof. Dr. Christian Bruneau on the occasion of his 60th birthday

Keywords: Homogeneous catalysis / Iridium / Hydrogen bonds / Hydride ligands / Cooperative effects

We have synthesized a series of organometallic oxime complexes as novel metal–ligand cooperating bifunctional catalysts. The reaction of [{Cp*IrCl(μ_2-Cl)}$_2$] with ketoximes in the presence of sodium acetate afforded the half-sandwich chlorido iridium complexes **6** bearing a C–N chelate oxime ligand with a protic OH group in the β-position to the metal. Complex **6a**, derived from acetophenone oxime, reacted with silver triflate to give the triflate complex **7** and cationic nitrile complex **8** depending upon the reaction solvent. Complexes **6** also reacted with a base in dichloromethane to afford the oximato-bridged dinuclear complexes **9**, which were converted back to the chlorido complexes **6** upon treatment with an amine hydrochloride. In contrast, dehydrochlorination of **6** in 2-propanol as well as the reaction of **9** with 2-propanol yielded the hydrido-bridged dinuclear oxime–oximato complexes **10**. Crossover experiments revealed that **10** dissociates into the mononuclear hydrido–oxime complex **11** and unsaturated oximato complex **12**, which are interconvertible by reactions with hydrogen donors and acceptors. Owing to the metal–ligand cooperation, **10** effectively catalyzed transfer hydrogenation of ketones with 2-propanol.

Introduction

Hydrogen transfer reactions catalyzed by metal complexes offer a practical approach for the reduction of ketones and oxidation of alcohols with the advantages of operational simplicity and mild reaction conditions.[1] Bifunctional metal hydride catalysts bearing a protic cooperating ligand often dramatically accelerate such reactions through the coupled transfer of the proton and hydride with the substrates. For example, the protic amine complex with a chiral chelate auxiliary, **1**, efficiently catalyzes the asymmetric transfer hydrogenation of ketones as a result of the facile and reversible conversion to the coordinatively unsaturated amido complex **2** (Scheme 1, top).[2] The proton-delivering functional group and nucleophilic metal hydride are more separated in Shvo's catalyst **3**, a heterodimer of the reduced (**4**) and oxidized (**5**) forms, which are interconvertible through proton-coupled hydride transfer with the substrate (Scheme 1, bottom).[3] In these metal–ligand bifunctional catalysts, the Brønsted acidity of the protic group and the relative positions of the two functionalities are judiciously designed to realize high catalytic performance.

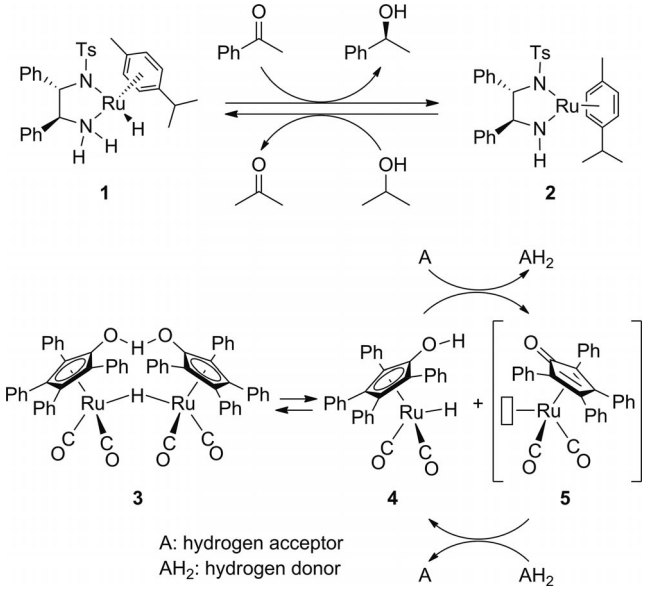

Scheme 1. Representative examples of bifunctional transfer hydrogenation catalysts.

We have continued our interest in the metal–ligand cooperating bifunctional catalysis of protic amine complexes typified by **1**.[4] Our recent efforts to modulate the catalytic activity and selectivity led to an investigation of C–N chelate amine complexes, in which the electron-donating σ-car-

[a] Department of Applied Chemistry, Graduate School of Science and Engineering, Tokyo Institute of Technology, O-okayama, Meguro-ku, Tokyo 152-8552, Japan
Fax: +81-3-5734-2637
E-mail: skuwata@apc.titech.ac.jp
tikariya@apc.titech.ac.jp

WILEY ONLINE LIBRARY
© 2012 Wiley-VCH Verlag GmbH & Co. KGaA, Weinheim

bon donor in the chelate increased the nucleophilic character of the substrate ligand;[5] these complexes are easily obtained by acetate-promoted cyclometalation of benzylic amines.[5,6] The cyclometalation methodology is also applicable to N-heteroaromatics, which leads to the formation of the structurally diverse bifunctional N-heterocyclic carbene[7] and pyrazole[8] complexes bearing an NH group in the β-position to the metal.[9] We have further explored such β-protic bifunctional catalysts[10] derived from the cyclometalation of appropriately designed ligand precursors. In this paper, we report cyclometalated ketoxime complexes as new β-OH bifunctional catalysts for the transfer hydrogenation of ketones.

Results and Discussion

Synthesis and Structure of C–N Chelate Oxime Complexes 6

We have recently demonstrated that the complex cationic N–N chelate oxime [Cp*IrCl(Py–NOH)]Cl (Cp* = η^5-C_5Me_5; Py–NOH = 2-acetylpyridine oxime) undergoes reversible deprotonation of the β-OH group.[11] The isoelectronic C–N chelate oxime complexes **6** were successfully obtained from the reaction of [{Cp*IrCl(μ_2-Cl)}$_2$] with acetophenone oximes in the presence of sodium acetate (Scheme 2). Quite recently, Davies and coworkers have synthesized a cyclometalated aldoxime complex in a similar manner.[9g] We also note that the cyclometalation of aromatic oximes has been long known[12] and is a key step in their C–H functionalization catalyzed by Cp*Rh complexes.[13] The ^{1}H NMR spectra of **6** exhibit a sharp singlet at around 9 ppm, which disappeared upon treatment with D_2O. The azomethine carbon atom resonance of **6a** is observed at 169.0 ppm. The detailed structure of **6a** was determined by X-ray analysis and is shown in Figure 1; selected interatomic distances and angles are listed in Table 1. Complex **6a** forms a centrosymmetric dimer connected by intermolecular hydrogen bonds between the crystallographically refined oxime hydrogen atom and the chlorido ligand. The hydrogen bond and the facile H–D exchange of the oxime hydrogen atom indicate the Brønsted acidity of the β-OH group, which should increase upon coordination.[14] The bond lengths in the chelate are very close to those in the related aldoxime complex mentioned above.[9g] The Ir–C1/C2 bonds *trans* to the σ-aryl ligand [2.250(5) and 2.252(6) Å] are noticeably longer than the rest of the Ir–C(cyclopentadienyl) bonds [2.155(5)–2.160(5) Å] in line with the strong *trans* influence. It should be noted that half-sandwich-type organometallic oxime complexes are rare[15] in contrast to the many Werner-type analogues reported to date.[14,16]

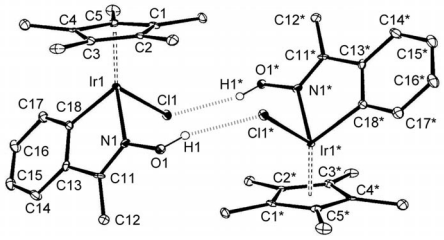

Figure 1. Dimeric structure of **6a** connected with hydrogen bonds. Hydrogen atoms except for the OH protons are omitted for clarity. Asterisks denote atoms generated by a symmetry operation (1 – *x*, 1 – *y*, 2 – *z*).

Table 1. Selected bond lengths [Å] and angles [°] for **6a**, **7**, and **8**.

	6a	**7**	**8**
Ir1–X_a[a]	2.4103(13)	2.224(5)	2.044(2)
Ir1–N1	2.059(4)	2.068(6)	2.067(3)
Ir1–C18	2.041(6)	2.052(6)	2.040(3)
N1–O1	1.410(7)	1.394(7)	1.395(4)
N1–C11	1.292(7)	1.299(8)	1.295(4)
O1–H1	0.87(8)	0.82	1.00(6)
X_b[a]···H1	2.31(8)	2.08	1.77(6)
X_b[a]···O1	3.126(4)	2.807(6)	2.748(4)
Ir1–N1–O1	122.5(3)	122.3(4)	122.8(2)
Ir1–N1–C11	121.5(4)	120.8(4)	121.2(2)
O1–N1–C11	116.0(4)	116.9(5)	115.9(3)

[a] X_a = Cl1 (**6a**), O2 (**7**), N2 (**8**); X_b = Cl1* (**6a**), O3 (**7**), O2 (**8**).

Reactions of 6a with Silver Triflate

When the chlorido–oxime complex **6a** was treated with silver triflate in dichloromethane, the triflato complex **7** was obtained in 45% yield, whereas the reaction in acetonitrile afforded the cationic nitrile complex **8** in 79% yield (Scheme 3). The OH resonance at 8.70 (**7**) and 10.20 (**8**) ppm in the ^{1}H NMR spectra was identified by D_2O exchange. Figure 2 depicts the crystal structures of **7** and **8**. Both complexes have a three-legged piano-stool structure with a C–N chelate oxime ligand. The bond lengths and angles, shown in Table 1, are unexceptional. The OH proton is engaged in a hydrogen bonding interaction with a triflate oxygen atom inside (**7**) or outside (**8**) the coordination sphere.

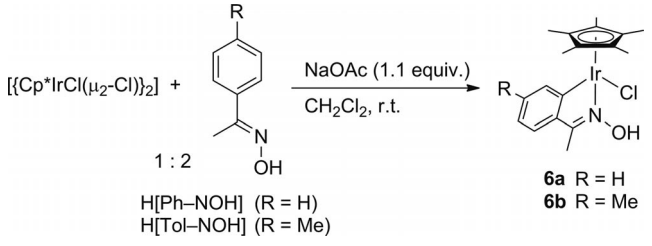

Scheme 2. Synthesis of C–N chelate oxime complexes **6**.

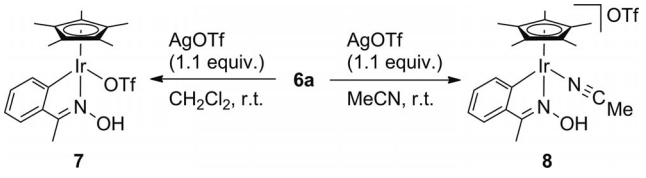

Scheme 3. Reactions of **6a** with silver triflate.

 © 2012 Wiley-VCH Verlag GmbH & Co. KGaA, Weinheim

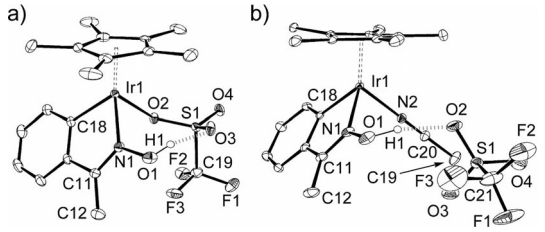

Figure 2. Structures of a) **7** and b) **8**. Hydrogen atoms except for the OH protons are omitted for clarity.

Dehydrochlorination of 6

Similar to the related β-protic pyrazole complex,[8] the chlorido–oxime complex **6** underwent facile dehydrochlorination with an equimolar amount of a base to afford the oximato-bridged dinuclear complexes **9**, as shown in Scheme 4. Complex **9a** reacted with an amine hydrochloride to regenerate **6a** as expected. An X-ray analysis of **9a** substantiated the dimeric structure with approximate C_2 symmetry (Figure 3 and Table 2). The oximato nitrogen and azomethine carbon atoms are perfectly planar as seen in **6a**. The N–O distances of 1.375 Å (mean) in the μ-oximato-κ*N*,κ*O* **9a** are close to those in the oxime complexes **6a**, **7**, and **8** [1.394(4)–1.410(7) Å] rather than that in the oximato-κ*N* complex [Cp*IrCl(Py–NO)] [1.291(5) Å], in which the N–O bond has some double bond character.[11] On the other hand, the Ir–O bond lengths of 2.131(2) and 2.141(2) Å are longer than those in [Cp*Ir(Ph)(OEt)(PMe_3)] [2.082(4) Å][17] and [Cp*Ir(H_2O)(Me_2CO)$_2$](BF_4)$_2$ [Ir–$OCMe_2$: 2.105(7) and 2.130(7) Å].[18] The large Ir–Ir separation of 3.9892(6) Å precludes any direct metal–metal bonding. The μ-κ*N*,κ*O* ligation of the oximate anion is found in a number of coordination compounds, some of which exhibit intriguing magnetic properties,[19] yet remains rare in organometallic compounds.[20] In the ^{1}H NMR spectra of **9**, the methyl group of the oximato ligand is shielded (1.13 ppm) due to the arene ring in the other half of the molecule, which suggests that the dimeric structure of **9** is preserved in solution. In fact, the reaction of **9a** and **9b** in [D_6]benzene at 55 °C did not yield the crossover product [(Cp*Ir)$_2$(Ph–NO)(Tol–NO)] (**9c**) at all after 23 h. The ^{13}C{^{1}H} NMR shift of the azomethine carbon atom in **9a** (169.9 ppm) is almost the same as that in the corresponding oxime complex **6a**, which contrasts with the upfield shift observed with the deprotonation of the cationic oxime complex [Cp*IrCl(Py–NOH)]Cl to the mononuclear oximato-κ*N* complex [Cp*IrCl(Py–NO)].[11]

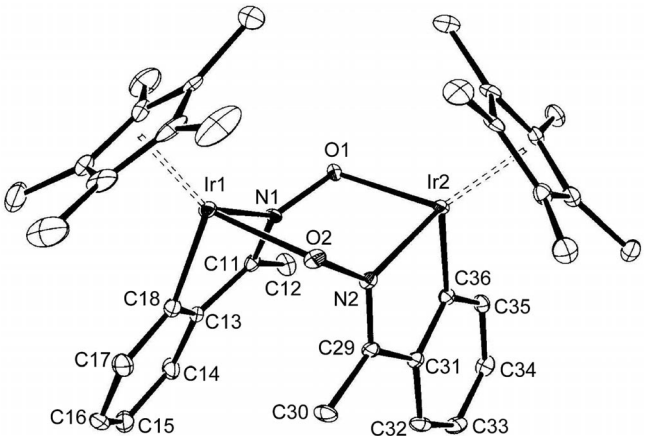

Figure 3. Structure of **9a**. Hydrogen atoms are omitted for clarity.

Table 2. Selected bond lengths [Å] for **9a** and **10a**.

	9a	**10a**
Ir1–N1/Ir2–N2	2.069(3)/2.066(3)	2.057(5)/2.036(7)
Ir1–O2/Ir2–O1	2.131(2)/2.141(2)	–
Ir1–C18/Ir2–C36	2.033(4)/2.026(4)	2.013(8)/2.024(7)
N1–O1/N2–O2	1.368(4)/1.382(4)	1.368(9)/1.355(9)
N1–C11/N2–C29	1.316(5)/1.297(5)	1.296(10)/1.315(11)

Synthesis and Reactions of Hydrido-Bridged Oxime–Oximato Complexes 10

In contrast, dehydrochlorination of **6** in a hydrogen donor solvent, 2-propanol, resulted in the formation of the hydrido-bridged oxime–oximato complexes **10** as shown in Scheme 5. The ^{1}H NMR spectra of **10** exhibit characteristic high- and low-field resonances with a 1 H intensity, which are ascribed to the hydrido and oxime ligands, respectively. The 30 H singlet of the Cp* ligand is somewhat shielded at 1.1 ppm, possibly due to the neighboring arene rings in the oxime ligands. The ^{13}C{^{1}H} signal of the azomethine carbon atoms in **10a** (159.2 ppm) is slightly upfield-shifted compared with those in the oxime complex **6a** and the oximato complex **9a**. The approximately C_2-symmetric dinuclear structure of **10a** was determined by single-crystal X-ray analysis as depicted in Figure 4. Although the hydrido and oxime hydrogen atoms could not be found in the difference Fourier map, these hydrogen atoms most likely bridge the two iridium atoms and two oxygen atoms through a three-center–two-electron bond and an OH···O hydrogen

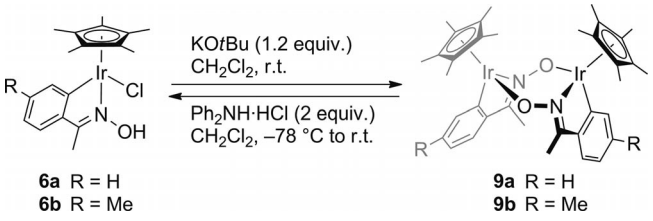

Scheme 4. Reversible dehydrochlorination of **6**.

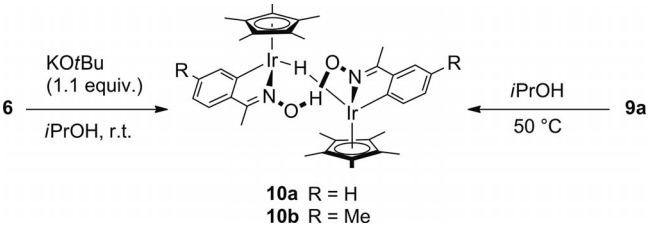

Scheme 5. Formation of **10**.

 © 2012 Wiley-VCH Verlag GmbH & Co. KGaA, Weinheim

bond, respectively, judging from the short Ir–Ir and O–O contacts [3.0026(4) and 2.455(9) Å, respectively]. The oxime and oximato ligands are almost indistinguishable from their metric parameters; the N–O distances of 1.368(9) and 1.355(9) Å in **10a** lie in the middle of those in the oxime and oximato-κ*N* complexes (vide supra).

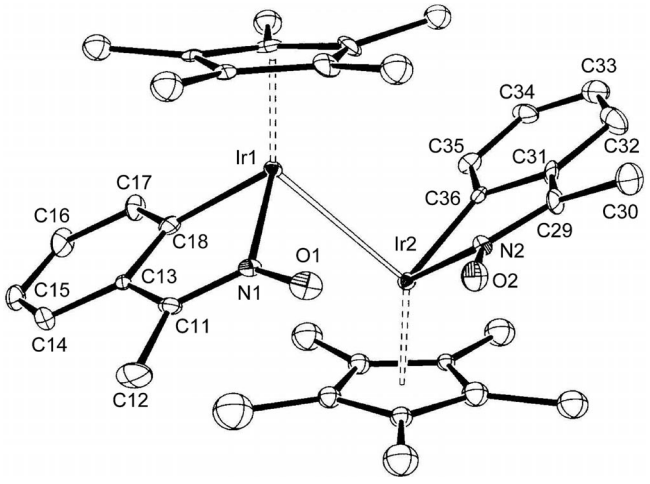

Figure 4. Structure of **10a**. Hydrogen atoms are omitted for clarity.

Complex **10a** could also be obtained cleanly by transfer hydrogenation of the oximato-bridged dinuclear complex **9a** with 2-propanol at 50 °C (Scheme 5). The fully-hydrogenated mononuclear hydrido–oxime complex [Cp*IrH(Ph–NOH)] (**11a**) was not produced even with extended reaction times. To gain more insight into the mechanism of this reaction, we carried out the following crossover experiments under milder conditions. When a mixture of the oximato-bridged complexes **9a** and **9b** in 2-propanol was stirred at room temperature for 17 h, ca. 15% of these complexes were converted into the mixed-ligand complex [(Cp*Ir)$_2$-(Ph–NOH)(Tol–NO)] (**10c**; the OH position is arbitrary) along with **10a** and **10b** in the expected statistical ratio, **10a/10c/10b** = 1:2:1. It is to be emphasized that the remaining **9** did not contain the crossover product **9c**, which suggests that cleavage of the dimeric structure of **9** is irreversible at least under these conditions. Furthermore, a separate crossover reaction of the hydrido-bridged complexes **10a** and **10b** in 2-propanol under the same conditions did not reach the statistical mixture; the observed ratio of **10a/10c/10b** was approximately 2:1:2.[21] Thus, the ligand scramble in the transfer hydrogenation of **9** is much faster than the crossover reactions of **9** and **10** themselves, indicating the presence of mononuclear intermediate(s) in the transfer hydrogenation. Scheme 6 illustrates the possible mechanism. Fragmentation of **9a**, which hardly occurs in nonpolar solvents as evidenced by the crossover experiment of **9a** and **9b** in [D$_6$]benzene (vide supra), may be facilitated by protonation with 2-propanol. Subsequent hydrogen transfer in a concerted or stepwise manner would generate the mononuclear hydrido–oxime complex **11a**, which immediately reacts with the concomitantly produced oximato complex **12a** to afford stable **10a** as the final product.

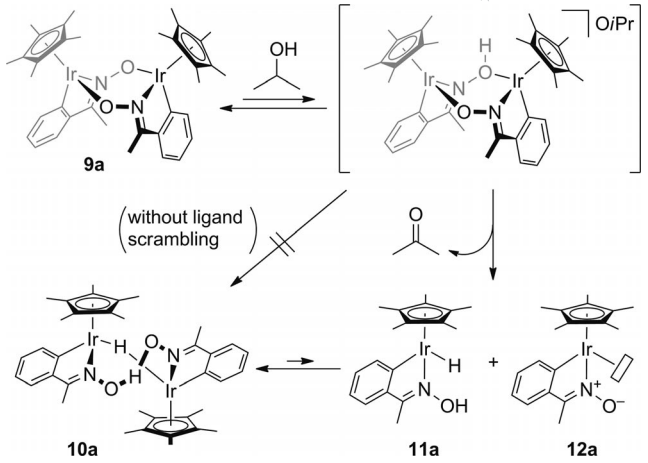

Scheme 6. Proposed mechanism for transfer hydrogenation of **9a**.

The crossover reaction of **10a** and **10b** demonstrated that the reaction of **11** and **12** to give **10** is reversible as in Shvo's catalyst (Scheme 1). We thus examined the dehydrogenation of the hydrido complex **10a** with a ketone as the oxidant. Treatment of **10a** with an equimolar amount of acetophenone in methanol at 50 °C afforded 1-phenylethanol in 63% yield (NMR). The ^{1}H NMR spectrum of the reaction mixture also revealed quantitative recovery of **10a** instead of dehydrogenation product **9a**, which implies that oxidation of methanol with **12a** is involved in the reaction. Notably, the reaction performed in toluene, a solvent without hydrogen donating ability, did not produce 1-phenylethanol. These observations indicate that hydrido–oxime **11a**, which would be generated by the splitting of **10a**, favors recombination with **12a** rather than the reaction with acetophenone. In methanol, however, **12a** is converted into **11a** through transfer hydrogenation with the solvent. The increased ratio of **11a** to **12a** leads to the hydrogen transfer from **11a** to acetophenone, which gives 1-phenylethanol and **12a**. Finally, **10a** would be regenerated from **11a** and **12a**.

Catalytic Transfer Hydrogenation of Ketones with 10a

The stoichiometric reactions mentioned above encouraged us to examine the catalytic transfer hydrogenation of ketones with the bifunctional oxime complexes. When a mixture of acetophenone and **10a** with a substrate/catalyst (S/C) ratio of 20:1 in 2-propanol was stirred at 50 °C, 1-phenylethanol was obtained quantitatively (Table 3, Entry 1). The reaction with an increased S/C ratio resulted in a lower yield (Entry 2). Various functionalized ketones with nitro, bromo, cyano, ester, and ether groups were reduced to the corresponding alcohols with these functional groups preserved (Entries 3–7). On the other hand, transfer hydrogenation of 4-aminoacetophenone did not proceed at all, possibly due to the coordination of the amino group (Entry 8).

 © 2012 Wiley-VCH Verlag GmbH & Co. KGaA, Weinheim

Table 3. Transfer hydrogenation of ketones with **10a**.

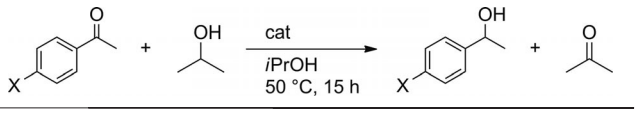

Entry	X	S/C	Yield [%]
1	H	20:1	100[a]
2	H	100:1	57[a]
3	NO_2	20:1	100[b]
4	Br	20:1	99[b]
5	CN	20:1	98[b]
6	OAc	20:1	87[b]
7	OMe	20:1	60[b]
8	NH_2	20:1	0[b]

[a] Determined by GC. [b] Determined by ^{1}H NMR spectroscopy.

Scheme 7 outlines the proposed mechanism for the catalytic transfer hydrogenation with **10a**. The hydrido-bridged dinuclear precatalyst **10a** dissociates into two catalytically active species **11a** and **12a**. The unsaturated oximato complex **12a** gains protons from 2-propanol to give the hydrido–oxime complex **11a**. Complex **11a** then reduces the ketone to the corresponding alcohol. The overall mechanism is quite similar to that of Shvo's catalyst, although formal redox of the metal and ligand is not involved in the β-protic oxime catalyst. It should be noted that cooperation of the oxime ligand is evident and essential in this catalysis in contrast to previously reported catalytic reactions with oxime complexes.[22]

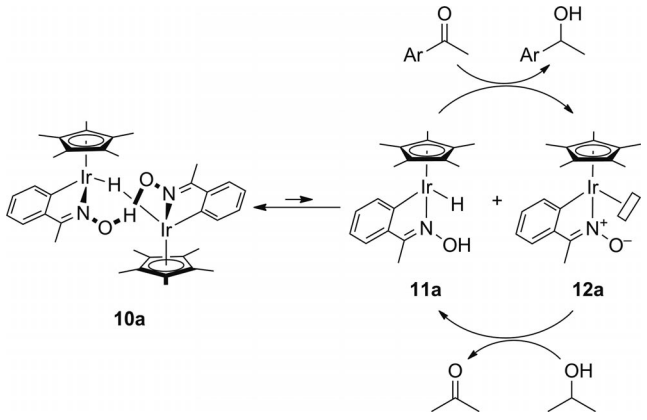

Scheme 7. Proposed mechanism for catalytic transfer hydrogenation with **10a**.

Conclusions

We have synthesized C–N chelate oxime complexes featuring a Brønsted acidic β-OH group as new metal–ligand bifunctional catalysts. Dehydrochlorination of the chlorido–oxime complex **6a** afforded the oximato complex **12a**, which is also bifunctional, with a Lewis acidic metal center and basic oximato ligand in a rigid framework. The organometallic frustrated Lewis pair[23] in **12a** is quenched in the dimer **9a** yet exerts a bifunctional effect in the reaction of **9a** with an amine hydrochloride and 2-propanol to give the parent chlorido complex **6a** and hydrido-bridged dinuclear oxime–oximato complex **10a**, respectively. We have further demonstrated that **10a** catalyzes the transfer hydrogenation of ketones with 2-propanol. A series of crossover experiments and stoichiometric reactions substantiated that **10a** splits into two spectroscopically elusive mononuclear species, i.e. **11a** and **12a**; these two species are interconvertible through reactions with hydrogen donors and acceptors and are responsible for the bifunctional catalysis. Further studies on the detailed mechanism of the hydrogen transfer from/to the mononuclear active species **11a** and **12a** as well as the development of new β-protic bifunctional catalysts are underway.

Experimental Section

General: All manipulations were performed under an atmosphere of argon using standard Schlenk technique unless otherwise specified. Solvents were dried by heating to reflux with sodium benzophenone ketyl (THF, toluene, diethyl ether, and hexane) or CaH_2 (acetonitrile, dichloromethane, and 2-propanol) and distilled before use. Ketoximes[24] and $[\{Cp^*IrCl(\mu_2\text{-}Cl)\}_2]$[25] were prepared according to the literature. ^{1}H and $^{13}C\{^1H\}$ NMR spectra (399.78 and 100.53 MHz) were obtained with a JEOL JNM-ECX400 spectrometer. The azomethine carbon signals were assigned by ^{1}H-^{13}C heteronuclear multiple quantum coherence (HMQC) and heteronuclear multiple-bond connectivity (HMBC) spectroscopy. Infrared spectra were recorded with a JASCO FT/IR-610 spectrometer. GC analyses were carried out using a Shimadzu GC-17A with an INNOWAX column. Elemental analyses were performed with a Perkin–Elmer 2400II CHN analyzer.

[Cp*IrCl(Ph–NOH)] (6a): To a solution of $[\{Cp^*IrCl(\mu_2\text{-}Cl)\}_2]$ (955.3 mg, 1.1991 mmol) and acetophenone oxime (325.0 mg, 2.4045 mmol) in dichloromethane (40 mL) was added sodium acetate (217.0 mg, 2.6452 mmol), and the mixture was stirred for 19 h at room temperature. After removal of the solvent in vacuo, the orange residue was extracted with dichloromethane (3× 10 mL) and filtered through a Celite pad. The resultant orange solution was evaporated to dryness. Recrystallization from dichloromethane/hexane (30 mL/50 mL) afforded **6a** as orange crystals (670.0 mg, 1.3480 mmol, 56%). ^{1}H NMR (CD_2Cl_2, –80 °C): δ = 1.74 (s, 15 H, Cp*), 2.54 (s, 3 H, N=CMe), 7.03, 7.13 (m, 1 H each, aryl), 7.33 (d, J = 8.6 Hz, 1 H, aryl), 7.67 (d, J = 7.3 Hz, 1 H, aryl), 9.42 (s, 1 H, OH) ppm. $^{13}C\{^1H\}$ NMR (CD_2Cl_2): δ = 8.9 [$C_5(CH_3)_5$], 11.5 [N=C(CH_3)], 89.6 [$C_5(CH_3)_5$], 121.6, 126.0, 130.3, 134.9, 142.8, 162.7, 169.0 (C=NOH) ppm. IR (KBr): $\tilde{\nu}$ = 1607, 1576, 1547, 1513 cm^{-1}. $C_{18}H_{23}ClIrNO$ (497.06): calcd. C 43.50, H 4.66, N 2.82; found C 43.49, H 4.65, N 2.90.

[Cp*IrCl(Tol–NOH)] (6b): This complex was obtained from 1-(*p*-tolyl)ethanone oxime by a method similar to that for **6a**. Yield: 40%. ^{1}H NMR ($CDCl_3$): δ = 1.74 (s, 15 H, Cp*), 2.40, 2.54 (s, 3 H each, N=CMe and C_6H_3Me), 6.83, 7.20 (d, J = 7.7 Hz, 1 H each, aryl), 7.49 (s, 1 H, aryl), 8.14 (s, 1 H, OH) ppm. $C_{19}H_{25}ClIrNO$ (511.08): calcd. C 44.65, H 4.93, N 2.74; found C 44.44, H 4.96, N 2.95.

[Cp*Ir(OTf)(Ph–NOH)] (7): A mixture of **6a** (74.4 mg, 0.150 mmol) and silver triflate (42.2 mg, 0.164 mmol) in dichloromethane (10 mL) was stirred for 14 h at room temperature. After removal of the solvent in vacuo, the orange residue was extracted with dichloromethane (3× 2 mL). Evaporation of the extract and

 © 2012 Wiley-VCH Verlag GmbH & Co. KGaA, Weinheim

subsequent recrystallization from THF/hexane (1 mL/20 mL) afforded **7** as orange crystals (41.6 mg, 0.0681 mmol, 45%). ^{1}H NMR ($CDCl_3$): δ = 1.72 (s, 15 H, Cp*), 2.51 (s, 3 H, N=CMe), 7.12, 7.25 (m, 1 H each, aryl), 7.35 (d, J = 7.4 Hz, 1 H, aryl), 7.89 (d, J = 7.6 Hz, 1 H, aryl), 8.70 (s, 1 H, OH) ppm. $C_{19}H_{23}F_3IrNO_4S$ (610.67): calcd. C 37.37, H 3.80, N 2.29; found C 37.25, H 3.86, N 2.31.

[Cp*Ir(MeCN)(Ph–NOH)](OTf) (8): A mixture of **6a** (225.3 mg, 0.4533 mmol) and silver triflate (140.0 mg, 0.5449 mmol) in acetonitrile (20 mL) was stirred for 3 h at room temperature. After removal of the solvent in vacuo, the yellow residue was extracted with dichloromethane (4× 4 mL). Evaporation of the extract and subsequent recrystallization from dichloromethane/hexane (2 mL/20 mL) afforded **8** as yellow crystals (234.3 mg, 0.3595 mmol, 79%). ^{1}H NMR ($CDCl_3$): δ = 1.78 (s, 15 H, Cp*), 2.44, 2.58 (s, 3 H each, N=CMe and MeCN), 7.13, 7.18 (m, 1 H each, aryl), 7.36 (d, J = 7.2 Hz, 1 H, aryl), 7.59 (d, J = 6.9 Hz, 1 H, aryl), 10.20 (s, 1 H, OH) ppm. IR (KBr): $\tilde{\nu}$ = 2313 (C≡N), 1615, 1580, 1553, 1508 cm^{-1}. $C_{21}H_{26}F_3IrN_2O_4S$ (651.73): calcd. C 38.70, H 4.02, N 4.30; found C 38.69, H 4.00, N 4.26.

[{Cp*Ir(Ph–NO)}$_2$] (9a): A mixture of **6a** (109.0 mg, 0.2193 mmol) and KO*t*Bu (29.7 mg, 0.265 mmol) in dichloromethane (18 mL) was stirred for 17 h at room temperature. After removal of the solvent in vacuo, the red residue was extracted with diethyl ether (4× 2 mL). The extract was concentrated to ca. 2 mL and stored at –30 °C. The red crystals formed were collected by filtration and dried in vacuo (69.0 mg, 0.0749 mmol, 68%). ^{1}H NMR (CD_2Cl_2): δ = 1.13 (s, 6 H, N=CMe), 1.62 (s, 30 H, Cp*), 6.53 (d, J = 7.3 Hz, 2 H, aryl), 6.77, 6.82 (m, 2 H each, aryl), 7.84 (d, J = 7.3 Hz, 2 H, aryl) ppm. ^{13}C{^{1}H} NMR (CD_2Cl_2): δ = 9.3 [$C_5(CH_3)_5$], 11.4 [N=C(CH_3)], 87.0 [$C_5(CH_3)_5$], 120.8, 123.3, 126.6, 136.0, 145.8, 163.9, 169.9 (C=NOH) ppm. IR (KBr): $\tilde{\nu}$ = 1573, 1565 cm^{-1}. $C_{36}H_{44}Ir_2N_2O_2$ (921.19): calcd. C 46.94, H 4.81, N 3.04; found C 47.33, H 5.14, N 3.13.

[{Cp*Ir(Tol–NO)}$_2$] (9b): This complex was obtained from **6b** in a manner similar to that for **9a**. ^{1}H NMR (CD_2Cl_2): δ = 1.13 (s, 6 H, N=CMe), 1.61 (s, 30 H, Cp*), 2.36 (s, 6 H, C_6H_3Me), 6.43, 6.63 (d, J = 7.6 Hz, 2 H each, aryl), 7.66 (s, 2 H, aryl) ppm.

Crossover Experiments with 9a and 9b: In an NMR tube equipped with a J-Young valve, a mixture of **9a** (4.7 mg, 0.0051 mmol) and **9b** (4.8 mg, 0.0051 mmol) in C_6D_6 (0.5 mL) was kept at 55 °C. The ^{1}H NMR spectrum of the mixture exhibited no significant change during a period of 23 h.

Reaction of 9a with Ph_2NH·HCl: To a solution of **9a** (31.2 mg, 0.0339 mmol) in dichloromethane (4 mL) was added Ph_2NH·HCl (14.1 mg, 0.0686 mmol) at –78 °C, and the mixture was slowly warmed to room temperature with stirring. After 17 h, the mixture was evaporated to dryness. Recrystallization from dichloromethane/hexane (1.5 mL/20 mL) afforded **6a** (24.7 mg, 0.0497 mmol, 73%).

[(Cp*Ir)$_2$(μ_2-H)(Ph–NO)(Ph–NOH)] (10a): A mixture of **6a** (53.1 mg, 0.107 mmol) and KO*t*Bu (14.4 mg, 0.128 mmol) in 2-propanol (10 mL) was stirred for 18 h at room temperature. After removal of the solvent in vacuo, the red residue was extracted with toluene (4× 2 mL). Evaporation of the extract and subsequent recrystallization from THF/hexane (1 mL/20 mL) afforded **10a** as red crystals (11.3 mg, 0.0122 mmol, 23%). ^{1}H NMR (CD_2Cl_2): δ = –19.31 (s, 1 H, IrH), 1.06 (s, 30 H, Cp*), 2.62 (s, 6 H, N=CMe), 6.85, 6.90 (m, 2 H each, aryl), 7.13 (d, J = 7.4 Hz, 2 H, aryl), 7.66 (d, J = 7.0 Hz, 2 H, aryl), 18.50 (s, 1 H, OH) ppm. ^{13}C{^{1}H} NMR (CD_2Cl_2): δ = 8.3 [$C_5(CH_3)_5$], 12.0 [N=C(CH_3)], 92.6 [$C_5(CH_3)_5$], 120.7, 123.0, 126.1, 137.1, 146.6, 158.4, 159.2 (C=NOH) ppm. IR (KBr): $\tilde{\nu}$ = 1574, 1557 cm^{-1}. $C_{36}H_{46}Ir_2N_2O_2$ (923.21): calcd. C 46.84, H 5.02, N 3.03; found C 46.68, H 5.03, N 3.16.

[(Cp*Ir)$_2$(μ_2-H)(Tol–NO)(Tol–NOH)] (10b): This complex was obtained from **6b** in a manner similar to that for **10a**. ^{1}H NMR (CD_2Cl_2): δ = –19.33 (s, 1 H, IrH), 1.07 (s, 30 H, Cp*), 2.37 (s, 6 H, C_6H_3Me), 2.59 (s, 6 H, N=CMe), 6.72, 7.00 (d, J = 7.7 Hz, 2 H each, aryl), 7.50 (s, 2 H, aryl), 18.41 (s, 1 H, OH) ppm.

Reaction of 9a with 2-Propanol: A solution of **9a** (29.2 mg, 0.0317 mmol) in 2-propanol (5 mL) was stirred for 36 h at 50 °C. Evaporation of the solvent and subsequent recrystallization from THF/hexane (0.8 mL/20 mL) afforded **10a** as red crystals (4.4 mg, 0.0048 mmol, 15%).

Transfer Hydrogenation of 9a and 9b with 2-Propanol: A mixture of **9a** (6.5 mg, 0.0071 mmol) and **9b** (6.7 mg, 0.0071 mmol) in 2-propanol (10 mL) was stirred for 17 h at room temperature. The solvent was removed in vacuo, and the residue dissolved in CD_2Cl_2. The ^{1}H NMR spectrum using 1,3,5-trimethoxybenzene as an internal standard revealed that ca. 15% of complexes **9** were converted into **10a**, **10b**, and the mixed-ligand product **10c** with the **10a/10c/10b** ratio of 1:2:1.

10c: ^{1}H NMR (CD_2Cl_2): δ = –19.32 (s, 1 H, IrH), 1.07 (s, 30 H, Cp*), 2.37 (s, 3 H, C_6H_3Me), 2.61 (s, 6 H, N=CMe), 6.73 (d, J = 7.8 Hz, 1 H, aryl), 6.84, 6.90 (m, 1 H each, aryl), 7.02 (d, J = 7.8 Hz, 1 H, aryl), 7.13 (m, 1 H, aryl), 7.50 (s, 1 H, aryl), 7.67 (d, J = 7.4 Hz, 1 H, aryl), 18.41 (s, 1 H, OH) ppm.

Catalytic Transfer Hydrogenation of Ketones with 10a: A mixture of **10a** (2.9 mg, 0.0031 mmol) and ketone (0.0628 mmol) in 2-propanol (2 mL) was stirred at 50 °C for 15 h. The reaction mixture was filtered through a silica plug and subjected to GC and ^{1}H NMR analysis.

X-ray Diffraction Studies: Diffraction experiments were performed with a Rigaku Saturn CCD area detector with graphite-monochromated Mo-K_α radiation (λ = 0.71070 Å). Single crystals suitable for X-ray analysis were mounted on glass fibers. Intensity data were corrected for Lorentz–polarization effects and for absorption. Details of crystal and data collection parameters are summarized in Table 4. Structure solution and refinements were carried out using the CrystalStructure program package.[26] The heavy atom positions were determined by a direct method program (SIR92;[27] for **6a**, **7**, **8**, and **10a**) or a Patterson method program (DIRDIF99 PATTY;[28] for **9a**) and remaining non-hydrogen atoms were found by subsequent Fourier syntheses. The non-hydrogen atoms were refined anisotropically by full-matrix least-square techniques based on F^2. The severely disordered Cp* ligands in **10a** were refined as follows: the methyl carbon atoms in one Cp* group [C(6)–C(10)] were refined with isotropic thermal parameters, and the other Cp* group was located at two disordered positions with 60% and 40% occupancies and included in the refinements as rigid groups. The oxime hydrogen atoms in **6a** and **8** were refined isotropically, whereas that in **7** was included in the refinement with fixed isotropic thermal parameters. The rest of the hydrogen atoms, except for the hydrido and oxime hydrogen atoms in **10a**, were placed at calculated positions and included in the refinements using the riding model. The absolute structures of **9a** and **10a** were determined on the basis of the Flack absolute structure parameter.[29]

CCDC-837050 (for **6a**), -837051 (for **7**), -837052 (for **8**), -837053 (for **9a**), and -837054 (for **10a**) contain the supplementary crystallographic data for this paper. These data can be obtained free of charge from The Cambridge Crystallographic Data Centre via www.ccdc.cam.ac.uk/data_request/cif.

 © 2012 Wiley-VCH Verlag GmbH & Co. KGaA, Weinheim

Table 4. X-ray crystallographic data for **6a**, **7**, **8**, **9a**, and **10a**.

	6a	**7**	**8**	**9a**	**10a**
Emprical formula	$C_{18}H_{23}ClIrNO$	$C_{19}H_{23}F_3IrNO_4S$	$C_{21}H_{26}F_3IrN_2O_4S$	$C_{36}H_{44}Ir_2N_2O_2$	$C_{36}H_{46}Ir_2N_2O_2$
MW	497.06	610.67	651.72	921.20	923.21
Crystal system	monoclinic	monoclinic	monoclinic	orthorhombic	monoclinic
Space group	$P2_1/c$	$P2_1/n$	$P2_1/c$	$P2_12_12_1$	$P2_1$
Crystal size [mm^3]	$0.3\times0.1\times0.1$	$0.5\times0.5\times0.3$	$0.3\times0.1\times0.1$	$0.4\times0.1\times0.1$	$0.4\times0.2\times0.2$
a [Å]	14.926(6)	10.407(5)	12.463(2)	10.9515(17)	11.130(3)
b [Å]	14.875(6)	20.157(9)	13.157(3)	14.237(2)	11.290(3)
c [Å]	8.334(4)	10.471(5)	15.710(3)	20.811(3)	12.929(4)
α [°]	90	90	90	90	90
β [°]	112.447(6)	110.669(6)	113.863(2)	90	95.964(4)
γ [°]	90	90	90	90	90
V [Å^3]	1710.1(13)	2055.0(16)	2356.0(8)	3244.7(9)	1615.9(7)
Z	4	4	4	4	2
T [K]	93	123	123	123	123
Density (calcd.) [g cm^{-3}]	1.930	1.974	1.837	1.886	1.897
μ [mm^{-1}]	7.986	6.669	5.824	8.251	8.284
F(000)	960	1184	1272	1776	892
Transmission factors	0.266–0.450	0.065–0.135	0.365–0.559	0.196–0.438	0.105–0.191
Independent reflections (R_{int})	3844 (0.040)	4711 (0.060)	5389 (0.029)	7383 (0.037)	7064 (0.029)
Parameters	225	287	319	425	327
$R1$ [$I > 2\sigma$ (I)]	0.0250	0.0415	0.0214	0.0184	0.0334
$wR2$ (all data)	0.0917	0.1069	0.0749	0.0452	0.0913
Goodness-of-fit	1.000	1.002	1.001	1.005	1.002
Largest difference peak/hole [e Å^{-3}]	1.96/–1.50	2.86/–2.06	1.49/–1.12	1.48/–1.94	9.49/–4.59

Acknowledgments

This work was supported by Grant-in-Aid for Scientific Research (S) from the Ministry of Education, Culture, Sports, Science and Technology, Japan (22225004).

[1] a) T. Ikariya, A. J. Blacker, *Acc. Chem. Res.* **2007**, *40*, 1300–1308; b) J. S. M. Samec, J.-E. Bäckvall, P. G. Andersson, P. Brandt, *Chem. Soc. Rev.* **2006**, *35*, 237–248.

[2] T. Ikariya, K. Murata, R. Noyori, *Org. Biomol. Chem.* **2006**, *4*, 393–406.

[3] a) M. C. Warner, C. P. Casey, J.-E. Bäckvall, *Top. Organomet. Chem.* **2011**, *37*, 85–125; b) B. L. Conley, M. K. Pennington-Boggio, E. Boz, T. J. Williams, *Chem. Rev.* **2010**, *110*, 2294–2312.

[4] a) T. Ikariya, *Bull. Chem. Soc. Jpn.* **2011**, *84*, 1–16; b) M. Ito, T. Ootsuka, R. Watari, A. Shiibashi, A. Himizu, T. Ikariya, *J. Am. Chem. Soc.* **2011**, *133*, 4240–4242; c) M. Ito, A. Shiibashi, T. Ikariya, *Chem. Commun.* **2011**, *47*, 2134–2136.

[5] a) S. Arita, T. Koike, Y. Kayaki, T. Ikariya, *Angew. Chem.* **2008**, *120*, 2481–2483; *Angew. Chem. Int. Ed.* **2008**, *47*, 2447–2449; b) S. Arita, T. Koike, Y. Kayaki, T. Ikariya, *Organometallics* **2008**, *27*, 2795–2802; c) S. Arita, T. Koike, Y. Kayaki, T. Ikariya, *Chem. Asian J.* **2008**, *3*, 1479–1485.

[6] a) J.-B. Sortais, V. Ritleng, A. Voelklin, A. Holuigue, H. Small, L. Barloy, C. Sirlin, G. K. M. Verzijl, J. A. F. Boogers, A. H. M. de Vries, J. G. de Vries, M. Pfeffer, *Org. Lett.* **2005**, *7*, 1247–1250; b) J.-B. Sortais, N. Pannetier, A. Holuigue, L. Barloy, C. Sirlin, M. Pfeffer, N. Kyritsakas, *Organometallics* **2007**, *26*, 1856–1867; c) J.-B. Sortais, N. Pannetier, N. Clément, L. Barloy, C. Sirlin, M. Pfeffer, N. Kyritsakas, *Organometallics* **2007**, *26*, 1868–1874.

[7] K. Araki, S. Kuwata, T. Ikariya, *Organometallics* **2008**, *27*, 2176–2178.

[8] Y. Kashiwame, S. Kuwata, T. Ikariya, *Chem. Eur. J.* **2010**, *16*, 766–770.

[9] β-NH-free azametallacycles derived from base-promoted cyclometalation of N-heterocycles are much more prevalent: a) W. Bauer, M. Prem, K. Polborn, K. Sünkel, W. Steglich, W. Beck, *Eur. J. Inorg. Chem.* **1998**, 485–493; b) D. L. Davies, O. Al-Duaij, J. Fawcett, M. Giardiello, S. T. Hilton, D. R. Russell, *Dalton Trans.* **2003**, 4132–4138; c) C. Scheeren, F. Maasarani, A. Hijazi, J.-P. Djukic, M. Pfeffer, S. D. Zari′c, X.-F. Le Goff, L. Ricard, *Organometallics* **2007**, *26*, 3336–3345; d) L. Li, W. W. Brennessel, W. D. Jones, *J. Am. Chem. Soc.* **2008**, *130*, 12414–12419; e) Y. Boutadla, O. Al-Duaij, D. L. Davies, G. A. Griffith, K. Singh, *Organometallics* **2009**, *28*, 433–440; f) J.-P. Djukic, J.-B. Sortais, L. Barloy, M. Pfeffer, *Eur. J. Inorg. Chem.* **2009**, 817–853; g) J. F. Hull, D. Balcells, J. D. Blakemore, C. D. Incarvito, O. Eisenstein, G. W. Brudvig, R. H. Crabtree, *J. Am. Chem. Soc.* **2009**, *131*, 8730–8731; h) Y. Boutadla, D. L. Davies, R. C. Jones, K. Singh, *Chem. Eur. J.* **2011**, *17*, 3438–3448; i) E. F. Flegeau, C. Bruneau, P. H. Dixneuf, A. Jutand, *J. Am. Chem. Soc.* **2011**, *133*, 10161–10170; j) L. Bernet, R. Lalrempuia, W. Ghattas, H. Mueller-Bunz, L. Vigara, A. Llobet, M. Albrecht, *Chem. Commun.* **2011**, *47*, 8058–8060.

[10] a) S. Kuwata, T. Ikariya, *Chem. Eur. J.* **2011**, *17*, 3542–3556; b) Y. Kashiwame, M. Watanabe, K. Araki, S. Kuwata, T. Ikariya, *Bull. Chem. Soc. Jpn.* **2011**, *84*, 251–258.

[11] M. Watanabe, Y. Kashiwame, S. Kuwata, T. Ikariya, *Chem. Lett.* **2010**, *39*, 758–759.

[12] a) H. Onoue, K. Minami, K. Nakagawa, *Bull. Chem. Soc. Jpn.* **1970**, *43*, 3480–3485; b) H. Onoue, I. Moritani, *J. Organomet. Chem.* **1972**, *44*, 189–195; c) M. Nonoyama, *J. Organomet. Chem.* **1975**, *92*, 89–95; d) A. J. Nielson, *J. Chem. Soc., Dalton Trans.* **1981**, 205–211; e) A. D. Ryabov, G. M. Kazankov, A. K. Yatsimirsky, L. G. Kuz'mina, O. Yu. Burtseva, N. V. Dvortsova, V. A. Polyakov, *Inorg. Chem.* **1992**, *31*, 3083–3090; f) H. Werner, A. Höhn, M. Dziallas, T. Dirnberger, *Dalton Trans.* **2006**, 2597–2606.

[13] a) A. S. Tsai, M. Brasse, R. G. Bergman, J. A. Ellman, *Org. Lett.* **2011**, *13*, 540–542; b) X. Zhang, D. Chen, M. Zhao, J. Zhao, A. Jia, X. Li, *Adv. Synth. Catal.* **2011**, *353*, 719–723.

[14] V. Yu. Kukushkin, D. Tudela, A. J. L. Pombeiro, *Coord. Chem. Rev.* **1996**, *156*, 333–362.

[15] a) U. Kölle, E. Raabe, C. Krüger, F. P. Rotzinger, *Chem. Ber.* **1987**, *120*, 979–985; b) E. Steckhan, S. Herrmann, R. Ruppert, E. Dietz, M. Frede, E. Spika, *Organometallics* **1991**, *10*, 1568–1577; c) H. Werner, T. Daniel, W. Knaup, O. Nürnberg, *J. Or-*

 © 2012 Wiley-VCH Verlag GmbH & Co. KGaA, Weinheim

ganomet. Chem. **1993**, *462*, 309–318; d) T. Daniel, W. Knaup, M. Dziallas, H. Werner, *Chem. Ber.* **1993**, *126*, 1981–1993; e) R. Lampeka, R. Bergs, R. Krämer, K. Polborn, W. Beck, *Z. Naturforsch. B* **1994**, *49*, 225–232; f) R. Bergs, R. Lampeka, C. Robl, W. Beck, *Z. Naturforsch. B* **1994**, *49*, 483–488; g) R. Lampeka, R. Bergs, R. Fernández de Bobadilla, K. Polborn, S. Mihan, W. Beck, *J. Organomet. Chem.* **1995**, *491*, 203–214; h) P. Kumar, A. K. Singh, S. Sharma, D. S. Pandey, *J. Organomet. Chem.* **2009**, *694*, 3643–3652.

[16] a) M. E. Keeney, K. Osseo-Asare, K. A. Woode, *Coord. Chem. Rev.* **1984**, *59*, 141–201; b) A. G. Smith, P. A. Tasker, D. J. White, *Coord. Chem. Rev.* **2003**, *241*, 61–85; c) C. J. Milios, T. C. Stamatatos, S. P. Perlepes, *Polyhedron* **2006**, *25*, 134–194.

[17] J. C. M. Ritter, R. G. Bergman, *J. Am. Chem. Soc.* **1998**, *120*, 6826–6827.

[18] H. Amouri, C. Guyard-Duhayon, J. Vaissermann, M. N. Rager, *Inorg. Chem.* **2002**, *41*, 1397–1403.

[19] a) P. Chaudhuri, *Coord. Chem. Rev.* **2003**, *243*, 143–190; b) T. C. Stamatatos, G. Christou, *Inorg. Chem.* **2009**, *48*, 3308–3322; c) M. Prinz, K. Kuepper, C. Taubitz, M. Raekers, S. Khanra, B. Biswas, T. Weyhermüller, M. Uhlarz, J. Wosnitza, J. Schnack, A. V. Postnikov, C. Schröder, S. J. George, M. Neumann, P. Chaudhuri, *Inorg. Chem.* **2010**, *49*, 2093–2102; d) B. Cordero, O. Roubeau, S. J. Teat, A. Escuer, *Dalton Trans.* **2011**, *40*, 7127–7129.

[20] a) M. Langenbahn, H. Stoeckli-Evans, G. Süss-Fink, *J. Organomet. Chem.* **1990**, *397*, 347–358; b) J. S.-Y. Wong, W.-T. Wong, *New J. Chem.* **2002**, *26*, 94–104; c) J. A. Cabeza, I. del Río, V. Riera, M. Suárez, C. Álvarez-Rúa, S. García-Granda, S. H. Chuang, J. R. Hwu, *Eur. J. Inorg. Chem.* **2003**, 4159–4165; d) J. S.-Y. Wong, Y.-J. Gu, L. Szeto, W.-T. Wong, *CrystEngComm* **2008**, *10*, 29–33.

[21] The ligand scrambling completed to give the statistical mixture after 17 h in both 2-propanol and toluene at 50 °C.

[22] a) D. A. Alonso, C. Nájera, *Chem. Soc. Rev.* **2010**, *39*, 2891–2902; b) D. Yang, H. Fu, *Chem. Eur. J.* **2010**, *16*, 2366–2370; c) S. Mukherjee, B. A. Patel, S. Bhaduri, *Organometallics* **2009**, *28*, 3074–3078.

[23] G. Erker, *Dalton Trans.* **2011**, *40*, 7475–7483.

[24] N. Jain, A. Kumar, S. M. S. Chauhan, *Tetrahedron Lett.* **2005**, *46*, 2599–2602.

[25] C. White, A. Yates, P. M. Maitlis, *Inorg. Synth.* **1992**, *29*, 228–234.

[26] *CrystalStructure 3.8*, Rigaku/MSC, The Woodlands TX, USA, **2000**–**2006**.

[27] A. Altomare, G. Cascarano, C. Giacovazzo, A. Guagliardi, M. Burla, G. Polidori, M. Camalli, *J. Appl. Crystallogr.* **1994**, *27*, 435.

[28] P. T. Beurskens, G. Admiraal, H. Behm, G. Beurskens, J. M. M. Smits, C. Smykalla, *Z. Kristallogr. (Suppl. 4)* **1991**, 99.

[29] H. D. Flack, *Acta Crystallogr., Sect. A* **1983**, *39*, 876.

Received: July 30, 2011
Published Online: October 10, 2011

 © 2012 Wiley-VCH Verlag GmbH & Co. KGaA, Weinheim

DOI: 10.1002/ejic.201100868

Snapshots of a Reversible Metal–Ligand Two-Electron Transfer Step Involving Compounds Related by Multiple Types of Isomerism

Cristina Tejel,*[a] Laura Asensio,[a] M. Pilar del Río,[a] Bas de Bruin,[b] José A. López,[a] and Miguel A. Ciriano[a]

Keywords: Rhodium / Iridium / Mixed-valent compounds / Imines / Electron transfer / Redox noninnocent ligands

An unusual and very fast equilibrium between two isomers, $[(cod)Rh^{-I}\{(bpa - 2H)^{0}\}Ir^{I}(cod)] \rightleftharpoons [(cod)Rh^{I}\{(bpa - 2H)^{2-}\}Ir^{I}(cod)]$, which simultaneously display multiple types of isomerism: ligand–metal redox (electromerism), linkage, bond-stretch and ring-slippage isomerism, has been studied by NMR spectroscopy and DFT calculations. Both isomers have been isolated by making rational use of their thermodynamic parameters ($\Delta H° = +1.93$ kcal mol^{-1}; $\Delta S° = +7.8$ cal mol^{-1} K^{-1}), and have been characterized by X-ray diffraction methods. The equilibrium that involves a two-electron exchange between a redox noninnocent ligand, which transforms from a deprotonated amido form into an imine, and a metal that is reduced, could elucidate a thus far obscure step in the oxidative dehydrogenation of amines to imines.

Introduction

The transition metal-promoted oxidation of organic ligands, including amines and alcohols, has been studied extensively in both chemical and biological systems.[1] Widespread in biochemistry,[2] but less developed in synthetic chemistry, the oxidative dehydrogenation of amines is a very important process, which leads to imines,[3] diazo compounds[4] and nitriles.[5] This reaction involves a series of subsequent proton and electron transfer steps and is an important example of reactions that allow the build up of multiple redox equivalents. Such reactions provide low energy reaction pathways that avoid high energy intermediates.[6]

Mechanistic details are not yet fully understood at the molecular level, although two distinct pathways seem to be operative. Coordination of the amine to metals, such as Cu, Fe and Ru, is followed by the release of protons and a one- or two-electron transfer from the N-donor ligands to reduce the metal,[3a–3c] which may remain as such in the product or become oxidized by oxygen to complete the catalytic cycle. Alternatively, catalytic dehydrogenation of amines to nitriles by complexes of late transition metals with pincer ligands follows a hydride route starting with the oxidative addition of the amine N–H bond followed by β-elimination and dehydrogenation, which is spontaneous or induced by a sacrificial hydrogen acceptor.[1a,5c] No clear agreement exists on the details of the electron and proton transfer steps in the mechanism of the oxidative dehydrogenation of amines,[3a–3c] and different intermediates and their metal and ligand oxidation states have been postulated. We report an unusual equilibrium between two isomers, which simultaneously display multiple forms of isomerism: ligand–metal redox (electromerism), linkage, bond-stretch and ring-slippage isomerism. This equilibrium is associated with a ligand-to-metal electron transfer step, which relates to (and provides a model for) one of the important steps in the oxidative dehydrogenation of amines to imines.

Results and Discussion

We recently reported a unique family of mixed-valent (M^{-I},M^{I}) dinuclear complexes $[(diolefin)M^{-I}\{(bpa - 2H)^{0}\}M^{I}(diolefin)]$ (M = Rh, Ir), which contain a doubly-deprotonated (at the amine nitrogen atom and the adjacent methylene group) bis(2-picolyl)amine (bpa) ligand.[7,8] These complexes are best described as mixed-valent compounds that consist of a tetrahedral M^{-I} metal, which is π-coordinated to the C=N bond of an imine group, and a *N*,*N*′-chelating, square-planar, d^8 M^{I} centre (Figure 1). These species are formed upon addition of a $[M^{I}(cod)]^{+}$ (cod = 1,5-cyclooctadiene) fragment to the corresponding anionic complex $[M^{I}\{(bpa - 2H)^{2-}\}(cod)]^{-}$,[9] which are unique because they contain a dearomatized pyridine group and a negative charge delocalized in the metallacycle, i.e. the dianionic ligand $\{bpa - 2H\}^{2-}$ (which is in fact a 2-iminopyridine ligand in its $2e^{-}$ reduced form: L^{2-}).

Taking the above electronic description, the reaction involves an internal redox process: the two-electron reduction

[a] Instituto de Síntesis Química y Catálisis Homogénea (ISQCH), Departamento de Química Inorgánica, CSIC – Universidad de Zaragoza,
Pedro Cerbuna 12, 50009 Zaragoza, Spain
Fax: +34-976-761187
E-mail: ctejel@unizar.es
[b] Van 't Hoff Institute for Molecular Sciences, University of Amsterdam,
Science Park 904, 1098 XH, Amsterdam, the Netherlands
Supporting information for this article is available on the WWW under http://dx.doi.org/10.1002/ejic.201100868.

© 2012 Wiley-VCH Verlag GmbH & Co. KGaA, Weinheim

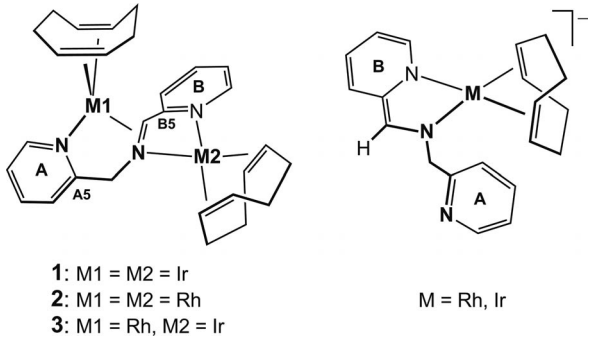

Figure 1. Representation of $[(cod)M^{I}\{(bpa - 2H)^{0}\}M^{I}(cod)]$ (left), in which the pyridine rings and *ipso* carbon atoms are labelled, and $[M^{I}\{(bpa - 2H)^{2-}\}(cod)]^{-}$ (right).

of one of the metal ions with oxidation of the ligand $\{bpa - 2H\}^{2-}$ to the corresponding neutral imine $PyCH_2$–N=CHPy [$\{bpa - 2H\}^{0}$, the oxidized form of the ligand: L^{0}].

The Rh, Ir heterodinuclear complex [(cod)Rh(bpa – 2H)-Ir(cod)] (**3**), which was prepared by this route, displayed unexpected behaviour in its NMR spectra with unforeseen and unusual temperature-dependent chemical shifts compared to the corresponding homonuclear Rh,Rh and Ir,Ir analogues, $[(cod)M^{I}\{(bpa - 2H)^{0}\}M^{I}(cod)]$ [M = Ir (**1**); Rh (**2**)], which called for additional investigation.[8]

The information given by the NMR spectra seemed to be ambivalent. One apparent inconsistency came from the $^{13}C\{^{1}H\}$-attached proton test (APT) spectrum of **3**, in which unexpected coupling constants, *J*(C,Rh), were observed on processing at high resolution. Thus, the couplings of the carbon atoms C^{A5} and C^{B5} from both pyridine rings and HC=N with ^{103}Rh were indicative for coordination of the three atoms to rhodium (Figure S1, Supporting Information). These couplings remain even at low temperature, with broadening starting at nearly –20 °C (Figure S2). However, the coupling of rhodium with C^{B5} was not observed in homodinuclear rhodium complex **2**. Moreover, the chemical shifts of the C^{B5} and HC=N carbon atoms in **3** (Figure 2) are largely shifted to high and low field, respectively, relative to those of **1** and **2**.[8] The chemical shift for C^{B5} in **3** (134.6 ppm) is identical to the C^{B5} resonances found for $[M^{I}\{(bpa - 2H)^{2-}\}(cod)]^{-}$ [134.4 (Ir) and 134.7 ppm (Rh)], which both contain a dearomatized pyridine ring (Py^{B}, Figure 1). This suggests the involvement of the $2e^{-}$ reduced form of the ligand $\{bpa - 2H\}^{2-}$ (L^{2-}) in the electronic structure of **3**.

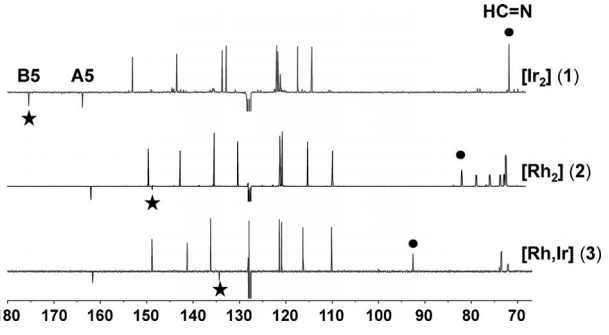

Figure 2. Selected region of the $^{13}C\{^{1}H\}$-APT spectra of **1**, **2** and **3**.

From these data, we wondered whether **3** has a static (electronic) structure, very different from those of **1** and **2**, or a similar (electronic) structure but is involved in a dynamic equilibrium with an isomeric form that has a completely different electronic structure. We were able to discriminate between these possibilities by studying the variable temperature (VT) ^{1}H NMR spectra of **3** (Figure 3), in which the broadening of the signal from the imine proton and other resonances with decreasing temperature (Figure S3) suggests the existence of a fast dynamic equilibrium between two species that cannot be frozen in solution even at –100 °C in [D_8]toluene. In addition to the broadening effects, the chemical shift for the imine proton largely moves to high field with decreasing temperature, which points to a temperature-dependent molar ratio of **3a** and **3b**, i.e. to a chemical equilibrium. The VT-NMR spectroscopic data were analyzed with a Van 't Hoff plot, which provided the following thermodynamic parameters associated with the equilibrium **3a** ⇌ **3b**: $\Delta H° = +1.93\ kcal\,mol^{-1}$ and $\Delta S° = +7.8\ cal\,mol^{-1}\,K^{-1}$, which results in $\Delta G°_{373} = -0.92\ kcal\,mol^{-1}$ and $\Delta G°_{173} = +0.57\ kcal\,mol^{-1}$ (Table S1 and Figure S4). The wide range of temperatures in which the dynamic equilibrium can be observed is remarkable and is a result of the fact that **3a** and **3b** have very similar energy and entropy values. The small value of $\Delta G°$ in the range 173–373 K with a reversal of the equilibrium position from predominantly **3b** at higher temperatures to predominantly **3a** at lower temperatures prompted us to try to crystallize **3** under different conditions.

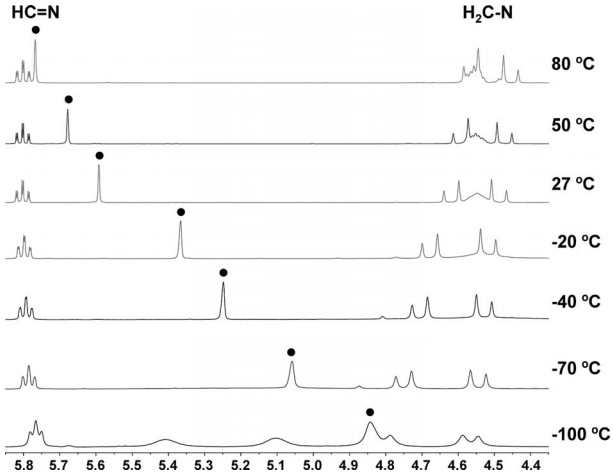

Figure 3. Selected region of the VT ^{1}H NMR spectra of **3** showing the strong effect of the temperature on the chemical shift of the HC=N proton.

Reproducibly, checked by X-ray analysis of crystals from several batches, dark orange single crystals of **3a** were obtained by cooling diluted hexane solutions of **3** (–35 °C) for three days. Moreover, dark red single crystals of **3b**, which had a metallic lustre, were grown by slow cooling (from 80 to 30 °C) of concentrated solutions of **3** in hexane. These solutions were obtained from the reaction of equimolar

 © 2012 Wiley-VCH Verlag GmbH & Co. KGaA, Weinheim

amounts of the rhodium and iridium complexes [{M(cod)(μ-OMe)}$_2$] with bpa. As anticipated, both types of crystals gave identical NMR spectra to those shown in Figures 2 and 3 when dissolved in [D$_8$]toluene. Their solid state X-ray structures are markedly different. The molecular structure of **3a**, the major isomer at lower temperatures, reveals coordination geometries, bond lengths and bond angles that fit best the mixed-valent [(cod)Rh^{-I}{(bpa – 2H)^0}-Ir^I(cod)] description with rhodium in the formal –I oxidation state (Figure 4). Most notable are the almost tetrahedral Rh centre and the characteristic intraligand bond lengths of bpa – 2H in its oxidized form: (bpa – 2H)^0 = PyCH$_2$–N=CHPy (bpi).

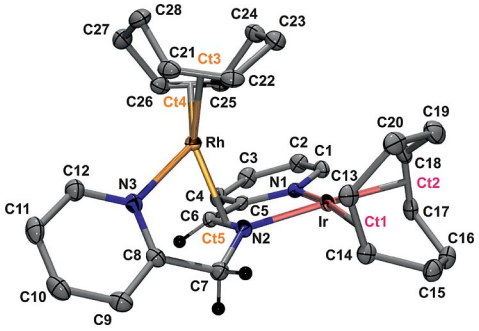

Figure 4. Structure of **3a** (ORTEP at 50% level). Rh is depicted in gold, and Ir in pink.

The iridium centre retains the square-planar geometry, which is typical for Ir^I. As reported previously, the M^{-I} oxidation state is less stabilized for iridium than for rhodium.[8] This leads to a preference of Rh for the imine compartment of the heteroditopic bpa – 2H ligand, which is confirmed by the X-ray structure of **3a**. In fact, all tested crystals of **3a** proved to be the [Rh^{-I},Ir^I] isomer with no evidence for the presence of the [Ir^{-I},Rh^I] isomer. The metal ions are separated by 3.3796(3) Å, which is too long for any metal–metal bonding interaction. The structural parameters of **3a** are comparable to those found in the structures of **1** and **2**.[8]

The molecular structure of **3b**, the major component at higher temperatures, is depicted in Figure 5. The pyridine-A (N3), which was bound to Rh in **3a**, has dissociated from

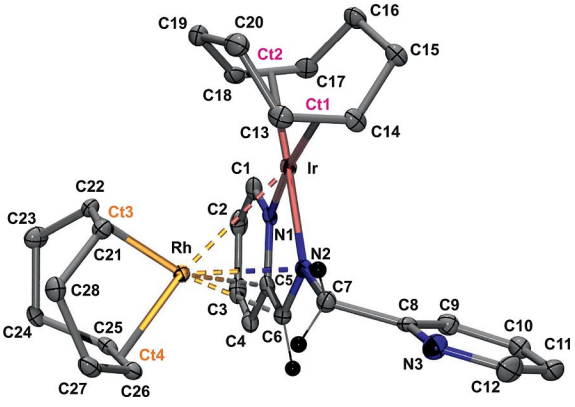

Figure 5. Structure of **3b** (ORTEP at 50% level). Rh is depicted in gold, and Ir in pink.

the metal in **3b**. The iridium atom in **3b** remains coordinated to the N1 and N2 nitrogen atoms, which are *trans* to the centroids of the two cod moieties in a square-planar geometry. The rhodium atom in **3b** adopts an unusual coordination geometry. In addition to the typical coordination of the cod ligand, the rhodium atom seems to interact with the imine carbon atom [Rh–C6 2.103(4) Å], the central nitrogen atom N2 [Rh–N2 2.384(3) Å], the *ipso* carbon atom of the coordinated pyridine C5 [Rh–C5 2.380(4) Å] and the iridium atom [Rh–Ir 2.8773(4) Å] (Figure 6). The short Rh–C6 bond length could point to a σ-Rh–C bond, but the geometry around this carbon atom is closer to a sp^2-type carbon atom than to that expected for a tetrahedral geometry (sp^3-hybridization) for a real σ-bond [angles around C6: C5–C6–H6 120(2), C5–C6–N2 116.2(3) and N2–C6–H6 121(2)°, Σ = 357(2)°]. In addition, no pyramidalization was found for C5 [Σ = 360.0(4)°] or N2 [Σ = 359.5(3)°].

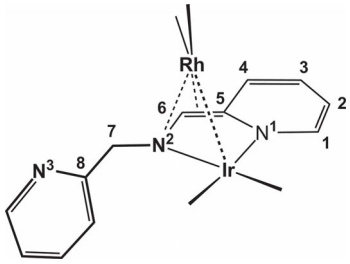

Figure 6. Representation of the bonding interactions in **3b**.

Therefore, the rhodium atom can be considered as interacting with an "iridaazabutenyl" moiety and the cod ligand. From this perspective, **3b** is best described as [(cod)Rh^I{(bpa – 2H)$^{2-}$}Ir^I(cod)] with rhodium in the +1 oxidation state, which interacts with the reduced form of the bridging ligand (bpa – 2H)$^{2-}$. It should be noted that if we exclude the Rh–N2 interaction, an almost square-planar geometry exists around rhodium with cod, the centroid of the C5=C6 double bond and iridium as binding motifs (Figure 6), which points to a [(cod)Rh^I{(bpa – 2H)$^{2-}$}-Ir^I(cod)] electronic structure. The Rh–N1 distance [2.685(2) Å] is too long to be considered as a bond, which excludes a description based on a η^5-interaction of the five-membered iridametallacycle with the rhodium atom (similar to a cyclopentadienyl ligand).

On the other hand, the C5–C6–N2 moiety belonging to the iridacycle can also be considered as an azaallyl ligand. Curiously, the structures of only three compounds of Rh, Ir, Pd and Pt with this type of ligand can be found in the CCDC library.[10] These, and other complexes with η^3-coordinated azaallyl ligands, typically show shorter M–C and M–N distances, but sometimes longer than those described here, and thus, it is difficult to assign the type of bonding in **3b** on the basis of structural data.[11]

Mayer bond orders (B.O.) determined from the DFT optimized geometry of **3b** (Table 1) are in full support of a bonding description as depicted in Figure 6.

 © 2012 Wiley-VCH Verlag GmbH & Co. KGaA, Weinheim

Table 1. DFT calculated (BP86, def2-TZVP) Mayer B.O., calculated bond lengths (DFT) and experimental bond lengths (X-ray) of the "iridaazabutenyl" fragment in **3b**.

Bond	B. O.	DFT [Å]	X-ray [Å]
Rh–N2	0.297	2.427	2.384(3)
Rh–C6	0.423	2.145	2.136(4)
Rh–C5	0.177	2.490	2.380(4)
Rh–Ir	0.180	2.970	2.8773(4)
Rh–N1	0.068	2.842	2.685(2)
N2–C6	0.941	1.393	1.396(5)
C5–C6	1.080	1.431	1.416(5)
N2–C7	0.972	1.457	1.465(5)
C7–C8	0.963	1.525	1.515(5)
Ir–N1	0.571	2.085	2.054(3)
Ir–N2	0.519	2.038	2.021(3)

The thermodynamic differences between **3a** and **3b** as calculated by (gas phase) DFT ($\Delta H°$ = +0.01 kcal mol^{-1}, $\Delta S°$ = +14.2 cal mol^{-1} K^{-1}, $\Delta G°_{298}$ = –4.2 kcal mol^{-1}) are in good qualitative agreement with the experimental values in solution. The computed energy difference between **3a** and **3b** depends only marginally on the level of the calculations (functional and basis set).[12] The small discrepancy between the experimental and computed values are (in part) due to differences between the condensed phase (experimental data in solution) and the gas phase (DFT) environment of the molecules.

To obtain more information about these atypical complexes and to better understand their electronic structures, we have prepared and characterized the related complex [Ir^{I}(bpi)(cod)(PPh$_3$)]PF$_6$ ([**4**]PF$_6$), that contains the neutral imine PyCH$_2$–N=CHPy (bpi), which is the oxidized form of the bpa – 2H ligand, and thus has the same ligand oxidation state as the bridging ligand in **3a**: (bpa – 2H)^0. All attempts to isolate the square-planar complex [Ir^{I}(bpi)(cod)]PF$_6$ by reacting [Ir^{I}(cod)(NCMe)$_2$]PF$_6$ with bpi under different conditions produced complicated mixtures of unidentified complexes or insoluble materials. Nonetheless, if the reaction is carried out in the presence of PPh$_3$, [**4**]PF$_6$ is formed cleanly and was isolated as red microcrystals in good yield. Possibly due to blocking the fifth coordination site, the reaction of [{Ir(cod)(μ-Cl)}$_2$] with bpi in the presence of PF$_6^-$ gave the dinuclear species [{Ir(cod)}$_2$(μ-bpi)Cl]$^+$ with a pentacoordinate iridium centre, which is an is an effective precatalyst for water oxidation.[13]

The molecular structure of [**4**]$^+$ is shown in Figure 7 along with the labelling scheme used. The iridium atom is bonded to a chelating bpi (through N1 and N2), cod and the phosphorus atom of the triphenylphosphane in a nearly trigonal bipiramidal (TBPY-5) coordination geometry. The pyridine nitrogen atom from bpi (N1) and one of the olefinic bonds occupy the axial positions [N1–Ir–Ct2 172.15(11)°], whereas the other olefinic bond, imine nitrogen (N2) and phosphorus atoms occupy the equatorial positions. The olefinic C13–C14 bond length [1.435(5) Å] is longer than the related C17–C18 bond length [1.394(5) Å] at the axial position, which is expected due to stronger π-back donation in the equatorial positions.

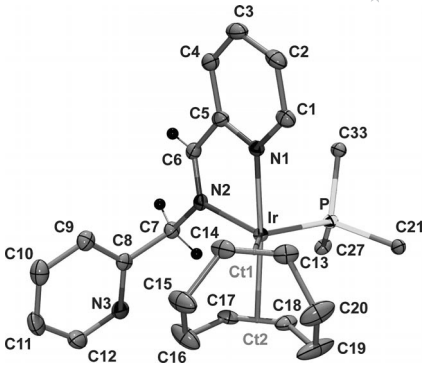

Figure 7. Structure of [**4**]$^+$ (ORTEP at 50% level). Only the C^{ipso} atoms of the phenyl groups from PPh$_3$ are shown for clarity.

The NMR spectra of [**4**]PF$_6$ are consistent with a similar structure in solution, which comprises a fluxional cod ligand (as expected for a five-coordinate geometry). The imine proton and carbon atom reveal typical chemical shifts [8.69 (^{1}H) and 168.3 ppm (^{13}C)], which are characteristic for an imine HC=N moiety without further π-coordination to a second metal.

For comparative purposes, the bond lengths of the iridium-α-pyridylimine moiety (N=C-Py^B) in **3a**, **3b**, [**4**]PF$_6$ and the anion in K*[Ir{(bpa – 2H)$^{2-}$}(cod)][9b] (K*[**5**], K* = potassium encapsulated in the cryptand 4,7,13,16,21,24-hexaoxa-1,10-diazabicyclo-[8.8.8]-hexacosane) obtained by X-ray analysis are collected in Table 2. The anion in K*[**5**] contains the reduced form of the N-donor ligand, {bpa – 2H}$^{2-}$, whereas the oxidized form {bpa – 2H}^{0} is found in the cation of [**4**]PF$_6$. In other words, [**4**]PF$_6$ and K*[**5**] incorporate the two redox extremes of the ligand (Figure 8).

Table 2. Bond lengths [Å] in the iridium-α-pyridylimine moiety (N=CH-Py^B) in [**4**]$^+$, **3a**, **3b** and [**5**]$^-$.

	[**4**]$^+$	**3a**	**3b**	[**5**]$^-$[a]
N1–C1	1.353(4)	1.361(4)	1.373(5)	1.372(12)
C1–C2	1.384(4)	1.367(4)	1.355(6)	1.340(13)
C2–C3	1.382(5)	1.403(4)	1.411(6)	1.421(14)
C3–C4	1.380(5)	1.372(4)	1.356(6)	1.335(13)
C4–C5	1.387(4)	1.414(4)	1.421(6)	1.446(12)
C5–N1	1.364(4)	1.374(4)	1.393(5)	1.414(11)
C5–C6	1.443(4)	1.429(4)	1.416(5)	1.382(13)
C6–N2	1.282(4)	1.423(4)	1.396(5)	1.368(11)
N2–C7	1.473(4)	1.456(4)	1.465(5)	1.469(11)
Ir–N1	2.095(2)	2.079(2)	2.054(3)	2.024(7)
Ir–N2	2.200(2)	2.019(2)	2.021(3)	1.969(8)
Ir–Ct1	2.066(3)	2.001(3)	2.001(4)	1.987(8)
Ir–Ct2	1.991(3)	1.987(3)	1.991(4)	1.953(9)

[a] Data taken from ref.[9b]

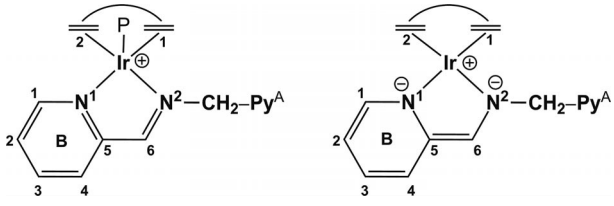

Figure 8. Representation of the oxidized and reduced forms of the ligand {bpa – 2H} in the iridium-α-pyridylimine moiety in [**4**]$^+$ (left) and [**5**]$^-$ (right).

 © 2012 Wiley-VCH Verlag GmbH & Co. KGaA, Weinheim

There is an excellent correlation between the ligand oxidation state and the expected intraligand bond length changes on going from $\{bpa - 2H\}^0$ in $[\mathbf{4}]^+$ to $\{bpa - 2H\}^{2-}$ in $[\mathbf{5}]^-$.[14] The corresponding bond lengths in **3a** and **3b** are in between these extremes, which provides a smooth transition in terms of the ligand redox states. The C6–N2 and (to a lesser extent) C5–C6 bonds are not diagnostic for the ligand oxidation state in **3a** and **3b** because π-coordination to rhodium has an intrinsic elongating effect on these bonds. However, all of the other bonds are diagnostic and show that the ligand in **3a** is close to the oxidized form $\{bpa - 2H\}^0$, whereas the reduced form $\{bpa - 2H\}^{2-}$ predominates in **3b**.

Consequently, **3a** and **3b** can be considered as redox or valence isomers. In **3a**, the rhodium fragment is best described as a $Rh^{-I}\{(bpa - 2H)^0\}$ moiety, whereas in **3b** it is best described as a $Rh^{I}\{(bpa - 2H)^{2-}\}$ moiety. Hence, simple ligand displacement leads to a completely different electronic structure, which is somewhat comparable to the electromeric forms of a recently reported rhodium(0) species.[15]

The observed redox or valence isomerism is not the only type of isomerism that relates **3a** and **3b** (Scheme 1). On going from **3a** to **3b**, a marked shortening of the rhodium–iridium bond length (ca. 0.5 Å) is observed, which points to the involvement of a metal–metal interaction or bond in **3b** that does not exist in **3a**. This is confirmed by a substantial Mayer B.O. between the metals as revealed by DFT (Table 1). Therefore both complexes are also metal–metal bond stretch isomers. Moreover, as evident from Figures 4 and 5, coordination/decoordination of the pendant pyridine (Py^A) is also involved in this transformation, so **3a** and **3b** are also linkage isomers, which elucidates the relevance of hemilabile ligands in the stabilization of unusual structures. Furthermore, all these structural changes are also associated with ring-slippage, which concerns the binding of rhodium to the C=N bond (**3a**) or to the iridaazabutenyl moiety (**3b**). Accordingly, **3a** and **3b** are thus multifaceted isomers that simultaneously incorporate redox changes of both the metal and the redox noninnocent ligand, metal–metal bond stretching, linkage and ring-slippage components, which together represent a new type of isomerism unknown to date.

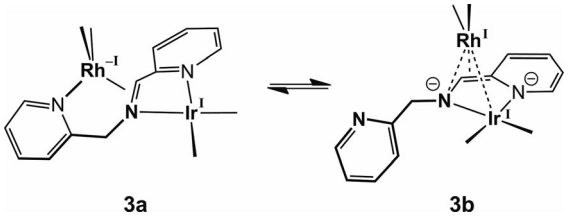

Scheme 1. Schematic representation of the structures and bonding of **3a** and **3b** in dynamic equilibrium.

The intrinsic reason for the isomerization of **3a** into **3b** (or vice versa, Scheme 1) is not evident. The thermodynamic parameters obtained experimentally for the **3a** ⇌ **3b** equilibrium (see above) clearly show that formation of **3a** is an exothermic process, whereas entropy governs (or is the driving force for) the formation of **3b**. The enthalpic stabilization of **3a** could well be related to the rearomatization of the pyridine ring (Py^B), which is an evident exothermic process, as well as the coordination of the pyridine. Such rearomatization requires the transfer of two electrons from the bridging ligand in **3b** [from $(bpa - 2H)^{2-}$ to $(bpa - 2H)^0$] to rhodium, which thereby transforms into a rhodium(–I) centre in an almost tetrahedral environment in this case. At this point, the two metals (Ir^I and Rh^{-I}) separate to avoid repulsion, breaking the metal–metal interaction, which causes a shift of the rhodium atom following a ring-slippage to become π-coordinated only to the C=N bond. Simultaneously, the pendant pyridine ring (Py^A) coordinates to the three-legged rhodium centre to achieve an 18 valence-electron count. In the reverse sense (from **3a** to **3b**), the dearomatization of Py^B [from $(bpa - 2H)^0$ to $(bpa - 2H)^{2-}$] is compensated by the entropy gained by decoordination of Py^A. This process regenerates a rhodium(I) centre but accumulates the negative charge in the iridametallacyle moiety. Most probably, the system solves this situation by moving it in part to the rhodium atom by coordination of the atoms in the iridacycle and through overlap of the *d*-orbitals between the two metals to form a metal–metal bond (Figure 9).

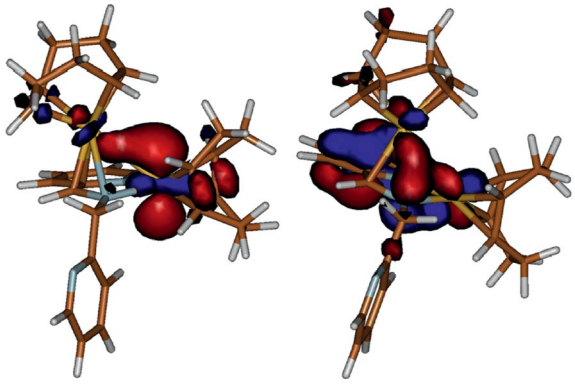

Figure 9. Highest occupied molecular orbital HOMO–1 (left) and HOMO–15 (right) Kohn–Sham-orbitals of the DFT optimized geometry of **3b**, which show examples of bonding overlap between the *d*-orbitals of the adjacent metals.

In spite of the complicated description, these concerted electron and metal movements take place with a low-energy barrier, which is thermally accessible in the wide range of temperatures studied. With the molecular structures in hand, all the NMR features that were misleading at the beginning fit under the consideration of a fast equilibrium between two exchanging species, **3a** and **3b**, with largely different (electronic) structures and in variable (temperature dependent) molar concentrations.

Conclusions

We have revealed an extremely fast and reversible isomerization between two complexes that involves both metal–ligand electron transfer and internal rearrangements of metal and ligand positions in the molecule. Both isomers

 © 2012 Wiley-VCH Verlag GmbH & Co. KGaA, Weinheim

have been isolated and characterized by X-ray diffraction. The study of the isomerization process by NMR methods gave thermodynamic parameters that are consistent with a low-barrier process between two species of similar energy, extended in a large range of temperatures and driven by entropy, which is in accordance with DFT calculations. The movements can be classified as a sequence of well known steps such as coordination/decoordination of a ligand, free rotation of C–C bonds and ring-slippage. In addition, there is a 2e⁻ transfer from an α-picolyamido ligand to a metal atom that transforms a deprotonated CH–N– amido group into an imine or vice versa, i.e. both isomers differ in the oxidation states of the metal and the ligand. Moreover, the isomers show distinct coordination geometries, hapticity and coordination of the donor atoms for one of the metals. The isomerism observed that simultaneously involves all these changes seems to be unique. Finally, the transfer of 2e⁻ from the ligand to the metal, spotted initially by subtle changes, elucidates the way in which a deprotonated amine can be oxidized to an imine, which provides a new, previously unsuspected, mechanistic step for the oxidation of amines by metal ions.

Experimental Section

General Methods: All procedures were performed under an argon atmosphere using standard Schlenk techniques. Solvents were dried and distilled under argon according to standard methods. NMR experiments were carried out with Bruker AV 500 and AV 400 instruments operating at 500 and 400 MHz for ^{1}H, respectively. Chemical shifts are reported in parts per million and referenced to $SiMe_4$, using the internal signal of the deuterated solvent as a reference. For the bpa and bpi numbering scheme see Figure S1. [{Rh(cod)(μ-OMe)}$_2$], [{Ir(cod)(μ-OMe)}$_2$][16] and PyCH$_2$–N=CHPy (bpi or {bpa – 2H}^{0})[17] were prepared according to literature methods. All other chemicals are commercially available and were used without further purification.

[(cod)Rh^{-I}{(bpa – 2H)^0}Ir^I(cod)] (3a): Addition of neat bpa (21.6 μL, 0.120 mmol) to a yellow suspension of [{Rh(cod)(μ-OMe)}$_2$] (29.2 mg, 0.060 mmol) and [{Ir(cod)(μ-OMe)}$_2$] (40.0 mg, 0.060 mmol) in diethyl ether (13 mL) at 0 °C produced a progressive dissolution of the solid and a colour change to dark red. After stirring for 1 h at 0 °C, hexane (15 mL) was added and the volume of the solution was reduced to 10 mL. The resulting solution was maintained undisturbed at –35 °C for three days. The crystals deposited (dark orange spheres made of small prisms) were studied by X-ray methods.

[(cod)Rh^I{(bpa – 2H)$^{2-}$}Ir^I(cod)] (3b): A mixture of [{Rh(cod)(μ-OMe)}$_2$] (29.2 mg, 0.060 mmol) and [{Ir(cod)(μ-OMe)}$_2$] (40.0 mg, 0.060 mmol) was dissolved in hexane (4 mL) at 65 °C with stirring by hand. Addition of neat bpa (21.6 μL, 0.120 mmol) produced an immediate colour change to dark red. The solution was maintained undisturbed to cool very slowly to room temperature. This methodology gives a concentrated solution of **3**, from which complex **3b** crystallized as dark red prisms with a green metallic lustre. The deposited crystals were studied by X-ray methods.

[Ir^I(bpi)(cod)(PPh$_3$)]PF$_6$ ([4]PF$_6$): Cationic [**4**]PF$_6$ was prepared in situ by reacting [{Ir(cod)(μ-Cl)}$_2$] (19.2 mg, 0.050 mmol) and AgPF$_6$ (25.28 mg, 0.100 mmol) in acetonitrile. The yellow suspension was filtered through celite and the solvents evaporated to dryness. The residue was dissolved in methanol (7 mL) and then triphenylphosphane (26.3 mg, 0.100 mmol) and bpi (17.8 μL, 0.100 mmol) were added successively to give a red solution from which a red solid started to crystallize almost immediately. The suspension was maintained undisturbed for 6 h, concentrated to ca. 3 mL and carefully layered with diethyl ether (10 mL). The solution was decanted, and the crystals deposited were washed with diethyl ether and vacuum-dried; yield 73.3 mg (81%). ^{1}H NMR (400.13 MHz, $CDCl_3$, –40 °C): δ = 8.69 (s, 1 H, *H*C=N), 8.63 [d, ^3J(H,H) = 5.5 Hz, 1 H, H^{B1}], 8.57 [d, ^3J(H,H) = 4.2 Hz, 1 H, H^{A1}], 7.78–7.75 (m, 3 H, H^{B4}, H^{A3} and H^{B3}), 7.36 (m, 3 H, ^{p}Ph$_3$P), 7.32–7.24 (m, 9 H, H^{A4}, ^{m}Ph$_3$P, H^{A2} and H^{B2}), 7.10 (t, 6H ^{o}Ph$_3$P), 5.57 (δ_A, 1 H) and 5.35 [δ_B, J(A,B) = 14.2 Hz, 1 H] (H_2C=N), 3.61 (br. t, 2 H, H^{14}, cod), 3.20 (br. t, 2 H, H^{13}, cod), 2.09 (m, 2 H, H^{15a}, cod), 1.83 (m, 2 H, H^{20a}, cod), 1.69 (m, 2 H, H^{20b}, cod), 1.48 (m, 2 H, H^{15b}, cod) ppm. ^{31}P{^{1}H} NMR (161.3 MHz, $CDCl_3$, –40 °C): δ = 6.15 (s, Ph$_3$P) ppm. ^{13}C{^{1}H} NMR (100.0 MHz, $CDCl_3$, –40 °C): δ = 168.3 (H*C*=N), 154.1 (C^{B5}), 153.9 (C^{A5}), 151.0 [d, ^3J(C,P) = 2.7 Hz, C^{B1}], 149.7 (C^{A1}), 138.7 (C^{B3}), 137.8 (C^{A3}), 132.9 [d, ^2J(C,P) = 10.8 Hz, ^{o}Ph$_3$P], 130.5 [d, ^4J(C,P) = 2.0 Hz, ^{p}Ph$_3$P], 129.8 [d, J(C,P) = 42.1 Hz, ^{i}Ph$_3$P], 129.4 (C^{B4}), 128.6 [d, ^3J(C,P) = 9.5 Hz, ^{m}Ph$_3$P], 128.5 (C^{A4}), 123.7 (C^{B2}), 123.4 (C^{A2}), 66.7 (H$_2$*C*-N), 63.7 (C^{14}), 63.5 [d, ^2J(C,P) = 10.6 Hz, C^{13}], 32.4 (C^{20}), 32.3 [d, ^3J(C,P) = 3.0 Hz, C^{15}] ppm.

X-ray Diffraction Studies on 3a·0.5(C$_6$H$_{14}$), 3b and [4]PF$_6$: Selected crystallographic data for the three complexes can be found in Table 3. Intensity measurements were collected with a Smart Apex diffractometer, with graphite-monochromated Mo-K_α radiation. A semiempirical absorption correction was applied to each data set with the multiscan[18] method. All non-hydrogen atoms were refined with anisotropic temperature factors except those corresponding to the disordered hexane [**3a**·0.5(C$_6$H$_{14}$)], which were refined with constrained isotropic thermal parameters. The hydrogen atoms were placed at calculated positions and refined isotropically in the riding mode, with the exception of the olefinic cod protons and the methine HC=N proton, which were found on the Fourier map and refined isotropically with free positional parameters. The

Table 3. Selected crystal, measurement and refinement data for **3a**·0.5(C$_6$H$_{14}$), **3b** and [**4**]PF$_6$.

	3a·0.5(C$_6$H$_{14}$)	**3b**	[**4**]PF$_6$
Empirical formula	$C_{31}H_{42}IrN_3Rh$	$C_{28}H_{35}IrN_3Rh$	$C_{38}H_{38}F_6IrN_3P_2$
FW	751.79	708.70	904.85
Temperature [K]	100(2)	100(2)	100(2)
Crystal system	monoclinic	monoclinic	monoclinic
Space group	$P2_1/c$	$P2_1/n$	$P2_1/c$
a [Å]	13.1530(6)	11.6496(7)	11.7427(6)
b [Å]	12.2190(5)	11.6787(7)	19.9448(10)
c [Å]	18.3195(8)	17.5824(11)	14.7344(7)
γ [°]	110.353(1)	99.338(1)	95.230(1)
V [Å^3]	2760.4(2)	2360.4(2)	3436.5(3)
Z	4	4	4
D_{calc} [g cm^{-3}]	1.809	1.994	1.749
μ [mm^{-1}]	5.439	6.354	4.045
F(000)	1484	1384	1792
Reflections collected	31025	14647	40540
Independent reflections	6018	5125	7491
R(int)	0.0262	0.0329	0.0415
GOF on F^2	1.034	1.018	1.049
Final R indices:			
R_1 [$I>2\sigma(I)$]	0.0198	0.0254	0.0235
wR_2 [all data]	0.0513	0.0528	0.0527

 © 2012 Wiley-VCH Verlag GmbH & Co. KGaA, Weinheim

structures were solved by direct methods and refined by full-matrix least-squares with the program SHELX97[19] in theWINGX[20] package.

DFT Geometry Optimizations: Geometry optimizations were carried out with the Turbomole program package[21] coupled to the PQS Baker optimizer[22] with the BOpt package[23] using the BP86 functional.[24] We used the def2-TZVP basis set[25] (small-core pseudopotentials on Rh and Ir)[26] for the geometry optimizations. The minima (no imaginary frequencies) were characterized by analytically calculating the Hessian matrix. Zero point energies and gas-phase thermal corrections (entropy and enthalpy, 298 K, 1 bar) were calculated from these analyses. Single point calculations at the DFT/b3-lyp[27] level (def2-TZVP basis set) gave similar results to those obtained at the DFT/BP86/def2-TZVP level. Relativistic effects were included implicitly through the use of ECPs for Rh and Ir. Mayer B.O.[28] were calculated from the Turbomole output files using the AOMix program.[29]

CCDC-839356 [for **3a**·0.5(C_6H_{14})], -839357 (for **3b**) and -839358 (for [**4**]PF_6) contain the supplementary crystallographic data for this paper. These data can be obtained free of charge from The Cambridge Crystallographic Data Centre via www.ccdc.cam.ac.uk/data_request/cif.

Supporting Information (see footnote on the first page of this article): Selected VT ^1H, $^{13}C\{^1H\}$ NMR spectra of **3**, Van 't Hoff plot for the equilibrium between **3a** and **3b**, representative NMR spectra for [**4**]PF_6 and DFT optimized geometries and energies (both at the BP86/def2-TZVP and b3-lyp/def2-TZVP levels) of **3a** and **3b**.

Acknowledgments

Generous financial support from the Ministerio de Ciencia e Innovación (MICINN)/Fondos Europeos para el Desarrollo Regional (FEDER) (Project CTQ2008-03860) and Gobierno de Aragón (GA), Project Number PI 155/08) is gratefully acknowledged. L. A. and P. R. thank MICINN/FEDER for a fellowship and a postdoctoral contract, respectively. This work was further supported by the European Research Council (grant agreement 202886, to B. d. B.) and the University of Amsterdam (to B. d. B.).

[1] a) J. Choi, A. H. R. MacArthur, M. Brookhart, A. S. Goldman, *Chem. Rev.* **2011**, *111*, 1761–1779; b) G. E. Dobereiner, R. H. Crabtree, *Chem. Rev.* **2010**, *110*, 681–703; c) B. Gnanaprakasam, J. Zhang, D. Milstein, *Angew. Chem.* **2010**, *122*, 1510–1513; *Angew. Chem. Int. Ed.* **2010**, *49*, 1468–1471; d) T. Zweifel, J.-V. Naubron, H. Grützmacher, *Angew. Chem.* **2009**, *121*, 567–571; *Angew. Chem. Int. Ed.* **2009**, *48*, 559–563; e) B. A. Steinhoff, S. S. Stahl, *J. Am. Chem. Soc.* **2006**, *128*, 4348–4355; f) I. W. C. E. Arends, R. A. Sheldon, in *Modern Oxidation methods* (Ed.: J.-E. Bäckvall), Wiley-VCH, Weinheim, Germany, **2004**, pp. 83–118; g) P. Gamez, I. A. Koval, J. Reedijk, *Dalton Trans.* **2004**, 4079–4088; h) *Advances in Catalytic Activation of Dioxygen by Metal Complexes* (Ed.: L. I. Simándi), in: *Catalysis by Metal Complexes*, vol. 26, Kluwer Academic, Dordrecht, The Netherlands, **2003**; i) K. Yamaguchi, N. Mizuno, *Chem. Eur. J.* **2003**, *9*, 4353–4361.

[2] a) J. Pang, N. S. Scrutton, S. P. de Visser, M. J. Sutcliffe, *Chem. Commun.* **2010**, *46*, 3104–3106; b) D. E. Edmondson, C. Binda, A. Mattevi, *Arch. Biochem. Biophys.* **2007**, *464*, 269–276; c) I. S. MacPherson, M. E. P. Murphy, *Cell Mol. Life Sci.* **2007**, *64*, 2887–2899; d) A. Roujeinikova, N. S. Scrutton, D. Leys, *J. Biol. Chem.* **2006**, *281*, 40264–40272; e) N. S. Scrutton, *Natl. Prod. Rep.* **2004**, *21*, 722–730; f) C. Binda, A. Mattevi, D. E. Edmondson, *J. Biol. Chem.* **2002**, *277*, 23973–23976; g) M. Mure, S. A. Mills, J. P. Klinman, *Biochemistry* **2002**, *41*, 9269–9278; h) J. P. Klinman, *Chem. Rev.* **1996**, *96*, 2541–2562.

[3] a) G. J. Christian, A. Llobet, F. Maseras, *Inorg. Chem.* **2010**, *49*, 5977–5985; b) J. P. Saucedo-Vázquez, V. M. Ugalde-Saldívar, A. R. Toscano, P. M. H. Kroneck, M. E. Sosa-Torres, *Inorg. Chem.* **2009**, *48*, 1214–1222; c) G. J. Christian, A. Arbuse, X. Fontrodona, M. A. Martinez, A. Llobet, F. Maseras, *Dalton Trans.* **2009**, 6013–6020; d) B. Zhu, M. Lazar, B. G. Trewyna, R. J. Angelici, *J. Catal.* **2008**, *260*, 1–6; e) A. Machkour, D. Mandon, M. Lachkar, R. Welter, *Eur. J. Inorg. Chem.* **2005**, 158–161; f) V. Amendola, L. Fabbrizzi, E. Mundum, P. Pallavicini, *Dalton Trans.* **2003**, 773–774; g) X. Gu, W. Chen, D. Morales-Morales, C. M. Jensen, *J. Mol. Catal. A* **2002**, *189*, 119–124; h) F. R. Keene, *Coord. Chem. Rev.* **1999**, *187*, 121–149.

[4] C. Zhang, N. Jiao, *Angew. Chem.* **2010**, *122*, 6310–6313; *Angew. Chem. Int. Ed.* **2010**, *49*, 6174–6177.

[5] a) S. Aiki, A. Taketoshi, J. Kuwabara, T. Koizumi, T. Kanbara, *J. Organomet. Chem.* **2011**, *696*, 1301–1304; b) A. Taketoshi, T. Koizumi, T. Kanbara, *Tetrahedron Lett.* **2010**, *51*, 6457–6459; c) W. H. Bernskoetter, M. Brookhart, *Organometallics* **2008**, *27*, 2036–2045; d) K. Yamaguchi, N. Mizuno, *Angew. Chem.* **2003**, *115*, 1518–1521; *Angew. Chem. Int. Ed.* **2003**, *42*, 1480–1483.

[6] J. S. M. Samec, A. H. Éll, J.-E. Bäckvall, *Chem. Eur. J.* **2005**, *11*, 2327–2334.

[7] C. Tejel, M. A. Ciriano, M. P. del Río, F. J. van den Bruele, D. G. H. Hetterscheid, N. Tsichlis i Spithas, B. de Bruin, *J. Am. Chem. Soc.* **2008**, *130*, 5844–5845.

[8] C. Tejel, M. P. del Río, L. Asensio, F. J. van den Bruele, M. A. Ciriano, N. Tsichlis i Spithas, D. G. H. Hetterscheid, B. de Bruin, *Inorg. Chem.* **2011**, *50*, 7524–7534.

[9] a) C. Tejel, M. A. Ciriano, M. P. del Río, D. G. H. Hetterscheid, N. Tsichlis i Spithas, J. M. M. Smits, B. de Bruin, *Chem. Eur. J.* **2008**, *14*, 10932–10936; b) C. Tejel, M. P. del Río, M. A. Ciriano, E. J. Reijerse, F. Hartl, S. Zális, D. G. H. Hetterscheid, N. Tsichlis i Spithas, B. de Bruin, *Chem. Eur. J.* **2009**, *15*, 11878–11889.

[10] a) S. Takemoto, S. Otsuki, Y. Hashimoto, K. Kamikawa, H. Matsuzaka, *J. Am. Chem. Soc.* **2008**, *130*, 8904–8905; b) S.-Y. Liu, I. D. Hills, G. C. Fu, *Organometallics* **2002**, *21*, 4323–4325; c) A. S. Batsanov, V. G. Andrianov, Y. T. Struchkov, V. S. Khandkarova, A. Z. Rubezhov, *Organomet. Chem. (USSR)* **1988**, *1*, 68.

[11] See for example: a) J. Hao, H. Liu, H.-Y. Yuan, *Acta Crystallogr., Sect. E* **2011**, *67*, m469; b) S. Yuan, S. Bai, D. Liu, W. H. Sun, *Organometallics* **2010**, *29*, 2132–2138; c) A. G. Avent, P. B. Hitchcock, M. F. Lappert, R. Sablong, J. R. Severn, *Organometallics* **2004**, *23*, 2591–2600; d) P. J. Daff, A. Monge, P. Palma, M. L. Poveda, C. Ruiz, P. Valerga, E. Carmona, *Organometallics* **1997**, *16*, 2263–2275.

[12] Values based on geometry optimizations at the b3-lyp/def2-TZVP level are similar: $\Delta H°$ = 1.1 kcal mol^{-1}, $\Delta S°$ = 13.1 cal mol^{-1} K^{-1}, $\Delta G°_{298}$ = –2.9 kcal mol^{-1}.

[13] W. I. Dzik, S. E. Calvo, J. N. H. Reek, M. Lutz, M. A. Ciriano, C. Tejel, D. G. H. Hetterscheid, B. de Bruin, *Organometallics* **2011**, *30*, 372–74.

[14] a) C. Tejel, L. Asensio, M. P. del Río, B. de Bruin, J. A. López, M. A. Ciriano, *Angew. Chem.* **2011**, *123*, 9001–9005; *Angew. Chem. Int. Ed.* **2011**, *50*, 8839–8843; b) C. C. Lu, E. Bill, T. Weyhermüller, E. Bothe, K. Wieghardt, *J. Am. Chem. Soc.* **2008**, *130*, 3181–3197.

[15] a) F. F. Puschmann, J. Harmer, D. Stein, H. Ruegger, B. de Bruin, B. H. Grützmacher, *Angew. Chem.* **2010**, *122*, 395–399; *Angew. Chem. Int. Ed.* **2010**, *49*, 385–389; b) F. F. Puschmann, H. Grützmacher, B. de Bruin, *J. Am. Chem. Soc.* **2010**, *132*, 73–75.

[16] R. Usón, L. A. Oro, J. A. Cabeza, *Inorg. Synth.* **1985**, *23*, 126–129.

[17] C. Incarvito, M. Lam, B. Rhatigan, A. L. Rheingold, C. J. Qin, A. L. Gavrilova, B. Bosnich, *J. Chem. Soc., Dalton Trans.* **2001**, 3478–3488.

 © 2012 Wiley-VCH Verlag GmbH & Co. KGaA, Weinheim

[18] G. M. Sheldrick, *SADABS*, Bruker AXS: Madison, WI, **1997**.
[19] G. M. Sheldrick, *SHELXL-97*, University of Göttingen, Germany, **1997**.
[20] L. J. Farrugia, *J. Appl. Crystallogr.* **1999**, *32*, 837–838.
[21] R. Ahlrichs, *Turbomole*, v. 6.3, Theoretical Chemistry Group, University of Karlsruhe, Germany.
[22] *PQS*, v. 2.4, **2001**, Parallel Quantum Solutions, Fayettevile, Arkansas (USA); the Baker optimizer is available separately from PQS upon request: I. Baker, *J. Comput. Chem.* **1986**, *7*, 385–395.
[23] P. H. M. Budzelaar, *J. Comput. Chem.* **2007**, *28*, 2226–2236.
[24] a) A. D. Becke, *Phys. Rev. A* **1988**, *38*, 3098–3100; b) J. P. Perdew, *Phys. Rev. B* **1986**, *33*, 8822–8824.
[25] a) F. Weigend, R. Ahlrichs, *Phys. Chem. Chem. Phys.* **2005**, *7*, 3297–3305; b) F. Weigend, M. Häser, H. Patzelt, R. Ahlrichs, *Chem. Phys. Lett.* **1998**, *294*, 143–152.
[26] a) Turbomole basis set library: *Turbomole*, v. 6; b) D. Andrae, U. Haeussermann, M. Dolg, H. Stoll, H. Preuss, *Theor. Chim. Acta* **1990**, *77*, 123–141.
[27] a) C. Lee, W. Yang, R. G. Parr, *Phys. Rev. B* **1988**, *37*, 785–789; b) A. D. Becke, *J. Chem. Phys.* **1993**, *98*, 1372–1377; c) A. D. Becke, *J. Chem. Phys.* **1993**, *98*, 5648–5652; d) Calculations were performed by using the Turbomole functional b3-lyp, which is not identical to the Gaussian B3LYP functional.
[28] a) I. Mayer, *Chem. Phys. Lett.* **1983**, *97*, 270–274; b) I. Mayer, *Chem. Phys. Lett.* **1984**, *110*, 440–444; c) I. Mayer, *Int. J. Quantum Chem.* **1986**, *29*, 73–84; d) I. Mayer, *Int. J. Quantum Chem.* **1986**, *29*, 477–483; e) A. J. Bridgeman, G. Cavigliasso, L. R. Ireland, J. Rothery, *J. Chem. Soc., Dalton Trans.* **2001**, 2095–2108.
[29] a) S. I. Gorelsky, *AOMix*, Program for Molecular Orbital Analysis, http://www.sg-chem.net/, University of Ottawa, v. 6.5, **2011**; b) S. I. Gorelsky, A. B. P. Lever, *J. Organomet. Chem.* **2001**, *635*, 187–196.

Received: August 19, 2011
Published Online: November 10, 2011

 © 2012 Wiley-VCH Verlag GmbH & Co. KGaA, Weinheim

DOI: 10.1002/ejic.201100803

Organochromium Complexes Bearing Noninnocent Diimine Ligands

Kevin A. Kreisel,[a] Glenn P. A. Yap,[a] and Klaus H. Theopold*[a]

Keywords: Chromium complexes / Diimine ligands / N ligands / Alkylation / Insertion

We have prepared several anionic and neutral organochromium complexes featuring noninnocent α-diimine ligands. All neutral and anionic complexes refrain from insertion of the C=N bonds of the diimine ligand into the chromium–carbon bonds, presumably due to the reduced nature of the diimine ligand. However, insertion can be facilitated by one-electron oxidation. Thus, oxidation of [(^{H}**L**^{iPr})CrR(THF)] [^{H}**L**^{iPr} = Ar–N=C(H)–(H)C=N–Ar in which Ar = 2,6-diisopropylphenyl and R = CH_2SiMe_3 or CH_3] with $[(C_5H_5)_2Fe]^+$ presumably forms [(^{H}**L**^{iPr})CrR(THF)]$^+$, which contains a neutral diimine ligand coordinated to Cr^{II}. This cationic complex apparently undergoes immediate insertion of the C=N bond of the diimine ligand into the Cr–alkyl bond, followed by C–H activation of the isopropyl substituent of an N–aryl group on the diimine ligand. DFT calculations confirm that [(^{H}**L**^{iPr})-CrR(THF)]$^+$ contains a neutral innocent diimine ligand that undergoes C=N bond insertion into the Cr–R bond.

Introduction

The recent interest in transition-metal complexes containing redox-active ligands has produced a remarkable number of reports detailing unusual electronic and geometric structures as well as unprecedented reactivity.[1] In most cases, the latter is best rationalized based on an assignment of the most appropriate electronic structure. Work by Wieghardt et al. and others has greatly improved our understanding of the noninnocence of a variety of ligands such as pyridinebis(imines),[2] catechols, 1,2-dioxolenes,[11] and α-diimines (also known as diazadienes).[3] Among the most frequently used of these ligands are the α-diimines, due to the ease of varying the sterics and electronics of these ligands. Pioneering work by van Koten showed the diversity in the reactivity of diimine ligands and established the potential noninnocence of the ligand by means of radical C–C coupling reactions between coordinated diimine ligands.[4] Arguably more interesting and perhaps mechanistically related to our work was the discovery of regioselective alkylation of diimine ligands by diorganozinc reagents.[5] Since then, the reactions of diimines with organozinc, organomagnesium, and organoaluminum reagents have been studied extensively.[5b,6] In many cases, these reactions lead to alkylation of the diimine ligand at various positions (see Scheme 1). More recently, there have been reports of transition metals mediating the alkylation of diimine ligands. Most relevant to our work are reports of the reactions of zirconium- and hafnium-alkyl compounds with diimine ligands and their use as catalysts in olefin polymerization.[7] Thus, the reaction of $M(CH_2Ph)_4$ (M = Zr or Hf) with *N*-aryl-substituted diimine ligands results in alkyl migration to the carbon atom of the diimine ligand and a 1,2-hydride shift, thereby leaving an amido–imine ligand coordinated to the metal. However, the mechanism of this rearrangement is still not entirely clear.

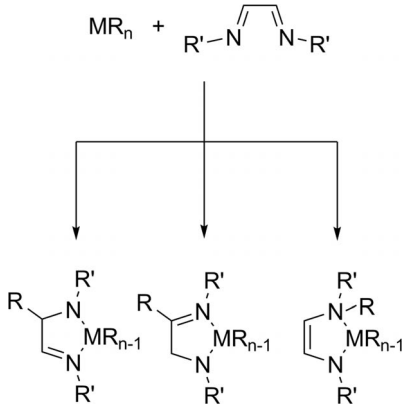

Scheme 1. Possible regioisomers produced by alkylation of a diimine ligand.

We recently reported a thorough investigation of the coordination chemistry of chromium-bearing diimine ligands utilizing both X-ray crystallography and density functional theory (DFT) calculations;[8] the present work extends this work to organometallic derivatives. An understanding of the electronic structure of these complexes facilitates a rationalization of their reactivity. Furthermore, the results presented here provide insight into the mechanism of alkyl

[a] Department of Chemistry and Biochemistry,
Center for Catalytic Science and Technology,
University of Delaware,
Newark, Delaware 19716, USA
Fax: +1-302-831-6335
E-mail: theopold@udel.edu

Supporting information for this article is available on the WWW under http://dx.doi.org/10.1002/ejic.201100803 or from the author.

WILEY ONLINE LIBRARY
© 2012 Wiley-VCH Verlag GmbH & Co. KGaA, Weinheim

migrations that have plagued organometallic diimine chemistry for decades.

Herein, we summarize our study of the organometallic chemistry of chromium supported by the diimine ligand, Ar–N=C(H)–(H)C=N–Ar ($^{H}L^{iPr}$; Ar = 2,6-diisopropylphenyl). The original intent of this work – in the context of Phillips catalysis of ethylene polymerization[9] – was to prepare cationic Cr^{II}-monoalkyls supported by bidentate nitrogen ligands, and to compare their catalytic activity for ethylene polymerization to alkyl-Cr^{III} compounds.[10] Although this goal was not realized, the results of our study shed light on a characteristic reaction pattern of diimine metal–alkyl complexes.

Results and Discussion

Our initial attempts to prepare dialkyl-Cr^{II} complexes of the type [($^{H}L^{iPr}$)CrR_2] by the reaction of [{($^{H}L^{iPr}$)Cr(μ-Cl)(Cl)}$_2$] with four equivalents of alkylating agents, such as PhMgCl or $(Me)_3SiCH_2Li$, indeed gave novel organometallic compounds, but in low yield. Full characterization of the reaction products revealed them to be formally Cr^{I}–dialkyl "ate" complexes of the general formula [($^{H}L^{iPr}$)-CrR_2]$^-$. Seeking to circumvent the apparent reduction of chromium by the electron-rich main-group alkyls, we eventually prepared the precursor [{($^{H}L^{iPr}$)Cr(μ-Cl)}$_2$] (**1**). As discussed elsewhere, the latter is best described as containing divalent chromium (Cr^{II}), coordinated by a singly reduced α-diimine radical anion.[8] Compound **1** is also an easily accessible synthon for the preparation of the aforementioned dialkyls in good yield (see Scheme 2). Upon addition of alkylating reagent (4 equiv.), excellent yields of [$Li(THF)_4$][($^{H}L^{iPr}$)Cr{$CH_2Si(CH_3)_3$}$_2$] (**2**) and [PhMg(THF)][($^{H}L^{iPr}$)$CrPh_2$] (**3a**) or [$Li(THF)_2$][($^{H}L^{iPr}$)$CrPh_2$] (**3b**) could be obtained. The molecular structures of **2** and **3a** were determined by X-ray crystallographic analysis; the molecular structures are depicted in Figures 1 and 2, respectively. Complex **2** crystallizes in the monoclinic space group $P2_1/n$ and displays a significantly distorted square-planar geometry. Its Cr–C bond lengths of 2.131(5) and 2.136(5) Å are in good agreement with other reported alkyl complexes of chromium. The Cr–N bond lengths of 1.994(4) and 2.004(4) Å are also similar to those of previously reported chromium diimine complexes. In addition, the THF-solvated lithium cation shows no signs of interaction with the chromate anion in the solid state [closest contact distance is 3.506(11) Å]. The phenyl derivative **3a** crystallizes in the monoclinic space group $P2_1/c$ and also exhibits distorted square-planar coordination geometry about chromium. The Cr–C bond lengths in **3a**, at 2.164(2) and 2.203(2) Å, are longer than those in **2**, presumably reflecting the pronounced bonding interaction of the phenyl groups with the magnesium counterion. The Cr–N bond lengths are also slightly elongated [2.0362(19) and 2.0613(19) Å]. The cation in **3a** {i.e., [PhMg(THF)]$^+$} is positioned close to the *ipso*-carbon atoms of both phenyl groups of the organochromium complex ion. When prepared from PhLi (see

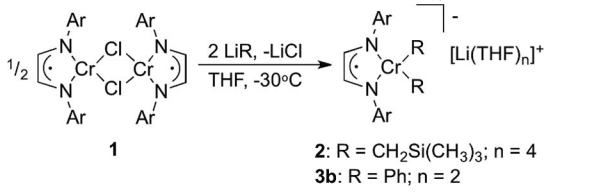

Scheme 2. Synthesis of complexes **2** and **3**.

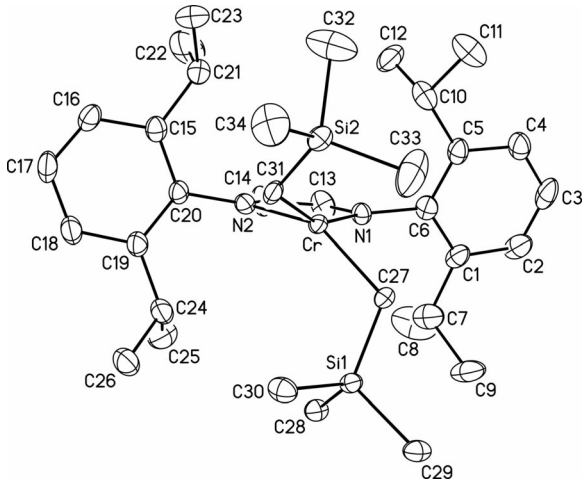

Figure 1. ORTEP plot of [$Li(THF)_4$][($^{H}L^{iPr}$)Cr{$CH_2Si(CH_3)_3$}$_2$] (**2**) at the 30% probability level. Hydrogen atoms and the $[Li(THF)_4]^+$ cation have been omitted for clarity. Selected structural parameters (distances in Å, angles in degrees): Cr–N1 2.004(4), Cr–N2 1.993(4), Cr–C27 2.131(5), Cr–C31 2.136(5), N1–C13 1.335(7), N2–C14 1.352(6), C13–C14 1.372(8); N1–Cr–N2 79.27(16), N1–Cr–C27 96.60(18), N1–Cr–C31 156.87(18), N2–Cr–C27 148.69(18), N2–Cr–C31 97.93(17), C27–Cr–C31 97.22(19).

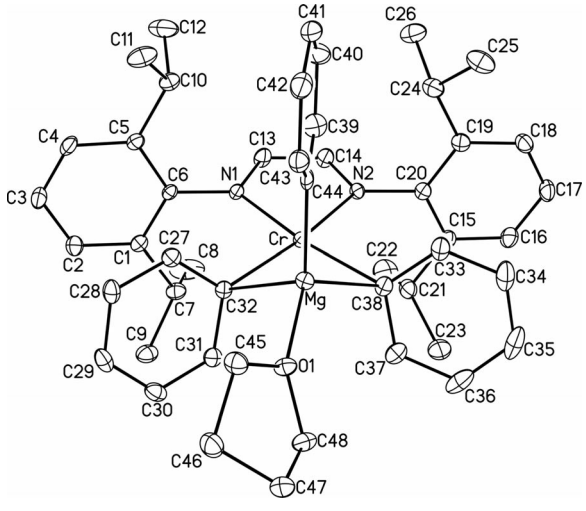

Figure 2. ORTEP plot of [PhMg(THF)][($^{H}L^{iPr}$)$CrPh_2$] (**3a**) at the 30% probability level. Hydrogen atoms have been omitted for clarity. Selected structural parameters (distances in Å, angles in degrees): Cr–N1 2.0362(19), Cr–N2 2.0613(19), Cr–C32 2.164(2), Cr–C38 2.203(2), N1–C13 1.335(3), N2–C14 1.335(3), C13–C14 1.383(3); N1–Cr–N2 78.61(8), N1–Cr–C32 92.21(8), N1–Cr–N38 172.45(8), N2–Cr–C32 170.54(8), N2–Cr–C38 94.01(8), C32–Cr–C38 95.23(9).

 © 2012 Wiley-VCH Verlag GmbH & Co. KGaA, Weinheim

Scheme 2), we assume that the lithium cation of **3b** also lies between the aryl rings and is coordinated by two THF ligands; this assertion is consistent with the elemental analysis (see the Exp. Section). X-ray quality crystals of **3b** were not attainable; however, the reaction was cleaner and resulted in higher yields. The diimine backbones of both **2** and **3a** show signs of reduction, consistent with one-electron reduced ligand-centered radicals.[8] Considering these bond lengths and the square-planar coordination favored by divalent chromium, the most appropriate assignment of an electronic structure to these complexes would be Cr^{II} (d^4, $S = 2$) with strong antiferromagnetic coupling to a ligand-centered radical, analogous to $[(^{H}\mathbf{L}^{i\mathrm{Pr}})CrCl_2]^-$ ($S = {}^3/_2$). Accordingly, room-temperature measurements of the effective magnetic moments (μ_{eff}) of **2** and **3b** gave 3.7(1) μ_B for both complexes, close to the spin-only moment for three unpaired electrons (3.87 μ_B).[11]

Interestingly, alkylation of **1** with MeLi (4 equiv.) did not give the expected $[Li(THF)_4][(^{H}\mathbf{L}^{i\mathrm{Pr}})Cr(CH_3)_2]$, but instead yielded dinuclear $[Li(THF)_4][\{(^{H}\mathbf{L}^{i\mathrm{Pr}})Cr\}_2(\mu\text{-}CH_3)_3]$ (**4**). In a similar manner, the reaction of **1** with an excess amount of $Li[BEt_3H]$ gave $[Li(THF)_4][\{(^{H}\mathbf{L}^{i\mathrm{Pr}})Cr\}_2(\mu\text{-}H)_3]$ (**5**), which is isostructural to **4**. Both **4** and **5** could also be prepared in good yield by addition of three equivalents of the appropriate alkylating reagent to **1** according to Scheme 3. Crystallizations from Et_2O at –30 °C gave blue crystals of **4** and purple crystals of **5**, respectively. The molecular structures of **4** and **5** are shown in Figures 3 and 4, respectively, along with selected interatomic distances and angles. Complex **4** crystallizes in the monoclinic space group $P2_1/c$ and contains two diimine chromium fragments joined by three bridging methyl ligands. The coordination geometry about each chromium atom is best described as trigonal bipyramidal, with the threefold axes approximated by C3–Cr1–N1 [168.23(16)°] and C1–Cr2–N3 [157.77(16)°]. The Cr–C distances range from 2.176(5) to 2.243(5) Å and are thus longer than those in the monomeric complexes described above, presumably due to three-center two-electron bonding. The bridging methyl ligands also fix the chromium atoms at a metal–metal distance of 2.469(1) Å, raising the possibility of metal–metal bonding. Indeed, the $[Cr_2(\mu\text{-}CH_3)_3]$ core of **4** is remarkably similar in structure to that of $[Cp^*_2Cr_2(\mu\text{-}CH_3)_3]BF_4$ (e.g., Cr–Cr 2.42 Å; Cp* = pentamethylcyclopentadienyl), to which we have attributed metal–metal bonding between its Cr^{III} centers many years ago.[12] The Cr–N distances in **4** [1.988(3) to 2.006(4) Å] are consistent with those in **1**. The THF-solvated lithium cation does not exhibit any close contacts with the anion; the closest internuclear distance between the two measures is 3.843(9) Å. The isostructural complex **5** crystallizes in the triclinic space group $P\bar{1}$, with each chromium also residing in a trigonal-bipyramidal coordination sphere – the axial vectors being defined by H1C–Cr1–N2 [168.8(9)°] and H1C–Cr2–N4 [168.8(9)°]. Although there is always a systematic error involved with hydride bond lengths established by X-ray crystallography,[13] the apparent Cr–H distances for the bridging hydride ligands range from 1.61(3)–1.78(3) Å and are comparable to other reported bridging hydrides of chromium.[14] The Cr–Cr distance of **5** is similar, although slightly shorter than that of **4**, measuring 2.4490(7) Å. The Cr–N distances in **5** are considerably shorter than in the previously mentioned complexes [1.952(2) to 1.957(2) Å]. Similar to **4**, the countercation of **5** is not closely associated with the chromate anion, with a distance of 3.594(5) Å between them. Both **4** and **5** show considerable disruption of the diimine π system and, based solely on bond lengths (**4**: $C–N_{av.}$ 1.375 Å; $C–C_{av.}$ 1.355 Å; **5**: $C–N_{av.}$ 1.371 Å; $C–C_{av.}$ 1.352 Å), the ligands appear to be closest to the dianionic enediamide electronic configuration. The latter would result in the assignment of +III as a formal oxidation state of chromium. Room-temperature magnetic measurements of **4** and **5** gave μ_{eff} values of 1.4(1) and 1.5(1) μ_B per Cr, respectively. These low values (the ex-

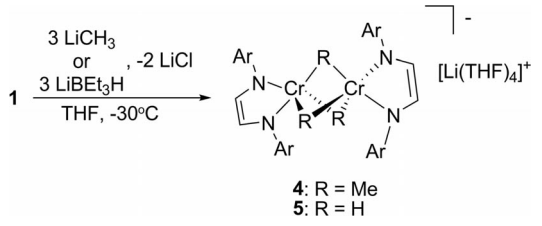

Scheme 3. Synthesis of bridging alkyl species **4** and **5**.

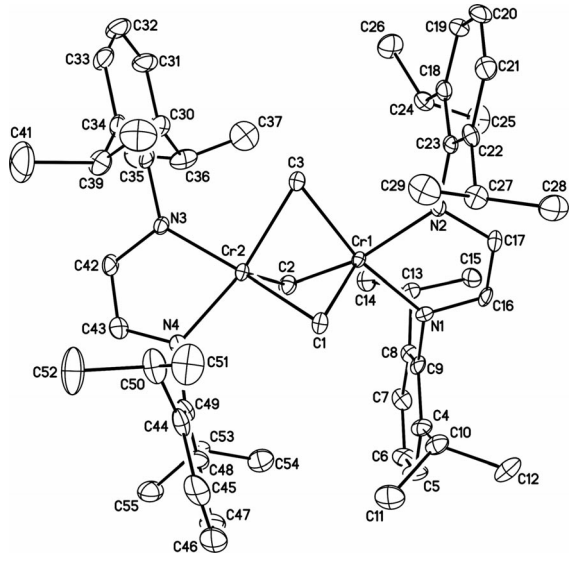

Figure 3. ORTEP plot of $[Li(THF)_4][\{(^{H}\mathbf{L}^{i\mathrm{Pr}})Cr\}_2(\mu\text{-}CH_3)_3]$ (**4**) at the 30% probability level. Hydrogen atoms and the $[Li(THF)_4]^+$ cation have been omitted for clarity. Selected structural parameters (distances in Å, angles in degrees): Cr1–Cr2 2.4690(10), Cr1–N1 2.006(4), Cr1–N2 2.002(3), Cr1–C1 2.192(4), Cr1–C2 2.235(5), Cr1–C3 2.202(5), Cr2–N3 1.990(4), Cr2–N4 1.988(3), Cr2–C1 2.243(5), Cr2–C2 2.176(5), Cr2–C3 2.221(5), N1–C16 1.366(6), N2–C17 1.393(6), N3–C42 1.367(5), N4–C43 1.374(6), C16–C17 1.349(6), C42–C43 1.361(7); Cr1–C1–Cr2 67.65(13), Cr1–C2–Cr2 68.07(14), Cr1–C3–Cr2 67.87(15), N1–Cr1–N2 79.51(14), N1–Cr1–C1 102.91(16), N1–Cr1–C2 93.16(17), N1–Cr1–C3 168.23(16), N2–Cr1–C1 116.96(17), N2–Cr1–C2 146.72(16), N2–Cr1–C3 90.37(16), N3–Cr2–N4 79.69(15), N3–Cr2–C1 157.77(16), N3–Cr2–C2 105.70(18), N3–Cr2–C3 93.41(16), N4–Cr2–C1 94.06(16), N4–Cr2–C2 106.69(17), N4–Cr2–C3 160.06(17).

 © 2012 Wiley-VCH Verlag GmbH & Co. KGaA, Weinheim

pected spin-only value for $S = {}^3/_2$ is 3.88 μ_B) are consistent with antiferromagnetic coupling between the chromium ions, metal–metal bonding, or a combination of the two.

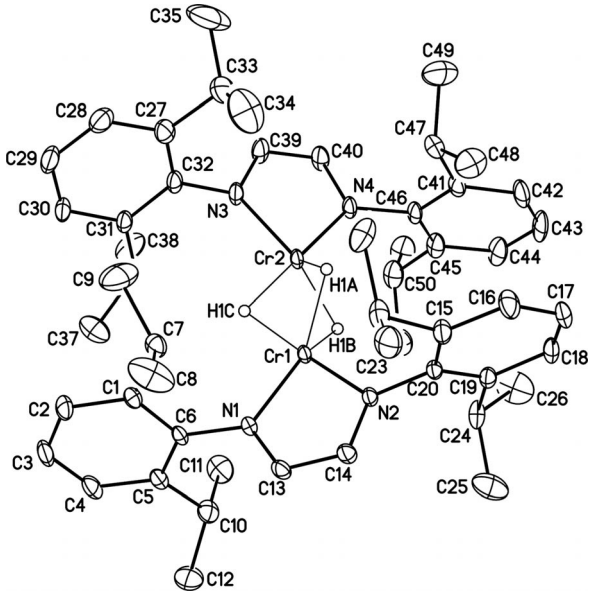

Figure 4. ORTEP plot of $[Li(THF)_4][\{(^HL^{iPr})Cr\}_2(\mu\text{-}H)_3]$ (**5**) at the 30% probability level. With the exception of the bridging hydride ligands, all hydrogen atoms and the $[Li(THF)_4]^+$ cation have been omitted for clarity. Selected structural parameters (distances in Å, angles in degrees): Cr1–Cr2 2.4490(7), Cr1–N1 1.9544(18), Cr1–N2 1.9524(19), Cr1–H1A 1.78(3), Cr1–H1B 1.72(3), Cr1–H1C 1.71(3), Cr2–N3 1.957(2), Cr2–N4 1.955(2), Cr2–H1A 1.61(3), Cr2–H1B 1.69(3), Cr2–H1C 1.68(3), N1–C13 1.374(3), N2–C14 1.372(3), N3–C39 1.3733, N4–C40 1.366(3), C13–C14 1.349(3) C39–C40 1.355(4); Cr1–H1A–Cr2 92.3(9), Cr1–H1B–Cr2 91.8(9), Cr1–H1C–Cr2 92.3(9), N1–Cr1–N2 80.42(8), N1–Cr1–H1A 147.5(9), N1–Cr1–H1B 141.0(9), N1–Cr1–H1C 97.9(9), N2–Cr1–H1A 103.5(9), N2–Cr1–H1B 112.7(9), N2–Cr1–H1C 168.8(9), N3–Cr2–N4 80.56(9), N3–Cr2–H1A 124.7(9), N3–Cr2–H1B 160.7(9), N3–Cr2–H1C 97.1(9), N4–Cr2–H1A 113.1(9), N4–Cr2–H1B 101.3(9), N4–Cr2–H1C 168.8(9).

Reaction of **1** with an excess amount of $LiCH_3$ resulted in the formation of a red product that was ultimately determined to be $[Li_2(THF)_3][(^HL^{iPr})Cr(CH_3)_3]$ (**6**) by X-ray crystallography (see Scheme 4). Interestingly, reaction of **1** with an excess amount of $Li[BEt_3H]$ only gave **5** in low yield; $[Li_2(THF)_3][(^HL^{iPr})CrH_3]$ was not isolated. Figure 5 depicts the results of the X-ray structure determination of **6**.

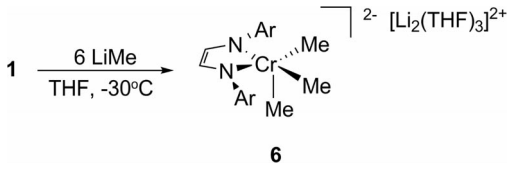

Scheme 4. Preparation of $[Li_2(THF)_3][(^HL^{iPr})Cr(CH_3)_3]$ (**6**).

The trialkyl crystallizes in the monoclinic space group *C*2/*c*. The geometry about the chromium in **6** is best described as square pyramidal with the angles between the apical ligand (C29) and the basal ones ranging from 91.2(2) to 103.9(1)°. The Cr–C distances [2.107(4), 2.150(5), and

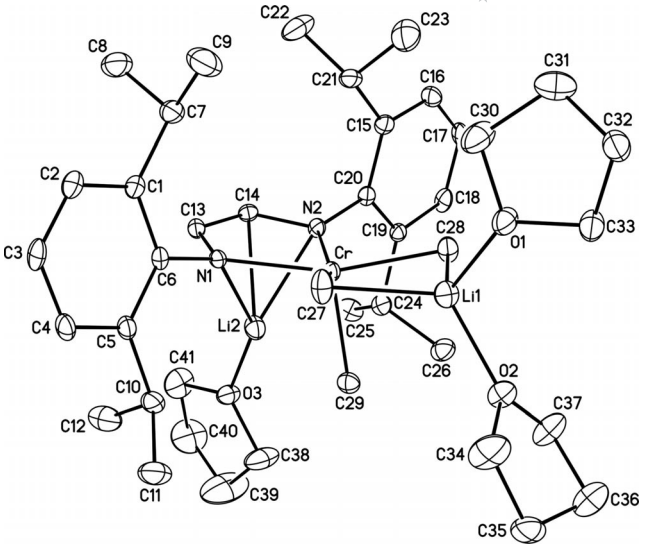

Figure 5. ORTEP plot of $[Li_2(THF)_3][(^HL^{iPr})Cr(CH_3)_3]$ (**6**) at the 30% probability level. Hydrogen atoms have been omitted for clarity. Selected structural parameters (distances in Å, angles in degrees): Cr–N1 2.081(3), Cr–N2 2.066(3), Cr–C27 2.159(5), Cr–C28 2.150(5), Cr–C29 2.107(4), N1–C13 1.402(4), N2–C14 1.401(4), C13–C14 1.344(5); N1–Cr–N2 76.7(1), N1–Cr–C27 89.7(2), N1–Cr–C28 161.7(2), N1–Cr–C29 103.9(1), N2–Cr–C27 159.1(2), N2–Cr–C28 90.2(2), N2–Cr–C29 102.6(2), C27–Cr–C28 99.0(2), C27–Cr–C29 96.0(2).

2.159(5) Å] are shorter than in the dinuclear complex **4** and more closely approximate the Cr–C bond lengths in **2** and **3**. Notably, the two lithium cations in **6** are closely associated with the chromate anion; one interacts with the two equatorial methyl ligands and the other is coordinated in a η^4 fashion by the reduced diimine ligand. This diimine coordination of the cation is rare, but some examples do exist.[15] Like complexes **4** and **5**, the C–N distances of 1.401(4) and 1.402(4) Å and the C–C distance of 1.344(5) Å are in accord with a heavily reduced diimine ligand, most likely to the extent of a dianionic, enediamide ligand. A magnetic susceptibility measurement of **6** gave a μ_{eff} of 3.8(1) μ_B, in accord with an $S = {}^3/_2$, Cr^{III} bound to a diamagnetic enediamide ligand.

Condensation of alkyl complexes **2**, **4**, and **6** with **1** in the proper stoichiometry readily furnishes neutral, monoalkyl complexes. Thus, reaction of two equivalents of **2** with **1** gives $[(^HL^{iPr})Cr\{CH_2Si(CH_3)_3\}(THF)]$ (**7**) in good yield (see Scheme 5). The results of an X-ray structure determination can be found in Figure 6.

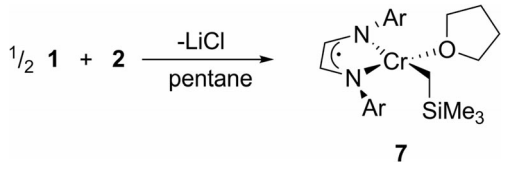

Scheme 5. Preparation of $[(^HL^{iPr})Cr\{CH_2Si(CH_3)_3\}(THF)]$ (**7**).

Complex **7** crystallizes in the monoclinic space group $P2_1/n$ with two crystallographically distinct, but chemically equivalent molecules (only one will be discussed). The dis-

 © 2012 Wiley-VCH Verlag GmbH & Co. KGaA, Weinheim

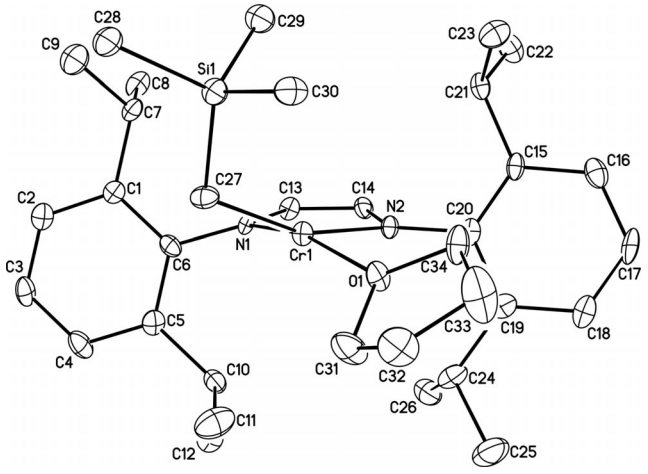

Figure 6. ORTEP plot of [(^{H}L^{iPr})Cr{$CH_2Si(CH_3)_3$}(THF)] (**7**) at the 30% probability level. Hydrogen atoms have been omitted for clarity. Selected structural parameters (distances in Å, angles in degrees): Cr1–N1 1.993(4), Cr1–N2 2.034(4), Cr1–C27 2.102(5), Cr1–O1 2.104(4), N1–C13 1.338(6), N2–C14 1.347(6), C13–C14 1.376(7); N1–Cr1–N2 78.90(18), N1–Cr1–C27 96.6(2), N1–Cr1–O1 164.59(16), N2–Cr1–C27 160.3(2), N2–Cr1–O1 95.26(16), C27–Cr1–O1 93.5(2).

torted square-planar geometry around the Cr in **7** is similar to that of its precursor, **2**. However, the Cr–C bond length of 2.098(6) Å is shorter than those in **2**, presumably due to the relief of the anionic charge buildup on the complex. The difference in the Cr–N distances of 1.995(5) Å (Cr–N1) and 2.035(5) Å (Cr–N2) can be attributed to a *trans* influence imparted by the alkyl group that is *trans* to N2. Like **2**, the reduction of the diimine ligand in **7** can be seen through the C–N bond lengths of 1.336(6) and 1.344(6) Å and the C–C bond length of 1.373(7) Å. This, and the room-temperature magnetic moment of 3.8(1) μ_B, are consistent with a $S = 2$, Cr^{II} complex strongly antiferromagnetically coupled to a ligand-centered radical.

In a similar manner, condensation of **1** with complex **4** or **6** in the proper stoichiometry yields the neutral, methyl-bridged dimer, [{(^{H}L^{iPr})Cr(μ-CH_3)}$_2$] (**8**) according to Scheme 6. The results of an X-ray analysis of **8** can be found in Figure 7.

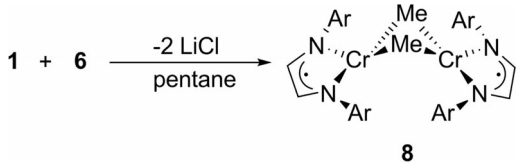

8

Scheme 6. Preparation of [{(^{H}L^{iPr})Cr(μ-CH_3)}$_2$] (**8**).

Complex **8** crystallizes in the monoclinic space group *C*2/*c* with a C_2 axis running perpendicular to the Cr–Cr vector and between the bridging methyl ligands. The geometry around each chromium atom is best described as distorted square planar with a dihedral angle of 20.1° between the N1–Cr1–N2 plane and the C1–Cr1–C1A plane. The two diimine chromium fragments are "folded" toward each other at the bridging methyl ligands at an angle of 53.0°

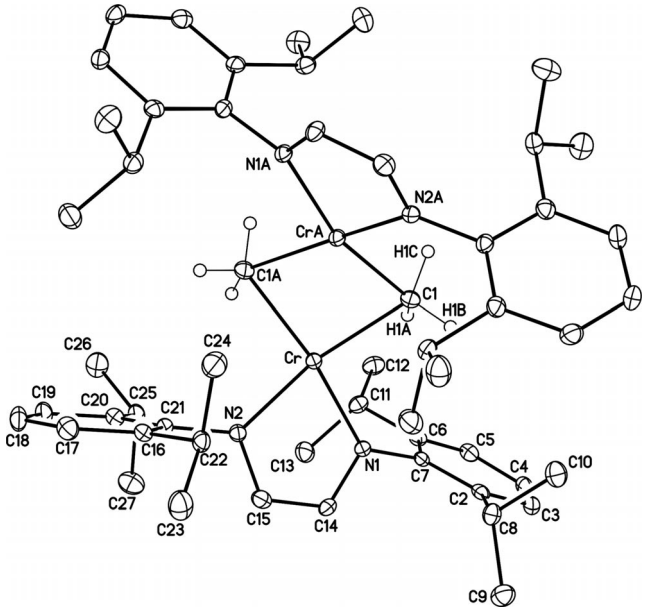

Figure 7. ORTEP plot of [{(^{H}L^{iPr})Cr(μ-CH_3)}$_2$] (**8**) at the 30% probability level. With the exception of the hydrogen atoms on the methyl ligands, all hydrogen atoms have been omitted for clarity. Selected structural parameters (distances in Å, angles in degrees): Cr–CrA 2.6649(8), Cr–N1 2.043(2), Cr–N2 2.026(2), Cr–C1 2.192(3), Cr–C1A 2.197(3), N1–C14 1.347(3), N2–C15 1.347(3), C14–C15 1.377(3); N1–Cr–N2 79.6(1), N1–Cr–C1 163.9(1), N1–Cr–C1A 93.6(1), N2–Cr–C1 95.3(1), N2–Cr–C1A 164.1(1), C1–Cr1–C1A 95.0(1).

(see Figure 7), which is likely due to some measure of Cr–Cr bonding, supported by the short metal–metal distance [Cr–Cr 2.6649(8) Å].[14d] The methyl ligands are symmetrically bridged with bond lengths of 2.192(3) and 2.197(3) Å. As in **4**, these long Cr–C distances are presumably a consequence of three-center two-electron bonding. Complex **8** has average C–N bond lengths of 1.347(3) Å and a diimine C–C bond length of 1.377(3) Å, making it most consistent with a high-spin Cr^{II} complex ($S = 2$) coupled to a ligand-centered radical. The room-temperature effective magnetic moment [1.8(1) μ_B per Cr] indicates appreciable metal–metal interactions, either Cr–Cr bonding or antiferromagnetic coupling or more likely a combination of both, much like in **4** and **5**. The solution behavior of **8** in C_6D_6 is in accord with the solid-state structure shown in Figure 7, with a very broad, isotropically shifted resonance at δ = 17.4 ppm and sharp resonances at δ = 8.49, 3.88, and 1.64 ppm in the ^{1}H NMR spectra. In [D_8]THF a dramatically different spectrum is obtained; thus, the broad resonance is shifted to –13.1 ppm while the others are located at 14.4, 2.69, and –1.91 ppm. We attribute these spectral differences to the formation of mononuclear [(^{H}L^{iPr})-Cr(Me)(THF)] in THF solution. The ^{1}H NMR spectrum of **8** in [D_8]THF is similar in appearance to that of its presumed analogue, complex **7** (see Exp. Section). A reaction of **5** with **1** was also attempted to generate a hydride species similar to **8**, namely, [{(^{H}L^{iPr})Cr(μ-H)}$_2$]. However, we found that the stronger Cr–H bonds in **5** would not give way as the Cr–C bonds in **4** and **6** had done. Other methods

 © 2012 Wiley-VCH Verlag GmbH & Co. KGaA, Weinheim

of generating [{(^{H}**L**$^{i\mathrm{Pr}}$)Cr(μ-H)}$_2$] from **1** (e.g., $AlEt_2Cl$, through β-hydrogen elimnation of an ethyl intermediate) produced a brown material with ^{1}H NMR spectroscopic resonances at 21.0, 2.17, 8.72, and –24.3 ppm. However, the reaction consistently produced intractable materials and structural characterization of the product was not achievable in this context {note, however, the initial isolation of [{(^{H}**L**$^{i\mathrm{Pr}}$)Cr}$_2$] from a related reaction}.[16]

With neutral alkyl complexes **7** and **8** in hand, oxidation was attempted to generate cationic alkylchromium complexes. Cr^{III} complexes of this type have proved to be very successful homogeneous ethylene polymerization catalysts.[10] However, oxidation of **7** with [$(C_5H_5)_2$Fe][BARF] [BARF = tetrakis(3,5-bis(trifluoromethyl)phenyl)borate] in Et_2O, intended to produce the cationic, formally Cr^{II} complex, [(^{H}**L**$^{i\mathrm{Pr}}$)Cr(CH_2SiMe_3)(THF)]$^+$, instead led to the product of a tortuous alkyl/hydride migration and C–H activation (see Scheme 7).

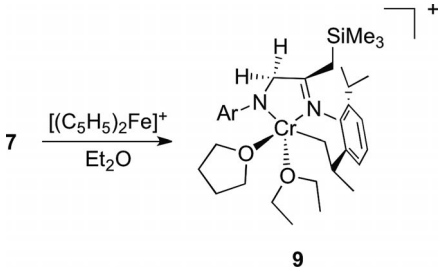

Scheme 7. Preparation of [(^{H,TMSM}**L***)Cr(THF)(Et_2O)][BARF] (**9**).

The ionic product isolated from the oxidation reaction, brown [(^{H,TMSM}**L***)Cr(THF)(Et_2O)][BARF] (**9**, in which ^{H,TMSM}**L** denotes alkyl migration to the backbone of what is now an iminoylamide ligand and **L*** denotes C–H activation of an isopropyl methyl group of an aryl substituent), crystallized in the triclinic space group $P\bar{1}$; the result of the structure determination is depicted in Figure 8. The structure of **9** is best described as square pyramidal with apical (C30) to basal bond angles ranging from 86.7(3) to 117.1(2)°. The Cr–C bond length is 2.053(6) Å and is thus consistent with typical Cr^{III}–C bond lengths. More interesting, however, is the apparent migration of the (trimethylsilyl)methyl group to the backbone of the diimine ligand. Close inspection of the bond lengths shows that the N1–C13 and C13–C14 bond lengths have lengthened to 1.451(8) and 1.480(9) Å, respectively, whereas the N2–C14 bond length is considerably shorter [1.306(7) Å] than the bond lengths in the precursor, complex **7**. Furthermore, the IR spectrum of **9** shows the appearance of a band at 1610 cm^{-1} consistent with a C=N vibration. These observations would suggest that the backbone of the ligand is in an imine–amide form with one C–N double bond, one C–N single bond, and a C–C single bond. Thus, the oxidation state ambiguity in the previous complexes has been removed and straightforward electron counting reveals a 13-electron, d^3, Cr^{III} complex ion. Accordingly, the experimentally determined magnetic moment was found to be 4.0(1) μ_B, consistent with the $S = {}^3/_2$ spin state of a typical Cr^{III} compound. Oxidation of the methyl-bridged **8** in THF also gave a brown solution that was proposed to be [(^{H,Me}**L***)Cr(THF)$_2$][BARF] (**10**) and has a similar ^{1}H NMR spectrum to that of **9** (see the Exp. Section).

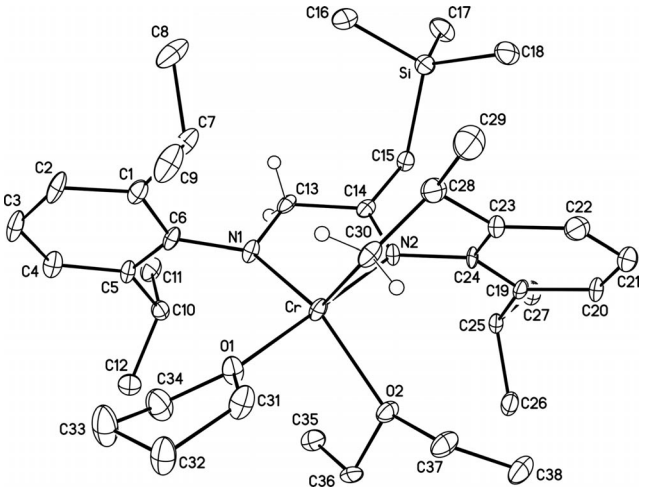

Figure 8. ORTEP plot of [(^{H,TMSM}**L***)Cr(THF)(Et_2O)][BARF] (**9**) at the 30% probability level. With the exception of the hydrogen atoms on C13 and C30, all hydrogen atoms and the [BARF]$^-$ anion have been omitted for clarity. Selected structural parameters (distances in Å, angles in degrees): Cr–N1 1.920(4), Cr–N2 2.013(5), Cr–C30 2.053(6), Cr–O1 2.065(4), Cr–O2 2.144(4), N1–C13 1.454(8), N2–C14 1.308(7), C13–C14 1.486(8), C14–C15 1.493(7); N1–Cr–N2 81.7(2), N1–Cr–C30 117.2(2), N1–Cr–O1 96.74(18), N1–Cr–O2 145.41(18), N2–Cr–C30 86.6(2), N2–Cr–O1 177.90(19), N2–Cr–O2 92.56(18), O1–Cr–O2 87.95(16), O1–Cr–C30 95.3(2), O2–Cr–C30 96.3(2).

Two mechanisms have been proposed for alkyl migration to C=N bonds in diimine ligands. The first involves homolytic cleavage of the metal–alkyl bond followed by recombination of the alkyl radical with a diimine ligand-centered radical. The second mechanism assumes 1,2-insertion of a C=N bond of the diimine ligand into a metal–alkyl bond. Either reaction step is then followed by a 1,2-hydride shift to engender unsaturation at the more substituted C–N bond. Assuming the HOMO of **7** houses the ligand-centered unpaired electron, oxidation would presumably produce [(^{H}**L**$^{i\mathrm{Pr}}$)Cr(CH_2SiMe_3)(THF)]$^+$, which contains a neutral diimine ligand and Cr^{II} (see Scheme 8). This intermediate could undergo either a 1,2-insertion of the alkyl ligand into the C–N double bond or homolytic cleavage of the alkyl and single-electron transfer to the diimine ligand, followed by radical recombination. Either of these steps is then followed by a hydride shift to the remaining imine carbon and reestablishment of the C–N double bond at the bulkier, alkyl-substituted side of the ligand. The resulting cationic Cr^{II} complex activates a C–H bond of an isopropyl substituent and a bimolecular reductive elimination of H_2 finally furnishes **9**. The C–H bond-activation step is an apparent consequence of the formation of a highly reactive, three-coordinate, cationic, Cr^{II} species.

 © 2012 Wiley-VCH Verlag GmbH & Co. KGaA, Weinheim

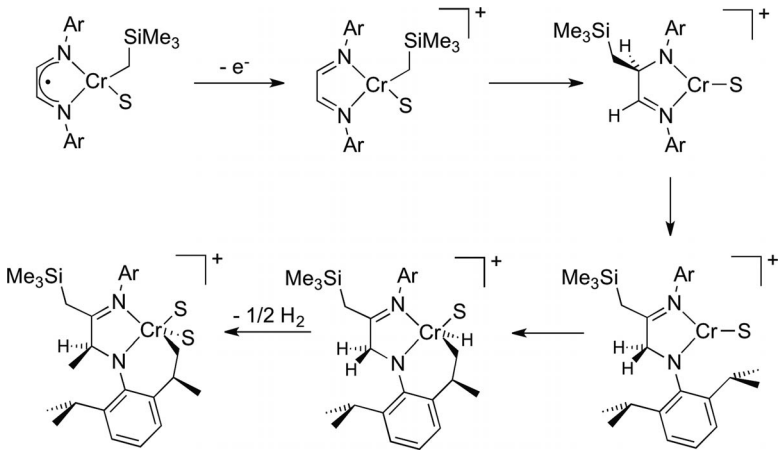

Scheme 8. Mechanism of formation of oxidation product **9** (S = THF, Et_2O).

For a better understanding of the relative propensity of metal alkyls such as **7** or its oxidized form towards alkyl migration, unrestricted DFT calculations at the B3LYP/6-311g level of theory were run on model complexes [(^{H}**L**^{Me})-Cr(Me)(THF)] (**7′**), [(^{H,Me}**L**^{Me})Cr(THF)] (**7′′**), [(^{H}**L**^{Me})-Cr(Me)(THF)]$^+$ (**8′**), and [(^{H,Me}**L**^{Me})Cr(THF)]$^+$ (**8′′**), in which the 2,6-diisopropylphenyl substituents and the alkyl ligand have all been replaced by methyl groups. A geometry optimization of **7′** gave metric parameters that are in excellent agreement (ΔC–N $<$ 0.020 Å; ΔC–C $\leq$ 0.022 Å; ΔCr–N $\leq$ 0.048 Å, ΔCr–C = 0.035 Å, ΔCr–O = 0.020 Å) with those of actual **7**, and its electronic structure is consistent with our assignment that chromium is in the +II oxidation state and the diimine ligand is reduced to a ligand-centered radical resulting in a $S = {}^3/_2$ ground state (see the Supporting Information).

An alkyl migration and subsequent hydride shift in **7′** would furnish **7′′** (see Figure 9). Single-point calculations of geometry-optimized structures of the $S = {}^5/_2$, ${}^3/_2$, and ${}^1/_2$ spin-state possibilities for **7′′** showed the quartet ($S = {}^3/_2$) to be most stable. Complex ^{4}**7′′** shows ligand bond lengths that are in accord with an iminoamide-type structure with unsaturation at the alkyl-substituted carbon position. Not only does this formulation result in an apparent reduction of the metal to Cr^{I}, a relatively unstable oxidation state for Cr, but most importantly, ^{4}**7′′** is calculated to be approximately 42 kcal mol^{-1} less stable than **7′**. In silico oxidation of **7′** to **8′** results in oxidation of the ligand-centered radical and formation of a high-spin diimine complex of Cr^{II} (d^4, $S = 2$). This spin state was found to be lower in energy than the corresponding triplet and singlet states. Complex ^{5}**8′** has bond lengths that are in accord with a neutral diimine ligand, that is, C–N distances of 1.2986 and 1.2964 Å and a C–C distance of 1.4617 Å. Furthermore, the Cr–O_{THF} and Cr–CH_3 bond lengths are shorter than those in **7′** due to the increase in formal charge on Cr. The calculation on the migratory insertion product of **8′**, namely **8′′**, produced metric parameters for the diimine ligand that are essentially identical to those in **7′′**; thus the ligand is clearly an iminoamide ligand. Like **8′**, complex **8′′** is also calculated to be a quintet ($S = 2$) Cr^{II} complex, this spin state being lower in energy than the $S = 1$ and $S = 0$ spin states. Unlike the **7′** to **7′′** rearrangement, the **8′** to **8′′** transformation is calculated to be energetically favorable by approximately 10 kcal mol^{-1}. These calculations are wholly consistent with our experimental observations, and they suggest that cationic alkyl-Cr^{II} complexes are subject to facile migratory insertions of unsaturated molecules into the chromium–carbon bond, at least in an intramolecular fashion.

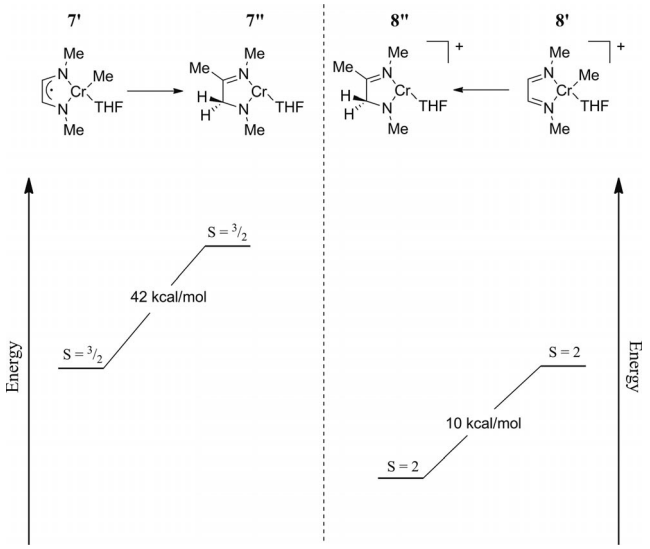

Figure 9. Relevant energies (not to scale), structures, and spin states for model complexes **7′**, **7′′**, **8′**, and **8′′**.

Conclusion

Several open-shell organometallic derivatives of chromium supported by a redox noninnocent diimine ligand have been prepared. These compounds feature reduced diimine ligands, with the extent of electron transfer depending on the particular compound. As the metal – which is only formally in the Cr^{I} oxidation state – finds itself in a more

 © 2012 Wiley-VCH Verlag GmbH & Co. KGaA, Weinheim

and more electron-rich coordination environment (i.e., the more alkyl ligands it has and the more negatively charged it is), the diimine radical anion accommodates the extra electron density to the point where it oxidizes even Cr^{II}, resulting in a formal Cr^{III}/enediamide pairing. Furthermore, we have shown that alkyl chromate and neutral organochromium complexes resist alkyl migration to the ligand, perhaps due to the reduced nature of the latter. However, upon oxidation to cationic alkyls, which feature neutral diimine ligands, migratory insertion of the C=N double bond into the metal–carbon bond becomes favorable and indeed facile. This suggests that organometallic diimine complexes of early transition metals will be most stable in the presence of appreciably reduced diimine ligands.

While α-diimines make excellent ancillary ligands for homogeneous olefin polymerization catalysts containing late-transition metals,[17] we anticipate that they will be less than "ancillary" when coordinated to metals on the left side of the periodic table.

Experimental Section

General: All manipulations were carried out with standard Schlenk, vacuum line, and glovebox techniques. Pentane, diethyl ether, and tetrahydrofuran were dried by passing the solvent through a column of activated alumina and sparging with N_2 to remove residual O_2 prior to use. [D_8]THF was predried with potassium metal and stored under vacuum over Na/K. C_6D_6 was predried with sodium metal and stored under vacuum over Na/K.

Starting Materials: [(Trimethylsilyl)methyl]lithium was purchased as a 1 M solution in pentane from Aldrich, was crystallized from solution at –30 °C, and was isolated as a white crystalline solid. All other alkyllithium and Gignard reagents were purchased from Aldrich and used as received. The preparations of **1** and [$(C_5H_5)_2$Fe][BARF] have been previously reported.[8]

Instrumentation: ^{1}H NMR spectra were recorded on a Bruker DRX-400 spectrometer and were referenced to the residual protons of the solvent ([D_8]THF, 1.73 and 3.58 ppm; C_6D_6, 7.15 ppm). FTIR spectra were recorded on a Mattson Alpha Centauri spectrometer with a resolution of 4 cm^{-1}. UV/Vis spectra were recorded on a Hewlett–Packard 8453 spectrophotometer. Mass spectroscopic data were collected at the University of Delaware Mass Spectrometry Facility in electron ionization mode (+15 eV), however no chromium containing fragments were detected for any of the complexes. Elemental analyses were performed by Desert Analytics. Room-temperature magnetic susceptibility measurements were carried out using a Johnson Matthey magnetic susceptibility balance. Molar magnetic susceptibilities were corrected for diamagnetism using Pascal constants.

[Li(THF)$_4$][(^{H}L^{iPr})Cr(CH$_2$SiMe$_3$)$_2$] (2): Complex **1** (0.150 g, 0.162 mmol) was dissolved in THF (15 mL) and cooled to –30 °C. $LiCH_2SiMe_3$ (0.061 g, 0.649 mmol) was then added and the solution was stirred at room temp. for 2 h. The THF was removed, and the residue was washed with pentane and extracted into Et_2O. The Et_2O was then removed to give analytically pure **2** in 72% yield (0.209 g). Green crystalline samples of **2** can be prepared by cooling a concentrated solution to –30 °C overnight. M.p. 110 °C (decomp.). ^{1}H NMR ([D_8]THF): δ = 15.5 (2 H, aromatic), 4.70 (24 H, *i*Pr), –13.2 (4 H, *i*Pr) ppm. IR (KBr disc): $\tilde{\nu}$ = 3050 (m), 2955 (s), 2928 (s), 2881 (s), 1460 (s), 1435 (s), 1380 (m), 1318 (m), 1250 (m), 1042 (m), 888 (w), 858 (m), 759 (m) cm^{-1}. UV/Vis (THF): λ_{max} (ε, M^{-1}cm^{-1}) = 467 (3674), 569 (2972), 741 (4560) nm. μ_{eff} (294 K) = 3.7(1) μ_B. Elemental analysis consistently gave values that were significantly low in carbon and hydrogen and high in nitrogen. The exact cause is unknown, but could be due to incomplete combustion of the cation/anion pair. Cation exchange with Et_4NCl led to poor solubility causing difficulty in separating the product from LiCl.

[Li(THF)$_2$][(^{H}L^{iPr})Cr(Ph)$_2$] (3b): A sample of **1** (0.195 g, 0.210 mmol) in THF (15 mL) was cooled to –30 °C. 1.8 M LiPh (0.44 mL) was added and the solution warmed to room temp. and stirred for 2 h. The resulting solution was stripped of THF, washed with pentane, and extracted into Et_2O. The ether solution was concentrated and cooled to –30 °C to give brown **3** in 56% yield (0.173 g). M.p. 184 °C (decomp.). ^{1}H NMR ([D_8]THF): δ = 17.0 (16 H, THF), 9.42 (2 H, aromatic), 6.54 (4 H, *i*Pr), 4.34 (24 H, *i*Pr) ppm. IR (KBr disc): $\tilde{\nu}$ = 3042 (m), 3033 (m), 2957 (s), 2925 (s), 2865 (s), 1464 (s), 1432 (s), 1382 (m), 1358 (s), 1318 (m), 1246 (m), 1197 (m), 1109 (w), 1039 (s), 887 (w), 759 (m), 730 (m), 708 (s) cm^{-1}. $C_{46}H_{62}CrLiN_2O_2$ (733.94): calcd. C 75.28, H 8.51, N 3.82; found C 75.36, H 8.38, N 3.50. UV/Vis (THF) λ_{max} (ε, M^{-1}cm^{-1}) = 477 (1007), 557 (841), 871 (450) nm. μ_{eff} (294 K) = 3.7(1) μ_B.

[Li(THF)$_4$][{(^{H}L^{iPr})Cr}$_2$(μ-Me)$_3$] (4): Compound **1** (0.223 g, 0.241 mmol) was placed in THF and cooled to –30 °C. A solution of LiMe (1.6 M, 0.45 mL) was added and the solution was stirred for 2 h at room temp. The solvent was removed from the blue solution, then it was washed with pentane and extracted into Et_2O. The solution was then concentrated and cooled to –30 °C overnight to yield **4** (0.182 g, 63%) as dark blue crystals. M.p. 184 °C (decomp.). ^{1}H NMR ([D_8]THF): δ = 7.47 (2 H, aromatic), 5.50 (4 H, *i*Pr), 1.19 (12 H, *i*Pr), 0.92 (12 H, *i*Pr) ppm. IR (KBr disc): $\tilde{\nu}$ = 3052 (w), 2959 (s), 2925 (m), 2865 (m), 1460 (m), 1437 (m), 1380 (m), 1359 (w), 1320 (m), 1253 (m), 1212 (w), 1105 (w), 1042 (m), 886 (w), 799 (w), 758 (m) cm^{-1}. $C_{71}H_{117}Cr_2LiN_4O_4$ (1201.65): calcd. C 70.97, H 9.81, N 4.66; found C 70.67, H 9.68, N 4.58. UV/Vis (THF): λ_{max} (ε, M^{-1}cm^{-1}) = 491 (3528), 631 (4737), 882 (3683) nm. μ_{eff} (294 K) = 1.4(1) μ_B per Cr.

[Li(THF)$_4$][{(^{H}L^{iPr})Cr}$_2$(μ-H)$_3$] (5): A solution of **1** (0.112 g, 0.121 mmol) in THF was cooled to –30 °C and a solution of $LiBEt_3H$ (0.36 mL, 1.0 M) was added to it. The solution was allowed to stir for 2 h at room temp. resulting in a violet solution. The THF was then removed, the residue was washed with pentane and extracted into Et_2O. The solution was then concentrated and cooled to –30 °C overnight to yield **5** (0.107 g, 77%) as dark violet crystals. M.p. 164 °C (decomp.).^{1}H NMR ([D_8]THF): δ = 7.76 (2 H, aromatic), 4.07 (4 H, *i*Pr), 1.88 (24 H, *i*Pr) ppm. IR (KBr disc): $\tilde{\nu}$ = 3048 (w), 2954 (s), 2928 (m), 2861 (m), 1460 (m), 1438 (m), 1375 (m), 1347 (w), 1320 (m), 1254 (m), 1210 (w), 1107 (w), 1080 (m), 1053 (m), 1037 (m), 756 (m) cm^{-1}. $C_{60}H_{95}Cr_2N_5$ {after [Li(THF)$_4$]$^+$ for [Et$_4$N]$^+$ exchange} (990.43): calcd. C 72.76, H 9.67, N 7.07; found C 72.31, H 9.59, N 7.28. UV/Vis (THF): λ_{max} (ε, M^{-1}cm^{-1})]: 490 (4332), 631 (3931), 816 (4042) nm. μ_{eff} (294 K) = 1.5(1) μ_B per Cr.

[Li$_2$(THF)$_3$][(^{H}L^{iPr})CrMe$_3$] (6): A solution of LiMe (1.6 M, 0.83 mL) was added to a –30 °C solution of **1** (0.176 g, 0.190 mmol) in THF (10 mL). The resulting red solution was allowed to stir at room temp. for 1 h. The solvent was then removed and the crude material was dissolved in Et_2O and filtered. The Et_2O was removed and the crude red material was dissolved in pentane and crystallized overnight at –30 °C to give a 81% yield of **6** (0.267 g) as red needles. M.p. 121 °C (decomp.). ^{1}H NMR ([D_8]THF): δ = 9.12 (8 H, THF), 3.91 (24 H, *i*Pr), 2.71 (8 H, THF) ppm. IR (KBr disc):

 © 2012 Wiley-VCH Verlag GmbH & Co. KGaA, Weinheim

$\tilde{\nu}$ = 3048 (w), 2958 (s), 2928 (m), 2864 (m), 1458 (m), 1435 (s), 1379 (w), 1353 (m), 1315 (m), 1248 (s), 1202 (m), 1104 (m), 1076 (m), 1041 (s), 890 (w), 759 (m) cm^{-1}. UV/Vis (THF): λ_{max} (ε, $M^{-1}cm^{-1}$) = 517 (928), 669 (334), 845 (449) nm. μ_{eff} (294 K) = 3.8(1) μ_B. Elemental analysis consistently resulted in values that were low in carbon and hydrogen content and high in nitrogen content. Upon cation exchange with an excess amount of Et_4NCl in THF, the solution turned blue and the anion of complex **4** was identified as the only product by ^1H NMR spectroscopy.

[(^{H}L^{iPr})Cr(CH_2SiMe_3)(THF)] (7): Compounds **1** (0.067 g, 0.072 mmol) and **2** (0.130 g, 0.145 mmol) were added to pentane (20 mL). The slurry was allowed to stir at room temp. overnight. The solvent was then removed and the residue was extracted with pentane, concentrated, and cooled to –30 °C overnight to give green **7** (0.169 g, 59% yield). M.p. 116 °C (decomp.).^1H NMR ([D_8]THF): δ = 19.5 (2 H, aromatic), 11.6 (9 H, $SiMe_3$), 2.15 (24 H, THF), –23.2 (4 H, *i*Pr) ppm. IR (KBr disc): $\tilde{\nu}$ = 3054 (w), 2957 (s), 2928 (s), 2865 (m), 1456 (m), 1439 (s), 1383 (w), 1360 (w), 1320 (m), 1254 (s), 1222 (w), 1102 (w), 860 (m), 800 (w), 757 (s) cm^{-1}. $C_{34}H_{55}CrN_2OSi$ (587.90): calcd. C 69.46, H 9.43, N 4.77; found C 69.56, H 9.59, N 5.05. UV/Vis (THF): λ_{max} (ε, $M^{-1}cm^{-1}$) = 499 (2672), 643 (2835) nm. μ_{eff} (294 K) = 3.8(1) μ_B.

[{(^{H}L^{iPr})Cr(μ-Me)}$_2$] (8): Pentane (25 mL) was added to **6** (0.155 g, 0.220 mmol) and **1** (0.208 g, 0.224 mmol). The slurry was allowed to stir at room temp. overnight. The solvent was removed from the resulting green solution and extracted with pentane, concentrated, and cooled to –30 °C overnight to give **8** (0.152 g, 52% yield). M.p. 162 °C (decomp.). ^1H NMR ([D_8]THF): δ = 14.4 (2 H, aromatic), 2.69 (24 H, *i*Pr), –1.91 (4 H, *i*Pr), –13.1 (6 H, CH_3) ppm. ^1H NMR (C_6D_6): δ = 17.2 (6 H, CH_3), 8.49 (2 H, aromatic), 3.88 (4 H, *i*Pr), 1.64 (24 H, *i*Pr) ppm. IR (KBr disc): $\tilde{\nu}$ = 3059 (w), 2959 (s), 2925 (m), 2866 (w), 1460 (m), 1441 (s), 1422 (m), 1383 (w), 1361 (w), 1323 (m), 1260 (s), 1222 (w), 1100 (w), 798 (w), 758 (s) cm^{-1}. $C_{59}H_{90}Cr_2N_4$ (959.37): calcd. C 73.87, H 9.46, N 5.84; found C 73.23, H 9.06, N 5.85. UV/Vis (pentane): λ_{max} (ε, $M^{-1}cm^{-1}$) = 491 (3421), 615 (1048) nm. μ_{eff} (294 K) = 1.8(1) μ_B per Cr.

[(^{H,TMSM}L*)Cr(THF)(Et_2O)][BARF] (9): Compound **7** (0.113 g, 0.192 mmol) was placed in Et_2O (20 mL). To this was slowly added a solution of [(C_5H_5)$_2$Fe][BARF] (0.200 g, 0.191 mmol) in Et_2O (10 mL). The solution was stirred for 2 h, then the Et_2O was removed, the residue was washed with pentane to remove ferrocene, then crystallized from Et_2O at –30 °C overnight to give **9** (0.120 g, 41% yield). M.p. 112 °C (decomp.). ^1H NMR ([D_8]THF): δ = 22.4 (2 H, aromatic), 7.69 (8 H, BARF), 7.49 (4 H, BARF), 3.76 (24 H, *i*Pr), –5.25 (9 H, $SiMe_3$), –23.1 (4 H, *i*Pr) ppm. IR (KBr disc): $\tilde{\nu}$ = 3071 (w), 2968 (m), 2932 (m), 2874 (m), 1610 (m), 1462 (m), 1440 (m), 1356 (s), 1277 (s), 1136 (s), 887 (m), 840 (s), 801 (w), 714 (m), 682 (m), 670 (m) cm^{-1}. $C_{70}H_{76}BCrF_{24}N_2O_2Si$ (1524.23): calcd. C 55.16, H 5.03, N 1.84; found C 55.01, H 4.86, N 2.00. UV/Vis (Et_2O): λ_{max} (ε, $M^{-1}cm^{-1}$) = 496 (748), 614 (350) nm. μ_{eff} (294 K) = 4.0(1) μ_B.

[(^{H,Me}L*)Cr(THF)$_2$][BARF] (10): Compound **8** (0.011 g, 0.012 mmol) and [(C_5H_5)$_2$Fe][BARF] (0.024 g, 0.024 mmol) were placed in a J. Young NMR spectroscopy tube followed by addition of [D_8]THF. The tube was then closed and a ^1H NMR spectrum was recorded. ^1H NMR ([D_8]THF): δ = 22.2 (2 H, aromatic), 7.78 (8 H, BARF), 7.57 (4 H, BARF), –0.41 (24 H, *i*Pr), –22.9 (4 H, *i*Pr) ppm.

Crystallographic Structure Determinations: A summary of the crystal data collection and refinement parameters for compounds **2**–**9** can be found in the Supporting Information. Suitable crystals were selected, mounted with viscous oil, and cooled to 120 K. Data were collected on a Bruker APEX CCD diffractometer using graphite-monochromated Mo-K_α radiation (λ = 0.71073 Å). Unit-cell parameters were obtained from three sets of 20 frames using 0.3° ω scans from different sections of the Ewald sphere. Data sets were corrected for absorption using SADABS multiscan methods.[18] No symmetry higher than triclinic was observed for complexes **5** and **9**. Systematic absences in the diffraction data and unit-cell parameters are consistent with $P2_1/n$ (=$P2_1/c$; no. 14), uniquely, for complexes **2**, **7**, **3**, and **4**; and, *Cc* (no. 9) and *C*2/*c* (no. 15) for complexes **6** and **8**. The centrosymmetric space group options yielded chemically reasonable and computationally stable results of refinement. Structures were solved by direct methods and refined with full-matrix least-squares methods based on F^2. Two symmetry unique but chemically similar molecules are located in the asymmetric unit for complex **7**. The compound molecule is located at a twofold axis in **8**. Four structures display cocrystallized solvent molecules: **2** (0.5 Et_2O); **5** (Et_2O); **8** (0.5 pentane); and **9** (pentane), each per asymmetric unit. Solvent molecules in **8** and **9** were treated as diffused contributions using Squeeze.[19] All non-hydrogen atoms were refined anistropically. All hydrogen atoms were treated as idealized contributions except for the bridging hydrides in **5**, the bridging methyl protons in **4**, **6**, and **7**, and the hydrogen atoms of the methylene C30 in **9**, which were located in difference maps. Located hydrogen atoms were positionally refined but with isotropic parameters constrained to 1.2U_{eq} of the attached carbon atom for the methyl and methylene groups, and of the chromium atoms for the hydrides. All atomic scattering factors are included in the SHELXTL program library.[18]

CCDC-837092 (for **2**), -837093 (for **3**), -837094 (for **4**), -837095 (for **5**), -837096 (for **6**), -837097 (for **7**), -837098 (for **8**), and -837099 (for **9**) contain the supplementary crystallographic data for this paper. These data can be obtained free of charge from The Cambridge Crystallographic Data Centre via www.ccdc.cam.ac.uk/data_request/cif.

Supporting Information (see footnote on the first page of this article): X-ray crystallographic data for complexes **2**–**9**, the details of the DFT calculations of **7′**, **7′′**, **8′**, and **8′′** and the complete citation for the Gaussian 03 software package.

Acknowledgments

We thank the University of Wisconsin-Madison's Chemistry Computer Center for computational assistance. This research was supported by grants from the Nation Science Foundation (NSF) (to K. H. T., grant numbers CHE-0616375 and CHE-0911081).

[1] a) P. J. Chirik, K. Wieghardt, *Science* **2010**, *327*, 794–795; b) D. Astruc, C. Ornelas, J. Ruiz, *Acc. Chem. Res.* **2008**, *41*, 841–856; c) J. L. Boyer, J. Rochford, M. K. Tsai, J. T. Muckerman, E. Fujita, *Coord. Chem. Rev.* **2010**, *254*, 309–330; d) A. K. Das, B. Sarkar, J. Fiedler, S. Zalis, I. Hartenbach, S. Strobel, G. K. Lahiri, W. Kaim, *J. Am. Chem. Soc.* **2009**, *131*, 8895–8902; e) A. Dei, D. Gatteschi, C. Sangregorio, L. Sorace, *Acc. Chem. Res.* **2004**, *37*, 827–835; f) A. Diez, E. Lalinde, M. T. Moreno, S. Sanchez, *Dalton Trans.* **2009**, 3434–3446; g) E. Evangelio, D. Ruiz-Molina, *Eur. J. Inorg. Chem.* **2005**, 2957–2971; h) S. I. Gorelsky, A. B. P. Lever, M. Ebadi, *Coord. Chem. Rev.* **2002**, *230*, 97–105; i) A. B. P. Lever, S. I. Gorelsky, *Struct. and Bonding* **2004**, *107*, 77–114; j) K. A. McNitt, K. Parimal, A. I. Share, A. C. Fahrenbach, E. H. Witlicki, M. Pink, D. K. Bediako, C. L. Plaisier, N. Le, L. P. Heeringa, D. A. V. Griend, A. H. Flood, *J. Am. Chem. Soc.* **2009**, *131*, 1305–1313; k) E. L. Rosen, C. D. Varnado, A. G. Tennyson, D. M. Khramov, J. W.

 © 2012 Wiley-VCH Verlag GmbH & Co. KGaA, Weinheim

Kamplain, D. H. Sung, P. T. Cresswell, V. M. Lynch, C. W. Bielawski, *Organometallics* **2009**, *28*, 6695–6706; l) P. Zanello, M. Corsini, *Coord. Chem. Rev.* **2006**, *250*, 2000–2022.
[2] a) S. C. Bart, K. Chlopek, E. Bill, M. W. Bouwkamp, E. Lobkovsky, F. Neese, K. Wieghardt, P. J. Chirik, *J. Am. Chem. Soc.* **2006**, *128*, 13901–13912; b) C. C. Lu, E. Bill, T. Weyhermuller, E. Bothe, K. Wieghardt, *J. Am. Chem. Soc.* **2008**, *130*, 3181–3197.
[3] a) N. Muresan, K. Chlopek, T. Weyhermüller, F. Neese, K. Wieghardt, *Inorg. Chem.* **2007**, *46*, 5327–5337; b) N. Muresan, T. Weyhermüller, K. Wieghardt, *Dalton Trans.* **2007**, 4390–4398; c) M. Ghosh, T. Weyhermüller, K. Wieghardt, *Dalton Trans.* **2008**, 5149–5151; d) M. Ghosh, S. Sproules, T. Weyhermüller, K. Wieghardt, *Inorg. Chem.* **2008**, *47*, 5963–5970; e) N. Muresan, C. C. Lu, M. Ghosh, J. C. Peters, M. Abe, L. M. Henling, T. Weyhermüller, E. Bill, K. Wieghardt, *Inorg. Chem.* **2008**, *47*, 4579–4590; f) M. M. Khusniyarov, T. Weyhermüller, E. Bill, K. Wieghardt, *J. Am. Chem. Soc.* **2009**, *131*, 1208–1221.
[4] G. Vankoten, K. Vrieze, *Adv. Organomet. Chem.* **1982**, *21*, 151–239.
[5] a) E. Wissing, S. Vanderlinden, E. Rijnberg, J. Boersma, W. J. J. Smeets, A. L. Spek, G. Vankoten, *Organometallics* **1994**, *13*, 2602–2608; b) M. Kaupp, H. Stoll, H. Preuss, W. Kaim, T. Stahl, G. Vankoten, E. Wissing, W. J. J. Smeets, A. L. Spek, *J. Am. Chem. Soc.* **1991**, *113*, 5606–5618; c) E. Wissing, E. Rijnberg, P. A. Vanderschaaf, K. Vangorp, J. Boersma, G. van Koten, *Organometallics* **1994**, *13*, 2609–2615; d) E. Wissing, M. Kaupp, J. Boersma, A. L. Spek, G. Vankoten, *Organometallics* **1994**, *13*, 2349–2356; e) E. Rijnberg, J. Boersma, J. Jastrzebski, M. T. Lakin, A. L. Spek, G. vanKoten, *Organometallics* **1997**, *16*, 3158–3164; f) E. Rijnberg, B. Richter, K. H. Thiele, J. Boersma, N. Veldman, A. L. Spek, G. van Koten, *Inorg. Chem.* **1998**, *37*, 56–63.
[6] a) P. J. Bailey, R. A. Coxall, C. M. Dick, S. Fabre, S. Parsons, L. J. Yellowlees, *Chem. Commun.* **2005**, 4563–4565; b) P. J. Bailey, C. M. Dick, S. Fabre, S. Parsons, L. J. Yellowlees, *Dalton Trans.* **2006**, 1602–1610; c) M. G. Gardiner, G. R. Hanson, M. J. Henderson, F. C. Lee, C. L. Raston, *Inorg. Chem.* **1994**, *33*, 2456–2461.
[7] a) P. De Waele, B. A. Jazdzewski, J. Klosin, R. E. Murray, C. N. Theriault, P. C. Vosejpka, J. L. Petersen, *Organometallics* **2007**, *26*, 3896–3899; b) R. D. J. Froese, B. A. Jazdzewski, J. Klosin, R. L. Kuhlman, C. N. Theriault, D. M. Welsh, K. A. Abboud, *Organometallics* **2011**, *30*, 251–262; c) H. Tsurugi, R. Ohnishi, H. Kaneko, T. K. Panda, K. Mashima, *Organometallics* **2009**, *28*, 680–687; d) H. Kaneko, H. Tsurugi, T. K. Panda, K. Mashima, *Organometallics* **2010**, *29*, 3463–3466; e) K. Mashima, R. Ohnishi, T. Yamagata, H. Tsurugi, *Chem. Lett.* **2007**, *36*, 1420–1421.
[8] K. A. Kreisel, G. P. A. Yap, K. H. Theopold, *Inorg. Chem.* **2008**, *47*, 5293–5303.
[9] a) J. P. Hogan, *J. Polym. Sci. Polym. Chem. Ed.* **1970**, *8*, 2637–2652; b) E. Groppo, C. Lamberti, S. Bordiga, G. Spoto, A. Zecchina, *Chem. Rev.* **2005**, *105*, 115–183.
[10] L. A. MacAdams, G. P. Buffone, C. D. Incarvito, A. L. Rheingold, K. H. Theopold, *J. Am. Chem. Soc.* **2005**, *127*, 1082–1083.
[11] R. L. Carlin, *Magnetochemistry*, Springer, Berlin, **1986**.
[12] C. Janiak, J. Silvestre, K. H. Theopold, *Chem. Ber.* **1993**, *126*, 631–643.
[13] R. Bau, M. H. Drabnis, *Inorg. Chim. Acta* **1997**, *259*, 27–50.
[14] a) R. A. Heintz, B. S. Haggerty, H. Wan, A. L. Rheingold, K. H. Theopold, *Angew. Chem.* **1993**, *105*, 1136; *Angew. Chem. Int. Ed. Engl.* **1992**, *31*, 1077–1079; b) R. A. Heintz, B. S. Haggerty, H. Wan, A. L. Rheingold, K. H. Theopold, *Angew. Chem.* **1992**, *104*, 1100; *Angew. Chem. Int. Ed. Engl.* **1992**, *31*, 1077–1079; c) R. A. Heintz, T. F. Koetzle, R. L. Ostrander, A. L. Rheingold, K. H. Theopold, P. Wu, *Nature* **1995**, *378*, 359–362; d) R. A. Heintz, R. L. Ostrander, A. L. Rheingold, K. H. Theopold, *J. Am. Chem. Soc.* **1994**, *116*, 11387–11396.
[15] X. J. Yang, J. Yu, Y. Y. Liu, Y. M. Xie, H. F. Schaefer, Y. M. Liang, B. Wu, *Chem. Commun.* **2007**, 2363–2365.
[16] K. A. Kreisel, G. P. A. Yap, O. Dmitrenko, C. R. Landis, K. H. Theopold, *J. Am. Chem. Soc.* **2007**, *129*, 14162–14163.
[17] S. D. Ittel, L. K. Johnson, M. Brookhart, *Chem. Rev.* **2000**, *100*, 1169–1203.
[18] G. M. Sheldrick, *Acta Crystallogr., Sect. A* **2008**, *64*, 112–122.
[19] A. L. Spek, *J. Appl. Crystallogr.* **2003**, *36*, 7–13.

Received: August 1, 2011
Published Online: September 27, 2011

 © 2012 Wiley-VCH Verlag GmbH & Co. KGaA, Weinheim

DOI: 10.1002/ejic.201100698

Radical Chemistry of Iminepyridine Ligands

Peter H. M. Budzelaar*[a]

Keywords: N ligands / Imines / Radicals / Electron transfer / Density functional calculations

The reactivity of metal fragments MeLi(THF), Me_2Mg, Me_2Zn and Me_3Al with a variety of imine/pyridine ligands was studied by DFT methods. Ligands having at least two such groups in conjugation very effectively accept an electron from a metal–carbon bonding orbital and thus assist alkyl dissociation: the M–Me dissociation free energy ΔG_d decreases by about 45 kcal/mol for the Li, Mg and Zn fragments, and by 60–70 kcal/mol for Me_3Al. Paths for transfer of an alkyl group to the ligands were also explored. Paths for transfer to ligand carbon atoms were found to have high barriers, and such transfers are instead proposed to proceed via initial M–Me dissociation. Direct alkyl transfer to ligand nitrogen atoms is somewhat easier, and for the most electropositive metal Li such a transfer might compete with radical chemistry. For Dimpy, the most stable products are the C3 and C4 alkylation ones. However, the observed regioselectivity of alkyl transfer (often to N_{py} or C2) does not correlate with product stability and is likely to be a complicated function of radical stability, steric factors and unpaired electron density distribution. The results illustrate that Dimpy and related ligands should be considered strong, reversible oxidants.

Introduction

Amine donors, whether monodentate or multidentate, are typically fairly strong σ-donors with negligible π-acceptor capabilities. Thus, they tend to stabilize metals in medium to high oxidation states. In this respect, pyridine still functions mostly like an ordinary amine donor. As soon as two or three imine/pyridine units are linked together to form a bidentate or terdentate ligand, the resulting extended conjugated π-system becomes a strong π-acceptor, stabilizing metals in unusually low oxidation states. Anomalous chemistry of main-group metal alkyl complexes of α-diimine and imine-pyridine ligands was already noted in the early 1980's,[1] and was attributed to easy generation of alkyl free radicals and ligand radical anions.[2] Detailed studies suggested the possibility of more complicated mechanisms also involving electron transfer reactions.[3]

More recently, both main group metal and transition metal complexes of the Dimpy ligand have been studied extensively,[4] and here too radical chemistry seems to be a recurring theme.[5] Free radical chemistry has also been suggested to be involved in the *N*-alkylation of Dimpy ligands by lithium, magnesium and zinc alkyls.[6] However, in an early study of the reaction of MeLi with Dimpy, we found that alkyl transfer to N is easy and can be described without invoking free radicals.[7] In the present work, we report a systematic computational (DFT: b3-lyp) study of the main group metal alkyl fragments MeLi(THF), Me_2Mg, Me_2Zn and Me_3Al reacting with a series of π-acceptor ligands (Scheme 1); selected reactions with related ligands are included for comparison. The results shed light on the competing formation of free radicals (via one-electron transfer to the ligand) and "regular" alkyl transfer to nitrogen, and explain the dependence of both reactions on the choice of metal and ligand.

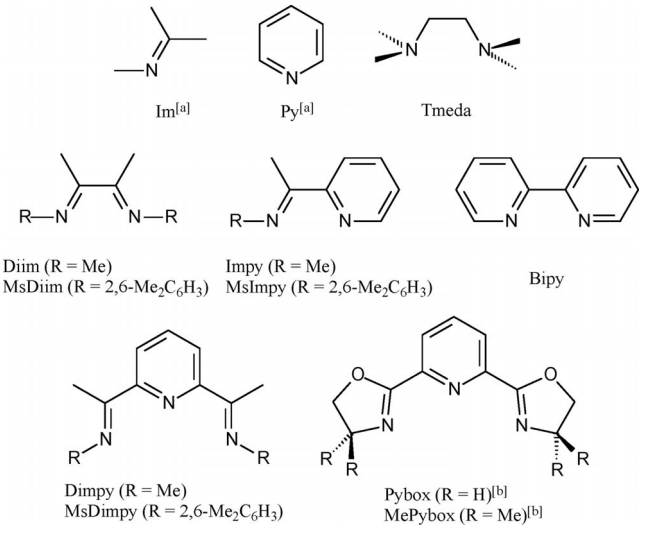

Scheme 1. Ligands studied. [a] Only with Me_3Al. [b] Only with Me_2Zn.

[a] Department of Chemistry, University of Manitoba, Winnipeg, MB R3T 2N2, Canada
Fax: +1-204 474 7608
E-mail: Peter_Budzelaar@umanitoba.ca

Supporting information for this article is available on the WWW under http://dx.doi.org/10.1002/ejic.201100698 or from the author.

© 2012 Wiley-VCH Verlag GmbH & Co. KGaA, Weinheim

Results and Discussion

Stabilization of Low Oxidation States – Loss of Alkyl

Table 1 shows calculated free energy changes for the loss of alkyl radicals from metal alkyl fragments and their complexes. The absolute M–C dissociation energies are not likely to be very accurate, since absolute dissociation energies are in general hard to predict with high accuracy. However, the numbers do not seem to depend much on the choice of functional (b-p values for Me_3Al and its Tmeda and Dimpy complexes are included in the Table), providing some confidence in the numbers. Also, relative values for the different ligands should still be meaningful. Inspection of the Table shows that homolytic cleavage of the M–alkyl bond in uncomplexed metal–alkyl fragments is highly endergonic, varying from +46 kcal/mol for MeLi(THF) to +72 kcal/mol for Me_3Al. Coordination of the pure σ-donor amine ligand TMEDA does not assist this dissociation at all. Simple mono-imine and mono-pyridine ligands stabilize the Me_2Al fragment by about 10 kcal/mol. However, coordination of any of the conjugated C/N ligands studied here reduces the dissociation energy drastically, by about 45 kcal/mol for MeLi(THF), Me_2Mg and Me_2Zn, and by around 60–70 kcal/mol for Me_3Al. The weakening of the M–C bond is so extreme that loss of alkyl becomes accessible as a reaction step at or around room temperature.

Table 1. Net M–Me bond dissociation free energies (ΔG_d) and barriers for Me transfer to pyridine/imine N ($\Delta G^‡$) in kcal/mol.[a]

Ligand	MeLi(THF)		Me_2Mg		Me_2Zn		Me_3Al	
	ΔG_d	$\Delta G^‡$	ΔG_d	$\Delta G^‡$	ΔG_d	$\Delta G^‡$	ΔG_d	$\Delta G^‡$
(none)	46.3		52.4		61.1		71.5 (71.0[c])	
Tmeda	49.5		59.0		60.3		73.8 (72.3[c])	
Im							60.2	77.6
Py							59.3	77.0
Diim	5.4	9.4	14.7	21.4	17.5	26.2	2.0	22.5
MsDiim	–1.1	14.6	10.2	28.9	13.0	34.2	4.7	43.4
Impy	6.1	18.5	18.7	32.3	21.8	37.2	7.9	27.4
MsImpy	3.3	16.4	16.7	31.3	20.0	35.7	7.7	32.7
Bipy	8.1	20.7	22.8	37.3	25.6	42.3	11.1	34.0
Dimpy	2.5[b]	11.3	11.3	19.8	17.3	28.8	–0.1 (–2.0[c])	18.2 (9.1[c])
MsDimpy	–3.6	5.9	6.9	16.1	13.7	25.7	16.1	32.7
Pybox					23.6	33.6		
MePybox					23.9	33.9		

[a] Relative to the coordination complex. [b] Using broken-symmetry solution for (Dimpy)Li(Me)(THF). [c] Calculated using the b-p functional for comparison.

Imine groups seem to be more effective than pyridines in assisting M–Me dissociation (by about 3 kcal/mol). Interestingly, the central pyridine ring in Dimpy does not appear to play a large role in this respect (other than to allow conjugation between the two terminal imine groups), since the M–C bond weakening by Dimpy is not much larger than that by the simpler Diim ligand. It should be noted here that the preferred ligand coordination mode is in most cases different for the original metal alkyl and its alkyl dissociation product. For example, Dimpy coordinates in monodentate fashion to Me_3Al but binds κ^3 to the Me_2Al fragment. In all cases, the low-valent metal fragment formed by loss of alkyl transfers its "extra" electron to a π*-orbital of the ligand. Thus, loss of alkyl does not result in metal reduction but instead reduces the ligand. Put differently, the ligand is a strong enough oxidant to oxidize the relatively high-energy M–C bond.

For most of the metal alkyl complexes studied, loss of alkyl does not have a barrier: on increasing one M–C distance, the energy increases monotonically to the dissociation limit. For short M–Me distances, a closed-shell configuration is preferred, but on stretching the bond the wavefunction switches to a broken-symmetry solution at some point, with significant transfer of electron density from the M–Me σ-bond to the ligand π* LUMO. One exception to this general trend is (Dimpy)LiMe(THF), where already at the equilibrium structure a slightly broken-symmetry solution ($<S^2>$ = 0.11) is preferred. The various Me_3Al complexes form a different kind of exception: they appear to have an actual barrier associated with M–C dissociation. The dissociation product has a higher ligand hapticity than the starting Me_3Al complex, and in some cases a barrier is found where an incoming nitrogen donor atom of the ligand "displaces" the metal-bound alkyl. However, the various transition states are only a few kcal/mol higher in energy than the final dissociation products, and some barrierless paths were also found for different initial arrangements of the alkyl group and nitrogen donors. For complexes of Dimpy with the other three metal fragments, hapticity also increases on Me dissociation, but this does not result in a barrier.

In all cases considered, loss of alkyl radical is endothermic, but the entropy gain on Me radical dissociation makes the reaction nearly neutral in free energy for some cases (e.g., Dimpy/Me_3Al). The energy of M–Me bond cleavage increases in the order MeLi(THF) < Me_2Mg < Me_2Zn: more electropositive metals have the higher-energy M–C bonding orbitals and hence constitute the most favourable situation for electron transfer from this bond to the ligand π* orbital. Interestingly, some of the Me_3Al complexes do not follow this trend and actually have net M–Me dissociation free energies rather similar to the MeLi(THF) complexes. It should be noted that for Al these "dissociations" are accompanied by a compensating change in ligand hapticity from η^1 to η^2 (Diim, Impy, Bipy) or η^3 (Dimpy). Replacement of methyl groups at ligand imine functionalities by the more realistic 2,6-dimethylphenyl groups reduces the donor strength of the ligands somewhat (1–5 kcal/mol). The effect of aryl introduction on the ease of alkyl radical loss also appears to be small (0–6 kcal/mol), except for (MsDimpy)$AlMe_3$ where Me loss is about 16 kcal/mol more difficult than for the parent Dimpy ligand.

Ligand Alkylation Reactions

Reaction of imine/pyridine ligands with metal alkyls often results in alkylation of the ligand skeleton. For Dimpy

 © 2012 Wiley-VCH Verlag GmbH & Co. KGaA, Weinheim

ligands, alkylation at nearly every position of the ligand skeleton (Scheme 2) has been observed, the sole exception being the imine nitrogen (presumably for steric reasons: virtually all Dimpy ligands studied so far have bulky groups at the imine nitrogens). The calculated product stability (Table 2; see Figure 1 for calculated geometries of $AlMe_3$ adducts) seems to be governed by the location of the negative charge on the mono-alkylated ligand anion. Structures with the negative charge delocalized over the extended π-system (positions 3 and 4) are preferred to those where alkylation has interrupted the conjugation (positions 2, iC). Alkylation at N and C2, which introduces strain in the ligand skeleton, is less favourable. With xylyl groups at the imine nitrogens, alkylation at iN becomes difficult because the xylyl groups are forced towards the central ring (see Figure 1). Alkylation at the pyridine N by Me_3Al seems to be particularly unfavourable (compared to other alkylation positions), most likely again for steric reasons.

Table 2. Stabilities of Dimpy alkylation products (Δ*G*, kcal/mol).[a]

Ligand	Pos.	MeLi(THF)	Me_2Mg	Me_2Zn	Me_3Al
Dimpy	iN	–18.7	–5.5	–1.6	–13.8
	iC	–19.9	–8.6	–6.1	–19.3
	N	–19.3	–5.6	–0.9	–7.4
	2	–17.9	–6.1	–3.1	–18.8
	3	–28.4	–14.3	–8.4	–26.5
	4	–25.3	–15.8	–10.5	–28.9
MsDimpy	iN	–10.2	–5.9	7.0	20.8
	iC	–19.3	–17.7	–4.1	–1.6
	N	–20.9	–18.8	–1.2	11.1
	2	–18.3	–19.5	–4.3	–2.0
	3	–32.6	–29.6	–10.7	–9.9
	4	–27.5	–29.7	–14.2	–12.7

[a] Relative to the coordination complex.

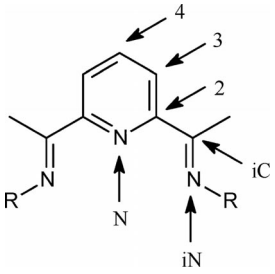

Scheme 2. Labelling of Dimpy alkylation positions.

In some cases, alkylation appears to be reversible, with a less favourable product rearranging on heating to a more favourable product. So far, no explanation has been given for the initial selectivities observed with various metal alkyl fragments, although it seems clear that steric factors play a significant role. In particular, there is no correlation of selectivity with product stability. The C3 and C4 adducts

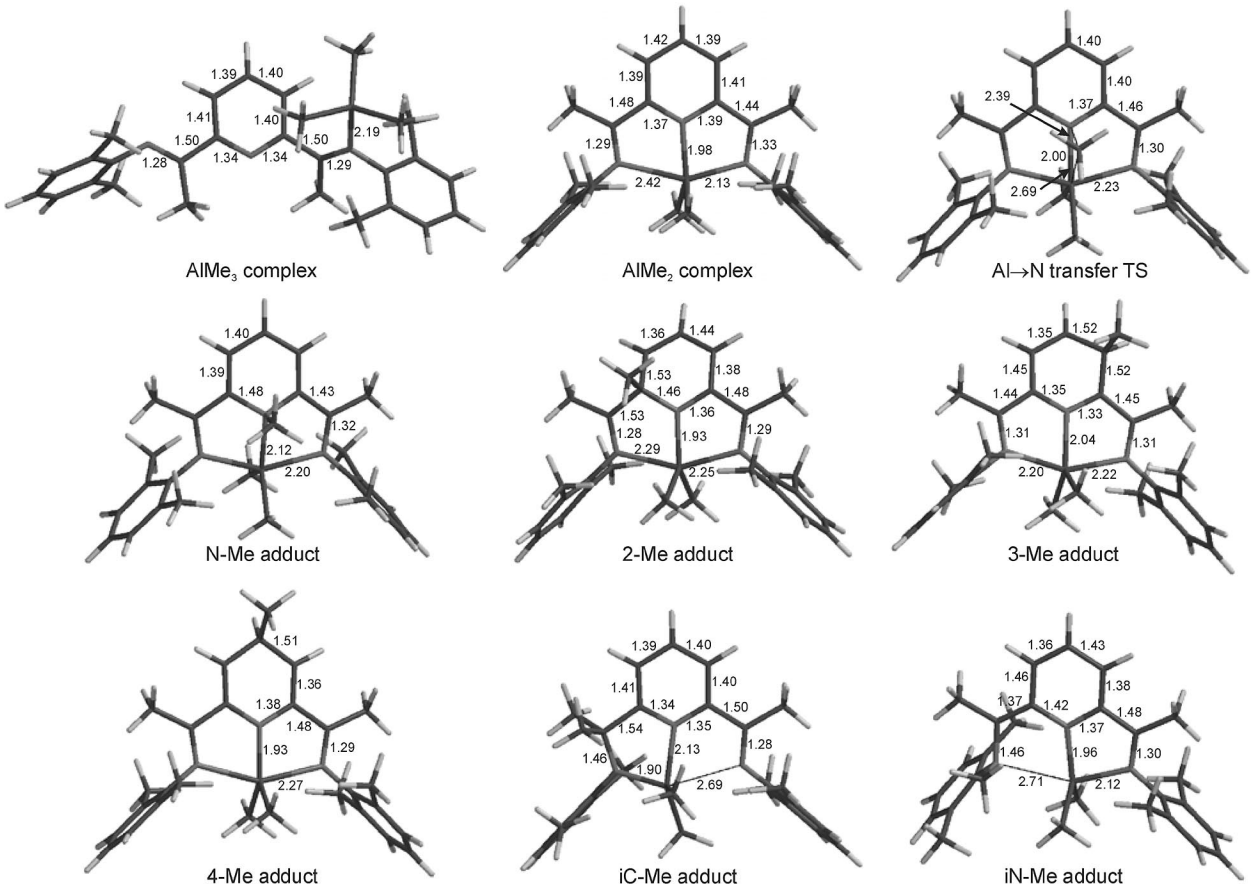

Figure 1. Geometries of relevant species in the reaction of MsDimpy with $AlMe_3$. Bond lengths [b3-lyp/SV(P)] in Å.

 © 2012 Wiley-VCH Verlag GmbH & Co. KGaA, Weinheim

are usually similar in energy and much more stable than any of the other adducts, but so far C3 addition has only been observed in two rather exceptional cases (Ca,[8] V[9]). In contrast, the much less stable C2-alkylation product seems to form easily, and the pyridine *N*-alkylation product has been observed for Li, Mg and Zn.[6,7] Rearrangement on heating does seem to follow the calculated product stabilities in the sense that for all cases reported so far, the rearranged product is calculated to be lower in energy than the initial product.

We have searched extensively for plausible reaction paths leading to the various Dimpy alkylation products. So far, the only reaction that can follow a simple alkyl transfer mechanism is, surprisingly, transfer to the pyridine nitrogen. This has a rather low barrier for Li, but the barrier becomes higher for less electropositive metals like Zn (relevant barriers are included in Table 1). Interestingly, this transfer does not involve an biradical-like transition state: even with the MeLi(THF) fragment, where a broken-symmetry solution is preferred for the simple coordination complex (Dimpy)Li(Me)(THF), the transition state for *N*-alkylation is purely closed-shell. In all cases considered, the calculated free-energy barrier for Me transfer to N is higher than the Me radical dissociation energy, typically by at least 10 kcal/mol. Therefore, it seems likely that even alkyl transfer to N will in most cases involve a radical mechanism; only for the very electropositive metal Li are the two paths close enough in energy to leave some room for doubt.

For all other alkylations, including those at the imine carbon or pyridine C2, transition state searches for intramolecular transfer led to unreasonably high barriers and to geometries that contain a virtually dissociated alkyl group. More complicated mechanisms involving a second metal alkyl fragment were also investigated. Polar mechanisms [e.g. via (Dimpy)$AlMe_2^+$ Me_4Al^-] show low barriers for transfer of a methyl group from anion to cation, but the energy cost of forming such ion pairs in the first place is high. Also, the calculated selectivity for this type of transfer does not agree with experiment but instead mostly follows product stability. Bridged bimetallic structures with concerted alkyl transfers also did not result in acceptable mechanisms.

Finally, sequential alkyl migration along the ligand skeleton was ruled out: this, too, results in nearly complete dissociation of the alkyl at the "transition states", which are again higher in energy than the simple Me radical dissociation product. In the end, we believe the most reasonable explanation of the observed reactivity is that all alkyl transfers *except possibly to the pyridine nitrogen* involve free radicals. An alkyl radical first dissociates from the metal, and then attacks the ligand radical anion formed at the same time. There seems to be no significant enthalpic barrier for attack at any position of the ligand except the sterically protected imine nitrogen. Selectivity would be determined by distance of the target atom from the metal center, by steric factors (e.g. protection of the iN and iC positions by a 2,6-disubstituted aryl group), and by distribution of unpaired electron density over the ligand radical anion. Figure 2 shows the SOMO of (Dimpy)$AlMe_2$: the electron density is largest on N, iC, C2 and C4, but rather low on C3, suggesting that an approaching radical might have a lower tendency to attack at C3.

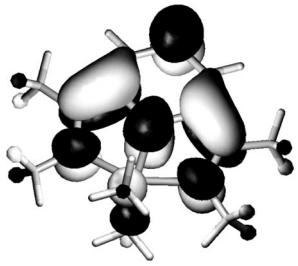

Figure 2. SOMO of (Dimpy)$AlMe_2$.

Further rearrangement on heating would be due to reversibility of the C–C coupling, with no need for the alkyl to first migrate back to the metal. The pyridine *N*-alkylation product could directly dissociate an alkyl radical, or first transfer back to the metal (these two options are close in energy). Once a stable C3 or C4 adduct has formed, alkyl dissociation is no longer thermally accessible.

Conclusions

Metal alkyl complexes of imine/pyridine ligands easily undergo electron transfer from an M–C bond to the ligand and concomitant loss of an alkyl radical; the radical may then be simply lost, but more often it alkylates the ligand at various positions. The reasons for the observed selectivity dependence on metal and alkyl are not completely clear yet but most likely involve steric factors as well as unpaired electron density distribution over the ligand.

Alkyl transfer to the pyridine nitrogen atom seems to be the only alkylation reaction that *might* sometimes happen via a path not involving free radicals. The balance between this reaction and radical loss is a rather subtle one and depends on the choice of metal alkyl, with the more electropositive metals more easily undergoing *N*-alkylation. Alkylation at any position of the pyridine ring involves loss of aromaticity of the ligand. Alkylation at N and C2 is not highly exothermic and can therefore be reversed, leading to isomerization of some alkylation products at higher temperatures. Dimerization of the C4 alkylation product constitutes a thermodynamic sink.[10]

The results described here should apply equally to transition metal complexes. The Dimpy ligand has been amply demonstrated to stabilize low-valent transition metal complexes via intramolecular transfer of 1–3 electrons. Loss of alkyl radicals could lead to the same types of ligand alkylation as observed for main group metals. One significant difference is that a transition metal could significantly affect the unpaired electron distribution over the ligand. The Dimpy ligand has two π* orbitals of nearly equal energy but different symmetry. Antiferromagnetic coupling of an unpaired electron at the metal with an electron in a π* orbital would result in much lower unpaired electron density

 © 2012 Wiley-VCH Verlag GmbH & Co. KGaA, Weinheim

at the ligand for that π* orbital; this might explain the lack of ligand alkylation upon loss of an alkyl radical from (Dimpy)CoR_2.[11]

Experimental Section

General: All calculations used the program Turbomole[12] in combination with the external Baker optimizer.[13] All geometries were initially fully optimized at the b3-lyp[14]/SV(P)[15] level. All basic systems (containing Diim, Impy, Bipy and Dimpy ligands) were then reoptimized at the b3-lyp/TZVP[16] level. For the 2,6-dimethylphenyl-substituted systems, TZVP-level re-optimization was not feasible. Instead, final-energy changes resulting from the SV(P) to TZVP re-optimization for the small (N-Me) systems were added as correction to the large (N-2,6-$Me_2C_6H_3$) systems. Vibrational analyses (analytical second derivatives) were carried out to check the nature of all stationary points (minima or transition states), and to calculate thermal corrections (enthalpy and entropy, gas phase, 273 K 1 bar). Since the calculations were not intended to model any specific experiment, no solvent corrections were applied, but entropies were scaled by a factor of 0.67 to represent the effect of reduced freedom in solution.[17] For all systems, improved single-point energies at the optimized geometries were then calculatedat the b3-lyp/TZVPP[18] level. Final free energies were obtained by combining the b3-lyp/TZVPP electronic energy with the enthalpy and scaled entropy values obtained at the b3-lyp/SV(P) or b3-lyp/TZVP levels. For systems where a broken-symmetry solution was found (primarily transition states for breaking the M–C bond), the "true singlet" energy was estimated from the energy of the broken-symmetry solution and the triplet energy evaluated at the same geometry according to ref.[19] (see below).

$$E_s = \frac{2E_{BS} - \langle S_{BS}^2 \rangle E_t}{2 - \langle S_{BS}^2 \rangle}$$

For testing sensitivity to the choice of functional, calculations for Me_3Al and its Tmeda and Dimpy complexes were repeated with the b-p functional[20] in combination with the TZVP and TZVPP basis sets; the results (included in the Supporting Information) were found to be very similar to the b3-lyp results. Orbital plots were generated using molden.[21]

Supporting Information (see footnote on the first page of this article): Tables of total energies, thermal corrections, and coordinates files for all species studied.

Acknowledgments

Financial aid from the Canada Foundation for Innovation and the Manitoba Research and Innovation Fund is gratefully acknowledged.

[1] a) J. T. B. H. Jastrzebski, J. M. Klerks, G. Vankoten, K. Vrieze, *J. Organomet. Chem.* **1981**, *210*, C49–C53; b) G. Vankoten, T. B. H. Jastrzebski, K. Vrieze, *J. Organomet. Chem.* **1983**, *250*, 49–61; c) A. L. Spek, J. T. B. H. Jastrzebski, G. Vankoten, *Acta Crystallogr., Sect. C* **1987**, *43*, 2006–2007.
[2] a) E. Wissing, H. Kleijn, J. Boersma, G. Vankoten, *Recl. Trav. Chim. Pays-Bas* **1993**, *112*, 618–626; b) E. Wissing, S. Vanderlinden, E. Rijnberg, J. Boersma, W. J. J. Smeets, A. L. Spek, G. Vankoten, *Organometallics* **1994**, *13*, 2602–2608; c) E. Wissing, K. Vangorp, J. Boersma, G. Vankoten, *Inorg. Chim. Acta* **1994**, *220*, 55–61.
[3] E. Wissing, M. Kaupp, J. Boersma, A. L. Spek, G. Vankoten, *Organometallics* **1994**, *13*, 2349–2356.
[4] a) V. C. Gibson, C. Redshaw, G. A. Solan, *Chem. Rev.* **2007**, *107*, 1745–1776; b) Q. Knijnenburg, S. Gambarotta, P. H. M. Budzelaar, *Dalton Trans.* **2006**, 5442–5448.
[5] D. Zhu, I. Thapa, I. Korobkov, S. Gambarotta, P. H. Budzelaar, *Inorg. Chem.* **2011**, DOI: 10.1021/ic2002145.
[6] I. J. Blackmore, V. C. Gibson, P. B. Hitchcock, C. W. Rees, D. J. Williams, A. J. P. White, *J. Am. Chem. Soc.* **2005**, *127*, 6012–6020.
[7] I. Khorobkov, S. Gambarotta, G. P. A. Yap, P. H. M. Budzelaar, *Organometallics* **2002**, *21*, 3088–3090.
[8] M. Arrowsmith, M. S. Hill, G. Kociok-Kohn, *Organometallics* **2010**, *29*, 4203–4206.
[9] D. Reardon, F. Conan, S. Gambarotta, G. Yap, Q. Y. Wang, *J. Am. Chem. Soc.* **1999**, *121*, 9318–9325.
[10] a) Q. Knijnenburg, J. M. M. Smits, P. H. M. Budzelaar, *Cr. Chim.* **2004**, *7*, 865–869; b) H. Sugiyama, G. Aharonian, S. Gambarotta, G. P. A. Yap, P. H. M. Budzelaar, *J. Am. Chem. Soc.* **2002**, *124*, 12268–12274.
[11] D. Zhu, F. F. B. J. Janssen, P. H. M. Budzelaar, *Organometallics* **2010**, *29*, 1897–1908.
[12] a) R. Ahlrichs, M. Bär, H.-P. Baron, R. Bauernschmitt, S. Böcker, M. Ehrig, K. Eichkorn, S. Elliott, F. Furche, F. Haase, M. Häser, C. Hättig, H. Horn, C. Huber, U. Huniar, M. Kattannek, A. Köhn, C. Kölmel, M. Kollwitz, K. May, C. Ochsenfeld, H. Ohm, A. Schäfer, U. Schneider, O. Treutler, K. Tsereteli, B. Unterreiner, M. Von Arnim, F. Weigend, P. Weis, H. Weiss, *Turbomole*, 5 ed., Theoretical Chemistry Group, University of Karlsruhe, **2002**; b) O. Treutler, R. Ahlrichs, *J. Chem. Phys.* **1995**, *102*, 346–354.
[13] a) J. Baker, *J. Comput. Chem.* **1986**, *7*, 385–395; b) J. Baker, *PQS*, 2.4 ed., Parallel Quantum Solutions, Fayetteville, AR, **2001**.
[14] a) A. D. Becke, *J. Chem. Phys.* **1993**, *98*, 5648–5652; b) A. D. Becke, *J. Chem. Phys.* **1993**, *98*, 1372–1377; c) C. T. Lee, W. T. Yang, R. G. Parr, *Phys. Rev. B* **1988**, *37*, 785–789.
[15] A. Schafer, H. Horn, R. Ahlrichs, *J. Chem. Phys.* **1992**, *97*, 2571–2577.
[16] A. Schafer, C. Huber, R. Ahlrichs, *J. Chem. Phys.* **1994**, *100*, 5829–5835.
[17] a) R. Raucoules, T. de Bruin, P. Raybaud, C. Adamo, *Organometallics* **2009**, *28*, 5358–5367; b) S. Tobisch, T. Ziegler, *J. Am. Chem. Soc.* **2004**, *126*, 9059–9071.
[18] F. Weigend, F. Furche, R. Ahlrichs, *J. Chem. Phys.* **2003**, *119*, 12753–12762.
[19] a) L. Noodleman, *J. Chem. Phys.* **1981**, *74*, 5737–5743; b) L. Noodleman, C. Y. Peng, D. A. Case, J. M. Mouesca, *Coord. Chem. Rev.* **1995**, *144*, 199–244; c) A. A. Ovchinnikov, J. K. Labanowski, *Phys. Rev. A* **1996**, *53*, 3946–3952; d) C. Adamo, V. Barone, A. Bencini, F. Totti, I. Ciofini, *Inorg. Chem.* **1999**, *38*, 1996–2004.
[20] a) J. P. Perdew, *Phys. Rev. B* **1986**, *33*, 8822–8824; b) A. D. Becke, *Phys. Rev. A* **1988**, *38*, 3098–3100.
[21] G. Schaftenaar, J. H. Noordik, *J. Comput. Aid. Mol. Des.* **2000**, *14*, 123–134.

Received: July 7, 2011
Published Online: September 29, 2011

 © 2012 Wiley-VCH Verlag GmbH & Co. KGaA, Weinheim

DOI: 10.1002/ejic.201100569

Synthesis and Electronic Structure of Reduced Bis(imino)pyridine Manganese Compounds

Sarah K. Russell,[a] Amanda C. Bowman,[b] Emil Lobkovsky,[c] Karl Wieghardt,[b] and Paul J. Chirik*[a]

Keywords: Manganese / Catalysts / Chelates / Redox chemistry / Non-innocent ligands

The synthesis and electronic structure of reduced aryl-substituted bis(imino)pyridine manganese compounds have been explored. Stirring a THF slurry of [(^{iPr}PDI)$MnCl_2$] {^{iPr}PDI = 2,6-(2,6-*i*Pr_2–C_6H_3N=CMe)$_2C_5H_3N$} with excess Na and catalytic (0.5 mol-%) naphthalene furnished the bis(THF) compound [(^{iPr}PDI)$Mn(THF)_2$]. Performing the reduction with excess Na(Hg) in toluene furnished the bis(chelate) manganese compound [(^{iPr}PDI)$_2$Mn]. For both compounds, a combination of EPR spectroscopy, magnetic measurements and metrical parameters determined from X-ray diffraction established high-spin Mn^{II} compounds with reduced, redox-active bis(imino)pyridine ligands. Substitution of the THF ligands with carbon monoxide yielded [(^{iPr}PDI)$Mn(CO)_2$], a low-spin Mn^{I}, d^6 compound with an experimentally observed bis(imino)pyridine-centred radical. Oxidation and reduction of this compound furnished [(^{iPr}PDI)$Mn(CO)_3]^+$ and [(^{iPr}PDI)$Mn(CO)_2]^-$, respectively, and provided a series of three manganese carbonyl compounds over three oxidation states. Elucidation of the electronic structure of these compounds established that oxidation events within the series are ligand- rather than manganese-based, most likely a result of the stable low-spin Mn^{I}, d^6 electron configuration imparted by the strong-field carbonyl ligands.

Introduction

Aryl-substituted bis(imino)pyridine ligands, ^{Ar}PDI [(*Ar*–N=CMe)$_2C_5H_3N$; *Ar* = aryl group], have received renewed attention in first-row transition-metal chemistry because of their relative ease of synthesis,[1] structural modularity[2] and ability to support a range of catalytically active compounds.[3,4] One notable feature of this ligand class is its so-called "redox-activity" or "non-innocence" whereby the conjugated π system of the ligand engages in reversible electron-transfer events with the metal.[5–8] Accordingly, many reduced bis(imino)pyridine metal compounds have formal oxidation states that are deceiving. Prominent among these compounds are first-row metal dinitrogen derivatives and examples are now known for vanadium,[9] chromium,[10] iron,[11] cobalt,[12] nickel[13] and a second-row example, ruthenium.[14] Reduced bis(imino)pyridine manganese examples are a conspicuous absence in this family of compounds and the electronic structure and possible catalytic activity of such species are of interest.

[a] Department of Chemistry, Princeton University, Princeton, New Jersey, 08544 USA
Fax: +1-609-258-6746
E-mail: pchirik@princeton.edu
[b] Max-Planck Institute for Bioinorganic Chemistry, Stiftstrasse 34-46, 45470 Mülheim an der Ruhr, Germany
[c] Department of Chemistry and Chemical Biology, Cornell University, Ithaca, New York, 14853 USA

Early investigations into the electronic structure of bis(imino)pyridine manganese compounds were pioneered by Wieghardt and coworkers.[8] A one-electron reduction of the high-spin, Mn^{II} bis(chelate) complex [($^{4-OMe}$PDI)$_2$Mn](PF$_6$)$_2$ {$^{4-OMe}$PDI = 2,6-(4-OMe-C_6H_4N=CMe)$_2C_5H_3N$} to the corresponding monocation resulted in two single-electron reductions of the bis(imino)pyridine chelates and oxidation of the metal to yield the low-spin Mn^{III} compound [($^{4-OMe}$PDI^{1-})$_2Mn^{III}$](PF$_6$). Crystallographic characterization of both compounds has provided reference values for the bond length distortions of a neutral and monoreduced chelate in bis(imino)pyridine manganese chemistry.

The high activity of [(^{iPr}PDI)$FeCl_2$] and [(^{iPr}PDI)$CoCl_2$] {^{iPr}PDI = 2,6-(2,6-*i*Pr_2–C_6H_3N=CMe)$_2C_5H_3N$} when activated with methylaluminoxane (MAO) in olefin polymerization[15,16] prompted a similar evaluation of the corresponding manganese compound. Gambarotta and coworkers synthesized [(^{iPr}PDI)$MnCl_2$] and established its structure as a five-coordinate, pseudo-square-pyramidal compound with a neutral bis(imino)pyridine chelate, similar to the iron and cobalt analogues.[17,18,19] No activity for ethylene polymerization was observed upon activation with MAO, behaviour attributed to the high-spin Mn^{II} (S = 5/2) ground state. Alkyl complexes were also explored and the four-coordinate, distorted-planar methyl complex [(^{iPr}PDI)$MnCH_3$] was synthesized and crystallographically characterized. Performing the alkylation of [(^{iPr}PDI)$MnCl_2$] with $LiCH_2SiMe_3$ yielded an anionic manganese alkyl, [(^{iPr}PDI)-

 © 2012 Wiley-VCH Verlag GmbH & Co. KGaA, Weinheim

$Mn(CH_2SiMe_3)]^-$, along with a bimetallic alkyl complex resulting from C–C coupling of deprotonated imine methyl groups. This reactivity highlights the chemical non-innocence of the bis(imino)pyridine ligand in addition to its redox activity.

Cámpora and coworkers have also explored bis(imino)pyridine manganese alkyl chemistry with the goal of understanding the lack of polymerization activity. Addition of the free bis(imino)pyridine ligand, ^{iPr}PDI, to various Mn^{II} dialkyl precursors resulted in migration of one of the alkyl groups to the *para*-pyridine position of the chelate. This route, following oxidative hydrolysis, provides a convenient synthetic route to 4-alkyl-substituted bis(imino)pyridines.[20] Use of β-silyl-substituted alkyls such as $[CH_2SiMe_3]$ enabled the isolation of a rare bis(imino)pyridine manganese dialkyl complex, $[(^{iPr}PDI)Mn(CH_2SiMe_3)_2]$, which over time in solution underwent migration of one of the alkyl ligands to the *para*-pyridine position of the bis(imino)pyridine, supporting the intermediacy of the manganese dialkyl compounds in the rearrangement process.[21] Synthesis of the pyridine-stabilized bis(imino)pyridine manganese alkyl cation $[(^{iPr}PDI)Mn(CH_2SiMe_3)(py)]^+$ was accomplished by protonation of the corresponding neutral dialkyl. Unlike the analogous bis(imino)pyridine iron[22] and cobalt[23] alkyl cations, the manganese compounds are inactive to ethylene polymerization, again attributed to the $S = 5/2$ ground state.

Bis(imino)pyridine manganese bis(triflato) compounds $[(^{iPr}PDI)Mn(OTf)_2]$ and $[(^{Mes}PDI)Mn(OTf)_2]$ {^{Mes}PDI = 2,6-(2,4,6-Me_3–C_6H_2N=CMe)$_2C_5H_3N$} have been reported by Britovsek and coworkers and explored in oxidation catalysis.[24] Once again, no catalytic turnover was observed, which was attributed to the high-spin d^5 configuration of the Mn^{II} centre.

As part of our continuing efforts in bis(imino)pyridine chemistry with reduced first-row metal ions, the reduction of $[(^{iPr}PDI)MnCl_2]$ was of interest. On the basis of the rich catalytic chemistry observed with $[(^{iPr}PDI)Fe(N_2)_2]$,[11a,11c,25] we sought to prepare a manganese analogue either with dinitrogen or other suitable neutral, labile ligands.[24,26] Given the lack of catalytic activity observed previously with high-spin bis(imino)pyridine manganese(II) complexes, two-electron reduced manganese compounds were targeted. However, we were curious as to whether the redox-active bis(imino)pyridine would prevent formation of low-oxidation state manganese compounds. Here we describe several synthetic strategies for the two-electron reduction of $[(^{iPr}PDI)MnCl_2]$ and elucidation of the electronic structure of the isolated products. Metal- versus bis(imino)pyridine-centred reductions are evaluated as a function of the additional ligands in the coordination sphere of the manganese ion.

Results and Discussion

Our studies commenced with the reduction of $[(^{iPr}PDI)MnCl_2]$ using methods that have proven successful with related iron[11a,11c] and cobalt compounds.[12] Stirring a THF solution of $[(^{iPr}PDI)MnCl_2]$[17] with 2 equiv. of sodium metal and a catalytic quantity of naphthalene (0.05 equiv.) in the presence of 1 atm of dinitrogen for 16 hours furnished a dark brown solid identified as the bis(imino)pyridine manganese bis(THF) compound, $[(^{iPr}PDI)Mn(THF)_2]$, in 61% yield [Equation (1)]. Analysis of the solid by infrared spectroscopy did not reveal any strong bands diagnostic of N_2 coordination.

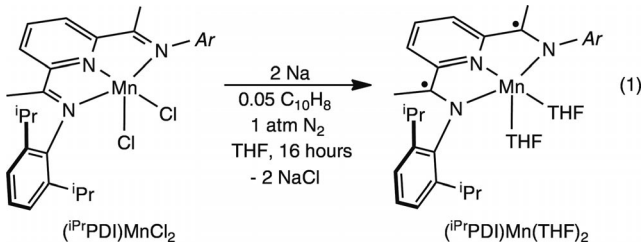

(1)

The ^{1}H NMR spectrum of $[(^{iPr}PDI)Mn(THF)_2]$ recorded in [D_6]benzene at 23 °C proved uninformative; only broad and featureless peaks were observed that were not readily assigned. Routine characterization was accomplished by aqueous degradation and integration of 1 equiv. of free bis(imino)pyridine ligand to a number of equivalents of liberated THF. A consistent ratio of 1:2 bis(imino)pyridine/THF was observed from batch to batch. Repeating the aqueous degradation with D_2O produced no observable ^{2}H NMR signals, confirming that the bis(imino)pyridine remains intact during the reduction procedure.

Single crystals of $[(^{iPr}PDI)Mn(THF)_2]$ suitable for X-ray diffraction were obtained from a concentrated diethyl ether solution stored at –35 °C. A representation of the solid-state structure is presented in Figure 1 and selected bond lengths and angles are reported in Table 1. The overall molecular geometry of the compound is best described as pseudo-square pyramidal with THF molecules occupying both the basal and apical positions. The bond lengths of the bis(imino)pyridine chelate are diagnostic of a two-electron reduction[5,6] with elongated N_{imine}–C_{imine} bond lengths of 1.367(3) and 1.340(3) Å. Accordingly, the C_{ipso}–C_{imine} bond

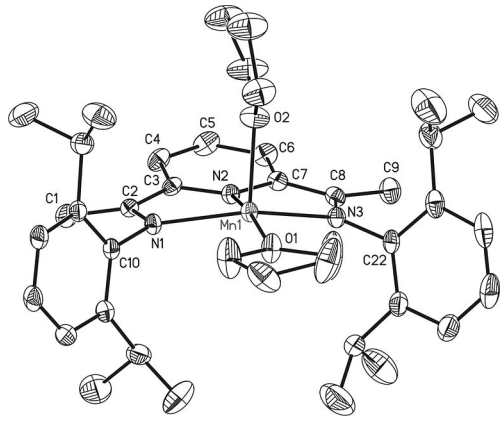

Figure 1. Representation of the solid-state structure of $[(^{iPr}PDI)Mn(THF)_2]$ at 30% probability ellipsoids. Hydrogen atoms are omitted for clarity.

 © 2012 Wiley-VCH Verlag GmbH & Co. KGaA, Weinheim

lengths are shortened to 1.441(3) and 1.421(3) Å. The Mn–N_{imine} distances of 2.1213(15) and 2.1946(15) Å along with the Mn–N_{py} bond length of 2.0514(17) Å are consistent with a high-spin Mn^{II} compound.

Table 1. Selected bond lengths [Å] and angles [°] for [(^{iPr}PDI)Mn(THF)$_2$].

Mn(1)–N(1)	2.1213(15)	N(1)–C(2)	1.367(3)
Mn(1)–N(2)	2.0514(17)	N(3)–C(8)	1.340(3)
Mn(1)–N(3)	2.1946(15)	C(2)–C(3)	1.441(3)
Mn(1)–O(1)	2.1909(15)	C(7)–C(8)	1.421(3)
Mn(1)–O(2)	2.1998(16)	N(2)–C(3)	1.363(2)
		N(2)–C(7)	1.374(2)
N(2)–Mn(1)–N(1)	75.92(6)	O(1)–Mn(1)–O(2)	93.85(6)
N(2)–Mn(1)–N(3)	74.68(6)	N(2)–Mn(1)–O(1)	169.19(7)
N(1)–Mn(1)–N(3)	146.13(6)	N(2)–Mn(1)–O(2)	96.84(7)

The solid-state magnetic moment of [(^{iPr}PDI)Mn(THF)$_2$] was determined by a magnetic susceptibility balance and produced a value of 3.7 μ_B at 23 °C, consistent with an S = 3/2 ground state. The magnetic behaviour of [(^{iPr}PDI)Mn(THF)$_2$] was also studied using SQUID magnetometry. A plot of μ_{eff} vs. temperature is presented in Figure 2. A fit of the data yielded an average g value of 2.10 and E/D = 0.21 and D = 0.61 cm^{-1}.

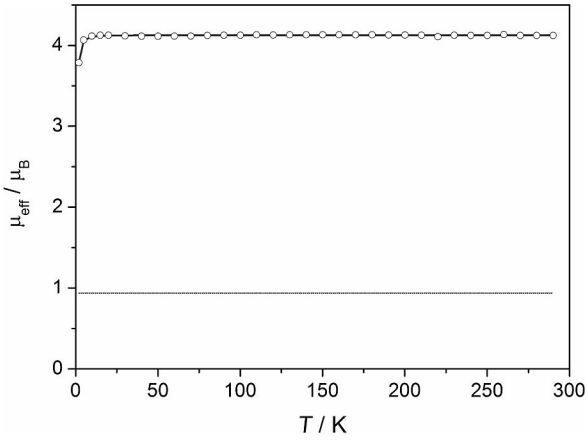

Figure 2. Variable temperature SQUID magnetization data for [(^{iPr}PDI)Mn(THF)$_2$]. Experimental data are represented by the open circles, the simulation is the top curve and the bottom line the paramagnetic impurity (see text). The data are corrected for underlying diamagnetism.

These data, in combination with the metrical parameters determined from X-ray diffraction, suggest that the electronic structure of [(^{iPr}PDI)Mn(THF)$_2$] is best described as a high-spin Mn^{II}, d^5 compound (S_{Mn} = 5/2), antiferromagnetically coupled to a bis(imino)pyridine triplet diradical (S_{PDI} = 1). The toluene/pentane glass (1:1) EPR spectrum of the compound, recorded at 10 K and presented in Figure 3, also supports this electronic structure description. A rhombic signal corresponding to an S = 3/2 compound is observed for the major species, while a second signal is present in small amounts (≈1%) for a second unidentified minor component. Variable amounts of the second minor component were observed in every sample of [(^{iPr}PDI)Mn(THF)$_2$] and was also observed in approximately 2–3% by SQUID magnetometry (Figure 2). A fit of the data for the major component yielded E/D = 0.209 and a small zero-field splitting parameter (D) of 0.604 cm^{-1}, in agreement with the values obtained from SQUID magnetometry. For the major component, the large g-anisotropy is consistent with manganese-centred spins and principally metal-based SOMOs.

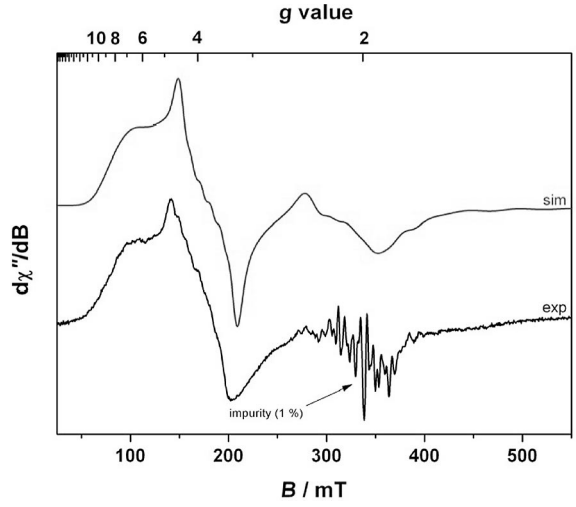

Figure 3. Experimental (bottom) and simulated (top) EPR spectra for [(^{iPr}PDI)Mn(THF)$_2$]. Data collected at 10 K in 1:1 toluene/pentane glass (microwave frequency 9.44 GHz, microwave power 0.32 mW, modulation 25 G). g_x = 2.829, g_y = 2.471, g_z = 2.302; A_{xx} = 176 × 10^{-4} cm^{-1}, A_{yy} = 352 × 10^{-4} cm^{-1}, A_{zz} = 150 × 10^{-4} cm^{-1}; D = 0.61 cm^{-1}, E/D = 0.21.

The catalytic performance of [(^{iPr}PDI)Mn(THF)$_2$] was evaluated in olefin hydrogenation and diene cycloisomerization reactions and compared to the corresponding iron and cobalt dinitrogen compounds.[11a,12b] Attempts to hydrogenate 1-hexene or cyclohexene in the presence of 10 mol-% [(^{iPr}PDI)Mn(THF)$_2$] at both 23 and 65 °C with 4 atm of H_2 produced no turnover. Likewise, α, ω-dienes such as diallyl *tert*-butylamine and diethyl diallyl malonate produced no [2+2] cyclization in the presence of 10 mol-% [(^{iPr}PDI)Mn(THF)$_2$] at 65 °C. The lack of reactivity is probably due to the high-spin Mn^{II} centre in [(^{iPr}PDI)Mn(THF)$_2$].

In an attempt to obviate formation of the bis(THF) manganese complex, the reduction of [(^{iPr}PDI)MnCl$_2$] was carried out in the absence of THF. Stirring a pentane slurry of [(^{iPr}PDI)MnCl$_2$] with an excess of 0.5% Na(Hg) for two days under a dinitrogen atmosphere followed by filtration and recrystallization of the product from diethyl ether at –35 °C resulted in isolation of a red solid identified as [(^{iPr}PDI)$_2$Mn] in 46% yield [Equation (2)].

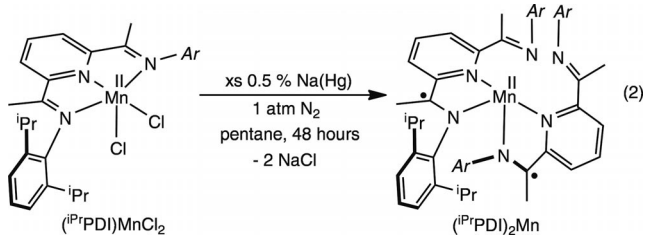

 © 2012 Wiley-VCH Verlag GmbH & Co. KGaA, Weinheim

As with [(^{iPr}PDI)Mn(THF)$_2$], the [D$_6$]benzene ^{1}H NMR spectrum of [(^{iPr}PDI)$_2$Mn] is uninformative exhibiting only broad and featureless resonances. Single crystals suitable for X-ray diffraction were obtained from a concentrated diethyl ether solution at –35 °C and a representation of the solid-state structure is presented in Figure 4. Selected bond lengths and angles are reported in Table 2. The overall molecular geometry is best described as a *cis*-divacant octahedron with pseudo *trans*-imine arms of each bis(imino)pyridine outside the primary coordination sphere of the manganese centre. The presence of two κ^2 rather than traditional κ^3 chelates is likely steric in origin and a consequence of the large 2,6-diisopropyl aryl rings that prevent formation of a six-coordinate idealized octahedral compound. A similar coordination geometry was observed in the bis(chelate) iron compound [(^{Et}PDI)$_2$Fe] {^{Et}PDI = 2,6-(2,6-Et$_2$–C$_6$H$_3$N=CMe)$_2$C$_5$H$_3$N}, while the compound with the smaller aryl substituents, ($^{4–OMe}$PDI)$_2$Fe, is hexacoordinate with two κ^3 chelates.[27]

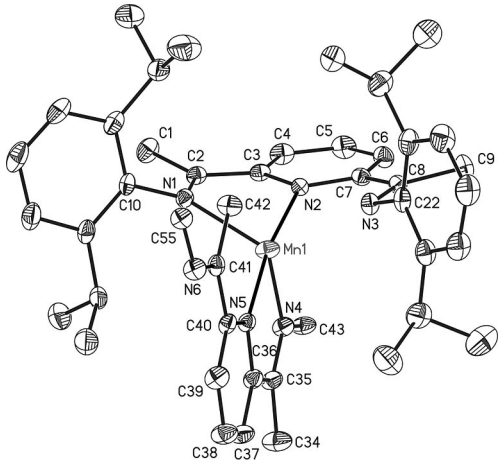

Figure 4. Representation of the solid-state structure of [(^{iPr}PDI)$_2$Mn] at 30% probability ellipsoids. Hydrogen atoms and aryl groups are omitted for clarity.

Table 2. Selected bond lengths [Å] and angles [°] for [(^{iPr}PDI)$_2$Mn].

Mn(1)–N(1)	2.2637(18)	C(2)–C(3)	1.450(3)
Mn(1)–N(2)	2.0320(16)	C(7)–C(8)	1.468(3)
Mn(1)–N(4)	2.1406(19)	N(3)–C(8)	1.298(3)
Mn(1)–N(5)	2.1311(16)	N(6)–C(41)	1.281(3)
N(1)–C(2)	1.324(3)	C(35)–C(36)	1.430(3)
N(4)–C(35)	1.338(4)	C(40)–C(41)	1.489(3)
N(2)–Mn(1)–N(5)	171.05(7)	N(1)–Mn(1)–N(2)	74.33(7)
N(2)–Mn(1)–N(4)	95.26(7)	N(1)–Mn(1)–N(5)	114.13(7)
N(4)–Mn(1)–N(5)	79.40(7)	N(1)–Mn(1)–N(4)	109.11

The metrical parameters of the bis(imino)pyridine chelate are consistent with a one-electron reduction (Table 2). Care must be exercised when interpreting these data and comparing them to compounds with traditional κ^3-bis(imino)pyridines. A more reasonable metrical comparison is to bidentate, redox-active α-iminopyridines.[28] For the portions of the chelates coordinated to the manganese centre, the N_{imine}–C_{imine} bond lengths are slightly elongated to 1.324(3) and 1.338(3) Å while the C_{imine}–C_{ipso} bond lengths are shortened to 1.450(3) and 1.430(3) Å. The free imine arms have N_{imine}–C_{imine} bond lengths of 1.298(3) and 1.281(3) Å, consistent with a neutral ligand.

A magnetic moment of 3.9 μ_B was measured in the solid state (23 °C) for [(^{iPr}PDI)$_2$Mn], consistent with three unpaired electrons and an overall S = 3/2 ground state. SQUID magnetization data were also collected on a polycrystalline sample between 2 and 300 K (Figure 5). At temperatures below 20 K a rise in the effective magnetic moment is observed due to intermolecular ferromagnetic coupling in the solid state. Overall, these interactions are weak as evidenced by the Weiss constant of 0.96 K. At temperatures above 25 K, the value of μ_{eff} plateaus at 3.9 μ_B, consistent with both the value measured on the magnetic susceptibility balance and the spin-only value for three unpaired electrons. Simulation of the data also yielded an average g value of 1.990, a D value of –1.759 cm^{-1} and an E/D value of 0.30.

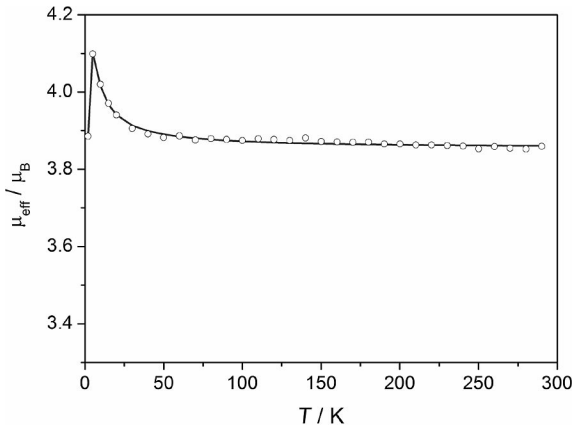

Figure 5. Variable temperature SQUID magnetization data for [(^{iPr}PDI)$_2$Mn]. Experimental data are represented by the open circles; data are corrected for underlying diamagnetism. The simulation is the curve.

The EPR spectrum of the compound, recorded in 1:1 toluene/pentane glass (Figure 6), exhibits a rhombic signal. The observation of large (and relatively isotropic) Mn hyperfine values is consistent with a Mn^{II} centre with principally metal-based SOMOs. On the basis of these data along with the metrical parameters from X-ray diffraction studies, [(^{iPr}PDI)$_2$Mn] is best described as a high-spin Mn^{II} (S_{Mn} = 5/2) compound antiferromagnetically coupled to two bis(imino)pyridine radical anions.

During the synthesis of [(^{iPr}PDI)Mn(THF)$_2$] and [(^{iPr}PDI)$_2$Mn] by a two-electron reduction of [(^{iPr}PDI)MnCl$_2$], an immediate colour change to dark orange-red was observed in both cases, suggesting a common intermediate. On the basis of a precedent from both bis(imino)pyridine iron[11] and cobalt[12] chemistry, [(^{iPr}PDI)MnCl] seemed a likely one-electron reduced intermediate. To test this possibility, an independent synthetic route to the compound was sought. Stirring a THF slurry of [(^{iPr}PDI)MnCl$_2$] with an equimolar quantity of [(^{iPr}PDI)Mn-

 © 2012 Wiley-VCH Verlag GmbH & Co. KGaA, Weinheim

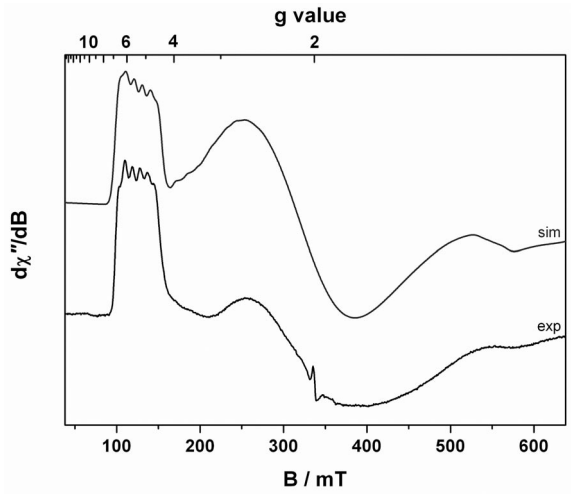

Figure 6. Experimental (bottom) and simulated (top) EPR spectra for [(^{iPr}PDI)$_2$Mn]. Data collected at 10 K in 1:1 toluene/pentane glass. A_{xx} = -85×10^{-4} cm^{-1}, A_{yy} = -78×10^{-4} cm^{-1}, A_{zz} = -92×10^{-4} cm^{-1}; D = –0.5 cm^{-1}, E/D = 0.33; $\sigma(E/D)$ = 0.07.

(THF)$_2$] furnished a dark-red solid identified as [(^{iPr}PDI)-MnCl(THF)] in 91% yield [Equation (3)]. This compound was also isolated from reduction of [(^{iPr}PDI)MnCl$_2$] with sodium metal in the presence of 5 mol-% naphthalene. When using this synthetic route, the reaction was initiated in THF solution to generate $NaC_{10}H_8$ and the solvent was then replaced with diethyl ether to avoid a two-electron reduction to [(^{iPr}PDI)Mn(THF)$_2$]. Even with this precaution, some decomposition and two-electron reduction was observed and thus the comproportionation method is the preferred synthetic route.

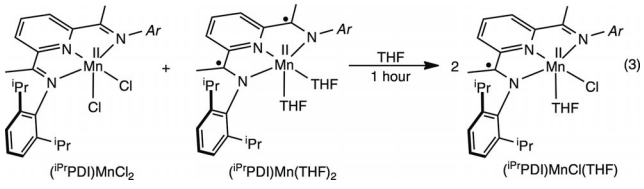

The [D$_6$]benzene ^{1}H NMR spectrum of [(^{iPr}PDI)-MnCl(THF)] at 20 °C exhibits five paramagnetically broadened and shifted resonances between –10 and 50 ppm, which are useful for routine characterization of the compound. Aqueous degradation liberated 1 equiv. of THF per equiv. of free bis(imino)pyridine, confirming THF coordination in bulk samples. Attempts to isolate a THF-free version of the compound by recrystallization from diethyl ether or pentane have been unsuccessful, resulting in the decomposition and isolation of an unidentified, insoluble white powder.

Single crystals of [(^{iPr}PDI)MnCl(THF)] suitable for X-ray diffraction analysis were obtained from layering pentane on to a THF solution of the compound at –35 °C. A representation of the solid-state structure is presented in Figure 7 and selected bond lengths and angles are reported in Table 3. There are two independent molecules in the asymmetric unit each with a crystallographically imposed mirror plane. The values reported in the table reflect the two molecules and the symmetry element. Also included are the corresponding metrical parameters for the related bis(imino)pyridine iron bromide compound [(^{iPr}PDI)-FeBr(THF)].[29] The overall molecular geometry is best described as idealized square pyramidal with the THF ligand occupying the apical position.

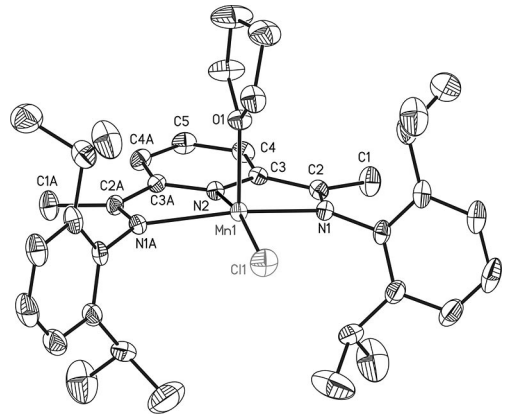

Figure 7. Representation of the solid-state structure of [(^{iPr}PDI)-MnCl(THF)] at 30% probability ellipsoids. Hydrogen atoms are omitted for clarity.

Table 3. Selected bond lengths [Å] and angles [°] for [(^{iPr}PDI)-MnCl(THF)] and [(^{iPr}PDI)FeBr(THF)].

	[(^{iPr}PDI)MnCl(THF)]	[(^{iPr}PDI)FeBr(THF)]
M–N$_{py}$	2.065(2)	2.008(3)
	2.058(2)	
M–N$_{imine}$	2.283(2)	2.172(3)
	2.314(2)	2.150(3)
M–X (X = Cl, Br)	2.293(1)	2.416(1)
	2.298(1)	
N$_{imine}$–C$_{imine}$	1.293(2)	1.299(4)
	1.296(3)	1.306(4)
C$_{ipso}$–C$_{imine}$	1.454(3)	1.446(5)
	1.441(3)	1.433(5)
N$_{py}$–M–O	95.27(8)	92.64(15)
	102.39(9)	
N$_{py}$–M–X	163.12(7)	167.89(9)
	160.63(7)	

The N$_{imine}$–C$_{imine}$ bond lengths of 1.293(2) and 1.296(3) Å are slightly elongated from the corresponding values of 1.273(2) and 1.279(8) Å reported for [(^{iPr}PDI)-MnCl$_2$][17] and fall between the accepted values for a neutral and monoreduced chelate,[5,6] rendering the ligand oxidation state assignment ambiguous. The C$_{imine}$–C$_{ipso}$ distances of 1.454(3) and 1.441(3) Å are a more pronounced distortion and are clearly more consistent with a one-electron bis(imino)pyridine reduction.[5,6] Similar bond perturbations are present in the related iron compound, [(^{iPr}PDI)-FeBr(THF)],[29] where a high-spin ferrous ion was assigned with a monoreduced bis(imino)pyridine chelate. We therefore conclude that [(^{iPr}PDI)MnCl(THF)] also contains a bis(imino)pyridine radical anion that is antiferromagnetically coupled to a high-spin Mn^{II} centre producing an overall S = 2 ground state. The high-spin, d^5 configuration

 © 2012 Wiley-VCH Verlag GmbH & Co. KGaA, Weinheim

is corroborated by the relatively long Mn–N_{py} and Mn–N_{imine} bond lengths (Table 3). Accordingly, a solid-state magnetic moment of 4.6 μ_B was measured at 23 °C, consistent with an $S = 2$ ground state. However, it should be noted that a traditional high-spin Mn^I description with a neutral chelate would also produce a magnetic moment consistent with four unpaired electrons.

Bis(imino)pyridine Manganese Carbonyl Compounds

Reduced bis(imino)pyridine manganese compounds with strong-field organometallic ligands were also explored with the goal of accessing lower metal oxidation and spin states.[30] Addition of 4 atm of carbon monoxide to a toluene solution of [(^{iPr}PDI)Mn(THF)$_2$] followed by solvent removal and subsequent recrystallization from diethyl ether at –35 °C furnished a dark-pink solid identified as [(^{iPr}PDI)Mn(CO)$_2$] in 87% yield [Equation (4)]. The infrared spectrum exhibits two strong bands centred at 1915 and 1860 cm^{-1} in pentane solution. These bands are observed at 1896 and 1836 cm^{-1} in the solid state (KBr pellet). Comparing the pentane values to the corresponding bands for [(^{iPr}PDI)Fe(CO)$_2$] (ν_{CO} = 1974 and 1914 cm^{-1}) establishes a more reducing metal centre in the manganese complex. A summary of all carbonyl stretching frequencies determined by infrared spectroscopy for the compounds in this work is reported in Table 4.

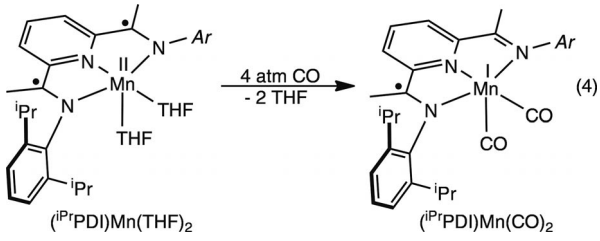

Table 4. Solid-state infrared stretching frequencies [ν(CO)] for bis(imino)pyridine manganese compounds prepared in this work. Data for [(^{iPr}PDI)Fe(CO)$_2$] taken from ref.[11a]

	ν(CO) [cm^{-1}]
[Na(OEt$_2$)$_3$][(^{iPr}PDI)Mn(CO)$_2$]	1806, 1719
[(^{iPr}PDI)Mn(CO)$_2$]	1896, 1836, 1915, 1860[a]
[(^{iPr}PDI)Mn(CO)$_3$][BPh$_4$]	2052, 1967, 1943
[(^{iPr}PDI)Fe(CO)$_2$]	1974, 1914[a]

[a] Recorded in pentane.

The solid-state structure of [(^{iPr}PDI)Mn(CO)$_2$] was determined by X-ray diffraction and is presented in Figure 8 and selected bond lengths and angles are reported in Table 5. The overall molecular geometry is best described as square pyramidal with carbonyl ligands in the apical and one of the basal positions, similar to the geometry of the iron analogue [(^{iPr}PDI)Fe(CO)$_2$]. The Mn–N_{imine} bond lengths of 1.988(1) and 1.996(1) Å and the Mn–N_{py} distance of 1.916(1) Å are significantly shorter than the metal–nitrogen bonds in [(^{iPr}PDI)MnCl$_2$], [(^{iPr}PDI)Mn(THF)$_2$] or [(^{iPr}PDI)$_2$-Mn], suggesting a low-spin state. The N_{imine}–C_{imine} bond lengths of 1.325(2) and 1.321(2) Å are elongated from the neutral chelate and are diagnostic of a monoreduced bis(imino)pyridine radical anion.[5,6] Accordingly, the C_{imine}–C_{ipso} distances of 1.443(2) and 1.445(2) Å also support this ligand oxidation state assignment.

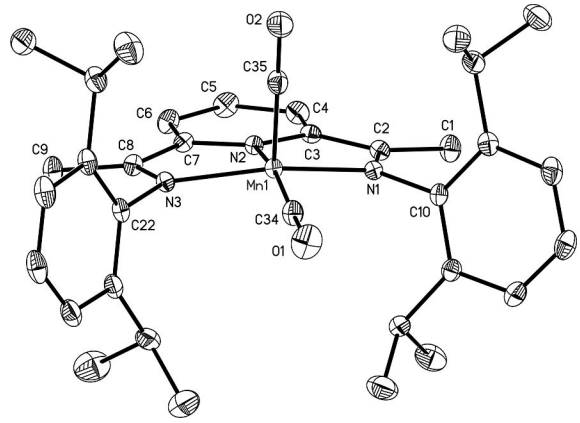

Figure 8. Representation of the solid-state structure of [(^{iPr}PDI)Mn(CO)$_2$] at 30% probability ellipsoids. Hydrogen atoms are omitted for clarity.

Table 5. Selected bond lengths [Å] for the series of bis(imino)pyridine manganese carbonyl complexes prepared in this study.

	[(^{iPr}PDI)Mn(CO)$_2$]$^-$	(^{iPr}PDI)Mn(CO)$_2$	[(^{iPr}PDI)Mn(CO)$_3$]$^+$
Mn(1)–N(1)	1.983(2)	1.988(1)	2.054(3)
Mn(1)–N(2)	1.886(2)	1.916(1)	1.961(3)
Mn(1)–N(3)	1.979(2)	1.996(1)	2.093(3)
Mn(1)–C(34)	1.752(3)	1.782(1)	1.858(4)
Mn(1)–C(35)	1.771(3)	1.762(1)	1.784(4)
N(1)–C(2)	1.343(3)	1.325(2)	1.298(4)
N(3)–C(8)	1.351(3)	1.321(2)	1.294(4)
C(2)–C(3)	1.411(4)	1.443(2)	1.476(5)
C(7)–C(8)	1.399(4)	1.445(2)	1.477(5)
N(2)–C(3)	1.388(3)	1.363(2)	1.350(4)
N(2)–C(7)	1.389(3)	1.360(1)	1.352(4)

To further explore the ground-state electronic structure of [(^{iPr}PDI)Mn(CO)$_2$], a solid-state magnetic moment was recorded at 23 °C. An effective magnetic moment of 1.8 μ_B was measured, consistent with an $S = 1/2$ ground state and the short metal–ligand bond lengths observed in the X-ray structure. The doublet ground state was also confirmed by EPR spectroscopy. The spectrum was collected at 10 K in 1:1 toluene/pentane glass and is presented in Figure 9. A rhombic signal was observed and simulation of the data produced manganese hyperfine coupling constants (I_{55Mn} = 5/2) of $A_{xx} = 23 \times 10^{-4}$ cm^{-1}, $A_{yy} = 8.0 \times 10^{-4}$ cm^{-1} and $A_{zz} = 32.5 \times 10^{-4}$ cm^{-1}. These values are relatively small and suggest a principally ligand, rather than metal-based SOMO. By comparison, low-spin Mn^{II} compounds with manganese-based SOMOs typically exhibit A values larger than 100 cm^{-1}.[31] The relatively small g-anisotropy (g = 2.007, 2.202, 1.998) is also consistent with this electronic structure description.

 © 2012 Wiley-VCH Verlag GmbH & Co. KGaA, Weinheim

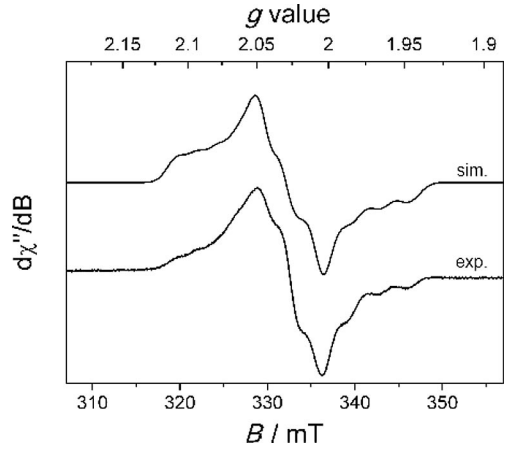

Figure 9. Experimental (bottom) and simulated (top) EPR spectra for [(^{iPr}PDI)Mn(CO)$_2$]. Data collected at 10 K in 1:1 toluene/pentane glass. $g_x = 2.070$, $g_y = 2.202$, $g_z = 1.998$; $A_{xx} = 23 \times 10^{-4}$ cm^{-1}, $A_{yy} = 8.0 \times 10^{-4}$ cm^{-1}, $A_{zz} = 32.5 \times 10^{-4}$ cm^{-1}.

On the basis of the crystallographic, magnetic and EPR spectroscopic data, the electronic structure of [(^{iPr}PDI)Mn(CO)$_2$] is best described as a low-spin Mn^{I}, d^6 compound with a bis(imino)pyridine radical anion as the SOMO. The d^6 electronic configuration at the manganese centre is well suited for π backbonding with the carbonyl ligands and accounts for the low infrared stretching frequencies as compared to the iron congener. It is also interesting to consider that a "simple" ligand-substitution reaction of the σ-donor THF for the π-acceptor CO induces a change in the metal oxidation state where [(^{iPr}PDI^{2-})Mn^{II}(THF)$_2$] transforms to [(^{iPr}PDI^{-})Mn^{I}(CO)$_2$].

Attempts to prepare [(^{iPr}PDI)Mn(CO)$_2$] by a sodium amalgam reduction of [(^{iPr}PDI)MnCl$_2$] under an atmosphere of carbon monoxide, which was also used to prepare [(^{iPr}PDI)Fe(CO)$_2$],[11a] did not yield the manganese dicarbonyl but rather the corresponding anion [Na(OEt$_2$)$_3$][(^{iPr}PDI)Mn(CO)$_2$] as a yellow solid [Equation (5)]. Decreasing the amount of sodium amalgam from 5 to 2 equiv. also furnished the manganese dicarbonyl anion along with remaining [(^{iPr}PDI)MnCl$_2$] starting material.

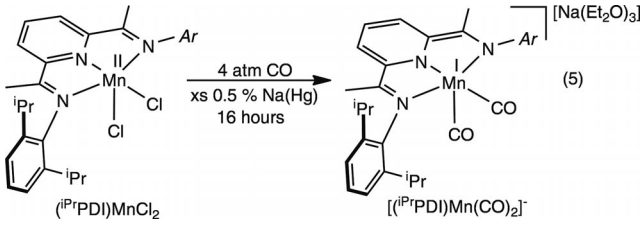

Diamagnetic [Na(OEt$_2$)$_3$][(^{iPr}PDI)Mn(CO)$_2$] was readily characterized by ^{1}H and ^{13}C NMR spectroscopy. Because of a limited solubility in hydrocarbon solvents, spectra were recorded in [D$_8$]THF. The imine methyl groups appear at δ = 2.62 ppm and the *meta*-pyridine at δ = 8.12 ppm, as expected for a diamagnetic compound with no contributions from low-lying paramagnetic excited states. The solid-state (KBr) infrared spectrum of [Na(OEt$_2$)$_3$][(^{iPr}PDI)Mn(CO)$_2$] exhibits two strong CO bands at 1806 and 1719 cm^{-1}, indicative of a high degree of reduction from the electron-rich manganese centre.

Single crystals suitable for X-ray diffraction were obtained from a concentrated diethyl ether solution at –35 °C. A representation of the solid-state structure is presented in Figure 10 and selected bond lengths and angles are reported in Table 5. The overall molecular geometry is best described as distorted-trigonal pyramidal, with the two carbonyl ligands occupying the equatorial positions, likely to maximize π-backbonding interactions. The sodium cation is ligated by three disordered diethyl ether molecules and is also coordinated to one of the oxygen atoms of the carbonyl ligands.

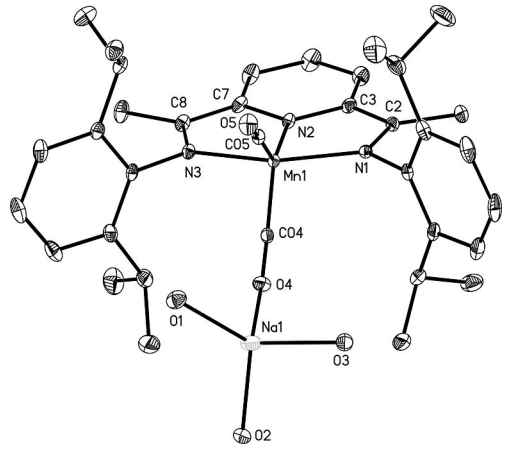

Figure 10. Truncated representation of the solid-state structure of [Na(OEt$_2$)$_3$][(^{iPr}PDI)Mn(CO)$_2$] at 30% probability ellipsoids. The diethyl ether carbon and hydrogen atoms are omitted for clarity.

The bond lengths of the bis(imino)pyridine chelate are diagnostic of a two-electron reduction. The N$_{imine}$–C$_{imine}$ bonds elongate to 1.343(3) and 1.351(3) Å, while the C$_{ipso}$–C$_{imine}$ distances shorten to 1.411(4) and 1.399(4) Å. These are the largest distortions observed in the family of bis(imino)pyridine manganese compounds prepared to date and likely indicative of the closed shell dianion [^{iPr}PDI]$^{2-}$ (S = 0).

The one-electron oxidation of [Na(OEt$_2$)$_3$][(^{iPr}PDI)Mn(CO)$_2$] was explored as an alternative synthetic route to [(^{iPr}PDI)Mn(CO)$_2$]. Addition of 1 equiv. of AgBPh$_4$ to a benzene solution of [Na(OEt$_2$)$_3$][(^{iPr}PDI)Mn(CO)$_2$] cleanly furnished the neutral manganese dicarbonyl [(^{iPr}PDI)Mn(CO)$_2$].

To complete a series of bis(imino)pyridine manganese carbonyl compounds over three different oxidation states, the oxidation of the neutral compound was also explored. Addition of 1 equiv. of [Cp$_2$Fe][BPh$_4$] to a benzene solution of [(^{iPr}PDI)Mn(CO)$_2$] followed by addition of pentane resulted in precipitation of a tan solid identified as a new bis(imino)pyridine manganese compound albeit in low yield. Analysis of the isolated solid by infrared spectroscopy revealed three strong carbonyl stretches centred at 2052,

 © 2012 Wiley-VCH Verlag GmbH & Co. KGaA, Weinheim

1967 and 1943 cm^{-1}, suggesting that the oxidation product was in fact the bis(imino)pyridine manganese tricarbonyl cation $[(^{iPr}PDI)Mn(CO)_3][BPh_4]$. With this information in hand, the procedure was repeated in the presence of 1 atm of carbon monoxide and furnished the desired $[(^{iPr}PDI)Mn(CO)_3][BPh_4]$ compound in near quantitative yield [Equation (6)]. The 18-electron manganese compound is diamagnetic and accordingly exhibits sharp ^1H and ^{13}C NMR spectra in $[D_8]$THF (see Experimental Section).

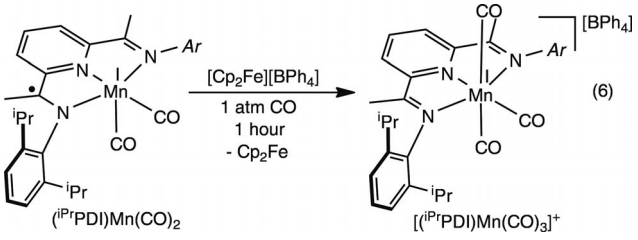

Single crystals suitable for X-ray diffraction were obtained from a fluorobenzene solution layered with pentane and stored at –35 °C. A representation of the solid-state structure is presented in Figure 11 and selected bond lengths and angles are reported in Table 5. The overall molecular geometry is best described as an idealized octahedron with a meridional arrangement of the three carbonyl ligands. The metrical parameters of the bis(imino)pyridine are consistent with a neutral chelate (Table 5). These values, coupled with the relatively short Mn–N bond lengths are consistent with a low-spin Mn^I compound, suggesting that the oxidation of $[(^{iPr}PDI^{1-})Mn^I(CO)_2]$ is principally ligand based.[30]

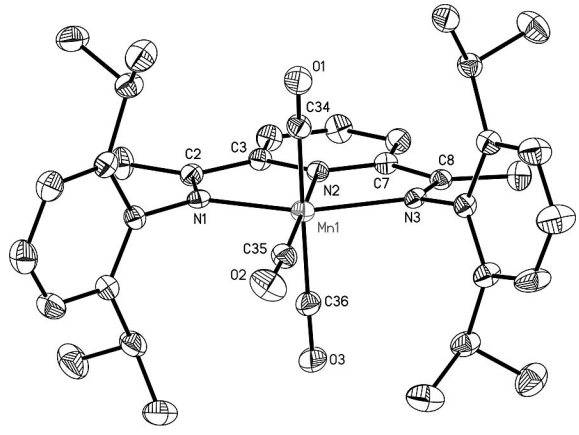

Figure 11. Truncated representation of the solid-state structure of $[(^{iPr}PDI)Mn(CO)_3][BPh_4]$ at 30% probability ellipsoids. The $[BPh_4]^-$ anion and the hydrogen atoms are omitted for clarity.

Having prepared examples of bis(imino)pyridine manganese carbonyl complexes that vary by three oxidation states, comparison of the electronic structures is useful to determine the site (metal vs. ligand) of reduction. A summary of the electronic structures is presented in Figure 12. A one-electron reduction of the cation $[(^{iPr}PDI^0)Mn^I(CO)_3]^+$ to $[(^{iPr}PDI^{1-})Mn^I(CO)_2]$ occurs at the bis(imino)pyridine chelate and with loss of a carbon monoxide ligand. Likewise, subsequent one-electron reduction of the neutral compound $[(^{iPr}PDI^{1-})Mn^I(CO)_2,]$ is also ligand-based and furnishes $[(^{iPr}PDI^{2-})Mn^I(CO)_2]^-$, where the bis(imino)pyridine is in its dianionic form. Similar ligand-based redox events have been reported for pincer manganese carbonyl compounds.[30]

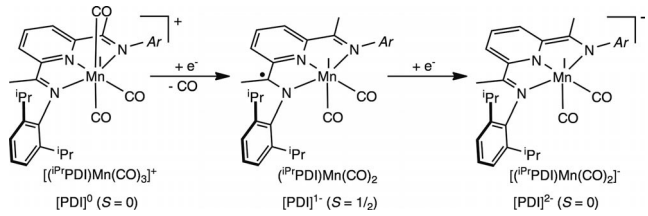

Figure 12. Electronic structure summary of a series of bis(imino)pyridine manganese carbonyl complexes that vary by three oxidation states. The oxidation and reduction processes are ligand- rather than metal-based and all compounds are low-spin Mn^I.

A similar series of bis(imino)pyridine iron carbonyl complexes that differ by three oxidation states has also been prepared and the electronic structures determined by a combination of X-ray diffraction, spectroscopic experiments and DFT calculations.[32] The neutral compound $[(^{iPr}PDI)Fe(CO)_2]$ is highly covalent and the best electronic structure description involves resonance structures between the $[(^{iPr}PDI^0)Fe^0(CO)_2]$ and $[(^{iPr}PDI^{2-})Fe^{II}(CO)_2]$ canonical forms, where in the latter case the bis(imino)pyridine chelate is in its closed shell dianionic form. Reducing the neutral carbonyl compound by one electron produced the anionic complex $[(^{iPr}PDI^{2-})Fe^I(CO)_2]^-$, where the reduction is iron-based and furnished a low-spin Fe^I compound with a dianionic chelate. Oxidation of $[(^{iPr}PDI)Fe(CO)_2]$ yielded the corresponding cation $[(^{iPr}PDI^0)Fe^I(CO)_2]^+$, which is also a low-spin Fe^I compound with a neutral bis(imino)pyridine chelate. For iron, redox chemistry within the carbonyl series of compounds involves cooperative metal and ligand oxidation and reduction events whereas in the corresponding manganese derivatives, the redox chemistry is principally ligand-based. For the latter, it is likely that the low-spin Mn^I, d^6 configuration is preferred for the strong-ligand field imparted by the carbonyl ligands (and also favours π backbonding), which in turn relegates redox events to the bis(imino)pyridine chelate.

Conclusions

A family of reduced bis(imino)pyridine manganese complexes have been synthesized and the role of the redox-active ligand on the overall electronic structure of the compounds established. Attempts to prepare a manganese dinitrogen derivative have been unsuccessful, likely due to the preferred electronic structure of the metal ion in a weak ligand field. For a principally σ-donating ligand such as THF, a high-spin Mn^{II} compound results with a doubly reduced bis(imino)pyridine diradical. Substitution of the THF ligands by carbon monoxide results in a reduction of the metal to low-spin Mn^I, d^6 with a concomitant oxidation

 © 2012 Wiley-VCH Verlag GmbH & Co. KGaA, Weinheim

of the ligand to its radical anion form. The bis(imino)pyridine radical is the SOMO of [(^{iPr}PDI)Mn(CO)$_2$] and was observed by EPR spectroscopy providing direct experimental evidence for the redox activity of the chelate. Oxidation and reduction of the neutral manganese dicarbonyl compound was also carried out and the Mn^{I}, d^6 electronic configuration was maintained throughout a series of compounds that vary by three oxidation states.

Experimental Section

General Considerations: All air- and moisture-sensitive manipulations were carried out using a standard vacuum line, Schlenk and cannula techniques, or in an MBraun inert atmosphere dry box containing an atmosphere of purified nitrogen. Solvents for air- and moisture-sensitive manipulations were initially dried and deoxygenated using literature procedures. [D$_6$]Benzene was purchased from Cambridge Isotope Laboratories and dried with 4 Å molecular sieves. The complexes [(^{iPr}PDI)MnCl$_2$] and [Cp$_2$Fe][BPh$_4$] were prepared according to literature procedures.[17,18]

^{1}H NMR spectra were recorded with Varian Mercury 300, Inova 400, 500 and 600 spectrometers operating at 299.76, 399.78, 500.62 and 599.78 MHz, respectively. ^{13}C NMR spectra were recorded with an Inova 500 spectrometer operating at 125.893 MHz. All ^{1}H and ^{13}C NMR chemical shifts are reported relative to SiMe$_4$ using the ^{1}H (residual) and ^{13}C chemical shifts of the solvent as a secondary standard. For diamagnetic complexes, many assignments were made based on COSY and HSQC NMR experiments. Solution magnetic moments were determined by Evans method using a ferrocene standard and are the average value of at least two independent measurements. Gouy balance measurements were performed with a Johnson Matthey instrument that was calibrated with HgCo(SCN)$_4$. Peak widths at half heights are reported for paramagnetically broadened and shifted resonances. Infrared spectra were collected with a Thermo Nicolet spectrometer. Elemental analyses were performed at Robertson Microlit Laboratories, Inc., in Madison, NJ.

Single crystals suitable for X-ray diffraction were coated with polyisobutylene oil in a drybox, transferred to a nylon loop and then quickly transferred to the goniometer head of a Bruker X8 APEX2 diffractometer equipped with a molybdenum X-ray tube (λ = 0.71073 Å). Preliminary data revealed the crystal system. A hemisphere routine was used for data collection and determination of lattice constants. The space group was identified and the data were processed using the Bruker SAINT+ program and corrected for absorption using SADABS. The structures were solved by direct methods (SHELXS) completed by subsequent Fourier synthesis and refined by full-matrix least-squares procedures.

SQUID magnetization data of crystalline powdered samples were recorded with a SQUID magnetometer (Quantum Design) at 10 kOe between 5 and 300 K for all samples. Values of the magnetic susceptibility were corrected for the underlying diamagnetic increment by using tabulated Pascal constants[33] and the effect of the blank sample holders (gelatin capsule/straw). Samples used for magnetization measurements were recrystallized multiple times and checked for chemical composition by ^{1}H NMR spectroscopy. The program julX written by E. Bill was used for (elements of) the simulation and analysis of magnetic susceptibility data.

X-band EPR data were collected with a Bruker ELEXSYS E500 spectrometer equipped with the Bruker standard cavity (ER4102ST) and a helium flow cryostat (Oxford Instruments ESR 910). Microwave frequencies were calibrated with a Hewlett–Packard frequency counter (HP5352B), and the field control was calibrated with a Bruker NMR field probe (ER035M). The spectra were simulated with the program GFIT (by E. Bill) for the calculation of powder spectra with effective g values and anisotropic line widths (Lorentzian line shapes were used). In each case a 2 mM solution of the complex was prepared in toluene. Data were recorded at 296 K with a frequency of 9.43 GHz, a modulation amplitude of 10 G and a microwave power of 1.26 mW. Simulations were conducted using the W95EPR software package.

[(^{iPr}PDI)Mn(THF)$_2$]: A 100 mL round-bottomed flask was charged with [(^{iPr}PDI)MnCl$_2$] (1.00 g, 1.65 mmol), sodium metal (0.078 g, 3.37 mmol, 2.05 equiv.) and naphthalene (0.010 g, 0.082 mmol, 0.05 equiv.). THF (approximately 20 mL) was added to the flask and the resulting reaction mixture was stirred for 16 h. During this time a colour change from orange to brown was observed. After reduction was complete (as indicated by the formation of the brown solution), the THF was removed in vacuo. The resulting solid was dissolved in diethyl ether and filtered through Celite. The filtrate was collected, concentrated, stored at –35 °C and yielded 0.687 g (61%) of a dark brown solid identified as [(^{iPr}PDI)Mn(THF)$_2$]. Crystals suitable for X-ray analysis were obtained from a diethyl ether solution stored at –35 °C. $C_{41}H_{59}MnN_3O_2$ (680.87): calcd. C 75.89, H 9.16, N 6.48; found C 76.14, H 9.20, N 6.36. Magnetic susceptibility: μ_{eff} = 3.7 μ_B (magnetic susceptibility balance, 23 °C).

[(^{iPr}PDI)$_2$Mn]: A 100 mL round-bottomed flask was charged with mercury (45.41 g, 226.38 mmol) and pentane (approximately 30 mL). Sodium metal (0.227 g, 9.87 mmol) was cut into pieces and added to the flask. The amalgam was stirred for 10 min, then solid [(^{iPr}PDI)MnCl$_2$] (1.00 g, 1.65 mmol) was added. The reduction was stirred for 48 h during which time a colour change in the solution from orange to brown was observed. After 48 h the solution was decanted from the amalgam and filtered through Celite. The remaining product was extracted into diethyl ether and filtered through Celite. Recrystallization from diethyl ether at –35 °C yielded 0.386 g (46%) of a red solid identified as [(^{iPr}PDI)$_2$Mn]. Crystals suitable for X-ray analysis were obtained from a diethyl ether solution stored at –35 °C. $C_{66}H_{86}MnN_6$ (1018.38): calcd. C 77.84, H 8.51, N 8.25; found C 77.94, H 8.52, N 8.39. Magnetic susceptibility: μ_{eff} = 3.9 μ_B (magnetic susceptibility balance, 23 °C).

[(^{iPr}PDI)MnCl(THF)]: A 100 mL round-bottomed flask was charged with [(^{iPr}PDI)Mn(THF)$_2$] (0.500 g, 0.734 mmol) and [(^{iPr}PDI)MnCl$_2$] (0.450 g, 0.741 mmol). THF (approximately 20 mL) was added to the flask and the resulting reaction mixture was stirred for 16 h. During this time a colour change from brown to dark red was observed. Following removal of the THF in vacuo, the product was extracted into diethyl ether and filtered through Celite. The solution was evaporated to dryness to yield 0.673 g (91%) of a dark-red solid identified as [(^{iPr}PDI)MnCl(THF)]. $C_{37}H_{51}ClMnN_3O$ (644.22): calcd. C 69.28, H 7.58, N 7.34; found C 69.01, H 8.22, N 7.32. Magnetic susceptibility: μ_{eff} = 4.6 μ_B (magnetic susceptibility balance, 23 °C). ^{1}H NMR ([D$_6$]benzene, 20 °C): δ = –7.91 (J = 530 Hz), –1.80 (J = 1013 Hz), 4.92 (J = 656 Hz), 10.17 (J = 954 Hz), 43.23 (J = 1701 Hz) ppm.

[(^{iPr}PDI)Mn(CO)$_2$]: A thick-walled glass vessel was charged with of [(^{iPr}PDI)Mn(THF)$_2$] (0.500 g, 0.734 mmol) and toluene (approximately 20 mL). The vessel was removed from the dry box and submerged in liquid nitrogen. On the high vacuum line, the vessel was evacuated and 4 atm of CO were added. The solution was warmed to room temperature and stirred for 1 h. During this time, a pink solution formed. The excess CO was removed on the high vacuum

 © 2012 Wiley-VCH Verlag GmbH & Co. KGaA, Weinheim

line and the vessel placed back in the box. The solution was filtered through Celite and all solvent removed in vacuo to yield 0.378 g (87%) of a dark-pink solid identified as [(^{iPr}PDI)Mn(CO)$_2$]. Crystals suitable for X-ray diffraction were grown from a diethyl ether solution stored at –35 °C. $C_{35}H_{43}MnN_3O_2$ (592.68): calcd. C 70.93, H 7.31, N 7.09; found C 70.70, H 7.37, N 6.91. Magnetic susceptibility: μ_{eff} = 1.9 μ_B ([D$_6$]benzene, 23 °C). ^{1}H NMR ([D$_6$]benzene, 20 °C): δ = –2.41 (J = 633 Hz), 3.52 (J = 87 Hz), 5.98 (J = 108 Hz), 7.24 (J = 40 Hz), 13.34 (J = 157 Hz) ppm. IR: $\tilde{\nu}$(CO) 1836, 1896 cm^{-1} (KBr); 1860, 1915 cm^{-1} (pentane).

[(^{iPr}PDI)Mn(CO)$_2$][Na(OEt$_2$)$_3$]: A thick-walled glass vessel was charged with mercury (45.41 g, 226.38 mmol) and toluene (approximately 50 mL). Sodium metal (0.227 g, 9.87 mmol) was cut into pieces and added to the vessel. The amalgam was stirred for 10 min and then solid [(^{iPr}PDI)MnCl$_2$] (1.00 g, 1.65 mmol) was added. The vessel was submerged in liquid nitrogen and 4 atm of carbon monoxide were added on the high vacuum line. The reaction mixture was warmed to room temperature and stirred for 48 h during which time a colour change from orange to dark yellow was observed. After 48 h the vessel was degassed and placed in the glove box. The solution was decanted from the amalgam and filtered through Celite. The remaining product was extracted into diethyl ether and filtered through Celite. Recrystallization from diethyl ether at –35 °C yielded 0.772 g (92%) of dark-yellow crystals identified as [(^{iPr}PDI)Mn(CO)$_2$][Na(OEt$_2$)$_3$]. Crystals suitable for X-ray diffraction were obtained from a concentrated diethyl ether solution at –35 °C. ^{1}H NMR ([D$_6$]benzene, 20 °C): δ = 0.99 [d, J = 7.6 Hz, 12 H, CH(CH_3)], 1.29 [d, J = 7.6 Hz, 12 H, CH(CH_3)], 1.38 (br. s, 8 H, THF), 2.62 [s, 6 H, C(CH_3)], 2.85 [sept, J = 7.6 Hz, 4 H, CH(CH$_3$)], 3.49 (br. s, 8 H, THF), 7.09 (br. s, 6 H, *m-Ar* and *p-Ar*), 7.34 (t, J = 7.6 Hz, 1 H, *p-py*), 8.12 (d, J = 7.6 Hz, 2 H, *m-py*) ppm. ^{13}C NMR ([D$_6$]benzene, 20 °C): δ = 17.48 [C(*C*H$_3$)], 24.54 [CH(*C*H$_3$)$_2$], 25.54 [CH(*C*H$_3$)$_2$], 27.87 [*C*H(CH$_3$)$_2$], 117.47 (*m-py*), 123.02 (*m-Ar*), 124.85 (*p-Ar*), 126.41 (*p-py*), 140.09, 142.86, 146.81, 154.47 (quaternary carbons), 232.93 (*C*O) ppm. IR (KBr): $\tilde{\nu}$ = (CO) 1719, 1806 cm^{-1}.

[(^{iPr}PDI)Mn(CO)$_3$][BPh$_4$]: A thick-walled glass vessel was charged with [(^{iPr}PDI)Mn(CO)$_2$] (0.200 g, 0.337 mmol) and [Cp$_2$Fe][BPh$_4$] (0.170 g, 0.337 mmol). The vessel was then evacuated on the high vacuum line and benzene (approximately 10 mL) was added at liquid-nitrogen temperature. While the reaction remained frozen, 4 atm of carbon monoxide were added. The solution was warmed to room temperature and stirred for 30 min during which time a colour change from purple to tan was observed. The vessel was degassed and placed in the drybox where the solution was transferred to a vial and pentane (approximately 10 mL) was added. Collection of the precipitate yielded 0.233 g (76%) of a tan solid identified as [(^{iPr}PDI)Mn(CO)$_2$][BPh$_4$]. $C_{60}H_{63}BMnN_3O_3$ (939.92): calcd. C 76.67, H 6.67, N 4.47; found C 76.39, H 6.91, N 4.38. ^{1}H NMR ([D$_8$]THF): δ = 1.08 [d, J = 5.2 Hz, 12 H, CH(CH_3)$_2$], 1.36 [d, J = 5.2 Hz, 12 H, CH(CH_3)$_2$], 2.17 [s, 6 H, C(CH_3)], 2.57 [sept, J = 5.2 Hz, 4 H, CH(CH$_3$)$_2$], 6.73 (br. s, 8 H, BPh$_4$), 6.87 (br. s, 8 H, BPh$_4$), 7.38 (br. s, 4 H, BPh$_4$), 7.07 (m, 6 H, *Ar*), 7.74 (m, 3 H, *m-py* and *p-py*) ppm. IR (KBr): $\tilde{\nu}$ = (CO) 1943, 1967, 2052 cm^{-1}.

CCDC-827876 {for [(^{iPr}PDI)Mn(THF)$_2$]}, -827877 {for [(^{iPr}PDI)$_2$-Mn)]}, -827878 {for [(^{iPr}PDI)Mn(CO)$_3$][BPh$_4$]}, -827879 {for [(^{iPr}PDI)Mn(CO)$_2$][Na(OEt$_2$)$_3$]}, -827880 {for [(^{iPr}PDI)Mn-(CO)$_2$]}, -844416 {for [(^{iPr}PDI)MnCl(THF)]} contain the supplementary crystallographic data for this paper. These data can be obtained free of charge from The Cambridge Crystallographic Data Centre via www.ccdc.cam.ac.uk/data_request/cif.

Acknowledgments

We thank the U. S. National Science Foundation and the Deutsche Forschungsgemeinschaft (DFG) for a Cooperative Activities in Chemistry between U. S. and German Investigators grant. We also thank Eckard Bill for assistance with the simulations of EPR data.

[1] E. C. Alyea, P. H. Merrel, *Inorg. Met. Org. Chem.* **1974**, *4*, 535.
[2] V. C. Gibson, C. Redshaw, G. A. Solan, *Chem. Rev.* **2007**, *107*, 1745.
[3] a) P. J. Chirik, in: *Catalysis Without Precious Metals* (Ed.: R. M. Bullock), Wiley-VCH, Weinheim, Germany, **2010**, pp. 83–106; b) P. J. Chirik, K. Wieghardt, *Science* **2010**, *327*, 5967.
[4] a) C. Bianchini, G. Giambastiani, I. G. Rios, G. Mantovani, A. Meli, A. M. Segarra, *Coord. Chem. Rev.* **2006**, *250*, 1391; b) T. Matsugi, T. Fujita, *Chem. Soc. Rev.* **2008**, *37*, 1264.
[5] Q. Knijnenburg, S. Gambarotta, P. H. M. Budzelaar, *Dalton Trans.* **2006**, 5442.
[6] S. C. Bart, K. Chlopek, E. Bill, M. W. Bouwkamp, E. Lobkovsky, F. Neese, K. Wieghardt, P. J. Chirik, *J. Am. Chem. Soc.* **2006**, *128*, 13901.
[7] K. P. Butin, E. K. Beloglazkina, N. V. Zyk, *Russ. Chem. Rev.* **2005**, *74*, 531.
[8] B. de Bruin, E. Bothe, T. Weyhermüller, K. Wieghardt, *Inorg. Chem.* **2000**, *39*, 2936.
[9] Vanadium: I. Vidyaratne, S. Gambarotta, I. Korobkov, P. H. M. Budzelaar, *Inorg. Chem.* **2005**, *44*, 1187.
[10] Chromium: I. Vidyaratne, J. Scott, S. Gambarotta, P. H. M. Budzelaar, *Inorg. Chem.* **2007**, *46*, 7040.
[11] Iron: a) S. C. Bart, E. Lobkovsky, P. J. Chirik, *J. Am. Chem. Soc.* **2004**, *126*, 13794; b) J. Scott, I. Vidyaratne, I. Korobkov, S. Gambarotta, P. H. M. Budzelaar, *Inorg. Chem.* **2008**, *47*, 896; c) S. K. Russell, J. M. Darmon, E. Lobkovsky, P. J. Chirik, *Inorg. Chem.* **2010**, *49*, 2782.
[12] Cobalt: a) V. C. Gibson, M. J. Humphries, K. P. Tellmann, D. F. Wass, A. J. P. White, D. J. Williams, *Chem. Commun* ; b) A. C. Bowman, C. Milsmann, C. C. Atienza, E. Lobkovsky, K. Wieghardt, P. J. Chirik, *J. Am. Chem. Soc.* **2010**, *132*, 1676.
[13] Nickel: D. Zhu, I. Thapa, I. Korobkov, S. Gambarotta, P. H. M. Budzelaar, *Inorg. Chem.* (ASAP) **2011**.
[14] Ruthenium: M. Gallagher, N. L. Wieder, V. K. Dioumaev, P. J. Carroll, D. H. Berry, *Organometallics* **2010**, *29*, 591.
[15] a) B. L. Small, M. Brookhart, *J. Am. Chem. Soc.* **1998**, *120*, 7143; b) B. L. Small, M. Brookhart, A. M. A. Bennett, *J. Am. Chem. Soc.* **1998**, *120*, 4049; c) A. M. A. Bennett (Dupont) WO 98/27124, 1998; *Chem. Abstr.* **1998**, *129*, 122973x.
[16] a) G. J. P. Britovsek, V. C. Gibson, B. S. Kimberely, P. J. Maddox, S. J. McTavish, G. A. Solan, A. J. P. White, D. J. Williams, *Chem. Commun.* **1998**, 849; b) G. J. P. Britovsek, M. Bruce, V. C. Gibson, B. S. Kimberely, P. J. Maddox, S. Mastroianni, S. J. McTavish, C. Redhsaw, G. A. Solan, S. S. Stromberg, A. J. P. White, D. J. Williams, *J. Am. Chem. Soc.* **1999**, *121*, 8728.
[17] D. Reardon, G. Aharnian, S. Gambarotta, G. P. A. Yap, *Organometallics* **2002**, *21*, 786.
[18] H. Sugiyama, D. Reardon, G. Aharnian, S. Gambarotta, G. P. A. Yap, P. H. M. Budzelaar, *J. Am. Chem. Soc.* **2002**, *124*, 12268.
[19] For a related bis(aldimino)pyridine-manganese dibromide compound, see: D. A. Edwards, M. F. Mahon, W. R. Martin, K. C. Molloy, *J. Chem. Soc., Dalton Trans.* **1990**, 3161.
[20] a) J. Cámpora, C. M. Pérez, A. Rodríguez-Delgado, A. M. Naz, P. Palma, E. Álvarez, *Organometallics* **2007**, *26*, 1104; b) J. Cámpora, P. Palma, C. M. Pérez, A. Rodríguez-Delgado, E. Álvarez, E. Gutiérrez-Puebla, *Organometallics* **2010**, *29*, 2960.
[21] C. M. Pérez, A. Rodríguez-Delgado, P. Palma, E. Álvarez, E. Gutiérrez-Puebla, J. Cámpora, *Chem. Eur. J.* **2010**, *16*, 13834.
[22] a) M. W. Bouwkamp, E. Lobkovsky, P. J. Chirik, *J. Am. Chem. Soc.* **2005**, *127*, 9660; b) A. M. Tondreau, C. Milsmann, A. D.

 © 2012 Wiley-VCH Verlag GmbH & Co. KGaA, Weinheim

Patrick, H. M. Hoyt, E. Lobkovsky, K. Wieghardt, P. J. Chirik, *J. Am. Chem. Soc.* **2010**, *132*, 15046.
[23] C. C. H. Atienza, C. Milsmann, E. Lobkovsky, P. J. Chirik, *Angew. Chem. Int. Ed.* **2011**, *50*, 8143.
[24] G. J. P. Britovsek, J. England, S. K. Spitzmesser, A. J. P. White, D. J. Williams, *Dalton Trans.* **2005**, 945.
[25] a) M. W. Bouwkamp, A. C. Bowman, E. Lobkovsky, P. J. Chirik, *J. Am. Chem. Soc.* **2006**, *128*, 13360; b) K. T. Sylvester, P. J. Chirik, *J. Am. Chem. Soc.* **2009**, *131*, 8772; c) S. K. Russell, P. J. Chirik, *J. Am. Chem. Soc.* **2011**, *133*, 8858.
[26] S. C. Bart, E. Lobkovsky, E. Bill, K. Wieghardt, P. J. Chirik, *Inorg. Chem.* **2007**, *46*, 7055.
[27] B. M. Wile, R. J. Trovitch, S. C. Bart, A. M. Tondreau, E. Lobkovsky, C. Milsmann, E. Bill, K. Wieghardt, P. J. Chirik, *Inorg. Chem.* **2009**, *48*, 4190.
[28] C. C. Lu, E. Bill, T. Weyhermüller, E. Bothe, K. Wieghardt, *J. Am. Chem. Soc.* **2008**, *130*, 3181.
[29] R. J. Trovitch, E. Lobkovsky, P. J. Chirik, *J. Am. Chem. Soc.* **2008**, *130*, 11631.
[30] A. T. Radosevich, J. G. Melnick, S. A. Stoian, D. Bacciu, C.-H. Chen, B. M. Foxman, O. V. Ozerov, D. G. Nocera, *Inorg. Chem.* **2009**, *48*, 9214.
[31] P. H. Rieger, *Coord. Chem. Rev.* **1994**, *135–136*, 203.
[32] A. M. Tondreau, C. Milsmann, E. Lobkovsky, P. J. Chirik, *Inorg. Chem.*, in press.
[33] G. A. Bain, J. F. Berry, *J. Chem. Educ.* **2008**, *85*, 532.

Received: June 4, 2011
Published Online: October 5, 2011

 © 2012 Wiley-VCH Verlag GmbH & Co. KGaA, Weinheim

DOI: 10.1002/ejic.201101091

Ruthenium Hydride Complexes with Zwitterionic Quinonoid Ligands – Isomer Separation, Structural Properties, Electrochemistry, and Catalysis

Stephan Hohloch,[a] Pierre Braunstein,*[b] and Biprajit Sarkar*[a]

Keywords: Quinones / Ruthenium / Hydrides / Noninnocent ligands / Redox chemistry / Transfer hydrogenation catalysis

Reactions of $[Ru(PPh_3)_3(CO)(H)Cl]$ with the zwitterionic *p*-benzoquinonemonoimine-type ligands 4-(*n*-butylamino)-6-(*n*-butylimino)-3-oxocyclohexa-1,4-dien-1-olate (**Q^1**), 4-(isopropylamino)-6-(isopropylimino)-3-oxocyclohexa-1,4-dien-1-olate (**Q^2**), and 4-(benzylamino)-6-(benzylimino)-3-oxocyclohexa-1,4-dien-1-olate (**Q^3**) in the presence of a base led to the formation of mononuclear complexes $[Ru(PPh_3)_2(CO)(H)(\mathbf{Q^1}_{-H})]$ (**1a** and **1b**), $[Ru(PPh_3)_2(CO)(H)(\mathbf{Q^2}_{-H})]$ (**2a** and **2b**), and $[Ru(PPh_3)_2(CO)(H)(\mathbf{Q^3}_{-H})]$ (**3a** and **3b**), respectively. The positional isomers (**a** and **b**) that were formed in each case were separated by preparative TLC. The structural characterization of **2a** and **3a**·MeCN helped to identify the isomers, and established the distorted octahedral coordination geometry around the ruthenium center. The bond lengths in the complexes are consistent with localization of the double bonds in $\mathbf{Q^2}_{-H}$ and $\mathbf{Q^3}_{-H}$ in both their monodeprotonated and metal-coordinated forms. The Ru–C–O(carbonyl) bond angle is almost linear. Cyclic voltammetry of the complexes showed one oxidation and one reduction process. These are predominantly centered on the quinonoid ligands, which shows their redox-noninnocent character. Studies of transfer hydrogenation with **2a** as a precatalyst showed that, in the presence of KOH, acetophenone could be converted to 1-phenylethanol within 10 h in over 90 % yield.

Introduction

Quinones have fascinated chemists for decades,[1] and their interaction with transition metals has relevance to biological systems.[2–4] The redox noninnocence of such molecules imparts many interesting properties to them.[5–12] Thus, metal complexes of quinonoid ligands have been extensively investigated due to their valence ambiguity and captivating electronic structures,[13–18] their engrossing magnetic properties,[19–22] their use as bridges for molecular and supramolecular systems,[19,23–36] and in homogeneous catalysis.[37–40] In recent years, we have developed the chemistry of the potentially antiaromatic zwitterionic quinonoid ligands **Q**[41–44] (Scheme 1) and their metal complexes. Metal complexes of these ligands, where the 6π + 6π zwitterionic form is more stable than the canonical forms, have found use in homogeneous catalysis,[45,46] redox[47–49] and supramolecular chemistry,[44] and as spacers for "metal–metal coupling".[50,51]

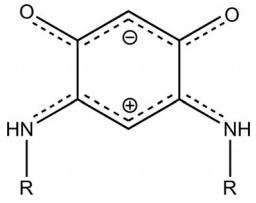

Scheme 1. Zwitterionic quinonoid ligands.

In this work we have extended the chemistry of these zwitterionic ligands to new ruthenium hydride complexes and probed their use as catalysts for transfer hydrogenation reactions. Hydride complexes of transition metals are intermediates in a variety of useful chemical transformations.[52] The syntheses of $[Ru(PPh_3)_2(CO)(H)(\mathbf{Q^1}_{-H})]$ (**1a** and **1b**), $[Ru(PPh_3)_2(CO)(H)(\mathbf{Q^2}_{-H})]$ (**2a** and **2b**), and $[Ru(PPh_3)_2(CO)(H)(\mathbf{Q^3}_{-H})]$ (**3a** and **3b**), where **Q^1**, **Q^2**, and **Q^3** are 4-(*n*-butylamino)-6-(*n*-butylimino)-3-oxocyclohexa-1,4-dien-1-olate, 4-(isopropylamino)-6-(isopropylimino)-3-oxocyclohexa-1,4-dien-1-olate, and 4-(benzylamino)-6-(benzylimino)-3-oxocyclohexa-1,4-dien-1-olate, respectively, are presented. The separation of the positional isomers (**a** and **b** in each case) of these complexes is reported and discussed. Results obtained from elemental analysis, mass spectrometry, ^{1}H NMR and IR spectroscopy, and structural analysis have been used to establish the formulation of these metal complexes. Cyclic voltammetry studies have been carried out to elucidate the redox properties of these complexes. Finally, the use of these complexes as precatalysts for transfer hydrogenation is presented and explained.

Results and Discussion

Synthesis, Spectroscopy, and Structures

Q^1–**Q^3** were deprotonated by using KO*t*Bu. Reactions of these deprotonated ligands with $[Ru(PPh_3)_3(Cl)(CO)(H)]$

[a] Institut für Anorganische Chemie, Universität Stuttgart, Pfaffenwaldring 55, 70550 Stuttgart, Germany
Fax: +49-711-68564165
E-mail: sarkar@iac.uni-stuttgart.de
[b] Laboratoire de Chimie de Coordination, Institut de Chimie (UMR 7177 CNRS), Université de Strasbourg, 4 rue Blaise Pascal, 67081 Strasbourg Cedex, France

Supporting information for this article is available on the WWW under http://dx.doi.org/10.1002/ejic.201101091.

WILEY ONLINE LIBRARY © 2012 Wiley-VCH Verlag GmbH & Co. KGaA, Weinheim

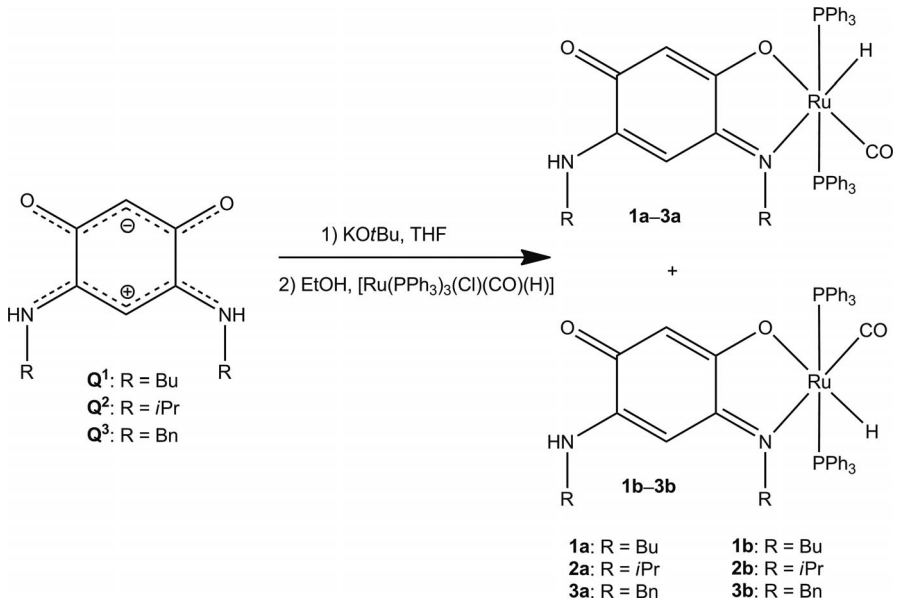

Scheme 2. Synthesis of the complexes.

under reflux conditions led to the formation of the metal complexes shown in Scheme 2.

Initial ^{1}H NMR spectroscopy (particularly the hydride signals) of the crude products indicated the formation of two different products in each case. Preparative TLC was used to separate these two fractions to obtain pure forms of **1a**–**3a**, **1b**, and **3b**. Unfortunately, the yield of **2b** was not high enough to warrant further investigation. During the reaction, one PPh_3 ligand dissociated from the precursor as a result of its high steric demand. Additionally, the chlorido ligand was abstracted as KCl with the K^+ ion associated with the deprotonated ligand. This process afforded six-coordinate, neutral ruthenium(II) complexes.

Complexes with the formula $[Ru(PPh_3)_2(CO)(H)(\mathbf{Q_{-H}})]$ can exist as various positional isomers. The ^{31}P NMR spectra of all the isolated complexes showed only one signal. Hence, the two PPh_3 ligands must be *trans* to each other, which also makes sense on steric grounds. With the two PPh_3 ligands *trans* to each other, $[Ru(PPh_3)_2(CO)(H)(\mathbf{Q_{-H}})]$ can exist as two different positional isomers, because the $\mathbf{Q_{-H}}$ ligands bind to the ruthenium center through an O and an N atom. The final identity of such isomers was established by single-crystal X-ray diffraction studies.

Complex **2a** crystallized at –10 °C from a dichloromethane solution layered with *n*-hexane (1:4), and **3a** crystallized by slow concentration of a CD_3CN solution under ambient conditions (Figures 1 and 2). Complex **2a** crystallized in the monoclinic $P2_1/n$ space group, and **3a**·MeCN crystallized in the triclinic $P\bar{1}$ space group. Crystallographic details are given in Table 4, and selected bond lengths and bond angles are listed in Table 1.

In both complexes, the ruthenium center is in a distorted octahedral environment and is coordinated by the O and N atoms of $\mathbf{Q_{-H}}$, two P atoms from PPh_3, a C atom from CO, and a hydrido ligand. The distortion from octahedral geometry is imposed by the chelating nature of $\mathbf{Q_{-H}}$ and

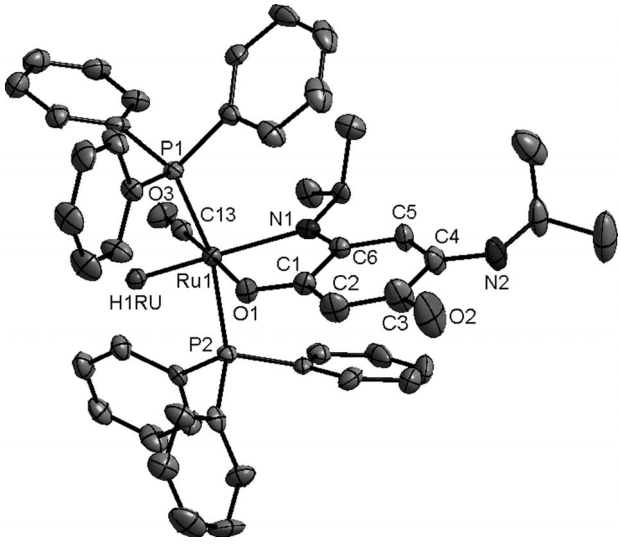

Figure 1. ORTEP plot of **2a**. Ellipsoids are drawn at 50% probability.

probably by the steric bulk of the two PPh_3 groups. Thus, the O1–Ru–N1 angle is 75.7(2) and 75.2(1)°, and the P2–Ru–P1 angle is 164.1(1) and 158.0(1)° in **2a** and **3a**·MeCN, respectively. The CO ligand in **2a** and **3a**·MeCN is *trans* to the O atom of $\mathbf{Q_{-H}}$. Hence, the identity of the red isomers **2a** and **3a**·MeCN was unambiguously established from the structural data. Extrapolation of these results to the red **1a** and the yellow **1b**–**3b** also helped to determine their identity.

Inspection of the bond lengths within $\mathbf{Q_{-H}}$ in **2a** and **3a**·MeCN shows that the C1–O1 distances of 1.276(8) and 1.290(3) Å are slightly longer than the C3–O2 distances of 1.263(9) and 1.244(3) Å, respectively. Accordingly, the C1–C2 distances of 1.398(10) and 1.382(3) Å for **2a** and **3a**·MeCN are slightly shorter than the C2–C3 distances of

 © 2012 Wiley-VCH Verlag GmbH & Co. KGaA, Weinheim

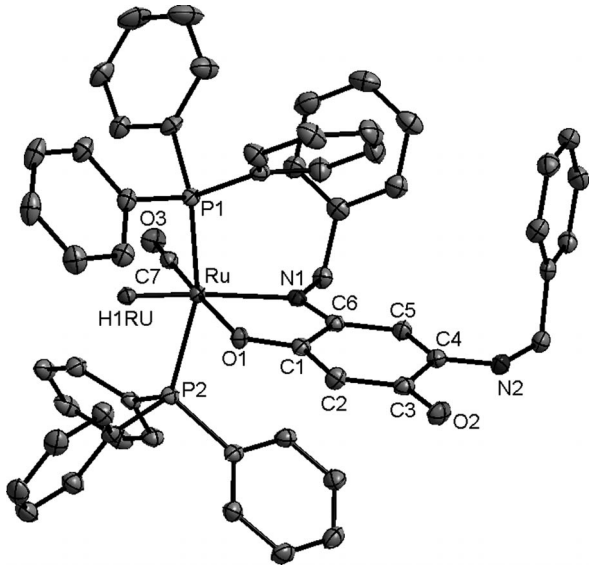

Figure 2. ORTEP plot of **3a**·MeCN. Ellipsoids are drawn at 50% probability.

Table 1. Selected bond lengths [Å] and angles [°].

	2a	**3a**·MeCN
C1–C2	1.398(10)	1.382(3)
C2–C3	1.420(13)	1.420(3)
C3–C4	1.528(12)	1.510(3)
C4–C5	1.372(9)	1.368(3)
C5–C6	1.427(9)	1.428(3)
C6–C1	1.490(9)	1.504(3)
C1–O1	1.276(8)	1.290(3)
C3–O2	1.263(9)	1.244(3)
C6–N1	1.298(8)	1.307(3)
C4–N2	1.347(9)	1.340(3)
C13–O3	1.148(9)	–
C7–O3	–	1.157(3)
Ru–O1	2.107(5)	2.138(2)
Ru–N1	2.185(5)	2.153(2)
Ru–H	1.73(9)	1.54(3)
Ru–P1	2.366(2)	2.3634(6)
Ru–P2	2.345(2)	2.3428(5)
Ru–C13	1.832(8)	–
Ru–C7	–	1.817(2)
N1–Ru–O1	75.7(2)	75.2(1)
O1–Ru–H	102.0(3)	99.0(1)
H–Ru–C13	77.0(3)	–
H–Ru–C7	–	85.0(1)
C13–Ru–N1	105.4(3)	–
C7–Ru–N1	–	99.8(1)
P1–Ru–P2	164.1(1)	158.0(1)
Ru–O1–C1	116.6(4)	116.4(1)
Ru–N1–C6	114.6(4)	117.5(1)

1.420(13) and 1.420(3) Å, respectively. A look at the C–N distances shows a related trend. The C6–N1 distances of 1.298(8) and 1.307(3) Å for **2a** and **3a**·MeCN, respectively, are shorter than the C4–N2 distances of 1.347(9) and 1.340(3) Å. This pattern is also reflected in the C5–C6 distances of 1.427(9) and 1.428(3) Å for **2a** and **3a**·MeCN, respectively, which are longer than the C4–C5 distances of 1.372(9) and 1.368(3) Å. Thus, the double bonds within the $\mathbf{Q}_{-\mathbf{H}}$ ligands became localized upon metal coordination, which is in contrast to the free ligands where the double bonds are delocalized within the "upper" and "lower" parts of the molecule (Scheme 2). The C1–C6 distances of 1.490(9) and 1.504(3) Å and the C3–C4 distances of 1.528(12) and 1.510(3) Å for **2a** and **3a**·MeCN, respectively, correspond to typical C–C single bonds and are comparable to the values found in the free ligands. These results are consistent with trends found in reported mononuclear complexes with these zwitterion-derived ligands.[47,49,51] The C–O distances of the carbonyl ligand of 1.148(9) and 1.157(3) Å for **2a** and **3a**·MeCN, respectively, are consistent with a C≡O triple bond. This is also reflected in the nearly linear Ru–C–O(carbonyl ligand) angle of 178.2 and 176.8° for **2a** and **3a**·MeCN, respectively.

In **3a**·MeCN, the phenyl rings of the benzyl groups are perpendicular to the plane of the benzoquinonemonoimine ring as well as perpendicular to each other. If we consider a plane that passes through C2 and C5 that is perpendicular to the plane containing the benzoquinonemonoimine ring, then the phenyl ring on the noncoordinated side of the ligand is parallel to this plane and that on the coordinated side is perpendicular to it. This probably happens to reduce the steric hindrance between the phenyl ring of the benzyl substituents and those of the PPh_3 group.

The positional isomers show significant differences in their ^{1}H NMR and IR spectroscopic signatures. The C–O stretching vibration for the carbonyl ligand attached to the ruthenium center appears at 1911 cm^{-1} for **1a** and at 1920 cm^{-1} for **1b** (Figure S1). A similar trend is also seen in **3a/3b** and **2a** (see Exp. Sect.). The CO ligand is *trans* to the O donor of $\mathbf{Q}^{\mathbf{1}}_{-\mathbf{H}}$ in **1a** and to the N donor in **1b** (Scheme 1). Structural analyses have shown that the donor atoms in the quinonoid ligands in their monometalated forms are best described as an O^- and a neutral imine N atom. A negatively charged O^- atom is expected to be a better π donor than a neutral imine N atom. Hence, in the case of **1a**, backbonding from the ruthenium center to the carbonyl ligand is larger than that in **1b**, which results in a lower carbonyl stretching frequency in **1a** than **1b**.

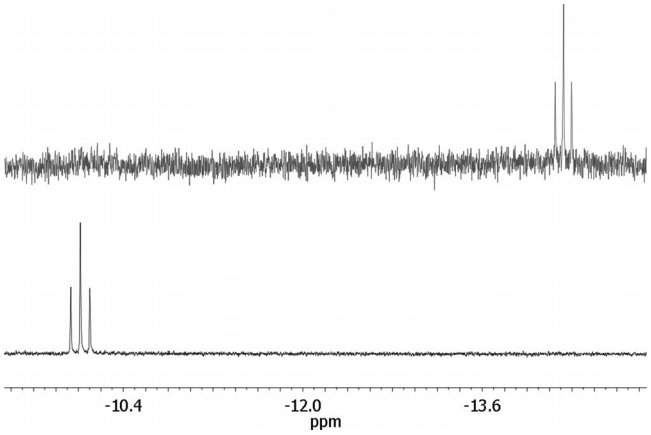

Figure 3. ^{1}H NMR (hydride region) spectra of **3a** (bottom) and **3b** (top).

 © 2012 Wiley-VCH Verlag GmbH & Co. KGaA, Weinheim

The influence of the different local electronic structures in the two positional isomers is also seen in the chemical shifts of the hydride in their ^{1}H NMR spectra. Thus, the hydride resonance appears at δ = –10 and –14.53 ppm in the spectra of **3a** and **3b**, respectively (Figure 3). Both signals are triplets because of coupling with the two equivalent P nuclei of PPh_3. In the case of **3b**, the hydrido ligand is *trans* to the better π-donating O^- donor. Because of the reasons stated above, its resonance shifts to higher fields compared to that of **3a**. Similar trends are also observed for the isomers of the other complexes (see Exp. Sect.).

Cyclic Voltammetry

The presence of a redox-active ruthenium center as well as a redox-active noninnocent quinonoid ligand provides an opportunity to probe the electron-transfer properties of the complexes. Cyclic voltammetry was carried out on **1a**–**3a**, **1b**, and **3b** in CH_2Cl_2/Bu_4NPF_6 (0.1 M). All the complexes show one oxidation and one reduction step, both of which are electrochemically and chemically irreversible at 295 K at all studied scan rates (50–1000 mV/s). The irreversibility of the processes is probably related to the presence of the hydrido ligand on the ruthenium center and the acidic N–H group in the $\mathbf{Q_{-H}}$ ligands. On lowering the temperature to 223 K, the reduction step became reversible, which can be seen from the peak separation of the forward and reverse waves and their heights (Figure 4). However, the oxidation step remained irreversible, and one can see further follow-up peaks on the anodic side (not shown in Figure 4), which are probably an effect of the first oxidation step.

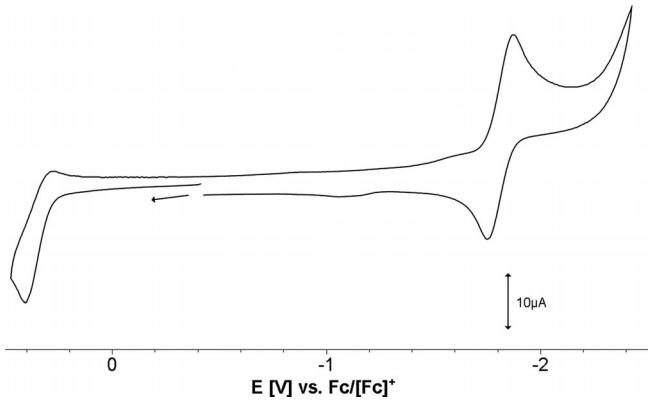

Figure 4. Cyclic voltammogram of **2a** in CH_2Cl_2/Bu_4NPF_6 (0.1 M) at 223 K. Scan rate: 100 mV/s.

The redox potentials for **1a**, **1b**, and **2a** are comparable, which is to be expected because of the similar electronic properties of the *n*-butyl and isopropyl groups. Positional isomers are also known to show virtually identical responses in their cyclic voltammograms. In contrast, the redox potentials of **3a** and **3b** are positively shifted compared to those of the other complexes (Table 2), which is expected because of the larger +I effect of *n*-butyl and isopropyl groups compared to the benzyl group. As the redox processes were not reversible at room temperature, our instrumental set up did not allow us to carry out detailed spectroelectrochemical measurements on these systems. In the absence of such data we can only speculate on the site of electron transfer in comparison to systems reported in the literature. The reduction step can be safely assigned to a reduction that predominantly takes place on $\mathbf{Q_{-H}}$. Metal complexes reported with such ligands usually show reduction steps at relatively high negative potentials.[47–49,51] Additionally, the free forms of such ligands also display such reduction processes.[47] Assignment of the oxidation step is more tricky because of the presence of the redox-active ruthenium(II) center and the noninnocent $\mathbf{Q_{-H}}$ ligands. Both these entities are known to undergo oxidation processes at comparatively low potentials.[51] As the oxidation step is irreversible even at low temperatures, one is tempted to assign it to an oxidation of the $\mathbf{Q_{-H}}$ ligand. However, we cannot totally rule out the oxidation of the ruthenium(II) center or a mixed situation.

Table 2. Redox potentials [V] obtained from cyclic voltammetry experiments.[a]

Complex	E_{pa} (ox)	$E_{1/2}$(red)
1a	0.32	–1.90
1b	0.35	–1.85
2a	0.40	–1.85
3a	0.55	–1.70
3b	0.57	–1.72

[a] Potentials vs. Fc/Fc^+. From measurements in CH_2Cl_2/Bu_4NPF_6 (0.1 M).

Catalytic Transfer Hydrogenation

Ruthenium hydride complexes are intermediates in many catalytic processes,[52] and transfer hydrogenation is an important example of such a process.[53] This reaction continues to attract considerable interest for both academic and industrial applications, because it allows hydrogenation without the use of H_2 gas.[54–64] In order to test the utility of our ruthenium hydride complexes as catalysts in the transfer hydrogenation reaction, we chose **2a** because of its relatively high yield compared to that of the other complexes. Acetophenone was chosen as the substrate and 2-propanol as the hydride source. The reaction is shown in Scheme 3.

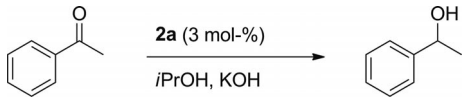

Scheme 3. Transfer hydrogenation reaction catalyzed by **2a**.

Initial attempts to perform the reaction without a base failed at room temperature as well as at a higher temperature. However, in the presence of excess base, 93% conversion to 1-phenylethanol was observed when the reaction was carried out at 70 °C (Table 3).

 © 2012 Wiley-VCH Verlag GmbH & Co. KGaA, Weinheim

Table 3. Results of catalytic experiments.

Catalyst	Base	Temperature	Time	Conversion
2a	–	r.t.	15 h	–
2a	–	80 °C	15 h	2%
2a	KOH	r.t.	15 h	0%
2a	KOH	70 °C	5 h	82%
2a	KOH	70 °C	10 h	93%

The question arises as to which mechanism this reaction follows. The outer-sphere and the inner-sphere mechanisms are both well established for transfer hydrogenation catalysis.[65–67] It is also known that the distinction between the two mechanisms is sometimes not straightforward.[68] Because of the presence of an additional N–H group in $\mathbf{Q}_{-H}$, it is tempting to propose an outer-sphere mechanism that follows a Noyori-type metal–ligand bifunctional route.[53] The required amide could be generated by an internal tautomeric transformation from a predominant *p*-benzoquinonemonoimine form to an *o*-benzoquinonemonoimine form. However, the experimental conditions that were used here point to an inner-sphere mechanism because of the high temperature that is required for the catalysis to proceed. This is probably related to the generation of a free coordination site at the ruthenium center by the dissociation of a PPh_3 ligand, for example. Addtionally, excess KOH is required for the catalysis to work well, which points to the requirement of a certain concentration of 2-propanolate for the catalysis to occur. Finally, the fact that the hydrido ligand is *trans* to the possible amide site in **2a** is not in favor of an outer-sphere metal–ligand bifunctional mechanism. Although the mechanism remains to be clarified in detail, with the present data we would like to propose an inner-sphere mechanism for the transfer hydrogenation reaction.

Conclusions

We have reported the mononuclear ruthenium hydride complexes of noninnocent quinonoid ligands derived from zwitterions that are characterized by 6π + 6π delocalized systems. The positional isomers of these complexes were separated for each of the complexes. Structural data helped to unambiguously establish isomer identity and showed the relocalization of the π systems within the quinonoid ligands, which resulted in the alternation of single and double bonds. Correlations could be made between local electronic effects and the carbonyl stretching frequencies in the IR spectra as well as the hydride chemical shifts observed in the ^{1}H NMR spectra of the isomers. The complexes show one oxidation and one reduction processes in their cyclic voltammograms, both of which are tentatively assigned to electron-transfer steps on the quinonoid ligands. One of the complexes was tested for its activity as a catalyst precursor in the transfer hydrogenation reaction of acetophenone, for which it shows good activity. Initial studies of the reaction conditions point to a possible inner-sphere mechanism for this reaction. However, detailed description of the reaction steps will have to await elaborate mechanistic studies.

Experimental Section

General Considerations: All commercially available reagents were used as received. Solvents were dried and distilled according to standard procedures. The syntheses of the organic compounds were carried out under air, and the ruthenium complexes were synthesized under argon. $\mathbf{Q^1}$–$\mathbf{Q^3}$[47]and $[Ru(PPh_3)_3(CO)(H)(Cl)]$[69] were prepared according to literature procedures.

Instrumentation: The ^{1}H and ^{31}P{^{1}H} NMR spectra were recorded with a Bruker AC 250 spectrometer. Elemental analysis was performed with a Perkin–Elmer Analyzer 240. Mass spectrometry experiments were carried out with a Bruker Daltronics Mictrotof-Q mass spectrometer. IR spectra were obtained with a Nicolet 6700 FTIR instrument. Cyclic voltammetry was carried out in Bu_4NPF_6 (0.1 M) solutions by using a three-electrode configuration (glassy carbon working electrode, Pt counter electrode, Ag wire as psuedo-reference) and a PAR 273 potentiostat and function generator. The ferrocene/ferrocenium couple served as the internal reference. For the catalytic conversions and yields, a gas chromatograph 7890A from Agilent technologies was used.

Syntheses

$[RuH(CO)(PPh_3)_2(Q^1_{-H})]$ (1a and 1b): $\mathbf{Q^1}$ (1 equiv., 0.1 mmol, 0.025 g) and KO*t*Bu (1 equiv., 0.1 mmol, 0.011 g) were mixed in a Schlenk flask under argon. To the mixture was added dry tetrahydrofuran (THF, 10 mL), and it was stirred at room temperature for 12 h. The violet solution turned orange, and an orange precipitate was formed. After 12 h, the THF was evaporated under high vacuum, and the solid dried under high vacuum for 30 min. $[Ru(PPh_3)_3(CO)(H)(Cl)]$ (1 equiv., 0.1 mmol, 0.095 g) was added to the orange solid followed by dry ethanol (20 mL). The mixture was heated to reflux under Ar overnight. The ethanol was evaporated under high vacuum. The solid was dissolved in CH_2Cl_2 (2 mL) in air and purified by preparative alumina TLC using 25% MeCN in CH_2Cl_2 as eluent. After purification, a red and a yellow fraction were obtained, which were identified as the positional isomers in a red/yellow ratio of 7:3. The overall yield was 30%. **1a** (red fraction): ^{1}H NMR (250 MHz, CD_3CN): δ = 7.64–7.57 (m, 12 H), 7.45–7.33 (m, 18 H), 5.97 (t, J = 5.75 Hz, 1 H), 4.79 (s, 1 H), 4.75 (s, 1 H), 3.04 (q, J = 6.5 Hz, 2 H), 2.90 (t, J = 8.5 Hz, 2 H), 1.62–1.51 (m, 3 H), 1.42–1.29 (m, 3 H), 1.07–0.85 (m, 7 H), 0.68 (t, J = 6 Hz, 3 H), –10.01 (t, J = 21.25 Hz, 1 H) ppm. ^{31}P{^{1}H} NMR (120 MHz, $CDCl_3$): δ = 43.5 ppm. MS: m/z = 905.2 $[M]^+$. $C_{51}H_{53}N_2O_3P_2Ru$ (905.26): calcd. C 67.76, H 5.80, N 3.10; found C 68.33, H 5.50, N 3.24. IR: $\tilde{\nu}$ = 3054 (w), 2958 (w), 2923 (w), 2362 (br.), 1911 (vs), 1735 (s), 1555 (s), 1497 (s), 1480 (s), 1090 (s) cm^{-1}. **1b** (yellow fraction): ^{1}H NMR (250 MHz, CD_3CN): δ = 7.75–6.95 (m, 70 H), 6.22 (t, J = 6.25 Hz, 1 H), 4.88 (s, 1 H), 4.5 (s, 1 H), 3.00 (q, J = 6.75 Hz, 2 H), 2.32 (t, J = 7.38 Hz, 2 H), 1.60–1.47 (m, 4 H), 1.41–1.31 (m, 4 H) 1.01–0.82 (m, 8 H), 0.59 (t, J = 7.25 Hz, 3 H), –14.32 (t, J = 17.5 Hz, 1 H) ppm. ^{31}P{^{1}H}NMR (120 MHz, CD_3CN): δ = 43.6 ppm. MS: m/z = 905.2 $[M]^+$. $C_{51}H_{53}N_2O_3P_2Ru$ (905.26): calcd. C 67.76, H 5.80, N 3.10; found C 66.95, H 5.94, N 2.99. IR: $\tilde{\nu}$ = 3055 (w), 2954 (s), 2924 (s), 2853 (br.), 1921 (vs), 1735 (s), 1495 (s), 1481 (s), 1433 (s), 1091 (s) cm^{-1}.

$[RuH(CO)(PPh_3)_2(Q^2_{-H})]$ (2a and 2b): $\mathbf{Q^2}$ (1 equiv., 0.1 mmol, 0.022 g) and KO*t*Bu (1 equiv., 0.1 mmol, 0.011 g) were mixed in a Schlenk flask under argon. To the mixture was added dry THF

 © 2012 Wiley-VCH Verlag GmbH & Co. KGaA, Weinheim

(10 mL), and it was stirred at room temperature for 12 h. The violet solution turned orange, and an orange precipitate was obtained. After 12 h, the THF was evaporated under high vacuum, and the residue was dried under high vacuum for 30 min. $[Ru(PPh_3)_3(CO)(H)(Cl)]$ (1 equiv., 0.1 mmol, 0.095 g) was added to the orange solid followed by dry ethanol (20 mL). The mixture was heated to reflux overnight under Ar. The ethanol was evaporated under high vacuum. The reddish solid was dissolved in CH_2Cl_2 (2 mL) in air and purified by preparative alumina TLC using 25% MeCN in CH_2Cl_2 as eluent. Two fractions were obtained, a red and a yellow fraction, which were identified as positional isomers in a ratio of 100:1. Because of the extremely low yield of the yellow fraction (**2b**) it was not possible to characterize it. The overall yield of both isomers was 35%. **2a** (red fraction): ^{1}H NMR (250 MHz, CD_3CN): δ = 7.53–7.45 (m, 13 H), 7.33–7.25 (m, 17 H), 5.83 (d, J = 7.5 Hz, 1 H), 5.02 (s, 1 H), 4.86 (s, 1 H), 3.59 (sept, J = 6.25 Hz, 1 H), 3.42 (sept, J = 6.5 Hz, 1 H), 1.19 (d, J = 6.25 Hz, 6 H), 0.77 (d, J = 6.5 Hz, 6 H), –10.75 (t, J = 22.5 Hz, 1 H) ppm. $^{31}P\{^1H\}$ NMR (120 MHz, CD_3CN): δ = 40.4 ppm. MS: m/z = 876.2 $[M]^+$. $C_{49}H_{49}N_2O_3P_2Ru$ (876.23): calcd. C 67.19, H 5.52, N 3.20; found C 66.76, H 5.35, N 3.07. IR: $\tilde{\nu}$ = 3054 (w), 2968 (w), 2928 (w), 2361 (br.), 1909 (vs), 1732 (s), 1579 (s), 1493 (s), 1433 (s), 1277 (s), 1090 (s) cm^{-1}. **2b** (yellow fraction, not isolated): ^{1}H NMR (250 MHz, CD_3CN): δ = 7.55–7.42 (m, 13 H), 7.33–7.28 (m, 17 H), 5.83 (d, J = 7.5 Hz, 1 H), 5.15 (s, 1 H), 4.78 (s, 1 H), 3.53 (sept, J = 6.25 Hz, 1 H), 3.38 (sept, J = 6.5 Hz, 1 H), 1.19 (d, J = 6.25 Hz, 6 H), 0.77 (d, J = 6.5 Hz, 6 H), –14.52 (t, J = 17.5 Hz, 1 H) ppm. $^{31}P\{^1H\}$ NMR (120 MHz, CD_3CN): δ = 41.5 ppm.

$[RuH(CO)(PPh_3)_2(Q^3_{-H})]$ (3a and 3b): Q^3 (1 equiv., 0.1 mmol, 0.032 g) and KO*t*Bu (1 equiv., 0.1 mmol, 0.011 g) were mixed in a Schlenk flask under argon. To the mixture was added dry THF (10 mL), and it was stirred at room temperature for 12 h. The violet solution turned orange, and an orange precipitate was obtained. After 12 h, the THF was evaporated under high vacuum, and the residue was dried under high vacuum for 30 min. $[Ru(PPh_3)_3(CO)(H)(Cl)]$ (1 equiv., 0.1 mmol, 0.095 g) was added to the orange solid followed by dry ethanol (20 mL). The mixture was heated to reflux under Ar overnight. The ethanol was evaporated under high vacuum. The reddish solid was dissolved in CH_2Cl_2 (2 mL) in air and purified by preparative alumina TLC using 25% MeCN in CH_2Cl_2 as eluent. Two fractions were obtained, a red and a yellow one, which were identified to be positional isomers in a red/yellow ratio of 7:3. The overall yield was 37%. **3a** (red fraction): ^{1}H NMR (250 MHz, CD_3CN): δ = 7.42–7.25 (m, 36 H), 7.07 (t, J = 7.5 Hz, 2 H), 6.84 (t, J = 7.5 Hz, 2 H), 6.63 (d, J = 7.5 Hz, 2 H), 5.12 (s, 1 H), 4.84 (s, 1 H), 4.36 (d, J = 6.5 Hz, 2 H), 4.05 (s, 2 H), –10.00 (t, J = 22.5 Hz, 1 H) ppm. $^{31}P\{^1H\}$ (120 MHz, CD_3CN): δ = 41.5 ppm. MS: m/z = 973.2 $[M]^+$. $C_{57}H_{49}N_2O_3P_2Ru$ (973.26): calcd. C 70.43, H 4.98, N 2.88; found C 70.13, H 5.05, N 2.77. IR: $\tilde{\nu}$ = 3057 (w), 2955 (s), 2924 (s), 2853 (s), 2360 (s), 2342 (s), 1915 (vs), 1735 (s), 1556 (s), 1258 (s), 1091 (br.), 1009 (br.) cm^{-1}. **3b** (yellow fraction): ^{1}H NMR (250 MHz, CD_3CN): δ = 7.70–7.24 (m, 35 H), 6.92 (d, J = 7.25 Hz, 3 H), 6.54 (t, J = 7.25 Hz, 3 H), 4.80 (s, 1 H), 4.78 (s, 1 H), 4.38 (d, J = 6.25 Hz, 2 H), 3.8 (s, 2 H), –14.53 (t, J = 17.25 Hz, 1 H) ppm. $^{31}P\{^1H\}$ NMR (120 MHz, CD_3CN): δ = 43.1 ppm. MS: m/z = 973.2 $[M]^+$. $C_{57}H_{49}N_2O_3P_2Ru$ (973.26): C 70.43, H 4.98, N 2.88; found C 70.18, H 4.86, N 2.75. IR: $\tilde{\nu}$ = 2959 (s), 2925 (s), 2216 (w), 2127 (w), 1926 (vs), 1736 (vs), 1436 (s), 1258 (s), 1091 (br.), 1006 (br.) cm^{-1}.

General Procedure for the Catalysis: The catalyst (0.03 equiv., 0.015 mmol, 0.013 g) was dissolved in 2-propanol (5 mL) and the mixture stirred for 5 min. KOH (0.33 equiv., 0.17 mmol, 0.009 g) was added, and the mixture was stirred for 5 min. Acetophenone (1 equiv., 0.5 mmol, 0.061 g), dissolved in 2-propanol (5 mL), was added. The mixture was and stirred under Ar at 70 °C for 5 h or overnight. After completion of the reaction, the mixture was filtered through cotton wool, and the conversion was analyzed by gas chromatography.

X-ray Crystallography: Data collection was performed with a Kappa CCD diffractometer. The measurements were carried out at 173 K by using Mo-K_α radiation (graphite monochromator). The structures were solved and refined by full-matrix least-squares techniques on F^2 with SHELX-97.[70] A severe disorder of the solvent was observed in **2a**; attempts to model the disorder failed. A SQUEEZE procedure[71] was applied on 586 Å^3 of solvent-accessible voids and 286 e/cell. The acetonitrile molecules in **3a** are disordered (Table 4). CCDC-804975 (for **2a**) and -804977 (for **3a**) contain the supplementary crystallographic data for this paper. These data can be obtained free of charge from The Cambridge Crystallographic Data Centre via www.ccdc.cam.ac.uk/data_request/cif.

Supporting Information (see footnote on the first page of this article): IR spectra of the complexes.

Table 4. Crystallographic details.

	2a	**3a**·MeCN
Empirical formula	$C_{49}H_{48}N_2O_3P_2Ru$	$C_{60}H_{49}N_3O_3P_2Ru$
M_r	875.90 g mol^{-1}	1013.03 g mol^{-1}
Crystal system, space group	monoclinic, $P2_1/n$	triclinic, $P\bar{1}$
a, b, c [Å]	12.2122(7), 15.6578(5), 13.9000(8)	13.1210(3), 13.5752(2), 15.7258(4)
α, β, γ [°]	90, 108.663(3), 90	112.9880(10), 98.2500(10), 103.0220(10)
V [Å^3]	2518.1(2)	2427.20(9)
Z	2	2
Density [g cm^{-3}]	1.155	1.386
F(000)	908	1048
Radiation type	Mo-K_α	Mo-K_α
μ [mm^{-1}]	0.412	0.439
Crystal size	0.25 × 0.15 × 0.15 mm	0.25 × 0.10 × 0.15
Measured reflections	6433	20522
Independent reflections	3524	11556
Observed [$I > 2\sigma(I)$] reflections	4857	10301
R_{int}	0.0789	0.0380
$R[F^2 > 2\sigma(F^2)]$, $wR(F^2)$, S	0.0545, 0.1483, 1.070	0.0296, 0.1092, 1.177
$\Delta\rho_{max}$, $\Delta\rho_{min}$ [e Å^{-3}]	0.589, –1.047	0.573, –1.272

 © 2012 Wiley-VCH Verlag GmbH & Co. KGaA, Weinheim

Acknowledgments

Baden-Württemberg Stiftung, Fonds der Chemischen Industrie, and Deutsche Forschungsgemeinschaft are kindly acknowledged for financial support of this work. We thank Dr. Roberto Pattacini and Dr. Falk Lissner for the measurement and solution of the crystal structures. We are very grateful to S. Schuster and Prof. Dr. E. Klemm for the measurement and interpretation of the gas-chromatography results.

[1] S. D. Thomson, *Naturally Occurring Quinones IV*, Springer, The Netherlands, **1996**, vol. IV.
[2] H. Decker, T. Schweikardt, F. Tuczek, *Angew. Chem.* **2006**, *118*, 4658; *Angew. Chem. Int. Ed.* **2006**, *45*, 4546.
[3] G. F. Z. da Silva, L.-J. Ming, *Angew. Chem.* **2007**, *119*, 3401; *Angew. Chem. Int. Ed.* **2007**, *46*, 3337.
[4] W. Kaim, B. Schwederski, *Coord. Chem. Rev.* **2010**, *254*, 1580.
[5] C. G. Pierpont, *Coord. Chem. Rev.* **2001**, *216–217*, 95.
[6] C. G. Pierpont, C. W. Lange, *Prog. Inorg. Chem.* **1994**, *41*, 331.
[7] D. Herebian, E. Bothe, F. Neese, T. Weyhermüller, K. Wieghardt, *J. Am. Chem. Soc.* **2003**, *125*, 9116.
[8] M. D. Ward, J. A. McCleverty, *J. Chem. Soc., Dalton Trans.* **2002**, 275.
[9] B. G.-d. Bonneval, K. I. M.-C. Ching, F. Alary, T.-T. Bui, L. Valade, *Coord. Chem. Rev.* **2010**, *254*, 1457.
[10] M. Nomura, T. Cauchy, M. Fourmigué, *Coord. Chem. Rev.* **2010**, *254*, 1406.
[11] P. Zanello, *Coord. Chem. Rev.* **2006**, *250*, 2000.
[12] A. I. Poddel'sky, V. K. Cherkasov, G. A. Abakumov, *Coord. Chem. Rev.* **2009**, *253*, 291.
[13] K. Ray, T. Petrenko, K. Wieghardt, F. Neese, *Dalton Trans.* **2007**, 1552.
[14] S. Bhattacharya, P. Gupta, F. Basuli, C. G. Pierpont, *Inorg. Chem.* **2002**, *41*, 5810.
[15] B. Sarkar, R. Huebner, R. Pattacini, I. Hartenbach, *Dalton Trans.* **2009**, 4653.
[16] A. Paretzki, H. S. Das, F. Weisser, T. Scherer, D. Bubrin, J. Fiedler, J. E. Nycz, B. Sarkar, *Eur. J. Inorg. Chem.* **2011**, 2413.
[17] N. Deibel, D. Schweinfurth, J. Fiedler, S. Zalis, B. Sarkar, *Dalton Trans.* **2011**, *40*, 9925.
[18] S. Patra, B. Sarkar, S. M. Mobin, W. Kaim, G. K. Lahiri, *Inorg. Chem.* **2003**, *42*, 6469.
[19] S. Kitagawa, S. Kawata, *Coord. Chem. Rev.* **2002**, *224*, 11.
[20] C. Carbonera, A. Dei, J.-F. Létard, C. Sangregorio, L. Sorace, *Angew. Chem.* **2004**, *116*, 3198; *Angew. Chem. Int. Ed.* **2004**, *43*, 3136.
[21] J. S. Miller, K. S. Min, *Angew. Chem.* **2009**, *121*, 268; *Angew. Chem. Int. Ed.* **2009**, *48*, 262.
[22] D. N. Hendrickson, C. G. Pierpont, *Top. Curr. Chem.* **2004**, *234*, 63.
[23] W.-G. Jia, Y.-F. Han, Y.-J. Lin, L.-H. Weng, G.-X. Jin, *Organometallics* **2009**, *28*, 3459.
[24] S. Kar, B. Sarkar, S. Ghumaan, D. Janardanan, J. v. Slageren, J. Fiedler, V. G. Puranik, R. B. Sunoj, W. Kaim, G. K. Lahiri, *Chem. Eur. J.* **2005**, *11*, 4901.
[25] J. Mattsson, P. Govindaswamy, A. K. Renfrew, P. J. Dyson, P. Stepnicka, G. S.-Fink, B. Therrien, *Organometallics* **2009**, *28*, 4350.
[26] H. Masui, A. L. Freda, M. C. Zerner, A. B. P. Lever, *Inorg. Chem.* **2000**, *39*, 141.
[27] M. Leschke, M. Melter, H. Lang, *Inorg. Chim. Acta* **2003**, *350*, 114.
[28] G. Margraf, T. Kretz, F. F. d. Biani, F. Laschi, S. Losi, P. Zanello, J. W. Bats, B. Wolf, K. R. Langer, M. Lang, A. Prokofiev, W. Assmus, H.-W. Lerner, M. Wagner, *Inorg. Chem.* **2006**, *45*, 1277.
[29] Y.-F. Han, H. Li, G.-X. Jin, *Chem. Commun.* **2010**, *46*, 6879.
[30] A. Pitto-Barry, N. P. E. Barry, O. Zava, R. Deschenaux, B. Therrien, *Chem. Asian J.* **2011**, *6*, 1595.
[31] S. Maji, B. Sarkar, S. M. Mobin, J. Fiedler, F. A. Urbanos, R. J.-Aparicio, W. Kaim, G. K. Lahiri, *Inorg. Chem.* **2008**, *47*, 5204.
[32] D. Kumbhakar, B. Sarkar, S. Maji, S. M. Mobin, J. Fiedler, F. A. Urbanos, R.-J. Aparicio, W. Kaim, G. K. Lahiri, *J. Am. Chem. Soc.* **2008**, *130*, 17575.
[33] D. Kumbhakar, B. Sarkar, A. Das, A. K. Das, S. M. Mobin, J. Fiedler, W. Kaim, G. K. Lahiri, *Dalton Trans.* **2009**, 9645.
[34] H. S. Das, F. Weisser, D. Schweinfurth, C.-Y. Su, L. Bogani, J. Fiedler, B. Sarkar, *Chem. Eur. J.* **2010**, *16*, 2977.
[35] D. Schweinfurth, H. S. Das, F. Weisser, D. Bubrin, B. Sarkar, *Inorg. Chem.* **2011**, *50*, 1150.
[36] F. Weisser, R. Huebner, D. Schweinfurth, B. Sarkar, *Chem. Eur. J.* **2011**, *17*, 5727.
[37] D. Zhang, G.-X. Jin, *Organometallics* **2003**, *22*, 2851.
[38] S. Scheuermann, B. Sarkar, M. Bolte, J. W. Bats, H.-W. Lerner, M. Wagner, *Inorg. Chem.* **2009**, *48*, 9385.
[39] A. I. Nguyen, K. J. Blackmore, S. M. Carter, R. A. Zarkesh, A. F. Heyduk, *J. Am. Chem. Soc.* **2009**, *131*, 3307.
[40] M. R. Ringenberg, S. L. Kokatam, Z. M. Heiden, T. B. Rauchfuss, *J. Am. Chem. Soc.* **2008**, *130*, 788.
[41] O. Siri, P. Braunstein, *Chem. Commun.* **2002**, 208.
[42] O. Siri, P. Braunstein, M.-M. Rohmer, M. Benard, R. Welter, *J. Am. Chem. Soc.* **2003**, *125*, 13793.
[43] Q. Z. Yang, O. Siri, P. Braunstein, *Chem. Commun.* **2005**, 2660.
[44] Q. Z. Yang, O. Siri, P. Braunstein, *Chem. Eur. J.* **2005**, *11*, 7237.
[45] J.-P. Taquet, O. Siri, P. Braunstein, R. Welter, *Inorg. Chem.* **2004**, *43*, 6944.
[46] Q. Z. Yang, A. Kermagoret, M. Agostinho, O. Siri, P. Braunstein, *Organometallics* **2006**, *25*, 5518.
[47] P. Braunstein, D. Bubrin, B. Sarkar, *Inorg. Chem.* **2009**, *48*, 2534.
[48] A. Paretzki, R. Pattacini, R. Huebner, P. Braunstein, B. Sarkar, *Chem. Commun.* **2010**, *46*, 1497.
[49] N. Deibel, D. Schweinfurth, R. Huebner, P. Braunstein, B. Sarkar, *Dalton Trans.* **2011**, *40*, 431.
[50] F. A. Cotton, J.-Y. Jin, Z. Li, C. A. Murillo, J. H. Reibenspies, *Chem. Commun.* **2008**, 211.
[51] H. S. Das, A. K. Das, R. Pattacini, R. Huebner, B. Sarkar, P. Braunstein, *Chem. Commun.* **2009**, 4387.
[52] G. J. Kubas, *Chem. Rev.* **2007**, *107*, 4152.
[53] R. Noyori, M. Yamakawa, S. Hashiguchi, *J. Org. Chem.* **2001**, *66*, 7931.
[54] G. Zassinovich, G. Mestroni, S. Gladiali, *Chem. Rev.* **1992**, *92*, 1051.
[55] J. S. M. Samec, J. E. Bäckvall, P. G. Andersson, P. Brandt, *Chem. Soc. Rev.* **2006**, *35*, 237.
[56] O. Pàmies, J. E. Bäckvall, *Chem. Eur. J.* **2001**, *7*, 5052.
[57] T. Ikariya, K. Murata, R. Noyori, *Org. Biomol. Chem.* **2006**, *4*, 393.
[58] P. Braunstein, F. Naud, *Angew. Chem.* **2001**, *113*, 702; *Angew. Chem. Int. Ed.* **2001**, *40*, 680.
[59] J. E. Bäckvall, *J. Organomet. Chem.* **2002**, *652*, 105.
[60] P. Braunstein, M. D. Fryzuk, F. Naud, S. J. Rettig, *J. Chem. Soc., Dalton Trans.* **1999**, 589.
[61] P. Braunstein, F. Naud, A. Pfaltz, S. J. Rettig, *Organometallics* **2000**, *19*, 2676.
[62] W. Baratta, F. Benedetti, A. Del Zotto, L. Fanfoni, F. Feluga, S. Magnolia, E. Putihano, P. Rigo, *Organometallics* **2010**, *29*, 3563.
[63] W. Baratta, G. Bossi, E. Putiguano, P. Rigo, *Chem. Eur. J.* **2011**, *17*, 3474.
[64] W. Baratta, R. Herdtweck, K. Siega, M. Toniutti, P. Rigo, *Organometallics* **2005**, *24*, 1660.
[65] Y. Jiang, Q. Jiang, X. Zhang, *J. Am. Chem. Soc.* **1998**, *120*, 3817.
[66] S. E. Clapham, A. Hadzovic, R. H. Morris, *Coord. Chem. Rev.* **2004**, *248*, 2201.

 © 2012 Wiley-VCH Verlag GmbH & Co. KGaA, Weinheim

[67] L. T. Ghoochany, S. Farsadpour, Y. Sun, W. R. Thiel, *Eur. J. Inorg. Chem.* **2011**, 3431.
[68] C. P. Casey, S. W. Singer, D. R. Powell, R. K. Hayashi, M. Kavana, *J. Am. Chem. Soc.* **2001**, *123*, 1090.
[69] T. Joseph, S. S. Deshpande, S. B. Halligudi, A. Vinu, S. Ernst, M. Hartmann, *J. Mol. Catal. A: Chem.* **2003**, *206*, 13.
[70] G. M. Sheldrick, *SHELXS-97, Program for Solution of Crystal Structures*, University of Göttingen, Germany, **1997**.
[71] A. L. Spek, *J. Appl. Crystallogr.* **2003**, *36*, 7.

Received: October 10, 2011
Published Online: December 13, 2011

 © 2012 Wiley-VCH Verlag GmbH & Co. KGaA, Weinheim

DOI: 10.1002/ejic.201101044

Aerobic Alcohol Oxidations Catalyzed by Oxorhenium Complexes Containing Redox-Active Ligands

Cameron A. Lippert,[a] Korbinian Riener,[a] and Jake D. Soper*[a]

Keywords: Redox-active ligands / Homogeneous catalysis / Oxidation / Rhenium / Proton-coupled electron transfer

The capacity of five-coordinate oxorhenium(V) anions with redox-active catecholate ligands to homolyze O_2 and afford dioxorhenium(VII) products is utilized for the development of new aerobic alcohol oxidation catalysts. The reaction of $[Re^{VII}(O)_2(cat)_2]^-$ with benzyl alcohol (BnOH) affords the expected products of net H_2 transfer: $[Re^{V}(O)(cat)_2]^-$, benzaldehyde, and presumably H_2O. However, mechanistic studies reveal that the formation of the active oxidant requires both the dioxo and monooxo species, so BnOH oxidation by $[Re^{VII}(O)_2(cat)_2]^-$ exhibits an unexpected catalytic dependence on $[Re^{V}(O)(cat)_2]^-$. Attempts to oxidize more thermodynamically challenging primary alcohols, which include CH_3OH, using the $[Re^{VII}(O)_2(cat)_2]^-$ + $[Re^{V}(O)(cat)_2]^-$ system did not yield aldehyde products. However, experiments performed in CH_3OH allowed the observation of a catalytically active intermediate species, which provides an insight into the mechanism of catalytic action and catalyst degradation. Based on these observations, complexes that contain a more oxidatively robust $[Br_4cat]^{2-}$ ligand were shown to exhibit higher catalytic activity as measured by total turnover number. The requirement for a redox-active ligand for catalyst function has both benefits and limitations that are discussed in the context of aerobic alcohol oxidation catalysis.

Introduction

Recent progress in the elaboration of complexes with redox-active ligands for selective bond making and breaking[1,2] has precipitated the development of an array of new catalytic methods for small molecule transformations, which include hydrogenation and dehydrogenation,[3,4] alcohol oxidation,[5] nitrene transfer,[6] and C–C bond formation.[3c,7,8] In addition to some of these, we are interested in expanding the utility of redox-active ligands for selective O_2 reduction in aerobic oxidation catalysis.[5c] Towards this goal, a recent study from our laboratory described the details of O_2 homolysis by oxorhenium(V) anions with redox-active ligands to generate dioxorhenium(VII) products (Scheme 1a).[9] Notably, the capacity of catechol- and aminophenol-derived ligands to undergo reversible 1e⁻ redox changes is a critical feature of O_2 homolysis reactions because multielectron O_2 cleavage proceeds by a series of 1e⁻ Re–O bond formation steps that generate superoxo and peroxo complex intermediates. Accordingly, the coordination of a redox-active ligand lowers the kinetic barrier to O_2 activation by allowing the 1e⁻ Re–O bond formation reactions to occur at the oxorhenium(V) centers without generating high-energy oxorhenium(VI) intermediates.

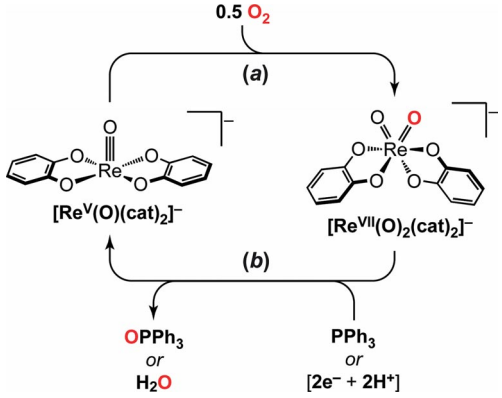

Scheme 1. Redox-active ligand-mediated O_2 homolysis at $[Re^{V}(O)(cat)_2]^-$ for oxo transfer catalysis.

Because high-valent metal–oxo compounds are ubiquitous in oxidation catalysis,[10] facile generation of a terminal Re^{VII}=O from O_2 presaged the development of new aerobic oxidation catalytic cycles. In our initial report, we noted that the dioxorhenium(VII) anions were efficiently reduced by PPh_3 to yield $OPPh_3$ and the corresponding monooxorhenium(V) species (Scheme 1b).[9] The sum of these stoichiometric reactions comprises a complete cycle for catalytic aerobic phosphane oxidation (Scheme 1). However, the practical utility of the rhenium complexes with redox-active ligands as oxo transfer reagents is limited by the thermodynamic stability of the Re^{VII}=O bonds, which require strong oxo acceptor substrates for catalytic turnover. In an attempt to expand the scope of O_2-derived oxo transfer ca-

[a] School of Chemistry and Biochemistry, Georgia Institute of Technology,
Atlanta, GA 30332-0400, USA
E-mail: jake.soper@chemistry.gatech.edu

Supporting information for this article is available on the WWW under http://dx.doi.org/10.1002/ejic.201101044.

WILEY ONLINE LIBRARY
© 2012 Wiley-VCH Verlag GmbH & Co. KGaA, Weinheim

talysis, we turned our attention to oxidase-type oxidations, in which the net addition of H_2 (or $2e^- + 2H^+$) to the oxo fragment might provide a more accessible kinetic pathway for reduction of the dioxorhenium(VII) complexes. We took inspiration from previous reports of catalytic alcohol oxidations that used high-valent rhenium complexes along with stoichiometric cooxidants, such as H_2O_2 and PhIO,[11] to pursue an aerobic variant of this chemistry based on facile O_2 homolysis by oxorhenium(V) compounds with redox-active ligands.[12]

This manuscript describes our first efforts to use O_2-derived dioxorhenium(VII) complexes with redox-active ligands for aerobic alcohol oxidation catalysis. The conditions for stoichiometric and catalytic oxidations of benzyl alcohol to afford benzaldehyde are reported. Attempts to oxidize more challenging alcohols, including CH_3OH, did not yield aldehyde products, but allowed the observation of a catalytically active intermediate species. Mechanistic investigations of oxidations by the dioxorhenium(VII) complexes revealed a surprising requirement for catalytic oxorhenium(V) and highlighted the necessity of the redox-active ligand for catalyst function. The utility and scope of this new methodology within these constraints are discussed.

Results

Aerobic Oxidation of $[Re^{V}(O)(cat)_2]^-$ to $[Re^{VII}(O)_2(cat)_2]^-$ in CH_3OH

Exposure of a green CH_3OH solution of $[Et_4N][Re^{V}(O)(cat)_2]$ ($[cat]^{2-}$ = 1,2-catecholate) to dry air results in the formation of a bright blue intermediate species (**I_B**) in ca. 100 min followed by slow conversion to a bright purple solution over 50 h (Figure 1). Comparison of the UV/Vis spectrum of the resulting purple solution with that of an authentic sample of $[Et_4N][Re^{VII}(O)_2(cat)_2]$, confirmed that $[Re^{VII}(O)_2(cat)_2]^-$ was the only observable colored product of the reaction. However, at UV/Vis concentrations (ca. 0.5 mM) in CH_3OH the aerobic oxidation of $[Re^{V}(O)(cat)_2]^-$ produced $[Re^{VII}(O)_2(cat)_2]^-$ in moderate yields (ca. 30%). The yield of $[Re^{VII}(O)_2(cat)_2]^-$ increased to ca. 75% when the reaction was performed using higher initial concentrations of $[Re^{V}(O)(cat)_2]^-$ (10–15 mM) in [D4]methanol, which was determined by ^1H NMR spectroscopy. In contrast, the same reaction performed in CH_2Cl_2 or CH_3CN gave quantitative conversion to $[Re^{VII}(O)_2(cat)_2]^-$ at all concentrations without the observation of **I_B**.[9]

Reduction of $[Re^{VII}(O)_2(cat)_2]^-$ to $[Re^{V}(O)(cat)_2]^-$ in Air-Free Alcohol Solutions

The UV/Vis spectra of CH_3OH solutions of pure $[Re^{VII}(O)_2(cat)_2]^-$ were stable under N_2 for weeks at ambient temperature, but we observed that samples that contained trace $[Re^{V}(O)(cat)_2]^-$ impurity underwent a series of color changes (from purple to blue to green) over several days,

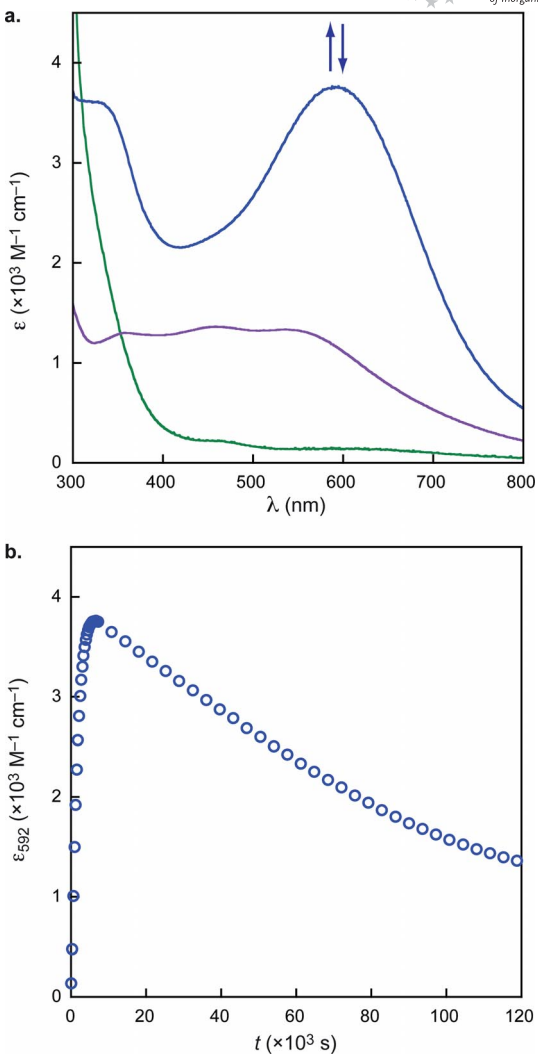

Figure 1. Selected UV/Vis absorption data from a reaction of 4.5×10^{-4} M $[Re^{V}(O)(cat)_2]^-$ with 1 atm dry air in CH_3OH at 25 °C. Spectra were selected at time points that correspond to the maximum yield of each observable species, which was measured by the change in absorption intensity at their respective λ_{max} values. (a) The reaction occurs in two phases; the first phase converts $[Re^{V}(O)(cat)_2]^-$ (green line) into **I_B** (blue line) in 100 min. The second phase affords $[Re^{VII}(O)_2(cat)_2]^-$ (purple line) in ca. 30% yield after 3000 min. (b) Time resolved absorption data at 592 nm for the formation and decay of **I_B**.

which appeared to correspond to the reverse of the oxidation described above. These color changes were reproduced by addition of 1 equiv. of $[Re^{V}(O)(cat)_2]^-$ to a purple solution of pure $[Re^{VII}(O)_2(cat)_2]^-$ in CH_3OH under N_2, which yielded a bright blue solution immediately with a UV/Vis spectrum identical to that of **I_B** observed in the reaction of $[Re^{V}(O)(cat)_2]^-$ with air in CH_3OH (vide supra). Over several days the blue solution gradually reformed pale green $[Re^{V}(O)(cat)_2]^-$, which was evidenced by its characteristic ^1H NMR spectrum. Similarly prepared solutions that contained $[Re^{V}(O)(cat)_2]^-$ and $[Re^{VII}(O)_2(cat)_2]^-$ in CH_3CN, tetrahydrofuran, dimethylsulfoxide, or CH_2Cl_2 gave no reaction that could be observed by UV/Vis or ^1H NMR spec-

 © 2012 Wiley-VCH Verlag GmbH & Co. KGaA, Weinheim

troscopy over several days, which suggests that CH_3OH is a critical component of the reduction.

Because both $[Re^{V}(O)(cat)_2]^-$ and $[Re^{VII}(O)_2(cat)_2]^-$ were required for the reaction under N_2, we initially suspected that the blue intermediate $\mathbf{I_B}$ observed in CH_3OH was a dimer of the oxorhenium(V) and dioxorhenium(VII) anions. All attempts to isolate and structurally characterize $\mathbf{I_B}$ were unsuccessful, which prompted us to pursue a spectroscopic investigation of its reaction kinetics and stoichiometry.[13] Surprisingly, experiments performed with varying initial proportions of $[Re^{V}(O)(cat)_2]^-$ and $[Re^{VII}(O)_2(cat)_2]^-$, but at constant total rhenium concentration, revealed that the yield of $\mathbf{I_B}$ scales linearly with the initial $[Re^{VII}(O)_2(cat)_2]^-$ concentration (Figure 2a). Furthermore, at constant concentrations of $[Re^{VII}(O)_2(cat)_2]^-$, the yield of $\mathbf{I_B}$ was independent of the initial concentration of $[Re^{V}(O)(cat)_2]^-$ (Figure 2b) but its relative rate of formation was a function of initial $[Re^{V}(O)(cat)_2]^-$ concentration (Figure 2c). These data imply that $[Re^{V}(O)(cat)_2]^-$ is a catalyst for the net reduction of $[Re^{VII}(O)_2(cat)_2]^- \rightarrow \mathbf{I_B} \rightarrow [Re^{V}(O)(cat)_2]^-$ in CH_3OH under N_2 but $[Re^{V}(O)(cat)_2]^-$ is not itself a component of $\mathbf{I_B}$.

Interestingly, the blue spectrum characteristic of $\mathbf{I_B}$ was independently generated by treating CH_3OH solutions of pure $[Re^{VII}(O)_2(cat)_2]^-$ with 1 equiv. of $LiOCH_3$ under N_2 (Figure 3). This suggests that $\mathbf{I_B}$ may be an $[OCH_3]^-$ adduct to $[Re^{VII}(O)_2(cat)_2]^-$ (discussed below), and the role of $[Re^{V}(O)(cat)_2]^-$ is to deliver a $[OCH_3]^-$ fragment to $[Re^{VII}(O)_2(cat)_2]^-$.

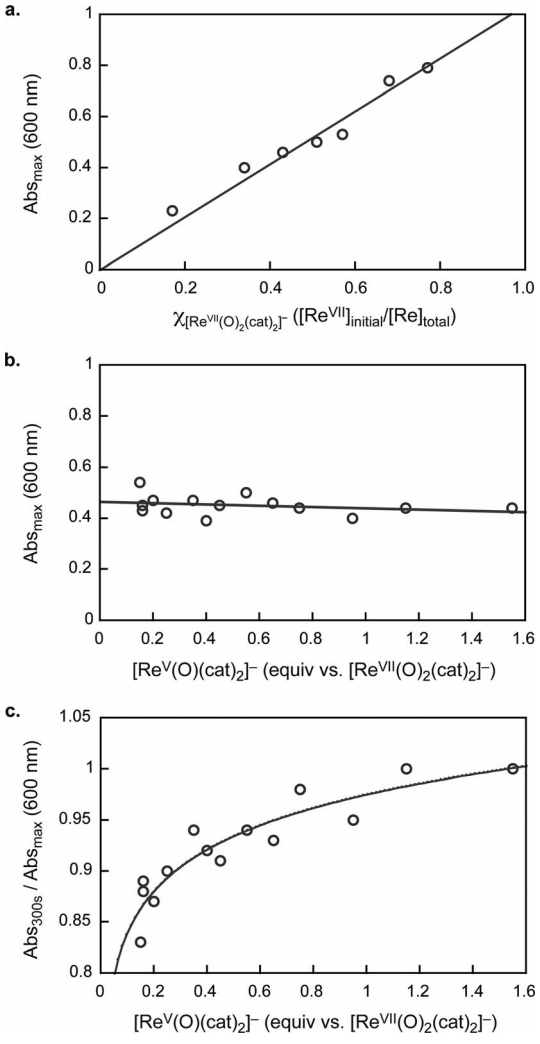

Figure 2. Selected UV/Vis absorption data from reactions of $[Re^{VII}(O)_2(cat)_2]^-$ with $[Re^{V}(O)(cat)_2]^-$ in CH_3OH to produce the blue intermediate $\mathbf{I_B}$ with λ_{max} = 600 nm. (a) Yield of $\mathbf{I_B}$ as a function of initial $[Re^{VII}(O)_2(cat)_2]^-$ concentration for reactions performed at constant total [Re] = 4.0×10^{-4} M. (b) Yield of $\mathbf{I_B}$ from reactions of 1.5×10^{-4} M $[Re^{VII}(O)_2(cat)_2]^-$ performed with varying amounts of added $[Re^{V}(O)(cat)_2]^-$. (c) Ratio of the yield of $\mathbf{I_B}$ at t = 300 s to the maximum $\mathbf{I_B}$ yield observed in reactions of 1.5×10^{-4} M $[Re^{VII}(O)_2(cat)_2]^-$ performed with varying amounts of added $[Re^{V}(O)(cat)_2]^-$.

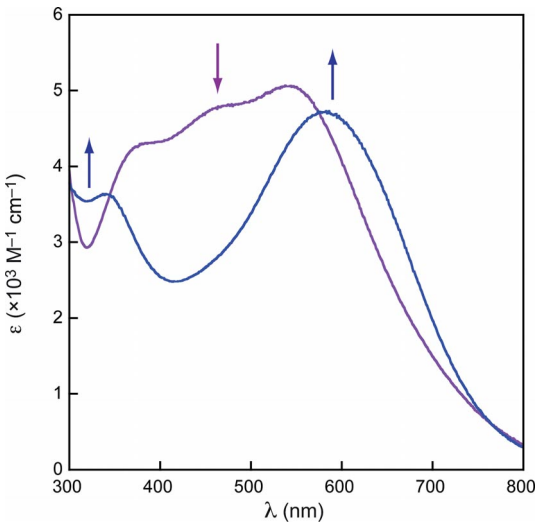

Figure 3. UV/Vis absorption spectra of 2.7×10^{-4} M $[Re^{VII}(O)_2(cat)_2]^-$ (purple line) and $\mathbf{I_B}$ (blue line) in CH_3OH obtained ca. 10 h after addition of 1.0 equiv. $LiOCH_3$ under N_2 at 25 °C.

The addition of 0.1 equiv. of $[Re^{V}(O)(cat)_2]^-$ to a benzyl alcohol (BnOH) solution of $[Re^{VII}(O)_2(cat)_2]^-$ under N_2 effected a color change from purple to green over 1 h at ambient temperature. Monitoring by UV/Vis spectroscopy gave no evidence of a blue intermediate species analogous to $\mathbf{I_B}$ during the reaction. Analysis of the resulting green solution by ^{1}H NMR spectroscopy confirmed that $[Re^{V}(O)(cat)_2]^-$ was the only observable catecholate-containing product, which was isolated in 62% yield by selective precipitation. The balance of the rhenium was apparently in the form of perrhenate $[ReO_4]^-$, which does not have a ^{1}H NMR spectrum but was observed at m/z = 250 in negative ion mode ESI–MS analyses of the crude reaction mixture. Analysis of the same product mixture by GC–MS showed benzaldehyde as the only organic product, which was formed in 58% yield based on limiting $[Re^{VII}(O)_2(cat)_2]^-$ (Table 1, Entry 1).

The marked increase in the rate of the $[Re^{VII}(O)_2(cat)_2]^- \rightarrow [Re^{V}(O)(cat)_2]^-$ reduction in BnOH vs. CH_3OH and the observation of PhCHO in the BnOH reaction mixtures implied that that $[Re^{VII}(O)_2(cat)_2]^-$ oxidizes alcohols according to Equation (1).

 © 2012 Wiley-VCH Verlag GmbH & Co. KGaA, Weinheim

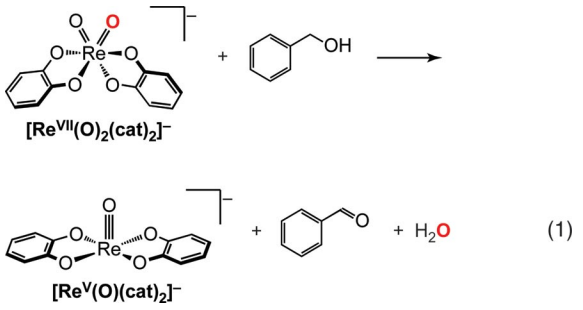

Table 1. Stoichiometric and catalytic oxidations of BnOH to PhCHO using dioxorhenium(VII) complexes with redox-active ligands.[a]

Entry	Oxidant[b]	$[Re^{VII}]_{initial}$ [mM]	$[Re^{V}]_{initial}$ [mM]	Yield [%][c]
1	$[Re^{VII}(O)_2(cat)_2]^- + N_2$	9.7	1.0	58
2	$[Re^{VII}(O)_2(cat)_2]^- + O_2$	0	8.8	118
3	$[Re^{VII}(O)_2(Br_4cat)_2]^- + N_2$	9.4	0.9	93
4	$[Re^{VII}(O)_2(Br_4cat)_2]^- + O_2$	0	8.4	707

[a] All reactions were performed in neat BnOH at 25 °C. [b] Catalytic oxidations using O_2 were performed under 1 atm dry air. [c] The yield was determined by GC analysis vs. a calibrated internal standard as described in the Experimental Section. All yields are the average of at least two independent experiments and are calculated based on limiting rhenium.

Consequently, NMR tubes containing $[Re^{VII}(O)_2(cat)_2]^-$ and 0.1 equiv. of $[Re^{V}(O)(cat)_2]^-$ in [D4]methanol with 5 equiv. of BnOH as an oxidizable substrate rapidly produced a blue solution under N_2 that slowly faded to a pale green over several days at ambient temperature. Formation of the blue intermediate was accompanied by the appearance of new resonances at 6.74 and 6.41 ppm in the ^1H NMR spectrum, which do not match those expected for $[Re^{V}(O)(cat)_2]^-$ or $[Re^{VII}(O)_2(cat)_2]^-$ and cannot be assigned to free $[cat]^{2-}$ or its oxidized derivatives. The new resonances subsequently decreased in intensity as $[Re^{V}(O)(cat)_2]^-$ was produced with concomitant formation of PhCHO. Integration of the ^1H NMR resonances for PhCHO and $[Re^{V}(O)(cat)_2]^-$ indicated that 50% of the initial $[Re^{VII}(O)_2(cat)_2]^-$ was converted to $[Re^{V}(O)(cat)_2]^-$ and a corresponding 0.5 equiv. of aldehyde was formed, which is consistent with the reaction stoichiometry in Equation (1) (Figure S1). H_2O was not found in the reaction mixture, but rapid H/D exchange with [D4]methanol likely obscured its observation by ^1H NMR spectroscopy. As above, the fate of the residual rhenium was apparently $[ReO_4]^-$, as evidenced by its presence in the ESI–MS spectra of the reaction mixtures and the observation free $[cat]^{2-}$ oxidation products in the ^1H NMR spectra at 6.64 and 6.55 ppm. To verify that these decomposition products were not the active species in the alcohol oxidation, solutions of $[ReO_4]^-$, $[ReO_4]^- + [Re^{V}(O)(cat)_2]^-$, and $[ReO_4]^- + [Re^{VII}(O)_2(cat)_2]^-$ in BnOH or MeOH were independently prepared and monitored by ^1H NMR, UV/Vis spectroscopy, and GC–MS. In all cases, no aldehyde was produced and no blue intermediate was observed within 15 h at ambient temperature. These data imply that alcohol oxidation results from a reaction with an intact oxorhenium complex that contains $[cat]^{2-}$ ligands and not from oxidative decomposition products, such as $[ReO_4]^-$ or derivatives thereof, which are produced during the course of the reaction. Consistent with this hypothesis, the addition of excess BnOH to a preformed blue solution of $\mathbf{I_B}$, which was generated from $[Re^{VII}(O)_2(cat)_2]^-$ and 0.1 equiv. $[Re^{V}(O)(cat)_2]^-$ in MeOH, gave an immediate color change to pale green accompanied by the formation of PhCHO, which suggested that $\mathbf{I_B}$ is the species responsible for BnOH oxidation, or a direct precursor to the active oxidant.

Aerobic Alcohol Oxidations Catalyzed by Catecholate-Containing Oxorhenium Complexes

The sum of the alcohol oxidation reaction in Equation (1) and the O_2 homolysis reaction in Scheme 1a comprises a complete catalytic cycle for aerobic alcohol oxidation based on the interconversion of $[Re^{VII}(O)_2(cat)_2]^-$ and $[Re^{V}(O)(cat)_2]^-$. Accordingly, stirring a BnOH solution of $[Re^{V}(O)(cat)_2]^-$ under 1 atm of dry air at ambient temperature gave a slow color change from pale green to dark purple. Analysis of the reaction mixture by ^1H NMR spectroscopy after 24 h showed $[Re^{VII}(O)_2(cat)_2]^-$ and no resonances for $[Re^{V}(O)(cat)_2]^-$, and GC–MS analysis of the same reaction mixture indicated that PhCHO was produced in 118% yield, which corresponds to slightly >1 turnover (Table 1, Entry 2). Although this is approximately double the PhCHO obtained in the stoichiometric reactions of BnOH with $[Re^{VII}(O)_2(cat)_2]^-$ (Table 1, Entry 1), the catalytic activity is poor.

The observation of $[ReO_4]^-$ and catechol-derived oxidation products in the reactions of BnOH with $[Re^{VII}(O)_2(cat)_2]^-$ suggested that the yields and rates of alcohol oxidation may be improved by substitution of the redox-active ligand with one that is more difficult to oxidize. Accordingly, addition of 0.1 equiv. of $[Re^{V}(O)(OPPh_3)(Br_4cat)_2]^-$ ($[Br_4cat]^{2-}$ = tetrabromo-1,2-catecholate) to a BnOH solution of $[Re^{VII}(O)_2(Br_4cat)_2]^-$ under N_2 produced a color change from dark purple to pale green over 90 min at ambient temperature. Analysis of the resulting green solutions by UV/Vis spectroscopy and ESI-MS confirmed that $[Re^{VII}(O)_2(Br_4cat)_2]^-$ was completely consumed in the reaction, and GC–MS of the same reaction mixture showed that PhCHO was the only organic product, which was formed in 93% yield (Table 1, Entry 3). Performing the reaction under dry air gave PhCHO in >700% yield after 7 d, based on the initial $[Re^{V}(O)(OPPh_3)(Br_4cat)_2]^-$ concentration, which corresponds to a sixfold increase in catalytic efficacy compared to the parent catecholate complexes.

Discussion

Formation and Composition of the Blue Oxidant $\mathbf{I_B}$

Formation of $\mathbf{I_B}$ in CH_3OH solution required at least two components: $[Re^{VII}(O)_2(cat)_2]^-$ and 1 equiv. $[OCH_3]^-$ or

 © 2012 Wiley-VCH Verlag GmbH & Co. KGaA, Weinheim

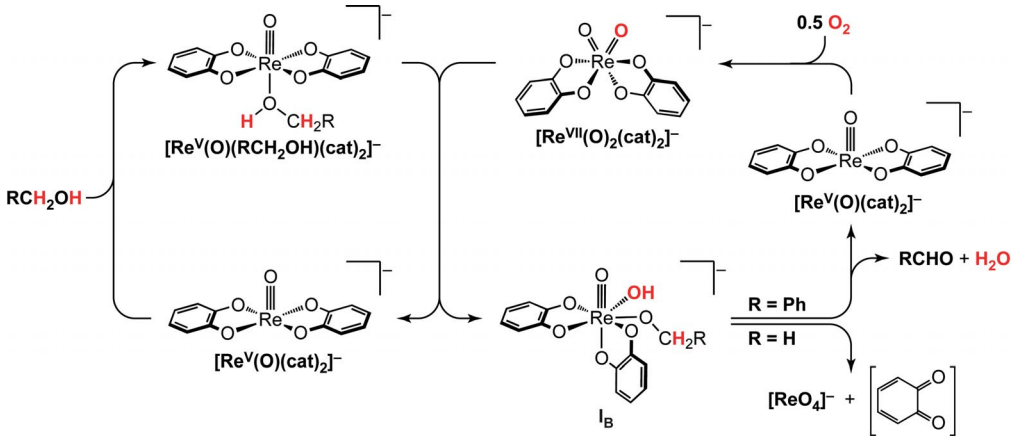

Scheme 2. Proposed mechanism for aerobic alcohol oxidations catalyzed by $[Re^{V}(O)(cat)_2]^-$ + $[Re^{VII}(O)_2(cat)_2]^-$ via $\mathbf{I_B}$.

trace $[Re^{V}(O)(cat)_2]^-$. Accordingly, the same $\mathbf{I_B}$ species was generated both during O_2 homolysis by $[Re^{V}(O)(cat)_2]^-$ and alcohol reduction by $[Re^{VII}(O)_2(cat)_2]^-$ because at intermediate reaction times both CH_3OH solutions contain mixtures of $[Re^{V}(O)(cat)_2]^-$ and $[Re^{VII}(O)_2(cat)_2]^-$. The observation that $\mathbf{I_B}$ was obtained from the reaction of $[Re^{VII}(O)_2(cat)_2]^-$ with either stoichiometric $[OCH_3]^-$ or catalytic $[Re^{V}(O)(cat)_2]^-$ suggests that the function of $[Re^{V}(O)(cat)_2]^-$ is to supply a $[OCH_3]^-$ fragment to $[Re^{VII}(O)_2(cat)_2]^-$. As a result, mixtures of $[Re^{V}(O)(cat)_2]^-$ and $[Re^{VII}(O)_2(cat)_2]^-$ produce $\mathbf{I_B}$ only in CH_3OH because the solvent itself is a component of the reaction. Addition of 1 equiv. of $[OCH_3]^-$ to $[Re^{VII}(O)_2(cat)_2]^-$ did not afford $\mathbf{I_B}$ in solvents such as CH_2Cl_2 or CH_3CN, perhaps due to the lack of accessible H^+, as discussed below.

A blue species analogous to $\mathbf{I_B}$ was also not observed in any reaction that contained BnOH, and the addition of BnOH to a blue solution of $\mathbf{I_B}$ resulted in the immediate formation of PhCHO and $[Re^{V}(O)(cat)_2]^-$. These data rationalize why $\mathbf{I_B}$ only accumulated to observable concentrations in CH_3OH: because $\mathbf{I_B}$ is competent to oxidize BnOH, generation of $\mathbf{I_B}$ (or its $[OBn]^-$ congener) is followed by rapid reduction to $[Re^{V}(O)(cat)_2]^-$. With the less easily reduced CH_3OH, $\mathbf{I_B}$ is unable to generate the corresponding aldehyde, so slow catabolism of the oxorhenium complex affords $[ReO_4]^-$ and free oxidized ligand.

Although the structure of $\mathbf{I_B}$ is not known, it likely contains both $[Re^{VII}(O)_2(cat)_2]^-$ and $[OCH_3]^-$ or CH_3OH. Alkoxide addition to $[Re^{VII}(O)_2(cat)_2]^-$ requires the oxorhenium(VII) center to accommodate a seventh ligand, which is not unreasonable. Computational studies of O_2 activation at $[Re^{V}(O)(cat)_2]^-$ suggest that a stable seven-coordinate η^2-peroxo complex $[Re^{VII}(O)_2(O_2^{2-})(cat)_2]^-$ is the minimum energy dioxygen adduct,[9] and seven-coordinate oxorhenium(VII) complexes have been inferred as intermediates in H_2O_2/CH_3ReO_3 oxidations.[14]

Scheme 2 presents a mechanism for aerobic alcohol oxidation by $[Re^{VII}(O)_2(cat)_2]^-$ + $[Re^{V}(O)(cat)_2]^-$, which is consistent with all of our experimental observations. In this mechanism, the $[Re^{V}(O)(cat)_2]^-$ catalyst is proposed to mediate the formation of $\mathbf{I_B}$ by binding and delivering CH_3OH to $[Re^{VII}(O)_2(cat)_2]^-$. In this respect, it is noteworthy that the color of the $[Re^{V}(O)(cat)_2]^-$ anion is visibly different in CH_3OH (green) vs. noncoordinating solvents (pale tan). We have previously discussed the capacity of $[Re^{V}(O)(cat)_2]^-$ to accommodate a sixth ligand,[9] and the reported single-crystal X-ray data for a CH_3OH adduct to the perchlorinated homolog $[Re^{V}(O)(CH_3OH)(Cl_4cat)_2]^-$ ($[Cl_4cat]^{2-}$ = tetrachloro-1,2-catecholate) provides strong support for the capacity of the $[Re^{V}(O)(cat)_2]^-$ to bind alcohols in this manner.[15] It is conceivable that such a coordinated CH_3OH ligand might hydrogen bond to a catechol oxygen atom of $[Re^{VII}(O)_2(cat)_2]^-$, and the close contact interaction leads to methanol transfer and the generation of $\mathbf{I_B}$. This hypothesis is supported by previous reports of isolated dinuclear rhenium complexes that are bridged by Lewis bases and/or hydrogen bonding interactions.[16]

As discussed above, the formulation of $\mathbf{I_B}$ as an alkoxide complex dianion, $[Re^{VII}(O)_2(OCH_3)(cat)_2]^{2-}$, is consistent with the observation that $\mathbf{I_B}$ is produced by the addition of $[OCH_3]^-$ to $[Re^{VII}(O)_2(cat)_2]^-$. Accordingly, generation of $[Re^{VII}(O)_2(OCH_3)(cat)_2]^{2-}$ from a reaction of $[Re^{VII}(O)_2(cat)_2]^-$ with $[Re^{V}(O)(CH_3OH)(cat)_2]^-$ would require the loss of a proton to solvent or adventitious base. An alternative assignment for $\mathbf{I_B}$ (shown in Scheme 2) is $[Re^{VII}(O)(OH)(OCH_3)(cat)_2]^-$ derived from a net [2+2] addition of CH_3OH across one Re=O bond. In this formulation for $\mathbf{I_B}$, the dianionic $[Re^{VII}(O)_2(OCH_3)(cat)_2]^{2-}$ complex generated from $[Re^{VII}(O)_2(cat)_2]^-$ + 1 equiv. $[OCH_3]^-$ must be a reasonably strong Brønsted base.

Alcohol Oxidation by $\mathbf{I_B}$

The generation of aldehyde and $[Re^{VII}(O)_2(cat)_2]^-$ products from the putative $[Re^{VII}(O)(OH)(OCH_2R)(cat)_2]^-$ intermediates requires the formal removal of $[H]^-$ from the bound alkoxide fragment by transfer of $2e^-$ to the oxorhenium(VII) center and $1H^+$ to the coordinated hydroxide ligand. A plausible mechanism for this transformation is presented in Scheme 3. It invokes a five-membered ring transition state that is strongly reminiscent of alcohol oxidation

 © 2012 Wiley-VCH Verlag GmbH & Co. KGaA, Weinheim

by chromic acid and Dess–Martin periodinane.[10] It is likely that generation of the aldehyde product occurs in a single $1H^+ + 2e^-$ step because protonation of the coordinated hydroxide ligand significantly enhances the oxidizing power of the oxorhenium(VII) center, and reduction of the rhenium(VII) ion makes the hydroxide ligand a much stronger base. Accordingly, coupling proton and electron transfer allows the net reaction to occur without the generation of high-energy species that would result from a stepwise process.

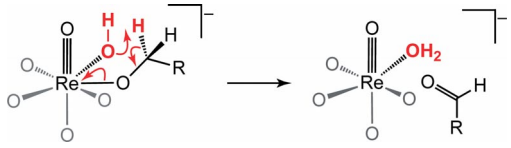

Scheme 3. Intramolecular proton transfer to a hydroxide ligand in $[Re^{VII}(O)(OH)(OCH_2R)(cat)_2]^-$ (**I_B**) for $[OCH_2R]^-$ oxidation.

The generation of PhCHO from BnOH solution establishes net H_2 addition and specifically proton-coupled electron transfer (PCET) as a viable alternative to strong O atom acceptors for the production of $[Re^{V}(O)(cat)_2]^-$ from $[Re^{VII}(O)_2(cat)_2]^-$. However, $[Re^{VII}(O)_2(cat)_2]^-$ does not efficiently oxidize CH_3OH to formaldehyde. Assuming that both $[Re^{VII}(O)(OH)(OCH_2R)(cat)_2]^-$ intermediates have similar steric constraints for the formation of the five-membered ring transition state shown in Scheme 3, the inability of $[Re^{VII}(O)_2(cat)_2]^-$ to oxidize CH_3OH cannot arise from kinetic factors. Rather, its disparate reactivity with CH_3OH vs. BnOH is apparently a function of the relative reducing power of the two alcohols.[17]

Limitations of Redox-Active Ligands for Rhenium Aerobic Alcohol Oxidation Catalysis

Because of their role in mediating O_2 homolysis by $[Re^{V}(O)(cat)_2]^-$, redox-active ligands are a crucial component of oxidase- or oxygenase-type catalytic cycles based on the interconversion of $[Re^{V}(O)(cat)_2]^-$ and $[Re^{VII}(O)_2(cat)_2]^-$ with dioxygen. Unfortunately, the data presented here suggest that the capacity of catecholate ligands to be oxidized at modest potentials also limits the practical utility of the $[Re^{VII}(O)_2(cat)_2]^-$ + $[Re^{V}(O)(cat)_2]^-$ system for catalytic alcohol oxidations.

Foremost among these limitations is catalyst stability. Under all of the conditions examined, alcohol oxidation by $[Re^{VII}(O)_2(cat)_2]^-$ yielded at most 50% of the intact, reduced $[Re^{V}(O)(cat)_2]^-$ and substantial quantities of nonalcohol oxidation products. Substitution of $[cat]^{2-}$ with electron-poor $[Br_4cat]^{2-}$ increased the yield of PhCHO to >90% in stoichiometric reactions of BnOH with $[Re^{VII}(O)_2(Br_4cat)_2]^-$ and gave a substantial increase in catalyst stability as measured by total turnover numbers. However, even the more robust $[Re^{VII}(O)_2(Br_4cat)_2]^-$ anion preferentially oxidizes a $[Br_4cat]^{2-}$ ligand over CH_3OH. Moreover, the perbrominated catalyst system has its own drawbacks. Specifically, the oxidizing $[Br_4cat]^{2-}$ ligands in $[Re^{V}(O)(Br_4cat)_2]^-$ significantly retard the O_2 homolysis reaction as compared to the $[cat]^{2-}$ congener, which makes the turnover frequency exceptionally sluggish. The turnover-limiting step changes based on the nature of the ligand employed, but this presents a different problem. For the $[cat]^{2-}$ ligand, the turnover-limiting step is apparently BnOH oxidation by $[Re^{VII}(O)_2(cat)_2]^-$. Because the alcohol oxidation by $[Re^{VII}(O)_2(cat)_2]^-$ requires a steady-state, nonzero concentration of $[Re^{V}(O)(cat)_2]^-$, the rapid reaction of $[Re^{V}(O)(cat)_2]^-$ with O_2 effectively deactivates the catalyst by depleting the solution of $[Re^{V}(O)(cat)_2]^-$.

Conclusions

The capacity of oxorhenium(V) anions that contain redox-active catecholate ligands to homolyze O_2 and generate dioxorhenium(VII) products has been shown to facilitate oxidase-type aerobic oxidations of BnOH to PhCHO. Although $[Re^{VII}(O)_2(cat)_2]^-$ is the net H_2 acceptor in the reaction, it does not react directly with alcohols. Rather, catalytic quantities of $[Re^{V}(O)(cat)_2]^-$ are required to generate the active oxidant, which we speculate may be a hydroxoalkoxo rhenium(VII) complex, formed by the intramolecular delivery of alcohol from $[Re^{V}(O)(CH_3OH)(cat)_2]^-$ to $[Re^{VII}(O)_2(cat)_2]^-$. Demonstration of net H_2 addition to $[Re^{VII}(O)_2(cat)_2]^-$ establishes PCET as a method for direct production of $[Re^{V}(O)(cat)_2]^-$ that does not require a strong O atom acceptor substrate, opening new avenues to utilize the $[Re^{VII}(O)_2(cat)_2]^-/[Re^{V}(O)(cat)_2]^-$ oxo transfer couple for aerobic oxidation catalysis. However, $[Re^{VII}(O)_2(cat)_2]^-$ is a poor catalyst for BnOH oxidation because it undergoes oxidative decomposition during the alcohol oxidation reaction and because the rapid reoxidation of $[Re^{V}(O)(cat)_2]^-$ by O_2 is actually detrimental to the catalytic function. The use of a perbrominated $[Br_4cat]^{2-}$ ligand provides enhanced catalyst stability and increased turnover number, but turnover frequency is low due to the slow kinetics of O_2 homolysis by $[Re^{V}(O)(Br_4cat)_2]^-$. The development of more useful oxidase-type alcohol oxidations based on O_2 homolysis by $[Re^{V}(O)(cat)_2]^-$-like species will require a balance of these competing trends so that the rate of O_2 activation matches the rate of the alcohol oxidation.

Experimental Section

General Considerations: Unless otherwise specified, all manipulations were performed under anaerobic conditions using standard vacuum line techniques or in an inert atmosphere glove box under purified nitrogen. Routine NMR spectra were acquired with a Varian Mercury 300 spectrometer (300.323 MHz for ^1H). All chemical shifts are reported in ppm relative to Me_4Si with the residual solvent peak serving as an internal reference. UV/Vis absorption spectra were acquired with a Varian Cary 50 spectrophotometer. Unless otherwise noted, all electronic absorption spectra were obtained at ambient temperatures in 1 cm quartz cells. Mass spectra were recorded at the Georgia Institute of Technology Bioanalytical Mass Spectrometry Facility. ESI-MS was carried out with BnOH solutions with a Micromass Quattro LC spectrometer. GC–MS was

 © 2012 Wiley-VCH Verlag GmbH & Co. KGaA, Weinheim

performed with an Agilent 6890 GC equipped with an autosampler and a Restek Rxi-5ms column (30 m × 0.25 mm internal dimensions, 0.25 μm film thickness). 1 μL injections were made at a 50:1 split ratio. The GC oven program consisted of a hold at 30 °C for 1 min, followed by a 15 °C min^{-1} ramp to 300 °C, and a hold at 300 °C for 11 min. The mass spectrometer used in tandem was a Micromass AutoSpec electroionization (EI) detector.

Methods and Materials: Anhydrous CH_3CN and CH_2Cl_2 for air- and moisture-sensitive manipulations were purchased from Sigma–Aldrich and further dried by passage through columns of activated alumina, degassed by at least three freeze–pump–thaw cycles, and stored under N_2 prior to use. CH_3OH (anhydrous, 99.0%) was purchased from Honeywell Burdick and Jackson. [D_4]Methanol was used as received from Cambridge Isotope Laboratories and stored under a dry N_2 atmosphere prior to use. $(Et_4N)[Re^{V}(O)(cat)_2]$,[18] $(Et_4N)[Re^{VII}(O)_2(cat)_2]$,[18] $(Et_4N)[Re^{V}(O)(OPPh_3)(Br_4cat)_2]$,[15] and $(Et_4N)[Re^{VII}(O)_2(OPPh_3)(Br_4cat)_2]$[9] were prepared by literature methods. All characterization data matched those referenced. All other reagents were purchased from Sigma–Aldrich and were used as received.

Reactions with Dioxygen in CH_3OH: In a representative procedure, a 1.0 cm quartz cuvette fitted with a Kontes high-vacuum Teflon valve was charged with $[Re^{V}(O)(cat)_2]^-$ (2.0 mL, 0.90 mmol, 0.45 mM) in CH_3OH and sealed under N_2. The solution was degassed on a high-vacuum line by three freeze–pump–thaw cycles and an initial spectrum was acquired. The cuvette was then backfilled with 1 atm of dry air, shaken vigorously, placed in a Peltier UV/Vis cell holder with a magnetic stirrer, and stirred to maintain a constant concentration of dissolved O_2 throughout the reaction. The reaction progress was monitored by UV/Vis spectroscopy (200–900 nm) for 3000 min at 5 min intervals. For NMR kinetics studies, a J. Young NMR tube with a Teflon screw cap was used in place of the cuvette.

Determination of I_B Yields with Varying Ratios of $[Re^{VII}(O)_2(cat)_2]^-$/$[Re^{V}(O)(cat)_2]^-$: A 1.0 cm quartz cuvette fitted with a Kontes high-vacuum Teflon valve was charged with freshly prepared CH_3OH solutions of $[Re^{VII}(O)_2(cat)_2]^-$ and $[Re^{V}(O)(cat)_2]^-$ to make the final concentrations 0.15 mM and 0.02–0.24 mM, respectively. The cuvette was sealed under N_2, shaken vigorously, and placed in a Peltier UV/Vis cell holder. The reaction progress was monitored by UV/Vis spectroscopy (300–1000 nm) at 2 min intervals, and the yield of I_B was determined by measurement of the maximum absorbance at 600 nm (λ_{max} for I_B).

Stoichiometric Alcohol Oxidations: In a representative procedure, $[Re^{VII}(O)_2(cat)_2]^-$ (4.0 mL, 48 mmol, 12.1 mM) in BnOH and $[Re^{V}(O)(cat)_2]^-$ (1.0 mL, 5.0 mmol, 5 mM) in BnOH were combined in a 20 mL scintillation vial, sealed under N_2, and stirred at ambient temperature for 15 h. For GC–MS analysis a 1 mL aliquot was transferred to a 2 mL GC autosampler vial and *n*-decane (1 μL) was added to serve as an internal standard. The vial was sealed under N_2 with a Teflon-lined septum cap prior to GC–MS analysis as described above. The organic products were quantified by comparison of the EI-MS detector response against calibration curves derived from pure materials and by comparison to the detector response for the *n*-decane internal standard. For NMR studies, $[Re^{V}(O)(cat)_2]^-$ (2 mM) was added to a [D_4]MeOH solution of $[Re^{VII}(O)_2(cat)_2]^-$ (20 mM) and BnOH (100 mM) in a J. Young NMR tube with a Teflon screw cap. The reaction was monitored over 48 h.

Catalytic Alcohol Oxidations: For catalytic alcohol oxidation experiments, solutions were prepared and analyzed exactly as described above for the stoichiometric variants, but the reaction mixtures were stirred under 1 atm dry air rather than N_2.

Supporting Information (see footnote on the first page of this article): ^1H NMR spectra from a reaction of $[Re^{VII}(O)_2(cat)_2]^-$ and 0.1 equiv. of $[Re^{V}(O)(cat)_2]^-$ with 6 equiv. BnOH at 25 °C in [D_4]methanol.

Acknowledgments

We gratefully acknowledge financial support from a Defense Advanced Research Projects Agency (DARPA) Young Faculty Award (Grant N6600 1-09-1-2094 to J. D. S.), the Fulbright Program (K. R.), and the Georgia Institute of Technology. We thank David Bostwick for mass spectrometry analyses.

[1] P. J. Chirik, K. Wieghardt, *Science* **2010**, *327*, 794–795.
[2] For recent examples, see: "Forum on Redox Active Ligands", *Inorg. Chem.* **2011**, *50*, 9737–9914.
[3] a) S. C. Bart, E. Lobkovsky, P. J. Chirik, *J. Am. Chem. Soc.* **2004**, *126*, 13794–13807; b) R. J. Trovitch, E. Lobkovsky, E. Bill, P. J. Chirik, *Organometallics* **2008**, *27*, 1470–1478; c) K. T. Sylvester, P. J. Chirik, *J. Am. Chem. Soc.* **2009**, *131*, 8772–8774.
[4] K. J. Blackmore, N. Lal, J. W. Ziller, A. F. Heyduk, *J. Am. Chem. Soc.* **2008**, *130*, 2728–2729.
[5] a) W. B. Tolman in *Comprehensive Coordination Chemistry II* (Eds.: I. A. McCleverty, T. J. Meyer), Elsevier Pergamon, Boston, **2004**, vol 8, pp. 715–737; b) P. Chaudhuri, K. Wieghardt, T. Weyhermüller, T. K. Paine, S. Mukherjee, C. Mukherjee, *Biol. Chem.* **2005**, *386*, 1023–1033; c) L. M. Mirica, X. Ottenwaelder, T. D. P. Stack, *Chem. Rev.* **2004**, *104*, 1013–1045; d) C. J. Rolle III, K. I. Hardcastle, J. D. Soper, *Inorg. Chem.* **2008**, *47*, 1892–1894.
[6] a) A. I. Nguyen, R. A. Zarkesh, D. C. Lacy, M. K. Thorson, A. F. Heyduk, *Chem. Sci.* **2011**, *2*, 166–169; b) A.F. Heyduk, R. A. Zarkesh, A. I. Nguyen, *Inorg. Chem.* **2011**, *50*, 9849–9863.
[7] a) W. I. Dzik, X. Xu, X. P. Zhang, J. N. H. Reek, B. de Bruin, *J. Am. Chem. Soc.* **2010**, *132*, 10891–10902; b) W.I. Dzik, X. P. Zhang, B. de Bruin, *Inorg. Chem.* **2011**, *50*, 9896–9903.
[8] A. L. Smith, K. I. Hardcastle, J. D. Soper, *J. Am. Chem. Soc.* **2010**, *132*, 14358–14360.
[9] C. A. Lippert, S. A. Arnstein, C. D. Sherrill, J. D. Soper, *J. Am. Chem. Soc.* **2010**, *132*, 3879–3892.
[10] a) R. A. Sheldon, J. K. Kochi, *Metal-Catalyzed Oxidations of Organic Compounds*, Academic Press, New York, **1981**; b) W. J. Mijs, C. R. H. I. De Jonge (Eds.), *Organic Syntheses by Oxidation with Metal Compounds*, Plenum, New York, **1986**; c) B. M. Trost, I. Flemming (Eds.), *Comprehensive Organic Synthesis: Selectivity, Strategy and Efficiency in Modern Organic Chemistry, Volume 7: Oxidation*, Pergamon, Oxford, **1991**.
[11] a) P. Praskevopoulou, N. Psaroudakis, S. Koinis, P. Stavropoulos, K. Mertis, *J. Mol. Catal. A* **2005**, *240*, 27–32; b) W. A. Hermann, J. P. Zoller, R. W. Fischer, *J. Organomet. Chem.* **1999**, *579*, 404–407; c) T. H. Zauche, J. H. Espenson, *Int. J. Chem. Kinet.* **1999**, *31*, 381–385; d) T. H. Zauche, J. H. Espenson, *Inorg. Chem.* **1998**, *37*, 6827–6831; e) J. H. Espenson, Z. Zhu, T. H. Zauche, *J. Org. Chem.* **1999**, *64*, 1191–1196; f) J. B. Arterburn, M. Liu, M. C. Perry, *Helv. Chim. Acta* **2002**, *85*, 3225–3236.
[12] For some reviews of recent progress in transition-metal-mediated aerobic alcohol oxidations, see: a) S. S. Stahl, *Angew. Chem.* **2004**, *116*, 3480; *Angew. Chem. Int. Ed.* **2004**, *43*, 3400–3420; b) M. J. Schultz, M. S. Sigman, *Tetrahedron* **2006**, *64*, 8227–8241; c) I. E. Marko, P. R. Giles, M. Tsukazaki, A. Gautier, R. Dumeunier, K. Dodo, F. Philippart, I. Chelle-Regnault, J.-L. Mutonkole, S. M. Brown, C. J. Urch in *Transition Metals for Organic Synthesis 2nd Edition* (Eds.: M. Beller, C. Bolm), Wiley-VCH, Weinheim, **2005**.

 © 2012 Wiley-VCH Verlag GmbH & Co. KGaA, Weinheim

[13] Because $\mathbf{I_B}$ is only transiently formed, spectroscopic yield (as measured by the maximum UV/Vis absorbance at λ_{max} = 600 nm) was used as a proxy for absolute yields in these studies. Although this is not always acceptable, under the conditions employed herein the rate of the second reaction step to consume $\mathbf{I_B}$ is significantly lower than the rate of $\mathbf{I_B}$ formation, which makes the spectroscopic yield a reasonable approximation for the absolute yield of $\mathbf{I_B}$ in the reactions.
[14] a) W. A. Herrmann, R. W. Fischer, D. W. Marz, *Angew. Chem.* **1991**, *103*, 1706; *Angew. Chem. Int. Ed. Engl.* **1991**, *30*, 1638–1641; b) W. A. Herrmann, R. W. Fischer, W. Scherer, M. U. Rauch, *Angew. Chem.* **1993**, *105*, 1209; *Angew. Chem. Int. Ed. Engl.* **1993**, *32*, 1157–1160.
[15] C. F. Edwards, W. P. Griffith, A. J. P. White, D. J. Williams, *J. Chem. Soc., Dalton Trans.* **1992**, 957–962.
[16] a) B. Machura, J. O. Dziegielewski, S. Michalik, R. Kruszynksi, T. J. Bartczal, J. Kusz, *Trans. Met. Chem.* **2003**, *28*, 939–947; b) G. Backes-Dahmann, J. H. Enemark, *Inorg. Chem.* **1987**, *26*, 3960–3962; c) B. Machura, M. Jaworka, R. Kruszynski, *Inorg. Chim. Acta* **2006**, *359*, 1303–1313; d) M. Tadokoro, T. Inoue, S. Tamaki, K. Fujii, K. Isogai, H. Nakazawa, S. Takeda, K. Isobe, N. Koga, A. Ichimura, K. Nakasuji, *Angew. Chem.* **2007**, *119*, 6042; *Angew. Chem. Int. Ed.* **2007**, *46*, 5938–5942; e) J. Jacob, G. Lente, L. A. Guzei, J. H. Espenson, *Inorg. Chem.* **1999**, *38*, 3762–3763.
[17] F. G. Bordwell, W.-Z. Liu, *J. Am. Chem. Soc.* **1996**, *118*, 10823.
[18] J. R. Dilworth, S. K. Ibrahim, S. R. Khan, M. B. Hursthouse, A. A. Karaulov, *Polyhedron* **1990**, *9*, 1323–1329.

Received: September 30, 2011
Published Online: November 24, 2011

 © 2012 Wiley-VCH Verlag GmbH & Co. KGaA, Weinheim

DOI: 10.1002/ejic.201100814

Dirhodium Catalysts That Bear Redox Noninnocent Chelating Dicarboxylate Ligands and Their Performance in Intra- and Intermolecular C–H Amination

Katherine P. Kornecki[a] and John F. Berry*[a]

Keywords: Rhodium / Homogeneous catalysis / Amination / Redox chemistry / Chelates

We report two new analogues of the well-known C–H amination catalyst $[Rh_2(esp)_2]$ (**1**) (esp = α,α,α′,α′-tetramethyl-1,3-benzenedipropanoate) that bear redox-active supporting ligands that are structurally similar to esp. The redox-active ligands are 2-[3-(1-carboxy-1-methylethoxy)phenoxy]-2-methylpropanoic acid (H_2**L1**) and (3-methoxycarbonyl-2,5-di-*tert*-butylphenoxy)ethanoic acid (H_2**L2**), which react with $Rh_2(OAc)_4$ to form the catalysts $[Rh_2(\mathbf{L1})_2]$ (**2**) and $[Rh_2(\mathbf{L2})_2]$ (**3**). Both **2** and **3** have been characterized by X-ray crystallography and cyclic voltammetry, inter alia. Compounds **2** and **3** are structurally similar to **1** but show more complex electrochemical features. Whereas **1** has a single reversible redox wave that corresponds to the $Rh_2^{II,II}/Rh_2^{II,III}$ couple, **2** and **3** show multiple oxidations that are characteristic of ligand-centered oxidation. Catalysts **1**, **2**, and **3** perform well in a model intramolecular C–H amination reaction, and all three catalysts perform equally well during the first four hours of a model intermolecular reaction. After this point, **2** and **3** cease to function, whereas **1** continues to be active. These results support the hypothesis that intermolecular C–H amination utilizes two distinct mechanisms: (1) a nitrene interception/insertion mechanism that is fast but ceases to be operative after four hours, and (2) a one-electron mechanism that is more robust over extended time periods, but requires the catalyst to be able to undergo Rh_2-centered oxidation.

Introduction

Catalytic C–H amination by means of nitrene transfer mediated by dirhodium paddlewheel compounds has become an important synthetic tool.[1] This reaction is outlined in Scheme 1, and involves oxidative transformation of a nitrogen-containing substrate (typically a sulfamate or carbamate ester) into a nitrene equivalent, with subsequent insertion of this nitrene into a substrate C–H bond. The nitrene insertion can either be intramolecular, thereby yielding cyclized products, or intermolecular. Whereas intramolecular reactions are well established, it has been shown that not every Rh_2 catalyst can efficiently accomplish intermolecular reactions.[2] $[Rh_2(esp)_2]$ (**1**; esp = α,α,α′,α′-tetramethyl-1,3-benzenedipropanoate) has been shown to be the best catalyst for the intermolecular amination transformation,[3] a fact that has been attributed to the added stability of the catalyst due to the chelate effect of the bridging dicarboxylate ligands. Current mechanistic information on intramolecular C–H amination by **1** is consistent with the mechanism shown on the left side of Scheme 1 whereby an iminoiodinane intermediate [formed in the rate-limiting reaction of sulfamate ester with $PhI(OAc)_2$] transfers the ni-

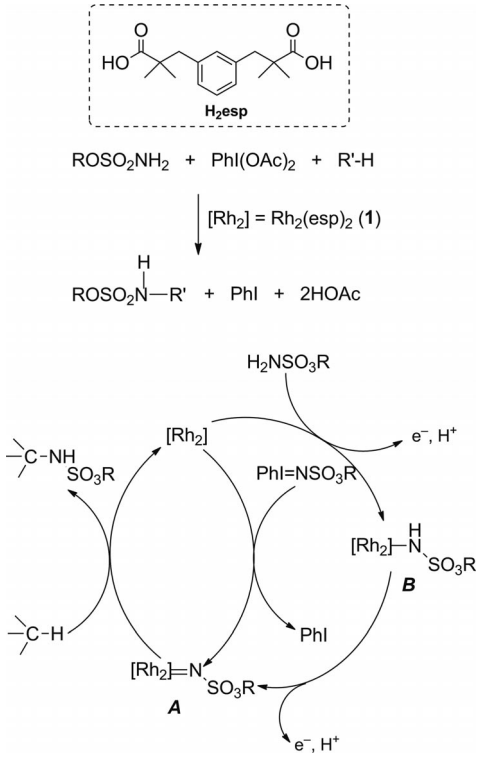

Scheme 1. Proposed catalytic cycle for dirhodium-catalyzed C–H amination: the inner mechanism involves direct nitrene transfer, and the outer mechanism (with amido intermediate **B**) corresponds to the one-electron pathway that dominates the intermolecular amination mechanism.

[a] Department of Chemistry,
University of Wisconsin, Madison
1101 University Avenue, Madison, WI 53706, USA
Fax: +1-608-262-6143
E-mail: berry@chem.wisc.edu

Supporting information for this article is available on the WWW under http://dx.doi.org/10.1002/ejic.201100814 or from the author.

WILEY ONLINE LIBRARY
© 2012 Wiley-VCH Verlag GmbH & Co. KGaA, Weinheim

trene to the dirhodium catalyst, thereby yielding the dirhodium nitrene intermediate **A**.[2] Intermediate **A** is then able to insert the nitrene directly into substrate C–H bonds to reform the original catalyst. For intermolecular C–H amination reactions, the iminoiodinane transfer mechanism appears to account for only around 30% of the product formation. The majority of the product has been proposed to form by means of the outer mechanism in Scheme 1, which involves single-electron redox steps.[4] The formation of C–H amination products by using the one-electron oxidant Ce^{4+} verifies the one-electron nature of this mechanism.[4]

Redox noninnocent ligands that are strongly coupled to a transition-metal center have been employed with success in catalytic reactions that involve redox transformations.[5] To the best of our knowledge, redox noninnocence has never been studied in the context of dirhodium complexes, or the possible implications to catalysis. Ferrocene-based redox auxiliaries in dirhodium complexes have been reported, but only their electrochemistry has been studied.[6] Because of the one-electron transformations involved in the outer mechanism for intermolecular C–H amination catalyzed by Rh_2 complexes, we have prepared Rh_2 catalysts that bear redox noninnocent ligands and describe their performance in intra- and intermolecular amination in this article.

Since the chelate effect is touted as the reason for the increased stability and selectivity of **1** as an intermolecular amination catalyst, we decided to study catalysts that are close structural analogues of **1**. The ligands **L1** {2-[3-(1-carboxy-1-methylethoxy)phenoxy]-2-methylpropanoate} and **L2** [(3-methoxycarbonyl-2,5-di-*tert*-butylphenoxy)ethanoate] (previously reported in the context of metallomacrocycle assembly)[7] have the same backbone chain-length as esp; however, the backbones of **L1** and **L2** contain a redox-active resorcinol-derived component (Scheme 2). Like the more well-known 1,2- or 1,4-dialkoxy-substituted benzenes,[8] 1,3-dialkoxybenzenes may be oxidized to the corresponding radical cations, as shown in Scheme 2.[9] The *meta*-disubstituted radical species are significantly less stable than their *ortho* or *para* congeners.[9,10] To the best of our knowledge, the *meta*-dialkoxybenzene motif has not yet been investigated as a redox-noninnocent ligand in coordination complexes, which further prompted this study.

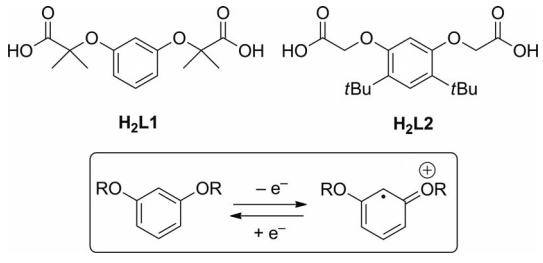

Scheme 2. Chelating dicarboxylate ligands and the redox capabilities of resorcinol-based compounds.

Results and Discussion

Synthesis

Both H_2**L1** and H_2**L2** were previously reported by Bonar-Law and co-workers,[7] and were prepared similarly herein with slight modifications to the synthesis of H_2**L2** (outlined in the Exp. Section). Treating the dicarboxylate ligands with dirhodium tetraacetate at 150 °C in dichlorobenzene affords the loss of acetic acid and the formation of complexes **1**–**3** in good yields (60–75%). Complex formation and purity were established by ^{1}H NMR spectroscopy, MALDI-MS, and elemental analysis. Crystals suitable for X-ray diffraction were obtained for complexes **2** and **3** as their diaquo and bis-acetone adducts, respectively (see Figures 1 and 2, vide infra). The axial ligands were removed under vacuum prior to the use of these compounds as catalysts.

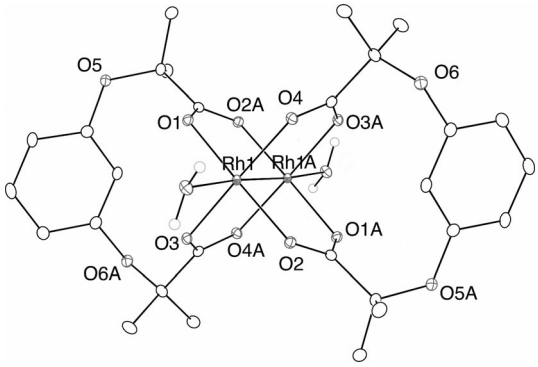

Figure 1. Thermal ellipsoid plot of catalyst **2**·2H_2O, with thermal ellipsoids drawn at the 30% probability level. Hydrogen atoms are omitted for clarity.

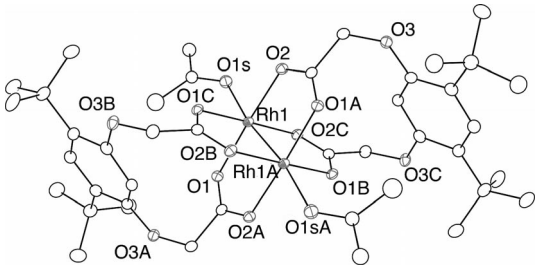

Figure 2. Thermal ellipsoid plot for **3**·2acetone, with thermal ellipsoids drawn at the 30% probability level. Hydrogen atoms are omitted for clarity.[12]

Crystallography

Crystal data for **2** and **3** are given in Table 1. The solid-state structures of **1**, **2**, and **3** are similar and show chelation of the dicarboxylate ligands to the metal–metal bonded dirhodium core. The Rh–Rh distances in all three catalysts range from 2.3817(9) to 2.3910(6) Å, which are effectively the same (see Table 2) and fall within the normal range for bond lengths in simpler $Rh_2^{II,II}$ carboxylate complexes.[11] The Rh–O bond lengths to the carboxylate ligands and ax-

 © 2012 Wiley-VCH Verlag GmbH & Co. KGaA, Weinheim

ial ligands are all normal. An interesting difference between the three structures presents itself in a comparison of the $O_{bound\ carboxylate}$–C–C–$O_{phenolate}$ torsion angles. There are two of these torsion angles in **1** that are crystallographically inequivalent; on one side of the bound carboxylate it is 57.301°, and it is 59.238° on the other, which are very close values and may not be considered to be significantly different in a chemical sense. This torsion angle in **3** is significantly smaller at only 18.79°. Interestingly, **2** differs from **1** and **3** in that its two crystallographically inequivalent smallest torsion angles on either side of the bound dicarboxylate are very different: 99.341 and 37.912°. If this difference in torsion angles is retained in solution, the nearly 90° torsion angle could play a role in facilitating hyperconjugation effects between the oxygen atom of the *meta*-dialkoxybenzene backbone and the carboxylate π orbitals, thus allowing for direct electronic communication to the rhodium center.

Table 1. Crystallographic parameters for **2** and **3**.

Compound	**2**·2 H_2O	**3**·2 acetone
Space group	$P\bar{1}$	$I4/m$
Crystal system	triclinic	tetragonal
a [Å]	12.520(3)	19.3634(5)
b [Å]	12.637(3)	19.3634(5)
c [Å]	14.577(4)	12.1982(4)
α [°]	91.372(4)	90
β [°]	100.240(4)	90
γ [°]	101.962(4)	90
V [Å^3]	2215.8(10)	4573.69(2)
Z	2	4
$R1$, $wR2$ [$(I) > 2\sigma(I)$]	0.0398, 0.0911	0.0302, 0.0736
$R1$, $wR2$ (all data)	0.0510, 0.0995	0.0446, 0.0793

Table 2. Selected bond lengths and angles in **1**, **2**, and **3**.

Compound	**1**·2 acetone[16]	**2**·2 H_2O	**3**·2 acetone
Rh–Rh [Å]	2.3817(9)	2.3873(6)	2.3910(6)
$Rh–O_{carboxylate}$ [Å]	2.0386(18)	2.0355(2)	2.036(2)
$Rh–O_{axial}$ [Å]	2.3042(19)	2.298(**7**)	2.286(4)
O–C–C–O (torsion) [°]	57.301, 59.238	37.912, 99.341	18.79

Electrochemistry

To test the redox activity of ligands **L1** and **L2**, cyclic voltammetric measurements were performed (Figures S1 and S2 in the Supporting Information). The H_2esp ligand, which lacks the *meta*-dialkoxybenzene moiety, shows no redox behavior in THF up to 2.1 V versus Fc/Fc$^+$. Under reducing conditions, an irreversible wave at –1.4 V is observed. Similar reductive waves are observed in THF for H_2**L1** and H_2**L2**, and it is thus reasonable to conclude that these waves correspond to electrochemical reduction and subsequent decarboxylation of the carboxylic acid functionalities. In addition to these reductive events, H_2**L1** and H_2**L2** show waves at positive potentials that correspond to oxidations that are absent in H_2esp. For H_2**L1**, multiple irreversible oxidation events are observed at potentials >1.2 V. In contrast, two discrete irreversible waves are observed for H_2**L2** at 0.9 and 1.1 V. The oxidations in H_2**L1** and H_2**L2** are safely assigned to the oxidation of the *meta*-dialkoxybenzene unit. The irreversibility of the oxidations is consistent with a fast decomposition process that occurs after the radical cation is generated.

The majority of dirhodium carboxylate paddlewheel complexes exhibit one reversible redox event that corresponds to the $Rh_2^{II,II}/Rh_2^{II,III}$ couple.[13] [Rh_2(esp)$_2$] (**1**) exhibits a perfectly reversible Rh-centered redox couple at $E_{1/2}$ = 0.82 V (versus Fc/Fc$^+$ in dichloromethane). Chemical oxidation and spectroelectrochemistry results indicate that this wave is centered at the Rh_2 unit and is assigned as the $Rh_2^{II,II}/Rh_2^{II,III}$ redox couple.[4] Compounds **2** and **3** feature more complexity in their cyclic voltammograms than does **1**. In contrast to the single, reversible wave observed for **1**, compound **2** displays multiple irreversible features at >1.2 V. The irreversibility of these features and their higher redox potential than **1** suggest that these oxidation events have a different origin than the $Rh_2^{II,II}/Rh_2^{II,III}$ couple of **1**. Since these redox events closely mirror the irreversible electrochemical behavior of the H_2**L1** ligand, it is reasonable to assign these as oxidations of the *meta*-dialkoxyphenylene moiety of the ligand backbone. Much like in the case of the free ligand itself, the radical cationic species that result from these oxidations are unstable and undergo a fast chemical reaction, likely radical/radical coupling, that renders the electrochemical signal irreversible. Like **2**, compound **3** shows multiple redox waves in its cyclic voltammogram. Unlike the irreversible behavior of **2**, the redox waves of **3** are reversible and appear at lower potentials. The CV of **3** shows a reversible two-electron wave at 0.97 V, and a further reversible one-electron wave at 1.3 V.

It is well established that phenoxyl radicals and phenoxyl radical complexes can be stabilized when bulky substituents protect the *ortho* and *para* positions of the aryl ring.[14] In a similar manner, addition of two *t*Bu substituents to the aryl ring of the ligands of **2** so as to form **3** leads to a greater stabilization of the corresponding radical cation [**L2**]$^{\cdot+}$. This stabilization is both a thermodynamic effect (reflected in the more accessible oxidation potential of **3**, 0.9 V, than **2**, >1.2 V) and a kinetic effect (the reversibility of the redox waves for **3** indicates that the chemical process responsible for rendering the **2** waves irreversible is now

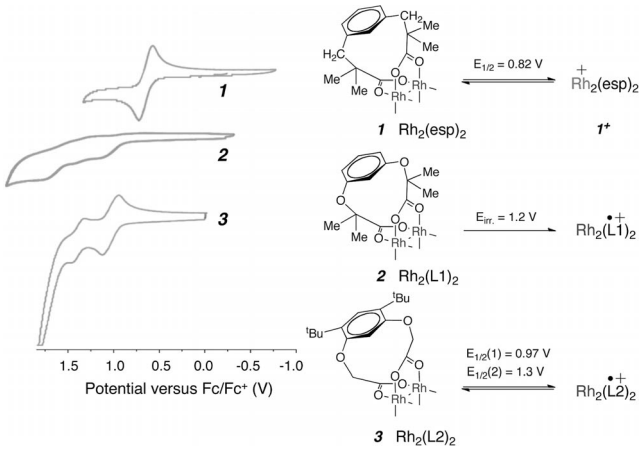

Figure 3. Redox features of chelate catalysts **1**, **2**, and **3**.

 © 2012 Wiley-VCH Verlag GmbH & Co. KGaA, Weinheim

slower than the scan time of the cyclic voltammogram) (Figure 3). It is not possible to tell if one of the multiple redox waves displayed by **2** or **3** is centered at the Rh_2 unit. However, in comparing the electrochemical data of **1**, **2**, and **3** we may note that any $Rh_2^{II,II}/Rh_2^{II,III}$ oxidations of **2** or **3** occur at substantially higher potential than in **1**, and that such an oxidation for **2** is not reversible. Given the general structural similarities between **1**, **2**, and **3**, it is not obvious why the $Rh_2^{II,II}/Rh_2^{II,III}$ couple would be less accessible in the latter two compounds, but this is certainly what happens.

Catalysis

As mentioned above, catalytic amination of C–H bonds is one of the primary applications of dirhodium complexes in which their redox chemistry is proposed to play an important role. Thus the catalytic activity of **1**, **2**, and **3** in intra- and intermolecular C–H amination reactions is of interest. The reaction shown in Scheme 3 has been a useful test reaction for the performance of dirhodium catalysts in intramolecular C–H aminations that target the benzylic C–H position.[15] Simple Rh_2 carboxylates such as $[Rh_2(oct)_4]$ (oct = octanoate) perform well as catalysts for this reaction with reported yields of approximately 84%.[15] Thus, chelating dicarboxylate ligands such as esp are not absolutely necessary for this transformation. Catalysts **1**, **2**, and **3** nevertheless perform intramolecular amination very well, particularly **1** and **3**. It is not entirely obvious why **2** gives a lower yield; however, catalyst **2** is not recoverable after the course of the reaction, thereby implying that radical reactions at the ligand may initiate catalyst degradation.

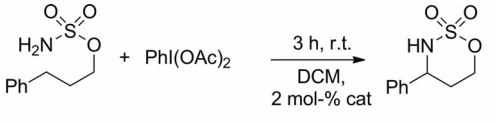

1 equiv.	1.1 equiv.	% Conv.
		1 95%
		2 76%
		3 97%

Scheme 3. Intramolecular reactivity of chelate catalysts. Percent conversion based on ^{1}H NMR spectroscopic integration versus concentration of uncyclized substrate.

To test the catalytic competence of **1**–**3** under intermolecular C–H amination conditions, conversion of ethyl benzene to the corresponding amination product by using H_2NTces (Tces = trichloroethylsulfamate) and $PhI(OAc)_2$ was used as a representative amination reaction (Scheme 4). Ethylbenzene is a particularly appropriate substrate since it presents benzylic C–H bonds similar to those in the intramolecular substrate described above. At four hours under these conditions, the three catalysts show comparable activity. However after this short timespan, **2** and **3** cease to function, whereas **1** continues to perform until a significant portion of the ethyl benzene is consumed. These results complement the report from Du Bois that $[Rh_2(S\text{-biTISP})_2]$ {S-biTISP = 1,3-[*N*,*N*′-bis(2,4,6-triisopropylbenzenesulfonyl)-(2*S*,2′*S*),(5*R*,5′*R*)-prolinate]benzene}, despite having chelating dicarboxylate ligands, is a poor intermolecular C–H amination catalyst.[2] Due to the structural analogy between **1**, **2**, and **3**, the poor catalytic performance of the latter two can be attributed to electronic rather than steric properties. Another important piece of information about these reactions is that the brilliant red color ascribed to one-electron oxidized $Rh_2^{II,III}$ species appears when catalyst **1** is used, but is absent for reactions that involve **3**, and appears but is short-lived for reactions that involve **2**.

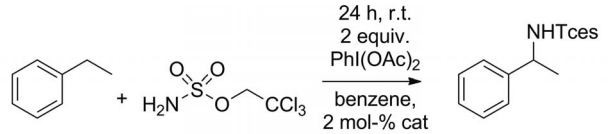

1.1 equiv.	1 equiv.	% Conv.
		1 31% after 4 h (72% final yield)
		2 30% (final yield)
		3 27% (final yield)

Scheme 4. Intermolecular reactivity of chelate catalysts. Percent conversion based on ^{1}H NMR spectroscopic integration versus an internal standard.

The catalytic results presented here can be rationalized in terms of the mechanism shown in Scheme 1 and provide further evidence to support this mechanism. Mechanistic data[15] on intramolecular C–H amination reactions are consistent with nitrene transfer from an iminoiodinane to the dirhodium catalyst, thereby forming the dirhodium nitrene complex **A**, which in turn is extremely electrophilic[16] and inserts the nitrene into the substrate C–H bond. This nitrene interception/insertion mechanism does not require any change in the oxidation state of the Rh_2 core, as long as **A** is considered to be an adduct of a neutral nitrene to an $Rh_2^{II,II}$ carboxylate core.[17]

At a 2 mol-% catalyst loading in the intramolecular cyclization reaction (Scheme 3), catalysts **1**, **2**, and **3** all seem to perform equally well and afford high yields of the product (>75%).

Magnesium oxide is an important additive that can affect the outcome of the reaction.[16] Table 3 gives a comparison of the yields of intramolecular C–H amination reactions catalyzed by 1 mol-% of **1**, **2**, and **3** (listed as turnover numbers) for the first 24 h of the reaction in the presence or absence of MgO. In general, catalyst performance is enhanced by this additive. We may expect that the function of MgO is to neutralize the acetic acid reaction byproduct, and that excessive amounts of acetic acid may be an important cause of catalyst arrest, particularly for **2** and **3**. Indeed, when no MgO is present, the initial green color of the dirhodium catalysts **2** and **3** quickly dissipates. Instead, the color of the reaction mixture becomes yellow, reminiscent of mononuclear Rh^{III} species. This is not the case when **1** is used as a catalyst, thereby indicating that some facet of

 © 2012 Wiley-VCH Verlag GmbH & Co. KGaA, Weinheim

its structure makes it more robust under the reaction conditions. In fact, when 1 equiv. of **1** is treated with 2 equiv. each of a sulfamate ester and $PhI(OAc)_2$ in dichloromethane, crystalline **1**·2HOAc (see Figure S4 in the Supporting Information) can be isolated after several days, which indicates that the catalyst is unchanged by acidic conditions. Acetic acid is clearly more detrimental to catalysts **2** and **3**, possibly implicating a protonation of the resorcinol-derived O atoms and subsequent destruction of the ligand, which is not feasible when **1** is used. Notwithstanding, when MgO is present, the reaction mixture will maintain its initial green color for **2** and **3**, thus allowing all three catalysts to remain active until complete product formation is achieved, which occurs at around 20 h for catalyst **1**, and after approximately 50 h for catalysts **2** and **3**.

Table 3. Turnover numbers (TON) for the intramolecular cyclization depicted in Scheme 3 using 1 mol-% catalyst loading after 24 h.

Catalyst	TON (3 equiv. MgO)	TON (MgO-free)
1	99	91
2	86[a]	56
3	69[a]	60

[a] > 90 after about 50 h.

We[4] and Du Bois[2,3] have noted that the nature of intermolecular C–H amination catalyzed by **1** is different at the beginning of the reaction than during the later stages of the reaction. Our current hypothesis for this behavior is that intermolecular C–H amination initially occurs by means of the interception/insertion mechanism described above, but after conversion of roughly 30% of the substrate this mechanism becomes inactive and the reaction continues by following a slower one-electron mechanism. This mechanism, which dominates product formation late in the reaction, involves oxidation of **1** in the presence of sulfamate ester substrate to yield a one-electron oxidized $Rh_2^{II,III}$-amido-type species **B**. Species **B** has a brilliant red color and is observable as an intermediate in the reaction. It undergoes a further one-electron oxidation to yield the nitrene intermediate **A**, which inserts the nitrene into the substrate C–H bond.

The hypothesis that the nitrene interception/insertion mechanism and the one-electron mechanism operate contemporaneously is supported by results we report here. Since the nitrene interception/insertion mechanism does not involve Rh_2-centered oxidation, we expect catalysts **1**, **2**, and **3** to perform equally well in the first stage of the catalytic reaction, just as the three catalysts all perform well in intramolecular C–H amination. Indeed, this is what happens. In the first four hours of the reaction, catalysts **1**, **2**, and **3** convert around 30% of the ethylbenzene to product. The one-electron mechanism for intermolecular C–H amination requires the catalyst to be oxidized to form **B**. Both **2** and **3** are more difficult to oxidize than **1** by at least 100 mV. Moreover, one-electron oxidation of **2** or **3** does not necessarily involve oxidation of the Rh_2 center from $Rh_2^{II,II}$ to $Rh_2^{II,III}$, but may instead involve oxidation of the *meta*-dialkoxybenzene ligand fragment. Neither **2** nor **3** is active in C–H amination beyond the initial four-hour period dominated by the nitrene interception/insertion mechanism. There are two possible explanations for this observation that are consistent with the working mechanistic hypothesis. First, it is possible that the one-electron oxidation of **2** or **3** occurs at such a high potential that these catalysts cannot be oxidized to **B** under the reaction conditions. The other possibility is that **2** or **3** can be oxidized under the reaction conditions, but that this oxidation is centered on the chelating dicarboxylate ligand rather than on the Rh_2 unit. If the ligand oxidation is strongly coupled to the metal center, we may anticipate that **B** could still be formed under these conditions. However, there is no π-conjugation pathway between the *meta*-dialkoxybenzene group and the Rh_2 center and a hyperconjugation pathway is doubtful, so the electronic coupling here is anticipated to be weak, thereby resulting in a one-electron oxidized species that resembles an uncoupled $Rh_2^{II,II}$ unit appended to an organic radical cation. Such a species would not be chemically equivalent to **B**, and therefore may not take part in the one-electron C–H amination mechanism. There is some indication that both of these possibilities are, in fact, occurring. When **2** is used as a catalyst, the red color characteristic of **B** appears briefly at the beginning of the reaction, then disappears. This observation is consistent with the first possibility outlined above in which initially the concentration of oxidant is high enough that **B** can be produced, but as the concentration of the oxidant wanes, the reaction mixture no longer has sufficient oxidizing power to utilize the one-electron mechanism. In contrast, when **3** is used as a catalyst, the red color of **B** is never observed. Thus, if **3** is oxidized under these conditions, then the oxidation must be ligand-centered and there must be little electronic coupling between the *meta*-dialkoxybenzene ligand fragment and the Rh_2 center. We interpret these results to mean that Rh_2 centered oxidation is necessary for the success of the one-electron intermolecular mechanism, and thereby for complete conversion of substrate.

Conclusion

For the first time, we have introduced redox noninnocent ligands as supporting ligands for metal–metal bonded compounds specifically to investigate their catalytic behavior. The *meta*-dialkoxybenzene motif in ligands **L1** and **L2** has been shown to engender the corresponding dirhodium complexes **2** and **3** with complex ligand-centered redox properties that are absent from the structurally analogous **1**. By assessing the differences in performance for catalysts **1**–**3**, it is evident that rhodium-centered oxidation is essential to the performance of dirhodium carboxylate catalysts in intermolecular C–H amination. Catalyst **1**, which has a reversible rhodium-centered redox couple, can access intermediate **B**, an $Rh_2^{II,III}$-amido species; catalysts **2** and **3** are more difficult to oxidize and are not successful in this one-electron mechanistic regime.

 © 2012 Wiley-VCH Verlag GmbH & Co. KGaA, Weinheim

Experimental Section

General: All reagents were obtained commercially unless otherwise noted. Reactions were performed using oven-dried glassware under an atmosphere of nitrogen, either in a glove box or using Schlenk techniques. Dichloromethane was dried with CaH_2 and distilled before use. [D_6]Benzene was dried on an activated alumina column prior to use. All other solvents were collected anhydrous from a Vacuum Atmospheres solvent system. The structures of known compounds were confirmed by ^{1}H NMR spectroscopy and ESI-MS. ^{1}H NMR spectra were collected on a 300 MHz Bruker spectrometer at room temperature.

Electrochemistry: All electrochemistry experiments were conducted under a nitrogen atmosphere in solutions (10 mL, 0.1 M) of tetrabutylammonium hexafluorophosphate in freshly distilled dichloromethane with a 0.001 M analyte concentration. The reference electrode consisted of a silver wire immersed in a 10 mM silver nitrate solution contained by a Vycor tip. The auxiliary electrode was a platinum wire. For cyclic voltammetry, data was referenced to the ferrocene/ferrocenium redox couple, and the working electrode was made of glassy carbon.

Ligands: H_2esp was prepared according to the synthesis described by Du Bois and co-workers.[18] H_2**L1** was prepared according to the synthesis reported by Bonar-Law and co-workers.[7] H_2**L2** was prepared similarly to the synthesis described by Bonar-Law and co-workers.[7] The differences are outlined below.

Synthesis of H_2L2: Et_2**L2**: A 100 mL Schlenk flask was charged with potassium carbonate (1.6 g, 11.6 mmol) and 4,6-di-*tert*-butylresorcinol (1.04 g, 4.7 mmol). Acetonitrile (50 mL) was added into the reaction, followed by the addition of α-iodoethyl acetate (1.1 mL, 9.3 mmol). The reaction was stirred at room temperature for 40 h. Solvent was removed in vacuo, and the residue was dissolved in dichloromethane. Particulates were filtered from the dichloromethane solution, which was subsequently concentrated. Purification was achieved by means of column chromatography on silica gel with gradient elution from 5–20% ethyl acetate in hexanes to yield a clear crystalline solid (0.9 g, 24%), the ethyl ester, Et_2**L2**. ^{1}H NMR ($CDCl_3$): δ = 7.229 (s, 1 H), 6.199 (s, 1 H), 4.576 (s, 4 H), 4.281 (q, 4 H), 1.387 (s, 18 H), 1.315 (t, 6 H) ppm. ESI/EMM: *m*/*z* calcd. 417.2248 $[M + Na]^+$; found 417.2243. H_2**L2**: NaOH (7 mL, 1 M), ethanol (5 mL), and acetone (2 mL) were added into a 25 mL round-bottomed flask charged with diester (0.4 g, 1.0 mmol). The flask was equipped with a reflux condenser and heated to 70 °C for 12 h. Any remaining ethanol was removed by rotary evaporation. A solution of 1.0 M HCl was added to the remaining reaction mixture, thereby resulting in a creamy white precipitate that was extracted into ethyl acetate (50 mL three times). The organic layer was dried with sodium sulfate, filtered, and concentrated. An off-white solid was isolated (0.31 g, 96%). ^{1}H NMR ([D_6]acetone): δ = 7.212 (s, 1 H), 6.563 (s, 1 H), 4.730 (s, 4 H), 1.392 (s, 18 H) ppm. ^{13}C NMR ([D_6]acetone): δ = 29.79, 34.32, 65.11, 99.24, 124.88, 129.78, 155.57, 169.55 ppm. ESI/EMM: *m*/*z* calcd. 337.1656 $[M - H]^-$; found 337.1657.

Synthesis of Dirhodium Chelate Complexes 1, 2, and 3: Dirhodium tetraacetate·2CH_3OH (100 mg, 0.197 mmol, 1 equiv.) and chelate ligand (2.5 equiv.) were added to an Erlenmeyer flask with anhydrous dichlorobenzene (30 mL). The flask was heated to 150 °C for 4 h, then allowed to cool completely. The solvent was removed by rotary evaporation, and the resulting green residue was subjected to chromatography on silica gel, gradient elution with acetone in dichloromethane, 0–25%. The complexes were afforded in 60–75% yields as microcrystalline green/green-blue solids.

Compound 1: Characterization data matched values previously reported by Du Bois and co-workers.[18]

Compound 2: ^{1}H NMR ($CDCl_3$ + 3 vol.-% [D_6]acetone): δ = 7.033 (t, 2 H), 6.464 (dd, 4 H), 6.108 (t, 2 H), 1.358 (s, 24 H) ppm. MALDI-MS: *m*/*z* calcd. 766.000; found 765.910. IR: $\tilde{\nu}$ = 2978.91, 2962.29, 1727.29, 1596.67, 1201.36, 961.30 cm^{-1}. Elemental analysis (**2** was dried at 100 °C under vacuum to afford the complex with no axial ligation): calcd. C 43.88, H 4.21, N 0.00; found C 43.83, H 4.55, N 0.09. Crystals suitable for X-ray diffraction were obtained by dissolving the purified material in hot dichlorobenzene and allowing the solution to cool slowly (around 70 h).

Compound 3: ^{1}H NMR ([D_6]acetone + 3 vol.-% $CDCl_3$): δ = 7.137 (s, 2 H), 5.202 (s, 2 H), 4.614 (s, 8 H), 1.343 (s, 36 H) ppm. MALDI-MS: *m*/*z* = calcd. 878.126; found 877.980. IR: $\tilde{\nu}$ = 2958.67, 2914.94, 2873.92, 1592.91, 1414.18, 919.83 cm^{-1}. Elemental analysis (**3** was dried at 100 °C under vacuum to afford the complex with no axial ligation); calcd. C 49.21, H 5.51, N 0.00; found C 49.28, H 5.79, N 0.13. Crystals suitable for X-ray diffraction were obtained by dissolving the purified material in a 1:1 mixture of acetone and dichloromethane followed by slow evaporation of the solvents.

Compound 1·2HOAc: Crystals suitable for X-ray diffraction were isolated from the treatment of **1** (30 mg, 0.039 mmol) with trichloroethylsulfamate (18 mg, 0.078 mmol) and $PhI(OAc)_2$ (25 mg, 0.078 mmol) in dichloromethane (5 mL). The red reaction mixture was layered with hexanes. After several days, blue-green crystals were harvested.

CCDC-837373 (for **2**), -837374 (for **3**), and -846682 (for **1**·2HOAc) contain the supplementary crystallographic data for this paper. These data can be obtained free of charge from The Cambridge Crystallographic Data Centre via www.ccdc.cam.ac.uk/data_request/cif.

Amination Reactions: Each of the three catalysts was tested in a prototypical intermolecular C–H amination reaction, as well as an intramolecular cyclization. For the intramolecular reaction, a prototypical reaction using the substrate depicted in Scheme 3 was performed in dichloromethane with the addition of 1.1 equiv. of hypervalent iodine oxidant, as reported in the literature.[15] The intramolecular reaction was typically complete after 4 h, as monitored by TLC. TONs were measured internally by ^{1}H NMR spectroscopy using a 1 mol-% catalyst loading over a 24 h period and by conducting the reaction described above in CD_2Cl_2. Product concentrations were determined against an internal cyclooctane standard.

Intermolecular reactions were performed in deuterated solvent and product formation was monitored over the course of 24 h in the presence of two equivalents of hypervalent iodine oxidant, as reported previously.[4] Final product conversion was done on the basis of ^{1}H NMR spectroscopic integration.

Supporting Information (see footnote on the first page of this article): Figures S1 and S2 show the cyclic voltammograms for H_2**L1** and H_2**L2**; and Figures S3 and S4 show the crystal structures of **3** and **1**·2HOAc.

Acknowledgments

We thank the Chemical Sciences, Geosciences, and Biosciences Division, Office of Basic Energy Sciences, Office of Science, U.S. Department of Energy for support (grant number DE-FG02-10ER16204).

 © 2012 Wiley-VCH Verlag GmbH & Co. KGaA, Weinheim

[1] a) D. N. Zatalan, J. Du Bois, *Top. Curr. Chem.* **2010**, *292*, 347–378; b) H. M. L. Davies, J. R. Manning, *Nature* **2008**, *451*, 417–424; c) H. M. L. Davies, M. S. Long, *Angew. Chem.* **2005**, *117*, 3584–3586; *Angew. Chem. Int. Ed.* **2005**, *44*, 3518–3520.
[2] K. W. Fiori, J. Du Bois, *J. Am. Chem. Soc.* **2007**, *129*, 562–568.
[3] D. N. Zatalan, J. Du Bois, *J. Am. Chem. Soc.* **2009**, *131*, 7558–7559.
[4] K. P. Kornecki, J. F. Berry, *Chem. Eur. J.* **2011**, *17*, 5827–5832.
[5] a) P. J. Chirik, K. Wieghardt, *Science* **2010**, *327*, 794–795; b) W. Kaim, *Inorg. Chem.* **2011**, *50*, 9752–9765.
[6] F. Estevan, P. Lahuerta, J. Latorre, E. Peris, S. Garcia-Granda, F. Gomez-Beltran, A. Aguirre, M. A. Salvado, *J. Chem. Soc., Dalton Trans.* **1993**, 1681–1688.
[7] J. Bickley, R. Bonar-Law, T. McGrath, N. Singh, A. Steiner, *New J. Chem.* **2004**, *28*, 425–433.
[8] J. K. Kochi, *Angew. Chem.* **1988**, *100*, 1331; *Angew. Chem. Int. Ed. Engl.* **1988**, *27*, 1227–1266, and references therein.
[9] a) M. Jonsson, J. Lind, T. Reitberger, T. E. Eriksen, *J. Phys. Chem.* **1993**, *97*, 11278–11282; b) J. Pavlinac, M. Zupan, S. Stavber, *Org. Biomol. Chem.* **2007**, *5*, 699–707; c) J. Pavlinac, M. Zupan, S. Stavber, *J. Org. Chem.* **2006**, *71*, 1027–1032.
[10] F. Marchetti, G. Pampaloni, C. Pinzino, *J. Organomet. Chem.* **2011**, *696*, 1294–1300.
[11] H. T. Chifotides, K. R. Dunbar, in: *Multiple Bonds Between Metal Atoms* (Eds.: F. A. Cotton, C. A. Murillo, R. A. Walton), Springer, New York, **2005**, pp. 465–567.
[12] The structure of **3** crystallizes with both acetone and dichloromethane as axial ligands with disorder 84% acetone/16% dichloromethane. The CH_2Cl_2 ligand was omitted from the thermal ellipsoid plot for clarity, and is shown in Figure S3 in the Supporting Information.
[13] K. Das, K. M. Kadish, J. L. Bear, *Inorg. Chem.* **1978**, *17*, 930–934.
[14] P. Chaudhuri, K. Wieghardt, *Prog. Inorg. Chem.* **2001**, *50*, 151–216.
[15] C. G. Espino, P. M. Wehn, J. Chow, J. Du Bois, *J. Am. Chem. Soc.* **2001**, *123*, 635–6936.
[16] K. W. Fiori, C. G. Espino, B. H. Brodsy, J. Du Bois, *Tetrahedron* **2009**, *65*, 3042–3051.
[17] J. F. Berry, *Dalton Trans.* **2011**, DOI: 10.1039/C1DT11434D.
[18] C. G. Espino, K. W. Fiori, M. Kim, J. Du Bois, *J. Am. Chem. Soc.* **2004**, *126*, 15378–15379.

Received: August 1, 2011
Published Online: November 17, 2011

 © 2012 Wiley-VCH Verlag GmbH & Co. KGaA, Weinheim

DOI: 10.1002/ejic.201100763

Insights into the Mechanism of the Ruthenium–Porphyrin-Catalysed Allylic Amination of Olefins by Aryl Azides

Daniela Intrieri,[a] Alessandro Caselli,[a] Fabio Ragaini,[a] Piero Macchi,[b] Nicola Casati,[c] and Emma Gallo*[a]

Keywords: Amination / C–H activation / Azides / Metalloporphyrins / Porphyrinoids / Homogeneous catalysis

This paper describes the synthesis of allylic amines by aryl azides (ArN_3) catalysed by [Ru(TPP)CO] (TPP = dianion of tetraphenylporphyrin). The employment of aryl azides renders the methodology sustainable as the formation of molecular nitrogen is the only stoichiometric byproduct. The isolation of catalytic intermediates and spectroscopic and kinetic studies revealed interesting information about the reaction mechanism, which could improve its catalytic efficiency in future research. An important result is the X-ray characterisation of $[Ru(TPP)(ArN)_2]$ [Ar = 3,5-$(CF_3)_2C_6H_3$], which is active in both stoichiometric and catalytic nitrene transfer reactions. The proposed involvement of carbonyl-monoimidoruthenium porphyrin complexes in the catalytic cycle is also derived from our kinetic and experimental results. All the data indicate the coexistence of two mechanisms, where the electronic nature of the engaged aryl azide and olefin concentration determine one mechanism or the other.

Introduction

The insertion of a nitrene "RN" functionality into a C–H bond represents a valuable tool to achieve a wide variety of nitrogen-containing fine chemicals, which frequently present pharmaceutical and/or biological properties.[1–6] Among the nitrogen sources available to perform amination reactions, organic azides (RN_3) occupy a prominent role. The activation of an organic azide by a transition-metal catalyst yields the reactive fragment "RN" with N_2 as the only stoichiometric byproduct. The generation of ecofriendly molecular nitrogen renders the process sustainable and atom efficient.[7–9] It is worth noting that the reaction of saturated hydrocarbons with organic azides, which is responsible for the direct transformation of a C–H into a C–N bond, is considered as a domain of high impact and extreme synthetic utility. Amongst the transition metal complexes employed as catalysts[4,10–12] for both intra- and intermolecular C–H aminations, metalloporphyrins[13–20] exhibit a very good catalytic activity and selectivity.

In view of the potential of porphyrin-based methodologies to transfer a nitrene moiety to a C–H bond, the comprehension of reaction mechanisms is crucial to plan new and more efficient catalytic systems in future. To date, some studies have been published on the mechanism of porphyrin-catalysed C–H amination,[21,22] and imido complexes of high-valent metals have often been suggested as key intermediates.[23–26]

Several years ago, we investigated the catalytic activity of porphyrinatocobalt complexes in the amination of benzylic substrates[27,28] by aryl azides, which were easily synthesised from commercially available anilines and showed a convenient reactivity–stability relationship. Since then, we have widely used aryl azides as nitrogen sources in aziridinations[29–32] and aminations[33,34] in the presence of porphyrinato-cobalt or -ruthenium complexes. Our kinetic and spectroscopic studies suggested that the benzylic and allylic aminations mediated by cobalt– porphyrins occur through the formation of an azido adduct intermediate.[28,33] Zhang and de Bruin et al.[35] have proposed, on the basis of DFT and electron paramagnetic resonance studies, that the azido adduct evolves into a radical nitrene intermediate before reacting with the hydrocarbon substrate. On the other hand, our data on porphyrinatoruthenium(II)-mediated C–H aminations by aryl azides[34,36] envisages the formation of ruthenium imido complexes as active intermediates, which is in accord with that proposed by Che et al.[23–26]

This report deals with a mechanistic study of allylic aminations by aryl azides catalysed by ruthenium porphyrin complexes. A catalytic cycle was proposed on the basis of kinetic and spectroscopic investigations. The isolation and characterisation of several compounds involved in the cata-

[a] Dipartimento di Chimica Inorganica, Metallorganica e Analitica, Università di Milano, and ISTM-CNR, via Venezian 21, 20133 Milano, Italy
Fax: +39-02-50314405
E-mail: emma.gallo@unimi.it
[b] Department of Chemistry & Biochemistry, University of Berne, Freiestrasse 3, 3012 Berne, Switzerland
[c] Diamond Light Source Ltd., Harwell Science and Innovation Campus, Chilton OX11 0DE, UK

Supporting information for this article is available on the WWW under http://dx.doi.org/10.1002/ejic.201100763 or from the author.

 © 2012 Wiley-VCH Verlag GmbH & Co. KGaA, Weinheim

lytic cycle shed light on the nitrene transfer reaction. A preliminary communication on the subject has recently been published.[36]

Results and Discussion

Synthetic Studies

Our recent study on the [Ru(TPP)CO]-mediated (TPP = dianion of tetraphenyl porphyrin) amination of benzylic substrates by aryl azides[34] prompted us to examine the amination of allylic substrates. The scope of the reaction reported in Scheme 1 was investigated by employing different allylic substrates and aryl azides (Table 1).

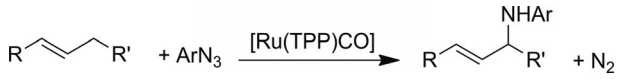

Scheme 1. Amination of allylic substrates catalysed by [Ru(TPP)CO].

The synthesis of allylic amines reported in Table 1 was firstly performed in benzene, employing the molar ratio [Ru(TPP)CO]/ArN_3/olefin = 1:50:250, and secondly with the neat olefin as the solvent. Data reported in Table 1 indicate that better yields are generally obtained by using the latter methodology. In particular, very high yields were achieved in olefin for the allylic amination of cyclohexene by almost every azide (Table 1, Run 1). The low yield observed in the reaction of 4-$OMeC_6H_4N_3$ with cyclohexene (Run 1, **1h**) is probably due to the coordination of the methoxy group to the ruthenium atom, which can partially inhibit the catalysis.[30] The reduced chemoselectivity of the amination of 1,2-dihydronaphthalene was because of the contemporaneous presence of both allylic and benzylic functionalities (Run 3).[34] The amination of 1-octene occurred only by a small extent because of its poor reactivity (Run 6). In all the reactions tested, the secondary products recovered were the aryl diazene and aniline corresponding to the azide employed.

In the belief that an important step for the improvement of the catalytic efficiency of the reported methodology is a comprehension of the reaction mechanism, we first studied the catalytic reactivity towards the components of a model reaction, cyclohexene and 3,5-$(CF_3)_2C_6H_3N_3$. No catalyst modification was observed by ^1H NMR when [Ru(TPP)CO] was suspended in cyclohexene and heated to reflux for several hours. However, the reaction between [Ru(TPP)CO] and an excess of Ar^aN_3 (3 equiv.) [Ar^a = 3,5-$(CF_3)_2C_6H_3$] yielded the bisimido complex [Ru(TPP)$(NAr^a)_2$] (**7**) in 70% yield (Scheme 2).

It is likely that **7** derives from the reaction of the monoimido [Ru^{IV}(TPP)(Ar^aN)CO] complex with another molecule of aryl azide. Unfortunately, the formation of **7** occurred without observable intermediates and every attempt to detect a ruthenium(IV) species failed. It is possible that the intermediate Ru^{IV} complex reacts with a second azide molecule at a much faster rate than the starting [Ru(TPP)(CO)]. However, [Ru^{IV}(TPP)(Ar^aN)CO] may also rapidly disproportionate to the bisimido **7** and [Ru(TPP)CO], analogous to that proposed for isostructural ruthenium(IV) oxo porphyrins.[37,38]

Table 1. The [Ru(TPP)CO]-mediated allylic amination by ArN_3.[a]

Run	Product[b]	Ar	Yield (%)[b]	Time (h)[c]
1	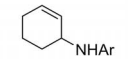	**1a**, 3,5-$(CF_3)_2C_6H_3$	26 (75)[d]	12(4)[d]
		1b, 4-$NO_2C_6H_4$	23 (70)[d]	5(6)[d]
		1c, 4-$^tBuC_6H_4$	13(89)[d]	6(7)[d]
		1d, 4-CNC_6H_4	35 (80)[d]	8(2)[d]
		1e, 4-$CF_3C_6H_4$	28 (85)[d]	7(4)[d]
		1f, 4$(CO_2Me)C_6H_4$	13 (85)[d]	6(8)[d]
		1g, 3,5-$Cl_2C_6H_3$	38 (90)[d]	10(3)[d]
		1h, 4-$MeOC_6H_4$	8 (33)[d]	7(7)[d]
2	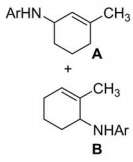	**2a**, 3,5-$(CF_3)_2C_6H_3$	**A**, 28, **B**, 15	10
		2b, 4-$NO_2C_6H_4$	**A/B**, 20	8
		2e, 4-$CF_3C_6H_4$	**A**, 17; **B**, 9	7
3	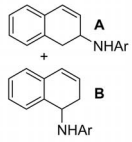	**3a**, 3,5-$(CF_3)_2C_6H_3$	**A**, 33, **B**, 24 (**A**, 51, **B**, 34)[d]	1 (0.3)[d]
		3b, 4-$NO_2C_6H_4$		3
			A, 32, **B**, 22 (**A**, 45, **B**, 28)[d]	(1)[d]
4	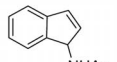	**4a**, 3,5-$(CF_3)_2C_6H_3$	42	3
		4b, 4-$NO_2C_6H_4$	30	3.5
		4e, 4-$CF_3C_6H_4$	30	5
5	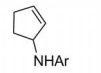	**5**, 4-$NO_2C_6H_4$	30	8
6	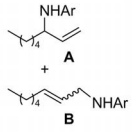	**6**, 3,5-$(CF_3)_2C_6H_3$	**A**, 9, **B**, 11	25

[a] General procedure for catalytic reactions: [Ru(TPP)CO] (10 mg, 1.34×10^{-2} mmol) in benzene (30 mL) heated to reflux; molar ratio catalyst/ArN_3/olefin = 1:50:250. [b] Determined by ^1H NMR (2,4-dinitrotoluene as the internal standard). [c] Time required to reach complete conversion of the starting ArN_3. [d] Reaction carried out in neat olefin heated to reflux.

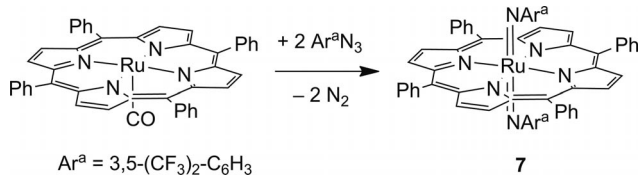

Scheme 2. Synthesis of **7**.

Complex **7** was fully characterised. It remained stable for a long period at room temperature and decomposed only when exposed to a coordinating solvent such as tetrahydrofuran. The NMR spectrum of **7** in $CDCl_3$ revealed a chemical shift of the aromatic azide hydrogen atoms due to the ring current effect of the porphyrin (see Supporting Information).

 © 2012 Wiley-VCH Verlag GmbH & Co. KGaA, Weinheim

Single-crystal X-ray diffraction confirmed the molecular structure of **7** (Figure 1; for crystallographic data and details see SI). The two ArN ligands are *syn*-periplanar (i.e. almost perfectly eclipsed about the N1···N2 axis). The Ru–N distances, 1.808(4) and 1.806(4) Å for N1 and N2, respectively, are in the range of double bonds, which confirms the imido nature of the ligand. The nitrogen lone pairs are available as demonstrated by the Ru–N–C angles, which are extremely bent [139.8(3) and 143.7(4)° for N1 and N2, respectively].[39] However, no intermolecular contact occurs between these two crystallographically independent atoms. This is certainly due to the absence of any H-bond donor and the almost hindered nature of the molecule. The porphyrin–Ru bonds are in the range 2.04–2.07 Å, and the porphyrin is not particularly distorted by the apical ligands.

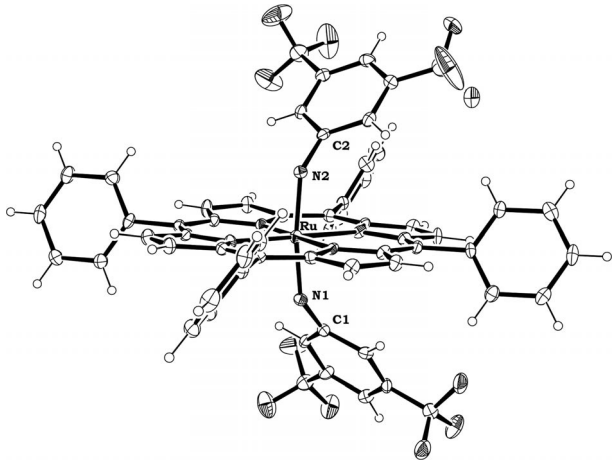

Figure 1. Molecular structure of **7**, ellipsoids are drawn at 30% probability.

In view of the nature of the imido–metal interaction in **7** (Figure 1), we investigated the reactivity of the nitrene transfer reaction by dissolving **7** (0.02 mmol) in cyclohexene (5 mL) at 75 °C. When TLC analysis showed the complete consumption of **7**, the reaction mixture was evaporated to dryness to eliminate the unreacted olefin and a ^{1}H NMR spectrum of the crude material was measured with 2,4-dinitrotoluene as the internal standard. The presence of the corresponding allylic amine in 52% yield indicated that the "Ar^{a}N" group had efficiently inserted into the C–H bond.

Following extensive research carried out by Che et al.[23] on the mechanism of stoichiometric reactions between imidoporphyrin complexes and hydrocarbons, we recently decided to study the catalytic activity of ruthenium–imidoporphyrins[36] to better assess their implication in Ru(TPP)-CO-catalysed C–H amination. Thus, we tested the catalytic activity of **7** in allylic aminations of several olefins by Ar^{a}N$_3$ (Table 2), despite the fact that other ruthenium–porphyrins are easier to handle and synthetically more accessible than **7**.[26,40]

Comparing the data in Table 2 with those reported in Table 1, we can conclude that in almost all cases the allylic amine yields are similar, or even better, which suggests the possible involvement of **7** in the catalytic cycle. If a phenyl group was present on the double bond of 1,2-dihydronaphthalene (Table 2, Run 6), the formation of the aziridine ring was also observed in accord with that already reported for the Ru(porphyrin)CO-catalysed aziridination of olefins.[30]

Table 2. Complex **7**-mediated allylic amination by Ar^{a}N$_3$.[a]

Run	Product[b]	Yield (%)[b]	Time (h)[c]
1	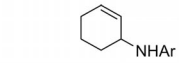	**1a**, 74(99)[d]	16(1)[d]
2	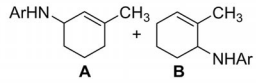	**2a**, **A**, 38(49)[d] **B**, 22(39)[d]	20(2)[d]
3	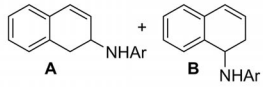	**3a**, **A**, 39 **B**, 21	1.5
4	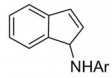	**4a**, 55(70)[d]	1.5(0.5)[d]
5	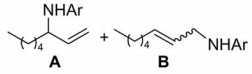	**6**, **A**, 5(11)[d] **B**, 6(11)[d]	40[e] (6)[d]
6	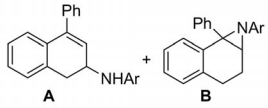	**8**, **A**, 33 **B**, 28	1.5

[a] General procedure for catalytic reactions: **7** (15 mg, 1.28×10^{-2} mmol) in benzene (30 mL) heated to reflux; molar ratio catalyst/Ar^{a}N$_3$/olefin = 1:50:250. [b] Determined by ^{1}H NMR (2,4-dinitrotoluene as the internal standard). [c] Time required to reach complete conversion of the starting Ar^{a}N$_3$. [d] Reaction carried out in neat olefin heated to reflux. [e] Ar^{a}N$_3$ conversion = 85%.

To better investigate the catalytic role of **7**, the reaction of cyclohexene with Ar^{a}N$_3$ was run in C_6D_6 (1 mL) at 65 °C in the presence of **7** (10 mg, 8.6×10^{-3} mmol) using a molar ratio of **7**/aryl azide/cyclohexene = 1:10:20. The progress of the reaction was monitored by ^{1}H NMR spectroscopy. The formation of the corresponding allylic amine was accompanied by the disappearance of the signals of **7** and signals attributed to a new ruthenium–porphyrin species **9** became evident. This new complex was visible by ^{1}H NMR spectroscopy until the aryl azide conversion was complete and then the formation of several signals in the porphyrin region indicated a decomposition process.

To isolate the complex observed during the NMR analysis, the reaction was performed on a larger scale (30 mg of **7**, 2.57×10^{-2} mmol) and followed by IR spectroscopy, which monitored the intensity of the 2116 cm^{-1} absorption of the N_3 group of the azide. The reaction was stopped at 90% of the aryl azide conversion to avoid the formation of decomposition products (vide supra) and the reaction mixture was refrigerated to yield a small amount of purple crystals.

 © 2012 Wiley-VCH Verlag GmbH & Co. KGaA, Weinheim

The X-ray structure reported in Figure 2 shows that **9** is the bisamido complex [Ru(TPP)($Ar^aNC_6H_9$)$_2$] (for crystallographic data and details see Supporting Information). The molecule sits on an inversion centre and the Ru–N1 distance is much larger than that in **7** [1.962(3) Å], which is in the range typical for amido bonds. The Ru1–N3–C31 and Ru1–N3–C41 angles have typical values of 122.2(3) and 124.0(3)°, respectively, with the N3–C31–C41 plane perpendicular to the TPP one. The N3–C31 bond length in **9** [1.417(5) Å] is longer than those of N1–C1 [1.361(6) Å] and N2–C2 [1.392(4) Å] in **7**. The porphyrin–Ru bonds are slightly shorter than those in **7** (2.042–2.047 Å). The intermolecular contacts are all quite long in the absence of strong interactions. Nevertheless, no empty volume is left in the crystal.

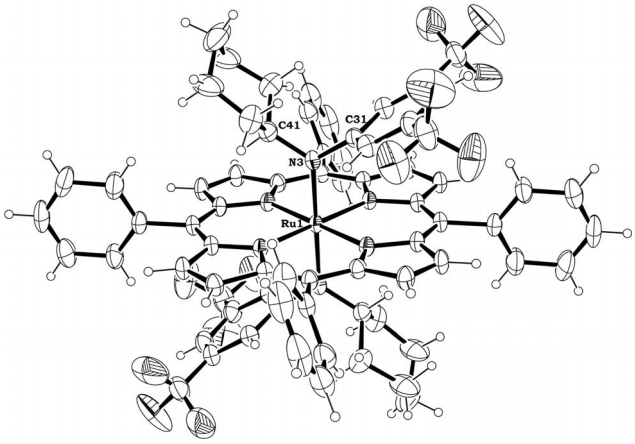

Figure 2. Molecular structure of **9**, ellipsoids are drawn at 30% probability.

We tried to synthesise **9** in large amounts but, because of its chemical instability, pure **9** was isolated in low yield (18%) together with the allylic amine and unidentified ruthenium species. Complex **9** is stable for a few days at –15 °C in the solid state and for some hours in a benzene solution and rapidly decomposes in the majority of solvents, especially coordinating ones. The diamagnetic behaviour of **9** indicates the formation of a ruthenium(IV) compound with $S = 0$. A recent DFT study is in accord with our experimental results.[41]

When **9** was left to stand in pure cyclohexene or benzene/cyclohexene, the fast formation of the corresponding allylic amine and uncharacterised ruthenium products was observed. Complex **9** could be accumulated in solution only under catalytic conditions in which both Ar^aN_3 and cyclohexene are present and the olefin concentration is larger than that of the azide. Conversely, when [Ar^aN_3] > [cyclohexene], **9** was completely converted into **7**. We have studied this reaction by dissolving **9** (6.85 mg, 5.15×10^{-3} mmol) in a C_6D_6 (1 mL) solution of Ar^aN_3 and cyclohexene in a molar ratio of **9**/aryl azide/cyclohexene = 1:50:10. The reaction was monitored by following the pyrrolic signals of the porphyrin in the ^{1}H NMR spectrum. After a few minutes at 65 °C, the formation of **7** was observed and after four hours, **9** was no longer detectable by ^{1}H NMR spectroscopy. If more cyclohexene (60 equiv.) was added to the mixture at this point, **9** was regenerated, which indicates a reversible process. The ^{1}H NMR spectra also disclosed the catalytic formation of the allylic amine.

To date, data collected suggest a mechanism for the allylic amination of cyclohexene in which both **7** and **9** are implicated (Scheme 3).

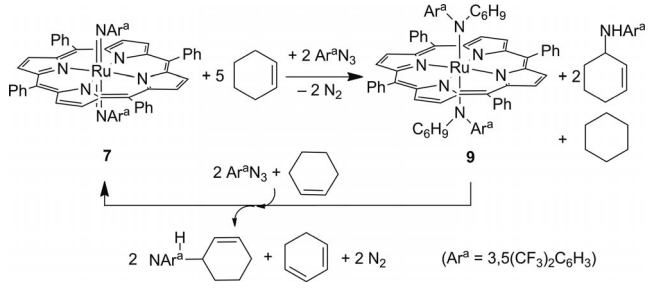

Scheme 3. Mechanistic hypothesis for the reaction between cyclohexene and Ar^aN_3 catalysed by **7**.

The synthesis of **9** requires the abstraction of two hydrogen atoms that, in our opinion, are associated with the **7**-mediated[42,43] reduction of a stoichiometric amount of cyclohexene to cyclohexane. The reduction of benzene is excluded because the allylic amination of cyclohexene also occurred in high yields in neat olefin (Table 2, Run 1). The complete inhibition of the reaction when the **7**-catalysed amination of cyclohexene was performed in the presence of TEMPO (2,2,6,6-tetramethylpiperidine *N*-oxide) indicates that the "NAr" insertion into the C–H bond proceeds via radical intermediates, which has been previously reported for similar catalytic systems.[23,35] The reversible **9** to **7** process occurs by a hydrogen atom transfer (HAT) reaction in which cyclohexene is oxidised to 1,3-cyclohexadiene, which was identified at the end of the catalytic reaction by GC–MS and ^{1}H NMR spectroscopy. 1,3-Cyclohexadiene was not present as an impurity in the starting cyclohexene, which was evidenced by the same techniques. Unfortunately, the presence of cyclohexane could not be detected by GC–MS spectroscopy because its signal overlaps with that of cyclohexene.

The hypothesis illustrated in Scheme 3 is supported by the ^{1}H NMR spectroscopic and GC–MS analyses of the amination of 1,2-dihydronaphthalene, which reveals, apart from the corresponding allylic amine, the presence of naphthalene and the benzylic amine of 1,2,3,4-tetrahydronaphthalene. The formation of the latter compound indicates that 1,2-dihydronaphthalene was partly reduced to 1,2,3,4-tetrahydronaphthalene that, being a benzylic substrate for the nitrene transfer reaction, was aminated. The involvement of the hydrocarbon substrate in the HAT process explains the need for an excess of olefin for the catalytic reaction to proceed. In fact, if allylic aminations were run with the olefin as the limiting reagent the consumption of Ar^aN_3 was not complete. It should be emphasised that the

 © 2012 Wiley-VCH Verlag GmbH & Co. KGaA, Weinheim

active role of **9** was further supported by its catalytic activity in the allylic amination of cyclohexene, which was maintained for two further runs when additional amounts of the reagents were added before the complete consumption of Ar^aN_3 to avoid the catalyst decomposition.

In order to assess if the formation of a bisimido complex is a general reaction, we have also studied the reactivity of [Ru(TPP)CO] towards other aryl azides. The reactions between [Ru(TPP)CO] and ArN_3 (Ar = 4-$CF_3C_6H_4N_3$, 4-$NO_2C_6H_4N_3$, 4-$CNC_6H_4N_3$) were monitored by ^{1}H NMR spectroscopy (C_6D_6). After the addition of the selected azide, an immediate modification of the NMR spectrum of [Ru(TPP)CO] was observed. The coordination of the nitrene ligand to the metal centre has been suggested on the basis of the change of the typical porphyrin region and for the appearance of signals in the same NMR region (2–7 ppm) where aromatic hydrogen atoms of the azide were detected for **7** (see SI). In every reaction tested, the newly formed complex was stable for a short time and the disappearance of the signals, which were attributed to the coordinated aryl group, indicated a decomposition process (see SI).

The reaction between [Ru(TTP)CO] and Ar^eN_3 (Ar^e = 4-$CF_3C_6H_4N_3$) was repeated on a larger scale and stopped after 30 min to avoid any decomposition. The purple complex [Ru(TPP)$(NAr^e)_2$] (**10**) was isolated in 60% yield and fully characterised. Unreacted [Ru(TPP)CO] was also present in the reaction mixture. Complex **10** was stable in the solid state under an inert atmosphere for several days but partially decomposed in solution, which made it difficult to determine its molecular structure by X-ray diffraction analysis. Nevertheless, we proposed the formation of the bisimido complex **10** on the basis of 1D and 2D NMR spectra, which showed a perfect similitude with those of **7**. The ^{1}H NMR spectrum (see SI) showed the presence of an AA′BB′ pattern for the aromatic azide moiety at 5.94 and 2.61 ppm. All the other analytical data agreed with the proposed structure.

Complex **10** was heated to reflux in cyclohexene for three hours to give the allylic amine (54%) and it was catalytically active in the reaction between cyclohexene and Ar^eN_3 using a catalytic molar ratio of **10**/azide = 1:50 in hot cyclohexene. After 2.5 hours the allylic amine **1e** was recovered in 55% yield. Complex **10** was also a competent catalyst in the allylic amination of 1-methylcyclohexene, indene and 1-octene by Ar^eN_3; the corresponding allylic amines were formed with yields comparable with those obtained using [Ru(TPP)CO] as the catalyst.

[Ru(TPP)CO] and 4 equiv. of Ar^eN_3 were heated to reflux in C_6H_6 for three hours to better understand the observed decomposition pathway. [Ru(TPP)(Ar^eNH_2)CO] (**11**) was isolated from the reaction mixture in 37% yield. Unidentified ruthenium compounds derived from the decomposition of **10** accounted for the rest of the reaction mass balance with respect to the starting [Ru(TPP)CO].

The structure of **11** was definitively assigned by comparing its analytical data with those of the reaction product from [Ru(TPP)CO] and 4-$CF_3C_6H_4NH_2$ (Scheme 4).

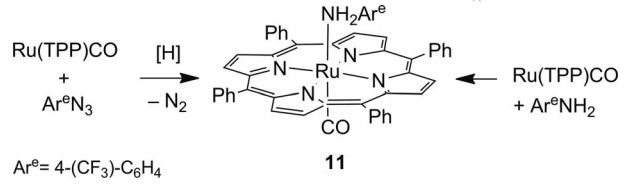

Scheme 4. Synthesis of **11**.

Complex **11** exhibited different spectra in $CDCl_3$ and in C_6D_6 due to the aromatic solvent-induced shift[44,45] effect (Figure 3); however, in both cases a signal at a negative chemical shift value was observed (–3.43 and –4.08 ppm in $CDCl_3$ and C_6D_6, respectively). The signal disappeared on addition of D_2O and the ^{2}H NMR spectrum in C_6D_6 disclosed the presence of a signal at –13.43 ppm; these data confirm the coordination of an arylamine to the ruthenium atom.

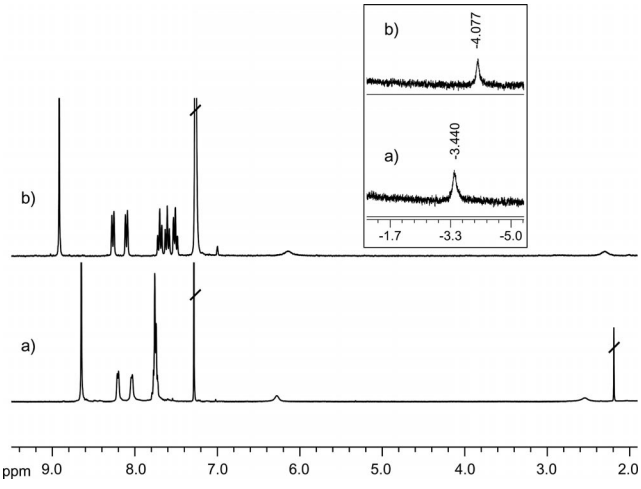

Figure 3. ^{1}H NMR spectra of **11** in $CDCl_3$ (a) and C_6D_6 (b).

To explain the formation of **11**, we propose that, as already suggested for the synthesis of **7**, the first step of the reaction between [Ru(TPP)CO] and Ar^eN_3 yields a monoimido ruthenium(IV) complex, which is too reactive to be detected. This intermediate can react with another molecule of aryl azide to yield **10** or can decompose to regenerate [Ru(TPP)CO]. The so-formed [Ru(TPP)CO] can be "trapped" by Ar^eNH_2 to yield **11**. The presence of Ar^eNH_2 in solution is due to partial aryl azide decomposition mediated by the ruthenium catalyst, which can promote hydrogen atom abstraction reactions.[35] Clearly, we cannot exclude that the direct reaction of [Ru(TPP)CO] with Ar^eNH_2 can also be responsible in part for the formation of **11**.

Considering that **11** can also be formed during the catalytic reaction, we have studied its catalytic activity in the allylic amination of several olefins using the same experimental conditions reported in Table 1. The data obtained (see experimental section) were comparable with those observed in [Ru(TPP)CO]-mediated reactions, which indicate that Ar^eNH_2, formed during the catalytic cycle, is not a catalyst inhibitor.

 © 2012 Wiley-VCH Verlag GmbH & Co. KGaA, Weinheim

Synthetic results described to date now suggest that, depending on the electronic nature of the employed aryl azide, both bis- and monoimido complexes can be involved in allylic aminations of cyclohexene and an active role is probably also played by monoimido species.

Kinetic Study

To shed some light on the [Ru(TPP)CO]-catalysed allylic amination of cyclohexene, a kinetic study was undertaken that employed Ar^eN_3 (Ar^e = 4-$CF_3C_6H_4N_3$) or Ar^aN_3 [Ar^a = 3,5-$(CF_3)_2C_6H_3N_3$] as nitrogen sources. The reactions were followed by IR spectroscopy, which monitored the intensity of the aryl azide absorption (Ar^eN_3 at 2102 cm^{-1} and Ar^aN_3 at 2116 cm^{-1}). All the kinetic experiments in this paper were run at 75 °C to avoid boiling benzene in the reactions in which it was present.

The rate of the reaction between cyclohexene and Ar^eN_3 showed a first-order dependence on azide and [Ru(TPP)CO] concentrations. However, a zero-order dependence on cyclohexene concentration (the other solvent was benzene) was observed (Figure 4). These data led to the kinetic equation $v = -d[Ar^eN_3]/dt = k_{obs}[Ru(TPP)CO][Ar^eN_3]$.

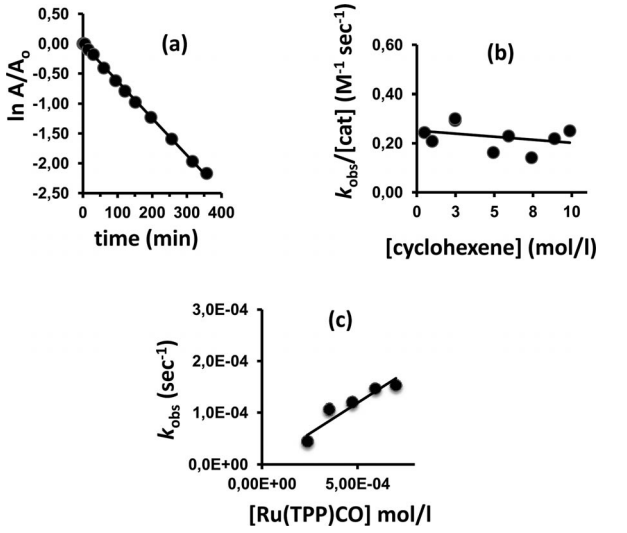

Figure 4. Kinetic dependence of the reaction rate with respect to the concentrations of 4-$CF_3C_6H_4N_3$ (a), cyclohexene (b) and [Ru(TPP)CO] (c).

Sampling the reaction mixture during the catalytic reaction and examining it by TLC allowed the observation of [Ru(TPP)(CO)(Ar^eNH_2)] as the only identifiable complex. Together with the observed kinetics, this observation is consistent with a reaction mechanism in which the rate-determining step is the formation of a monoimido complex that very quickly reacts with the olefin to form the allylic amine and regenerate [Ru(TPP)CO]. We suggest that [Ru(TPP)CO] reacts with aniline, a reaction by-product, yielding [Ru(TPP)(CO)(Ar^eNH_2)] (**11**) that was identified during the catalysis. This mechanistic hypothesis envisages that **11** should be the only product accumulated in solution, which is in accord with the experimental observation (Scheme 5).

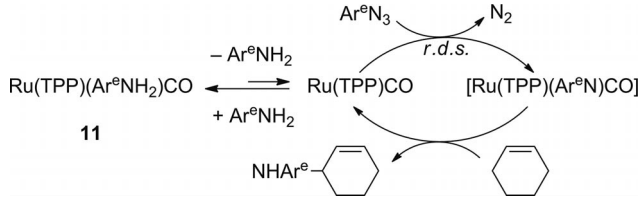

Scheme 5. Mechanistic hypothesis for the reaction between cyclohexene and 4-$CF_3C_6H_4N_3$ catalysed by [Ru(TPP)CO].

The active role of bisimido **10** under these conditions is not supported by the kinetic experiments. In particular, it would be difficult to explain the observation of a ruthenium carbonyl complex even at the end of the reaction if the coordinated CO had been lost in the formation of **10**.

The same kinetics have been observed for the reaction of 4-$NO_2C_6H_4N_3$ with cyclohexene catalysed by [Ru(TPP)CO] (see the Supporting Information for graphics).

The kinetics of the [Ru(TPP)CO]-catalysed reaction between Ar^aN_3 and cyclohexene were more complex than previously discussed. A first-order dependence on the aryl azide was observed but the rate order dependence on the olefin concentration is not unique. A first-order dependence was observed up to an olefin concentration of 3 M and then the reaction rate was almost independent from the quantity of cyclohexene present in solution (Figure 5a). This behaviour indicates the coexistence of at least two mechanisms that occur contemporaneously with the prevalence of one or the other depending on the olefin concentration.

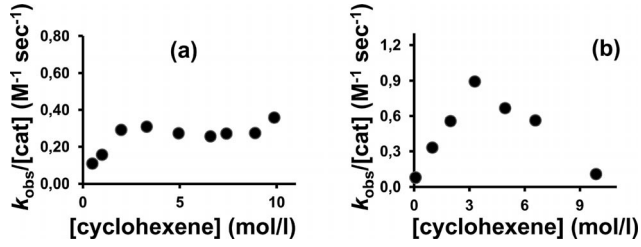

Figure 5. Kinetic dependence of the reaction rate with respect to olefin concentration in the reactions between cyclohexene and 3,5-$(CF_3)_2C_6H_3N_3$ catalysed by [Ru(TPP)CO] (a) or **7** (b).

The kinetics of the reaction between Ar^aN_3 and cyclohexene were also studied in the presence of **7**, and a first-order dependence with respect to the aryl azide concentration was observed. The rate dependence on the olefin concentration showed both similarities and differences with respect to that observed with [Ru(TPP)CO] as the catalyst. A first-order dependence on cyclohexene concentration was again obtained up to a 3 M concentration, but an inhibiting effect at higher concentrations was evident (Figure 5b) rather than the flat dependence visible in Figure 5a.

 © 2012 Wiley-VCH Verlag GmbH & Co. KGaA, Weinheim

Bearing in mind the results of the synthetic studies discussed above, all the experimental results can be accounted for in the general reaction scheme shown in Scheme 6.

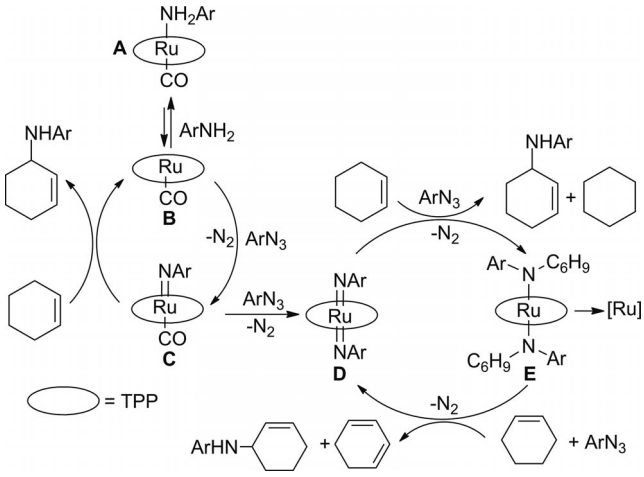

Scheme 6. Mechanistic hypothesis for the allylic amination of cyclohexene by aryl azides catalysed by [Ru(TPP)CO].

The reaction of [Ru(TPP)CO] (**B** in Scheme 6) with ArN_3 initially forms a monoimido complex (**C**). In the case of Ar = 4-$CF_3C_6H_4$, the reaction with cyclohexene to yield the allylic amine and regenerate **B** is faster than the reaction with a second azide molecule for all cyclohexene concentrations tested. Thus, the second cycle in Scheme 6 does not operate and the kinetics are clearly first order for the azide and ruthenium complex (r.d.s. formation of the monoimido complex **C**) and zero order with respect to cyclohexene (fast reaction). [Ru(TPP)CO], in equilibrium with **11**, is the resting state of the catalyst, which is in accord with the experimental observations. In the case of the stoichiometric reaction between [Ru(TPP)CO] and 4-$CF_3C_6H_4N_3$, which has been described previously, this clearly does not hold. In this case there is no olefin available to trap **C** and the reaction evolves to the bisimido complex **D**.

In the case of Ar = 3,5-$(CF_3)_2C_6H_3$, the situation is more complex. The higher reactivity of the bis-trifuoromethylated azide renders the formation of the bisimido complex **D** more competitive than when only a single electron-withdrawing group (CF_3 or NO_2) is present. The rate dependence of the catalytic reaction on olefin concentration shown in Figure 5 (a) can be explained by assuming that at low cyclohexene concentration formation of **D** is relevant during the reaction. The reaction of **D** with cyclohexene becomes rate determining and the kinetics are first order with respect to the olefin. At a higher cyclohexene concentration, the reaction of **C** with the olefin becomes faster than the reaction with another azide molecule and the same situation is observed in the case of Ar = 4-$CF_3C_6H_4$ (zero-order kinetics in cyclohexene).

When **7** was employed as the catalyst, the situation at low olefin concentration parallels that observed for [Ru(TPP)CO]. However, the two types of kinetics cannot give the same behaviour at high olefin concentration because no CO is present in the first case and a complex of type **C** cannot be formed. Under these conditions, in agreement with the results of the synthetic studies described in above, the resting state of the complex gradually shifts towards the bisamido complex **E**. The rate of the reaction should be independent of olefin concentration, but it must be considered that **E** has a low stability and easily decomposes. Thus, faster catalyst deactivation is observed when this type of complex is accumulated in solution. Such a gradual decomposition can be difficult to separate in any single kinetic experiment by the natural rate decrease due to azide consumption and it easily results in a lower apparent first-order kinetic constant.

It should be noted that the lower slope of the low cyclohexene concentration branch of Figure 5 (a) with respect to that shown in part b is consistent with the contemporaneous competition of two catalytic cycles in the first case, only one of which is accelerated by an increase in olefin concentration. In theory, it may be possible to calculate the relative weight of the two catalytic cycles by the observed differences, but the number of available data points does not allow us to perform this calculation reliably.

Conclusions

The allylic amination of cyclohexene catalysed by ruthenium porphyrin complexes occurs through at least two different mechanisms where one prevails over the other depending on the nature of the employed aryl azide and the olefin concentration. Experimental and kinetic data indicate that both mono- and bisimido species can be involved in the nitrene transfer reaction but the high reactivity of the monoimido derivative precluded any characterisation. However, the isolation of its decomposition products and kinetic data suggest that the monoimido complex is mainly responsible for the catalytic reaction when using aryl azides that show less electron-withdrawing behaviour. On the other hand, if an aryl azide that bears two strong electron-withdrawing substituents, such as two CF_3 groups, is employed, the monoimido complex rapidly reacts with the aryl azide to be further oxidised to the bisimido complex, which becomes the reaction catalyst.

To better clarify the role of mono- and bisimido complexes in the nitrene transfer reaction into an allylic C–H bond, a computational study is currently in progress.

Experimental Section

General: Unless otherwise specified, all reactions were carried out in a nitrogen atmosphere employing standard Schlenk techniques and magnetic stirring. Benzene and *n*-hexane were dried by an M. Braun SPS-800 solvent purification system. Cyclohexene and 1-octene were distilled from sodium benzophenone and kept under nitrogen. All the other starting materials were commercial products and used as received. Aryl azides,[30,46] tetraphenylporphyrin[47,48] and [Ru(TPP)CO][49] were synthesised by methods as reported in the literature or with minor modifications.[50] The purity of olefins

 © 2012 Wiley-VCH Verlag GmbH & Co. KGaA, Weinheim

and the aryl azides employed was confirmed by GC–MS or ^{1}H NMR spectroscopy. NMR spectra were recorded at room temperature with a Bruker AC-300 or a Bruker avance 300-DRX instruments operating at 300 MHz for ^{1}H, 75 MHz for ^{13}C and 282 MHz for ^{19}F, or with a Bruker Avance 400-DRX spectrometers operating at 400 MHz for ^{1}H and 100 MHz for ^{13}C. Chemical shifts (ppm) are reported relative to Me_4Si. The ^{1}H NMR signals of the compounds described below have been attributed by COSY and NOESY techniques. Assignments of the resonances in ^{13}C NMR spectra were made using the APT pulse sequence and heteronuclear single quantum coherence (HSQC) and HMBC techniques. GC–MS were performed with a Shimadzu QP5050A instrument. Infrared spectra were recorded with a Varian Scimitar FTS 1000 spectrophotometer. UV/Vis spectra were recorded with an Agilent 8453E instrument. Elemental analyses and mass spectra were recorded in the analytical laboratories of Milan University. CCDC-720709 (for **7**) and -720710 (for **9**) contain the supplementary crystallographic data for this paper. These data can be obtained free of charge from The Cambridge Crystallographic Data Centre via www.ccdc.cam.ac.uk/data_request/cif.

General Procedure for Catalytic Reactions

Method A: In a typical run, the catalyst (1.3×10^{-2} mmol) and the aryl azide (6.3×10^{-1} mmol) were added to a benzene (30 mL) solution of the olefin (3.2 mmol). The resulting solution was heated to reflux using a preheated oil bath. The consumption of the aryl azide was monitored by TLC up to the point that its spot was no longer observable, and then by IR spectroscopy, which measured the characteristic N_3 absorbance in the range 2095–2130 cm^{-1}. The reaction was considered to be finished when the absorbance of the azide measured was below 0.03 (by using a 0.5 mm thick cell). The solution was then evaporated to dryness and analysed by ^{1}H NMR spectroscopy with 2,4-dinitrotoluene as the internal standard. The residue was purified by flash chromatography on deactivated silica with 10% Et_3N added to the eluent (*n*-hexane/ethyl acetate) during the packing of the column.

Method B: The synthetic procedure reported above was repeated using the olefin as the reaction solvent.

***N*-(Cyclohex-2-enyl)-3,5-bis(trifluoromethyl)benzenamine (1a):**[51] 26% yield obtained by following method A with [Ru(TPP)CO] as catalyst; 75% yield by following method B with [Ru(TPP)CO] as catalyst; 74% yield by following method A with **7** as catalyst; 99% yield by following method B with **7** as catalyst.

Method C: Compound **9** (17 mg, 1.28×10^{-2} mmol) and trifluoromethylphenyl azide (166 mg, 6.51×10^{-1} mmol) were added to a benzene (30 mL) solution of cyclohexene (0.325 mL, 3.21 mmol). The solution was heated to reflux for 18 h, evaporated to dryness and analysed by ^{1}H NMR spectroscopy with 2,4-dinitrotoluene as the internal standard (70% of **1a**). Analytical data are in accord with the literature.

***N*-(Cyclohex-2-enyl)-4-nitrobenzenamine (1b):**[52] 23% yield obtained by following method A with [Ru(TPP)CO] as catalyst; 70% yield by following method B with [Ru(TPP)CO] as catalyst. $C_{12}H_{14}N_2O_2$ (218.11): calcd. C 66.04, H 6.47, N 12.84; found C 66.50, H 6.49, N 12.61. ^{1}H NMR (300 MHz, $CDCl_3$): δ = 8.10 (d, 2 H, J = 9.1 Hz, H_{Ar}), 6.55 (d, 2 H, J = 9.1 Hz, H_{Ar}), 5.97 (m, 1 H, CH=C*H*–CH_2), 5.73 (m, 1 H, C*H*=CH–CH_2), 4.51 (br. s, 1 H, NH), 4.10 (br. s, 1 H, C*H*NH), 2.09–2.01 (m, 2 H, CH_2), 1.98–1.92 (m, 1 H, CH_2), 1.80–1.67 (m, 2 H, CH_2), 1.63–1.57 (m, 1 H, CH_2) ppm. ^{13}C NMR (75 MHz, $CDCl_3$): δ = 152.7 (C), 132.2 (CH), 127.1 (CH), 126.9 (CH), 111.7 (CH), 48.1 (CH), 28.9 (CH_2), 25.3 (CH_2), 19.7 (CH_2) ppm. One quaternary carbon was not detected. EI-MS: m/z = 218 $[M]^+$.

4-*tert*-Butyl-*N*-(cyclohex-2-enyl)aniline (1c): 13% yield obtained by following method A with [Ru(TPP)CO] as catalyst; 89% yield by following method B with [Ru(TPP)CO] as catalyst. $C_{16}H_{23}N$ (229.18): calcd. C 83.79, H 10.11, N 6.11; found C 84.01, H 10.02, N 6.01. ^{1}H NMR (300 MHz, $CDCl_3$): δ = 7.21 (d, 2 H, J = 8.8 Hz, HAr), 6.59 (d, 2 H, J = 8.8 Hz, HAr), 5.85 (m, 1 H, CH=C*H*–CH_2), 5.80 (m, 1 H, C*H*=CH–CH_2), 3.97 (br. s, 1 H, C*H*NH), 3.55 (br. s, 1 H, NH), 2.06–2.03 (m, 2 H, CH_2), 1.95–1.90 (m, 2 H, CH_2), 1.70–1.62 (m, 2 H, CH_2), 1.29 [s, 9 H, C(C*H*$_3$)$_3$] ppm. ^{13}C NMR (75 MHz, $CDCl_3$): δ = 145.2 (C), 140.3 (C), 130.3 (CH), 129.3 (CH), 126.5 (CH), 113.3 (CH), 48.5 (CH), 34.2 (C), 32.0 (CH_3), 29.4 (CH_2), 25.6 (CH_2), 20.1 (CH_2) ppm. EI-MS: m/z = 229 $[M]^+$.

4-(Cyclohex-2-enylamino)benzonitrile (1d):[53] 13% yield obtained by following method A with [Ru(TPP)CO] as catalyst; 89% yield by following method B with [Ru(TPP)CO] as catalyst. Analytical data are in accord with the literature.

***N*-(Cyclohex-2-enyl)-4-(trifluoromethyl)benzenamine (1e):**[54] 28% yield obtained by following method A with [Ru(TPP)CO] as catalyst; 85% yield by following method B with [Ru(TPP)CO] as catalyst; 30% yield by following method A with **10** as catalyst; 55% yield by following method B with **10** as catalyst. 25% yield by following method A with **11** as catalyst; 99% yield by following method B with **11** as catalyst. Analytical data are in accord with the literature.

Methyl-4-(cyclohex-2-enylamino)benzoate (1f):[51] 13% yield obtained by following method A with [Ru(TPP)CO] as catalyst; 85% yield by following method B with [Ru(TPP)CO] as catalyst. Analytical data are in accord with the literature.

3,5-Dichloro-*N*-(cyclohex-2-enyl)benzenamine (1g):[51] 38% yield obtained by following method A with [Ru(TPP)CO] as catalyst; 90% yield by following method B with [Ru(TPP)CO] as catalyst. Analytical data are in accord with the literature.

***N*-(Cyclohex-2-enyl)-4-methoxybenzenamine (1h):**[54] 8% yield obtained by following method A with [Ru(TPP)CO] as catalyst; 33% yield by following method B with [Ru(TPP)CO] as catalyst. Analytical data are in accord with the literature.

3,5-Bis(trifluoromethyl)-*N*-(3-methylcyclohex-2-enyl)benzenamine (2aA) and 3,5-Bis(trifluoromethyl)-*N*-(2-methylcyclohex-2-enyl)-benzenamine (2aB): 43% yield (A/B = 65:35) obtained by following method A with [Ru(TPP)CO] as catalyst; 60% yield (A/B = 63:34) by following method A with **7** as catalyst; 88% (A/B = 56:44) yield by following method B with **7** as catalyst. **2aA** and **2aB:** $C_{15}H_{15}F_6N$ (323.11): calcd. C 55.73, H 4.68, N 4.33; found C 56.09, H 4.90, N 4.67. ^{19}F NMR (282 MHz, $CDCl_3$): δ = –63.56 ppm. EI-MS: m/z = 323 $[M]^+$. **2aA:** ^{1}H NMR (300 MHz, $CDCl_3$): δ = 7.11 (s, 1 H, H_{Ar}), 6.93 (s, 2 H, H_{Ar}), 5.44–5.43 (m, 1 H, C*H*=C–CH_3), 4.13 (br. s, 1 H, NH), 4.01 (br. s, 1 H, C*H*NH), 1.98–1.95 (m, 2 H, CH_2), 1.88–1.83 (m, 2 H, CH_2), 1.72 (s, 3 H, CH_3), 1.71–1.64 (m, 2 H, CH_2) ppm. ^{13}C NMR (75 MHz, $CDCl_3$): δ = 148.7 (C), 139.7 (C), 132.9 (q, J = 30.9 Hz, *C*–CF_3), 124.0 (q, J = 270.9 Hz, *C*F_3), 121.6 (CH), 112.5 (CH), 110.0 (CH), 48.7 (CH), 30.4 (CH_2), 28.5 (CH_2), 24.1 (CH_3), 20.0 (CH_2) ppm. **2aB:** (300 MHz, $CDCl_3$): δ = 7.11 (s, 1 H, H_{Ar}), 6.93 (s, 2 H, H_{Ar}), 5.68–5.66 (m, 1 H, C*H*=C–CH_3), 4.13 (br. s, 1 H, NH), 3.84 (br. s, 1 H, C*H*NH), 2.04–2.02 (m, 2 H, CH_2), 1.75 (m, 3 H, CH_3), 1.70–1.56 (m, 4 H, CH_2) ppm. ^{13}C NMR (75 MHz, $CDCl_3$): δ = 148.2 (C), 133.3 (C), 132.9 (q, J = 30.9 Hz, *C*–CF_3), 127.2 (CH), 124.0 (q, J = 270.9 Hz, CF_3), 112.2 (CH), 110.0 (CH), 51.4 (CH), 28.1 (CH_2), 25.5 (CH_2), 21.9 (CH_3), 18.2 (CH_2) ppm.

 © 2012 Wiley-VCH Verlag GmbH & Co. KGaA, Weinheim

***N*-(3-Methylcyclohex-2-enyl)-4-nitroaniline (2bA) and *N*-(2-methylcyclohex-2-enyl)-4-nitroaniline (2bB):**[33] 20% yield (**2bA** + **2bB**) obtained by following method A with [Ru(TPP)CO] as catalyst. Analytical data are in accord with the literature.

***N*-(3-Methylcyclohex-2-enyl)-4-trifluoromethylaniline (2eA) and *N*-(2-methylcyclohex-2-enyl)-4-trifluoromethylaniline (2eB):** 26% yield (A/B = 65:35) obtained by following method A with [Ru(TPP)CO] as catalyst; 30% yield (A + B) by following method A with **10** as catalyst; 42% yield (A/B = 66:34) by following method A with **11** as catalyst; 99% yield (A + B) by following method B with **11** as catalyst. **2eA:** ^{1}H NMR (300 MHz, $CDCl_3$): δ = 7.41 (d, 2 H, J = 8.4 Hz), 6.63 (d, 2 H, J = 8.4 Hz), 5.66 [br. s, 1 H, C*H*=C(CH_3)], 4.01 (br. s, 1 H, NH), 3.86 (br. s, 1 H, C*H*NH), 2.05–1.88 (m, 3 H, CH_2), 1.77 (s, 3 H, CH_3), 1.63–1.56 (m, 3 H, CH_2) ppm. ^{13}C NMR (100 MHz, $CDCl_3$): δ = 150.2 (C), 133.5 (C), 126.7 (CH), 126.4 (CH), 118.1 (*C*CF_3, q, J = 32.1 Hz), 111.8 (CH), 50.8 (CH), 28.0 (CH_2), 25.2 (CH_2), 21.6 (CH_3), 17.7 (CH_2) ppm, the CF_3 signal was not detected. **2eB:** ^{1}H NMR (300 MHz, $CDCl_3$): δ = 7.40 (d, 2 H, J = 8.7 Hz), 6.62 (d, 2 H, J = 8.7 Hz), 5.48 [br. s, 1 H, C*H*=C(CH_3)], 4.00 (m, 2 H, CHNH), 1.98 (m, 2 H, CH_2), 1.86–1.84 (m, 1 H, CH_2), 1.72 (s, 3 H, CH_3), 1.71–1.61 (m, 3 H, CH_2) ppm. ^{13}C NMR (75 MHz, $CDCl_3$): δ = 150.2 (C), 139.1 (C), 127.0 (CH), 122.4 (CH), 118.7 (q, J = 32.6 Hz, *C*CF_3), 112.5 (CH), 48.4 (CH), 30.4 (CH_2), 28.7 (CH_2), 24.2 (CH_3), 20.1 (CH_3) ppm, the CF_3 signal was not detected.

***N*-[3,5-Bis(trifluoromethyl)phenyl]-1,2-dihydronaphthalen-2-amine (3aA) and *N*-[3,5-Bis(trifluoromethyl)phenyl]-1,2-dihydronaphthalen-1-amine (3aB):** 57% yield (A/B = 58:42) obtained by following method A with [Ru(TPP)CO] as catalyst; 85% yield (A/B = 60:40) by following method B with [Ru(TPP)CO] as catalyst; 60% yield (A/B = 65:35) by following method A with **7** as catalyst. **3aA:** $C_{18}H_{13}F_6N$ (357.09): calcd. C 60.51, H 3.67, N 3.92; found C 60.80, H 3.82, N 4.00. ^{1}H NMR (300 MHz, $CDCl_3$): δ = 7.26–7.13 (m, 5 H, H_{Ar}), 6.95 (s, 2 H, H_{Ar}), 6.65 [d, 1 H, J = 9.3 Hz, C*H*=CH–CH(NH)], 6.08 [dd, 1 H, J = 9.3 Hz and 4.5 Hz, CH=C*H*–CH(NH)], 4.38 [1 H, dddd, J = 8.4, 6.3, 6.3 Hz and 4.5 Hz, C*H*(NH)], 4.16 (d, 1 H, J = 8.4 Hz, NH), 3.12 (dd, 1 H, J = 15.9 Hz and 6.3 Hz, CH_2), 3.02 (dd, 1 H, J = 15.9 Hz and 6.3 Hz, CH_2) ppm. ^{13}C NMR (75 MHz, $CDCl_3$): δ = 147.2 (C), 132.4 (q, J = 32.8 Hz, *C*–CF_3 overlapping with another quaternary carbon), 129.9 (CH), 128.6 (CH), 127.8 (CH), 127.1 (CH, two signals overlaid), 126.6 (CH), 123.4 (q, J = 270.8 Hz, *C*F_3), 112.1 (CH), 110.2 (CH), 46.4 (CH), 33.3 (CH_2) ppm. ^{19}F NMR (282 MHz, $CDCl_3$): δ = –63.17 ppm. EI-MS: m/z = 357 $[M]^+$. **3aB:** $C_{18}H_{13}F_6N$ (357.09): calcd. C 60.51, H 3.67, N 3.92; found C 60.61, H 3.88, N 3.97. ^{1}H NMR (400 MHz, $CDCl_3$): δ = 7.34–7.24 (m, 3 H, H_{Ar}), 7.19–7.17 (m, 2 H, H_{Ar}), 7.01 (s, 2 H, H_{Ar}), 6.62 (dt, 1 H, J = 9.6 Hz and 1.6 Hz, C*H*=CH–CH_2), 6.02 (dt, 1 H, J = 9.6 Hz and 4.3 Hz, CH=C*H*–CH_2), 4.76 (dt, 1 H, J = 8.6 Hz and 6.3 Hz, C*H*=NH), 4.37 (d, 1 H, J = 8.6 Hz, NH), 2.64 (ddd, 2 H, J = 6.3, 4.3 Hz and 1.6 Hz, CH_2) ppm. ^{13}C NMR (100 MHz, $CDCl_3$): δ = 147.7 (C), 134.5 (C), 133.3 (C), 132.6 (q, J = 32.8 Hz, *C*–CF_3), 128.5 (CH), 128.0 (CH), 127.8 (CH), 126.9 (CH, two signals overlaid), 125.7 (CH), 123.5 (q, J = 270.9 Hz, *C*F_3), 112.3 (CH), 110.3 (CH), 50.4 (CH), 29.4 (CH_2) ppm. ^{19}F NMR (282 MHz, $CDCl_3$): δ = –63.50 ppm. EI-MS: m/z = 357 $[M]^+$.

***N*-(4-Nitrophenyl)-1,2-dihydronaphthalen-2-amine (3bA) and *N*-(4-Nitrophenyl)-1,2-dihydronaphthalen-1-amine (3bB):** 54% yield (A/B = 59:41) obtained by following method A with [Ru(TPP)CO] as catalyst; 73% yield (A/B = 61:39) by following method B with [Ru(TPP)CO] as catalyst. **3bA** and **3bB:** $C_{16}H_{14}N_2O_2$ (266.11): calcd. C 72.16, H 5.30, N 10.52; found C 71.76, H 5.27, N 10.46. **3bA:** ^{1}H NMR (300 MHz, $CDCl_3$): δ = 8.11 (d, 2 H, J = 9.0 Hz, H_{Ar}), 7.27–7.16 (m, 4 H, H_{Ar}), 6.69 (d, 1 H, J = 9.6 Hz, C*H*=CH–CH), 6.58 (d, 1 H, J = 9.0 Hz, H_{Ar}), 6.10 (dd, 1 H, J = 9.6 Hz, J = 4.5 Hz, CH=C*H*–CH), 4.51 (m, 1 H, C*H*NH), 4.46 (m, 1 H, NH), 3.11 (m, 2 H, CH_2) ppm. ^{13}C NMR (75 MHz, $CDCl_3$): δ = 154.2 (C), 152.3 (C), 130.8 (CH), 129.2 (CH), 128.4 (CH), 127.7 (CH), 127.3 (CH), 126.9 (CH), 112.0 (CH), 47.1 (CH), 34.0 (CH_2) ppm, two quaternary carbon atoms were not detected. EI-MS: m/z = 266 $[M]^+$.

***N*-[3,5-Bis(trifluoromethyl)phenyl]-1*H*-inden-1-amine (4a):** 42% yield obtained by following method A with [Ru(TPP)CO] as catalyst; 55% yield by following method A with **7** as catalyst; 70% yield by following method B with **7** as catalyst. $C_{17}H_{11}F_6N$ (343.08): calcd. C 59.48, H 3.23, N 4.08; found C 59.68, H 3.38, N 4.05. ^{1}H NMR (300 MHz, $CDCl_3$): δ = 7.46 (d, 1 H, J = 7.5 Hz, H_{Ar}), 7.38–7.35 (m, 2 H, H_{Ar}), 7.27–7.24 (m, 1 H, H_{Ar}), 7.22 (s, 1 H, H_{Ar}), 7.04 (s, 2 H, H_{Ar}), 6.92 (dd, 1 H, J = 5.7 Hz and 1.8 Hz, C*H*=CH–CH), 6.53 (d, 1 H, J = 5.7 Hz and 1.8 Hz, CH=C*H*–CH), 5.16 (d, 1 H, J = 8.7 Hz, C*H*NH), 4.34 (d, 1 H, J = 8.7 Hz, N*H*) ppm. ^{13}C NMR (75 MHz, $CDCl_3$): δ = 148.5 (C), 144.0 (C), 143.2 (C), 135.3 (CH), 133.7 (CH), 132.8 (q, J = 33.4 Hz, *C*–CF_3), 128.8 (CH), 126.4 (CH), 123.7 (q, J = 273.0 Hz, *C*F_3), 123.4 (CH), 122.0 (CH), 112.8 (CH), 111.0 (CH), 61.2 (CH) ppm. ^{19}F NMR (282 MHz, $CDCl_3$): δ = –63.57 ppm. EI-MS: m/z = 343 $[M]^+$.

***N*-(4-Nitrophenyl)-1*H*-inden-1-amine (4b):** 42% yield obtained by following method A with [Ru(TPP)CO] as catalyst; 55% yield by following method A with **7** as catalyst; 70% yield by following method B with **7** as catalyst. $C_{15}H_{12}N_2O_2$ (252.09): calcd. C 71.42, H 4.79, N 11.10; found C 71.65, H 4.95, N 10.92. ^{1}H NMR (300 MHz, $CDCl_3$): δ = 8.12 (d, 2 H, J = 9.3 Hz, H_{Ar}), 7.45–7.50 (d, 1 H, J = 7.2 Hz, H_{Ar}), 7.36–7.39 (m, 2 H, H_{Ar}), 7.27–7.24 (m, 1 H, H_{Ar}), 6.94 (dd, 1 H, J = 5.6, J = 1.2 Hz, C*H*=CH–CH) 6.66 (d, 2 H, J = 9.3 Hz, H_{Ar}), 6.53 (dd, 1 H, J = 5.6, J = 1.8 Hz, CH=C*H*–CH), 5.21 (dd, 1 H, J = 8.4, J = 1.2 Hz, C*H*NH), 4.71 (d, 1 H, J = 8.4 Hz, NH) ppm. ^{13}C NMR (75 MHz, $CDCl_3$): δ = 153.3 (C), 144.0 (C), 143.4 (C), 139.6 (C), 135.4 (CH), 134.1 (CH), 129.1 (CH), 126.8 (CH), 126.7 (CH), 123.6 (CH), 122.4 (CH), 112.3 (CH), 61.2 (CH) ppm. EI-MS: m/z = 252 $[M]^+$.

***N*-[4-(Trifluoromethyl)phenyl]-1*H*-inden-1-amine (4e):** 30% yield obtained by following method A with [Ru(TPP)CO] as catalyst; 14% yield by following method A with **10** as catalyst; 17% yield by following method A with **11** as catalyst. $C_{16}H_{12}NF_3$ (275.09): calcd. C 69.81, H 4.39, N 5.09; found C 69.94, H 4.73, N 5.56. ^{1}H NMR (300 MHz, $CDCl_3$): δ = 7.50 (d, 1 H, J = 7.5 Hz, H_{Ar}), 7.45 (d, 2 H, J = 8.4 Hz, H_{Ar}), 7.37 (m, 2 H, H_{Ar}), 7.24 (m, 1 H, H_{Ar}), 6.90 (dd, 1 H, J = 5.7, J = 1.2 Hz, C*H*=CH), 6.74 (d, 2 H, J = 8.4 Hz, H_{Ar}), 6.57 (dd, 1 H, J = 5.7 Hz, J = 1.8 Hz, CH=C*H*), 5.18 (d, 1 H, J = 8.7 Hz, C*H*NH), 4.23 (d, 1 H, J = 8.7 Hz, NH) ppm. ^{13}C NMR (75 MHz, $CDCl_3$): δ = 150.2 (C), 144.4 (C), 143.0 (C), 135.9 (CH), 132.9 (CH), 126.9 (CH), 126.7 (C), 126.5 (CH), 112.7 (CH), 110.1 (C), 61.1 (CH) ppm. ^{19}F NMR (282 MHz, $CDCl_3$): δ = –61.40 ppm.

***N*-(Cyclopent-2-enyl)-4-nitroaniline (5):**[33] 30% yield obtained by following method A with [Ru(TPP)CO] as catalyst. $C_{11}H_{12}N_2O_2$ (204.09): calcd. C 64.69, H 5.92, N 13.72; found C 64.54, H 5.83, N 13.98. ^{1}H NMR (300 MHz, C_6D_6): δ = 8.12 (d, 2 H, J = 9.0 Hz, H_{Ar}), 5.97 (d, 2 H, J = 9.0 Hz, H_{Ar}), 5.75 (m, 1 H, C*H*=CH), 5.47 (m, 1 H, CH=C*H*), 4.01 (m, 1 H, C*H*NH), 3.73 (br. s, 1 H, NH), 2.20–2.12 (m, 2 H, CH_2), 1.93–1.91 (m, 1 H, CH_2), 1.30–1.24 (m, 1 H, CH_2) ppm. ^{13}C NMR (75 MHz, $CDCl_3$): δ = 152.5 (C), 138.8 (C), 135.2 (CH), 130.7 (CH), 126.5 (CH), 111.6 (CH), 59.1 (CH), 31.4 (CH_2), 31.1 (CH_2). EI-MS: m/z = 204 $[M]^+$.

 © 2012 Wiley-VCH Verlag GmbH & Co. KGaA, Weinheim

3,5-Bis(trifluoromethyl)-*N*-(oct-1-en-3-yl)benzenamine (6A) and (*E*/*Z*)-3,5-Bis(trifluoromethyl)-*N*-(oct-2-enyl)benzenamine (6B): 20% yield (A/B = 45:55) obtained by following method A with [Ru(TPP)CO] as catalyst; 11% yield (A/B = 45:55) by following method A with **7** as catalyst; 22% yield (A/B = 50:50) by following method B with **7** as catalyst. **6A:** $C_{16}H_{19}F_6N$ (339.14): calcd. C 56.63, H 5.64, N 4.13; found C 57.02, H 6.00, N 4.06. ^{1}H NMR (300 MHz, $CDCl_3$): δ = 7.13 (s, 1 H, H_{Ar}), 6.94 (s, 2 H, H_{Ar}), 5.72 (ddd, 1 H, J = 17.2, 10.3 Hz and 6.1 Hz, C*H*=CH_2), 5.23 (d, J = 17.2 Hz, 1 H, CH=CH_2), 5.20 (d, 1 H, J = 10.3 Hz, CH=CH_2), 4.09 (d, J = 6.9 Hz, 1 H, NH), 3.87–3.83 [m, 1 H, C*H*(NH)], 1.65–1.61 (m, 2 H, CH_2), 1.36–1.30 (m, 6 H, CH_2), 0.92 (3 H, pst, J = 6.9 Hz, CH_3) ppm. ^{13}C NMR (75 MHz, $CDCl_3$): δ = 148.5 (C), 138.9 (CH), 132.6 (q, J = 32.4 Hz, *C*–CF_3), 124.0 (q, J = 270.8 Hz, *C*F_3), 116.4 (CH_2), 112.8 (CH), 110.4 (br., CH), 56.4 (CH), 36.1 (CH_2), 32.0 (CH_2), 25.9 (CH_2), 22.9 (CH_2), 14.4 (CH_3) ppm. ^{19}F NMR (282 MHz, $CDCl_3$): δ = –63.57 ppm. EI-MS: m/z = 339 $[M]^+$. **6B:** E/Z = 63:37. $C_{16}H_{19}F_6N$ (339.14): calcd. C 56.63, H 5.64, N 4.13; found C 56.90, H 5.85, N 3.99. ^{1}H NMR (300 MHz, $CDCl_3$): *E* isomer: δ = 7.16 (s, 1 H, H_{Ar}), 6.96 (s, 2 H, H_{Ar}), 5.77–5.64 (m, 1 H, C*H*=CH), 5.54–5.51 (m, 1 H, C*H*=CH), 4.20 (br. s, 1 H, NH), 3.79–3.76 (m, 2 H, CH_2), 2.09–2.05 (m, 2 H, CH_2CH=CH), 1.40–1.20 (m, 6 H, CH_2), 0.93–0.89 (m, 3 H, CH_3) ppm; *Z* isomer: δ_H = 7.17 (s, 1 H, H_{Ar}), 6.96 (s, 2 H, H_{Ar}), 5.77–5.64 (m, 1 H, C*H*=CH), 5.54–5.51 (m, 1 H, C*H*=CH), 4.12 (br. s, 1 H, NH), 3.84–3.81 (m, 2 H, CH_2), 2.17–2.14 (m, 2 H, CH_2CH=CH), 1.40–1.20 (m, 6 H, CH_2), 0.93–0.89 (m, 3 H, CH_3) ppm. ^{13}C NMR (75 MHz, $CDCl_3$): δ = 148.7 (C), 134.8 (CH), 134.7 (CH), 132.3 (m, *C*–CF_3), 125.0 (CH), 124.9 (CH), 112.0 (CH), 111.9 (CH), 110.1 (CH), 45.7 (CH_2), 40.8 (CH_2), 32.3 (CH_2), 31.5 (CH_2), 31.3 (CH_2), 29.1 (CH_2), 28.8 (CH_2), 27.6 (CH_2), 22.4 (CH_2), 14.0 (CH_3) ppm. 19F NMR (282 MHz, $CDCl_3$): δ = –63.55 ppm. EI-MS: m/z = 339 $[M]^+$.

Synthesis of 7: 3,5-Bis(trifluoromethyl)phenyl azide (223 mg, 0.87 mmol) was added to a benzene (60 mL) suspension of [Ru(TPP)(CO)] (210 mg, 0.28 mmol). The resulting dark solution was heated to reflux under nitrogen for 4 h until the complete consumption of [Ru(TPP)(CO)] was observed by TLC (SiO_2, petroleum ether/CH_2Cl_2 = 7:3). The mixture was evaporated to dryness, and the residue was purified by chromatography (alumina, petroleum ether/dichloromethane = 8:2) to give **7** (230 mg, 70%). $C_{60}H_{34}N_6F_{12}Ru$ (1167.33): calcd. C 61.70, H 2.93, N 7.20; found C 61.34, H 2.99, N 7.55. UV/Vis (CH_2Cl_2): λ_{max} [log(ε/M^{-1} cm^{-1})] = 419 [5.03], 526 [4.00] nm. IR (ATR): $\tilde{\nu}$ = 1014 (oxidation marker), 877 (imido band) cm^{-1}; IR (CH_2Cl_2): $\tilde{\nu}$ = 1016 (oxidation marker) cm^{-1}; IR (nujol): $\tilde{\nu}$ = 1016 (oxidation marker), 878 (imido band) cm^{-1}. ^{1}H NMR (300 MHz, $CDCl_3$): δ = 8.87 (s, 8 H, H_β), 8.08 (d, J = 6.9 Hz, 8 H, H_o), 7.83–7.76 (m, 12 H, H_{m-p}), 6.60 (s, 2 H, H_{Ar}), 2.66 (s, 4 H, H_{Ar}) ppm. ^{1}H NMR (300 MHz, C_6D_6): δ = 9.00 (s, 8 H, H_β), 8.17 (d, J = 6.9 Hz, 8 H, H_o), 7.62–7.58 (m, 12 H, H_{m-p}), 6.58 (s, 2 H, H_{Ar}), 2.95 (s, 4 H, H_{Ar}) ppm. ^{13}C NMR (75 MHz, $CDCl_3$): δ = 151.9 (C), 142.5 (C), 141.9 (C), 134.6 (CH), 131.9 (CH), 129.7 (q, J = 33.2 Hz, *C*–CF_3), 128.4 (CH), 127.2 (CH), 123.6 (C), 122.3 (q, J = 271.7 Hz, *C*F_3), 118.1 (CH), 117.8 (CH) ppm. ^{19}F NMR (282 MHz, $CDCl_3$): δ = –64.06 ppm. ^{19}F NMR (282 MHz, C_6D_6): δ = –63.75 ppm. ESI-MS: m/z = 1169 $[M + 1]^+$.

***N*-[3,5-Bis(trifluoromethyl)phenyl]-1,2-dihydro-4-phenylnaphthalen-2-amine (8A) and 1-[3,5-Bis(trifluoromethyl)phenyl]-1a,2,3,7b-tetrahydro-7b-phenyl-1*H*-naphtho[2,1-*b*]azirine (8B):** 61% yield (A/B = 54:46) obtained by following method A with **7** as catalyst. **8A:** $C_{24}H_{17}F_6N$ (433.13): calcd. C 66.51, H 3.95, N 3.23; found C 66.65, H 4.01, N 3.18. ^{1}H NMR (300 MHz, $CDCl_3$): δ = 7.42–7.37 (m, 5 H, H_{Ar}), 7.28–7.25 (m, 3 H, H_{Ar}), 7.19 (s, 1 H, H_{Ar}), 7.14–7.12 (m, 1 H, H_{Ar}), 7.01 (s, 2 H, H_{Ar}), 6.10 [d, 1 H, J = 4.6 Hz, C(Ph)=C*H*–CH(NH)], 4.51 [m, 1 H, C*H*(NH)], 4.26 (d, 1 H, J = 8.9 Hz, NH), 3.22 (dd, 1 H, J = 15.4 Hz and 5.7 Hz, CH_2), 3.05 (dd, 1 H, J = 15.4 Hz and 7.2 Hz, CH_2) ppm. ^{13}C NMR (75 MHz, $CDCl_3$): δ = 147.8 (C), 142.5 (C), 139.8 (C), 134.2 (C), 134.1 (C), 133.0 (q, J = 32.8 Hz, *C*–CF_3), 129.3 (CH), 128.8 (CH), 128.4 (CH), 128.3 (CH), 127.4 (CH), 126.8 (CH), 126.6 (CH), 123.9 (q, J = 271.0 Hz, *C*F_3), 112.8 (CH), 110.8 (CH), 47.7 (CH), 34.7 (CH_2) ppm. ^{19}F NMR (282 MHz, $CDCl_3$): δ = –63.51 ppm. EI-MS: m/z = 433 $[M]^+$. Compound **8B** was isolated by chromatography as a mixture with 1-phenylnaphthalene because of the very similar R_f values of these compounds in several solvents on both alumina and silica. The presence of 1-phenylnaphthalene was confirmed by GC–MS analysis. The ^{1}H, ^{13}C and ^{19}F NMR spectra of this mixture are reported in the Supporting Information. The ^{1}H and ^{13}C NMR signals of **8B** have been attributed by COSY, NOESY, HSQC and HMBC techniques.

Synthesis of 9: Complex **7** (99 mg, 8.5×10^{-2} mmol) was added to a benzene (15 mL) solution of 3,5-bis(trifluoromethyl)phenyl azide (217 mg, 8.4×10^{-1} mmol) and cyclohexene (0.42 mL, 4.25 mmol). The resulting solution was stirred at 75 °C, and the aryl azide conversion was monitored by IR spectroscopy, which measured the characteristic N_3 absorbance at 2116 cm^{-1}. After 4 h (60% of ArN_3 conversion), TLC (alumina, petroleum ether/dichloromethane = 8:2) showed the complete consumption of **7**. The reaction mixture was concentrated to 2 mL and petroleum ether (20 mL) was added. The resulting suspension was filtered to eliminate a dark insoluble residue and concentrated to 10 mL. The resulting purple solid was collected by filtration and dried in vacuo (20 mg, 18%). GC–MS analysis of the solution revealed the presence of the allylic amine *N*-(cyclohex-2-enyl)-3,5-bis(trifluoromethyl)benzenamine. $C_{72}H_{52}F_{12}N_6Ru$ (1329.47): calcd. C 65.01, H 3.94, N 6.32; found C 65.20, H 4.03, N 6.20. UV/Vis (CH_2Cl_2): λ_{max} [log(ε/M^{-1} cm^{-1})] = 414 [480], 526 [3.92] nm; IR (nujol): $\tilde{\nu}$ = 1013 (oxidation marker) cm^{-1}; IR (ATR): $\tilde{\nu}$ = 1008 (oxidation marker) cm^{-1}. ^{1}H NMR (300 MHz, $CDCl_3$): δ = 8.44 (s, 8 H, H_β), 7.90–7.87 (m, 8 H, H_o), 7.75–7.71 (m, 12 H, H_{m-p}), 6.91 (s, 2 H, H_{Ar}), 4.30–4.26 (m, 2 H, CH–C*H*=CH), 2.85–2.82 (m, 2 H, H_{Ar}), 2.61–2.59 (m, 2 H, H_{Ar}), 1.60–1.54 (m, 2 H, CH=C*H*–CH_2 overlapping with H_2O), 0.88–0.82 (m, 2 H, CH=CH–C*H*H), 0.52–0.43 (m, 2 H, CH=CH–CH*H*), 0.13–0.09 (m, 2 H, CH_2–C*H*H–CH_2 overlapping with grease), –0.04 to –0.10 (m, 2 H, CH_2–CH*H*–CH_2), –1.57 to –1.62 (m, 2 H, N–CH–C*H*H), –1.91 to –1.95 (m, 2 H, N–CH–CH*H*), –2.10 to –2.13 (m, 2 H, N–CH) ppm. The ^{13}C NMR spectrum is not reported because **9** partly decomposed during the experiment. ^{19}F NMR (282 MHz, $CDCl_3$): δ = –63.25, –63.00 ppm. ESI-MS: m/z = 1331 $[M + 1]^+$.

Synthesis of 10: 4-(Trifluoromethyl)phenyl azide (74.0 mg, 0.393 mmol) was added to a benzene (50 mL) suspension of [Ru(TPP)CO] (145 mg, 0.197 mmol) to give a dark solution, which was heated to reflux under nitrogen for 30 min. The mixture was concentrated to 30 mL and filtered to eliminate unreacted [Ru(TPP)CO]. The resulting solution was evaporated to dryness and *n*-hexane (20 mL) was added. The purple solid was collected by filtration and dried in vacuo (88 mg, 44%). $C_{58}H_{37}F_6N_6Ru$ (1032.37): calcd. C 67.44, H 3.61, N 8.14; found C 67.87, H 3.98, N 8.05. UV/Vis (CH_2Cl_2): λ_{max} [log(ε/M^{-1} cm^{-1})] = 417 [5.42], 530 [4.27] nm. IR (ATR): $\tilde{\nu}$ = 1011 (oxidation marker), 838 (imido band) cm^{-1}; IR (CH_2Cl_2): $\tilde{\nu}$ = 1015 (oxidation marker) cm^{-1}; IR (nujol): $\tilde{\nu}$ = 1012 (oxidation marker), 842 (imido band) cm^{-1}. ^{1}H NMR (300 MHz, C_6D_6): δ = 9.00 (s, 8 H, H_β), 8.15 (d, 8 H, J = 9.1 Hz, H_o), 7.59–7.58 (m, 12 H, H_{m-p}), 5.94 (d, 4 H, J = 8.4 Hz,

 © 2012 Wiley-VCH Verlag GmbH & Co. KGaA, Weinheim

H_{Ar}), 2.61 (d, 4 H, J = 8.4 Hz, H_{Ar}). ^{13}C NMR (75 MHz, C_6D_6): δ = 154.0 (C), 144.5 (C), 142.9 (C), 142.6 (C), 142.0 (*C*CF_3, q, J = 27.2 Hz), 134.7 (CH), 131.5 (CH), 126.8 (CH), 122.9 (CH), 121.9 (CF_3, q, 185.9 Hz), 118.3 (CH) ppm, the complex partly decomposed during the analysis. ^{19}F NMR (282 MHz, C_6D_6): δ = –62.6 ppm. ESI-MS: m/z = 1033 $[M + 1]^+$.

Synthesis of 11. Method I: 4-(Trifluoromethyl)aniline (45.9 mg, 2.85×10^{-1} mmol) was added to a benzene (50 mL) suspension of [Ru(TPP)CO] (105.6 mg, 1.4×10^{-1} mmol). The resulting red solution was stirred at room temperature for 30 min, concentrated to 2 mL and *n*-hexane (15 mL) was added. The resulting red solid was collected by filtration and dried in vacuo (95 mg, 75%).

Method II: 4-(Trifluoromethyl)phenyl azide (151.2 mg, 8.08×10^{-1} mmol) was added to a benzene (50 mL) suspension of [Ru(TPP)CO] (149.9 mg, 2.02×10^{-1} mmol). The resulting dark solution was heated to reflux under nitrogen for 3 h and then filtered to remove insoluble products deriving from the decomposition of **10**. The solution was evaporated to dryness and *n*-hexane (15 mL) was added. The resulting solid was collected by filtration and dried in vacuo (67.5 mg, 37%). $C_{52}H_{34}F_3N_5ORu$ (902.34): calcd. C 69.17, H 3.80, N 7.77; found C 68.87, H 4.11, N 7.49. UV/Vis (CH_2Cl_2): λ_{max} [log (ε/M^{-1} cm^{-1})] = 411 [5.42], 530 [4.39] nm. IR (ATR): $\tilde{\nu}$ = 1964 (CO stretch), 1008 (oxidation marker) cm^{-1}; IR (CH_2Cl_2): $\tilde{\nu}$ = 1942 (CO stretch), 1009 (oxidation marker) cm^{-1}; IR (nujol): $\tilde{\nu}$ = 1965 (CO stretch), 1009 (oxidation marker) cm^{-1}. ^1H NMR (300 MHz, C_6D_6): δ = 8.93 (s, 8 H, H_β), 8.27 (d, 4 H, J = 7.5 Hz, H_o), 8.10 (d, 4 H, J = 7.5 Hz, $H_{o'}$), 7.70 (4 H, pst, J = 7.5 Hz, H_m), 7.61 (4 H, pst, J = 7.5 Hz, H_p), 7.51 (4 H, pst, J = 7.5 Hz, $H_{m'}$), 6.15 (m, 2 H, H_{Ar}), 2.29 (m, 2 H, H_{Ar}), –4.08 (br. s, 2 H, NH_2) ppm. The ^2H NMR spectrum showed a signal at –13.43 ppm due to coordinated $ArNH_2$. ^{13}C NMR (75 MHz, C_6D_6): δ = 144.6 (C), 143.0 (C), 135.2 (CH), 134.2 (CH), 132.7 (CH), 127.3 (CH), 126.8 (CH), 122.5 (C) ppm. ^{19}F NMR (282 MHz, C_6D_6): δ = –61.9 ppm. FAB-MS: m/z = 902.

Kinetic Measurements: To a Schlenk flask under a nitrogen atmosphere were added the catalyst, aryl azide and cyclohexene in this order. When required, benzene was added at this point. The flask was capped with a rubber septum and immediately placed in an oil bath preheated to 75 °C. The solution was stirred for one minute to dissolve all reagents and a sample (0.2 mL) was withdrawn for IR spectroscopic analysis. Consumption of the aryl azide was followed by IR spectroscopy (2095–2130 cm^{-1}) by withdrawing samples of the solution at regular time intervals. As all reactions were run in the presence of a large excess of olefin, the apparent first-order rate constants were fitted to the equation $-d[ArN_3]/dt = k_{app}[Ru(TTP)CO][ArN_3]$. The concentration of catalyst was calculated by the exact amount of catalyst weighed in each run and was considered to remain constant during the reaction.

Supporting Information (see footnote on the first page of this article): NMR spectra of all isolated compounds, kinetic and crystallographic data.

Acknowledgments

We thank the Ministero dell'Università e della Ricerca (MIUR) (Programmi di Ricerca Scientifica di Rilevante Interesse Nazionale) for financial support.

[1] H. M. L. Davies, J. R. Manning, *Nature* **2008**, *451*, 417–424.
[2] M. M. Diaz-Requejo, P. J. Pérez, *Chem. Rev.* **2008**, *108*, 3379–3394.
[3] P. Müller, C. Fruit, *Chem. Rev.* **2003**, *103*, 2905–2919.
[4] F. Collet, C. Lescot, P. Dauban, *Chem. Soc. Rev.* **2011**, *40*, 1926–1936.
[5] M. Minozzi, D. Nanni, P. Spagnolo, *Chem. Eur. J.* **2009**, *15*, 7830–7840.
[6] F. Collet, R. H. Dodd, P. Dauban, *Chem. Commun.* **2009**, 5061–5074.
[7] S. Cenini, E. Gallo, A. Caselli, F. Ragaini, S. Fantauzzi, C. Piangiolino, *Coord. Chem. Rev.* **2006**, *250*, 1234–1253.
[8] T. Katsuki, *Chem. Lett.* **2005**, *34*, 1304–1309.
[9] S. Bräse, C. Gil, K. Knepper, V. Zimmermann, *Angew. Chem.* **2005**, *117*, 5320; *Angew. Chem. Int. Ed.* **2005**, *44*, 5188–5240.
[10] S. Cenini, F. Ragaini, E. Gallo, A. Caselli, *Curr. Org. Chem.* **2011**, *15*, 1578–1592.
[11] T. G. Driver, *Org. Biomol. Chem.* **2010**, *8*, 3831–3846.
[12] K. Omura, M. Murakami, T. Uchida, R. Irie, T. Katsuki, *Chem. Lett.* **2003**, *32*, 354–355.
[13] S. Fantauzzi, A. Caselli, E. Gallo, *Dalton Trans.* **2009**, 5434–5443.
[14] H. Lu, X. P. Zhang, *Chem. Soc. Rev.* **2011**, *40*, 1899–1909.
[15] C.-M. Che, V. K.-Y. Lo, C.-Y. Zhou, J.-S. Huang, *Chem. Soc. Rev.* **2011**, *40*, 1950–1975.
[16] H. Lu, H. Jiang, L. Wojtas, X. P. Zhang, *Angew. Chem. Int. Ed.* **2010**, *49*, 10192–10196.
[17] Y. Liu, C.-M. Che, *Chem. Eur. J.* **2010**, *16*, 10494–10501.
[18] H. Lu, J. Tao, J. E. Jones, L. Wojtas, X. P. Zhang, *Org. Lett.* **2010**, *12*, 1248–1251.
[19] H.-J. Lu, V. Subbarayan, J.-R. Tao, X. P. Zhang, *Organometallics* **2010**, *29*, 389–393.
[20] J. V. Ruppel, R. M. Kamble, X. P. Zhang, *Org. Lett.* **2007**, *9*, 4889–4892.
[21] Y. Moreau, H. Chen, E. Derat, H. Hirao, C. Bolm, S. Shaik, *J. Phys. Chem. B* **2007**, *111*, 10288–10299.
[22] J.-L. Liang, S.-X. Yuan, J.-S. Huang, C.-M. Che, *J. Org. Chem.* **2004**, *69*, 3610–3619.
[23] S. K.-Y. Leung, W.-M. Tsui, J.-S. Huang, C.-M. Che, J.-L. Liang, N. Zhu, *J. Am. Chem. Soc.* **2005**, *127*, 16629–16640.
[24] S.-M. Au, W.-H. Fung, M.-C. Cheng, C.-M. Che, S.-M. Peng, *Chem. Commun.* **1997**, 1655–1656.
[25] S. K.-Y. Leung, J.-S. Huang, J.-L. Liang, C.-M. Che, Z.-Y. Zhou, *Angew. Chem.* **2003**, *115*, 354; *Angew. Chem. Int. Ed.* **2003**, *42*, 340–343.
[26] J.-L. Liang, J.-S. Huang, X.-Q. Yu, N. Zhu, C.-M. Che, *Chem. Eur. J.* **2002**, *8*, 1563–1572.
[27] S. Cenini, E. Gallo, A. Penoni, F. Ragaini, S. Tollari, *Chem. Commun.* **2000**, 2265–2266.
[28] F. Ragaini, A. Penoni, E. Gallo, S. Tollari, C. L. Gotti, M. Lapadula, E. Mangioni, S. Cenini, *Chem. Eur. J.* **2003**, *9*, 249–259.
[29] S. Fantauzzi, E. Gallo, A. Caselli, F. Ragaini, P. Macchi, N. Casati, S. Cenini, *Organometallics* **2005**, *24*, 4710–4713.
[30] S. Fantauzzi, E. Gallo, A. Caselli, C. Piangiolino, F. Ragaini, S. Cenini, *Eur. J. Org. Chem.* **2007**, 6053–6059.
[31] C. Piangiolino, E. Gallo, A. Caselli, S. Fantauzzi, F. Ragaini, S. Cenini, *Eur. J. Org. Chem.* **2007**, 743–750.
[32] E. Gallo, M. G. Buonomenna, L. Vigano, F. Ragaini, A. Caselli, S. Fantauzzi, S. Cenini, E. Drioli, *J. Mol. Catal. A* **2008**, *282*, 85–91.
[33] A. Caselli, E. Gallo, S. Fantauzzi, S. Morlacchi, F. Ragaini, S. Cenini, *Eur. J. Inorg. Chem.* **2008**, 3009–3019.
[34] D. Intrieri, A. Caselli, F. Ragaini, S. Cenini, E. Gallo, *J. Porphyrins Phthalocyanines* **2010**, *14*, 732–740.
[35] V. Lyaskovskyy, A. I. O. Suárez, H. Lu, H. Jiang, X. P. Zhang, B. de Bruin, *J. Am. Chem. Soc.* **2011**, *133*, 12264–12273.
[36] S. Fantauzzi, E. Gallo, A. Caselli, F. Ragaini, N. Casati, P. Macchi, S. Cenini, *Chem. Commun.* **2009**, 3952–3954.
[37] J. T. Groves, R. Quinn, *J. Am. Chem. Soc.* **1985**, *107*, 5790–5792.
[38] C.-J. Liu, W.-Y. Yu, C.-M. Che, C.-H. Yeung, *J. Org. Chem.* **1999**, *64*, 7365–7374.

 © 2012 Wiley-VCH Verlag GmbH & Co. KGaA, Weinheim

[39] A porphyrinato-bis(imido)osmium complex with similar bond lengths and angles, which is inactive in C–H nitrene insertions, has been reported: J. A. Smieja, K. Shirzad, M. Roy, K. Kittilstved, B. Twamley, *Inorg. Chim. Acta* **2002**, *335*, 141–146.
[40] J. W. W. Chang, P. W. H. Chan, *Angew. Chem.* **2008**, *120*, 1154; *Angew. Chem. Int. Ed.* **2008**, *47*, 1138–1140.
[41] E. Gonzalez, P. J. Brothers, A. Ghosh, *J. Phys. Chem. B* **2010**, *114*, 15380–15388.
[42] M. J. Zdilla, M. M. Abu-Omar, *Inorg. Chem.* **2008**, *47*, 10718–10722.
[43] M. J. Zdilla, J. L. Dexheimer, M. M. Abu-Omar, *J. Am. Chem. Soc.* **2007**, *129*, 11505–11511.
[44] H. Stamm, H. Jaeckel, *J. Am. Chem. Soc.* **1989**, *111*, 6544–6550.
[45] K. Nikki, H. Inakura, L. Wu, N. Suzuki, T. Endo, *J. Chem. Soc. Perkin Trans. 2* **2001**, 2370–2373.
[46] M. Tanno, S. Sueyoshi, S. Kamiya, *Chem. Pharm. Bull.* **1982**, *30*, 3125–3132.
[47] A. D. Adler, F. R. Longo, J. D. Finarelli, J. Goldmacher, J. Assour, L. Korsakoff, *J. Org. Chem.* **1967**, *32*, 476.
[48] J. S. Lindsey, I. C. Schreiman, H. C. Hsu, P. C. Kearney, A. M. Marguerettaz, *J. Org. Chem.* **1987**, *52*, 827–836.
[49] D. P. Rillema, J. K. Nagle, L. F. Barringer Jr, T. J. Meyer, *J. Am. Chem. Soc.* **1981**, *103*, 56–62.
[50] E. Gallo, A. Caselli, F. Ragaini, S. Fantauzzi, N. Masciocchi, A. Sironi, S. Cenini, *Inorg. Chem.* **2005**, *44*, 2039–2049.
[51] F. Ragaini, S. Cenini, F. Turra, A. Caselli, *Tetrahedron* **2004**, *60*, 4989–4994.
[52] S. Cenini, S. Tollari, A. Penoni, C. Cereda, *J. Mol. Catal. A* **1999**, *137*, 135–146.
[53] Y.-C. Hsu, K.-H. Gan, S.-C. Yang, *Chem. Pharm. Bull.* **2005**, *53*, 1266–1269.
[54] O. Lober, M. Kawatsura, J. F. Hartwig, *J. Am. Chem. Soc.* **2001**, *123*, 4366–4367.

Received: July 22, 2011
Published Online: November 15, 2011

 © 2012 Wiley-VCH Verlag GmbH & Co. KGaA, Weinheim